Assessment of the Effect of Climate Change in Anticipated Water Resources Availability in Arid Climate Zones

A thesis submitted in partial fulfillment of the requirements for the degree of Doctor of Philosophy

By

Ruqayah Kadhim Mohammed

B.Sc., M.Sc.

School of Computing Science and Engineering

University of Salford

Manchester

UK

September 2017

Table of Contents

List of Figures

List of Tables

Acknowledgements

I thank the most gracious, the most merciful **ALLAH** for giving me the ability and the patience to complet this study.

Primarily, I would like to express my special appreciation to my supervisor Professor **Miklas Scholz**, you have provided exceptional academic guidance. I would like to thank you for encouraging my research from the start, and your support throughout the study period has been priceless. I am grateful for the opportunity to have worked under your supervision on this subject, through which I have learnt so much in addition to the Ph.D. itself. You have supported my development in the research community through our publications in (peer-reviewed) journals and have supported my papers in many regional and international conferences.

Many thanks go to my colleagues in the School of Computer Science and Engineering, who helped me with their advice and experience. I wish to particularly thank Dr. Furat Al-Faraj, who supported my study from the beginning. I am also very grateful for the support from Amjad Hussain, Yassine Moktari, and Mohammed Nanekely. Other colleagues and friends at the University of Salford have also supported my development, and I am truly grateful.

Special thanks to my family. Words cannot express how grateful I am to the soul of my mother, I will miss you a lot. Your memory will always be with me and I hope that you are proud of my achievement. Your prayers for me during my study sustained me on this journey. May Allah have mercy on your soul. I am grateful to the soul of my father and my brother, and to my brothers and my sisters, for all of the sacrifices that you have made on my behalf.

Dedicated

To

My Mother

Who passed away recently

A strong and gentle soul who taught me to trust in Allah, believe in hard work, and that so much could be done with a little.

Published Journal Papers Declaration

Six papers have been published in the following (peer-reviewed) journals as a part of the current research achievements:

Paper 1 Mohammed R, Scholz M (2016) Impact of climate variability and streamflow alteration on groundwater contribution to the baseflow of the Lower Zab River (Iran and Iraq). *Environmental Earth Science* 21(75):1–11. doi:10.1007/s12665-016-6205-1

Authors contributions: The first author undertook the data collection and analysis and prepared the paper draft, which was revised by Miklas Scholz.

Paper 2 Mohammed R, Scholz M (2017a) Impact of evapotranspiration formulations at various elevations on the reconnaissance drought index. *Water Resources Management* 31(1):531–548. doi:10.1007/s11269-016-1546-9

Authors contributions: Ruqayah Mohammed pledged the data collection and analysis, results visualisation and discussion, in addition to preparing the paper draft, which was revised by Miklas Scholz.

Paper 3 Mohammed R, Scholz M, Nanekely MA, Moktari Y (2017a) Assessment of models predicting anthropogenic interventions and climate variability on surface runoff of the Lower Zab River. *Stochastic Environmental Research and Risk Assessment*. doi.10.1007/s00477-016-1375-7 (in press)

Authors contributions: The first author pledged the data collection and analysis, results visualisation and discussion, and prepared the paper draft, which was

revised by Miklas Scholz. Nanekely helped in collecting some required data, and Moktari undertaking part of the hydrological models.

Paper 4 Mohammed R, Scholz M, Mohammad ZK (2017b) Temporal hydrologic alterations coupled with climate variability and drought for transboundary river basins. *Water Resources Management* 31(5):1489–1502. doi:10.1007/s11269-017-1590-0

Authors contributions: Ruqayah Mohammed undertook the data (hydrological and meteorological) collection, investigation, and analysis, results visualisation and discussion, and prepared the paper draft. Miklas Scholz revised the paper draft. Kermani provided an article regarding the study area.

Paper 5 Mohammed R, Scholz M (2017b) The reconnaissance drought index as a climatic index for the detection of climatic variability for various geographical areas but with particular reference to arid environments. *Journal of Arid Environments* 144:181–191. doi:10.1016/j.jaridenv.2017.03.014

Authors contributions: Ruqayah Mohammed undertook the meteorological data collection, investigation, and analysis, results visualisation and discussion and prepared the draft paper, which was revised by Miklas Scholz.

Paper 6 Mohammed R, Scholz M (2017c) Adaptation strategy to mitigate the impact of climate change on water resources in arid and semi-arid regions: A case Study. *Water Resources Management*. 31:3557–3573. doi 10.1007/s11269-017-1685-7

Additional Published Journal Paper Outside the Current Research Topic

Paper 4

Mohammed R, Scholz M (2017) Review of salinity intrusion in rivers and estuaries: Potential impacts of freshwater flow and tidal mixing, human interventions and sea level rise. *Journal of Water and Climate Change*. doi:10.2166/wcc.2017.334.

Authors' contributions: The first author prepared the paper draft, including literature survey, and the paper sections structuring and writing. Miklas Scholz revised the draft of the paper.

Submitted Journal Papers Declaration

Four papers have been submitted for publication in the following (peer-reviewed) journals as a part of the current research achievements:

Paper 1 Mohammed R, Scholz M (2017) Integration of the flow duration curve into digital filtering algorithms simulating climate variability and human-induced impacts on the river baseflow. *Hydrological Sciences Journal*

Authors contributions: Ruqayah Mohammed undertook the paper work, such as data exploration and examination, results visualisation and discussion, and organised the paper draft. Whereas, Miklas Scholz revised the paper draft.

Paper 2 Mohammed R, Scholz M (2017) Evaluation of the climate variability and human-induced impacts on the hydrologic anomalies and river-groundwater exchange in a semi-arid area. *Stochastic Environmental Research and Risk Assessment*

Authors contributions: Ruqayah Mohammed undertook the paper work, such as the data exploration and examination, results visualisation and discussion and organised the paper draft. Miklas Scholz revised the paper draft.

Paper 3 Mohammed R, Scholz M (2017) Water resources in arid and semi-arid regions: climate change scenarios for impact assessment and adaptation strategies. *International Journal of Climatology*

Authors contributions: The first author undertook the paper work including data gathering and examination, results visualisation and discussion, and structured the paper draft. The second author revised the paper draft.

Conferences Declaration

The author participated in the following (local and international) conferences:

1. Ajman 4th International Environment Conference 2016

Mohammed R, Scholz M (2016) Impact of potential evapotranspiration methods at various altitudes on the reconnaissance drought index alpha form for arid and semi-arid regions

2. Shanghai 2016 International Conference on Water Resource and Environment (WRE2016)

Mohammed R, Scholz M (2016) The Reconnaissance Drought Index as a Climatic Index for the Detection of Climatic Variability for Various Geographical Areas

3. Salford Postgraduate Annual Research Conference (SPARC) 2016

Mohammed R, Scholz M, Yu Wang (2016) Assessment of the Potential Impact of Climate Variability Linked to Drought on the Temporal Hydrologic Alterations Shared River Basins. The University of Salford, Salford, Greater Manchester, United Kingdom, Salford Postgraduate Annual Research Conference (SPARC 2016) Book of Abstracts, 14–15 June 2016, MediaCityUK, ISBN: 978-1-907842-85-6

4. Computing Science and Engineering-Postgraduate Symposium (CSE-PGSym16)

Mohammed R, Scholz M, Yu Wang (2016) Evaluation of the Potential Impacts of Climate Change Coupled with Drought on the Temporal Hydrologic Alterations in Transboundary River Basins. The University of Salford, Salford, Greater

Manchester, United Kingdom, Proceeding of CSE 2016 Annual PGR Symposium (CSE-PGSym16), 27th April 2016, ISBN:978-1-907842-83-2

5. The Ninth Manchester Metropolitan University Postgraduate Research Conference (9th MMU PGR)

Mohammed R, Scholz M (2016) Evaluation the climate change and streamflow alteration impacts on groundwater involvements to the base flow of the Lower Zab River. The Ninth Manchester Metropolitan University Postgraduate Research Conference (9th PGR), Manchester Metropolitan University, Greater Manchester, United Kingdom, Wednesday, 22nd February 2017. 09:00 to 17:30 (GMT)

6. Computing Science and Engineering-Postgraduate Symposium 2017 (CSE-PGSym 17)

Mohammed R, Scholz M (2017) Evapotranspiration Techniques Impacts at Different Elevations on the Reconnaissance Drought Index. The University of Salford, Salford, Greater Manchester, United Kingdom, Proceeding of CSE 2017 Annual PGR Symposium (CSE-PGSym17) 17th March 2017, ISBN:978-1-1907842-94-8

7. Salford Postgraduate Annual Research Conference (SPARC) 2017

Mohammed R, Scholz M, Yu Wang (2017) Assessment of multi-model approach for runoff simulation in Shared River Basins. The University of Salford, Salford, Greater Manchester, United Kingdom, Salford Postgraduate Annual Research Conference (SPARC 2016) Book of Abstracts, 27th–29th June 2017, MediaCityUK, ISBN:978-1-907842-98-6

Abbreviations

AET	The long-term average annual actual evapotranspiration
a_i	Meteorological station area
ANOVA	One-way analysis of variance
BC	Blaney-Criddle method
bcm	Billion Cubic Meters
BF	Baseflow
BFI	Baseflow Index
BFI_{max}	Maximum baseflow index
C	Coefficient of deep percolation
C_a	Reservoir active capacity
CD	Coefficient of Dispersion
CFSR	Climate Forecasting System Reanalysis
CMI	Crop Moisture Index
CN	Continental
C_v	Coefficient of variation
DF	Direct runoff
dP	Delta perturbations in precipitation
dPET	Delta perturbations in potential evapotranspiration
DF	The Deviation Factor
DrinC	Drought Indices Calculator
D_t	The actual water yield over the period t
DP	Delta Perturbation
EFC	Environmental Flow Component
ET_o	Reference evapotranspiration
FAO	Food and Agricultural Organization of the United Nations
FDC	Flow Duration Curve
G(x)	Cumulative probability of gamma distribution
GADM	Global Administrative Areas Datasets
GCM	General Circulation Models
GGES	Greenhouse Gasses Emissions Scenarios

GIS	Geographic Information System
GLCF	Global and Land Cover Facility
GR4J	Ge´nie Rural a Daily 4 parameters model
H(x)	Cumulative probability
HadCM3	Hadley Centre Coupled Model, version 3
HBV	Hydrologiska Byråns Vattenbalansavdelning (The Water Balance Department of the Hydrological Bureau)
HG	Hargreaves method
HL	Highland
IHA	Indicators of Hydrologic alterations
IoA	Index of Agreement
IPCC	Intergovernmental Panel on Climate Change
LL	Lowland
LARS-WG	Long Ashton Research Station Weather Generator
LZRB	Lower Zab River Basin
mcm	million cubic meters
MAE	Mean Absolute Error
MBE	Mean Bias Error
MD	Mediterranean
Medbasin-D	Medbasin rainfall runoff Daily model
Medbasin-M	Medbasin rainfall runoff monthly model
M–K	Mann–Kendall analysis
NDVI	Normalised Difference Vegetation Index
NCEP	National Centres for Environmental Prediction
NOAA	National Oceanic and Atmospheric Administration
NSCE	Nash–Sutcliffe Coefficient of Efficiency
OPOF	Reservoir Operational Probability of Failure
P	Precipitation
P_a	Anthropogenic intervention period precipitation
P_{av}	Basin average precipitation
P_b	Observed precipitation of the baseline period
PDSI	Palmer Drought Severity Index

PET	Potential evapotranspiration
PET_a	Anthropogenic intervention period potential evapotranspiration
PET_b	Observed potential evapotranspiration of the baseline period
PHDI	Palmer Hydrological Drought Index
P_i	Average value of the station polygon precipitation
P_{ij}	Precipitation of the j-th month of the i-th water year
P_{ij}	Precipitation of the j-th month of the i-th water year
PM	FAO Penman-Monteith methodology
P_m	Average value of the basin precipitation
P_r	Probability that a particular flow will be equivalent to or greater than a particular time ratio
PR-DCC	Precipitation-Runoff Double Cumulative Curve
r	Coefficient of correlation
R	Streamflow
R^2	Coefficient of determination
R_a	Observed streamflow subject to anthropogenic interventions period
RAI	Rainfall Anomaly Index
R_{ar}	Rebuild runoff series for the anthropogenic interventions period
R_b	Observed streamflow of the baseline period
RCM	Regional Climate Models
RCY	Reservoir Capacity Yield
RDI	Reconnaissance Drought Index
RDI_n	Normalised Reconnaissance Drought Index
RDI_{st}	Standardised Reconnaissance Drought Index
$RDI_{\alpha k}$	Initial Reconnaissance Drought Index
R_e	Reservoir Reliability
RMSE	Root Mean Square Error
R_n	Net radiation at the crop surface
$R_{obs(i)}$	Observed streamflow
RRV	Reliability, resilience, vulnerability
R_{SAMt}	multi-model streamflow simulated by the simple average model (SAM) at time t

$R_{sim(i)}$	Predicted streamflow at time step i
$R_{simi,t}$	Model streamflow simulation for i model and t time
RVA	Range of Variability Approach
SAI	Standardised Anomaly Index
SAM	Simple Average Method
SD	Standard Deviation
SDI	Streamflow Drought Index
SDM	Statistical Downscaling Models
S_{ik}	Aggregate streamflow storage for the i-th water year and the k-th reference period
S_{max}	Total capacity of the soil storage
SMDI	Soil Moisture Drought Index
SPI	Standardised Precipitation Index
SPSS	Statistical Program for Social Sciences
S_t	Reservoir storage volumes at the beginning of a time-period t
S_{t+1}	Reservoir storage volumes at the end of a time-period t
SWSI	Surface Water Supply Index
t	Time step
TF	Total flow
TFPW	Trend free pre-whitening
ThW	Thornthwaite
T_m	Mean air temperature
TR	Tropical
u_2	Wind speed at 2-m elevation
UNECE	United Nations Economic Commission for Europe
UNESCO	United Nations Educational, Scientific and Cultural Organization
UN-ESCWA	United Nations Economic and Social Commission for Western Asia
V_{ij}	Streamflow storage time series of j-th month for a i-th water year
WG	Weather Generator
WMO	World Meteorological Organization
Y	Yield
y_i	$Ln(\alpha_{ki})$

α	Filter parameter
α_k	Initial value of reconnaissance drought index (RDI) index
β	Scale parameter
γ	Psychrometric constant
$\Gamma(\gamma)$	Gamma function
Δ	Slope vapour pressure curve
φ	Reservoir Resilience
υ	Vulnerability
GƆ	Coefficient of plant-available water related to the vegetation category

Abstract

Climate change impact and drought phenomena linked with anthropogenic pressure have become a growing concern for water resource managers and policy makers, particularly in arid and semi-arid regions. This research proposes generic methodologies to evaluate the prospective impact of such changes at a basin-scale. The Lower Zab River Basin, northern Iraq, has been selected as a representative case study. These methodologies have been achieved through the following: (1) Highlight the impact of potential evapotranspiration (PET) methods, elevation, and climatic conditions on the reconnaissance drought index (RDI) results, applying three of the most widespread PET estimates, which are Thornthwaite, Hargreaves, and Blaney-Criddle in addition to the Food and Agriculture Organization Penman-Monteith reference technique, using data from 24 stations cover different elevations and climatic conditions for the period from 1979 to 2014. The initial form of RDI is directly influenced by the selected PET method at different elevations for all regions. (2) Combine the results of the flow duration curve and the digital filtering algorithms to overcome the limitations of the traditional baseflow separation methods, and then determine the baseflow annual variations. The water yielded from the basin storage system during the dry seasons resulted in dissimilarities in the observed baseflow index between the pre-damming and post-damming periods of the streamflow. (3) Quantify the hydrological alterations of various flow characteristics utilise the Indicators of Hydrologic Alteration method, in addition to multi-regression, hydrologic sensitivity, and hydrologic model simulations. Climate change was the main factor reducing streamflow. (4) Compare the results of seven ensembles General Circulation Models (GCM) with the results of delta perturbation (DP) scenarios. Both scenarios predicted almost identical decreases in the mean monthly flows to the reservoir. The DP scenarios allow the sensitivity of the impact models to climate change to be more evidently determined compared to GCM scenarios so that they could be complemented GCM scenarios.

Chapter 1: INTRODUCTION

1.1 General Background

One of the most serious environmental issues facing the world today is climate change, it is widely accepted that global warming has the potential to affect many humans dramatically and adversely because of both natural and anthropogenic changes in temperature, precipitation, sea level, storms, air quality, and other climatic conditions (IPCC, 2014). The fifth assessment report of the intergovernmental panel on the climate change, IPCC, explained that the impacts of global warming on natural and human systems are observed on all continents and across the oceans (IPCC, 2014). Hydrological cycle alterations are considered to be one of the most climate change impacts, for example, floods, drought, and storms (IPCC, 2007; Suen, 2010; Ludwig et al., 2014; Doll and Zhang, 2010; Mittal et al., 2016). By the end of the 21st century, it is more likely that global mean air temperature will increase by 1.4 °C to nearly 5.8 °C (IPCC, 2001). However, the Middle East and North Africa (MENA) will likely encounter a decrease in rainfall and runoff between 10 and 25% and between 10 and 40%, respectively, and an increase in evaporation between 5 and 20% (Jagannathan et al., 2009).

Many arid and semi-arid areas, such as Mediterranean geographical regions, western USA, southern Africa, north-east Brazil, southern and eastern Australia have witnessed a decline in water resources as a result of climate change (IPCC, 2007, 2014). It is expected that by the mid of 21st century the annual mean streamflow to decline between 10 and 30% at many dry areas at mid-latitudes and dry tropics (IPCC, 2007; Wang et al., 2016). A growing number of studies have highlighted drought-prone areas and water stress are anticipated to increase in some parts of the world and flood risks are foreseen to rise in others owing to changing the climate (Sun and Feng, 2013; Jiang et al., 2014).

The third report of the IPCC confirmed that there are critical limitations in existing adaptation options assessment and the current knowledge of adaptation and adaptive capacity to climate variability is inadequate. Developing storage reservoirs and irrigation schemes, inter-basin water transfers by networks of pipes and canals, and further development of groundwater resources are some of the traditional adaptation strategies for arid and semi-arid areas (Ragab and Prudhomme, 2002; Wan et al., 2015). A precise evaluation of the implications of a wide range of potential climate change scenarios is needed to effectively handle possible climate alterations (Stagl and Hattermann, 2016). Additionally, adaptation to such change in a shared river catchment is not limited to the nation and sub-nation-based capacities but should be treated as an on-going and long-term process to be incorporated in all levels of planning and operation or implementation (Gibson et al., 2005).

1.2 Problem Statement

Climate change impacts and uncertainties have become a major concern facing water resources managers and decision makers, in particular in arid and semi-arid areas in developing countries. Increased population growth and a growing demand for water have noticeably worsened the disproportional and intense competition among transboundary river basins. Literature has highlighted gaps in the knowledge and the urgent need to develop a set of methodologies and equations to help water resources managers and policy makers to make informed and robust decision in facing many uncertainties about the future, which can help them to cope with and mitigate the potential adverse effects of climate change on water resources availability. The impact of climate change associated with a spectrum of uncertainties has become a growing concern, which presses heavily on water resources managers and decision makers, on how to handle and mitigate the present and the anticipated adverse effects on water resources availability.

The main questions that may arise are: How can the results of the hydrologic impact studies be best used to enable managers to make an informed and robust decision in facing many uncertainties about the future? What an effective decision that can practically be put in place to address the growing problem due to the increasing need for water in a changing climate?

In addition, how well would the water resources managers' decisions work across a spectrum of climate change uncertainty?

In order to study the problem and achieve the main research aim, the Lower Zab River Basin (LZRB) shared between Iraq and Iran has been selected as a case study. The magnitude of problems plaguing the LZRB has a great deal in common with other watersheds, such as Rhine, Volta, and Senegal, where the problems of shared water resources utilisation in a sustainable manner is expected to exacerbate under the collective impact of uncertainty surrounding climate change.

The drainage area of the LZRB occupies about 20,604.95 km^2, of which 76% is located in Iraq and 24% in Iran. In the latter region, substantial water withdrawal is currently taking place. There has been a noticeable growth in water storage facilities, and plans for additional control arrangements upstream. The basin covers a range of relatively large watershed and a wide range of climatic and hydrologic conditions. The upstream and downstream developments vary widely. This suggests a wide range of uncertainties in climate change impacts on water resources availability, which can be assessed. The proposed study aims at developing a set of practical methodologies and equations for integrated water management in river basin under future climate change storylines.

Findings are expected to significantly contribute to the knowledge of integrated water resources management in developing countries, in particular, arid and semi-arid areas under climate change uncertainties.

1.3 Aim and Objectives

The aim of the study is to provide engineers, planners, and policy makers with a meaningful ensemble of projected changes in water storage reliability with which to plan for the future, by developing a set of methodologies and equations to help with climate change adaptation and mitigation. To achieve the above aim, the following objectives are identified as shown in Figure 1.1.

1. To evaluate the sensitivity of the reconnaissance drought index to the potential evapotranspiration formulations at various elevations and climatic conditions and highlight the use of the reconnaissance drought index as an aridity and climatic index.

2. To assess the link between a flow duration curve and an Eckhardt (2005) digital filtering algorithm to overcome the limitations of the traditional approaches of baseflow separation.

3. To evaluate the spatiotemporal hydrologic alterations coupled with climate variability and drought events in a river basin.

4. To evaluate and compare the results of the general circulation models and the delta perturbation scenarios, to investigate how these scenarios differ from each other in terms of their ability to simulate streamflow and reservoir performance.

Figure 1.2 shows that the objectives of this research have been published in many (peer-reviewed) journals.

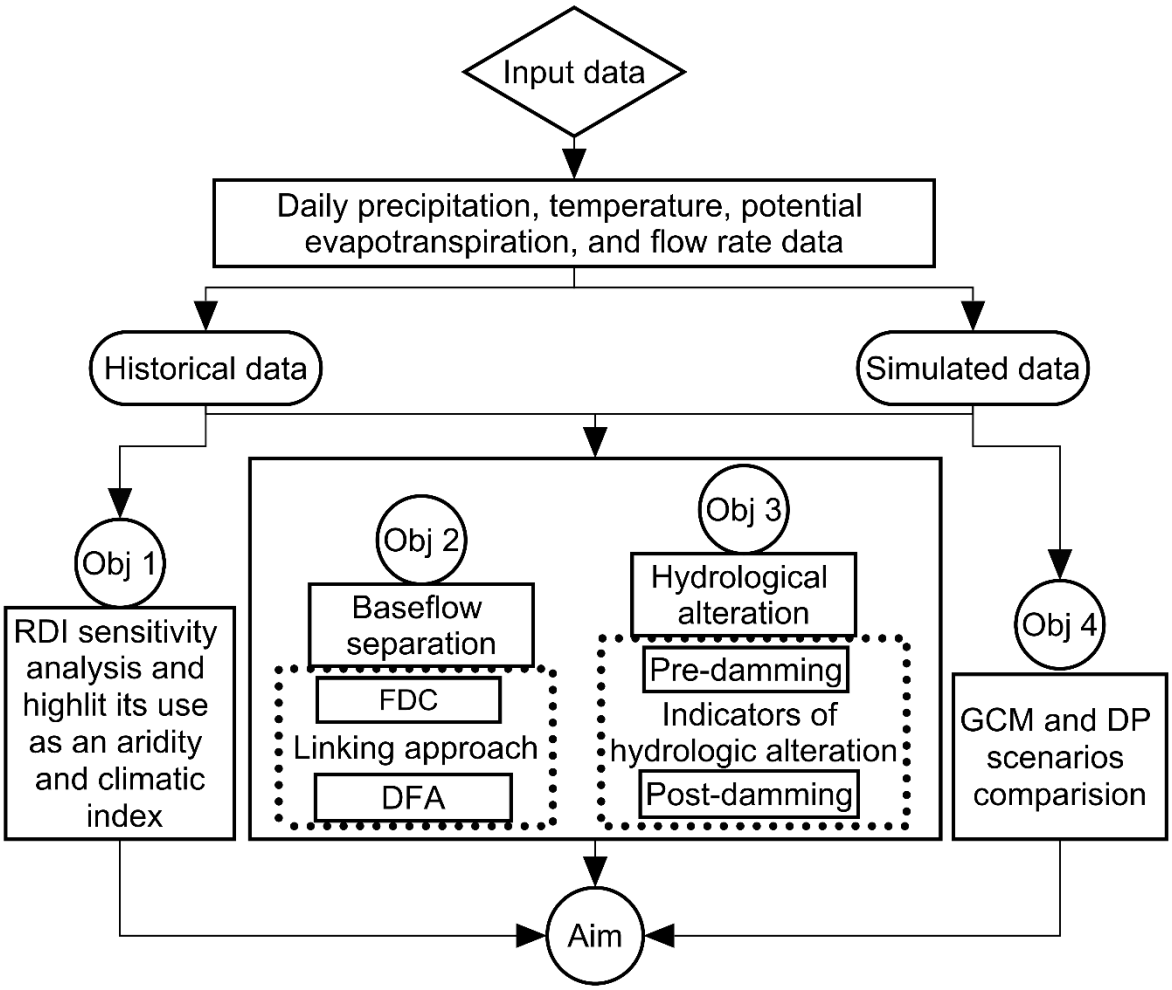

CC=Climate change;
DFA=Digital filtering algorithem;
DP=Delta perturbation climate scenario;
FDC=Flow duration curve;
GCM= General circulation models;
Obj=Objective; and
RDI=Reconnaissance drought index.

Figure 1.1 The advancement of the objectives to achieve the main research aim

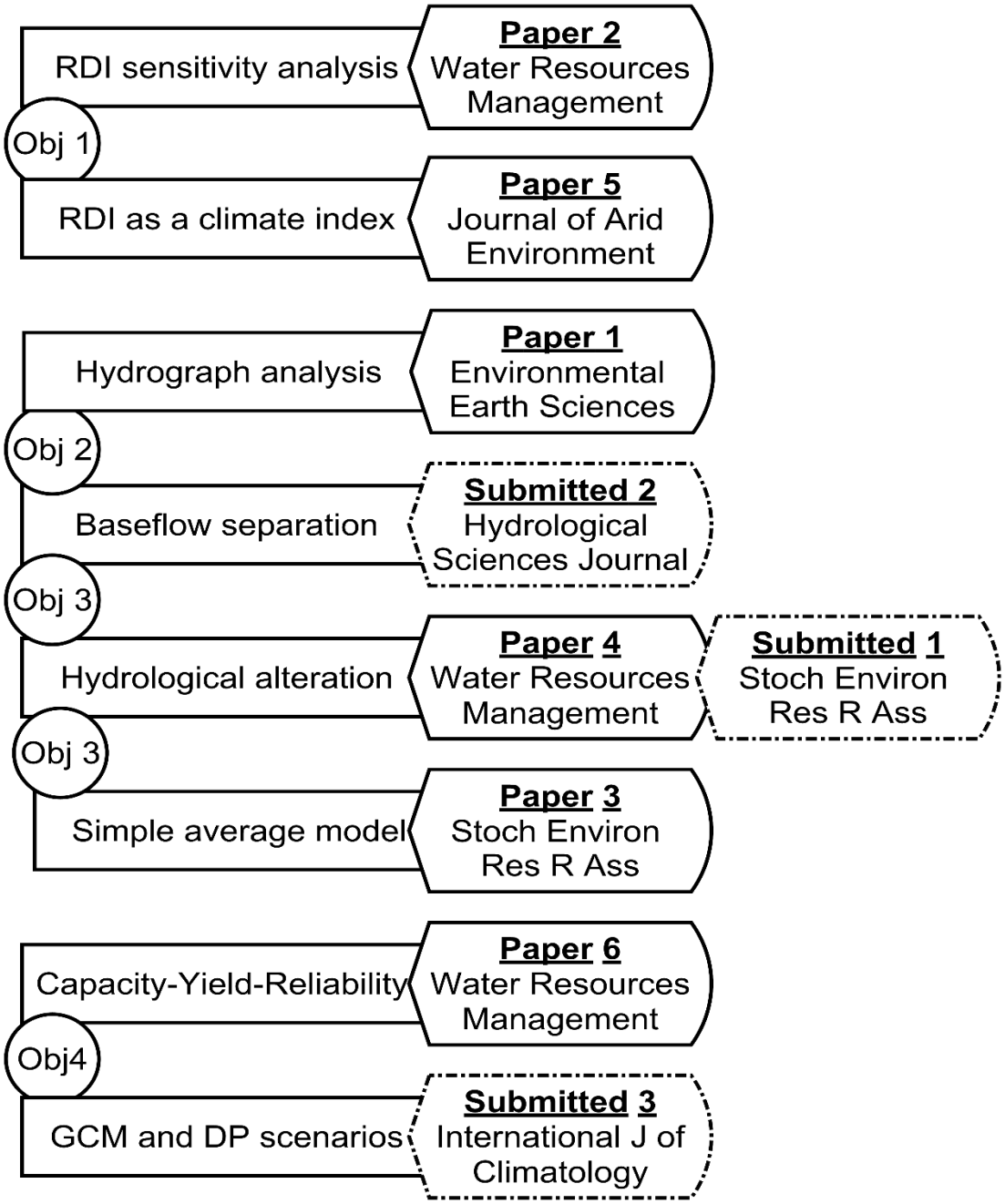

DFA = Digital filtering algorithem;
DP = Delta perturbation climate scenario;
FD = Flow duration curve;
GCM = General circulation model scenario;
J = Journal;
Obj = Objective;
RDI = Reconnaissance drought index; and
Stoch Environ Res R Ass = Stochastic Environmental Research and Risk Assessment.

Figure 1.2 Flowchart lists the published and the submitted journal papers based on the research objectives

1.4 Thesis Outline

This thesis has been organised into five Chapters as listed in the following:

Chapter 1: INTRODUCTION

The introduction represents the basis of the thesis as it presents the focus points of the research. The chapter involves the following sections: General Background, Problem Statement, Aim and Objectives, and Thesis Outline.

Chapter 2: CRITICAL LITERATURE REVIEW

Chapter two presents the research literature survey that has been critically reviewed. The chapter covers Overview, Hydro-Climatic Data Trend Analysis, Drought Analysis, Hydrograph Analysis, Hydrologic Alteration , Anthropogenic Interventions Evaluation, Climate Change Scenarios, Climate Change , Climate Forecasting System Reanalysis Data.

Chapter 3: METHODS, MODELS, AND APPLICATIONS

This chapter explores the details of the materials and the methodology. This chapter encompasses the following sections and sub-sections: Overview, Representative Case Study, Data Availability and Collection, Tools Implemented, Methodology (Hydro-Climatic Data Trend Analysis, Potential Evapotranspiration Estimation, Basin Average Precipitation Computation, Drought and Aridity Identification, Hydrograph Analysis, Hydrologic Alteration, Normal Years Identification, Rainfall-Runoff Simulation, Hydrologic Sensitivity Analysis Method, Multi-Regression Method, Separation Effect Framework, Climate Change Impact, Model Performance Criteria, Climate Change Scenarios, Reservoir Capacity-Yield-Reliability, and Long Ashton Research Station Weather Generator Model.

Chapter 4: RESULTS AND DISCUSSION

The results and the main findings are presented and discussed in detail. Chapter four consists the following sections: Hydro-Climatic Data Trend Analysis, Hydro-Climatic Data Change Point Detection, Basin Average Precipitation Computation, Drought Analysis (Drought Identification, Reconnaissance Drought Index Sensitivity Analysis, Impacts of Potential

Evapotranspiration Methods, Reconnaissance Drought Index as a Climatic Index, Drought and Aridity Trends, and Future Scenarios, Relationships between Meteorological and Hydrological Drought), Hydrograph Analysis (Flow Duration Curve Linked to Digital Filtering Algorithms (Upstream Sub-Basin and Downstream Sub-Basin), Impact, Climate Change and Drought Episode Impact on the Hydrograph, Seasonal Variations of the Baseflow Index), Hydrologic Alteration (Overview and Anthropogenic Intervention Impact of on the Streamflow), Anthropogenic Interventions Evaluation (General , Rainfall-Runoff Models Calibration and Validation, Multi-Regression Equation, Methods of Hydrologic Sensitivity Analysis, Methods of Hydrological Simulation, Simple Average Method and Single Model Predictions), Climate Change (Rainfall-Runoff Simulation, LARS-WG5.5 Calibration and Validation, Meteorological Variables, Drought Identification and Hydrologic Alteration (Delta Perturbation Scenario andGeneral Circulation Model Scenario), Reservoir Inflow, and Reservoir Capacity-Yield-Reliability Relationships.

<u>Chapter 5:</u> CONCLUSIONS AND RECOMMENDATIONS

Chapter five provides detailed: Conclusions (Drought Analysis, Hydrograph Analysis, Streamflow Alteration, Anthropogenic Interventions Evaluation, and Climate Change Evaluation), Recommendations for Future Research, and Limitations of the Study.

Chapter 2: CRITICAL LITERATURE REVIEW

2.1 Overview

Climate change affects the function and operation of existing water infrastructure as well as water management practices. Current water management practices are likely to be unable to reduce the negative impacts of climate change on water supply reliability, flood risk, health, energy, and aquatic ecosystems (Park and Kim, 2014). Considering the importance of basin storage reliability and its potential sensitivity to climate change, many studies have addressed these issues (Fowler et al., 2003; Li et al., 2010; Raje and Mujumdar, 2010; Watts et al., 2011; Bardsley et al., 2013; Chatterjee et al., 2014; Kiparsky et al., 2014; Park and Kim, 2014). They have investigated the hydrological regime alterations due to climate change impacts on water supply reliability. However, the majority of studies have only analysed the direct effect of such change on the hydrologic cycle, rather than assessing the impacts in terms of water resources management or developing methodology(s) and/or equation(s) that can help water resources policy makers in making an effective and robust decision in facing many uncertainties about the future.

Water supply reliability models have often been derived from historical climate data that may neither accurately represent the past nor future climatic conditions (Vicuna and Dracup, 2007). This disconnect has motivated interest in the formal integration of climate change into water resources planning and management, taking into consideration the uncertainties linked to such change. Although some studies attempted to investigate the climate change uncertainties on water resources (Payne et al., 2004; Minville et al., 2009; Li et al., 2010; Raje and Mujumdar, 2010; Bastola et al., 2012; Ashofteh et al., 2012; Matonse et al., 2013); they neither incorporated the adaptation measures into their resources models, nor

investigated how well would the water resources managers' decisions work across a spectrum of climate change uncertainty.

Therefore, the current research aims to bridge the gap in decision makers' understanding of climate change on surface water systems in arid climate zones by developing a set of methodologies and equations, considering the uncertainties involved in climate change projections. In order to study the problem and achieve the main research aim, the Lower Zab River Basin (LZRB) has been selected as a representative case study; this is located in the north of Iraq. The basin covers a relatively wide range of climatic and hydrological conditions. This suggests a wide range of uncertainties in climate change impacts on water resources availability.

Findings are expected to significantly contribute to knowledge in the field of water resources, by incorporating adaptation measures into a water resource model (supply and/or demand-side), in arid climate zones. Based on the research results, an adaptable operational approach can be implemented, where the decision makers adjust the operational rules on the basis of inflow prediction and the existing state of reservoir storage at each given time step, leading to more efficient and sustainable management of the basin storage system.

2.2 Hydro-Climatic Data Trend Analysis

Based on the non-normal distribution attributes of datasets, which is common in hydro-climatic datasets, two widespread distribution-free or non-parametric techniques (Mann–Kendall analysis – M-K – and the Pettitt test) are normally applied to identify the variations in hydro-climatic time series. The former is utilised for identifying monotonic trends or slow trends, whereas the latter is applied to identify sudden changes in the average level. A brief description of these two tests can be found below.

Firstly, for trend detection in the datasets, the M-K analysis can be considered. The M-K analysis is a distribution-free technique for evaluating if there is a monotonic upward or downward trend of the considered parameters over time (Dahamsheh and Aksoy, 2007; Gedikli et al., 2008; Gedikli et al., 2010; Seibert and Vis, 2012). A monotonic downward (upward) trend indicates that the parameter consistently decreases (increases) during the studied period. However, the trend may or may not be linear. The M-K analysis can be

applied instead of a parametric linear regression test, which can be used to analyse if the slope of the computed linear regression line is different from zero. The regression test requires that the residuals from the fitted regression line are normally distributed. Such an assumption is not required by the M-K test. Previous studies (Gedikli et al., 2008; Gedikli et al., 2010; Robaa and Al-Barazanji, 2013; Seibert and Vis, 2012) have detailed the M-K method and were referred to in the development of this thesis. The M–K test requires time series to be free of autocorrelation/serial correlation. The existence of serial correlation in the datasets will increase the possibility that the M-K analysis identifies a significant trend (Shadmani et al., 2012). This caused a disproportionate rejection of the null hypothesis of no trend, while the null hypothesis is true. Therefore, pre-whitening of the original dataset before applying the M–K test is recommended (Oguntunde et al., 2011; Shadmani et al., 2012).

Secondly, the Pettitt test is applied for change point identification. Change point identifications are considered as important in the analysis of runoff datasets for studying the impacts of anthropogenic interventions and climate change. The Pettitt test is also a distribution-free method to calculate the existence change point(s) for the average of a time series if the specific change time is unidentified. This analysis is commonly applied to assess alterations in hydro-climatic data (Velázquez et al., 2011; Zhang et al., 2001).

Furthermore, the precipitation-runoff double cumulative curve (PR-DCC) can illustrate the consistency of runoff and precipitation data (Jiang et al., 2011). In general, the curve is a straight line. A variation in the trend of the curve could deduce that the properties of streamflow or precipitation have altered. The PR-DCC technique can be applied to test the homogeneity of hydrological data and is often seen as an efficient tool for the detection of the hydrological system variations due to anthropogenic interventions (Huo et al., 2008; Velázquez et al., 2011; Zhang at al., 2001). As an auxiliary method for the change point detection in the precipitation and runoff series, the PR-DCC method can be used.

By using a change point test and trend analysis, the streamflow dataset can be divided into a baseline period dataset and an anthropogenic intervention period dataset (Jiang at al., 2011). In this study, the Pettitt test for change point identification of the streamflow time series is tested for re-approval of the change points identified using PR-DCC. Depending

on the separated periods, the impacts of anthropogenic intervention and climate change on streamflow can be divided by using streamflow simulation.

2.3 Drought Analysis

One of the main water-related hazards is drought (Giannikopoulou et al., 2014), which should be considered as a three-dimensional event characterised by its severity, duration, and affected area (Tsakiris and Vangelis, 2005; Vangelis et al., 2013; Zarch et al., 2015). Despite the fact that there is no commonly agreed definition of the term drought, a universally acceptable one describes the event as a considerable decline in the water availability during a lengthy time-period and over a spacious region (Tigkas, 2008).

For identifying, quantifying, and monitoring drought, there are different suggested methodologies. One of the most popular methods, which are distinctive collections of indicators involving meteorological, hydrological and other data, is the estimation of drought indices (Tsakiris and Vangelis, 2005; Tigkas, 2008; Vangelis et al., 2013; Giannikopoulou et al., 2014). Drought indices are categorised into two main groups: common indices and ones that are more detailed. The former gives an outline of the drought event and its strength, while the latter is generally beneficial for related drought occurrences to the prospective destruction from drought in different areas of the environment, society, and overall economy (Tigkas, 2008; Tigkas et al., 2012). The indices are vital and practical elements for characterising drought and supporting policy makers for moderating its impact on various water consumption sections since they facilitate intricate interrelationships between several climatic variables. Noticeably, indices make it easier to transfer climate anomaly information to a wide range of audiences and assisting scientists in quantitative weather abnormality evaluations, in terms of their intensity, frequency, areal extent, and duration (Vangelis et al., 2013; Giannikopoulou et al., 2014). Moreover, when drought indices are utilised, the time steps are adapted and the thresholds of each index selected are considered for representing the levels of drought severity.

A high number of meteorological drought indices with different levels of intricacy have been utilised in various climatic conditions throughout the world to achieve many objectives. Examples of some of the most common drought indices are as follows: Crop moisture index

(CMI), deciles, palmer drought severity index (PDSI), palmer hydrological drought index (PHDI), percent of normal, standardised anomaly index (SAI), rainfall anomaly index (RAI), standardised precipitation index (SPI), soil moisture drought index (SMDI), and surface water supply index (SWSI), as well as indices linked to the normalised difference vegetation index (NDVI). Several authors have reviewed the current and potential operational uses of remote sensing to aid decisions on drought assessment over the last few decades, for example, Heim (2002), McVicar and Jupp (1998), and AghaKouchak et al. (2015).

The World Meteorological Organization (WMO) has put forward SPI as a universal drought index because of its capacity to estimate for various reference periods, adapting to the different response times of typical hydrological parameters to precipitation shortages (Vicente-Serrano et al., 2015). The index allows detection of different drought categories affecting different systems and areas. However, there are deficiencies associated with its failure to identify drought conditions determined not by a shortage of precipitation, but by a higher than normal atmospheric evaporative demand. The failure of SPI to capture a raised evaporative demand associated with climate change is challenging (Tsakiris and Vangelis, 2005; Cook et al., 2014). Therefore, recent drought trend studies (Sheffield et al., 2012; Vicente-Serrano et al., 2014) and drought scenarios under potential climate change projections (e.g., Hoerling et al., 2012; Cook et al., 2014) depend on drought indices that take into account precipitation and the atmospheric evaporative demand. Applying such indices, Cook et al. (2014) showed that increased potential evapotranspiration not only intensifies dry weather in areas where precipitation is already decreased, it also drives regions into a drought that would otherwise not have been.

Tigkas et al. (2012, 2015) introduced a summary of the reconnaissance drought index (RDI) theory with some practical applications; RDI is founded on the precipitation, which is observed, and potential evapotranspiration, which is estimated. RDI can be calculated for any time step and can be effectively related to agricultural drought and directly linked to the climate conditions of the area. Generally, in the case of higher temperatures, water demand increase; therefore, RDI could be amended to be used as an indicator for future drought risk assessment, related to the various sectors of water use. This makes RDI suitable for climate instability studies.

When discussing drought, it is important to have an understanding of aridity and the difference between the two events. In terms of meteor-climatology, aridity is defined as the degree to which weather lacks effective moisture. Whereas, drought is defined as the period of abnormally dry climate, adequately extensive enough to cause a serious hydrological imbalance. Generally, aridity is measured by comparing long-term average precipitation to long-term average evapotranspiration. On average, the climate is considered arid if demand is greater than supply. Drought denotes the moisture equilibrium that occurs on a monthly basis. Drought is a temporary phenomenon, whereas aridity is a permanent phenomenon.

Drought severity and aridity evaluation are impacted by many factors, such as the potential impact of potential evapotranspiration methods, meteorological station elevation variations, and climate conditions. A growing number of researchers in the field of water resources have recently used RDI as a drought evaluation index (e.g., Tigkas et al., 2012; Vanglis et al., 2013; Giannikopoulou et al., 2014; Cai et al., 2015; Zarch et al., 2015). However, they only used the standardised form without taking into consideration the other forms of the index. In addition, the studies did not consider changes in the drought severity evaluation, which would occur if there are changes in the potential evapotranspiration methods, the different elevations of the weather stations within the same basin, or the impact of the regional climate conditions. For example, although Vangelis et al. (2013) assessed the impact of different potential evapotranspiration methods on the drought severity computed by RDI, they only used data from semi-arid climates of the Mediterranean region and only for two meteorological stations, without taking into consideration other semi-arid climatic conditions, such as tropical and continental, dry climates, such as the Sahara, and humid conditions. Furthermore, Vangelis et al. (2013) only focused on the standardised form of the index (RDI_{st}) without giving any attention to the other forms, such as the initial (alpha) form ($RDI_{\alpha 12}$). Therefore, to fill the knowledge gap, this study has focused, as one of its objectives in particular, in the alpha form, which is used for aridity evaluation, attempting to answer the following questions: (1) How can the potential evapotranspiration method(s) impact on the RDI index outcomes, which in turn can change the drought severity and aridity evaluation? (2) If the elevations of the meteorological stations that have been located within the same basin changed, how would this alter the evaluation of the drought and aridity of the basin? (3) In the assessment of the regional drought severity and aridity, does a change in climatic conditions require taking account of the potential evapotranspiration estimations?

Defining the climate of a region is normally based on the long-term pattern of variations in meteorological variables, such as mean air temperature, precipitation, humidity, and wind. The long-term impacts of climate change are expected to affect land use, agriculture, water resources, society, and environmental sustainability. Accordingly, such changes can strengthen present pressure and extreme events, thus increasing water resources system hazards and overall uncertainty (Loukas et al., 2008; Logan et al., 2010).

The fifth assessment report of the Intergovernmental Panel on Climate Change (IPCC) explained that the impacts of global warming on natural and human systems are observed on all continents and oceans (IPCC, 2014). Hydrological cycle alterations are considered one of the greatest climate change impacts, such as floods, drought, and storms (IPCC, 2007; Michel and Pandya, 2009). By the end of the 21st century, it is more likely that the global mean air temperature will increase by 1.4 °C to nearly 5.8 °C (IPCC, 2001). However, the Middle East and North Africa will likely encounter a decrease in rainfall and runoff between 10 and 25%, and between 10 and 40%, respectively, and an increase in evaporation between 5 and 20% (Jagannathan et al., 2009).

Both precipitation and mean air temperature can be basic parameters to characterise regional climate and designate alterations in climate. However, these parameters display changeable trends in various regions. Accordingly, a compound index that integrates these parameters can be very critical for analysis of the overall climate. potential evapotranspiration is considered as a more descriptive weather parameter for replacing air temperature in water resources management, owing to its involvement in water balance studies. Analysing long-term time series of both precipitation and potential evapotranspiration of a region can result in one of the following combinations: ++, +0, +-, 0+, 00, 0-, -+, -0 and --, where + indicates a rise, - indicates a decline, and 0 indicates no alteration for the considered parameters. It is not clear if alterations will lead to wetter or drier climates. Trends in the availability of water may be deduced by the recorded rise of precipitation and/or potential evapotranspiration. Accordingly, a more beneficial method would be to simultaneously study the two key variable alterations using a single index, which will respond positively, if potential evapotranspiration decreases, or precipitation increases and vice versa. A recently developed index, the RDI, has been suggested (Tsakiris and Vangelis, 2005; Tsakiris et al., 2007), the index is applied in many areas all over the word, in particular, in the semi-arid and arid

geographical regions, and it is gaining ground as a result of its high sensitivity and resilience, as well as its low data requirements (Tigkas et al., 2012; Asadi and Vahdat, 2013; Rossi and Cancelliere, 2013; Asadi Zarch et al., 2015; Vicente-Serrano et al., 2015). Tigkas et al. (2012, 2015) published brief explanations of the hypothetical basis for RDI and many other drought-related indices together with some practical applications with a specialised software package named Drought Indices Calculator (DrinC), which was established to provide a simple interface for the drought indices estimations.

Recently, many researchers have discussed and utilised RDI as a drought severity index. In order to detect the probable climatic change, Tigkas et al. (2012) suggested a single index: Alpha and normalised expressions of RDI. Additionally, Vangelis et al. (2013) assessed the potential evapotranspiration estimation methods effect on the characterisation of drought severity resulting from RDI. They compared the RDI outcomes for different reference periods using some widespread empirical PET approaches with low data needs. Based on their research analysis, they argued that no substantial impact on RDI was identified by applying the chosen potential evapotranspiration estimation approaches. Then, Shamsnia (2014) computed the indices of SPI and RDI applying twenty-nine points of weather data from the hydrological year 1981/1982 to 2009/2010 for five geographical regions. They concluded that wet and dry seasons on short time scales depend on precipitation and potential evapotranspiration, in addition to other meteorological variables, and suggested (for drought assessments) utilising the RDI index to select short reference periods, such as 1, 3, and 6 months. Cai et al. (2015) assessed the spatial and temporal drought characteristics based on monthly precipitation data from thirty-three meteorological stations over the time-period from 1960 to 2010. They applied the amended RDI to capture the patterns of drought and to estimate the drought severity for all studied locations.

A growing number of studies in the water resources field have discussed, applied, and explained the theoretical background of the RDI index for drought severity assessment. However, they particularly focused on the RDI_{st} form of the index, but they did not discuss or focus on the particular use of the alpha form of the index, neither as an aridity index, nor as a climate change detection index, and how this form can be efficiently used to investigate the climate change impacts on arid regional climates. Therefore, and to acknowledge the gap in understanding, this study assessed the climate variability occurrence and its effects

on the arid climate of a geographical region depending on the RDI forms (alpha and normalised) as a single climatic index.

2.4 Hydrograph Analysis

Separation of streamflow hydrographs into dry-weather or baseflow and direct run-off components, Figure 2.1, is a useful technique to understand the groundwater contribution to rivers, in particular when concerned with a varied range of water resources organisation matters (Brodie and Hostetler, 2005; Lu et al., 2015). Such techniques have also been utilised to quantify the groundwater element of hydrological budgets and to assist in the estimation of recharge rates. The direct run-off component represents the additional streamflow contributed by sub-surface flow and surface flow; whereas the baseflow component represents steady groundwater flow contributions to river discharge. Brodie and Hostetler (2005) argued that the exploration of groundwater inputs to watercourses is important when discussing matters, such as the water resources supply probability of failure, water distribution and design of water storage systems, hydroelectric power generation, and water needs for ecosystems.

Various techniques have been developed to separate the baseflow from the overall runoff hydrograph, which is traditionally categorised into three basic techniques: graphical baseflow separation, filtering algorithms frequency analysis, and recession analysis (Brodie and Hostetler, 2005; WMO, 2009; Welderufael and Woyessa, 2010). Tallaksen and van Lannen (2004) pointed out that Nathan and McMahon (1990) distinguished between methods for continuous separation regarding different components of flow.

Graphical methods separate the baseflow component on a discharge hydrograph by connecting an intersecting point of baseflow and direct flow upon the hydrograph's rising limb lowest flow point to a point on the falling limb where it is assumed all flows are changed to baseflow (Linsley et al., 1988; Welderufael and Woyessa, 2010). These techniques partition baseflow in different ways that vary in their complexity and involve a constant flow rate, as shown in Figure 2.1, constant slope and concave technique (Brodie and Hostetler, 2005). Conversely, Lim et al. (2005) confirmed that the main drawback of these techniques is that they do not provide consistent outcomes even with similar flow data.

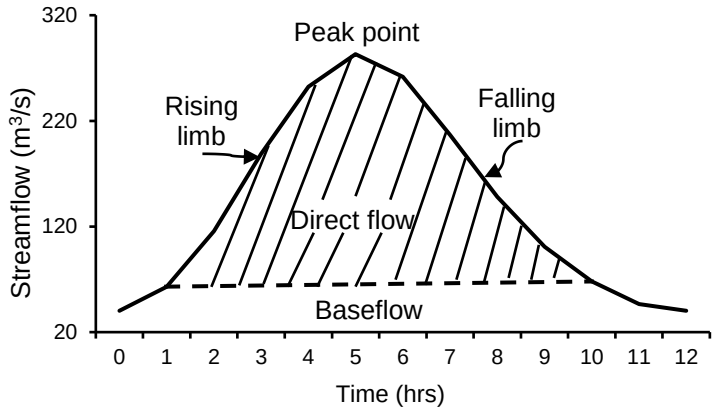

Figure 2.1 Constant flow rate graphical method for baseflow separation

The digital filtering techniques (DFA) are the most regularly used methods in river flow separation, which splits the baseflow by a filtering or processing procedure (Eckhardt, 2005; Lim et al., 2005, 2010; Welderufael and Woyessa, 2010; Mulder et al., 2015). These methods have been recommended for providing reproducible results, can easily be automated, and should be linked to the baseflow reach of a river basin (Arnold et al., 2000; Eckhardt, 2005). For the purpose of this study, two of the recursive digital filtering techniques have been used: the Eckhardt (2005) and Chapman (1999) methods. The latter is one of the most commonly used recursive filtering algorithms for baseflow separation.

The frequency duration or flow duration curve (FDC) method represents the relationship between the magnitude and the frequency of daily, weekly or monthly discharges for a specific river basin (Cigizoglu and Bayazit, 2000). It is another widespread approach to analyse the characteristics of a river and is used to estimate the time percentage the stream discharge is equal to or exceeds a historical period (Welderufael and Woyessa, 2010). FDC can be defined as a curve showing the percentage of time that a streamflow is likely to be equivalent or is greater than some specific values, Figure 2.2. This plot describes the capability of the basin to provide flows of various magnitudes. The lower and upper parts of the plot profile are essential in evaluating the channel and basin attributes. The high-flow area form indicates the type of flood that the basin is describing, while the form of the low-flow region describes the basin capacity to endure the low flow during the dry season.

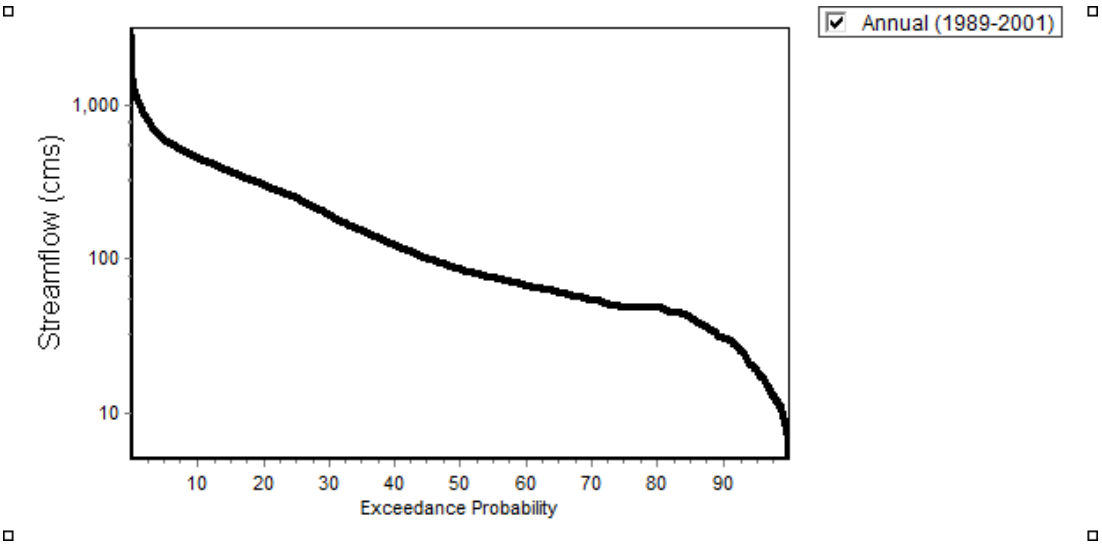

Figure 2.2 Flow duration curve for the Lower Zab River at the Dokan hydrological station for the water years from 1989 to 2001

The plot form is greatly impacted on by a simple time unit, which is applied in sketching it. For instance, when the mean flow at a daily base is applied, then the resulting curve will be sharp. However, when a monthly mean or any other long period average flow is applied, the resultant plot will be plane due to averaging of the short-term peaks with the intervening lesser flows over this month. Extreme data are gradually averaged out, as the duration increases; e.g., an FDC depends on annual streamflow at a station characterised by a long record.

If the contributions of groundwater are minor, the curve slope at the lower end tends to be steep, whereas a flat curve indicates significant baseflow. A number of indices can be provided by FDC to describe the streamflow rating or regionalization purposes. Normally, Q_{50} (the flow exceeds 50% of the time) is seen as the median flow (Gordon et al., 2004). A flow $\geq Q_{50}$ is understood as low flow. The Q_{90}/Q_{50} ratio represents a proportion of the river flow groundwater aquifers involvement or the corresponding proportion of the BF component (Smakhtin, 2001; Welderufael and Woyessa, 2010; Stewart, 2015).

Hydrograph recession analysis is considered as one of the widely used techniques for separation of the baseflow at a basin scale (Sujono et al., 2004). The main focus of a recession study is on the recession curve that is shown as the falling limb on the hydrograph which follows the stream crest when discharge reduces, as shown in Figure 2.3. Recession parts are chosen from the hydrographic value and can be separately or simultaneously analysed to obtain and understand the processes, which impact on dry-weather conditions.

For a single hydrograph recession, a semi-logarithmic plot is originally applied for separating a hydrograph into linear elements of river flow, interflow, and dry-weather flow. When assessing a set of hydrograph recessions at a certain basin at the same time, a master recession curve is usually applied. Along with the graphical method, the fitting procedure may also be performed mathematically.

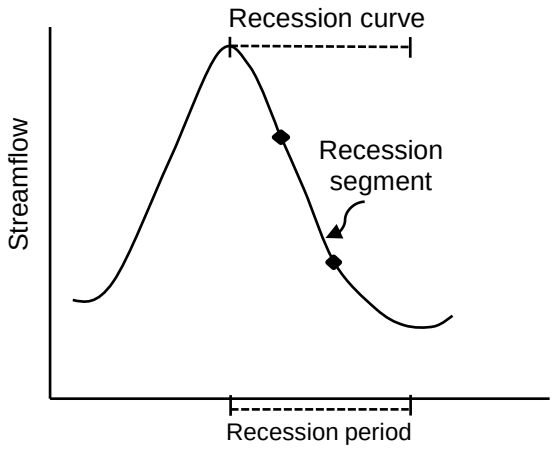

Figure 2.3 Recession curve, period, and segment

The baseflow index (BFI) is the percentage of baseflow to total flow estimated from a hydrograph separation approach. It was initially developed in a low flow analysis in the UK (Abebe and Foerch, 2006) for describing the hydrological reaction of soils and geology of the basin. A high BFI value would expose the basin's ability to feed flow of the stream during prolonged dry periods. The BFI is associated with many characteristics of the river basin, such as soil type and geology, topography, vegetation, and climate (Tallaksen and van Lannen, 2004; Longobardi and Villani, 2008; Welderufael and Woyessa, 2010; Price, 2011). The index can change between 0.15 and 0.20 for an impervious basin, to larger than 0.95 for a basin with a high storage volume and a steady flow system (WMO, 2009).

The BF timing and quantity can be impacted by many factors, such as climate, human activities (e.g., river damming), and basin characteristics. Recently, the vast majority of research in the field of water resources have analysed the BF contribution to streamflow (e.g., Partington et al., 2012; Fan et al., 2013; Mei and Anagnostou, 2015; Rumsey et al., 2015; Stewart, 2015; He et al., 2016; Miller et al., 2016; Lott and Stewart, 2016; Mohammed and Scholz, 2016). However, they only used and/or compared many traditional techniques without taking into consideration climate change, drought phenomena, and/or human-induced activities. More recently, Ebrahim and Villholth (2016) determined the annual

ground water storage availability applying the linear reservoir theory and traditional BF separation analysis. However, they did not consider the impacts of climate change, drought events, and human-induced activities on the groundwater input to the flow of rivers.

This study presents a generic methodology during which FDC results are linked to DFA results to estimate the best filter parameter (α) value. Subsequently, the outcomes are used to assess climate change, drought events, and human-induced impacts on the groundwater contributions to streamflow, by which the following question can be answered: To what extent can such a methodology overcome the DFA drawbacks, and can be used to assess the impacts of climate change and human-induced activity on BF? The proposed methodology will support engineers and water resources policy makers to make informed and robust decisions on adaptation and mitigation strategies in the face of climate variability.

2.5 Hydrologic Alteration

Alteration of seasonal rivers flow components, such as high and low flows caused by climate change and anthropogenic interventions, has created enormous concern for hydrologists, due to consequences for riverine ecosystems (Suen, 2010; Doll and Zhang, 2010; Mittal et al., 2016). Along with direct human-induced effects, climate change is anticipated to affect the water cycle and thus alter natural flow characteristics. An increasing mean air temperature will directly increase the rate of potential evapotranspiration, thereby decreasing streamflow (Zhang et al., 2009; Mittal et al., 2016). In general, due to climate change impacts, it is expected that arid and semi-arid regions will experience an increase in mean air temperature and a decrease in precipitation (IPCC, 2014). The annual average streamflow is likely to decline within the range from 10 to 30% over some arid areas at mid-latitudes in 2050 (IPCC, 2007). Many affected areas currently have water-stressed regions, and a rise in drought periods is also anticipated for mid-latitudes. Climate variability has the perspective to intensify water resource pressures for the majority of Asian areas (IPCC, 2014). The local projections of meteorological parameters in Asia founded on a so-identified A2 drove greenhouse gas emission scenario by the General Circulation Models; display that the precipitation reduction could stretch to -40% for periods between December and February, and to -50% for the months between June and August. However, the surge in air temperature might be in the range between +6 and +10% during summer and winter, respectively. It is

important to note that these forecasts might only be regarded as valid until the end of this century.

Doll and Zhang (2010) argued that by the mid 21st century it is expected that climate change would affect flow regime more than the effects of anthropogenic interventions. Climate change impacts are anticipated to interact with the current anthropogenic influences and thus lead to extra pressure to riverine environments (Mittal et al., 2016).

The Nature Conservancy (2009) has developed an easy tool for the natural and altered hydrologic systems estimation, which is the Indicator for Hydrologic Alteration (IHA) (Richter et al., 1998). The IHA uses daily streamflow data to calculate seventy-six parameters, which are divided into thirty-three within IHA and thirty-four within the Environmental Flow Component (EFC). The thirty-three IHA parameters are classified into five groups that addressing the magnitude, timing, frequency, duration, and rate of change (Richter et al., 1997; Richter et al., 1998; Yang et al., 2008; Jiang et al., 2014), which are described as follows:

The first group involves twelve-monthly median flows that describe the normal flow condition. The monthly magnitude of water conditions at any given time is a degree of suitability or availability of environment and defines such environment attributes as a wet area or habitat volume.

The second group consists of ten parameters that describe the magnitude and duration of annual extreme flows, comprising 1-, 3-, 7-, 30-, and 90-day annual maxima and minima to cover the daily, weekly, monthly and seasonal cycles.

The third group contains 1-day annual maximum and minimum Julian dates indicating the timing of annual extreme flows.

The fourth group consists of four parameters that refer to the frequency and duration of the high and low pulses incorporated within this group. The high pulses are periods within a year when the daily flows are above the 75th percentile of the pre-alteration time-period. In contrast, the low pulses are periods within a year when the daily flows are below the 25th percentile of the pre-alteration time-period.

The fifth group consists of four parameters (fall rate, rise rate, fall count, rise count) indicating the numbers and mean rates of both positive and negative changes of flow on two consecutive days.

As a starting point for the hydrologic alteration detection, an important choice will have to be made: whether to compare two separate time-periods or analyse trends over a single time-period. If the studied hydrologic system has experienced an abrupt alteration due to river regulation, such as dam building, the IHA can be used to determine how the flow regime was affected, through calculating the hydrologic parameters for the pre-alteration and post-alteration time-periods. However, for hydrologic regimes that have experienced a long-term accumulation of anthropogenic interventions, the IHA can calculate and draw linear regressions to assess the trend. The type of statistical analysis has to then be selected. Either parametric (mean/standard deviation) or nonparametric (percentile) can be decided. The non-parametric analysis is usually preferred, due to the skewed nature of many hydrologic datasets (a key assumption of parametric analysis is that the data are normally distributed). However, the parametric analysis may be preferable in certain cases, such as flood frequency or average monthly flow volumes.

To investigate the alteration between two periods, the IHA program supports customers to apply the Range of Variability Approach (RVA) defined by Richter et al. (1997). The RVA utilises the pre-development normal deviation of IHA parameters for describing to which extent the normal streamflow has been changed. The RVA analysis creates a series of Hydrologic Alteration factors, which quantify the alteration level of the thirty-three IHA variables. The RVA test is only obtainable for IHA variables, and results in an automatic delineation of three classes of the same size: the low class covers all values less than or equal to the 33^{rd} percentile; the middle class covers all values falling in the range of the 34^{th} to 67^{th} percentiles, and the high class covers all values larger than the 67^{th} percentile.

The software then calculates the anticipated rate at which the post-impact values of the IHA parameters should fall within each class. This anticipated rate is equivalent to the number of amounts in the class through the pre-alter period multiplied by the percentage of post-alter to pre-impact water years. Lastly, a hydrologic alteration factor is computed for each of the three classes as shown in equation (2.1).

$$\text{Hydrologic alteration (\%)} = \frac{\text{Observed} - \text{Expected}}{\text{Expected}} \times 100 \qquad (2.1)$$

When the recorded frequency of post-alteration annual values fall within the RVA objective range and equal the anticipated one, the hydrologic alteration is equivalent to zero. A positive variation refers to when the values of annual parameters fall within the RVA objective window more frequently than anticipated, whereas, negative values refer to when the value falls inside the RVA objective window less frequently than anticipated.

RVA analyses the temporal hydrologic alteration based on a point data. Such data and evaluations usually reflect hydrologic conditions over a wider area upstream and downstream of the river. Using point-based data to assess hydrological conditions in both directions of the gauge stations requires specific rules. Hydrologic alteration mapping can be visualised once such data have been analysed and their spatial applicability determined. There are a number of hydrologic alteration mapping strategies, such as categorising the numerical measures of the alteration into a few qualitative classes, assigning a different mapping pattern to each alteration class and displaying each mapped river segment with an appropriate pattern based on the level of hydrologic alteration detected within that river segment.

In 1998, Richter et al., for the hydrologic alteration mapping purposes, divided the ranges of alteration (0–100%) into three categories of equal range and allocated each category a different pattern: (1) 0–33% denotes slight or no alteration; (2) 34–67% denotes modest alteration; (3) 68–100% denotes a high degree of alteration. Because the measurement of hydrologic alteration is point based, i.e. measured at the stream gauge station, mapping conventions are necessary for characterizing the whole stream reach based on point source data. If the hydrologic alteration degree at a particular site is > 67%, it is suggested that the high level of alteration would extend upstream to the first dam location. Such an altered zone is also suggested to extend to the first confluence with a major tributary downstream. Slight or modest zones are suggested to extend downstream similarly to highly altered zones, however, at the upstream, it is expected to extend to either the first dam location, the first dammed major tributary location, or to a contact with a highly altered zone.

Furthermore, it is important to highlight the scorecard table, which involves a variety of statistics, such as the annual coefficient of variation (C_v), flow predictability, consistency (predictability), percentage of flood within a 60-day period, length of flood-free season, coefficient of dispersion (CD), significant count, deviation factor for the median and coefficient of distribution. The CD can be expressed mathematically by using equation (2.2).

$$\text{Coefficient of dispersion (CD)} = \frac{75^{\text{th}} \text{ percentile} - 25^{\text{th}} \text{ percentile}}{50^{\text{th}} \text{ percentile}} \tag{2.2}$$

where CD is the coefficient of dispersion, 75th percentile is the flow (m^3/s) that is equal to or exceeding 75% of the flow records, 25th percentile is the flow, which is equal to or exceeding 25% of the flow records, and 50th percentile is the flow that is equal to or exceeding 50% of the flow record. The deviation factor (DF) between two time-periods is mathematically represented using equation (2.3).

$$\text{Deviation factor (DF)} = \frac{|\text{Expected} - \text{Observed}|}{\text{Observed}} \times 100 \tag{2.3}$$

where DF is the deviation factor. DF is calculated for both the median and the coefficient of dispersion.

The significant count is similar to the *p*-value in parametric statistics (The Nature Conservancy, 2009). Subsequently, a minimum significant count (the lowest value is zero) means that the variance between the pre-impact and post-impact periods is extremely significant, and a highly significant count (the highest value is one) means that there is slight variance between the baseline and climatically impacted times.

Considerable research work has been carried out to study the impacts of anthropogenic perturbations on natural flow regimes and evaluate the hydrologic alterations (Jiang et al., 2014; Yan et al., 2010; Guo et al., 2014; Gao et al., 2013; Sun and Feng, 2013; Duan et al., 2007; Wang et al., 2013; Mohammed and Scholz, 2017b). Recent research has explored the climate change impacts on the streamflow alteration through utilising the IHA (Gibson et al., 2005; Suen, 2010; Doll and Zhang, 2010; Kim et al., 2011; Lee et al., 2014; Mittal et al.,

2014; Stagl and Hattermann, 2016; Mohammed et al., 2017b). However, most of these researchers have only focused on the ecological consequences on the stream than on the hydrological ones, which has been highlighted in this research. For example, Stagl and Hattermann (2016) evaluated future flow alterations by means of ecologically relevant flow indicators rather than by means of hydrological relevant flow indicators. Furthermore, Stagl and Hattermann (2016) did not incorporate the meteorological and hydrological drought episodes within their methodology; and they did not even evaluate how sensitive the baseflow would be to climate change and river alteration, which has been considered in this research.

2.6 Anthropogenic Interventions Evaluation

Alterations in streamflow, as a result of climate change linked with the anthropogenic interventions, have long been the main focus of hydrological studies (Guo et al., 2014; Jiang et al., 2011). Climate change is considered as the focal factor changing precipitation patterns. However, anthropogenic interventions have affected water resources temporally and spatially. The impacts of these two factors on streamflow are sensitive, particularly in semi-arid and arid geographical regions, and can result in serious environmental degradation and water crisis (Zhang et al., 2001; Miao et al., 2011; Cheng et al., 2016). Hence, assessing factors that impact on alterations of river flow have become paramount.

Figure 2.4 Dokan dam (35°57'14" N and 44°57'10" E), northern Iraq, represents an anthropogenic intervention on a river

A growing number of studies focus on evaluating the ratio of climate change and anthropogenic interventions, Figure 2.4, on basin streamflow (Jiang et al., 2011; Wang et al., 2013; Ye et al., 2013; Guo et al., 2014; Mao et al., 2015; Cheng et al., 2016). Such impacts vary based on geographical region; accordingly, they are commonly explored at a regional scale, such as on a sub-basin or basin scale. For instance, Ma et al. (2008) predicted that climate variability accounted for over 64% of the reduction in average yearly streamflow, mainly as a result of precipitation decline.

The impacts of anthropogenic interventions and climate variability can be quantified through adopting the following steps: firstly, determining the change points in climatic data since it would influence the results in assessing other factors (Cheng et al., 2016). Specifying such points can be achieved by using statistical methods, such as the M-K (Chen and Xu, 2005; Kahya and Kalayci, 2004; Gedikli et al., 2010; Mao et al., 2015), the Pettitt's analysis or the PR-DCC technique (Jiang et al., 2011; Guo et al., 2014; Vaheddoost and Aksoy, 2016). Accordingly, the hydrological years before the alteration are considered as a baseline, and then the impact of the climate change period can be separated from the baseline period. The second step is to apply methods that determine the climate change effects. Hence, the effects

are then attributed to other factors, such as land use land cover, direct withdrawal of water from the surface or subsurface flow for municipal, industrial production and irrigation purposes, and other different purposes which are considered as anthropogenic interventions (Zhao et al., 2010).

To identify the impacts of climate variability and anthropogenic interventions on streamflow, a large number of methodologies have been proposed (Li et al., 2007; Ma et al., 2008; Miao et al., 2011; Wang et al., 2013; Guo et al., 2014; Chang et al., 2015; Cheng et al., 2016). The rainfall-runoff model simulation is usually considered as the most widely spread method (Futter et al., 2015; Jiang et al., 2011; Jones et al., 2006; Zhang et al., 2001). For example, Li et al. (2007) suggested a framework to predict the mean runoff sensitivity on precipitation and potential evapotranspiration. The technique was then employed to evaluate the anthropogenic interventions and climate change impacts on streamflow (Li et al., 2007; Zhang et al., 2001). However, some modernistic endeavors have been developed to address this environmental issue using linear regression analysis (Li et al., 2007; Zhao et al., 2010).

A rainfall-runoff simulation is an estimated explanation of the problematical hydrologic phenomena that happen in the environment. Such a model is a potentially powerful tool to solve practical hydrological challenges. In addition, the model is considered as an effective method for understanding the complex water cycle processes.

Rainfall-runoff models have advanced from empirical models to conceptual ones and thus to distributed models. Hydrological estimation accuracy has improved over time. However, there are often diverse modeling uncertainties, such as model parameters as well as data and model structural errors (Jiang et al., 2014). Uncertainties in hydrological modeling have been studied previously (Ajami et al., 2007; Duan et al., 2007; Vallam et al., 2014; Zheng et al., 2014). Zheng et al. (2014) demonstrated that hydrological model parameter uncertainties have great impacts on model simulation results. The uncertainties in the model simulation during wet periods are relatively higher than those during dry periods.

Numerous rainfall-runoff models are available, and each model describes the processes of hydrological events. There is currently no single model that can describe the principles of basin rainfall-runoff covering all conditions. Therefore, multi-model approaches depend on

the results of several models can improve the accuracy of hydrological prediction through a reduction of the model structure uncertainty. This study focuses on applying a simple multi-model approach to performing streamflow simulations and uncertainty analyses.

The simple average technique (SAM) is considered the simplest method of combining the results of many single hydrological models (Ajami et al., 2006; Duan et al., 2007; Velázquez et al., 2011). An equal weight is assigned to the results of all of the considered models. This method can produce estimates that are better than those of the single models. The accuracy of the SAM method depends mainly on the number of models involved and on the actual estimating capability of the specific models included. The combined predicted streamflow (R) from N hydrological models can be computed by equation (2.4).

$$R_{SAM,t} = \frac{1}{N}\sum_{j=1}^{N} R_{sim_{i,t}} \tag{2.4}$$

where $R_{SAM,t}$ is the multi-model streamflow simulated by SAM at time t, N is the number of models under consideration and $R_{simi,t}$ is the model streamflow simulation for i model and t time.

2.7 Climate Change Scenarios

Recently, climate change has had noticeable influences on biological and physical systems (IPCC, 2014). Various General Circulation Models (GCM) regularly expect rises in magnitudes and frequency of maximum weather events and precipitation variability (IPCC, 2014), which might severely affect global future water resources (Chen et al., 2011; Wilby et al., 2014). Generally, to quantify the impacts of climate change at a basin scale, rainfall-runoff models are often utilised applying GCM data as inputs (Bozkurt et al., 2015; Mohammed and Scholz, 2017c). Yet, the main challenge of the GCM is the spatial resolution mismatch between GCM outputs and the data required for rainfall-runoff models (Semenov and Stratonovitch, 2010; Chen et al., 2011). Thus, for impact studies, it is vital to enhance these global scale models through implementing some post-processing. Accordingly,

downscaling methods, whether they are regional climate models, (RCM) or statistical (SDM) methods, are established to achieve this condition.

The RCM models are computationally expensive and they are only available for limited areas, yet, despite the developments, their results are still too coarse for many practical uses, such as basin hydrology. Thus, SDM methods were developed to overcome these problems. SDM comprises integrating large-scale variables (the predictors, GCM or RCM) with local scale variables (the predictands, basin or site scale). Such procedures are rather simple to apply and computationally inexpensive.

The SDM models are divided into three main classes: transfer function (regression), weather typing and weather generator (WG) (Chen et al., 2011; Trzaska and Schnarr, 2014). The first approach includes forming statistical regression relations between the large scale and the local scale variables. These techniques are rather simple to use, however, the main weakness is the non-existence of a constant relationship between predictors and predictands. The weather typing method comprises a combination of the predictands and its relation to varied classes of atmospheric circulation (Chen et al., 2011; Trzaska and Schnarr, 2014) with a key benefit being that the predictands are closely related to global circulation. Nevertheless, its reliability is based on a static relationship between large-scale circulation and regional climate. Particularly, there is commonly no solid relationship between daily precipitation and large-scale circulation. The third of the SDM categories, which is the WG, is grounded on the perturbation of its variables according to the variations estimated by climate models (Semenov et al., 2013). The major advantage of WG is its capability to quickly yield sets of climate scenarios to study the influences of exceptional weather phenomenon, and also to examine expected variability. Accordingly, this research implemented a stochastic weather generator, which is LARS-WG5.5 (Long Ashton Research Station Weather Generator). LARS-WG5.5 tested in various places in the world and proved its capability to simulate rainfall extremes with the realistic ability (Semenov et al., 2013).

A growing number of researchers have investigated climate change impacts based on the results of the GCM that have been downscaled to the basin-scale applying statistical or regional (i.e. dynamical) downscaling procedures. However, many researchers, such as Chen et al. (2011) stated that there are many sources of uncertainty involved in climate change studies; the major sources of uncertainty are linked to GCM and greenhouse gasses

emissions scenarios (GGES), in addition to the uncertainties that stem from a downscaling method. Therefore, to avoid the GCM and downscaling uncertainties and challenges, many studies (e.g., Tigkas et al., 2012; Vangelis et al., 2013; Reis et al., 2016; Mohammed and Scholz, 2017c) proposed and applied delta perturbation (change factor) (DP) concepts. Delta perturbation, incremental, arbitrary, or synthetic scenarios, all describe techniques where particular climatic variables (mean air temperature and/or precipitation) are perturbed incrementally (and rationally) through arbitrary amounts, as shown in equation (2.5). Changes in air temperature, for example, +1 or +4 °C, can be combined with precipitation changes of, say, -4 or -6% (or no change at all) to create an incremental scenario (IPCC, 2014).

$$AMV_t(mm) = OMV_t(mm) \pm RA(\%) \times OMV_t(mm) \quad (2.5)$$

in which AMV_t is the anticipated meteorological variable (mm) at a specific time step t, OMV_t is the observed meteorological variable (mm) at a specific time step t, RA is the added or subtracted ratio (%).

DP scenarios commonly assume a consistent yearly change in meteorological parameters over a study area. Despite the fact that this method has frequently been criticised for its failure to shape future changes in the distribution of probability and seasonality of climatic characteristics, and, therefore, the streamflow. The DP scenario is easy to use, provide data on a range of potential variations and can readily be applied in a reliable manner for different research areas.

Although the DP technique does not involve future changes in the distribution of probability concerning weather characteristics and seasonality, it is still a practical technique in identifying tipping points at which a reservoir is anticipated to fail catastrophically in supplying a pre-defined water need. The DP scenarios often represent a realistic set of variations that are physically reasonable; mostly if constant changes are applied over a very large area or if assumed changes in parameters are not physically consistent with each other. The prime application of the DP scenario is in system sensitivity exploration. Recently, numerous researchers have adopted the DP scenario (e.g., Tigkas et al., 2012; Al-Faraj and Scholz, 2014; Soundharajan et al., 2016; Reis et al., 2016; Mohammed and Scholz, 2017c).

For example, Mohammed and Scholz (2017c) have formulated the climatic scenarios for the streamflow alterations evaluation by shifting the historical potential evapotranspiration and precipitation values by steps of 2% within the range from 0 to +30% for PET and from 0 to −40% for P, as shown in Figure 2.5. In this way, they took into consideration all potential arrangements, around 336 scenarios formulated for the considered basin, comprising all the arrangements of P and PET variations that lie within the considered ranges. Such scenarios contain all the climate change predictions for the studied region.

Accordingly, the prime aim of this study is to quantify the influences of climate change on the LZRB in Iraq, taking into consideration the uncertainties that stem from GCM and DP techniques. Then, comparing the outcomes of these two scenarios, using an ensemble of seven GCM methods and perturbations of P (dP) by 0–40% (2% step) and PET perturbations (dPET) of 0–30% (2% step) to investigate how close these two climate change scenarios are, or how different they are from each other. A variety of scenarios is applied to detect the sensitivity of the water resources system to climate change and to support policy makers in climate change adaptation. Based on the literature review, this study can be considered as a first attempt to answer the following question: What would be the differences/and or the similarities in climate change assessment between two GCM and DP scenarios? Previous climate change assessment studies usually depend on just one climate change scenario, which is normally the GCM.

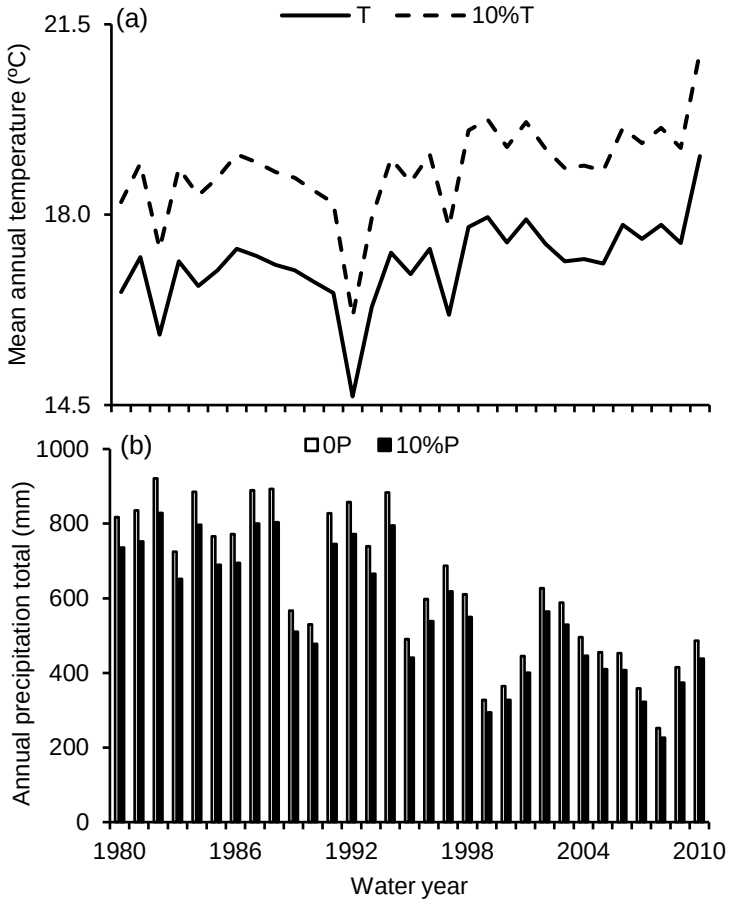

Figure 2.5 Application of the synthetic climate change scenario to the (a) Annual mean air temperature (T); and (b) Reduction in the annual precipitation (P) (mm), over the Lower Zab River Basin, northern Iraq

2.8 Climate Change Evaluation

It is expected that climate variability will intensify the pressure on present water resources (IPCC, 2014), such as the alteration in the river flow seasonality (Vicuna and Draup, 2007; Brekke et al., 2009; Minville et al., 2009) as well as reservoir planning and performance. Such change is most likely to result in a negative effect on any water resources system in nearly all regions of the world. However, the characteristics and severity of such an effect will differ considerably from one geographical area to another. These effects must be quantified for managing and operational purposes of water resources systems. A growing number of researchers have explored the climate change impacts in reservoirs (Fowler et al., 2003; Schaefli et al., 2007; Brekke et al., 2009; Li et al., 2010; Bosona and Gebresenbet, 2010; Alvarez et al., 2014; Park and Kim, 2014; Adeloye et al., 2016). More recently, Reis et al. (2016) quantified worsening reservoir reliability in the future. Only a few researchers

have focused on reservoir management adaptation to climate variability (e.g., Payne et al., 2004; McMahon et al., 2006; Li et al., 2010; Minville et al., 2009; Raje and Mujamdar, 2010) and confirmed that the impact of such change on streamflow should be considered through re-examination of reservoir operating rules.

Reservoir operation is a difficult task comprising several hydrological, environmental, economical, technical, and political concerns. In general, the selection of management methods depends on many factors, such as specific characteristics of a reservoir, the data availability, the objectives specified, and the limits imposed (Park and Kim, 2014). By considering either structural or non-structural adaptation, water resources managers and policymakers can mitigate climate change impacts. Structural adaptations include increasing the number and/or the size of dams, transferring water between basins and building desalination plants. However, non-structural adaptation may include reservoir operation modification, such as flood management and water supply (Watts et al., 2011).

Under different levels of water availability, each dam has its specific maximum operational rules that maximize its purpose. However, several dams would not be able to work efficiently under the anticipated climate change impacts (Park and Kim, 2014). In order to simulate the streamflow alteration and evaluate the reservoir operation performance due to climate change, reservoir models are a powerful approach for integrating hydrological data into climate change simulations (Li et al., 2010). Due to universal environmental changes, such as the intensity and frequency of floods and droughts, integrated with vegetation and land use alterations, in addition to the impacts of regional anthropogenic intervention, it is often necessary to change current dam operational strategies. This is because these rules are specified by the local climatic conditions. An assessment of water supply volumes is necessary, following an evaluation of the hydrologic effect on water demand in the future. Therefore, one of this research objectives is to assess the potential impacts of climate change on basin hydrology. In particular, the study considers the impacts on reservoir OPOF and storage in the water resource system at the Dokan multipurpose dam, in northern Iraq, attempting to answer the following question: How well would the adaptation measures, whether they are structural or non-structural, work across a range of climate change uncertainty? And can it, therefore, be used as a support for mitigating climate change impact on water resources. As far as the researcher is aware, this is the first attempt at testing various

options against the range of different future climate change scenarios to effectively manage the basin storage system.

2.9 Climate Forecasting System Reanalysis Data

Gathering representative weather data for basin-scale hydrological simulations might be challenging and take a lot of time. This is because the land-based meteorological stations do not usually adequately cover the climate observed over a basin for many reasons, such as they might be located far from the area of interest and are associated with missing data, which holds true for the case study area. Accordingly, this research introduces a procedure for utilising the CFSR global methodological dataset (Saha et al., 2014) to gain historical meteorological data and investigate its applicability for hydrologic alteration, drought severity assessment, and climate change studies. The CFSR data are based on a dataset created by the National Centres for Environmental Prediction (NCEP) as a part of a climate forecast system (Dile and Srinivasan, 2014; Saha et al., 2014). The CFSR dataset supersedes the previous National Centers for Environmental Prediction (NCEP)/National Center for Atmospheric Research (NCAR) reanalysis dataset that has been utilised widely in previous downscaling research (e.g., Michelangeli et al., 2009; Maurer et al., 2010). Recent research in water resources (Dile and Srinivasan, 2014; Sharp et al., 2015; Adeloye et al., 2016; Soundharajan et al., 2016; Mohammed and Scholz, 2017a) is dependent on the CFSR dataset. For example, Mohammed and Scholz (2017a) confirmed the CFSR data reliability by applying the dataset to evaluate the probable effect of potential evapotranspiration formulations at different elevations and climatic conditions on the RDI index. The CFSR dataset covers the period from 1979 to 2014 with a spatial resolution of 0.5° × 0.5° (Soundharajan et al., 2016). Concerning data reliability in watershed-scale modelling, Fuka et al. (2014) confirmed that applying the CFSR data as input to the hydrological model produces streamflow, which are as accurate as (or even better than) models derived through popular meteorological stations, particularly in cases where the stations are located greater than 10 km from the area of interest.

Chapter 3: METHODS, MODELS, AND APPLICATIONS

3.1 Overview

To achieve the prime aim of this study and support engineers and policy makers in climate change adaptation and mitigation, an investigation of the key parameters, such as basin characteristics and hydro-climatic data availability is essential. Therefore, this chapter presents a brief description of the materials and methods that were used in conducting the study. The chapter is divided into five sections: Sections 3.1 and 3.2 introduce the chapter and the Representative Case Study, respectively. Data Availability and Collection and the Tools Implemented are described in sections 3.3 and 3.4, respectively. While the Methodology is explained in section 3.5.

3.2 Representative Case Study

The Tigris River is the second largest river in western Asia with a basin shared by four countries: Iraq, Iran, Syria, and Turkey. It is mainly fed by numerous tributaries that rise in the Zagros Mountains in Iraq, Iran, and Turkey, in addition to the contributions from precipitation that stem from the Armenian highlands. The Tigris has a higher water yield compared to The Euphrates river. The natural annual flow of the Tigris at the Iraqi-Syrian-Turkish border was around 21 billion cubic meters (bcm) (UN-ESCWA, 2013). Over the last few years, the Tigris flow volume has been affected by large water development projects in Iraq and Turkey. The flow volume records for Kut show a significant negative trend. Water supplies to the Mesopotamian Marshlands have also dwindled over the past 40 years. In addition to Turkey's use of the Tigris River for the Southeastern Anatolia Project (GAP), Iraq has built several dams and diversion projects on the river, centering on the Tharthar

canal between the Euphrates and the Tigris. Water from the Tigris is mainly used for agriculture, with irrigation projects in all riparian countries.

The Tigris River Basin has a number of sub-basins, most of which are shared between Iraq and Turkey or between Iraq and Iran, which are the Fesh Khabour, the Greater Zab, the Lower Zab, and the Diyala, Table 3.1. Their contribution to the total Tigris River flow rate is significant, with more than 27 bcm (UN-ESCWA, 2013). In general, there is limited information on the Tigris tributaries and few in-depth studies exist on these rivers. The Fesh Khabour is shared between Iraq and Turkey and forms the smallest of the four tributaries, both in terms of river length and basin size. The Greater and the Lower Zab are not only the most prominent Tigris tributaries but also contribute the largest flow volume to the Tigris River. Finally, the Diyala, which is shared between Iraq and Iran, is regulated by four dams.

Table 3.1 The Tigris river tributaries with their important properties (UN-ESCWA, 2013)

Tributaries	Total Basin Area (km^2)	Tributary Length (km)	Mean annual flow volume (BCM)	Shared Area %		
				Iraq	Turkey	Iran
Fesh-Khabour	6143	181	2	43	57	—
Greater Zab	26310	462	12.7	65	35	—
Lower Zab	19780	302	7.8	76	-	24
Diyala	33240	574	4.6	75	-	25

The Greater and the Lower Zab Rivers are considered as the main contributors to the Tigris discharge that contributes 40-60% of the total Tigris flow in Baghdad. In general, the four shared tributaries exhibit similar flow regimes, with normal fluctuations of wet and dry years, around the average yearly flow rate. Despite the fact that both the Lower Zab and the Diyala have been regulated by dams since the 1960s, there is currently no evidence of a regulated streamflow regime. Water resources management differs from one shared basin to another. For instance, while the Greater Zab is, to date, unregulated, several of the dams and regulators on the Lower Zab and the Diyala support irrigated agriculture projects in the area.

The Lower Zab River is considered in this study as a representative case study for arid and semi-arid regions. The river has been selected based on its size, significance, hydrologic and climatic conditions, and the data availability.

The Lower Zab River (also known as Little or Lesser Zab) is one of the main tributaries of the Tigris River in the Erbeel governorate in the north-east of Iraq. The river and its tributaries are situated between latitudes 36°50' N and 35°20' N, and longitudes 43°25'00" E

and 45°50'00" E (Mohammed and Scholz, 2016), Figure 3.1. The river originates from the Zagros mountains in Iran and flows about 370 km south-east and south-west of Iran, and northern Iraq, before joining the Tigris near Fatha city, which is located about 220 km north of Baghdad (UN-ESCWA, 2013), with a total length of approximately 302 km and about 80 km south of the Greater Zab River. The catchment area of the River is approximately 20,605.0300 km^2 with nearly 76% located in Iraq. The mean annual storage of the river at Dokan and Altun Kupri-Goma is about 6 billion cubic meters (bcm) and 7.8 bcm in this order (UN-ESCWA, 2013; Mohammed et al., 2017a), Figure 3.1. The corresponding mean contribution to the Tigris of 191 m^3/s and 249 m^3/s for the two stations, respectively (UN-ESCWA, 2013). Figure 3.2 indicates the average annual flow variability of the River Zab, which is characterised by regular oscillation of dry and wet periods at both gauging stations (USGS, 2010). The mean, maximum, and minimum discharges of the Lower Zab are 227 m^3/s, 3420 m^3/s, and 6 m^3/s, respectively (USGS, 2010). The Lower Zab crosses rather diverse ecological and climatic zones. Annual precipitation (P) along the river course decreases from more than 1000 mm in the Iranian Zagros to less than 200 mm at the confluence with the River Tigris. Mean temperatures follow the same gradient. The mountain valleys are usually subjected to colder winters than the corresponding foothill areas. However, summers in the latter are usually hotter (NOAA, 2009).

Dokan (35°57'14" N and 44°57'10" E) is the main dam that has been constructed in the Iraqi portion of the Lower Zab River Basin, whereas Iran is recently constructing one dam with two others in the planning phase. The Dokan, which is a multi-purpose arch dam, was constructed between 1957 and 1961 upstream Dokan town with a maximum storage capacity of approximately 6,970 million cubic meters (mcm), crest height of 116 m above the river bed (516 m) and a length of 360 m. The main dam functions are to control the discharge of the Lower Zab River, store water for irrigation, and to provide hydroelectric power. There are a number of tributaries contributing to the river discharge, such as the Banah and Qazlaga.

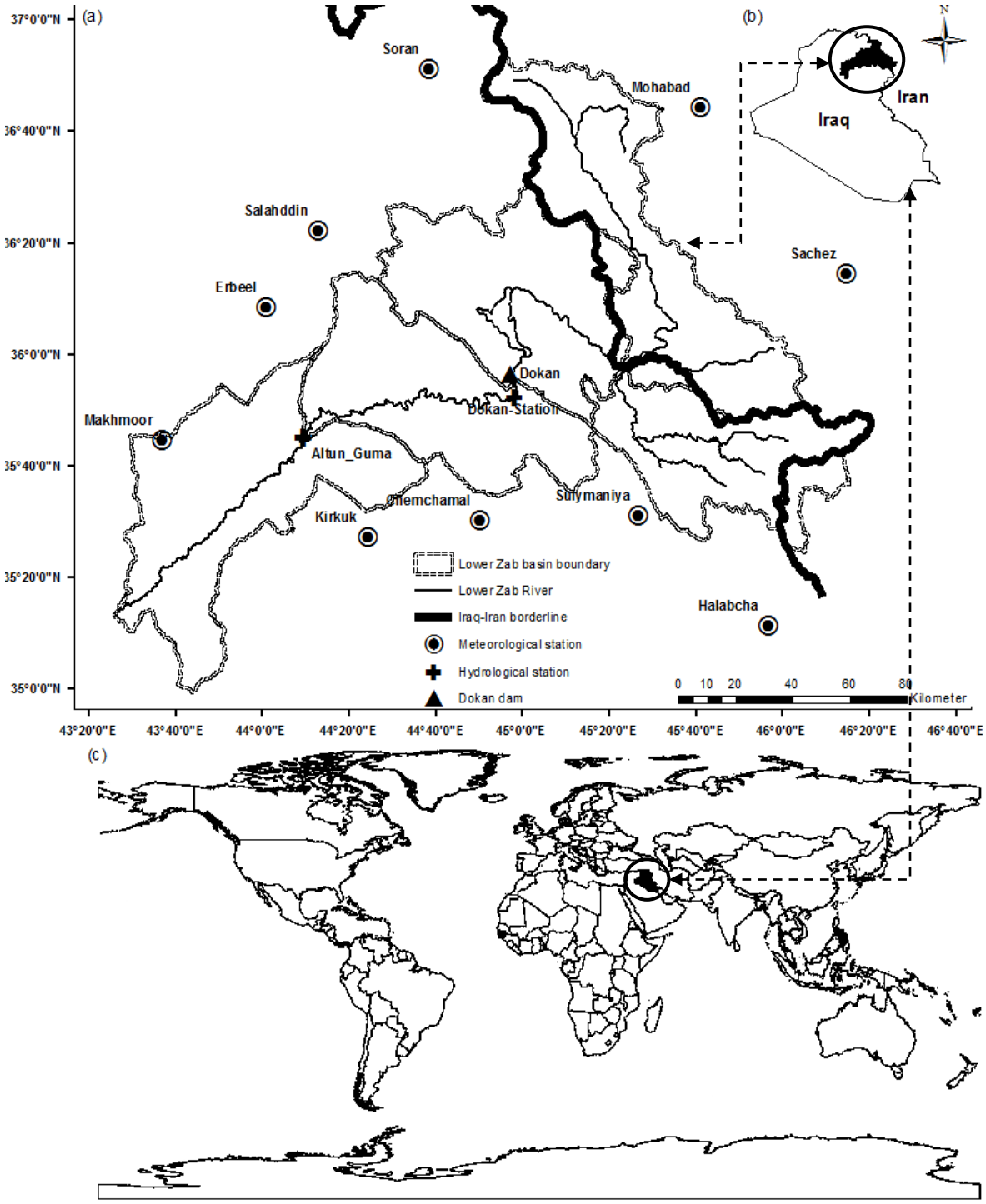

Figure 3.1 (a) The hydrographical network of the region studied is located in (b) Iraq, which is shown on the (c) world map

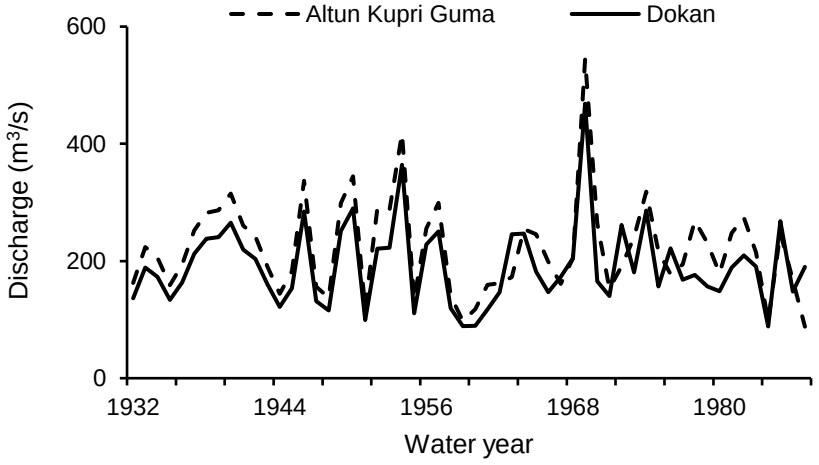

Figure 3.2 Mean annual discharges at the two main gauging stations along the Lower Zab River for the time-period between 1932 and 1987

3.3 Data Availability and Collection

1. Meteorological data: Daily meteorological data, such as precipitation, maximum and minimum air temperature, from ten stations were collected for the time-period between 1979/1980 to 2012/2013. The stations are distributed over the study basin with elevations ranging between 651 m and 1536 m (Table 3.2 and Figure 3.1a).

The climate forecasting system reanalysis (CFSR) data are based on a dataset created by the National Centres for Environmental Prediction (NCEP) as a part of the climate forecast system (Dile and Srinivasan, 2014; Saha et al., 2014). These data are applied in this study to gain historical data for different climatic conditions throughout the world, and to investigate its applicability for drought and aridity assessments. Before using the CFSR dataset, it is critical to assess its validity by assessing the correlation coefficients between these data sets and the data collected from land-based gauging stations. Table A1, Appendix A, indicates that there is a very good correlation between the CFSR and the land-based datasets. Therefore, the CFSR datasets can be considered and used in hydrological studies. The CFSR (CFSR, 2015; Retrieved 05th September 2015 from http://globalweather.tamu.edu/home/) dataset has been applied in this study for two different elevations representing typical lowland and mountainous stations that were selected from semi-arid (Mediterranean (MD), Tropical (TR), and Continental (CN)), Sahara, and humid climatic regions (Figure 3.3). Table 3.3 shows the categories and locations of the chosen meteorological stations. For

example, the gridded station labelled (HL) is situated at an elevation (1677 m) representing a mountainous area in the East of Al-Sudan (22° 0′ 36″N, 36° 15′ 0″E), while the station that is labelled (LL) is situated at a low elevation (40 m) in the UK (52° 55′ 12″ N, 3° 45′ 0″ W). Reliable monthly data of minimum and maximum temperature, precipitation, relative humidity, and wind speed were sourced.

Table 3.2 Address of the meteorological stations that are distributed over the Lower Zab River Basin

Sub-basin	Station ID	Latitude (°)	Longitude (°)	Elevation (m)
US[a]	Sulymaniya	35.53	45.45	885
	Halabcha	35.44	45.94	651
	Sachez	36.25	46.26	1536
	Mohabad	36.75	45.70	1356
	Salahddin	36.38	44.20	1088
	Soran	36.87	44.63	1132
DS[b]	Kirkuk	35.47	44.40	319
	Makhmoor	35.75	43.60	306
	Erbeel	36.15	44.00	1088
	Chemchamal	35.52	44.83	701

[a]Upstream; [b]Downstream

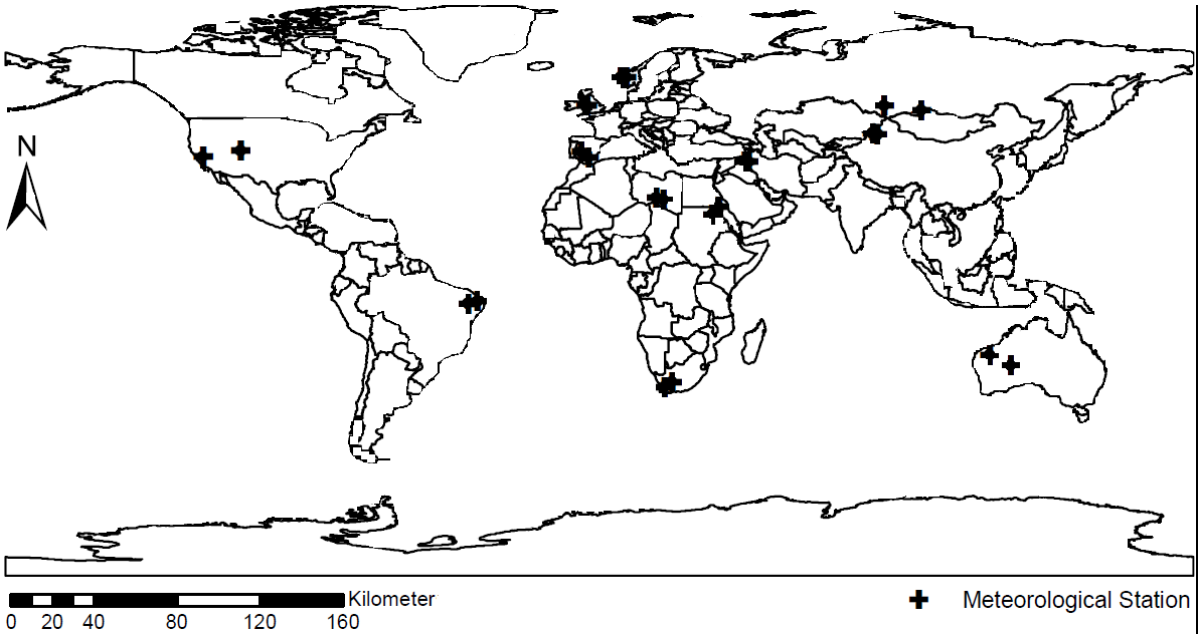

Figure 3.3 The locations of the selected gridded meteorological stations, Climate Forecast System Reanalysis (CFSR, 2015; Retrieved 05th September 2015 from http://globalweather.tamu.edu/home/)

Table 3.3 Categories of the selected gridded meteorological stations from different climatic conditions throughout the world

Climate	Station ID	Latitude (°)	Longitude (°)	Elevation (m)
Semi-arid				
Mediterranean				
South Africa	LL[a]	-32.63	19.69	485
	HL[b]	-31.07	22.19	1382
North Iraq	LL[a]	35.75	44.06	306
	HL[b]	35.75	45.25	1458
West Australia	LL[a]	-26.07	124.68	485
	HL[b]	-22.95	118.43	820
South USA	LL[a]	37.31	-120.00	361
	HL[b]	39.18	-108.75	1382
Tropical				
East China	LL[a]	44.49	82.81	409
	HL[b]	44.18	84.38	1316
East Brazil	LL[a]	-6.71	-36.88	440
	HL[b]	-7.34	-39.69	918
Continental				
South East Spain	LL[a]	38.87	-5.31	438
	HL[b]	36.99	-3.13	1208
South Russia	LL[a]	52.92	86.25	403
	HL[b]	51.36	97.50	1360
Arid				
Sahara	LL[a]	24.82	17.19	146
	HL[b]	24.20	19.38	604
Al-Sudan	LL[a]	19.83	34.34	390
	HL[b]	22.01	36.25	1677
Humid				
UK	LL[a]	52.92	-3.75	40
	HL[b]	52.92	-4.06	717
Norway	LL[a]	6.56	61.35	490
	HL[b]	8.13	61.35	1652

[a]Low Land; [b]High Land

2. Hydrological data: This study assessed the daily flow rate at two key hydrometric stations, which are Dokan (Latitude 35° 53′ 00″ N; Longitude 44° 58′ 00″ E) and Altun Kupri-Goma Zerdela (Latitude 35° 45′ 41″ N; Longitude 44° 08′ 52″ E) stations. The drainage region for the former is estimated to be 12,095.64 km^2 and data were available between 1931 and 2013, whereas the corresponding values for the latter are 8,509.39 km^2 for the period between 1931 and 1993 (Figure 3.1). The data were obtained from the Ministry of Agriculture and Water Resources in the Kurdistan region of Iraq, Appendix C.

3. Reservoir data: Reservoir capacity, water elevation, and surface water area for the Dokan are shown in Table 3.4.

Table 3.4 Dokan reservoir topographic features

Elevation (m)	Capacity ($10^9 m^3$)	Surface area (km^2)
458	0.000	0
468	0.646	45
470	0.742	51
475	1.034	67
480	1.418	87
485	1.909	110
490	2.524	137
495	3.279	166
500	4.188	198
505	5.260	231
510	6.495	263
511	6.800	270

4. Geospatial data: World borders, Iraqi boundaries, and the LZRB shape files have been downloaded from Thematic Mapping (2009), the Global Administrative Areas (GADM, 2012), and the Global and Land Cover Facility (GLCF, 2015) databases, respectively. GADM is a spatial database of the location of the world's administrative areas (or administrative boundaries), for use in GIS and similar software. GADM describes where these administrative areas are located, and for each area, it provides some attributes, such as the name and variant names. Whereas, GLCF is a center for land cover science with a concentrate on a study using remotely sensed satellite data and products to access land cover change for regional to universal systems, respectively.

3.4 Tools Implemented

1. ArcGIS 10.3: ArcGIS 10.3 was used for hydro-climatic station location projections, Thiessen network computations, and river and river basin delineations.

2. SPSS 23: Statistical analyses concerning the daily hydro-climatic datasets, comprising trend test, monthly and annual amounts, modifications, and the filling of data gaps were completed by the Statistical Program for Social Sciences (SPSS) 23.

3. Daniel's XL Toolbox: A one-way analysis of variance (ANOVA) analysis was achieved using Daniel's XL Toolbox. Daniel's XL Toolbox is an open-source Add-In for the common software Excel. This tool was also used to convert excel graphs to pictures with specific dimensions and resolutions.

4. DrinC 1.5.73: The Drought Indices Calculator (DrinC) 1.5.73 is user-friendly software for the estimation of a number of climatic drought indices such as the Reconnaissance Drought Index (RDI), the Streamflow Drought Index (SDI), the Standardised Precipitation Index (SPI) and the Rainfall Deciles. The common features of these indices are that they need a relatively low data for their calculation, and the outcomes can be simply understood and applied (Tigkas et al., 2012, 2015). DrinC offers a unit for the estimation of potential evapotranspiration (PET) with temperature based methods: Hargreaves (T_{min}, T_{max}), Thornthwaite (T_{mean}), Blaney – Criddle (T_{mean}). To produce reliable results for drought characterisation, time series data of at least 30 water years should be prepared.

5. ET_o 3.2: The reference evapotranspiration ET_o (mm) calculator version 3.2 (FAO, 2012) was used to estimate evapotranspiration by the Food and Agriculture Organization Penman-Monteith standard method (Allen et al., 1998).

6. IHA 7.1: To evaluate the natural flow regime alteration that is caused by climate variability linked to the human-induced activities, the Indicators of Hydrologic Alteration software version (IHA 7.1) was utilised (The Nature Conservancy, 2009).

7. *HydroOffice (2015):* For baseflow (BF) separation and flow duration curve estimation, HydroOffice (2015) (BFI+3.0 and FDC) (https://hydrooffice.org/Downloads?Items=Soft-ware) was used by applying the methodology that was developed by Mohammed and Scholz (2016).

8. Fortran90: For the application of reservoir capacity yield (RCY) model, a Fortran90 program was developed and used.

9. Medbasin 2.1(2016): Medbasin, which is a software package based on the deterministic, lumped, conceptual hydrological model (http://www.ewra.net/medbasin/) was used.

10. Ge´nie Rural a Daily 4 parameters (GR4J, 2016) model: Excel sheet for the GR4J hydrological model was downloaded and used (https://webgr.irstea.fr/modeles/journalier-gr4j-2/?lang=en).

11. RS MINERVE 2.5 (2016): To run the Hydrologiska Byråns Vattenbalansavdelning (HBV) rainfall-runoff model, RS MINERVE 2.5 (https://www.crealp.ch/down/rsm/install2

/archives.html) was used. RS MINERVE is free downloaded software for the simulation of free surface runoff flow formation and propagation (Foehn et al., 2016). It models complex hydrological and hydraulic networks according to a semi-distributed conceptual scheme. RS MINERVE contains different hydrological models for rainfall-runoff in addition to the HBV model. Several projects and theses have used and are using this program for study basins in Switzerland, Spain, Peru, Brazil, France, and Nepal. RS MINERVE was developed at the Laboratory of Hydraulic Constructions at the Ecole Polytechnique Fédérale de Lausanne (Dubois et al., 2000; García Hernández et al., 2007)

12. LARS-WG5.5: Long Ashton Research Station Weather Generator (LARS-WG5.5) was applied to downscaling meteorological data in addition to General Circulation Models (GCM) scenarios application (Rothamsted Research, 2017) (http://www.rothamsted.ac.uk/mas-models/larswg.php).

3.5 Methodology

3.5.1 Hydro-Climatic Data Trend Analysis

The normality of hydro-climatic datasets was investigated with the Kolmogorov–Smirnov analysis as a first step before conducting change tests using statistical techniques. Depending on the results of these tests, most hydro-climatic data series applied in this research does not follow a normal distribution at a significance level p of 0.05. Regarding the non-normal distribution attributes of datasets utilised in the current research, two widespread distribution-free nonparametric techniques (Pettitt test and Mann–Kendall (M–K) analysis) were applied to identify the variations in streamflow, precipitation, air temperature, and potential evapotranspiration time series in the LZRB. The former was utilised for identifying monotonic trends or slow trends, whereas the latter was applied to identify sudden changes in the average level. Before applying non-parametric analysis, the influence of serial correlation in the dataset was eliminated. This research applied the trend free pre-whitening (TFPW) method at 5% significant level (Oguntunde et al., 2011; Shadmani et al., 2012).

As an auxiliary method for the detection of the change point in the precipitation and runoff series, this study used the Precipitation Runoff Double Cumulative Curve (PR-DCC)

method. By using change point test and trend analysis, the streamflow dataset is divided into a baseline period dataset and an anthropogenic intervention period dataset (Jiang et al., 2011). In this study, Pettitt's test for change point identification of the streamflow time series is tested for reapproval of the change points identified using PR-DCC. Depending on the separated periods, the impacts of anthropogenic intervention and climate change on streamflow can be divided by using streamflow simulation methods.

3.5.2 Potential Evapotranspiration Estimation

The potential evapotranspiration estimation methods can be split into three main groups. The first group is known as hydrologic or water balance methods, which comprise physical techniques, and its application is restricted to laboratory conditions. The second group comprises analytical methods that are based on climatic parameters; in this group, potential evapotranspiration processes are expressed by equations, which concentrate on the two key climatic components of mass transport and energy balance. The Penman-Monteith (PM) and the Priestley-Taylor methodologies are recognised models of this group (Shahidian et al., 2012; Vangelis et al., 2013). Empirical methods belong to the last group. The underlying assumption is that temperature is a good indicator of the evaporative influence of the atmospheric temperature. These methods became very common because of their low data requirements. The Hargreaves (HG), Thornthwaite (ThW), and Blaney–Criddle (BC) equations are the most widely used methods representing this category.

The selection of the best potential evapotranspiration estimate for a specific climate and elevation is important. This is required since the application of different approaches may result in flaws in estimations of water resources availability. Therefore, one of the study objectives is to analyse potential evapotranspiration estimate impacts on aridity and drought evaluations at different climatic conditions throughout the world. To achieve this, HG, ThW, and BC potential evapotranspiration methods were selected and used with the FAO Penman-Monteith (PM) methodology for reference purposes. The following is a brief description for the aforementioned temperature-based in addition to PM methods:

3.5.2.1 Hargreaves Method

The Hargreaves method is a methodology for potential evapotranspiration estimation; it is simple and reliable, requires little data, is easy-to-compute and has a minimum impact associated with arid weather station results. This method is temperature-based, as it requires only the minimum and maximum values of temperature. Many researchers, such as Hargreaves and Samani (1982, 1985) have studied this method. For a specific latitude and day, solar radiation (R_A) is usually estimated from published tables or calculated applying a group of equations (Xu and Singh, 2001; Vangelis et al., 2013).

$$PET = 0.0230 \times R_A \times T_m^{1/2} \times (T_m + 17.80) \tag{3.1}$$

where PET is the potential evapotranspiration (mm), R_A is the total incoming extra-terrestrial solar radiation in the same units as evaporation (mm), T_m is the mean monthly temperature (ºC).

3.5.2.2 Thornthwaite Method

This method is one of the temperature-based empirical formulae for calculation of potential evapotranspiration, estimated on a monthly basis and is given by equation (3.2).

$$PET = 16 \times \left(\frac{N}{12}\right) \times \left(\frac{m}{30}\right) \times T_m^{1/2} \times \left(10 \times \frac{T_m}{I}\right)^{\eta} \tag{3.2}$$

where N is the average monthly possible sunshine hours (hr/day), m is the number of days of each month, T_m is the mean monthly temperature (ºC), and η is estimated by equation (3.3).

$$\eta = 6.75 \times 10^{-7} \times I^3 - 7.71 \times 10^{-5} \times I^2 + 1.79 \times 10^{-2} \times I + 0.49 \tag{3.3}$$

where I is a heat index for the year calculated according to equation (3.4).

$$I = \sum_{i=1}^{12} \left(\frac{T_i}{5}\right)^{1.514} \tag{3.4}$$

Given the observed monthly average temperatures at a meteorological station, a prediction of the monthly evaporation of the year can be obtained. Despite the fact that this formula is shown by many researchers to underestimate potential evapotranspiration, it has been widely accepted around the globe (Vangelis et al., 2013).

3.5.2.3 Blaney–Criddle Method

The Blaney–Criddle method is popular and widely used, especially in semi-arid and arid climates, due to its ease-of-use. The general form is shown in equations (3.5).

$$PET = k \times p \times (0.46 \times T_m + 8.13) \tag{3.5}$$

where PET is the potential evapotranspiration (mm) from the reference crop, T_m is the average temperature (°C), k is a monthly coefficient representing consumption, p is the ratio of the mean number of daylight hours in the day for the specified month over the total of daylight hours in the year, which is a function of the latitude of the study area and the month required. Despite the fact that the p value is normally estimated through tables, it can also be computed according to equation (3.6) (Vangelis et al., 2013).

$$p = 100 \times \left(\frac{\sum_{i=d_1}^{d_2} N_i}{\sum_{i=1}^{365} N_i}\right) \tag{3.6}$$

where N_i is the theoretical number of daytime hours; i, and d_1 and d_2 are the last days of a month.

3.5.2.4 Food and Agriculture Organization: Penman-Monteith Method

The FAO Penman-Monteith method is primarily applied to estimate the reference evapotranspiration (ET) as indicated in equation (3.7) according to McMahon et al. (2013).

$$ET = \frac{0.408 \times (R_n - G) + \gamma \times \frac{900}{T_m + 273} \times u_2 \times (e_s - e_a)}{\Delta + \gamma \times (1 + 0.34 \times u_2)} \quad (3.7)$$

where ET is the reference evapotranspiration (mm/day), R_n is the net radiation at the crop surface (MJ/m^2/day), G is the soil heat flux density (MJ/m^2×day), u_2 is the wind speed at 2-m elevation (m/s), e_s is the saturation vapour pressure (kPa), e_a is the natural vapour pressure (kPa), e_s-e_a is the saturation vapour pressure deficit (kPa), Δ is the slope vapour pressure curve (kPa/°C), and γ is the psychrometric constant (kPa/°C).

3.5.3 Basin Average Precipitation Computation

To accomplish a precise estimate of the spatial distribution of rainfall, it is necessary to use interpolation methods. The 'weighing means' technique is often considered as the most significant for engineering praxis (Akin, 1971). This technique assigns weights at each gauging station in proportion to the basin area, which is closest to that station (Diskin, 1970; Croley and Hartmann, 1985). The following steps are accomplished using ArcGIS 10.3. To set-up, the method: A shapefile of the named watershed polygons as a function of the land cover image can be created. This step is followed by the creation of two shape files. The first one is the basin border polygon, while the second is the point shapefile that represents meteorological stations. Each point representation is linked to a value of the long-term precipitation.

A Thiessen network 'weighting means' estimates the area of each station polygon (a_i). This has been achieved depending on the following: (1) Connection of the adjacent stations with lines. (2) Construction of perpendicular bisectors of each line. (3) Extension of the bisectors and applying them to form polygons around each station. (4) Hydro-climatic variable values for each gauging station multiplied by the area of each polygon (a_i, km^2). The next step required the computation of the average values of hydro-climatic value by summing-up of

all values obtained from the previous steps and dividing the corresponding number by the total basin area according to equation (3.8) (Akin, 1971).

$$M_m = \frac{\sum_{i=1}^{n} a_i \times M_i}{\sum_{i=1}^{n} a_i} \tag{3.8}$$

where M_m is the average basin hydro-climatic value, such as precipitation (mm), potential evapotranspiration (mm), the standardised precipitation index, the standardised expression of the reconnaissance drought index, and the standardised precipitation evapotranspiration index, a_i (km^2) is the meteorological station area, and M_i (mm) is the average value of the station polygon M.

3.5.4 Drought and Aridity Identification

For hydro-climatic drought and aridity identification, this study applied three of the widely used meteorological drought indices, which are standardised precipitation index, reconnaissance drought index, and standardised precipitation index. In addition to these, stream drought index was applied, which uses historical time series of a monthly streamflow values at a streamflow gauge station as an input data.

3.5.4.1 Standardised Precipitation Index

Standardised precipitation index (SPI) was established to define and monitor drought and has been applied by McKee et al. (1993). The estimation of SPI at a specific site depends on a series of accumulated precipitation for a reference time scale (e.g. 1, 3, 6, 9, and 12 months). Such a series is fitted to a probability distribution, which is then transformed into a normal distribution so that the mean SPI for the location and the desired period is zero (Edwards and McKee, 2015). Positive SPI values indicate greater than median precipitation, while negative values indicate less than median precipitation. The gamma distribution to fit well climatological precipitation time series (Vangelis et al., 2013). The gamma distribution is defined by its probability density function and is calculated as follows (3.9).

$$g(x) = \frac{1}{\beta^{\gamma} \times \Gamma(\gamma)} x^{\gamma-1} e^{-\frac{x}{\beta}} \text{ for } x > 0 \quad (3.9)$$

where γ and β are the shape and scale parameters, respectively, and $\Gamma(\gamma)$ is the gamma function. The spatiotemporal extent of the gamma probability distribution parameters γ and β can be predicted for 3, 6, 9, and 12 months. The γ and β are estimated by the maximum likelihood method as shown in equations (3.10) to (3.12).

$$\gamma = \frac{1}{4A}\left(1 + \sqrt{1 + \frac{4 \times A}{3}}\right) \quad (3.10)$$

$$\beta = \frac{\overline{x}}{\gamma} \quad (3.11)$$

$$A = \ln(\overline{x}) - \frac{\sum \ln(x)}{N} \quad (3.12)$$

When the cumulative precipitation datasets for the selected reference period contain zeros, the gamma function cannot be defined for x = 0. Therefore, a composite cumulative probability function (equation (3.13)) may be utilised. The resulting parameters are then used to compute the cumulative probability of a measure precipitation episode. Since the gamma function is undefined for x = 0 and a precipitation distribution may contain zeros, the cumulative probability H(x) is estimated according to equation (3.13).

$$H(x) = q + (1 - q) \times G(x) \quad (3.13)$$

where q is the likelihood of zero precipitation and G(x) is the gamma distribution cumulative probability. The probability of zero precipitation (q) can be computed by m/N if m is zero in the α_k time series. The gamma distribution cumulative probability G(x) is replaced by the cumulative probability H(x); in which q is the probability of a zero precipitation and G(x) is the cumulative probability of the incomplete gamma function.

Based on SPI, a drought phenomenon occurs when the index constantly reaches a value of ≤ -1.0. The phenomenon stops when the index becomes positive. Accordingly, each drought phenomenon has a duration defined by its start point and termination, and intensity for each month that the phenomenon continues. Moreover, being a standardised index, SPI is particularly suited to compare drought conditions among different periods and regions with different climatic conditions. A transformation is implemented such that the derived SPI values follow a normal distribution since monthly precipitation is not normally distributed. For a normally distributed random parameter, SPI is the number of standard deviations that the measured value would deviate from the long-term mean (Tigkas et al., 2015).

3.5.4.2 Reconnaissance Drought Index

The Reconnaissance Drought Index (RDI) can be formulated as the alpha/initial ($RDI_{\alpha k}$), normalised (RDI_n), and standardised (RDI_{st}) forms. The RDI_{st} is often used for drought severity assessments, whereas $RDI_{\alpha k}$ can be applied as an aridity index. This index is mainly founded on the aggregated precipitation and potential evapotranspiration theories (Vangelis et al., 2013). The $RDI_{\alpha k}$ is normally estimated using equation (3.14).

$$RDI_{\alpha_k^i} = \frac{\sum_{j=1}^{12} P_{ij}}{\sum_{j=1}^{12} PET_{ij}} \quad i = 1 \text{ to } N \text{ and } j = 1 \text{ to } 12 \tag{3.14}$$

where P_{ij} and PET_{ij} represent, respectively, precipitation (mm) and potential evapotranspiration (mm) of the j^{th} month of the i^{th} water year, which in Iraq begins in October, N is the total year number for weather data, and k is the considered time step.

The values of $RDI_{\alpha k}$ match both the gamma and the lognormal distributions in various positions for a variety of examined time scales (Tigkas, 2008). Through applying the former distribution, RDI_{st} can be computed applying equation (3.15).

$$RDI_{st}^i = \frac{y_i - \overline{y}}{\hat{\sigma}_y} \tag{3.15}$$

where y_i is the $\ln(RDI_{\alpha ki})$, $\bar{y}$ is its arithmetic mean and $\hat{\sigma}_y$ is the corresponding standard deviation.

Table 3.5 Drought and aridity classifications based on the standardised reconnaissance drought index (RDI_{st}) and the alpha reconnaissance drought index ($RDI_{\alpha 12}$) values

No.	RDI_{st} range	Drought classes	$RDI_{\alpha 12}$ range	Aridity classes
1	≥ 2.0	Extremely wet	≤ 0.03	Hyper-arid
2	1.99 – 1.50	Very wet	0.03 – 0.2	Arid
3	1.49 – 1.00	Moderately wet	0.2 – 0.5	Semi-arid
4	0.99 – 0.00	Normal	0.5 – 0.65	Dry sub-humid
5	0.00 to -0.99	Near normal	≥ 0.65	Humid
6	-1 – -1.49	Moderately dry		
7	-1.5 – -1.99	Severely dry		
8	≤ -2.0	Extremely dry		

Equations (3.9) to (3.13) can be used to calculate RDI_{st} in the gamma distribution application (Tigkas, 2008). RDI has been applied extensively for drought identification, quantification, and observation. The severity of drought can be evaluated through the estimation of RDI_{st}. This method is widely used, in particular, in semi-arid and arid geographical areas (Asadi Zarch et al., 2011; Tigkas et al., 2012).

A positive value of RDI_{st} relates to a wet period, whereas a negative value is indicative of a dry period compared to the natural climatic conditions of the study area. The drought severity can be classified into eight classes based on the RDI_{st} values and it increases when RDI_{st} numbers are minimal (Table 3.5). RDI is estimated for a water year in 1, 3, 6, 9, and 12 month reference time durations. This indicates a variable quality of RDI compared to other drought indices, since it is computed for pre-determined reference time-periods.

$RDI_{\alpha 12}$ is based on the ratio of annual precipitation and potential evapotranspiration, which makes it attractive in that it is conceptually and operationally simple and is based solely on the two main parameters that define aridity. UNESCO (1979) proposed a classification of climate zones based on aridity expressed as an index, in which arid regions are defined into many classes, based on the limited values of $RDI_{\alpha 12}$ as shown in Table 3.5.

3.5.4.3 Standardised Precipitation Evapotranspiration Index

The standardised precipitation evapotranspiration index (SPEI) is a simple multi-scalar drought index that incorporates precipitation and temperature values. The SPEI index is based on a monthly climatic water balance (precipitation-potential evapotranspiration). The

values are aggregated at different time scales and converted to standard deviations, with respect to average values. Given a value of potential evapotranspiration, the difference between precipitation and potential evapotranspiration for the month i can be calculated based on equation (3.16).

$$D_i = P_i - PET_i \tag{3.16}$$

in which P_i (mm) and PET_i (mm) are precipitation and potential evapotranspiration (mm) for the i^{th} month, respectively.

Equation (3.16) provides a simple measure of the water excess or shortage for the investigated month. The computed D_i values are accumulated at different time measures, following the same procedure as that for SPI. The difference in a given month j and year i depends on the chosen time scale k. For example, the accumulated difference for one month in a particular year i with a 12-month time scale is calculated using equations (3.17) and (3.18).

$$D_{i,j}^{k} = \sum_{a=13-k+j}^{12} D_{i-1,a} + \sum_{a=1}^{j} D_{i,,a} \quad \text{if } j < k \tag{3.17}$$

$$D_{i,j}^{k} = \sum_{a=j-k+1}^{j} D_{i,a} \quad \text{if } j \geq k \tag{3.18}$$

where $D_{i,\,1}$ is the precipitation and potential evapotranspiration difference in the first month of year i, (mm).

Vicente-Serrano et al. (2010) and Beguería et al. (2003) provided complete descriptions of the theory behind SPEI, the computational details, and comparisons with other popular drought indicators. Many researchers, such as Joetzjer et al. (2013) argued that SPEI does not represent soil water content compared to PDSI. However, the SPEI index is slightly different from the drought indices that involve a simple soil moisture budget, as the prime aim of SPEI is to represent departures in climatological drought, the balance between the water availability and the atmospheric water demand.

3.5.4.4 Stream Drought Index

Given monthly time series streamflow storage V_{ij} for a specific water year, the corresponding cumulative value can be obtained according to equation (3.19), which was developed by Nalbantis (2008).

$$S_{i,k} = \sum_{j=1}^{3k} V_{i,j} \quad \text{for } i = 1, 2, \ldots, n; j = 1, 2, \ldots, 12; k = 1, 2, 3, 4 \tag{3.19}$$

where S_{ik} is the aggregate streamflow storage for the i^{th} water year and the k^{th} reference period, k = 1 for the period October–December, k = 2 for October–March, k = 3 for October–June, and k = 4 for October–September.

Stream drought index (SDI) founded on the streamflow aggregated volumes $S_{i,k}$ for each period k of the i^{th} water year can be defined according to equation (3.20)).

$$SDI_{i,k} = \frac{S_{i,k} - \overline{M}_k}{SD_k} \quad \text{for } i = 1, 2, \ldots, n; \text{ and } k = 1, 2, 3, 4 \tag{3.20}$$

where $\overline{M}_k$ and SD_k is the cumulative streamflow storage means and the standard deviation of the period k, respectively, since they are calculated over a long time. Although many values founded on logical criteria could be used, the truncation level is set to $\overline{M}_k$ by this definition.

For most small basins, the streamflow follows a skewed probability distribution. This can be estimated by gamma distribution functions. The distribution is then converted into a normal distribution. Appling the two-parameter lognormal distribution, the SDI index is defined as shown in equation (3.21).

$$SDI_{i,k} = \frac{y_{i,k} - \overline{y}_k}{S_k} \quad \text{for } i = 1, 2, \ldots ; \text{ and } k = 1, 2, 3, 4 \tag{3.21}$$

where the natural logarithms of cumulative streamflow with mean $\bar{y}_k$ and standard deviation S_k, can be estimated according to equation (3.22).

$$y_{i,k} = \ln(S_{i,k}) \qquad \text{for } i = 1,2,\ldots.., \text{ and } k = 1, 2, 3, 4 \tag{3.22}$$

A value of SDI greater than zero relates to a non-drought period. In comparison, a negative value is indicative of a drought period in comparison to the natural conditions of the study region. The hydrological drought severity phenomena increase when SDI values are minimal, and it follows the same classification for drought severity is used as the one for the RDI index, Table 3.6. Usually, an integer number from 0 (non-drought) to 4 (extreme drought) is considered.

Table 3.6 Drought classifications based on the streamflow drought index (SDI) values

No.	SDI range	Drought classes
0	≥ 0.0	Non-drought
1	-0.99 – 0.01	Mild drought
2	-1.49 – -1.00	Moderately wet
3	-1.99 – -1.49	Severe drought
4	< -2	Extreme drought

3.5.5 Hydrograph Analysis

Particular activities that can affect dry-weather may contain river flow regulations, where river discharge is controlled through infrastructure elements, such as dams, weirs or locks. Discharges from surface water storage structures for downstream stakeholders can make up the bulk of a river during dry times, reducing the groundwater contribution, which in turn decreases the dry-weather index. Many researchers argue that dry-weather assessment should be performed in unregulated reaches or, at least, the regulated basin area should be ≤ 10% of the basin area of the river gauge (Al-Faraj and Scholz, 2014). This study explored the effects of weather variability and anthropogenic interventions on river flow alteration. The sensitivity of groundwater to such changes was then assessed.

A new generic methodology for studying the impacts of anthropogenic intervention (e.g. river damming) linked to climate change and drought events, on the groundwater contribution to river flow, has been developed. Two digital filtering algorithms (DFA) were

utilised. Eckhardt (2005) and Chapman (1999) developed the suggested generic methodology for BF separation from the daily average flow to the LZRB, which was observed at the Dokan and Altun Kupri-Goma Zerdela gauging stations, shown in Figure 3.1.

The Eckhardt (2005) approach is used to achieve low pass filtering of the flow hydrograph to separate the BF (equation (3.23)).

$$BF_t = \frac{(1 - BFI_{max}) \times \alpha \times BF_{t-1} + (1 - \alpha) \times BFI_{max} \times TF_t}{1 - \alpha \times BFI_{max}} \quad (3.23)$$

where BF (m^3/s) is the isolated baseflow, BFI is the baseflow index, which is the long-term ratio of BF to the total flow (TF), TF (m^3/s) is the total flow, α is the filter parameter, and t is the time step for $BF_t \leq TF_t$.

Chapman (1999) discussed the second recursive DFA that can be estimated by equation (3.24).

$$DF_t = \frac{3 \times \alpha^{-1}}{3 - \alpha} \times TF_{t-1} + \frac{2}{3 - \alpha} \times (TF_t - TF_{t-1}) \quad (3.24)$$

where DF (m^3/s) is the direct runoff, TF (m^3/s) is the total flow, α is the filter parameter, and t is known as the time step.

Two parameters are needed for the Eckhardt recursive method identification (Eckhardt, 2005): (i) The recession constant stemming from the recession curve of the hydrograph valuation, and (ii) The BFI_{max} that cannot be measured but enhanced based on the results of other methods. As a starting point, this study, BFI_{max} was taken as 0.25 (Eckhardt, 2005).

Based on the suggested approach, the outcomes of the FDC study have been combined with the results from equation (3.23) to gain α Eckhardt parameter value after considering BFI_{max} = 0.25 (Eckhardt, 2005) for perennial rivers with predominantly porous aquifers, as a starting point. First of all, the long-term average annual fraction of TF from BF was estimated after obtaining the Q_{90} and Q_{50} numbers by applying the FDC method, connecting equation (3.23)

with FDC (Al-Faraj and Scholz, 2014). Considering α = 0.925 as an initial value (Arnold and Allen, 1999; Smakhtin, 2001), the daily flow is filtered for various numbers of filter Eckhardt parameter (α) until the BFI is equivalent to the Q_{90}/Q_{50} ratio. Several BF time series were gained by applying the filtered α Eckhardt parameter value. Secondly, linear regression models were performed between the annual BFI and the annual runoff for all considered periods at both the upstream and downstream sub-basins to investigate climate change, drought events, and river regulating impacts on the BF contribution.

To explore the potential impact of stream regulation on the groundwater involvement to the total flow (TF) of streamflow, this part of the study considered the pre-damming, post-damming and integrated periods. At the basin inlet, the first period covered the water years from 1931 to 1965 (considered as pre-damming). The water years that span from 1966 to 2013 are considered as the post-damming period, and the integrated period covers the hydrological years between 1931 and 2013. However, the corresponding periods at the downstream location were 1931–1965, 1966–1993 and 1931–1993, respectively.

3.5.6 Hydrologic Alteration

The collective impact of the anthropogenic intervention and climate change on the river flow regime have been evaluated using the Indicators of Hydrologic Alteration (IHA) software version 7.1 (Richter et al., 1998).

A subset of the IHA indices was utilised in the evaluation of the extent to which the natural flow regime had been altered. The successive drought episodes were also considered in this analysis. Many indices were used, including the annual and monthly (mean and median) flows, magnitudes of annual extreme conditions (such as the 1-, 3-, 7-, 30-, and 90-days minima and maxima), and the lower and upper thresholds of percentiles (such as the 10^{th}, 25^{th}, 50^{th}, 75^{th}, and 90^{th} percentiles).

The daily Lower Zab River flow rate for the water years from 1931 to 2013 was measured at the Iraqi side of the river. The entire records were separated into two prime categories: natural flow period and changed flow period. The first hydrological alteration occurred in the water year 1965, which was considered as a reference water year. Accordingly, the period between 1931 and 1964 represents the pre-regulated period. However, the period that

covers the hydrologic years between 1965 and 2013 was considered as the post-regulated period. The time intervals selected depended on the degree of anthropogenic intervention, such as increasing water requirements and reservoir constructions, in addition to the impact of climate change. The first period, between 1965 and 2013, represents the entire period since the first reservoir was constructed. The period between 1979 and 2014 was characterised by variation in climate involving two sub-periods (1979–1987 and 1998–2008). These time scales depended on the level of alteration.

3.5.7 Normal Years Identification

Thirty-five hydrological years (1979–2013) were utilised to estimate the RDI_{st} values, to specify which period closely represented (on average) the normal climatic conditions. Such a period expressed the timeframe in which no extreme RDI_{st} values were recorded and when (on average) the RDI_{st} value was close to zero. The period of twelve water years (1988–2000), which characterised normal conditions, was applied to calibrate the HBV model and run the delta perturbation (DP) climatic scenarios. The regression coefficients a_1, b_1, a_2, and b_2 of equations (3.25) and (3.26) were also evaluated.

$$RDI_{st} = a_1 \times \ln(RDI_{\alpha 12}) + b_1 \tag{3.25}$$

$$SDI = a_2 \times \ln(runoff) + b_2 \tag{3.26}$$

where RDI_{st}, $RDI_{\alpha 12}$, and SDI are the RDI standardised form, the RDI alpha expression, and the stream drought index. Table 3.7 lists the average annual precipitation for the normal water years over the considered time-period.

Table 3.7 Precipitation (P) for normal hydrological years

Water year	Mean P (mm)	Water year	Mean P (mm)
1983–1984	768	2001–2002	599
1985–1986	732	2002–2003	650
1986–1987	800	2003–3004	572
1988–1989	557	2004–2005	558
1989–1990	718	2009–2010	588
1990–1991	700	2010–2011	597
1992–1993	763	2011–2012	658
1993–1994	816	2012–2013	788
1995–1996	562	2013–2014	635
1996–1997	568		

3.5.8 Rainfall-Runoff Simulation

For the purposes of planning, designing or management of river discharges, rainfall-runoff models have been used widely to acquire streamflow data, since such data are not easily available. These models comprise a series of equations that endeavor to mimic the diversity of the interrelated events, which participate in the hydrological process. The hydrological models might be categorised based on many criteria, such as procedure description, solution mechanism, and scale. Various categories are applied in the literature, for example lumped and distributed models, continuous-time, and event-based models, as well as conceptual and black-box models (Tigkas et al., 2004; Aksoy et al., 2016).

For the simulation of basin runoff, depending on a set of weather parameters, the current research utilises three of the most commonly used conceptual models, which are the Medbasin (Tigkas and Tskiris, 2004), Ge´nie Rural a Daily 4 parameters (GR4J) and the Hydrologiska Byråns Vattenbalansavdelning (HBV; The Water Balance Department of the Hydrological Bureau) rainfall-runoff models (Tabari and Taalaee, 2011; Tigkas et al., 2012). The Medbasin model integrates the two lumped hydrological models Medbasin-D and Medbasin-M for daily (D) and monthly (M) data, respectively, with tools for forecasting different climatic variations and drought scenarios. The Medbasin-M model is based on two calibration parameters, the total capacity of the soil storage S_{max} (mm) and the coefficient of deep percolation C. The monthly delay factor *a* adjusts the distribution of the monthly runoff (Tigkas and Tsakiris, 2004). A favorable computation of S_{max} (mm) can be accomplished by

equation (3.27). Monthly precipitation (mm) and potential evapotranspiration (mm) can be utilised as input data for the rainfall-runoff modeling process.

$$S_{max} = 25.4 \times \left(\frac{1000}{CN} - 10\right) \tag{3.27}$$

where S_{max} (mm) is the total capacity of the soil storage and CN is the curve number that is based on many factors, such as land use and land cover, previous moisture conditions in the basin, and soil infiltrability.

The GR4J is a daily-lumped four-parameter rainfall-runoff model that is used both for precipitation and potential evapotranspiration data as input for meteorological variables. The model belongs to the family of soil moisture accounting models; it shows a good robustness in comparative studies and was also extensively tested for various climatic regions including the USA, Australia, and France. The model calibration is relatively simple because of the low number of parameters (Perrin et al., 2003).

HBV is an example of a semi-distributed conceptual model simulating daily discharge depending on daily rainfall and air temperature and monthly estimates of potential evapotranspiration as input. Air temperature data are used for calculating snow accumulation.

As a first step for simulation of runoff, the rainfall-runoff models have to be calibrated depending on the recorded dataset of the baseline period. Subsequently, the usual time series of streamflow is rebuilt for the anthropogenic period. After that, the anthropogenic intervention impact on streamflow is estimated by subtracting the recorded streamflow from the rebuilt streamflow, as shown in equation (3.28).

$$\Delta R_{anthropogenic} = R_a - R_{ar} \tag{3.28}$$

where $\Delta R_{anthropogenic}$ (mm/month) indicates the change in the mean annual runoff, as a result of the anthropogenic intervention effect, R_a (mm/month) refers to the observed runoff of the

anthropogenic intervention period, and R_{ar} (mm/month) is the rebuilt runoff series for the anthropogenic intervention period.

3.5.8.1 Hydrologic Sensitivity Analysis Method

The analysis of hydrologic sensitivity is defined as the ratio variation in average streamflow in response to the average precipitation and potential evapotranspiration variations in an annual time step (Velázquez et al., 2011). The basin water balance can be expressed by the equation (3.29). The change of ΔS (mm) can reasonably be ignored on the average yearly time scale. It follows that ΔS can be set as zero for a lengthy time-period (i.e. 10 water years or more) (Guo et al., 2014; Jiang et al., 2014).

$$P = PET + R + \Delta S \tag{3.29}$$

where P (mm) is precipitation, PET (mm) represents potential evapotranspiration, R (mm) is streamflow, and ΔS (mm) is basin water volume change. According to Zhang et al. (2001), long-term average annual actual evapotranspiration (AET) can be calculated as depending on equations (3.29) and (3.14).

$$\frac{PET}{P} = \frac{1 + \omega \times RDI_{\alpha_k}^{-1}}{1 + \omega \times RDI_{\alpha_k}^{-1} + RDI_{\alpha_k}} \tag{3.30}$$

where PET (mm) is potential evapotranspiration, P (mm) is precipitation, GƆ is the coefficient of the available water for plants related to the vegetation type (Zhang et al., 2001), k is the time step, and $RDI_{\alpha_k^i}$ is defined in equation (3.14).

Note that GƆ is the coefficient of plant-available water as a function of the crop type (Zhang et al., 2001). The parameter GƆ can be calibrated with the support of the annual long-term AET estimated from equations (3.29) and (3.30). Precipitation and potential evapotranspiration perturbations can result in water balance alterations. Through considering a hydrologic sensitivity analysis, the average yearly streamflow alteration as a result of climate change can be predicted using equation (3.31) (Jiang et al., 2011).

$$\Delta R_{climate} = \beta \times \Delta P + \gamma \times \Delta PET \quad (3.31)$$

where $\Delta R_{climate}$ (mm/month), ΔP (mm) and ΔPET (mm) indicate variations in streamflow, precipitation, and potential evapotranspiration, respectively; β and γ are the streamflow coefficients of sensitivity to precipitation and potential evapotranspiration in this order, which can be expressed by equations (3.32) and (3.33) (Li et al., 2007).

$$\beta = \frac{1 + 2 \times RDI_{\alpha_{12}}^{-1} + 3 \times \omega \times RDI_{\alpha_{12}}^{-1}}{(1 + RDI_{\alpha_{12}}^{-1} + \omega \times (RDI_{\alpha_{12}}^{-1})^2)^2} \quad (3.32)$$

where β is the streamflow coefficient of sensitivity to precipitation, $RDI_{\alpha_{12}}^{-1}$ is the 1/annual dryness index and Ꞷ is the coefficient of available water for plants related to the vegetation category (Zhang et al., 2001).

$$\gamma = - \frac{1 + 2 \times \omega \times RDI_{\alpha_{12}}^{-1}}{\left(1 + RDI_{\alpha_{12}}^{-1} + \omega \times \left(RDI_{\alpha_{12}}^{-1}\right)^2\right)^2} \quad (3.33)$$

where γ is the streamflow coefficient of potential evapotranspiration, Ꞷ is the coefficient of plant-available water related to the vegetation category (Zhang et al., 2001) and $RDI_{\alpha 12}$ is the 1/annual dryness index.

3.5.8.2 Multi-Regression Method

In this method, streamflow is integrated with precipitation and potential evapotranspiration at a monthly time scale for the baseline time-period, as shown in equation (3.34).

$$R_b = a \times P_b + b \times PET_b + c \quad (3.34)$$

where R_b (mm/month) refers to the baseline period observed streamflow; P_b (mm) and PET_b (mm) represent the precipitation and potential evapotranspiration of the baseline period,

respectively; and a, b, and c are three constants predicted using least-square regression analysis.

Based on equation (3.34), the natural streamflow of the anthropogenic intervention can be expressed as shown in equations (3.35) and (3.36).

$$\overline{R_a} = a \times P_a + b \times PET_a + c \tag{3.35}$$

where $\overline{R_a}$ (mm/month) expresses the reconstructed streamflow for the anthropogenic intervention period; P_a (mm) and PET_a (mm) represent the anthropogenic interventions period precipitation and potential evapotranspiration, respectively; and a, b, and c are three parameters estimated using least-square regression analysis.

$$\Delta R_{anthropogenic} = R_a - \overline{R_a} \tag{3.36}$$

where $\Delta R_{anthropogenic}$ (mm/month) indicates the average annual streamflow alteration owing to the effects of the anthropogenic intervention, R_a (mm/month) represents the recorded streamflow subject to the anthropogenic intervention period, and $\overline{R_a}$ (mm/month) indicates the change in mean annual runoff due to anthropogenic interventions.

3.5.8.3 Separation Effect Framework

The impacts of climate change and anthropogenic intervention on streamflow can be estimated using the following equations (3.37) to (3.40).

$$\Delta R_{total} = R_a - R_b \tag{3.37}$$

$$\Delta R_{total} = \Delta R_{anthropogenic} + \Delta R_{climate} \tag{3.38}$$

$$E_{anthropogenic} = \frac{\Delta R_{anthropogenic}}{|\Delta R_{total}|} \times 100\% \quad (3.39)$$

$$E_{climate} = \frac{\Delta R_{climate}}{|\Delta R_{total}|} \times 100\% \quad (3.40)$$

where ΔR_{total} (mm/month) is the total change of streamflow, R_a (mm/month) represents the streamflow subject to anthropogenic intervention, R_b (mm/month) refers to the baseline period observed streamflow, $\Delta R_{anthropogenic}$ (mm/month) indicates the variation in the average annual streamflow alteration owing to the anthropogenic intervention effects, $\Delta R_{climate}$ (mm/month) indicates variations in streamflow, $E_{anthropogenic}$ (%) expresses the impact of anthropogenic intervention on streamflow, $|\Delta R_{total}|$ indicates the absolute value of ΔR_{total},.and $E_{climate}$ (%) indicates the impact of climate change on streamflow.

3.5.8.4 Climate Change Impact

The exposure of the prospective impacts of climate change on the hydro-climatic parameters is determined by the climate change and anthropogenic intervention impact analysis. The key result of climate change is that wet and dry years are categorised by maximum and minimum flows, respectively. In 2006, Yoo suggested that the proper times during which yearly basin precipitation is more than average precipitation (P_{av}) (P_{av}) + 0.75 × standard deviation (SD) are considered as wet years, whereas, years with annual precipitation of no more than P_{av} - 0.75 × SD are considered as dry. Consequently, years with precipitation amounts between these two thresholds are measured as typical years (Yang et al., 2008):

$$P_{av} - 0.75 \times SD \leq P \leq P_{av} + 0.75 \times SD \quad (3.41)$$

3.5.8.5 Model Performance Criteria

To test the rainfall-runoff models' effectiveness, the following criteria were applied, equations (3.42) to (3.46):

$$RMSE = \sqrt{\frac{1}{n}\sum_{i=1}^{n}[(R_{obs})_i - (R_{sim})_i]^2} \quad (3.42)$$

$$IoA = 1 - \frac{\sum_{i=1}^{n}\left[(R_{obs})_i - (R_{sim})_i\right]^2}{\sum_{i=1}^{n}[|(R_{obs})_i - \overline{R}_{obs}| + |(R_{sim})_i - \overline{R}_{sim}|]^2} \quad (3.43)$$

$$r = \sqrt{\frac{\sum_{i=1}^{n}\left[(R_{obs})_i - \overline{R}_{obs}\right][(R_{sim})_i - \overline{R}_{sim}]}{\{\sum_{i=1}^{n}[(R_{obs})_i - \overline{R}_{obs}]\}^{0.5}\{\sum_{i=1}^{n}[(R_{sim})_i - \overline{R}_{sim}]\}^{0.5}}} \quad (3.44)$$

$$MAE = \frac{1}{n}\sum_{i=1}^{n}\left|(R_{obs})_i - (R_{sim})_i\right| \quad (3.45)$$

$$NSCE = 1 - \frac{\sum_{i=1}^{n}\left[(R_{sim})_i - (R_{obs})_i\right]^2}{\sum_{i=1}^{n}\left[(R_{obs})_i - \overline{R_{obs}}\right]^2} \quad (3.46)$$

where RMSE is the root mean square error (dimensionless), IoA is the index of agreement (dimensionless), r is the correlation coefficient (dimensionless), MAE is the mean absolute error (dimensionless), NSCE is the Nash–Sutcliffe model efficiency coefficient (Nash and Sutcliffe, 1970), $R_{obs(i)}$ is the recorded streamflow (mm/month) at i time step, $R_{sim(i)}$ is the predicted streamflow (mm/month) at i time step, $\overline{R}_{obs}$ is the average amount of the recorded values (mm/month), and n is the data point number.

3.5.9 Climate Change Scenarios

For the evaluation of the climate change impact, this research utilised and compared the results of two of the commonly applied climate change scenarios, which are the GCM and DP. Regarding the former, the local-scale climate scenarios were based on the SRA2 emission scenario simulated by the selected seven GCM, shown in Table 3.8, generated by

using LARS-WG5.5 for the time-periods of 2011–2030 (near future), 2046–2065 (medium future), and 2080–2099 (far future) and a baseline period of 1980–2010, to predict the future change in weather data over the representative case study. This GCM are as follows: CNCM3, GFCM21, HADCM3, INCM3, IPCM4, MPEH5, and NCCCS. For the DP scenario, delta perturbations in precipitation (dP) of 0–40% (2% step) and potential evapotranspiration perturbations (dPET) of 0–30% (2% step) and a baseline period of 1988–2000 were used. Accordingly, 336 scenarios were developed representing the collective impact of alteration in precipitation and potential evapotranspiration values. These scenarios included all the possible climate change projections.

Then, to investigate how close the results of GCM and DP scenarios are, or how different they are from each other, in terms of their ability to simulate streamflow and reservoir performance, an evaluation and comparison of the results of these two scenarios was performed

3.5.10 Long Ashton Research Station Weather Generator Model

For the prediction of climate data at a single site under the present and future climatic situations, LARS-WG5.5 has been used. LARS-WG5.5 is a stochastic weather generator (WG) grounded on the series methodology (Semenov and Stratonovitch, 2010). This version of the LARS-WG incorporates predictions from 15 GCM used in the Intergovernmental Panel on Climate Change (IPCC) fourth assessment report (AR4) (Semenov and Stratonovitch, 2010). Table 3.8 lists important features of the GCM, contenting grid resolution, the reference time-periods for climate predictions, and available Special Report on Emission Scenarios (SRES). These models are referred to in LARS-WG by their acronyms used in AR4 (Table 3.8). The main assumptions of the SRES scenarios are given in Table 3.9.

LARS-WG model utilises daily data for a specified site to estimate a set of probability distribution parameters of weather variables, in addition to the relationships between them, which then is used to create artificial climate time series of random length by arbitrarily choosing values from the suitable distributions. Through perturbing variables of distributions for a location with the estimated alterations of climate resulting from a

universal or local climate model, a daily climatic scenario for this location could be created and applied, as well as a process based effect model for impacts evaluation. The weather generation model proved to have good performance in reproducing several climate data comprising extreme climate episodes (Semenov and Stratonovitch, 2010).

Table 3.8 Global climate models (GCM) from Intergovernmental Panel on Climate Change (IPCC) fourth assessment report (AR4) integrated into the Long Ashton Research Station Weather Generator (LARS-WG5.5); T_1: 2011–2030; T_2: 2046–2065; T_3: 2081–2100 (Adapted from: Semenov and Stratonovitch, 2010)

Global climate model	Model acronym	Grid (°)	Time-period	Country	Source
Special Report on Emissions Scenarios: SRA1B					
[a]CGCM33.1 (T_{47})	CGMR	2.8×2.8	T_1,T_2,T_3	Canada	McFarlane et al. (1992)
Special Report on Emissions Scenarios: SRA1B, SRB1					
[b]CSIRO-MK3.0	CSMK3	1.9×1.9	T_1,T_2,T_3	Australia	Gordon et al. (2002), CSMD (2005)
[c]FGOALS-g1.0	FGOALS	2.8×2.8	T_1,T_2,T_3	China	Wang et al. (2004)
[d]MRI-CGCM2.3.2	MIHR	2.8×2.8	T_1,T_2,T_3	Japan	K-1 Model Developers (2004)
[e]BCM2.0	BCM2	1.9×1.9	T_1,T_2,T_3	Norway	Déqué (1994)
[f]GISS-AOM	GIAOM	3×4	T_1,T_2,T_3	USA	Russell et al. (1995)
[g]PCM	NCPCM	2.8×2.8	T_1,T_2	USA	Kiehl et al. (1998), Kiehl and Gent (2004)
Special Report on Emissions Scenarios: SRA1B, SRA2					
[h]HadGEM1	HADGEM	1.3×1.9	T_1,T_2,T_3	UK	Martin et al. (2006), Ringer et al. (2006)
[i]CNRM-CM3	CNCM3	1.9×1.9	T_1,T_2,T_3	France	Déqué et al. (1994)
Special Report on Emissions Scenarios: SRA1B, SRA2, SRB1					
[j]GFDL-CM2.1	GFCM21	2.0×2.5	T_1,T_2,T_3	USA	GFDL-GAMDT (2004)
[k]HadCM3	HADCM3	2.5×3.75	T_1,T_2,T_3	UK	Gordon et al. (2000), Pope et al. (2000),
[l]INM-CM3.0	INCM3	4×5	T_1,T_2,T_3	Russia	Galin et al. (2003)
[m]IPSL-CM4	IPCM4	2.5×3.75	T_1,T_2,T_3	France	Hourdin et al. (2006)
[n]ECHAM5-OM	MPEH5	1.9×1.9	T_1,T_2,T_3	Germany	Roeckner et al. (1996)
[o]CCSM3	NCCCS	1.4×1.4	T_1,T_2,T_3	USA	Collins et al. (2004)

[a]Canadian Centre for Climate Modelling and Analysis; [b]Commonwealth Scientific and Industrial Research Organisation; [c]Institute of Atmospheric Physics; [d]National Institute for Environmental Studies; [e]Bjerknes Centre for Climate Research ; [f]Goddard Institute for Space Studies; [g]National Centre for Atmospheric; [h]UK Meteorological Office; [i]Centre National de Recherches Meteorologiques; [j]Geophysical Fluid Dynamics Lab; [k]UK Meteorological Office; [l]Institute for Numerical Mathematics; [m]Institute Pierre Simon Laplace; [n]Max-Planck Institute for Meteorology; [o]National Centre for Atmospheric

Table 3.9 Carbon dioxide (CO2) concentrations for selected climate scenarios specified in the Special Report on Emissions Scenarios (SRES) (Adopted from Semenov and Stratonovitch, 2010)

Scenario	Key assumptions	CO_2 concentration (part per million)		
		T_1	T_2	T_3
B_1 The sustainable world	Quick alteration in economic organisations, dematerialization comprising developed equity and ecological concern. There is a global concern regarding ecological and social sustainability and more effort in introducing clean technologies. The world people extents to 7 billion by 2100.	410	492	538
B_2 The world of technological inequalities	A heterogeneous society emphasising local solutions to economic, social and environmental sustainability rather than global solutions. Human welfare, equality, and environmental protection all have high priority.	406	486	581
A_1B The rich world	Characterised by very rapid economic growth (3% a year), low population growth (0.27% a year) and rapid introduction of new and more efficient technology. Globally there is economic and cultural convergence and capacity building, with a substantial reduction in regional differences in per capita income.	418	541	674
A_2 The separated world	Cultural characteristics distinct the diverse areas, making the world more heterogeneous and international cooperation less likely. 'Family values', local traditions and high population growth (0.83% a year) are emphasised. Less focus on economic development (1.65% a year) and material wealth.	414	545	754

LARS-WG5.5 utilises a semi-empirical distribution, which is defined as the cumulative probability distribution function, to approximate probability distributions of dry and wet series, daily extreme temperatures, precipitation, solar radiation and potential evapotranspiration. For each weather parameter v, a value of a weather parameter v_{ia} equivalent to the probability p_i is computed as in equation (3.47).

$$v_i = \min\{v{:}P(v_{obs} \leq v) \geq P_i\} \qquad i = 0,\ldots\ldots, n \tag{3.47}$$

where P() denotes probability deepened on recorded data $\{v_{obs}\}$. Two values p_0=0 and p_n = 1with the corresponding values of $v_0 = \min\{v_{obs}\}$ and $v_n = \min\{v_{obs}\}$ are fixed for each climatic variable. To estimate the maximum values of a climate parameter precisely, some p_i is assigned near to 0 for very low amounts of the parameter and near to 1 for very high amounts; the remaining values of p_i are distributed equally on the probability scale. For P, three values near to 1 are applied, which are as follows: $p_{n-1} = 0.999$, $p_{n-2} = 0.995$ and $p_{n-3} = 0.985$. These values permit a better estimate of events with very high daily P that occurs with very low probability, e.g. rainfall during hurricanes. Due to the probability of very low

daily precipitation (< 1 mm) for radiation are distributed similarly between low and high values, because of the physical limitations on low and high values of daily radiation.

The synthetic weather generation procedure is separated into three main steps: (1) Site analysis function, which is used for model calibration through analysis of the recorded meteorological data to estimate their statistical properties. The obtained results are saved in two parameter files; (2) Q_{Test} function is used for model validation during which the statistical properties of the recorded and artificial meteorological data are examined to investigate if there are any statistically significant variations; and (3) The generator function is used for synthetic meteorological data generation. The parameter files derived during the model calibration are used to produce artificial meteorological data having similar statistical properties as the recorded data, but different on a day-to-day basis. Artificial data equivalent to a specific climate change scenario may also be produced, by applying global climate model derived changes in temperature, precipitation, and solar radiation to the LARS-WG5.5 parameter files. Furthermore, a daily location climate scenario can be generated by changing variables of distributions for a location with the anticipated variations of weather resulting from global or local weather simulations. The generated climatic scenarios can then be utilised in combination with a procedure founded influence model for impacts evaluation.

To create weather scenarios for a specific site, future time-period, and an emission scenario, the LARS-WG5.5 baseline variables, which estimate the recorded weather data, are amended by the delta variations for the future period and the emissions projected by a GCM for each weather parameter for the network covering the location.

In this research, the regional scale climate scenarios are founded on the SRA2 scenario modeled by seven ensembles of GCM simulated by utilising LARS-WG5.5 for the 2011–2030, 2046–2065, and 2080–2099 periods to forecast the future alteration of temperature and precipitation in the LZRB.

To develop the reservoir capacity-yield-reliability relationships, many pre-processing steps for the inflow time series were performed. Firstly, to estimate the volume of precipitation and the evaporation, the elevation-area-capacity relationships were derived for precipitation and evaporation. This research suggested the following model represented the relationship

between the reservoir water level (elevation) or the water surface area and the capacity with an excellent correlation coefficient equation (3.48):

$$EA = a_3 + b_3 \times S + c_3 \times S^{d_3} \tag{3.48}$$

in which EA is either the reservoir water level (m) or the reservoir water surface area (km^2), S is the reservoir storage in (10^9 m^3); and a_3, b_3, c_3, d_3 are the regression coefficients; excel software was used to estimate these values. Figure 3.4 shows the relationships between the reservoir water level, surface area, and the capacity based on the topographic features of the Dokan reservoir, which are illustrated in Table 3.4.

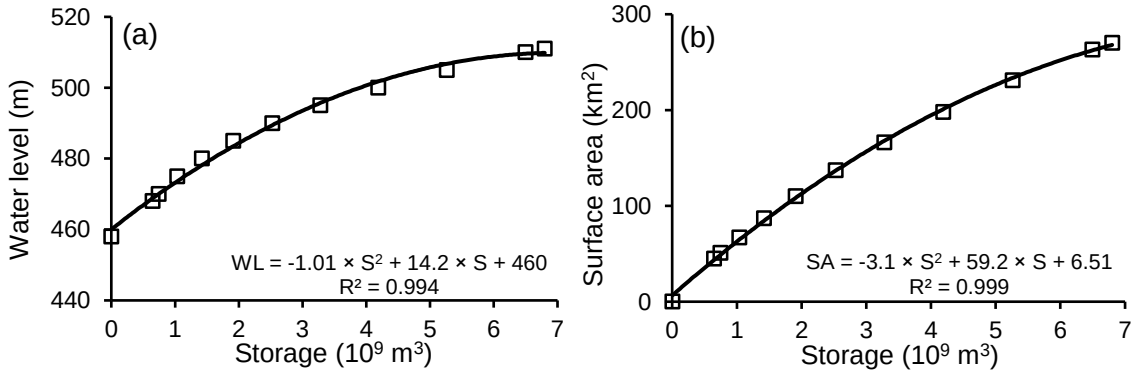

Figure 3.4 Water level-surface area-capacity relationships for the Dokan Reservoir; (a) Water level-capacity relationship; and (b) Surface area-capacity relationship

Then, the statistical properties of the inflow time series were investigated as they have a vital effect on the predicted measures of risk. Table 3.10 shows a summary of the main statistical properties of the reservoir inflow. The mean monthly runoff ranged from 444 m^3/s during April to 53.59 m^3/s during September. A high monthly correlation was recorded in November, with a value of less than 0.5. The monthly and annual inflows are skewed to the right as these values have a positive skewness.

Table 3.10 Statistical properties of the Dokan reservoir inflow

Month	Minimum (m^3/s)	Maximum (m^3/s)	Mean (m^3/s)	Standard deviation (m^3/s)	variation coefficient	Skewness coefficient	Lag-12 correlation coefficient
Oct	11.19	112.06	53.91	24.70	0.46	0.28	0.52
Nov	20.23	311.97	88.80	56.14	0.63	1.86	0.42
Dec	28.77	582.23	141.31	103.12	0.73	2.08	0.73
Jan	32.06	481.26	174.71	103.73	0.59	0.97	0.73
Feb	51.21	676.29	277.63	148.70	0.54	0.85	0.52
March	47.90	1569.16	418.80	292.87	0.70	2.10	0.77
April	40.33	1373.10	444.14	260.03	0.59	1.24	0.82
May	48.55	786.77	282.62	154.16	0.55	1.26	0.92
June	26.97	351.03	130.91	70.80	0.54	0.97	0.77
July	13.00	208.68	73.37	41.35	0.56	1.12	0.74
August	8.58	185.29	57.88	32.93	0.57	1.58	0.84
Sep	9.27	146.87	53.59	29.38	0.55	0.83	0.51
Annual	28.17	565.39	183.14	109.83	0.58	1.26	0.69

After that, the RCY model was utilised to develop the relationships of the capacity-yield-reliability, under the collective impacts of climate change. Three future time horizons, the 2020s, 2050s, and 2080s have been considered. Two relationships were developed which can be used to enable managers to make an informed and robust decision in facing many uncertainties about the future. The first relationship is the yield%-OPOF%, and the second is the capacity ($10^6 \times m^3$)-yield%. These relationships can be applied to test various options against the range of different future scenarios.

3.5.11 Reservoir Capacity-Yield-Reliability Relationship

As a first step for reservoir capacity-yield (RCY) performance evaluation, the Hydrologiska Byråns Vattenbalansavdelning (HBV) hydrological model is calibrated based on the baseline period observed dataset. Subsequently, the RCY simulation was performed applying equation (3.49) (McMahon and Adeloye, 2005).

$$S_{t+1} = S_t + R_t - D_t - \Delta E_t - L_t \tag{3.49}$$

$$\text{Subject to } 0 \leq S_{t+1} \leq C_a \tag{3.50}$$

where S_{t+1} and S_t are reservoir storage volumes at the end and the beginning of a time-period t, respectively; R_t is the inflow over the period t; D_t is the actual water yield over the period t; ΔE_t is the reservoir net evaporation loss within the period t; L_t represents other losses; and C_a is the reservoir active capacity.

During the simulation procedures, the reservoir S_o is typically assumed to be full (McMahon and Mein, 1978, 1986), and the downstream demand is usually considered as a specific fraction of the mean inflow. The usual period is one month, but any other period can be used. McMahon and Mein (1978) provided a complete method to calculate the reservoir operational probability of failure, which can be summarised as follows: (a) Assume the reservoir is initially full ($S_o = C_a$); (b) Apply equation (3.49) month by month on the historical or generated monthly flows; (c) Plot (S_{t+1}) against time on a monthly time scale; and (d) Compute the OPOF by using equation (3.51).

The storage size estimated through behavior analysis varies little with the starting month. By the behavior analysis, the vulnerability of the reservoir is estimated by ignoring the constraint on equation (3.49) and then choosing the maximum negative value of (S_{t+1}) during the analysis period, whereas the resilience is estimated by computing the maximum consecutive number of empty months during the analysis (Moy et al., 1986).

Following the simulation, three appropriate performance measures were assessed (McMahon and Adeloye, 2005; McMahon et al., 2006):

(1) The time-based reliability (R_e) can be defined as the percentage of the entire period under investigation during which a reservoir is capable of providing the full demand without any deficiencies, as indicated in equation (3.51).

$$R_e = 1 - OPOF \tag{3.51}$$

where R_e is the reservoir reliability(%) and OPOF(%) is the reservoir operational probability of failure, which is defined as the ratio of time units during which the reservoir is effectively empty to the total number of time units applied in the analysis (equation (3.52)).

$$OPOF = \frac{N_e}{N} \tag{3.52}$$

where OPOF is the reservoir operational probability of failure (%), N_e is the time units number during which the reservoir is empty, and N is the total number of time units in the streamflow time series. There is no limitation on the OPOF but many studies considered 5% to be an acceptable limitation (McMahon and Adeloye, 2005).

(2) The resilience φ describes the reservoir's ability to recover from failure, Moy et al. (1986) defined it as the maximum number of consecutive periods of shortage that occur prior to recovery, and can be expressed based on equation (3.53) as discussed previously (Hashimoto et al., 1982; Fowler et al., 2003; Park and Kim, 2014).

$$\varphi = \sum_{t=1}^{N} Y_t \tag{3.53}$$

where Y_t is the number of continuous shortage indicator, $Y_t = 1$ if there is a shortage in period (t) and $Y_t = 0$ otherwise, and t = 1, 2, ……, N, which is the total number of time units in the stream flow time series sequence of failure periods.

(3) The vulnerability υ is a criterion to determine the significance of failure. Mathematically, it is expressed by equation (3.54) as shown in the past (Fowler et al., 2003; Park and Kim, 2014).

$$\upsilon = \max (Df_t) \tag{3.54}$$

where υ is the system vulnerability, and Df_t is a deficit at time t (McMahon and Adeloye, 2005; McMahon et al., 2006).

Chapter 4: RESULTS AND DISCUSSION

4.1 Hydro-Climatic Data Trend Analysis

Long-term trends in hydrological processes are potentially influenced by a changing climate and anthropogenic interventions (Robaa and Al-Barazanji, 2013; Shadmani et al., 2012; Mohammed et al., 2017a). Investigating such trends might support the identification of anthropogenic intervention starting points. To detect the long-term trends in the annual mean air temperature, precipitation (P), potential evapotranspiration, and streamflow, this study applies the Mann-Kendall (M-K) test.

Table 4.1 contains the statistical properties of the key meteorological variables representing the M-K test for the decadal change for different climatic conditions, in addition to the semi-arid specific case study, which is the Lower Zab River Basin (LZRB). The table displays the three-dimensional distribution of trend rise and fall, as well as non-significant trends, for the studied areas. The mean air temperature time series shows that the majority of non-significant trends are situated in most of the Mediterranean (MD) and continental (CN) areas, while the tropical (TR), arid and most of the humid climatic conditions show significantly positive trends.

LZRB, which is considered as an example for representing semi-arid areas, displayed a rising trend of mean air temperature with a maximum value of 0.67 °C for one decade, while a declining precipitation trend (Figure 4.1a) with a maximum decrease of 151 mm per decade was noted. The LZRB annual precipitation is around 720 mm. The maximum precipitation (1222 mm) was recorded for 1987/1988, while the corresponding minimum (250 mm) was assigned to 2007/2008. The mean annual precipitation changed spatially from 56 mm at Kirkuk station, which is located in the lower part of the basin, to 1369 mm at Sulymaniya station, which is situated in the upper basin. This indicates that the upper sub-

basin, which is characterised by high elevations (compared to the lower part), had higher precipitation values than the lower. An evident trend of mean air temperature increase during the last half-century led to a significant ($p < 0.05$) rise in the potential evapotranspiration for the entire LZRB, Figure 4.1b and Table 4.1. The increase in potential evapotranspiration rate was 39 mm per decade. With an average value of about 1065 mm, the computed potential evapotranspiration for the basin changed from 962 mm in 1982/1983 to 1110 mm in 2007/2008 (Figure 4.1b). The obtained results indicate that the semi-arid climate, as represented by the specific case study, is getting warmer and drier due to climate change. The annual P decreased and the annual average air temperature increased (Table 4.1). The findings regarding LZRB are largely in agreement with previous studies (Fadhil, 2011; Robaa and AL-Barazanji, 2013). Figure 4.2 and Figure 4.3 display the spatial distribution of the long-term mean air temperature and precipitation over the LZRB, respectively. The basin mean air temperature varied between (6–13) ºC and (13–19) ºC at the upstream river sub-basin to more than 19 ºC at the downstream sub-basin. While the long-term precipitation over the basin changed spatially from 56 mm at Kirkuk station to 1369 mm at Sulymaniya station. It is important to note that the upper sub-basin had higher precipitation values than the lower one (Figure 4.3).

Furthermore, the ratios of the long-term average monthly precipitation to the long-term average annual precipitation for the studied hydrological year period, which started in October, are listed in Table 4.2. Data analysis outcomes show that the accumulated precipitation over the wet months, which are from October to May, accounts for approximately 99.5% of the entire annual precipitation. However, the aggregated P during the dry months, which are from June to September, contributes to just about 0.5% of the total precipitation. The obtained results indicate that the climate in the LZRB is getting warmer and drier. The annual precipitation and runoff depth decreased, whereas, the yearly average air temperature increased. These findings are largely in agreement with previous studies (Fadhil, 2011; Robaa and Al-Barazanji, 2013).

Table 4.1 Statistical properties of meteorological variables representing the non-parametric test for different climatic conditions, in addition to the Lower Zab River basin (LZRB) as semi-arid representative case study

Wider Region	Station ID	Meteorological parameter					
		T^a_m (°C)		P[b] (mm)		PET[c] (mm)	
		M-K[d]	*p*-value	M-K[d]	*p*-value	M-K[d]	*p*-value
Mediterranean							
South Africa	LL[e]	-0.005	0.966	0.264*	0.026	-0.240*	0.042
	HL[f]	-0.059	0.619	0.193	0.102	-0.247*	0.037
North Iraq	LL[e]	0.462**	<0.010	-0.536**	<0.010	0.243	0.040
	HL[f]	0.079	0.500	-0.328**	0.010	0.193	0.100
West Australia	LL[e]	0.103	0.386	-0.099	0.402	0.103	0.386
	HL[f]	0.227	0.055	0.334**	0.005	0.113	0.341
South USA	LL[e]	-0.005	0.966	0.025	0.831	0.129	0.274
	HL[f]	0.032	0.787	0.045	0.701	-0.015	0.898
Tropical							
East China	LL[e]	0.603**	<0.010	-0.365**	0.002	0.257*	0.030
	HL[f]	0.318**	0.007	-0.560**	<0.010	0.587**	<0.010
East Brazil	LL[e]	0.486**	<0.010	-0.066	0.580	0.129	0.274
	HL[f]	0.412**	0.001	-0.365**	0.002	-0.274*	0.012
Continental							
South East Spain	LL[e]	0.042	0.723	0.146	0.217	-0.092	0.435
	HL[f]	0.220	0.063	0.126	0.287	-0.045	0.701
South Russia	LL[e]	0.163	0.168	-0.055	0.639	0.19	0.108
	HL[f]	0.106	0.371	-0.277*	0.019	0.447**	<0.010
Arid							
Sahara	LL[e]	0.439**	<0.010	0.153	0.196	0.308**	0.009
	HL[f]	0.371**	0.002	0.069	0.560	0.153	0.196
Al-Sudan	LL[e]	0.250**	0.034	-0.008	0.943	0.106	0.371
	HL[f]	0.244**	0.039	-0.197	0.097	0.156	0.187
Humid							
UK	LL[e]	0.445**	<0.010	0.133	0.262	0.113	0.341
	HL[f]	0.455**	<0.010	0.113	-0.244	0.113	0.034
Norway	LL[e]	0.136	0.250	0.005	0.966	0.185	0.118
	HL[f]	0.069	0.560	0.002	0.989	0.185	0.118
Semi-arid climate							
LZRB case study (US[g])	Sulymanya	0.358**	<0.010	-0.301**	<0.010	0.201	0.090
	Halabcha	0.572**	<0.010	-0.522**	<0.010	0.316**	<0.010
	Sachez	0.079	0.500	-0.328**	0.010	0.193	0.100
	Mahabad	0.603**	<0.010	-0.573**	<0.010	0.525**	<0.010
	Salahddin	0.452**	<0.010	-0.472**	<0.010	0.220	0.060
	Soran	0.380**	<0.010	-0.426**	<0.010	0.241*	0.050
LZRB case study (DS[h])	Kirkuk	0.422**	<0.010	-0.553**	<0.010	0.420**	<0.01
	Makhmoor	0.462**	<0.010	-0.536**	<0.010	0.243	0.040
	Erbeel	0.351**	<0.010	-0.371**	<0.010	0.203	0.090
	Chemchamal	0.345**	<0.010	-0.412**	<0.010	0.139	0.240

[a]Mean air temperature; [b]Precipitation; [c]Potential evapotranspiration; [d]Mann–Kendall; [e] Lowland; [f]High land; [g]Upstream; and [h]Downstream

Note: Negative (−) and positive (+) values indicate the decreasing and increasing trends, respectively;

**Correlation is significant at the 0.01 level (2-tailed); and

*Correlation is significant at the 0.05 level (2-tailed)

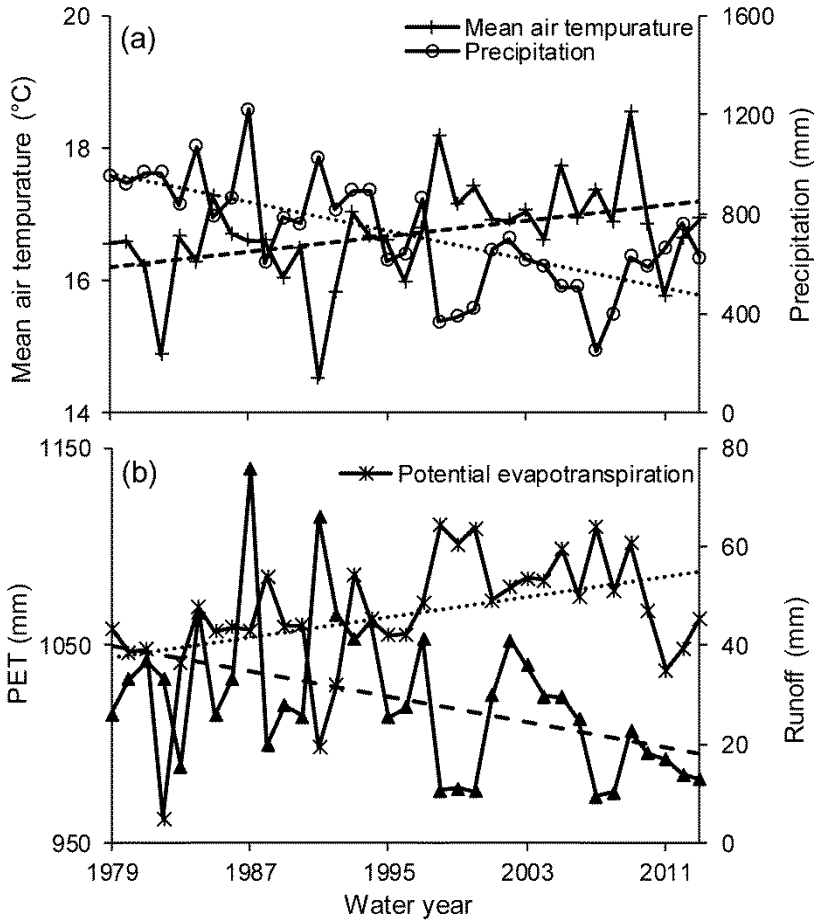

Figure 4.1 Annual values and trends of (a) Mean air temperature and precipitation, and (b) Potential evapotranspiration (PET) Lower Zab River Basin for the time-period between 1979 and 2013

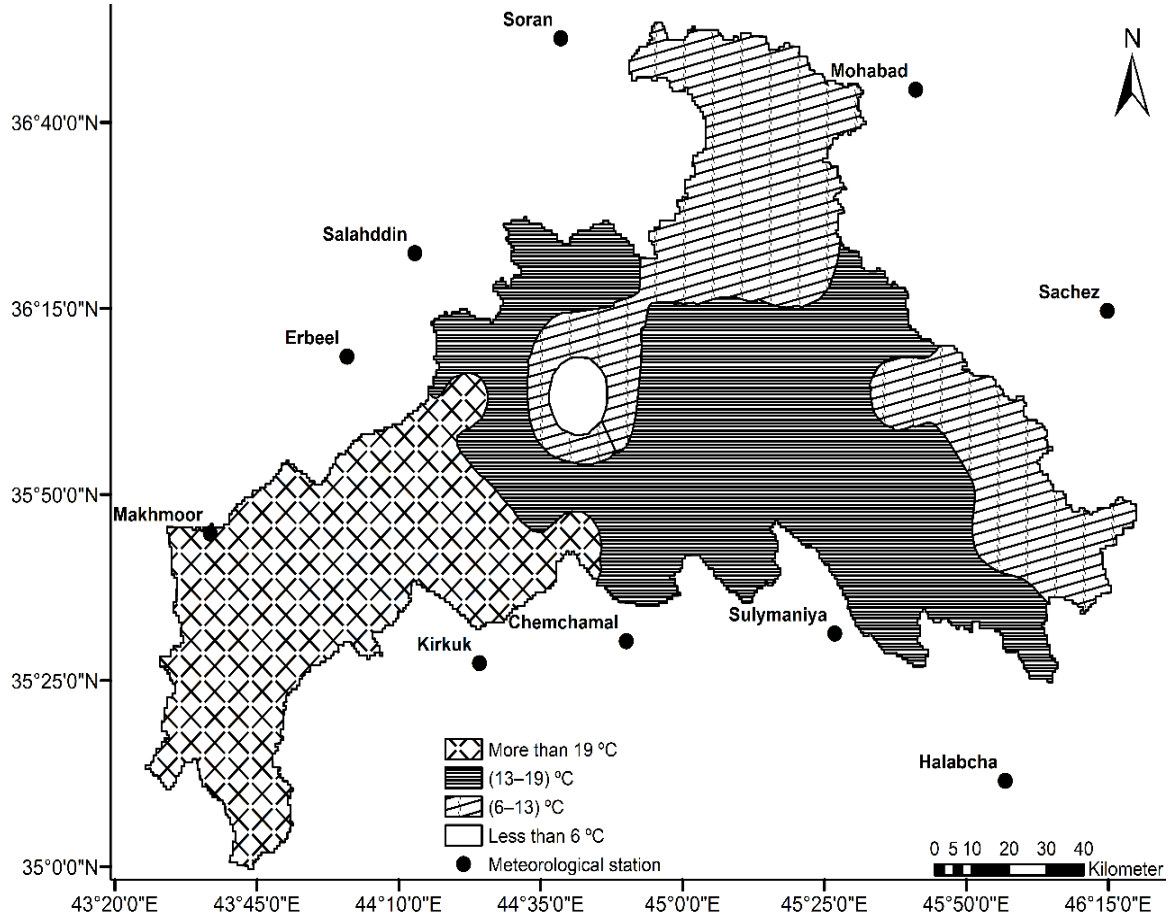

Figure 4.2 The long-term spatial distribution of the mean air temperature over the Lower Zab River Basin

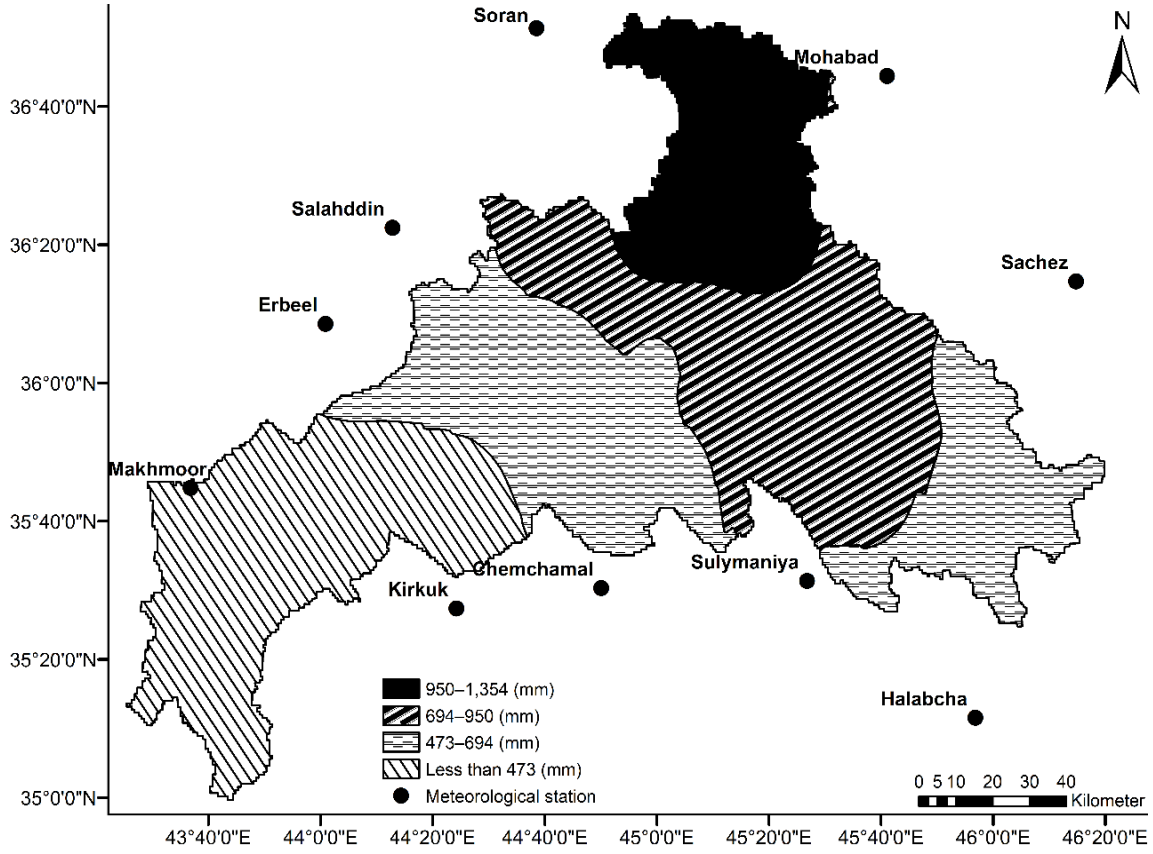

Figure 4.3 Spatial distribution of the long-term precipitation over the Lower Zab River Basin

Table 4.2 Long-term average monthly to long-term annual precipitation ratios

Sub-basin	Station name	Percentage of long-term annual precipitation ratio					
		Oct	Nov	Dec	Jan	Feb	Mar
US[a]	Sulymanya	4.53	12.16	16.42	18.63	17.42	16.83
	Halabcha	3.87	10.92	16.33	18.01	19.01	17.55
	Sachez	4.17	11.27	15.27	16.80	17.04	17.94
	Mohabad	5.88	11.91	14.26	15.76	16.19	16.65
	Salahddin	4.09	12.18	15.82	18.10	18.14	16.92
	Soran	5.04	12.19	13.78	13.91	15.62	16.66
DS[b]	Kirkuk	4.94	13.41	16.89	17.83	16.96	16.56
	Makhmoor	6.78	13.11	15.66	17.09	15.56	17.11
	Erbeel	5.87	12.93	15.91	17.27	16.53	16.48
	Chemchamal	5.17	13.14	16.53	17.48	16.91	16.21
Sub-basin	Station name	Percentage of long-term annual precipitation ratio					
		Apr	May	Jun	Jul	Aug	Sep
US[a]	Sulymanya	9.75	4.05	0.10	0.00	0.00	0.11
	Halabcha	10.64	3.39	0.12	0.02	0.00	0.14
	Sachez	11.20	5.78	0.25	0.05	0.01	0.22
	Mohabad	12.26	6.32	0.41	0.07	0.05	0.25
	Salahddin	10.82	3.70	0.10	0.00	0.00	0.13
	Soran	14.74	6.91	0.73	0.08	0.11	0.23
DS[b]	Kirkuk	9.06	4.09	0.17	0.00	0.00	0.10
	Makhmoor	9.53	4.73	0.17	0.00	0.00	0.25
	Erbeel	10.26	4.31	0.18	0.00	0.00	0.26
	Chemchamal	9.92	4.38	0.13	0.00	0.00	0.12

[a]Upstream; [b]Downstream

The coefficient of runoff is expressed as the percentage of the streamflow compared to the P over a specific period and has been selected to represent the LZRB hydro-climatic conditions (Figure 4.4). The decline in the coefficient of runoff (Figure 4.4) indicates that the streamflow yield has become weaker during the last four decades as estimated previously (Kahya and Kalayci, 2004; Mohammed et al., 2017a).

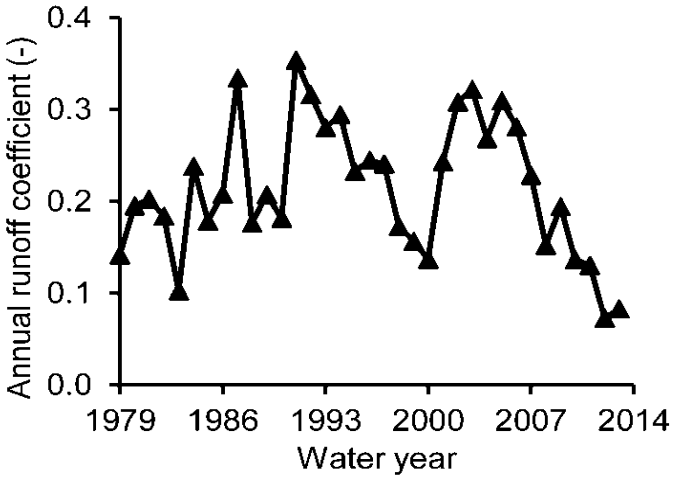

Figure 4.4 Annual runoff coefficient for the 1979–2014 period in Lower Zab River Basin

4.2 Hydro-Climatic Data Change Point Detection

The upstream annual runoff of the LZRB has an average of 169 m^3/s for the 35-year hydrological period (1979 to 2013). The minimum was 54 m^3/s for the water year 2007/2008. Nearly, 436 m^3/s was noticed as the maximum for the year 1987/1988 (Figure 4.1). Over the studied period, mean streamflow runoff of the LZRB exhibited a significant decline (-0.334 at $\alpha = 95\%$) at a rate of -38 m^3/s per decade.

The change point of the annual runoff series was determined using the Pettitt and precipitation-runoff double cumulative curve (PR-DCC) tests. Figure 4.5 and Figure 4.6 show the change point years of the runoff and precipitation time series by using the Pettitt and PR-DCC methods, respectively. The water year 1997/1998 is considered as a change point for the studied time series. The obtained results are found to be consistent with the findings of many other researchers with respect to this study area. For example, Sen et al. (2011) explained, through an analysis based on NCEP/NCAR reanalysis data that due to climate change, the study region

witnessed a statistically ($p < 0.05$) significant shift in the streamflow during the same period of time. In addition, Bozkurt and Sen (2013) investigated the hydro-climatic effects of future climate change in the study region using the results of different dynamically down-scaled General Circulation Models (GCM) (ECHAM5, CCSM3, and HadCM3) and emission scenario (A1FI, A2, and B1) simulations. They found that the annual surface runoff of the headwater area declined dramatically by about 25 to 55%.

The aggregate yearly runoff and precipitation shown in Figure 4.6a indicate that before 1997, runoff and precipitation were relatively regular, but after 1997, the properties of runoff or precipitation altered. Integrating the PR-DCC analysis and the Pettitt test, the year 1997 could be seen as the change point reflecting the impact of both climate change and anthropogenic intervention on the runoff and precipitation. Accordingly, the period between 1979 and 1997 was considered as the baseline period during which the anthropogenic intervention impacted on runoff were less recognisable. To fully appreciates the effects of climate and other influences on streamflow over the two periods, the variations in the correlation of streamflow and precipitation were investigated (Figure 4.6b).

The period from 1998 to 2013 was seen as the anthropogenic interventions period, and was grouped into three hydrological sub-periods: 1998–2002, 2003–2008 and 2009–2013. For these hydrological periods, changes in average yearly streamflow, P, and potential evapotranspiration were estimated (Table 4.3). During the periods 1998–2002, 2003–2008, and 2009–2013, the mean annual precipitation declined by -42, -43 and -30%, and the potential evapotranspiration increased by 4, 3.5, and 1%, whereas streamflow decreased by -44, -37, and -55% in this order.

The runoff intra-annual alteration is associated with the monthly cycle of precipitation, mean air temperature and catchment water-related non-climatic drivers. To further comprehend the intra-annual availability of streamflow and precipitation, the mean monthly precipitation and streamflow data between the baseline period (1979–1997) and the anthropogenic interventions period (1998–2013) have been compared with each other (Figure 4.7). Noticeable changes in both precipitation and streamflow were seen for the two considered time-periods. The average monthly precipitation and streamflow between 1998 and 2013 declined compared with the corresponding data for the baseline period. The decreases were greatest for June, July, and August (irrigation season), and were smallest during the winter months. Hence, the decrease in

streamflow within the post-alteration period may be due to basin-related non-climate drivers as indicated in the past.

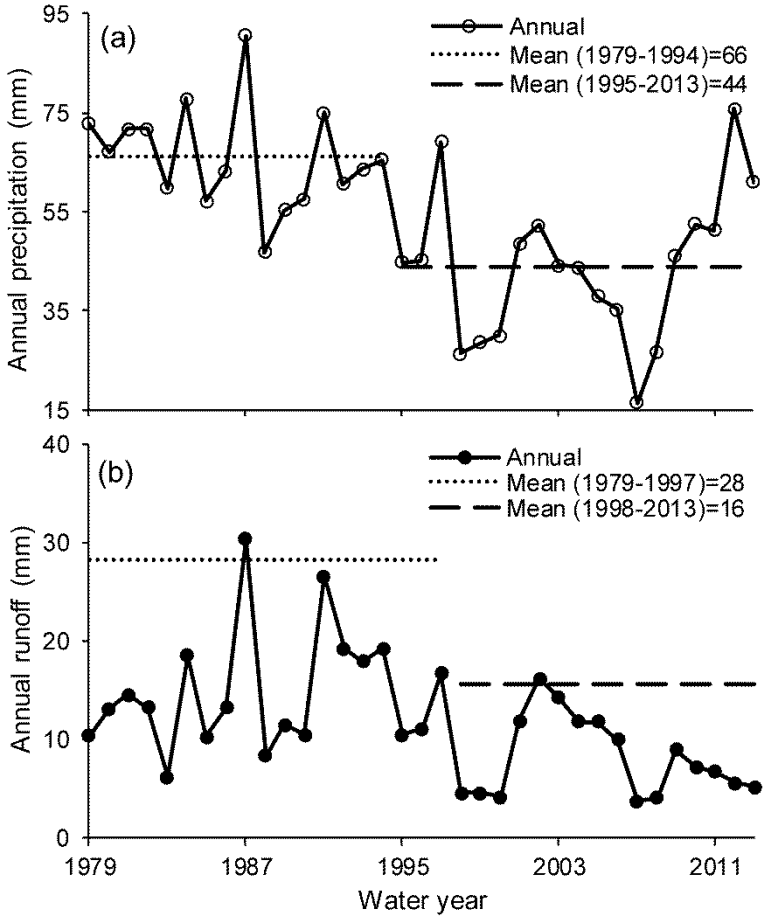

Figure 4.5 Pettitt test for detecting a change in the annual: (a) precipitation; and (b) runoff

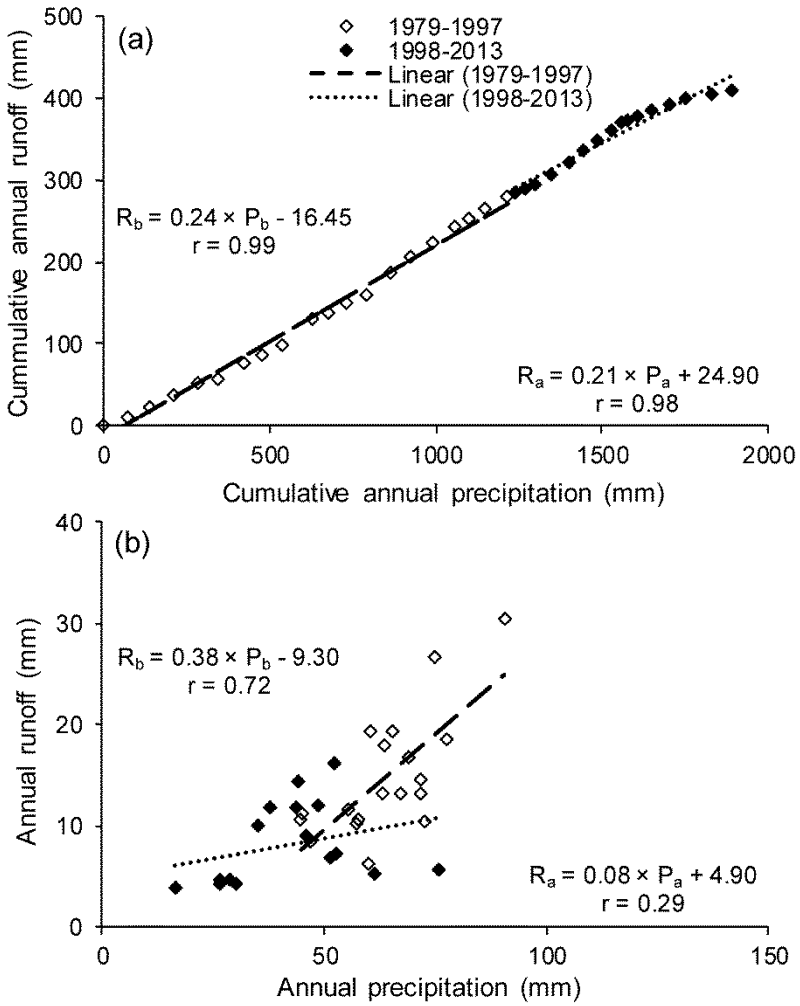

Figure 4.6 (a) Precipitation-runoff double cumulative curve (PR-DCC) of annual precipitation and runoff in the Lower Zab River basin; and (b) correlation between precipitation and runoff for the two considered time-period

Table 4.3 Changes in mean annual precipitation, potential evapotranspiration, and runoff during recent hydrological periods

Duration	Unit	1998–2002	2003–2008	2009–2013
Precipitation	mm/a	507	496	611
	Change in mm/a	-83.98	-36.3	-90.9
	Relative change in %	-42	-43	-30
Potential evapotranspiration	mm/a	1106	1088	1064
	Change in mm/a	-7.79	6.53	-9.51
	Relative change in %	+4	+3.5	+1
Recorded runoff	mm/a	8	9	7
	Change in mm/a	-2.90	-2.67	-0.96
	Relative change in %	-44	-37	-55

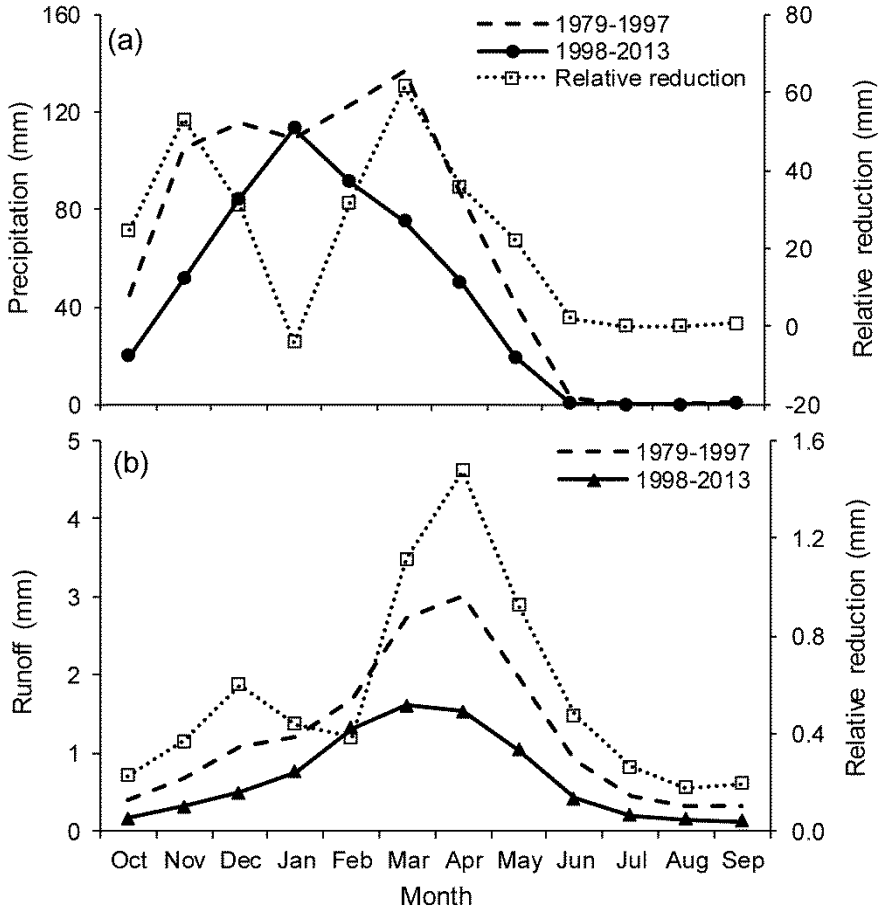

Figure 4.7 Average monthly (a) precipitation; and (b) runoff for the baseline (1979–1997) and the altered periods between 1998 and 2013

4.3 Basin Average Precipitation Computation

To accomplish a precise estimation of the spatial distribution of rainfall over the LZRB, Thiessen network has been implemented. This technique assigns weights at each gauging station in proportion to the basin area, which is closest to that station. In this research, a Thiessen network was created to estimate the area of each station polygon (ai, km^2), Table 4.4. Rainfall values for each gauging station were multiplied by the area of each polygon (ai, km^2). Meteorological stations are distributed both inside and outside basin polygons, Figure 4.8. The figure displays how the whole basin area divided into ten sub-areas each of which belongs to a specific meteorological station.

Table 4.4 Station addresses with corresponding average precipitations and the sub area sizes

Sub-basin	Station ID	Sub-area (a_i) (km^2)	Av[a] P[b] (mm)	Av[a] PET[c] (mm)
US[d]	Sulymaniya	4479.57	772	1989
	Halabcha	735.60	585	980
	Sachez	1182.79	462	1550
	Mohabad	2593.31	886	920
	Salahddin	1641.07	652	2058
	Soran	1463.30	813	1433
DS[e]	Kirkuk	1693.76	342	897
	Makhmoor	3008.41	361	934
	Erbeel	979.76	575	935
	Chemchamal	2827.46	738	2075

[a]Average; [b]Precipitation; [c]Potential evapotranspiration; [d]Upstream; and [e]Downstream

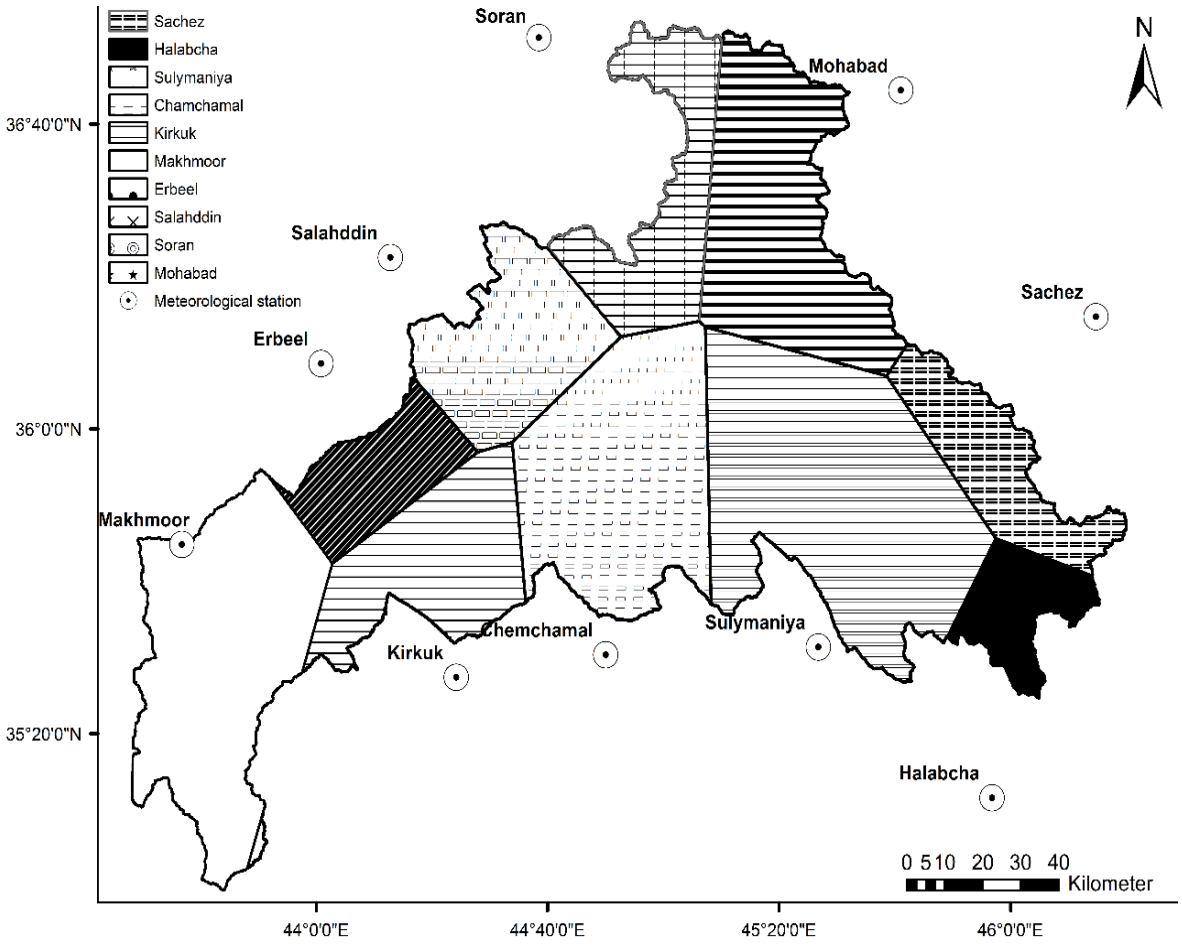

Figure 4.8 The sub-basins areas based on the application of Thiessen network analysis to compute the basin average precipitation

4.4 Drought Analysis

4.4.1 Drought Identification

The study applied three of the widely used meteorological drought indices that are the standardised precipitation index (SPI), the standardised reconnaissance drought index RDI_{st}, and the standardised precipitation evapotranspiration index (SPEI). Table 4.5 summarises the M-K analysis results and person correlation coefficient (r) for the annual values of SPI, RDI_{st}, and SPEI. Substantial tendencies for the drought indices were witnessed at 1% significance level. Additionally, Table 4.5 results illustrate a comparison between the indices, which shows that the three indicators were adjacent to each other, but the correlation between RDI_{st} and SPI was the best, and RDI_{st} and SPEI correlation was better than between SPEI and SPI. Accordingly, RDI_{st} is considered in this study for meteorological drought detection and can be selected for further drought analysis within the region.

Table 4.5 The distribution-free analysis for the three of the widely used meteorological drought indices in addition to the person correlation coefficient r, over the studied basin

Sub-basin	Station name	SPI[c]		RDI_{st}[d]		SPEI[e]		Person (r) correlation		
		M-K[f]	*p*-value	M-K[f]	*p*-value	M-K[f]	*p*-value	1[g]	2[h]	3[i]
US[a]	Sulymanya	-405**	<0.01	-267*	<0.05	-203	0.086	0.89	0.96	0.75
	Halabcha	-503**	<0.01	-524**	<0.01	-341**	<0.01	0.82	0.99	0.82
	Sachez	-333**	<0.01	-308**	<0.01	-284*	0.016	0.85	0.99	0.84
	Mahabad	-571**	<0.01	-513**	<0.01	-523**	<0.01	0.94	0.97	0.93
	Salahddin	-182	0.125	-194	0.102	-281*	<0.05	0.95	0.99	0.94
	Soran	-573**	<0.01	-563**	<0.01	-595**	<0.01	0.76	0.91	0.70
DS[b]	Kirkuk	-553**	<0.01	-539**	<0.01	-425**	<0.01	0.83	0.92	0.91
	Makhmoor	-539**	<0.01	-554**	<0.01	-486**	<0.01	0.90	1.00	0.90
	Erbeel	-405**	<0.01	-406**	<0.01	-395**	<0.01	0.83	0.92	0.91
	Chemchamal	-405**	<0.01	-371**	<0.01	-332**	<0.01	0.91	0.99	0.88

[a]Upstream; [b]Downstream; [c]The standardised precipitation index; [d]The standardised reconnaissance drought index; [e]The standardised precipitation evapotranspiration index; [f]Mann–Kendall distribution-free test; [g]RDI_{st} vs SPEI correlation; [h]RDI_{st} vs SPI correlation; and [i]SPEI vs SPI correlation.
Note: Negative (-) and positive values indicate the decreasing and increasing trends, respectively;
**Correlation is significant at the 0.01 level (2-tailed); and
*Correlation is significant at the 0.05 level (2-tailed). Note: Values of M-K are multiplied by 10^{-3}

To demonstrate the relationships between meteorological and hydrological drought, the calculations for the annual reference period for SPI, RDI_{st}, and SPEI have been performed (Figure 4.9). These data were correlated with the SDI annual values. Figure 4.9 reveals linear relationships between the two types of drought indices over the time-period from 1979/1980 to 2013/2014. It can be concluded that the equations show better fits between SDI and RDI_{st} than

between SDI and SPEI as indicated by higher correlation coefficients. Despite the fact that this method involves substantial uncertainty, it is useful since the proactive processes to moderate consequences of drought are based on the classification of the predicted drought and not on the total value of SDI.

Furthermore, to assess the occurrence of drought events within the studied geographical area, SPI, RDI_{st}, and SPEI were calculated using the available precipitation data and the estimated potential evapotranspiration. Figure 4.10a and Figure 4.10b present the indices calculated for the water years between 1979 and 2014 incorporated with the long-term basin average precipitation (P_{av}) and potential evapotranspiration, respectively. A non-regular cyclical configuration of drought and rainy times was detected. Droughts on a cyclical basis were detected for five years over the considered dataset; mostly for 1998/1999, 1999/2000, 2000/2001, 2007/2008, and 2008/2009 (for example, corresponding RDI_{st} mean values were -1.68, -1.54, -1.26, -2.95 and -1.49 in this order). Similar findings were also reported by many earlier research studies within the region (Fadhil, 2011; UNESCO, 2014). Drought usually happens at the beginning of the rainy season, which is reflected by either a decline in precipitation coupled with potential evapotranspiration increase or a delay in precipitation events. As the RDI_{st} analysis shows, the basin drought severity has dramatically worsened over the past twelve years. In particular, during the years from 1998 to 2011, the drought severity increased as the number of months with extended periods of precipitation shortages and potential evapotranspiration growths increased. Figure 4.11 and Figure 4.12 visualise the areal extent of the worst drought and the aridity episode, respectively, that the LZRB experienced during the water year 2007/2008.

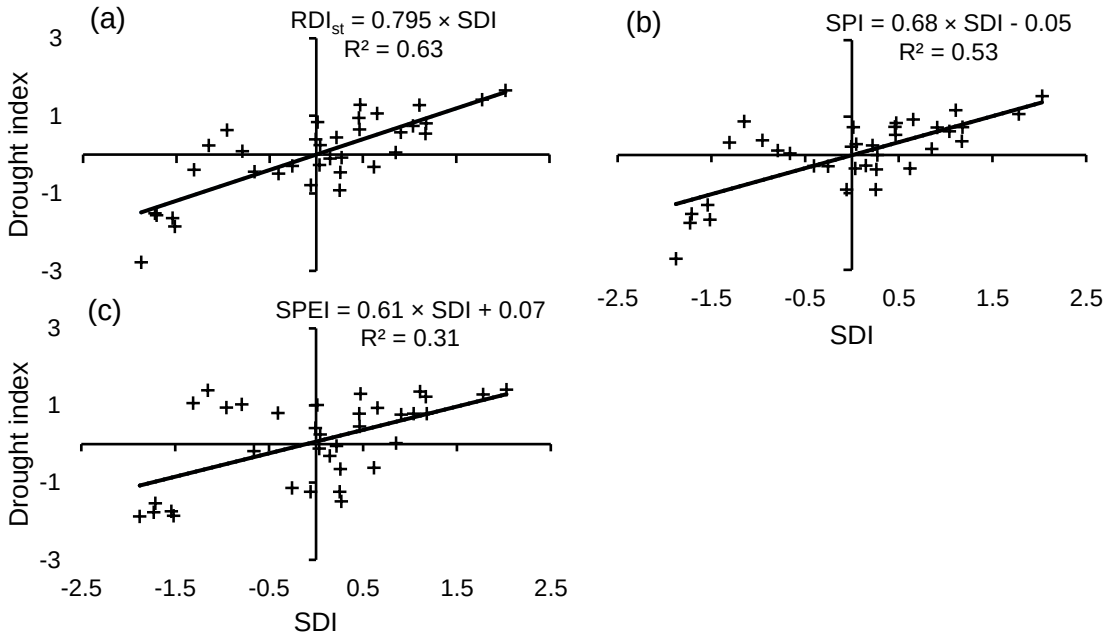

Figure 4.9 Predicted annual streamflow drought index (SDI) equations based on (a) the standardised precipitation index (SPI); (b) the standardised reconnaissance drought index (RDI_{st}); and (c) the standardised precipitation evapotranspiration index (SPEI) for annual reference periods concerning the Lower Zab River Basin

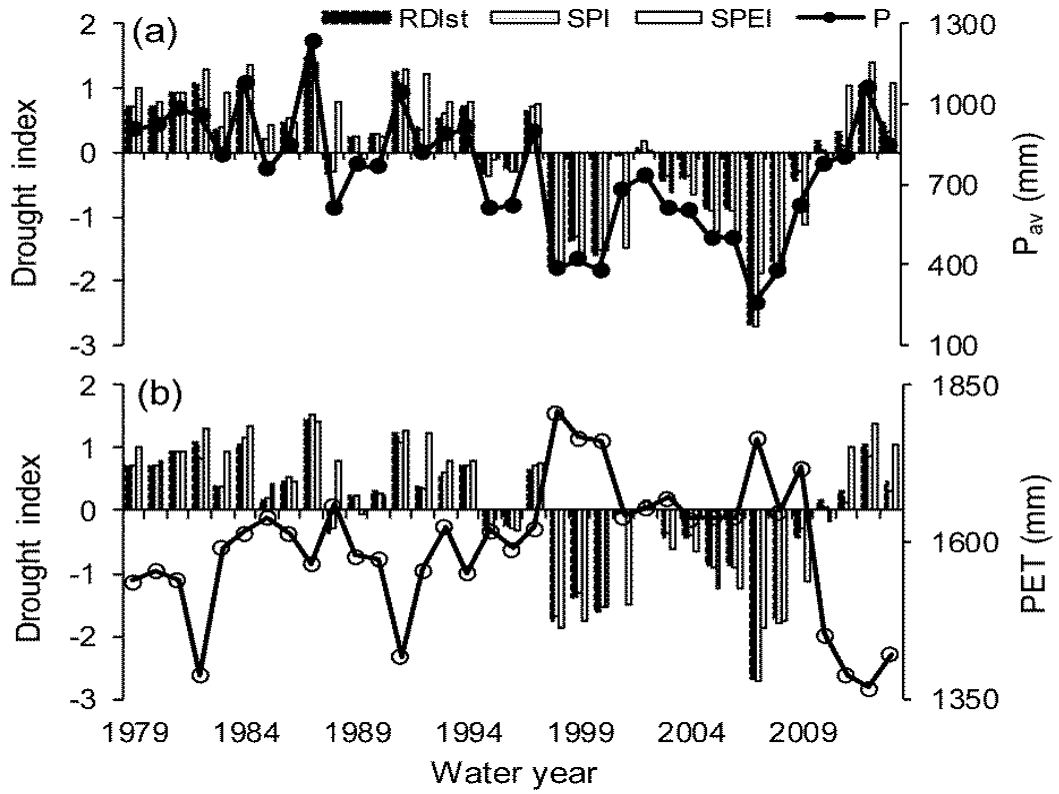

Figure 4.10 Temporal variations of the standardised reconnaissance drought index (RDI_{st}), standardised precipitation index (SPI), and standardised precipitation evapotranspiration index (SPEI) coupled with the long-term average; (a) precipitation (P_{av}) for the Lower Zab River Basin (LZRB) for the period from 1979 to 2014; and (b) potential evapotranspiration (PET) for the LZRB for the period from 1979 to 2014

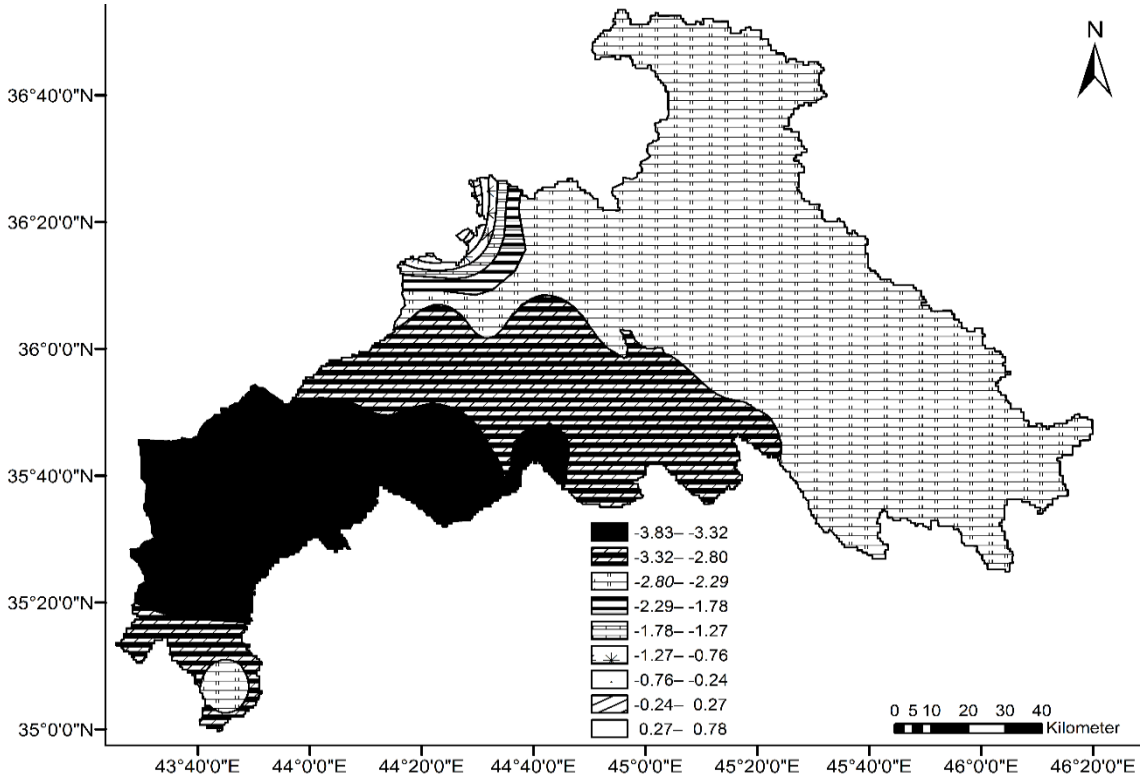

Figure 4.11 The spatial distribution of the worst drought that occurred over the Lower Zab River Basin during the water year 2007/2008

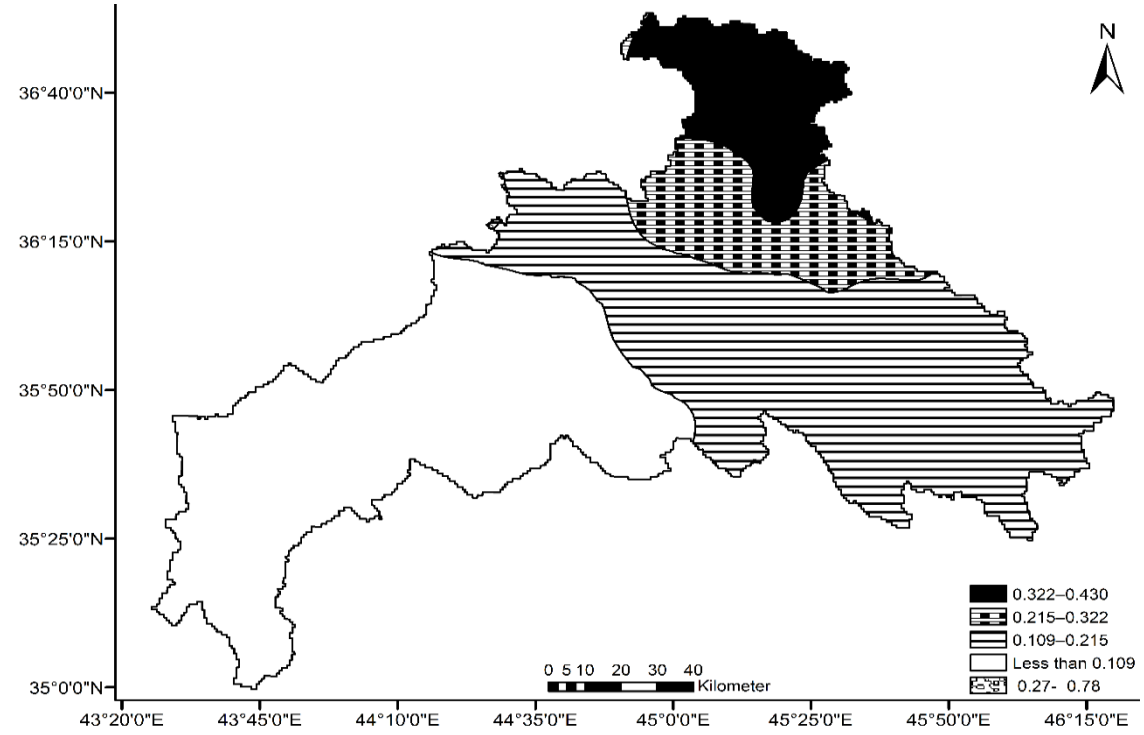

Figure 4.12 The spatial distribution of the long-term aridity over Lower Zab River Basin during the water year 2007/2008

4.4.2 Reconnaissance Drought Index Sensitivity Analysis

The focus of this part of the research is in the sensitivity analysis of the spatiotemporal variability of RDI to the prospective impact of potential evapotranspiration methods, meteorological station elevation variations, and climate conditions. The motivation to study RDI index is the fact that, the index is depended on the combination of precipitation and potential evapotranspiration, which is considered more realistic than using precipitation only. In addition, RDI is a newly developed drought index and is used in several areas throughout the world, particularly in semi-arid and arid regions, and became the acquisitions base as a result of its low data requirements, high sensitivity, resilience, and suitability for climate instability (Rossi and Cancelliere, 2013; Vicente-Serrano et al., 2015; Zarch et al., 2015). RDI provides physically thorough theoretical grounds for evaluation of the meteorological drought severity and aridity assessment. Therefore, it is important to evaluate potential evapotranspiration estimation impact, meteorological station elevation variations, and climate conditions on the aridity and drought severity characterization estimated by this index.

Accordingly, the main purpose of this part of the research is to investigate the results of the three basic components of the RDI index, in particular, its $RDI_{\alpha 12}$ form. The investigation included, firstly analyses the sensitivity of RDI and highlight the use of such index as an aridity and a climatic index. Then, compare the results of the HG, ThW, and BC potential evapotranspiration methods with the results of PM methodology for reference purposes. In addition to assessing the impact of meteorological station elevation variations for different climate conditions on the results of this particular index.

To address these objectives, meteorological data from twenty-four stations throughout the world describing semi-arid (MD, TR, and CN), Sahara, and humid climatic conditions, representing both mountainous regions and lowlands, have been selected, Figure 4.13 (http://globalweather.tamu.edu/home/). Table 4.6 shows the categories and locations of the chosen gridded meteorological stations. For example, the gridded station labelled “HL”, is situated in the East of Al-Sudan (22° 0′ 36″N, 36° 15′ 0″E), representing a mountainous area with an elevation of 1677 m, while the station that is labelled “LL”, is situated in the UK (52° 55′ 12″ N, 3° 45′ 0″ W), representing low elevation of 40 m. The average yearly precipitation and temperature for the first location are 1118 mm and 24.7 °C, respectively. The corresponding means for the second station are 155 mm and 9.1 °C, respectively. Reliable monthly data of

minimum and maximum temperature, precipitation, relative humidity, and wind speed were sourced.

Initially, the data were examined for their validity. Minor emendations and filling of some minor gaps in the datasets were implemented depending on customary statistical practices. Then, 35-year datasets for these stations were produced. After that, potential evapotranspiration was estimated by the considered methods, Figure 4.14. The next step involved the calculation of annual values of $RDI_{\alpha 12}$, RDI_{st}, and RDI_{n} depending on potential evapotranspiration values estimated by various methods with the aid of the software tool called drought indices calculator (DrinC) as reported by Tigkas et al. (2015).

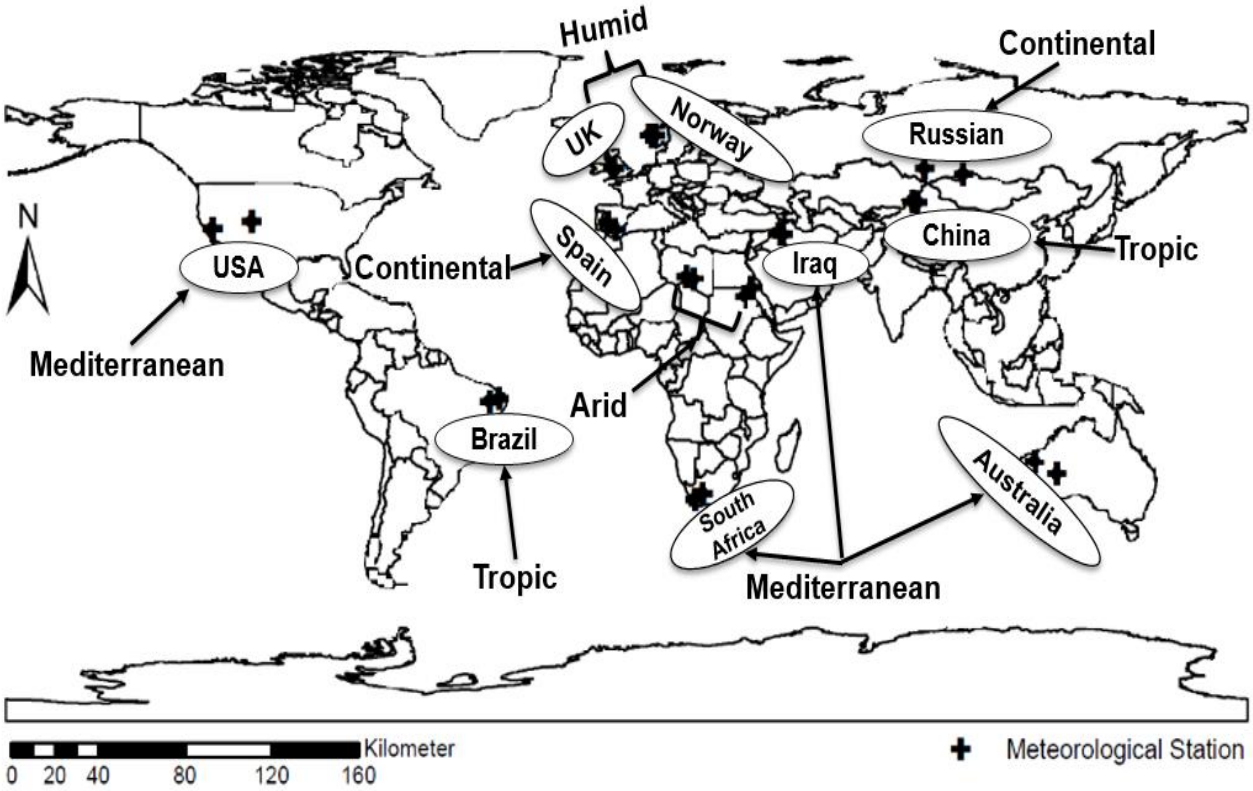

Figure 4.13 The locations of the selected gridded meteorological stations based on the Climate Forecasting System reanalysis dataset (CFSR, 2015) (http://globalweather.tamu.edu/home/)

Table 4.6 Statistical performance indicators of the annual reconnaissance drought index (RDI_n) for the normalised values estimated by various potential evapotranspiration methods against the reference method, for different locations all over the world

Wider region	St[a] ID	Lat[b] (°)	Long[c] (°)	El[d] (m)	RMSE[e]			MBE[f]		
					1[g]	2[h]	3[i]	1[g]	2[h]	3[i]
Mediterranean										
South Africa	LL[j]	-32.63	19.69	485	42	54	50	2	3	2
	HL[k]	-31.07	22.19	1382	33	33	36	1	1	1
North Iraq	LL[j]	35.75	44.06	306	18	57	29	0	3	1
	HL[k]	35.75	45.25	1458	36	37	52	1	1	3
West Australia	LL[j]	-26.07	124.68	485	51	90	48	3	8	2
	HL[k]	-22.95	118.43	820	54	91	54	3	8	3
South USA	LL[j]	37.31	-120.00	361	57	47	51	3	2	3
	HL[k]	39.18	-108.75	1382	50	43	54	3	2	3
Tropical										
East China	LL[j]	44.49	82.81	409	71	82	84	5	7	7
	HL[k]	44.18	84.38	1316	109	112	110	12	13	12
East Brazil	LL[j]	-6.71	-36.88	440	49	79	53	2	6	3
	HL[k]	-7.34	-39.69	918	36	42	61	1	2	4
Continental										
South Russia	LL[j]	38.87	-5.31	403	102	57	62	10	3	4
	HL[k]	36.99	-3.13	1360	369	108	107	136	12	11
South East Spain	LL[j]	52.92	86.25	438	35	40	43	1	2	2
	HL[k]	51.36	97.50	1208	68	58	57	5	3	3
Arid										
Sahara	LL[j]	24.82	17.19	146	26	74	21	1	6	0
	HL[k]	24.20	19.38	604	25	59	21	1	4	0
Al-Sudan	LL[j]	19.83	34.34	390	48	150	26	2	23	1
	HL[k]	22.01	36.25	1677	42	55	27	2	3	1
Humid										
UK	LL[j]	52.92	-3.75	40	25	59	21	1	4	0
	HL[k]	52.92	-4.06	717	26	74	21	1	6	0
Norway	LL[j]	6.56	61.35	490	50	86	82	2	7	7
	HL[k]	8.13	61.35	1652	53	115	112	3	13	13

[a]Station; [b]Latitude; [c]Longtude; [d]Elevation; [e]Root Mean Square Error; [f]Mean Bias Error; [g]Hargreaves Method; [h]Thornthwaite Method; [i]Blaney-Criddle method; [j]Low Land; [k]High Land. Note: Values of RMSE and MBE are multiplied by 10^{-3}

4.4.2.1 Impacts of Potential Evapotranspiration Methods

The selection of the best potential evapotranspiration estimate for a specific climate and elevation is important. This is required since the application of different approaches may result in flaws in estimations of water resources availability. Therefore, this part of the research emphasis on the analysis of the potential evapotranspiration estimate and its impact on the aridity and drought evaluations. It is critical to note that for all climatic conditions, ThW produced lower values, except for humid climate as HG is linked to lower potential evapotranspiration values, whereas PM had the highest ones Figure 4.14. Differences of about 1000, 500, 750, 1000, and 1250 mm in terms of mean values were calculated for MD, TR, CN,

Sahara, and humid climates, respectively. The HG and PM formulas follow the same annual pattern with rather alike variations around their average numbers in the same periods. However, a diverse variation pattern is followed by ThW. This result confirms findings by Vangelis et al. (2013).

The difference among all locations is that the amounts estimated by ThW are mostly lower than the values calculated by the other two methods for MD, TR, CN, and Sahara climates. Moreover, it can be observed that ThW strongly underestimates potential evapotranspiration under dry and arid conditions and at elevated elevations, since the equation does not take into account the air saturation deficit, it is mainly calibrated for temperate climates at low elevations. Whereas BC estimates rather accurately with no large under- or over-estimates the majority of the time series, the obtained results using BC are close to the numbers produced by HG, particularly for MD, TR, and CN regions. Moreover, for the humid regions, the BC methodology was linked to the best findings (similar to the full equation of PM). Accordingly, HG could be considered as the main method to estimate potential evapotranspiration for almost all the selected regions due to its suitability for climate change studies. The superiority of HG is supported by several research studies in the field (Vangelis et al., 2013; Tigkas et al., 2015).

Then, and to investigate the potential impacts of the potential evapotranspiration methods on the drought severity assessment, Table 4.7 and Table 4.8 show RDI_n and RDI_{st} values, which could be considered approximately the same regardless of elevation and potential evapotranspiration estimation used for most of MD, TR, and Sahara climates. Slight variations, which appear for few years are not significant because they do not influence drought severity as indicated by the RDI index. The different numbers, despite their variations, are in the same drought severity category without surpassing a drought severity threshold. No significant differences ($p > 0.05$) were noted for RDI_n and RDI_{st} values produced by the numerous potential evapotranspiration methodologies for most of MD, TR, and Sahara areas. However, this could not the case for smaller periods, such as 3, 6, and 9 months, therefore, it is suggested to use such periods for further research in this index. Furthermore, RDI_{st} and RDI_n values for many other geographical regions, such as South Russia, UK, and East Brazil are significantly ($p < 0.05$) different for various elevations using the three potential evapotranspiration methods compared to PM (Table 4.7 and Table 4.8). The differences are considered important since they affect drought severity reported by RDI_{st}, and different values give completely different drought

severity categories for almost all periods. This would become even clearer for shorter periods, such as 3, 6, and 9 months, which is why it is highly recommended to use such periods for future research.

Regional aridity evaluations can alter due to many factors, such as the specific potential evapotranspiration method used and weather station elevations. Table 4.8 reveals that no significant aridity variations were found with respect to different potential evapotranspiration estimates for different elevations in the West Australia, East Brazil, Sahara, and Al-Sudan geographical regions.

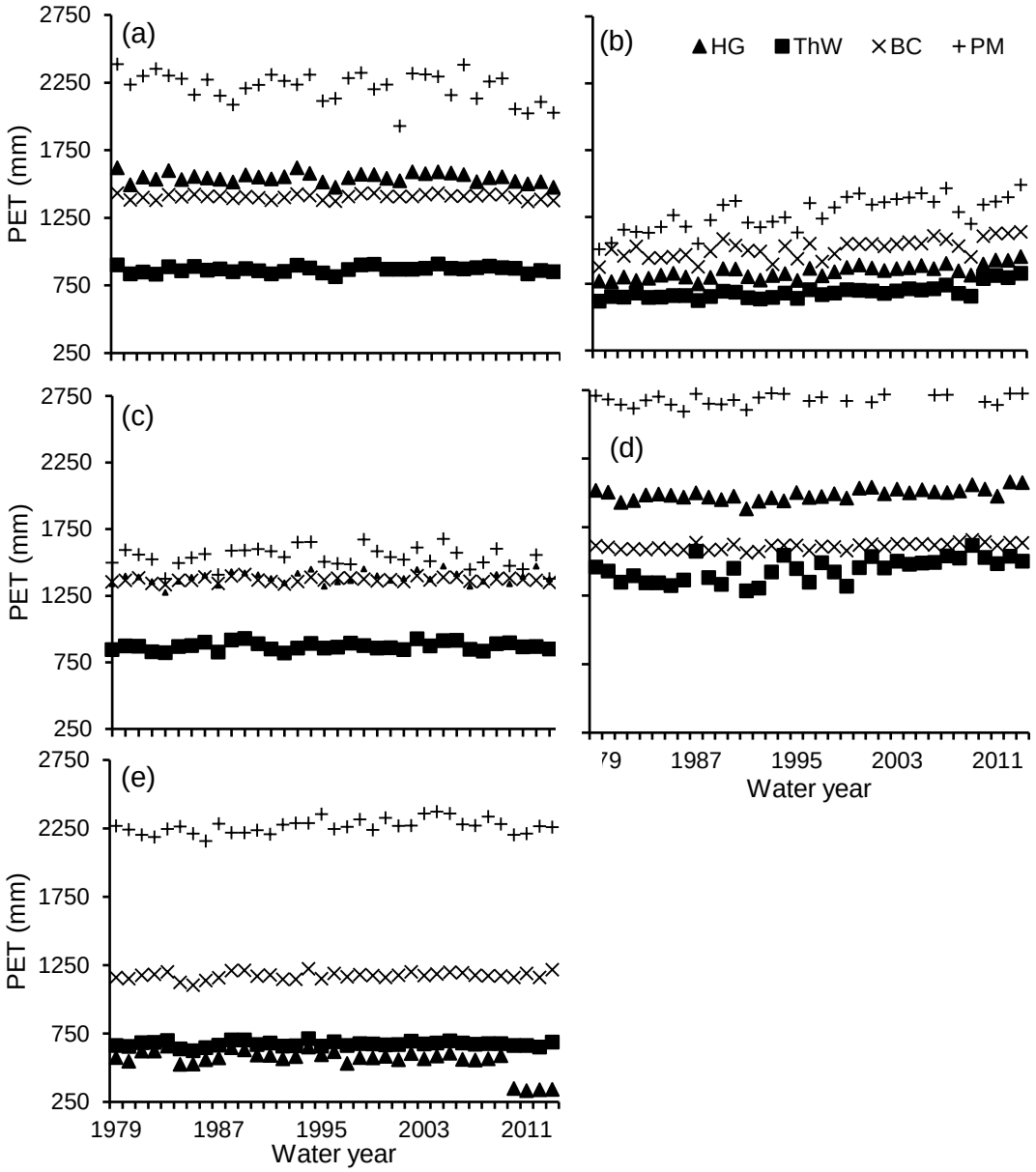

Figure 4.14 Potential evapotranspiration (PET) estimated by Hargreaves (HG), Thornthwaite (ThW) and Blaney-Criddle (BC) methods with the results of FAO Penman-Monteith (PM) methodology for reference for different climatic conditions: (a) Mediterranean, (b) tropical, (c) continental, (d) Sahara, and (e) humid

Table 4.7 Statistical performance indicators of the annual reconnaissance drought index for the standardised values (RDI_{st}) estimated by various potential evapotranspiration methods against the reference method for different locations throughout the world

Wider region	Station ID	El[a] (m)	RMSE[b]			MBE[c]		
			1[d]	2[e]	3[f]	1[d]	2[e]	3[f]
Mediterranean								
South Africa	LL[g]	485	2	3	3	21	34	26
	HL[h]	1382	66	70	69	4	5	5
North Iraq	LL[g]	306	34	92	40	1	8	2
	HL[h]	1458	111	75	126	12	6	16
West Australia	LL[g]	485	78	140	78	6	20	6
	HL[h]	820	91	174	83	8	32	7
South USA	LL[g]	361	99	89	49	10	8	2
	HL[h]	1382	142	108	159	20	12	25
Tropical								
East China	LL[g]	409	62	102	91	4	10	8
	HL[h]	1316	240	162	164	58	26	27
East Brazil	LL[g]	440	213	302	214	41	91	45
	HL[h]	918	6	83	68	3	7	5
Continental								
South East Spain	LL[g]	438	70	60	63	5	4	39
	HL[h]	1208	154	97	93	24	9	9
South Russia	LL[g]	403	543	199	247	295	40	61
	HL[h]	1360	417	122	124	174	15	15
Arid								
Sahara	LL[g]	146	23	49	31	1	2	1
	HL[h]	604	12	30	10	0	1	0
Al-Sudan	LL[g]	390	23	40	18	1	2	0
	HL[h]	1677	70	67	38	5	4	1
Humid								
UK	LL[g]	40	1320	533	504	1742	284	254
	HL[h]	717	698	433	447	488	188	200
Norway	LL[g]	490	180	307	298	32	94	89
	HL[h]	1652	232	596	607	54	355	368

[a]Elevation; [b]Root Mean Square Error; [c]Mean Bias Error; [d]Hargreaves Method; [e]Thornthwaite Method; [f]Blaney-Criddle method; [g]Low Land; and [h]High Land.
Note: Values of RMSE and MBE are multiplied by 10^{-3}

Table 4.8 Statistical performance indicators of the annual reconnaissance drought index for the initial values α_k at k=12 months ($RDI_{\alpha 12}$) estimated by various potential evapotranspiration methods against the reference method for different locations throughout the world

Wider region	St[a] ID	El[b]	RMSE[c]			MBE[d]			ANOVA[e]		
			1[f]	2[g]	3[h]	1[f]	2[g]	3[h]	1[f]	2[g]	3[h]
Mediterranean											
South Africa	LL[i]	485	52	187	69	50	35	5	*	*	*
	HL[j]	1382	31	115	41	29	13	2	*	*	*
North Iraq	LL[i]	306	40	79	56	37	6	3	61	*	*
	HL[j]	1458	63	599	208	58	359	43	125	*	*
West Australia	LL[i]	485	25	49	23	-23	2	1	213	69	270
	HL[j]	820	89	31	77	-78	1	6	*	581	*
South USA	LL[i]	361	79	299	86	71	89	7	72	*	*
	HL[j]	1382	29	293	74	24	86	5	227	*	*
Tropical											
East China	LL[i]	409	111	186	52	102	35	3	*	*	144
	HL[j]	1316	385	900	167	369	811	28	*	*	622
East Brazil	LL[i]	440	166	247	229	159	61	53	*	*	*
	HL[j]	918	87	341	130	84	116	17	91	*	*
Continental											
South Russia	LL[i]	403	137	245	271	-50	60	73	404	*	*
	HL[j]	1360	2273	632	190	1583	399	36	*	*	944
South East Spain	LL[i]	438	24	171	25	23	29	6	270	*	230
	HL[j]	1208	183	502	47	172	251	2	*	*	280
Arid											
Sahara	LL[i]	146	16	4	3	1	0	0	280	*	81
	HL[j]	604	2	5	3	1	0	0	150	*	*
Al-Sudan	LL[i]	390	5	3	9	2	0	0	180	*	61
	HL[j]	1677	2	8	7	2	0	0	140	*	*
Humid											
UK	LL[i]	40	209	403	1437	-124	162	2064	268	*	*
	HL[j]	717	478	549	1703	-458	302	2901	*	*	*
Norway	LL[i]	490	644	1326	2891	-515	1758	8355	141	*	*
	HL[j]	1652	279	395	893	231	156	797	106	388	*

[a]Station; [b]Elevation; [c]Root Mean Square Error; [d]Mean Bias Error; [e]One-way analysis of variance (ANOVA) at 0.05 significant level; [f]Hargreaves Method; [g]Thornthwaite Method; [h]Blaney-Criddle method; [i]Low Land; [j]High Land.

Note: Values of RMSE, MBE, and ANOVA are multiplied by 10^{-3}; *< 0.05

Figure 4.15a and b show the results for only West Australia, as an example. Marginal differences, which are revealed for many years, cannot be seen as important since they do not influence aridity evaluation. The different numbers, despite their fluctuations, stay constant for the two main elevations in the same aridity class without exceeding any threshold value. However, this could not be the case for smaller time-periods. This is why $RDI_{\alpha 12}$ values for shorter reference periods than the annual one are recommended. For the MD and CN climatic conditions in South Africa, South USA, and South East Spain, Figure 4.15c, d as well as Table 4.8 present results for South Africa, as an example, confirming that there is a considerable variation in the $RDI_{\alpha 12}$ values for different elevations using different potential

evapotranspiration estimates, which in turn affect significantly regional aridity assessments. Despite the fact that values of $RDI_{\alpha 12}$ produced by the HG and BC methods are not similar to the results of the reference method, they are rather identical and the most significant ($p < 0.05$) deviations are shown by the ThW method. Moreover, no significant ($p > 0.05$) differences were detected in the $RDI_{\alpha 12}$ values estimated by the potential evapotranspiration methods (particularly, the HG method) at low elevations in North Iraq (Figure 4.15e, f), East China, and South Russia. Whereas at mountainous locations, significant ($p < 0.05$) $RDI_{\alpha 12}$ values were noted using different potential evapotranspiration estimates as shown in Table 4.8. Regarding $RDI_{\alpha 12}$ for humid climatic conditions, such as the UK, Figure 4.15g, h as well as Table 4.8 show that at both elevations the selected methods are underestimating potential evapotranspiration (particularly, the BC method) so that using such methods can lead to completely different aridity categories for mountainous locations.

Furthermore, Figure 4.16a shows the $RDI_{\alpha 12}$ values for different climatic conditions. Note that $RDI_{\alpha 12}$ is significantly ($p < 0.05$) higher for humid areas regarding the whole time series and linked to higher fluctuations compared to other climatic conditions. Furthermore, $RDI_{\alpha 12}$ is higher for the mountainous locations, for the complete time series, and related to higher variability compared with lowland locations (Figure 4.16b). Eventually, and for explanation purposes, Figure 4.16c and Figure 4.16d represent how RDI_{st} and RDI_{n} values at a specific region and climate condition can be changed with considerable fluctuations corresponding to different elevations.

Apart from the above, the author suggests using any of the examined potential evapotranspiration methods for RDI_{st} and RDI_{n} estimations with the aim to circumvent the ThW equation, particularly for mountainous locations. Furthermore, the HG method provides the most accurate results. Since RDI utilises the critical part of potential evapotranspiration but retaining the need for data to a minimum, the HG and BC methods are the most appropriate choices for computing potential evapotranspiration for RDI in many regions (particularly in semi-arid and arid). However, in the case of the long-term reliable datasets availability of several weather parameters, researchers should use PM estimates.

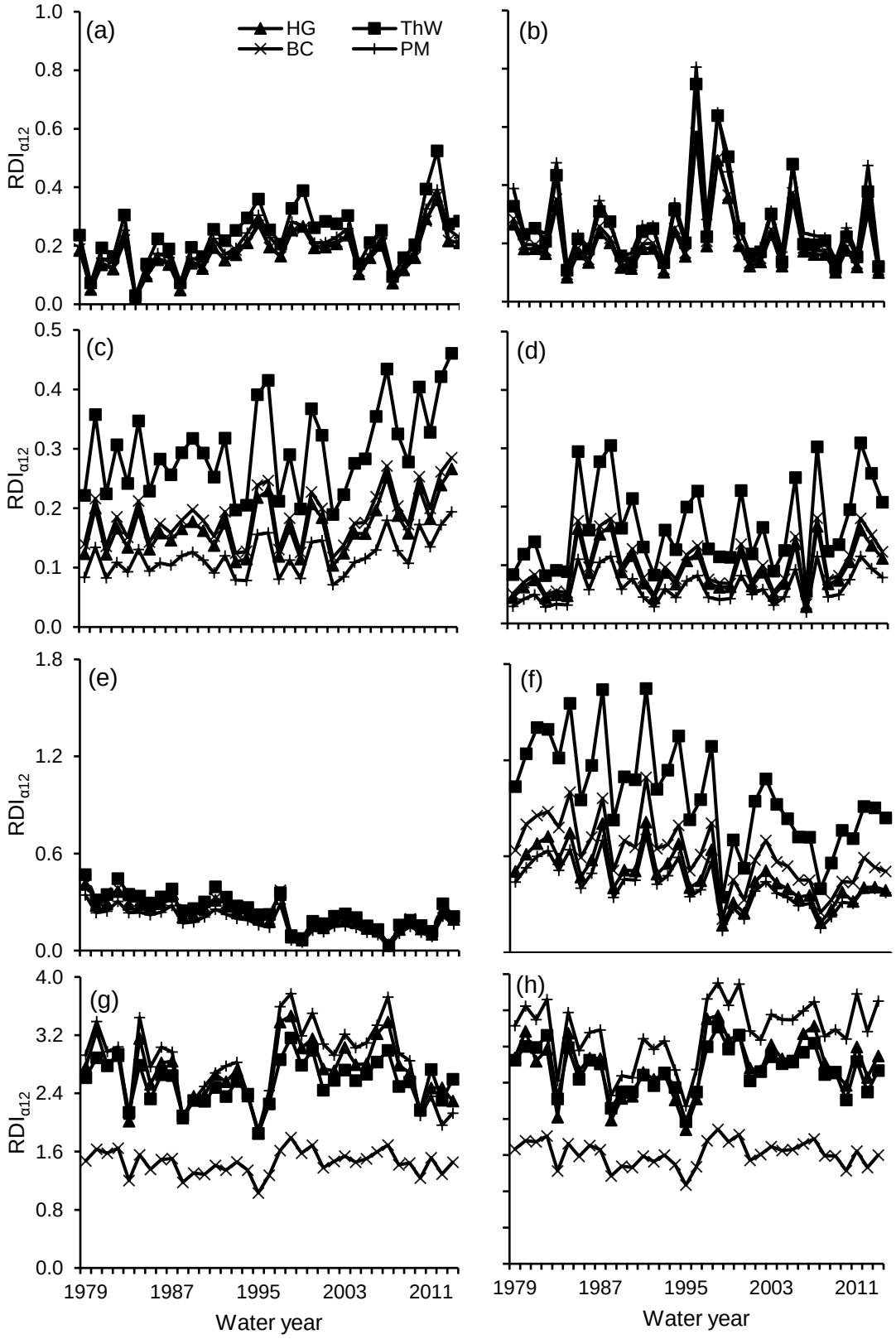

Figure 4.15 The alpha reconnaissance drought index ($RDI_{\alpha 12}$) values estimated by Hargreaves (HG), Thornthwaite (ThW), and Blaney-Criddle (BC) potential evapotranspiration methods with the results of FAO Penman-Monteith (PM) methodology for reference for two different elevations each in (a) and (b) West Australia, (c) and (d) South Africa, (e) and (f) North Iraq, and (g) and (h) UK

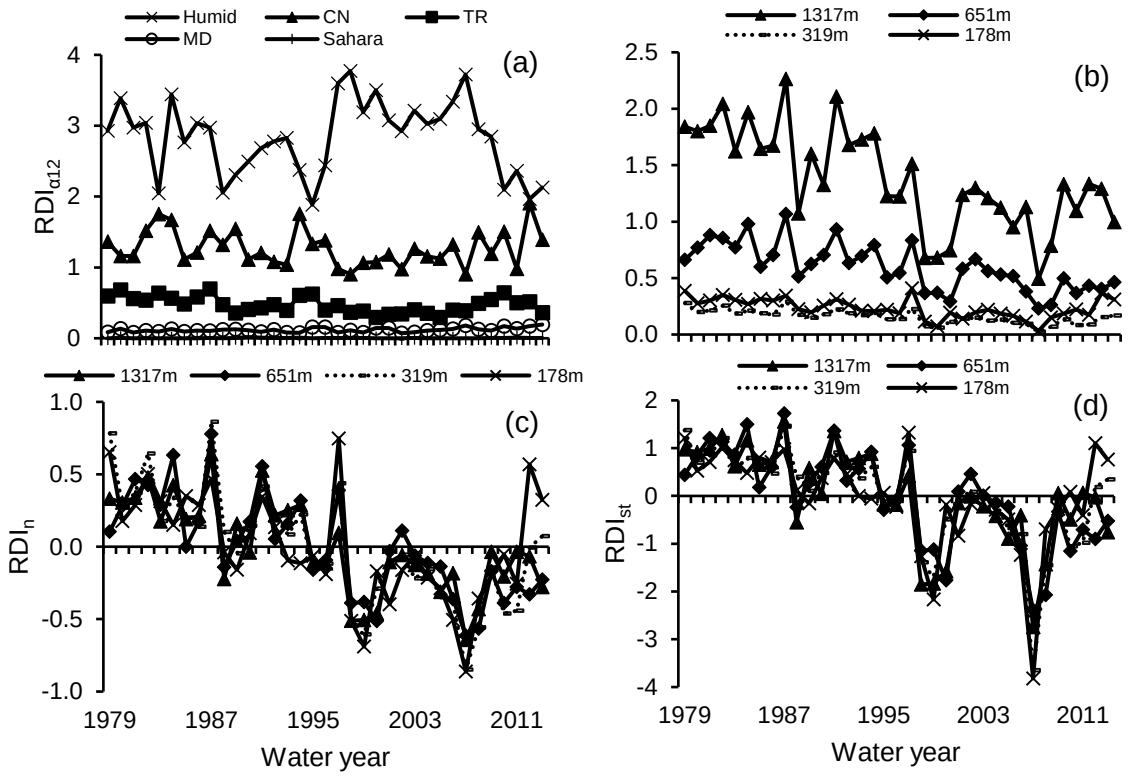

Figure 4.16 (a) The annual reconnaissance drought index alpha form ($RDI_{\alpha 12}$) form values for Mediterranean (MD), tropical (TR), conventional (CN), Sahara, and humid climatic conditions; (b) different elevations;(c) The normalised annual reconnaissance drought index (RDI_n) values for different elevations; and (d) The standardised annual reconnaissance drought (RDI_{st}) index values for different elevations

4.4.2.2 Reconnaissance Drought Index as a Climatic Index

Currently, there have been recommendations that variations in the regularity of extreme events may accompany climate variability. General circulation models forecast a noticeable alteration in precipitation (IPCC, 2001, 2007), supported by measurements of precipitation trends, showing reduced winter precipitation and improved variability (IPCC, 2001). There is an indication that climate variabilities are now represented by meteorological and hydrologic droughts. In contrast to various drought studies of streamflow, bounded drought research depends on meteorological drought indices with minimum data requirements concerning land use, hydrology, meteorology, agro-hydrology, and water management (Blenkinsop and Fowler, 2007; Loukas et al., 2008). Accordingly, this part of the research will investigate whether the increasing trend of droughts and regional aridity (IPCC, 2001), as explained above, is likely to remain in the future, investigating aridity and severity of droughts as the prime indicators. The author trying to understand the past and present severity of aridity and associated drought

conditions by rebuilding climatic records of climate change to estimate future aridity and drought severity using simple regression equations. This should help to understand whether aridity and droughts increase or decrease in severity in the future.

Therefore, to highlight the use of RDI as a climate index, in particular, its initial and normalised forms and evaluate the climate change impacts on aridity and droughts assessment on different climatic conditions; meteorological data from twenty-four stations throughout the world describing different climatic conditions have been used (Figure 4.13).

A geographical regional climate is usually quantified by utilisation of weather data. For the temporal evaluation of climate change, a climatic index may be valuable for management and operational uses. This index should be founded on the key parameters for climate change identification, which are precipitation and mean air temperature. Because of being based on precipitation and potential evapotranspiration, the alpha form of RDI is appropriate for evaluating the regional climatic conditions. Consequently, this part of the research presents examples of applying the RDI alpha form, as well as the normalized one as a climatic index. Using meteorological data from twenty-four locations representing different climatic conditions, such as arid, semi-arid (MD, TR, and CN), and humid conditions, in addition to considering the LZRB as a geographical case study region for the purpose of an accurate and more detailed assessment have been utilised.

Examples of the use of RDI as a climate index are presented in this sub-section. To highlight this function of the RDI index, Figure 4.17 shows the alpha values for five geographical regions concerning various climatic conditions representing MD, TR, CN, Sahara, and humid climate, respectively. The most important point is that the $RDI_{\alpha 12}$ values are considerably higher for the humid areas regarding the whole time series and associated with higher variability in comparison with other climatic conditions. Moreover, a more comprehensive exposure to climate change could be performed through assessing shorter reference periods compared to the annual period.

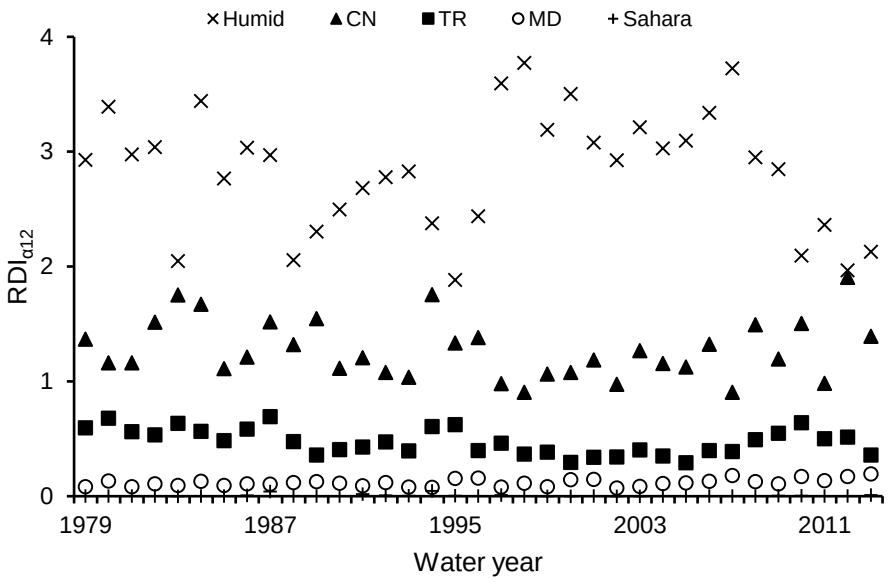

Figure 4.17 The time series of 35 water years of the alpha form of the reconnaissance drought index ($RDI_{\alpha 12}$) representing Mediterranean (MD), tropical (TR), conventional (CN), Sahara, and humid climate conditions

Figure 4.18 and Figure 4.19 present a thirty-five-year time series of $RDI_{\alpha 12}$ for winter and summer seasons at different locations for various climatic conditions. Due to a steep reduction in precipitation during summer time, the alpha values are much lower than the corresponding winter values for nearly all the considered locations and climatic conditions. The alpha form of RDI incorporates both cumulative precipitation and potential evapotranspiration. Therefore, it has been used in the above example as a climate alteration detection index.

RDI_n would be applied additionally for the identification of substantial trends, therefore, displaying signals of climatic variability. Figure 4.20 presents the annual and the 6-months periods (October to March; April to September) for the RDI_n values concerning different geographical regions and various climatic conditions.

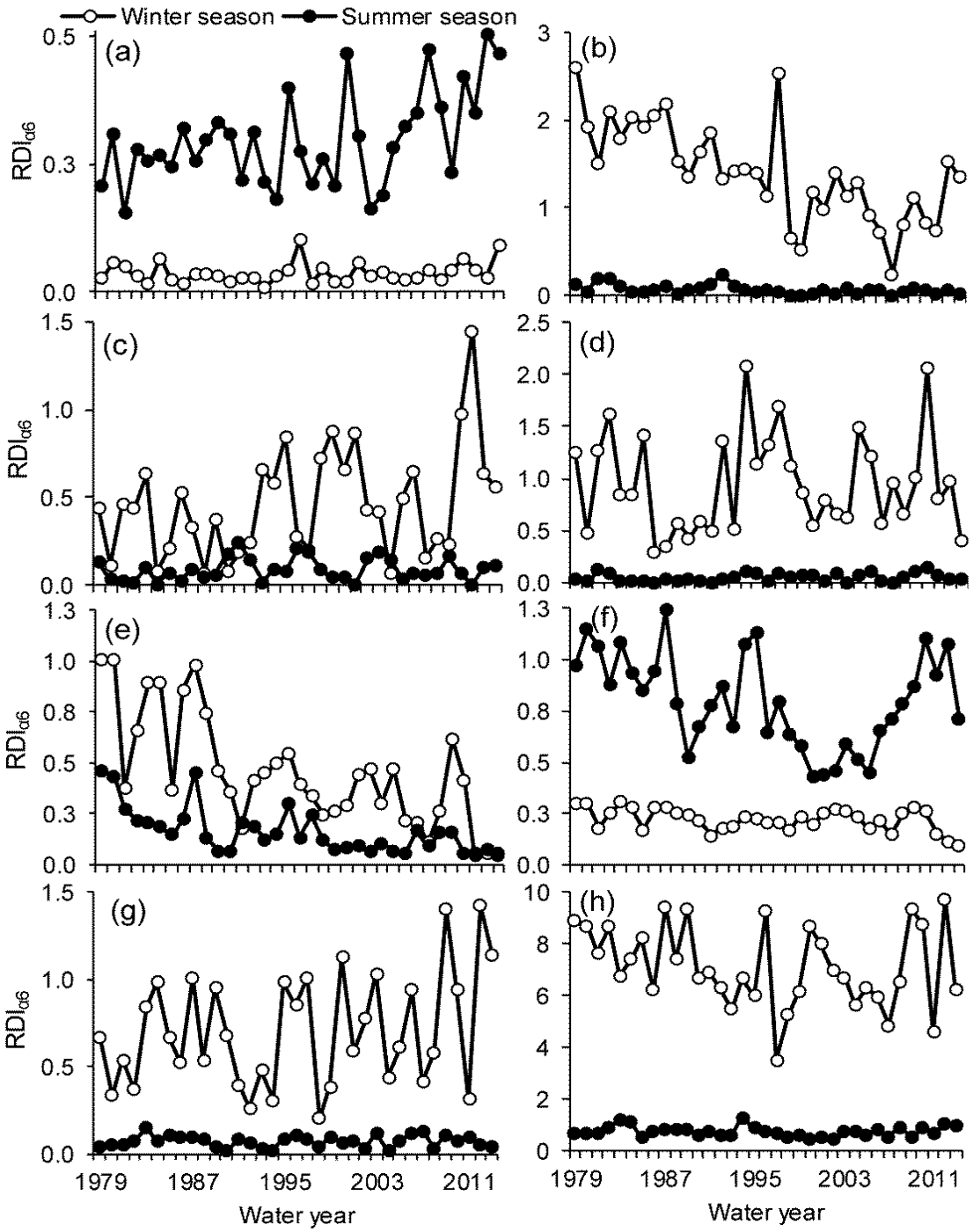

Figure 4.18 Time series for 35 water years of the alpha form of the reconnaissance drought index ($RDI_{\alpha 6}$) seasonal values for (a) South Africa; (b) North Iraq; (c) West Australia; (d) South USA; (e) East China; (f) East Brazil; (g) South-East Spain; and (h) South Russia

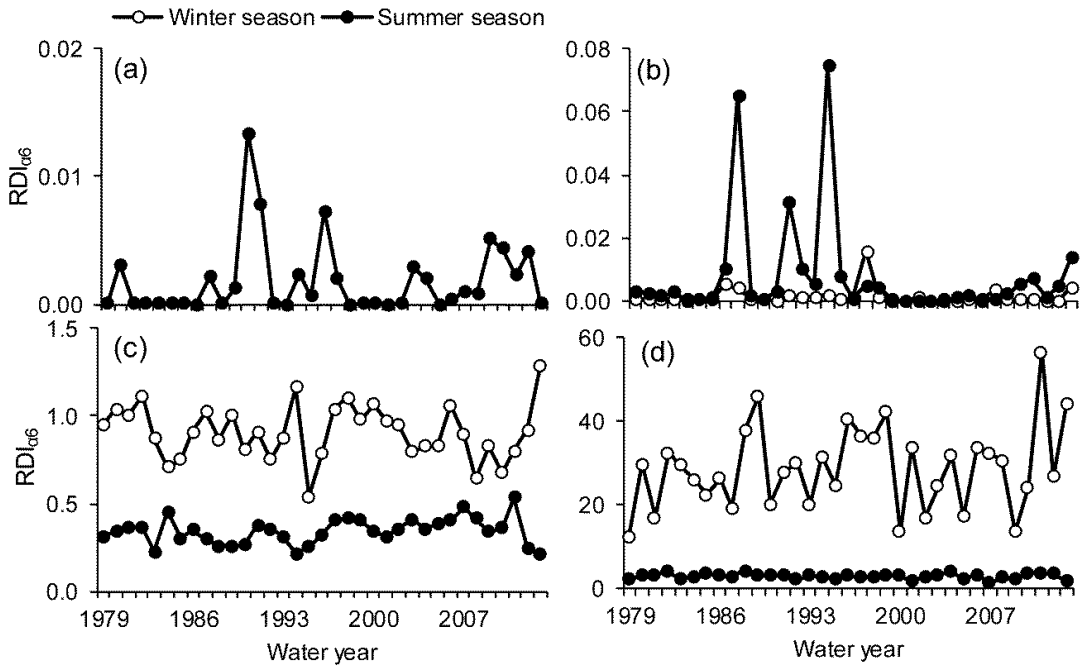

Figure 4.19 Time series of 35 water years of the alpha form of the reconnaissance drought index ($RDI_{\alpha 6}$) seasonal values, representing arid and humid climates: (a) Libya; (b) Al-Sudan; (c) the United Kingdom; and (d) Norway

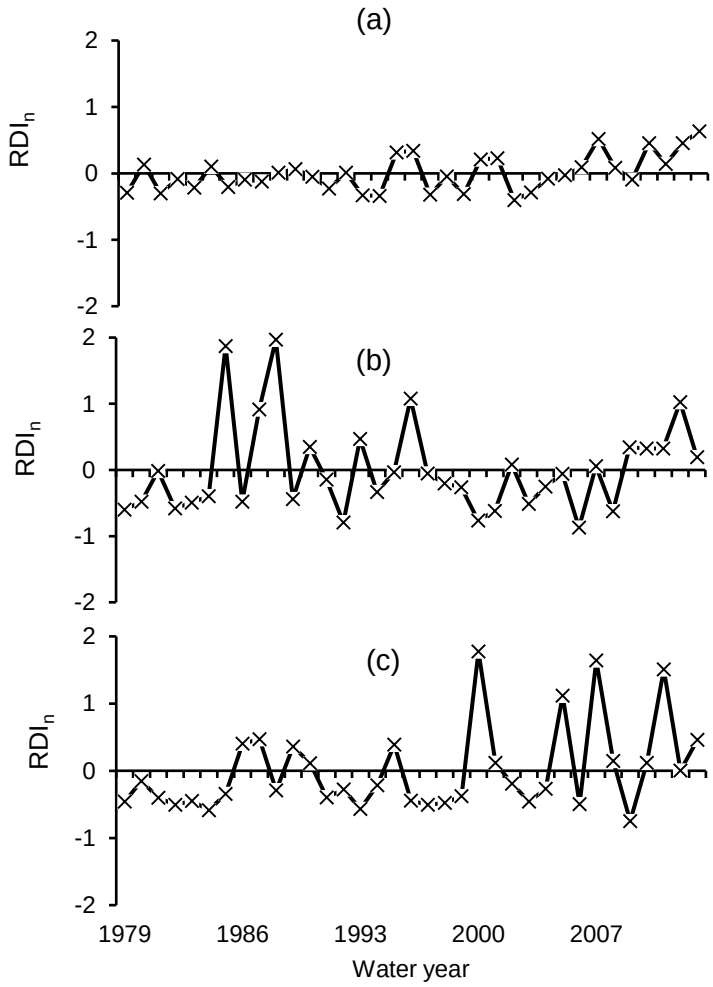

Figure 4.20 The normalized reconnaissance drought index (RDI_n) concerning a time series of 35 water years for (a) an annual reference period; (b) the winter season (October to March); and (c) the summer season (April to September)

4.4.2.3 Drought and Aridity Trends, and Future Scenarios

For the purpose of trend identification in both the $RDI_{\alpha 12}$ and RDI_{st} time series, linear regression tests have been applied. The trend analysis outcomes were used to shape drought and aridity scenarios (optimistic scenario) referring to the next three decades, assuming that these trends will continue without change (Table 4.9 and Table 4.10). The percentage of severe and extreme drought years will remain approximately the same for arid regions and decrease in humid regions, whereas semi-arid areas will transform from normal to extremely dry conditions.

The RDI_{a12} values coincided with the aridity index that is applied for climate classification. In general, the decreasing trend of precipitation and increasing trend of potential

evapotranspiration resulted in a negative aridity trend and vice versa. In most studied cases, the regional aridity trends showed the same trends as for precipitation, indicating that the aridity trends could mainly be determined by the precipitation trends and to a lesser extent by the potential evapotranspiration trends (Figure 4.21 and Figure 4.22). The humid areas showed an increasing trend in the annual RDI_{a12} index, which means that these regions became wetter, while some of the semi-arid locations showed decreasing trends in RDI_{a12}. At some stations, the increasing trends in potential evapotranspiration were accompanied with increasing trends in precipitation, which requires further research to determine the parameters that contributed to such change. A trend analysis of the most sensitive parameters of potential evapotranspiration may highlight some of the causes of increasing and decreasing trends in potential evapotranspiration.

Through highlighted semi-arid regions, in particular, those that are more vulnerable to the impact of climate change, a case study has been selected. Table 4.9 and Table 4.10 show that the Dokan, which is the upstream sub-basin, has been classified as moderately wet-normal, while it is categorised as nearly normal-moderately dry at the present time. However, it is expected to become extremely dry over the next thirty years. The downstream sub-basin has altered from moderately wet to normal over the past three decades to near normal-moderately dry at present, and it is expected to convert to moderately-extremely dry during the next thirty years. Taking into consideration the past, the present, and the future aridity variations over the LZRB, it can be noticed that the upstream sub-basin is expected to become semi-arid over the next few decades as a result of human-induced links to climate change (Table 4.10). However, the downstream sub-basin is most likely to change from semi-arid to arid and/or hyper-arid.

Table 4.9 Trend analysis representing climate change impact on drought index calcification for different climate conditions throughout the world, in addition to the Lower Zab River Basin (LZRB) as a specific semi-arid case study

Wider Region	Station ID	Time			Change /decadal
		Past	Present	Future	
Mediterranean					
South Africa	LL[c]	-0.710[5]	0.662[4]	1.838[2]	0.392
	HL[d]	-0.433[5]	0.411[4]	1.134[3]	0.241
North Iraq	LL[c]	1.130[3]	-1.080[6]	-2.020[8]	-0.063
	HL[d]	0.730[4]	-0.710[5]	-1.940[7]	-0.410
West Australia	LL[c]	-0.780[5]	0.736[4]	2.04[1]	0.433
	HL[d]	0.111[3]	-0.110[5]	-0.296[5]	-0.062
South USA	LL[c]	0.024[4]	0.070[4]	0.031[4]	-0.013
	HL[d]	-0.130[5]	0.119[4]	0.332[4]	0.071
Tropical					
East China	LL[c]	1.390[3]	-1.310[6]	-3.620[8]	-0.770
	HL[d]	0.960[4]	-0.895[5]	-2.490[8]	-0.530
East Brazil	LL[c]	0.970[4]	-0.920[5]	-2.540[8]	-0.540
	HL[d]	0.360[4]	-0.340[5]	-0.940[5]	-0.200
Continental					
South East Spain	LL[c]	-0.311[5]	0.295[4]	0.814[4]	0.173
	HL[d]	-0.224[5]	0.214[4]	0.589[4]	0.125
South Russia	LL[c]	-0.079[5]	0.075[4]	0.207[4]	0.044
	HL[d]	0.743[4]	-0.710[5]	-1.949[7]	-0.413
Arid					
Sahara	LL[c]	-0.423[5]	0.179[4]	0.695[4]	0.172
	HL[d]	-0.423[5]	0.179[4]	0.695[4]	0.172
Al-Sudan	LL[c]	-0.423[5]	0.179[4]	0.695[4]	0.172
	HL[d]	-0.423[5]	0.179[4]	0.695[4]	0.172
Humid					
UK	LL[c]	-0.985[5]	0.929[4]	2.570[1]	0.547
	HL[d]	-0.937[5]	0.883[4]	2.443[1]	0.520
Norway	LL[c]	0.319[4]	-0.304[5]	-0.838[5]	-0.178
	HL[d]	0.292[4]	-0.276[5]	-0.762[5]	-0.162
Semi-arid climate					
LZRB case study (US[a])	Sulymanya	0.660[4]	-0.640[5]	-1.750[7]	-0.370
	Halabcha	1.260[3]	-1.190[6]	-2.240[8]	-0.070
	Sachez	0.730[4]	-0.710[5]	-1.940[7]	-0.410
	Mahabad	1.210[3]	-1.130[6]	-3.150[8]	-0.670
	Salahddin	0.230[4]	-0.220[5]	-0.420[5]	-0.013
	Soran	1.000[3]	0.800[4]	0.630[5]	-0.056
LZRB case study (DS[b])	Kirkuk	1.140[3]	-1.070[6]	-2.010[8]	-0.063
	Makhmoor	1.130[3]	-1.080[6]	-2.020[8]	-0.063
	Erbeel	0.830[4]	-0.780[5]	-1.470[6]	-0.046
	Chemchamal	0.860[4]	-0.820[5]	-2.260[8]	-0.480

[a]Upstream; [b]Downstream; [c]Low Land; [d]High Land; [1]Extremely wet (≥ 2); [2]Very wet (1.99 — 1.50); [3]Moderately wet (1.49 — 1.00); [4]Normal (0.99 — 0.00); [5]Near normal (0.00 — 0.99); [6]Moderately dry (–1.00 — –1.49); [7]Severely dry (–1.50 — –1.99); and [8]Extremely dry (≤ –2)

Table 4.10 Trend analysis representing climate change impacts on the aridity calcification ($RDI_{\alpha 12}$) for different climate conditions throughout the world, in addition to the Lower Zab River Basin (LZRB) as a specific semi-arid case study

Wider Region	Station ID	Time			Change/ decade
		Past	Present	Future	
Mediterranean					
South Africa	LL[c]	0.136[2]	0.199[2]	0.253[3]	0.018
	HL[d]	0.074[2]	0.110[2]	0.137[3]	0.009
North Iraq	LL[c]	0.580[4]	0.200[3]	0.030[1]	-0.010
	HL[d]	0.380[3]	0.240[3]	0.120[3]	-0.040
West Australia	LL[c]	0.113[2]	0.229[3]	0.328[3]	0.030
	HL[d]	0.210[3]	0.203[3]	0.197[2]	-0.002
South USA	LL[c]	0.385[3]	0.354[3]	0.327[3]	-0.009
	HL[d]	0.305[3]	0.326[3]	0.344[3]	0.006
Tropical					
East China	LL[c]	0.531[4]	0.958[5]	1.324[5]	0.122
	HL[d]	2.428[5]	1.406[5]	0.530[4]	-0.292
East Brazil	LL[c]	0.781[5]	0.491[3]	0.242[3]	-0.083
	HL[d]	0.612[4]	0.521[4]	0.442[4]	-0.026
Continental					
South East Spain	LL[c]	0.212[3]	0.272[3]	0.323[3]	0.017
	HL[d]	0.570[3]	0.675[5]	0.765[5]	0.030
South Russia	LL[c]	1.206[5]	1.241[5]	1.271[5]	0.011
	HL[d]	4.933[5]	1.815[5]	-0.858[1]	-0.891
Arid					
Sahara	LL[c]	0.003[1]	0.004[1]	0.005[1]	0.000
	HL[d]	0.004[1]	0.004[2]	0.004[1]	0.000
Al-Sudan	LL[c]	0.011[1]	0.004[1]	-0.002[1]	-0.002
	HL[d]	0.022[1]	0.012[1]	0.003[1]	-0.003
Humid					
UK	LL[c]	2.202[5]	3.749[5]	5.075[5]	0.442
	HL[d]	2.230[5]	3.700[5]	4.960[5]	0.420
Norway	LL[c]	6.263[5]	5.528[5]	4.898[5]	-0.210
	HL[d]	3.660[5]	3.350[5]	3.083[5]	-0.089
Semi-arid climate					
LZRB case study (US[a])	Sulymanya	1.130[5]	0.750[5]	0.420[3]	-0.110
	Halabcha	0.860[5]	0.340[3]	0.110[3]	-0.150
	Sachez	0.380[3]	0.240[3]	0.120[3]	-0.040
	Mahabad	0.620[4]	0.240[3]	0.570[4]	-0.110
	Salahddin	0.300[3]	0.350[3]	0.380[3]	0.000
	Soran	0.800[5]	0.790[5]	0.430[3]	-0.120
LZRB case study (DS[b])	Kirkuk	0.230[3]	0.080[2]	0.020[1]	0.000
	Makhmoor	0.580[4]	0.200[3]	0.030[1]	-0.010
	Erbeel	0.320[3]	0.150[3]	0.070[2]	-0.010
	Chemchamal	0.480[3]	0.270[3]	0.090[2]	-0.060

[a]Upstream; [b]Downstream; [c]Low Land; [d]High Land;[1]Hyperarid (≤ 0.03); [2]Arid ($0.03 - 0.20$); [3]Semi-arid ($0.20 - 0.50$); [4]Dry sub-humid ($0.50 - 0.65$); and [5]Humid (≥ 0.65)

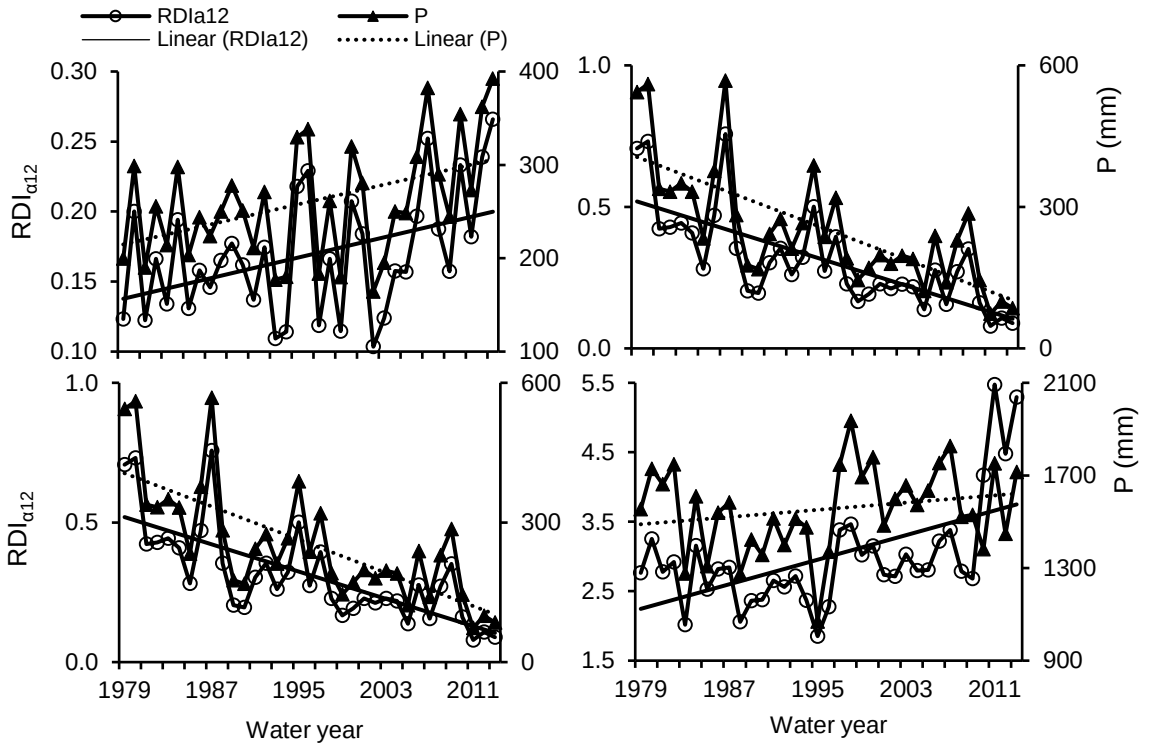

Figure 4.21 Annual values and trends of aridity index ($RDI_{\alpha 12}$) and precipitation (P) for (a) Mediterranean; and (b) tropical; (c) conventional; and (d) humid, climatic conditions for the time-period between 1979 and 2014

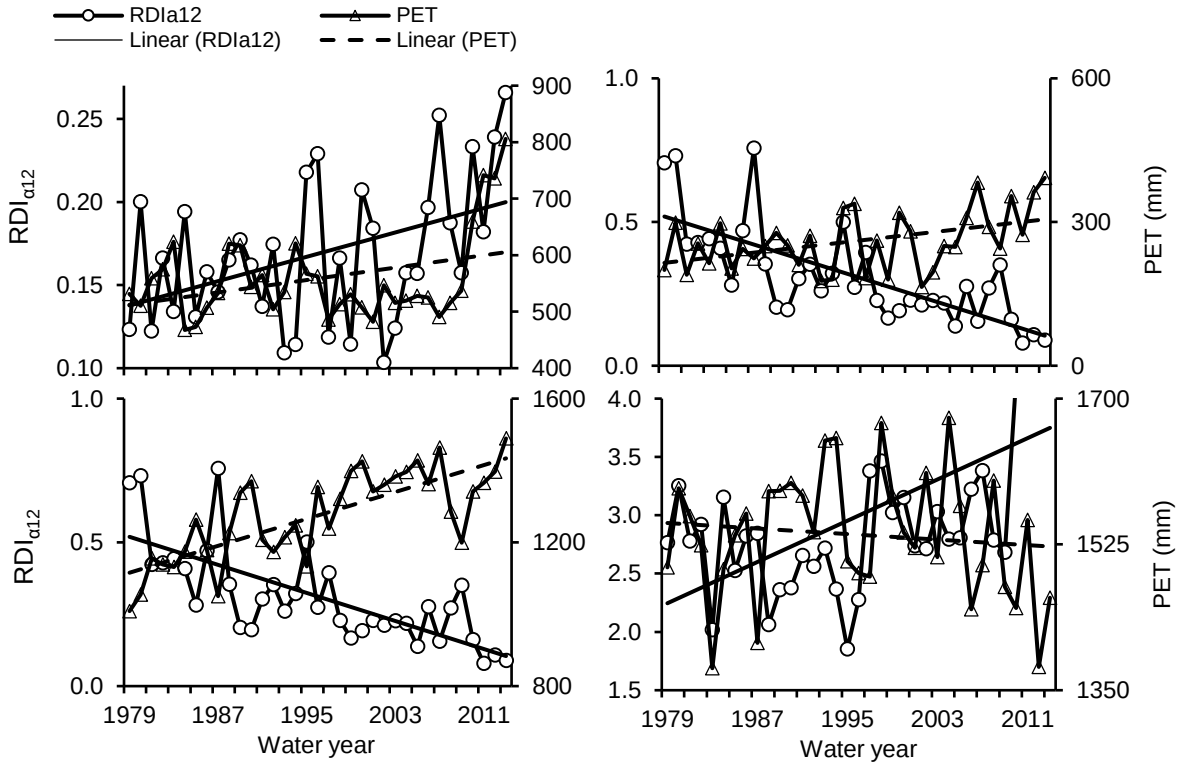

Figure 4.22 Annual values and trends of aridity index ($RDI_{\alpha 12}$) and potential evapotranspiration (PET) for (a) Mediterranean; and (b) tropical; (c) conventional; and (d) humid, climatic conditions for the time-period between 1979 and 2014

4.4.3 Relationships between Meteorological and Hydrological Drought

The meteorological drought estimations were achieved for the reference periods of 3, 6, and 12 months. The linear regression relations between RDI_{st} (3, 6, and 12 months) and SDI (12 months) for the water years 1979/1980 to 2013/2014 are presented in Figure 4.23. As the reference periods become longer, the equations of regression reveal better fits, as represented by the higher value of correlation coefficients, Figure 4.23. This can be expected because an improved correlation is obtained by including more data related to the hydrological drought of the assessed year. This is achieved for a reference period of up to 9 months by which precipitation and streamflow co-exist. Regression equations can introduce predicts with rather high uncertainty. Accordingly, each prediction of SDI should be treated only as a representative value, particularly if it is calculated applying data from the first trimester of the water year. It follows that this relatively simple method, which introduces findings with substantial uncertainty, proves to be useful since pro-active measures, to mitigate the effects of droughts, are decided upon the class of severity category of the expected drought event and not on the absolute SDI value.

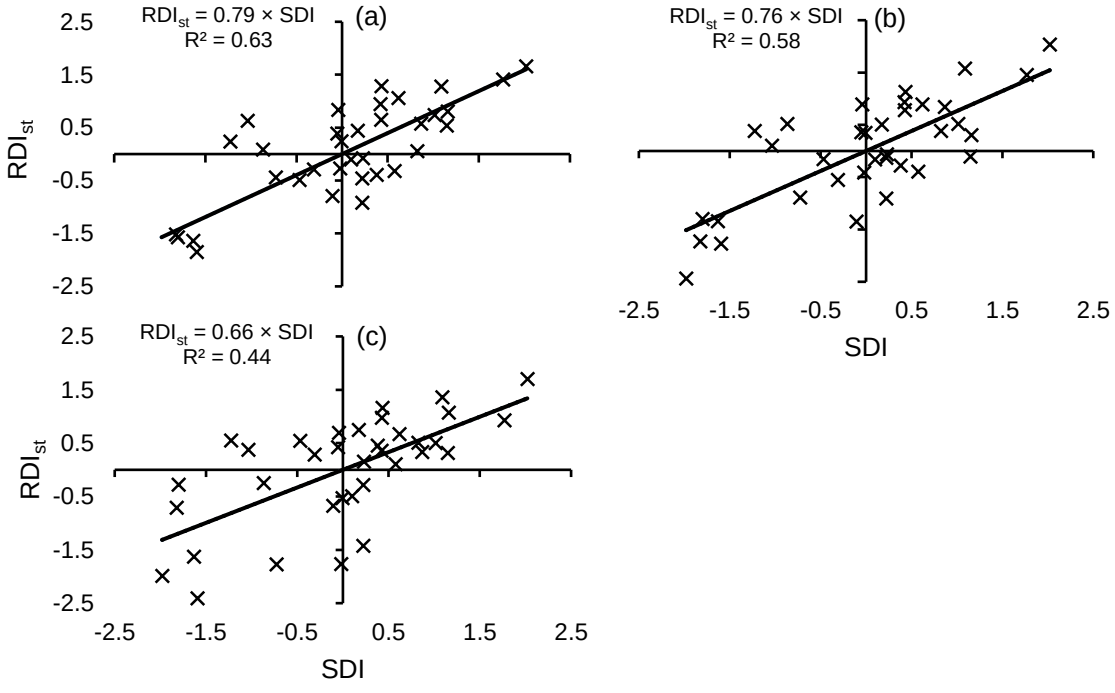

Figure 4.23 Annual streamflow drought index (SDI) forecasting equations based on the standardised reconnaissance drought index (RDI_{st}) for the reference time-periods of 12, 6, and 3 months: (a) RDI_{st} (12 months) – SDI (12 months), (b) RDI_{st} (6 months) – SDI (12 months) and (c) RDI_{st} (3 months) – SDI (12 months), respectively

4.5 Hydrograph Analysis

A generic methodology during which the results of the flow duration curve (FDC) are linked to the results of digital filtering algorithm (DFA), to estimate the best filter parameter (α) value has been developed. Subsequently, the outcomes are used to assess climate change, drought events, and human-induced impacts on the below-ground water contributions to streamflow by which the following question can be answered: "To what extent can such methodology overcome the DFA drawbacks, and can be used to assess the impacts of climate change and human-induced on BF? Figure 4.24 shows the flow chart of the developed methodology.

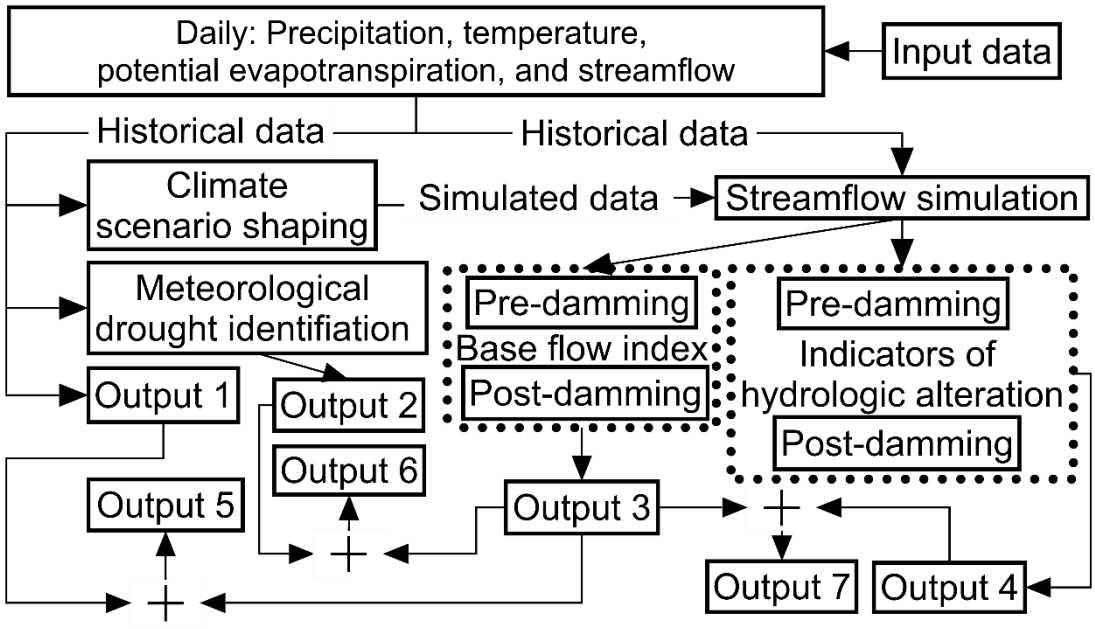

Figure 4.24 New methodology for assessing the impacts of river damming as well as climate change and drought events on the groundwater contribution to river flow, which belongs to objectives four and five

By providing a full picture of the prospective impacts of climate change and the expected human-induced as well as the possibility of such effects. The study results should be beneficial for engineers and policy-makers so that they can develop an effective adaptation strategy to cope with and mitigate the potential impacts of such changes. Therefore, the proposed methodology can address the challenge whether a simple implementation, although applied to one regime, would be easily replicated to other water resources systems. As far as the author is aware, this is the only substantial research presenting such a methodology and characterising the impacts of both climate change, human-induced, and drought phenomena on ground water contributions.

4.5.1 Flow Duration Curve Linked to Digital Filtering Algorithms

4.5.1.1 Upstream Sub-Basin

Based on the outcomes of equation (3.23), a 0.982 value of α yielded BFI equivalent to the value resulting from the low flow index. After considering this value in the separation technique, the following information has been gained: Firstly, over the hydrological period that spans from 1931 to 2013, the separated annual BF values varied from 0.448 (2006) to 3.54 billion cubic meters (bcm). The equivalent annual BF varied from nearly 37 to almost 293 mm. However, the long-term BF value and the equivalent standard deviation (SD) were 1.43 and 0.60 bcm in this order. Accordingly, BF long-term average yearly value and the corresponding SD were predicted to be around 118 and about 50 mm, respectively. Secondly, Figure 4.25a, Figure 4.25b, Figure 4.25c and equations (4.1), (4.7) and (4.13) in Table 4.11 show a strong correlation between the separated BF and TF, depending on the developed linear regression models. Furthermore, Figure 4.25d shows that the annual temporal values of BFI fluctuated from 0.26 (1958) to 0.42 (1997), and BFI long-term value in addition to the equivalent SD were 0.35 and 0.027 in this order. Outcomes expose that around 70% of the yearly BFI values were located within the mean±SD ranges.

Additionally, and referring to equation (3.25), results expose that a 0.925 value of α yields BFI that is equivalent to the value gained from the created FDC. Therefore, the annual BF values during the period between 1931 and 1993 changed from 0.84 (2006) to 7.26 bcm (1968). The equivalent annual BF varied from about 69 to closely 600 mm. BF long-term average annual value and the equivalent SD were 2.86 and 1.23 bcm, correspondingly. BF long-term average yearly value and the corresponding SD were 237, and around 102 mm in this order. Figure 4.25a, Figure 4.25b, and Figure 4.25c show the separated BF linked with TF. The developed linear models (equations (4.2), (4.8), and (4.14), Table 4.11) show a strong correlation. BFI annual temporal variability ranged from 0.51 (1968) to 0.54 (1972). The average long-term BFI value and the matching SD were 0.53 and 0.01, in that order. Accordingly, roughly 61% of the BFI yearly values were expected to be within the mean±SD ranges. Furthermore, the results demonstrated a good relationship between equations (3.23) and (3.24) as shown in Table 4.11 (equations (4.3), (4.9), and (4.15)).

4.5.1.2 Downstream Sub-Basin

The results from equation (3.23) show that a 0.925 value for α Eckhardt parameter yields BFI equating to the one obtained from FDC. During the years from 1931 to 1993, the annual BF magnitude changed between 0.01 (1993) and 4.20 (1968) bcm. BF long-term average yearly value and the equivalent SD were 1.60 and 0.76 bcm, respectively. Figure 4.25a, Figure 4.25b, and Figure 4.25c show the separated BF and TF relationships. The estimated linear model represented by equations (4.4), (4.10), and (4.16) in Table 4.11 show a good correlation. However, Figure 4.25d displays that the annual temporal values of BFI varied from 0.26 (1968) to 0.82 (1992) with 0.30 and 0.12, long-term BFI and SD, respectively. Outcomes indicate that nearly 94% of the yearly BFI values are placed within the mean±SD ranges.

Based on equation (3.24), a 0.925 value for α Eckhardt parameter creates BFI that is equivalent to the value estimated by the created FDC. During the hydrological years between 1931 and 1993, the annual BF values varied from 0.01 (1993) to 8.42 (1968) bcm. The long-term average yearly BF value and SD were 3.08 and 1.61 bcm, respectively. The values of BFI varied between 0.21 (1989) and 0.82 (1992), while BFI long-term value was 0.51±0.11. Around 94% of BFI annual values are placed within the mean±SD ranges, and the developed equation (4.5), (4.11) and (4.17), Table 4.11, show a robust coefficient of determination (R^2). The results also demonstrate a strong relationship between equations (3.23) and (3.24) as shown in Table 4.11 (equations (4.6), (4.12), and (4.18)).

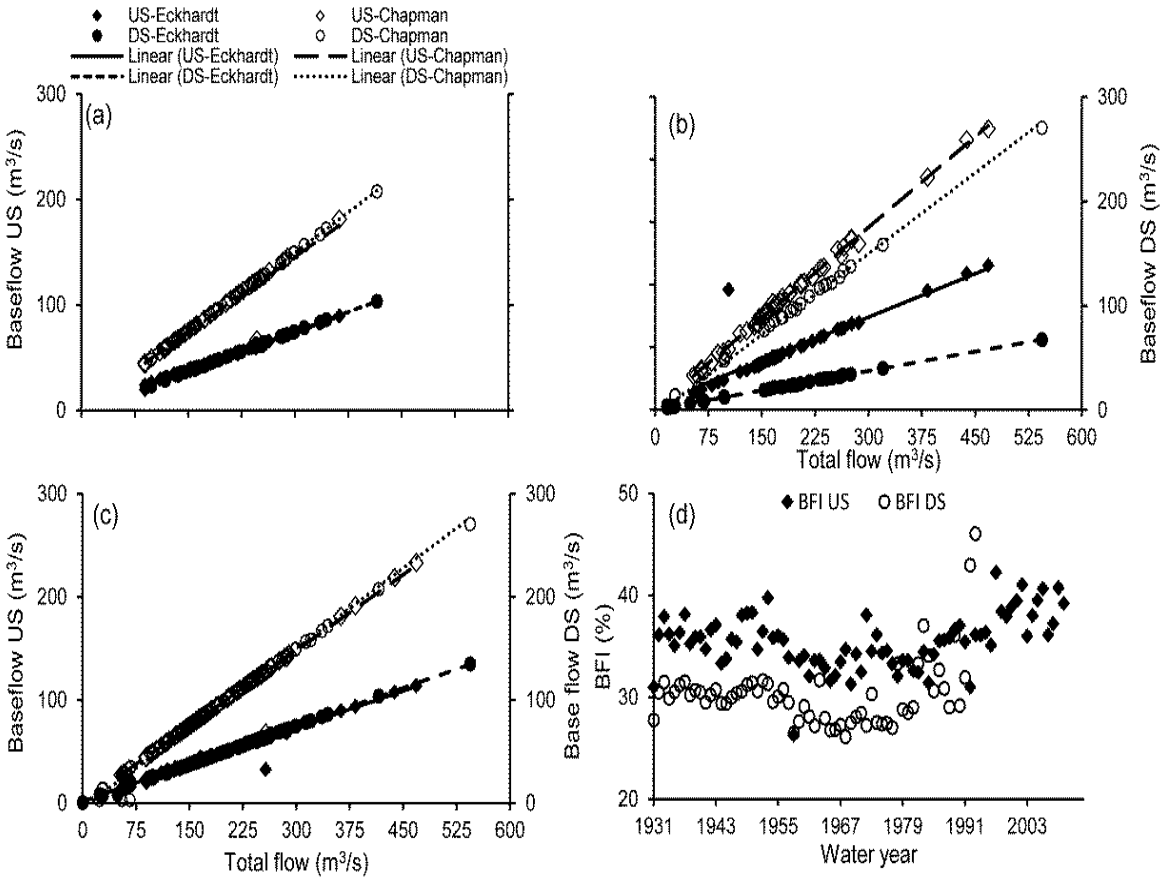

Figure 4.25 Linear regression models for the relationships between the separated baseflow using Eckhardt and Chapman methods, and the total runoff at upstream (US) and downstream (DS) sub-basins for (a) pre-damming; (b) post-damming; and (c) integrated, time-periods; and (d) annual baseflow index (BFI) variability as a function of time for US and DS sub-basins, estimated by the Eckhardt recursive digital filtering algorithms coupled with the flow duration curve

Table 4.11 The developed linear regression models for the upstream and downstream sub-basins at the three considered periods using both the Eckhardt algorithm linked to the flow duration curve and the Chapman digital algorithm

Time-period	Sub-basin	Algorithm	Equation		
			Formulation	R^2	No.
Pre-damming	Upstream	Eckhadt	$BF^a=0.24\times TF^b+1.3$	0.99	4.1
		Chapman	$BF^a=0.48\times TF^b+2.7$	0.92	4.2
		Eckhadt-Chapman	$BF^a_{Eckhadt}=1.95\times BF^a_{Chapman}+0.65$	0.91	4.3
	Downstream	Eckhadt	$BF^a=0.25\times TF^b+0.1$	0.99	4.4
		Chapman	$BF^a=0.51\times TF^b-3.6$	0.97	4.5
		Eckhadt-Chapman	$BF^a_{Eckhadt}=2.10\times BF^a_{Chapman}-3.73$	0.97	4.6
Post-damming	Upstream	Eckhadt	$BF^a=0.23\times TF^b+5.0$	0.80	4.7
		Chapman	$BF^a=0.48\times TF^b+1.3$	0.99	4.8
		Eckhadt-Chapman	$BF^a_{Eckhadt}=1.70\times BF^a_{Chapman}+11.1$	0.80	4.9
	Downstream	Eckhadt	$BF^a=0.12\times TF^b+0.2$	0.99	4.10
		Chapman	$BF^a=0.52\times TF^b-5.2$	0.99	4.11
		Eckhadt-Chapman	$BF^a_{Eckhadt}=4.20\times BF^a_{Chapman}-6.2$	0.99	4.12
Integrated	Upstream	Eckhadt	$BF^a=0.24\times TF^b+1.8$	0.97	4.13
		Chapman	$BF^a=0.52\times TF^b-5.2$	0.99	4.14
		Eckhadt-Chapman	$BF^a_{Ekhadt}=2.10\times BF^a_{Chapman}-5.2$	0.99	4.15
	Downstream	Eckhadt	$BF^a=0.25\times TF^b+1.3$	0.99	4.16
		Chapman	$BF^a=0.49\times TF^b+1.0$	0.97	4.17
		Eckhadt-Chapman	$BF^a_{Ekhadt}=2.10\times BF^a_{Chapman}-6.9$	0.98	4.18

[a]Baseflow and [b]Total runoff

4.5.2 Anthropogenic Intervention Impact on the Hydrograph

To explore the potential impact of the stream regulation by dams on the groundwater involvement to TF of streamflow, this part of the study considered the pre-damming, post-damming, and integrated time-periods. At the basin inlet, the first period covers the water years from 1931 to 1965 (considered as pre-damming). The water years that span from 1966 to 2013 are considered as the post-damming period, and the integrated period covers the hydrological years between 1931 and 2013. However, the corresponding periods at the downstream location were 1931–1965, 1966–1993 and 1931–1993, respectively.

Consequently, the daily FDC outcomes at the Dokan site for the three periods pointed out that Q_{90} and Q_{50} flow rates were 35 and 101, 31 and 100, and 33 and 100 m^3/s, correspondingly. Therefore, Q_{90}/Q_{50} ratios, which represent the BFI values, were about 35, 31 and 33% in that order, representing water capacities that the stream may obtain from groundwater recharge and/or other delayed low groundwater resources concerning the considered time-periods. Based on daily FDC results at the Altun Kupri-Goma Zerdela site for the three periods, Q_{90} and Q_{50} values were 40 and 132, 17 and 127, and 31 and 129 m^3/s, respectively, so that BFI were nearly 30, 14, and 24% in this order. This shows that the pre-damming BFI was dramatically larger

compared to the estimated numbers for both the post-damming period and the combined periods, which can be attributed to the decrease of the sub-surface water contribution to the entire LZRB flow, due to water yielded from the Dokan reservoir over the dry months, decreasing BFI. Consequently, more attention has to be given to appraise the aquifer properties and understand the features potentially causing variations for developing the basin groundwater flow management.

Considering the pre-damming period, a 0.982 value for α Eckhardt parameter has been produced by equation (3.23). The annual BF volume period varies from 0.632 (1958) to 2.826 (1953) bcm. The corresponding annual BF values are between 30 to 132 mm. The long-term BF average annual value was 1.478±0.512 bcm. However, the annual BF magnitudes estimated by equation (3.24) during the same period varied from 1.38 (1958) to 5.71 (1953) bcm. The equivalent annual BF was between 65 and 266 mm. The long-term annual mean BF was 2.91±1.05 bcm. Applying equation (3.23), the annual BF values varies from 0.437 (2006) to 3.647 (1968) bcm for the post-damming period. The equivalent annual BF changed from about 21 to 170 mm. The long-term annual mean BF volume was 1.45±0.70 bcm. Using equation (3.24), annual BF values varied from 0.871 (2006) to 7.077 (1968) bcm. The equivalent annual BF changed from approximately 40 to 330 mm. The long-term annual average BF value was 2.88±1.31 bcm.

Furthermore, Figure 4.26 displays the variations of TF, the separated BF values, and BFI for the three periods and both sub-basins. Findings indicate that the derived BF values for the three studied periods display similar patterns. Variations have been witnessed for BFI concerning the post-damming period, in particular, concerning the upstream sub-basin (Figure 4.26a), which can be attributed to the water yield from the Dokan reservoir during the dry season.

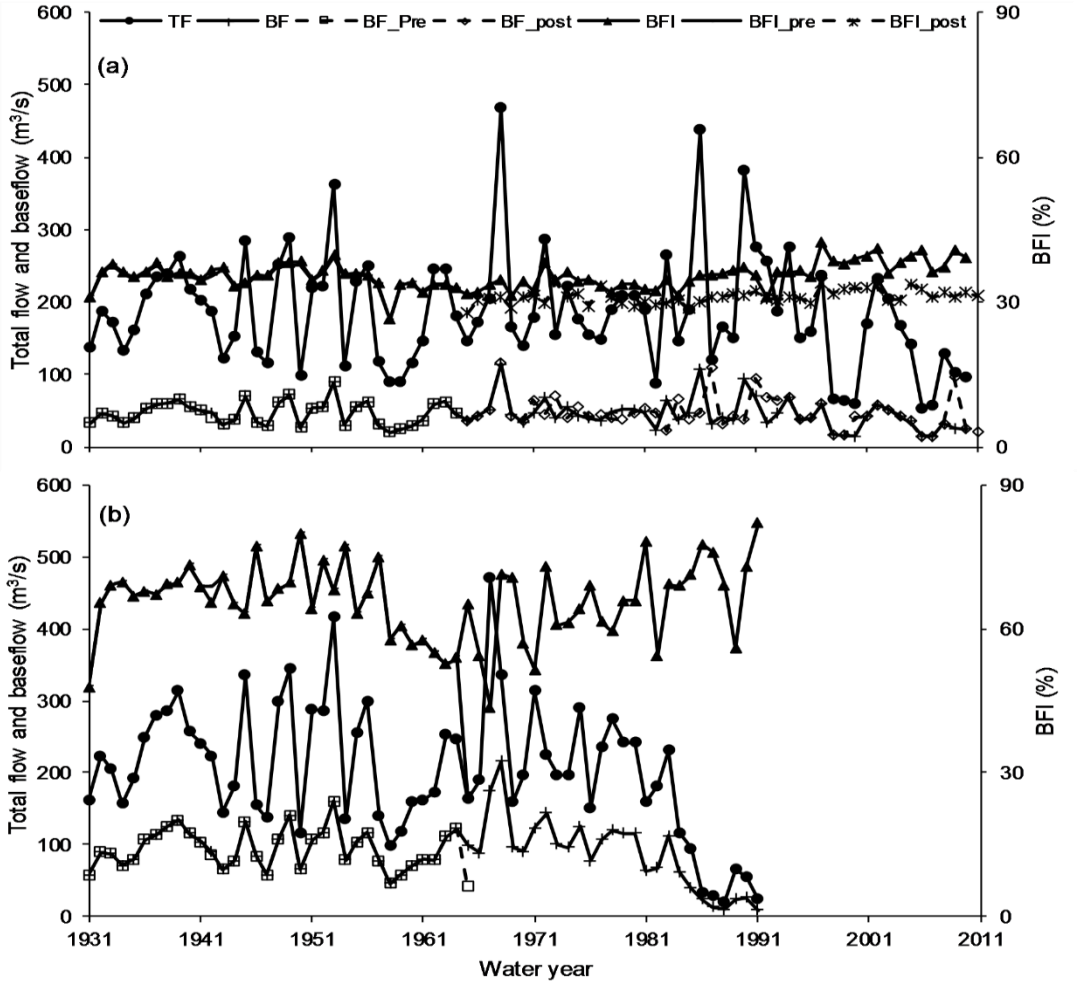

Figure 4.26 Long-term monthly variation of total flow (TF), baseflow (BF), and the baseflow index (BFI) estimated by the Eckhardt filtering algorithm coupled with the flow duration curve (FDC) for the pre-alteration and post-alteration time-periods at (a) Dokan hydrometric station and (b) Altun Kupri-Goma Zerdela station

4.5.3 Climate Change and Drought Episode Impact on the Hydrograph

The potential effects of climate change and drought event detection on the hydro-climatic variables and BFI over the studied basin should be seen as an important milestone, in the study of the influence of these events on the water resources availability in the basin. The key climate variability outcome is that rainy and dry years are determined by maximum and minimum flows, respectively.

Figure 4.27 displays wet and dry years thresholds coupled with the BFI time series. A significant ($p < 0.01$) rise in the sub-basin P_{av} of nearly 44% was noticed for the water year 1987. A noteworthy change in the flow of about 118% resulted from an increase in the amount

of precipitation, which in turn reduced the groundwater involvement to TF. In contrast, for the years from 1998 to 2001 and from 2006 to 2008, a steep drop in the sub-basin P_{av} of about 40 and 60%, respectively, was calculated. A reduction of about 66, 77 and 79% (corresponding yearly average flow values of 0.35×10^9 m^3, 0.31×10^9 m^3, and 0.34×10^9 m^3) for the years 1998/1999, 2000/2001, and 1999/2000 in river flow resulted from P_{av}. This led to a corresponding increase in the involvement of groundwater (represented by BFI). Nevertheless, 52, 80 and 83% streamflow decreases (equivalent to 0.76×10^9, 0.29×10^9, and 0.31×10^9 m^3 annual mean flow volumes) were observed during the water years 2006/2007, 2007/2008, and 2008/2009, respectively. Additionally, a steep drop during which the flow change ranged between 75 and 86% (equivalent to 0.31×10^9 m^3 and 1.24×10^9 m^3) indicated the absolute minimum and maximum annual mean storage volumes, which occurred between 1991 and 2013. Therefore, the BFI rose from about 31% to almost 35%. Figure 4.28 shows that there is a wide variability in the simulated TF, BF, and BFI values, respectively. For example, the simulated values of TF, BF, and BFI based on the Future 6 (F_6) (10% P reduction linked with 10% PET increase) scenario could be as low as 36, 34, and 22%, respectively, which reflects the severity of climate change in the study area. The climate change impact on the runoff estimations generally follows the impact on both BF and BFI. C_v for the simulated TF, the separated BF, and BFI are as high as 0.45, 0.51, and 0.31, respectively. This coefficient can be regarded as an indication of the variability or uncertainty of these values.

Figure 4.29a and Figure 4.29b present the RDI_{st} values estimated for the studied sub-basins, showing that a non-symmetric seasonal drought pattern and wet periods were detected, particularly in the upper sub-basin. Droughts were identified on a regular basis at the upstream sub-basin for the water years 1998/1999, 1999/2000, 2000/2001, 2007/2008, and 2008/2009 (Figure 4.29a). The corresponding mean RDI values were -1.84, -1.67, -1.45, -2.91, and -1.53. These findings complement several earlier studies (Fadhil, 2011; UNESCO, 2014). Depending on the detected drought event concerning the upstream sub-basin, sub-surface contributions increased from about 30 to 35%. However, no drought episodes have been recorded for the downstream sub-basin (Figure 4.29b).

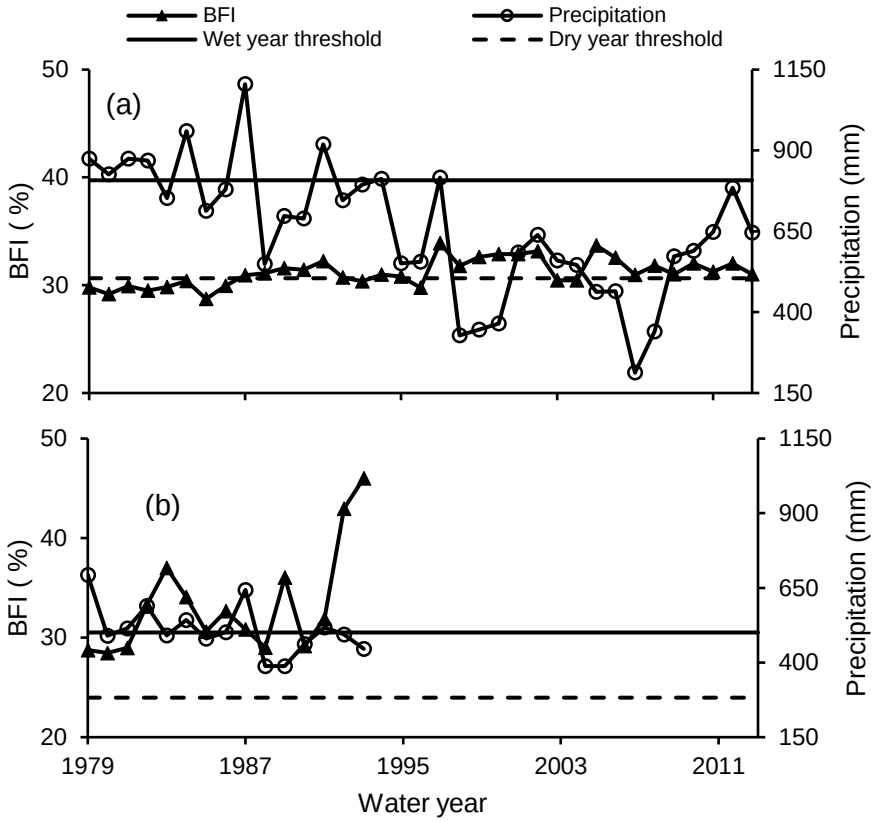

Figure 4.27 Long-term baseflow index (BFI) with both wet and dry year thresholds coupled with long-term average precipitation for the periods between 1979 and 2013 for (a) Dokan and (b) Altun Kupri-Goma Zerdela stations, respectively

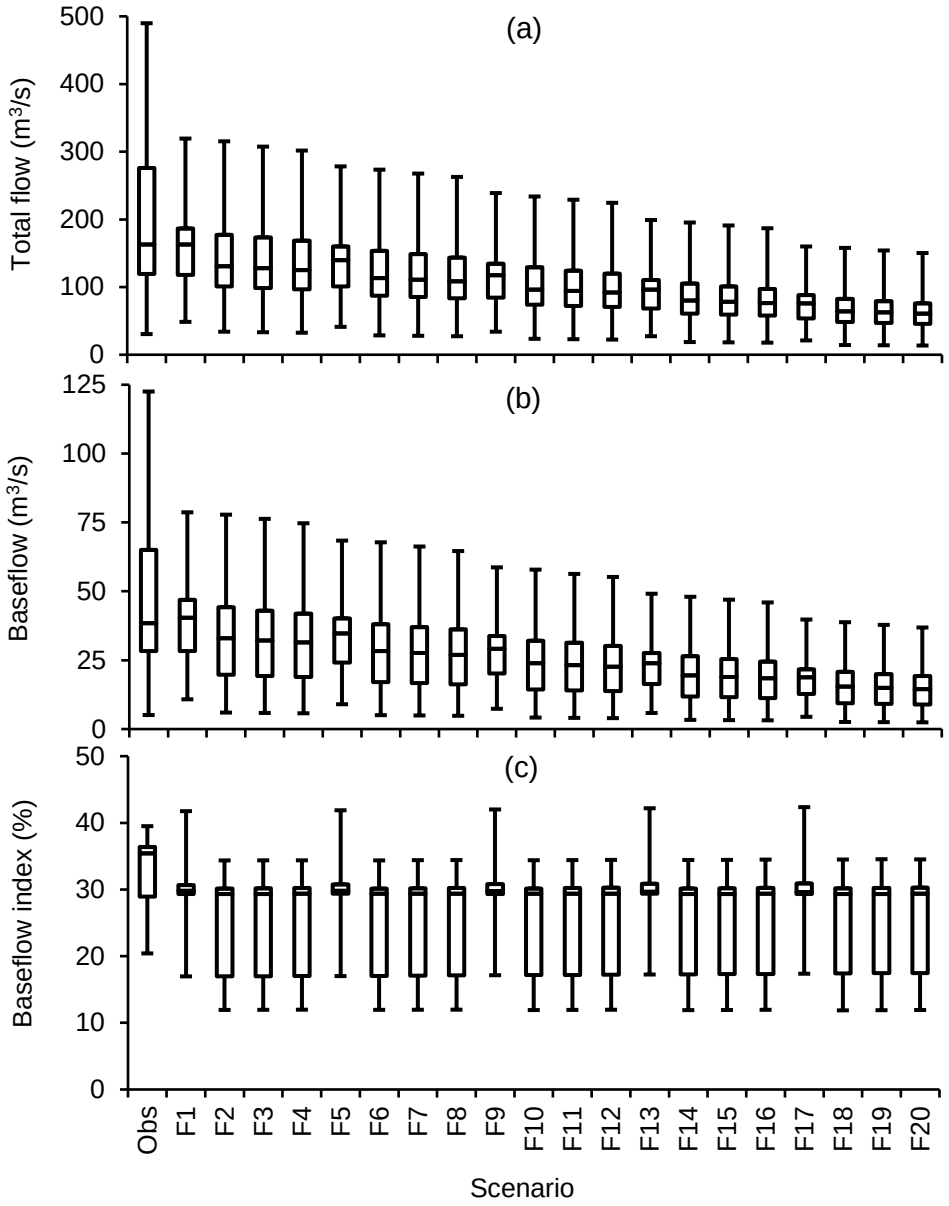

Figure 4.28 Box plot indicating (a) the total runoff; (b) the baseflow; and (c) the baseflow index at the inlet of the basin based on the delta perturbation climate scenario. Note: future F_1 to F_4 (0% reduction in precipitation (P) linked with 0,10, 20, and 30% increase in potential evapotranspiration (PET), respectively), F_5 to F_8 (10% reduction in P linked with 0,10, 20, and 30% increase in PET, respectively), F_9 to F_{12} (20% reduction in P linked with 0,10, 20, and 30% increase in PET, respectively), F_{13} to F_{16} (30% reduction in P linked with 0,10, 20, and 30% increase in PET, respectively), F_{17} to F_{20} (40% reduction in P linked with 0,10, 20, and 30% increase in PET, respectively). Note: Obs = Observed

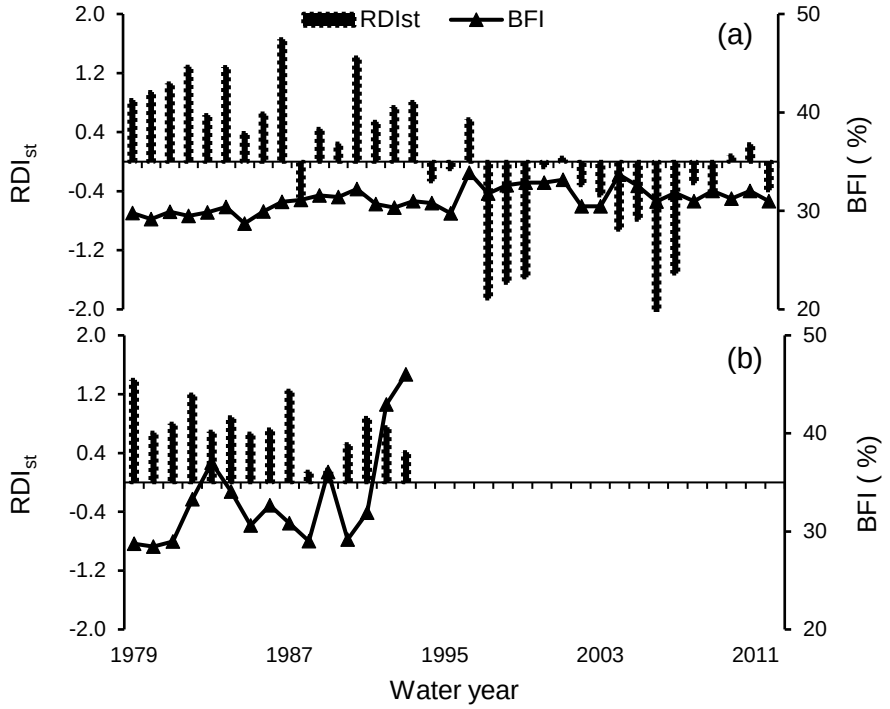

Figure 4.29 The standardised reconnaissance drought index (RDI) coupled with the long-term baseflow index (BFI) for the Lower Zab River basin between 1979 and 2013 for (a) Dokan and (c) Altun Kupri-Goma Zerdela stations in this order

4.5.4 Seasonal Variations of the Baseflow Index

Results of the seasonal BFI variability at the upstream sub-basin (Figure 4.30a) show that the Dokan sub-basin is likely to recharge LZRB with groundwater from aquifers. This contribution started to rise significantly ($p < 0.05$) from April until obtaining an absolute maximum number by the end of June. This level of recharge continued without change until the mid of August. A marginal drop for September was noted. Additionally, BFI entries usually showed high variations over the dry period.

Figure 4.30b reveals that the downstream sub-basin long-term BFI is nearly doubled that of the upstream sub-basin values for the months from October to April, whereas they are close to each other for the remaining period. This variability in BFI may result from the difference in the periods studied. The period horizon for the Dokan sub-basin spanned from 1931 to 2013 (82 years), whereas for the Altun Kupri-Goma Zerdela sub-basin, it ranged from 1931 to 1993 (62 years). Despite the fact that the catchment area of the Dokan sub-basin (12,096 km^2 is larger than the Altun Kupri-Goma Zerdela one (8,509 km^2), the former is characterised by both a higher P rate (Table 4.4) and elevation. This may increase the contribution of both runoff and

the interflow to TF of the Dokan sub-basin, which in turn decreases the contribution of BF to LZRB discharge. The research findings specify that through the last few years, climate variability and drought events have harmfully affected the availability of the LZRB storage water.

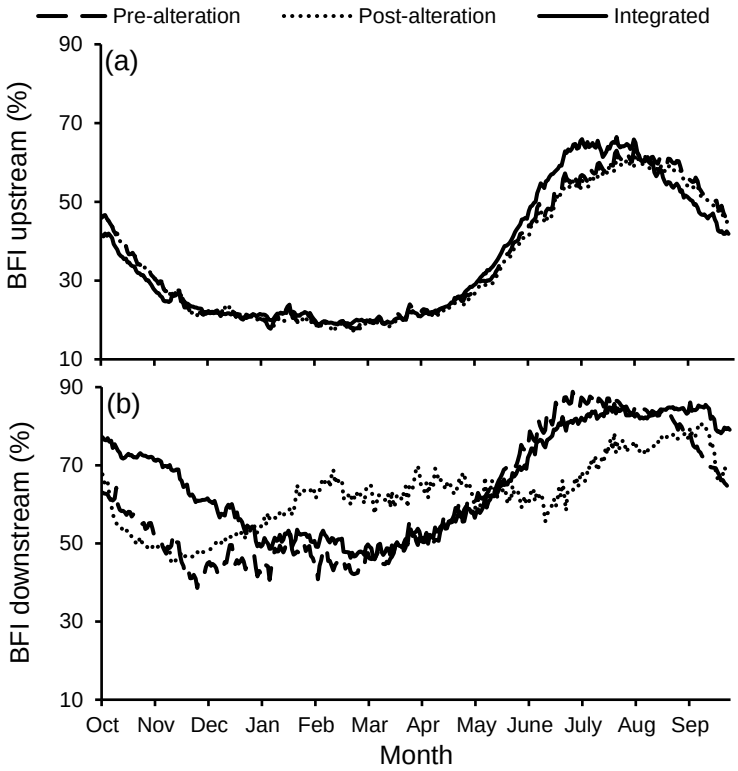

Figure 4.30 Seasonal variations of the BFI estimated by the Eckhardt filtering algorithm coupled with the flow duration curve for the three studied time-periods at (a) Dokan and (b) Altun Kupri-Goma Zerdela stations, respectively

4.6 Hydrologic Alteration

4.6.1 Overview

Due to universal environmental changes, such as the intensity and frequency of floods and droughts, integrated with vegetation and land use alterations, in addition to the impacts of regional anthropogenic intervention, it is often necessary to evaluate such changes on the hydrologic alteration. Therefore, this part of the research highlights the assessment of the potential impacts of human-induced and climate change on the LZRB hydrology, attempting to address: "To what extent would the climate change and anthropogenic intervention alter a basin

hydrological properties?" In addition to predicting hydrological drought for relatively small basins based on meteorological data. Subsequently, the research can be considered as a comparative study during which climate change impacts, human interventions, precipitation, potential evapotranspiration, RDI_{st}, SPI, SPEI, and streamflow alteration are assessed as shown in Figure 4.31.

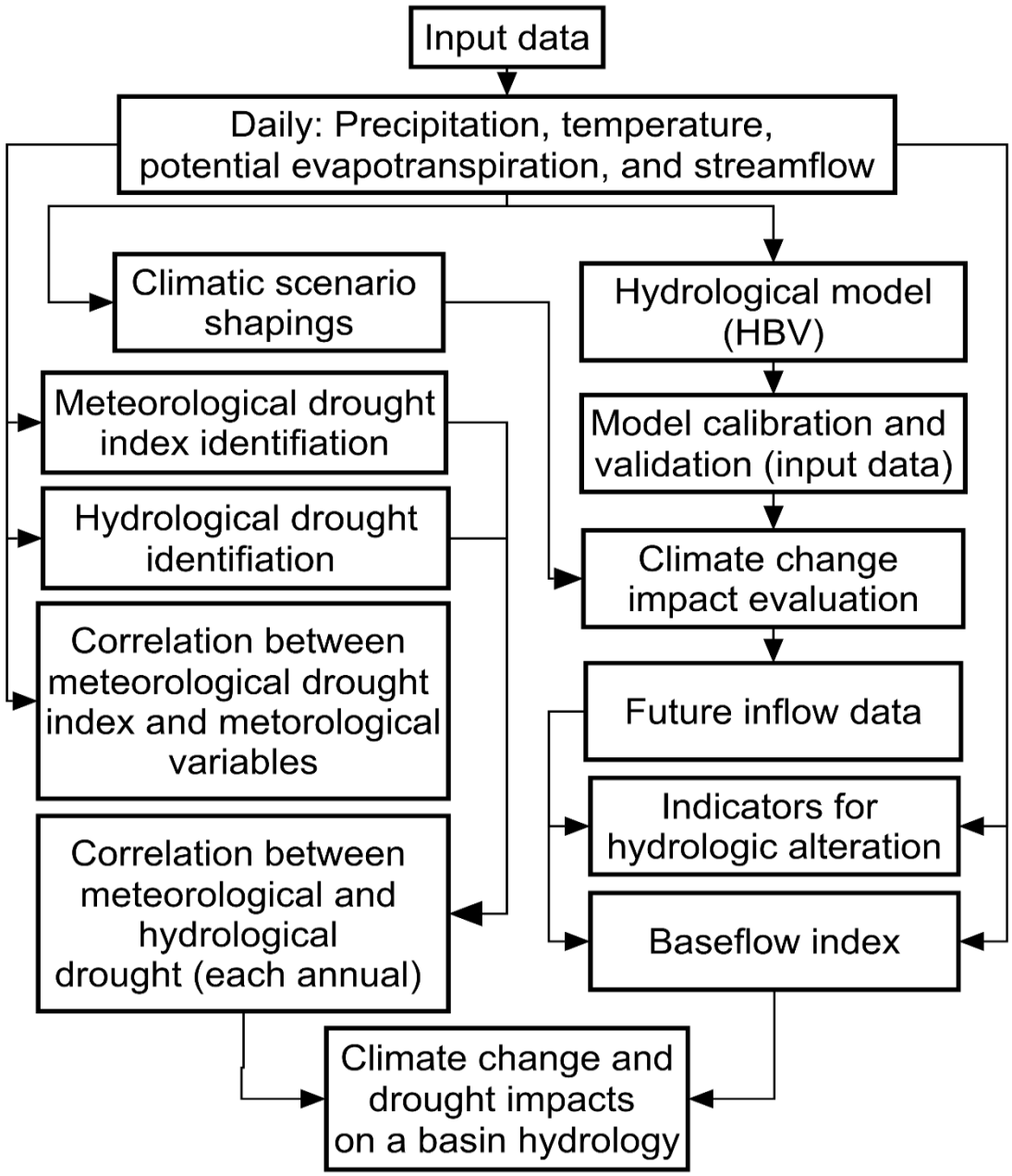

Figure 4.31 The detailed advancement of the objective five

4.6.2 Anthropogenic Intervention Impact of on the Streamflow

Figure 4.32 displays the annual alteration ratio of the changed timespan (1965–2013), compared to the long-term median yearly discharge for the unchanged period (1932–1965) was calculated according to equation (2.1), corresponding to normal years with both wet and dry years thresholds. Additionally, Figure 4.32 shows the alterations of the median annual flow for the post-damming condition based on the long-term pre-damming median annual flow. It is important to note that the water year 1987 observed a substantial rise in the basin Pav of almost 44% more than the typical yearly extreme threshold, which results in about 118% alteration in the streamflow with the corresponding annual mean flow volume of 2.31×10^9 m^3, Table 4.12. However, a contrast was detected for the periods 1998–2001 and 2006–2008 as Table 4.12 displays.

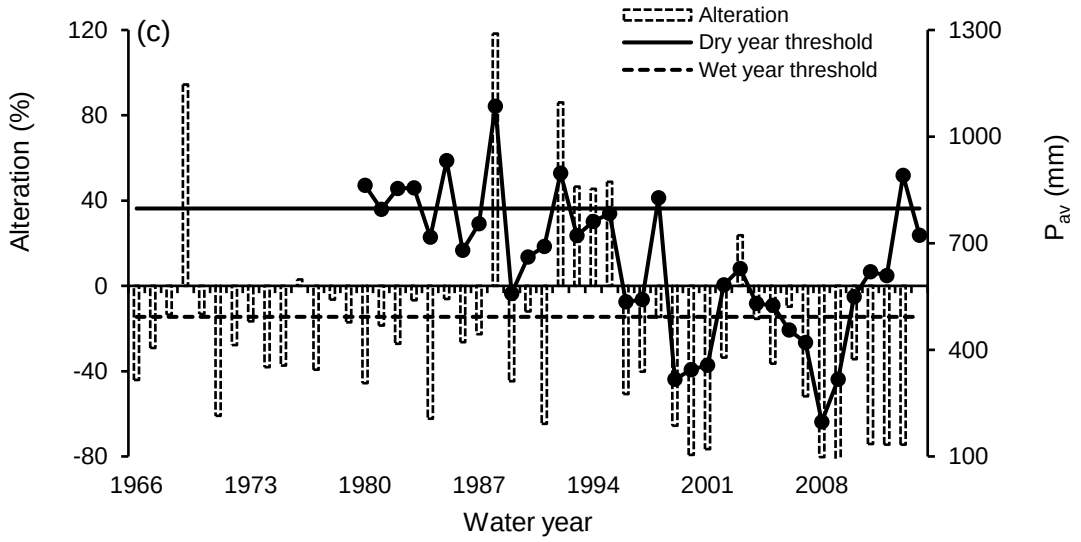

Figure 4.32 Annual median anomaly for the period between 1966 and 2014 with both wet and dry year thresholds coupled with long-term average precipitation over the study area for the time span between 1979 and 2014

These two hydrological years observed a sharp decrease in the basin P_{av} to almost 40 and 60% in this order. P_{av} reduction resulted in a dramatic decrease in the LZRB streamflow by around 66, 77 and 79% with the corresponding yearly average flow capacities of 0.35×10^9, 0.31×10^9, and 0.34×10^9 m^3 for the period between 1998 and 2001, Table 4.12. However, the period between 2006 and 2008 observed about 52, 80, and 83% streamflow decreases with 0.76×10^9, 0.29×10^9, and 0.31×10^9 m^3 annual mean flow volumes. Additionally, between 1991 and 2013,

the normal flow system has observed a sudden drop during which the streamflow anomaly fluctuated from 75 to 86 with 0.31×10^9 and 1.24×10^9 m^3 maximum and minimum annual average storage capacities in this order, Table 4.12. Findings proved that during the past few decades, climate change has negatively affected the LZRB water storage availability.

Moreover, the alteration in monthly median flows corresponding to the long-term natural flow regime and the three changed time scales and their related alteration is visualised in Figure 4.33. The alteration during the two altered time spans of the periods 1965–2013 and 1979–1987 could be considered relatively close to each other, particularly through the rainy months. The small variations can be assigned to the climate change impacts, which was noticeable from the water year 1998 onward. The dramatic alteration during the non-rainy months assigned to the effect of human-induced and climate change pressure, in the upper part of the studied area, which in turn decreases the basin water resources availability.

To investigate the potential impacts of human-induced (i.e. river damming) on the hydrological characteristics of LZRB, a comparison of monthly percentiles between the pre-damming and the post-damming periods for the (a) 10^{th}, (b) 25^{th}, (c) 50^{th}, (d) 75^{th} and (e) 90^{th} percentiles has been conducted, Figure 4.34. Generally, between January and June, the alteration can be considered relatively small. In contrast, during the non-rainy months, there were considerable streamflow alterations that can be attributed to the effect of human-induced and climate change pressures, which decreased the basin water resources availability.

Furthermore, Table 4.13 reveals that the 1-day to 7-day minimum flows remained almost the same, whereas there was a marked increase in the 30-day minimum flow of about 38%. The 1-day to 90-day maximum flows declined considerably. The corresponding declines ranged from 6 to 37%. This type of flow alteration can be attributed to river regulation activities.

Table 4.12 Annual river flows, storages, means of changed to unchanged storage ratios, and median anomalies between the periods from 1979–1980 to 1987–1988 and from 1998–1999 to 2008–2009

Water year	Flow (m^3/s)	Storage ($\times 10^9$ m^3)	Percentage change	
			Long-term mean yearly storage	Anomaly
Time-periods between 1979–1980 and 1987–1988				
1979–1980	148	4.68	0.79	-46
1980–1981	189	5.96	1.00	-19
1981–1882	210	6.61	1.11	-27
1982–1983	190	6.00	1.01	-7
1983–1984	88	2.79	0.47	-62
1984–1985	268	8.46	1.42	-6
1985–1986	148	4.66	0.78	-26
1986–1987	190	5.98	1.01	-23
1987–1988	436	13.75	2.31	+118
Time-periods between 1998–1999 and 2008–2009				
1998–1999	66	2.08	0.35	-66
1999–2000	65	2.04	0.34	-79
2000–2001	59	1.87	0.31	-77
2001–2002	171	5.40	0.91	-34
2002–2003	233	7.36	1.24	+24
2003–2004	205	6.46	1.09	-15
2004–2005	170	5.37	0.90	-37
2005–2006	170	5.38	0.90	-10
2006–2007	144	4.53	0.76	-52
2007–2008	54	1.70	0.29	-80

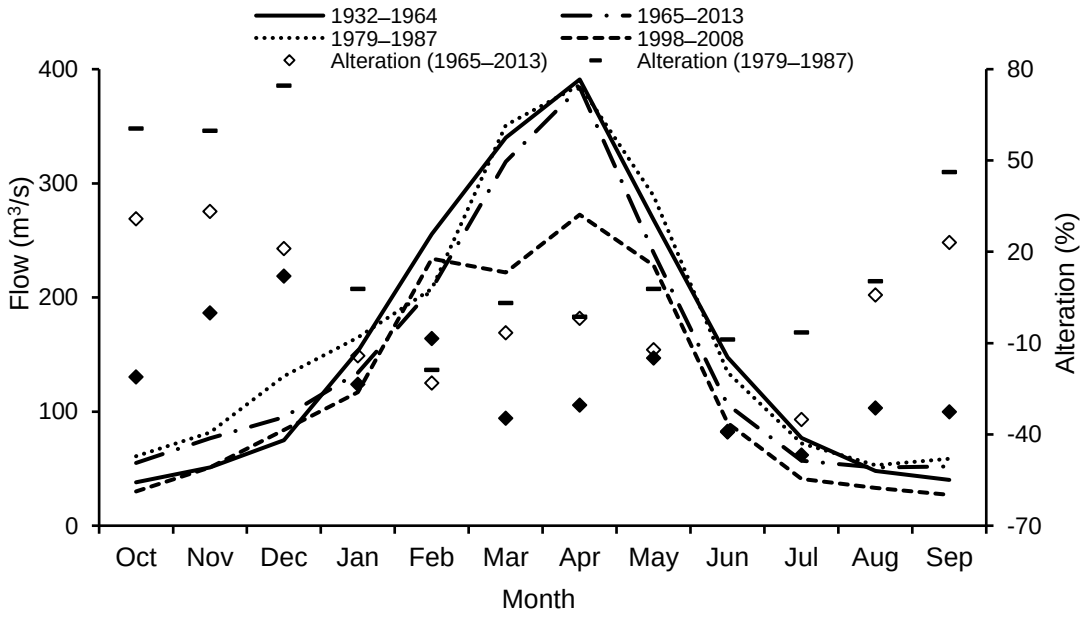

Figure 4.33 The long-term median monthly flows of the pre-altered and the three altered time scales coupled with their anomalies

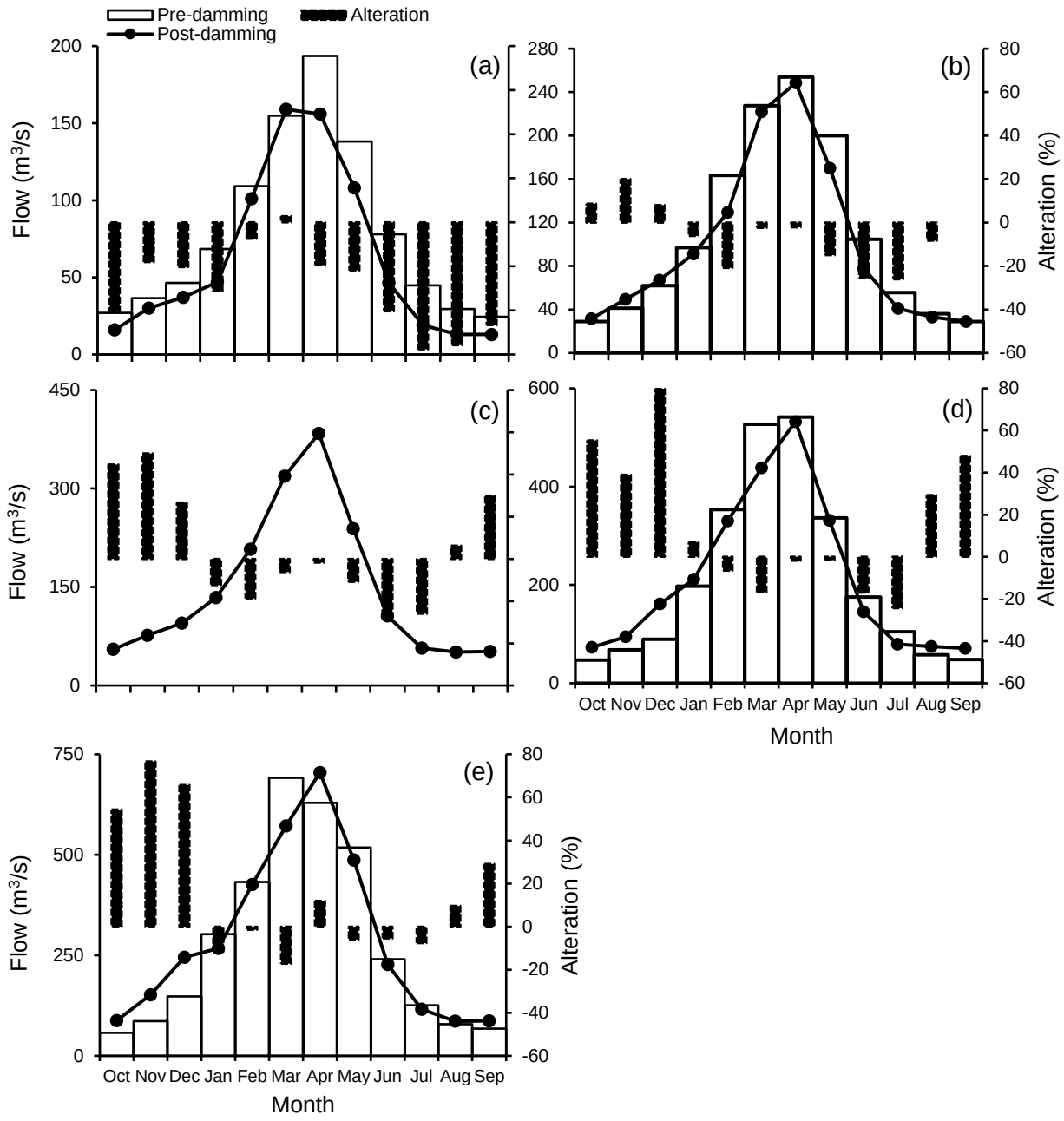

Figure 4.34 Comparison of monthly percentiles between pre-damming and post-damming periods coupled with the alteration ratio for the (a) 10th; (b) 25th; (c) 50th; (d) 75th; and (e) 90th percentiles

Table 4.13 The alteration ratio for the annual median, minima, and maxima flow for the pre-damming and post-damming periods

Runoff (m^3/s)	Pre-damming	Post-damming	Alteration %
n		n-day minima	
1-	25.00	25.00	0
3-	27.00	27.33	1
7-	28.00	31.00	11
30-	31.13	43.00	38
90-	54.32	55.41	2
n		n-day maxima	
1-	1279.00	820.00	-36
3-	1018.00	798.70	-22
7-	765.60	660.70	-14
30-	539.50	505.80	-6
90-	440.70	365.70	-17
BFI[a]	0.16	0.17	6

[a]Baseflow index

4.7 Anthropogenic Interventions Evaluation

4.7.1 General

Land use and land cover have been demonstrated universally to be the main factors impacting on river basin flow (Li et al., 2007; Huo et al., 2008; Miao et al., 2011; Wang et al., 2013; Guo et al., 2014; Chang et al., 2015). However, detailed assessments of the long-term change in streamflow to the LZRB and the distinct contribution of anthropogenic interventions and climate change have not been reported upon. The main target of this part of this study is to answer the following question: "To what extent do anthropogenic interventions and climate change impact on the alteration of runoff within LZRB?" The answer depends on three of the most commonly accepted runoff simulation methods applied, which are the Medbasin, GR4J, and HBV models. Accordingly, this section included the results of the analysis of the basin streamflow temporal variations, the critical change points, and trends of annual basin streamflow detection, the relative contributions of climate change and anthropogenic interventions, such as land use change, reservoir construction, and in-channel damming on basin streamflow; and the evaluation of how the accuracy of multi-model simulation is influenced by the seasonal variations of hydrological processes, and the accuracy level of individual member models. The models applied (Section 3.5.8) have different structural assumptions and data requirements. They were selected to ensure that they cover a wide range of possibilities to maximise the benefits obtained from combining their outputs.

The results can be used for regional water resources evaluation and utilisation as well as managing benchmarks by shading light on the abrupt changes and trends of historical hydrological data for the whole studied geographical region and similar ones elsewhere.

4.7.2 Rainfall-Runoff Models Calibration and Validation

Figure 4.35 displays scatter diagram relationships between monthly runoff and precipitation for the time-periods 1979–1997 (r = 0.50) and 1998–2013 (r = 0.44). The correlation between monthly runoff and precipitation for 1979–1997 is better than that for 1998–2013. The coefficients of runoff for the baseline period were more than the ones for the climate change and anthropogenic intervention periods. The obtained results demonstrated that the runoff was considerably affected by drought events due to climate change linked to upstream non-climatic drivers, such as river regulation, land use changes, water withdrawal and inter-basin water transfer schemes.

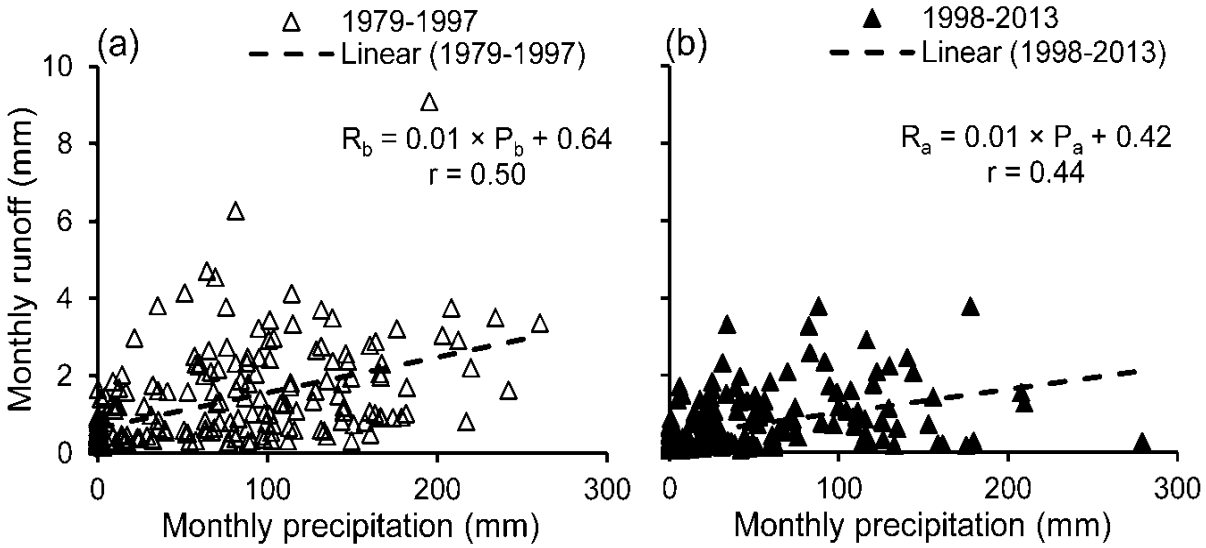

Figure 4.35 Monthly relationship between precipitation and runoff for the (a) 1979–1997, and (b) 1998–2013 periods

4.7.3 Multi-Regression Equation

Depending on the monthly precipitation and potential evapotranspiration of the baseline period, a multi-regression equation was developed as indicated by equation (4.19).

$$R = 0.013 \times P + 0.0034 \times PET - 0.05 \quad (4.19)$$

where R (mm) is the monthly streamflow, P (mm) is precipitation, and PET (mm) represents the potential evapotranspiration.

Figure 4.36a and Figure 4.36b indicate good promise between monthly recorded and predicted streamflow data applying equation (4.19) for the Dokan hydrologic station during the considered time-periods 1979–1997 and 1998–2013, respectively. The value of the coefficient of correlation was 0.52 at a significance level of 0.001. The Nash-Sutcliffe Coefficient (NSCE) was 0.30. The obtained measures of performance show that the multi-regression model may not predict streamflow precisely. The natural runoff series was rebuilt after considering the P and potential evapotranspiration of the anthropogenic interventions period as input. Using the rebuild runoff time series, the impacts of human activities and climate variability on streamflow were tested.

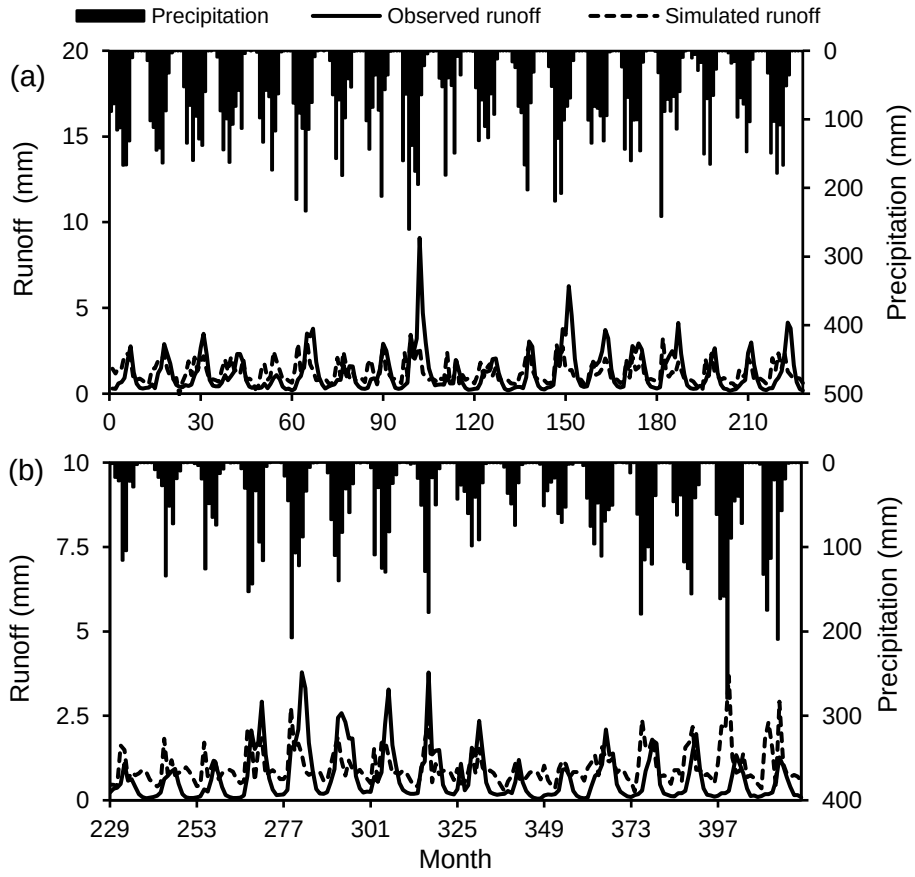

Figure 4.36 Monthly observed and simulated runoff by multi-regression method at the Dokan hydrologic station for the (a) 1979–1997; and (b) 1998–2013 periods, respectively

4.7.4 Methods of Hydrologic Sensitivity Analysis

The coefficient of plant-available water to crop type GO is the main variable in the hydrologic sensitivity analysis. This parameter has been calibrated by equating long-term annual AET computed using equation (3.29) and the baseline period for the water balance. Considering GO = 1, the outcomes of yearly AET predicted by equation (3.29) are acceptable and reasonable (Figure 4.37). Thus GO = 1 has been specified for LZRB. When GO is set to 1, the coefficients of sensitivity values $\frac{\partial R}{\partial P}$ and $\frac{\partial R}{\partial ET}$ (where R (mm/month) is the monthly streamflow) were 0.0167 and 0.0141 in this order, which indicates that the runoff change was more subtle to precipitation compared to potential evapotranspiration.

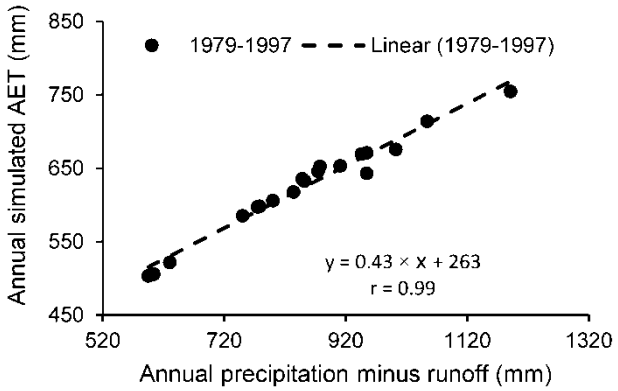

Figure 4.37 Scatter diagram and correlation of annual actual evapotranspiration (AET) estimated from a water balance equation and predicted using equation (3.29) for the time-period between 1979 and 1997

4.7.5 Methods of Hydrological Simulation

The calibration period for the hydrologic model was 1988–2000, while 1979–1986 was the validation period. The obtained results from the three used models show a good promise between monthly recorded and predicted runoff data at the Dokan hydrologic station from 1979 to 1997 (Figure 4.38a). Table 4.14 shows the performance measures for the calibration and validation periods using GR4J, Medbasin, and HBV simulation models. The calibrated rainfall-runoff model was used to rebuild the streamflow datasets for the anthropogenic interventions period between 1998 and 2013 (Figure 4.38b) with actual weather and hydrologic input data. With the rebuild streamflow dataset of the anthropogenic intervention period and the corresponding recorded streamflow dataset, it makes it possible to quantitatively assess the

impacts of non-climate drivers and climate variability on streamflow. Figure 4.36b and Figure 4.38b compared recorded and predicted streamflow data for the Dokan hydrologic station for the hydrological years between 1998 and 2013. The impacts of anthropogenic interventions and climate variability on streamflow were assessed depending on both the conceptual framework and the simulated findings of the various applied models. The simulation methods provided relatively consistent computations of the mean streamflow ratio change for the hydrological period between 1998 and 2013 (Table 4.15). The data show that climate change makes the greatest impact.

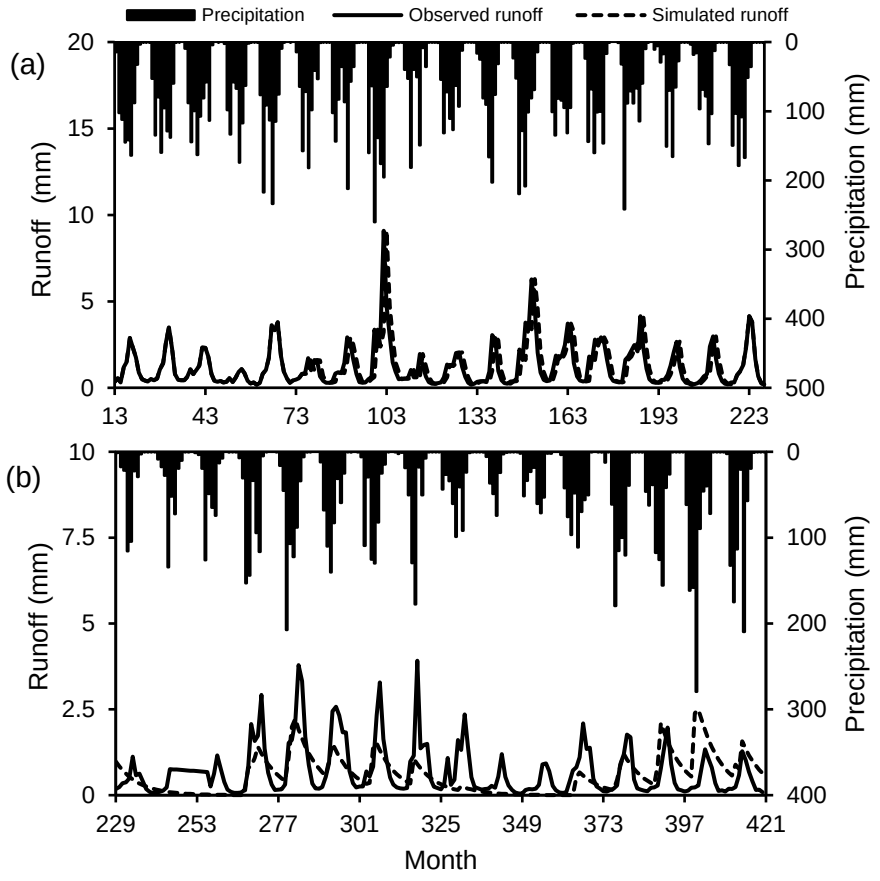

Figure 4.38 Monthly observed and simulated runoff using simple average multi-model technique at the Dokan hydrological station for the: (a) 1979–1997 and 1998–2013 periods

Table 4.14 Performance measures for the calibration and validation time-periods using the Ge´nie Rural a Daily 4 parameters (GR4J), Medbasin, and Hydrologiska Byråns Vattenbalansavdelning (HBV) simulation models

Model	Time-period	Statistical performance			
		RMSE[a]	IoA[b]	r[c]	NSCE[d]
Medbasin	Calibration	2.69	0.96	0.94	88
	Validation	5.99	0.66	0.50	83
GR4J	Calibration	0.79	0.90	0.82	67
	Validation	1.00	0.90	0.84	50
HBV	Calibration	0.73	0.99	0.93	80
	Validation	0. 68	0.99	0.84	50

[a]Root mean square error; [b]Index of agreement; [c]Correlation coefficient; and [d]Nash–Sutcliffe coefficient

Table 4.15 Climate change and anthropogenic interventions impacts on mean annual runoff (R) during recent hydrological periods using different rainfall-runoff simulation methods

Duration		Unit	1998–2002	2003–2008	2009–2013
Runoff total alteration		mm/a	-6.54	-5.52	-8.08
Multi-regression method	$\Delta R_{anthropogenic}$	mm/a	-1.93	-1.88	-0.97
		%	-30	-34	-12
	$\Delta R_{climate}$	mm/a	-4.61	-3.64	-7.11
		%	-71	-66	-88
Hydrological sensitivity	$\Delta R_{anthropogenic}$	mm/a	-1.94	1.41	3.27
		%	-30	-26	-40
	$\Delta R_{climate}$	mm/a	4.60	4.10	4.81
		%	-70	-74	-60
Medbasin model	$\Delta R_{anthropogenic}$	mm/a	-0.29	-0.67	-2.36
		%	-4	-12	-29
	$\Delta R_{climate}$	mm/a	-6.25	-4.85	-5.72
		%	-96	-88	-71
GR4J[a] model	$\Delta R_{anthropogenic}$	mm/a	-1.03	-0.72	-0.43
		%	-16	-14	-5
	$\Delta R_{climate}$	mm/a	-5.51	-4.73	-7.65
		%	-84	-86	-95
HBV[b] model	$\Delta R_{anthropogenic}$	mm/a	-0.60	-0.14	-3.10
		%	-9	-3	-38
	$\Delta R_{climate}$	mm/a	-5.94	-5.38	-4.98
		%	-91	-97	-62
SAM[c]	$\Delta R_{anthropogenic}$	mm/a	-0.35	-0.23	-0.69
		%	-5	-4	-8
	$\Delta R_{climate}$	mm/a	-6.19	-5.29	-7.39
		%	-95	-96	-92

[a]Ge´nie Rural a Daily 4 parameters; [b]Hydrologiska Byråns Vattenbalansavdelning; [c]Simple average method

4.7.6 Comparison of Simple Average Method and Single Model Predictions

To examine the simple average method (SAM) performance, firstly, a set of numerical experiments were computed using the three hydrological models. Figure 4.39a shows the linear regression between observed and simulated runoff for various model predictions regarding the Dokan hydrological station. Figure 4.39b reveals that HBV is the best (B) model in terms of

correlation coefficient, whereas the Medbasin model is the weakest (W). Then, the SAM has been utilised to estimate the streamflow (Figure 4.39b). Figure 4.39 reveals that the statistics from the single model simulations are almost always worse than those of SAM, W, and B simulations. The results confirm that just simply averaging the single model simulations would lead to an enhancement of the simulation level of accuracies, which is consistent with previous research findings (Ajami et al., 2006; Georgakakos et al., 2004). Hence, excluding the worst performing model leads to an improvement of the correlation compared to the single hydrological model.

Furthermore, hydrological parameters, such as flow rate are known to have a special annual cycle. The hydrologic model simulation accuracies for different months often mimic this yearly cycle (Figure 4.20), which shows the performance of the individual model simulations for the studied basin during various months for the two considered periods. Figure 4.40 reveals that a model might perform well for some months, but poorly for other months, when compared to competing models.

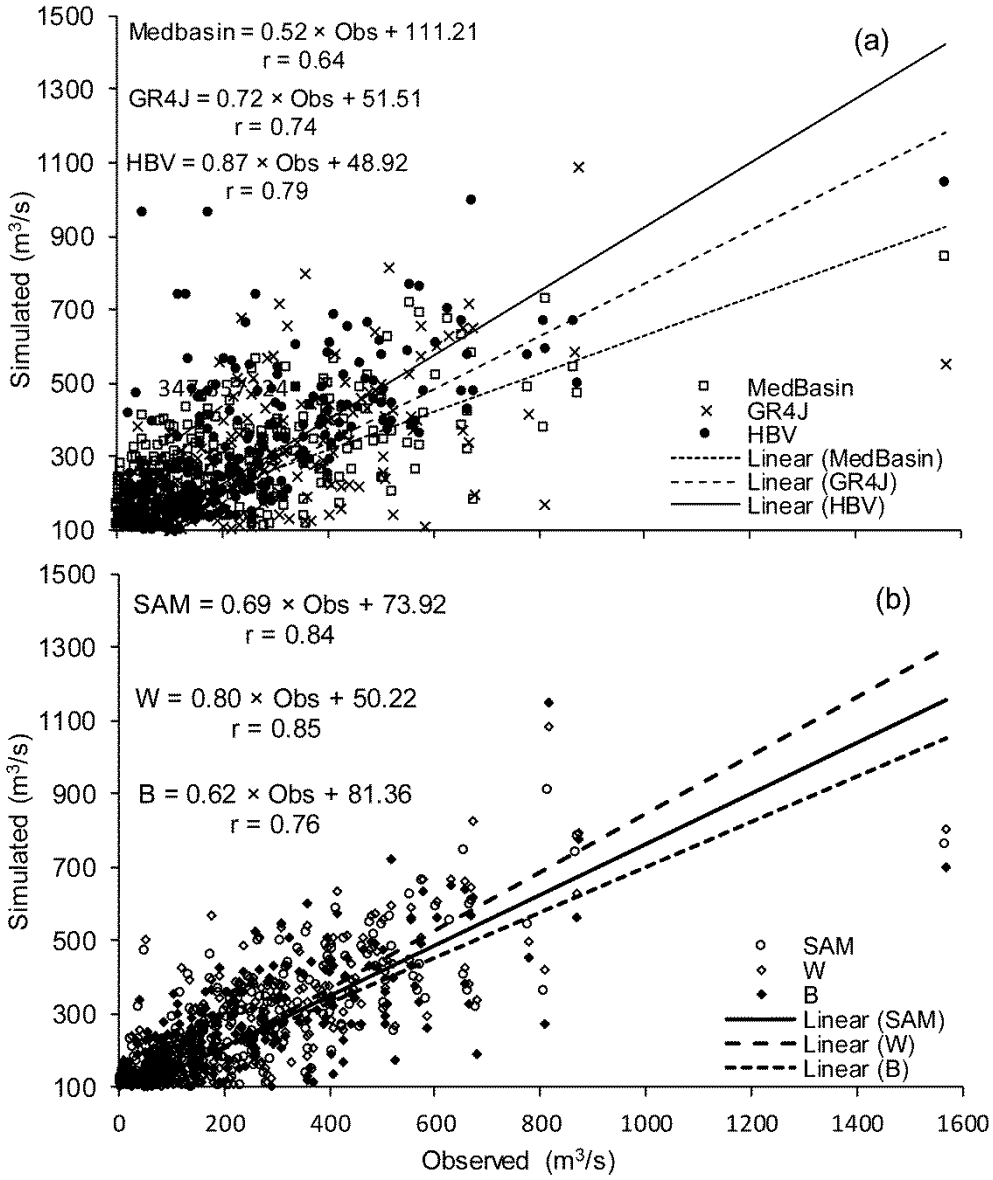

Figure 4.39 Linear regression between observed and simulated runoff: (a) Medbasin, Ge´nie Rural a Daily 4 parameters (GR4J), and Hydrologiska Byråns Vattenbalansavdelning (HBV) models; (b) simple average model (SAM), excluding the best model (B) and the worst model (W) simulation results, for the Dokan hydrological station

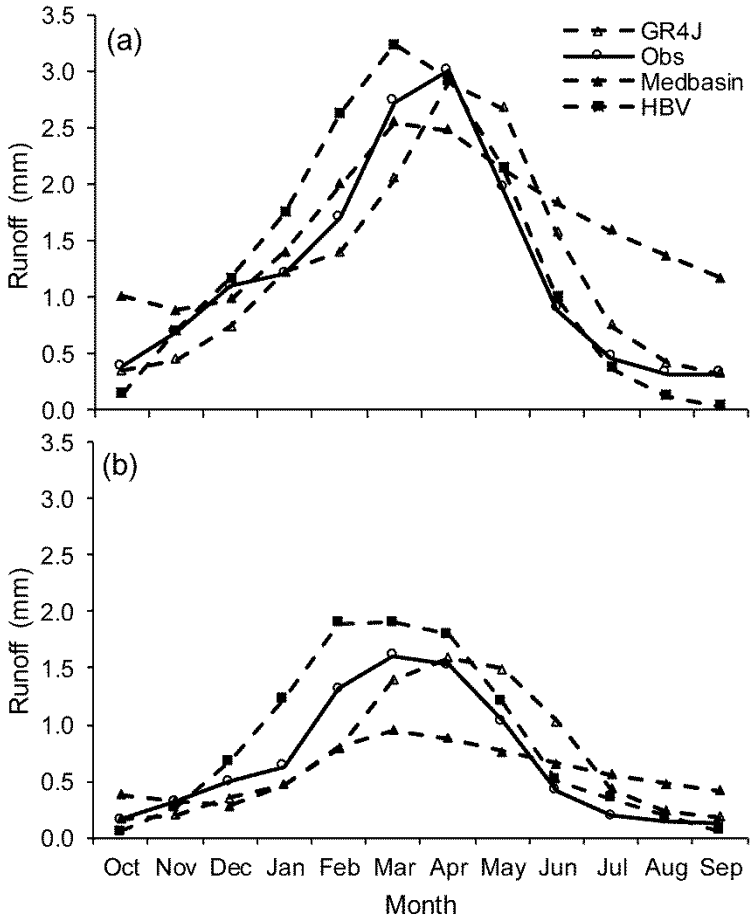

Figure 4.40 Monthly observed (Obs) and simulated runoff using Medbasin, Ge´nie Rural a Daily 4 parameters (GR4J), and Hydrologiska Byråns Vattenbalansavdelning (HBV) models at the Dokan hydrological station for the (a) 1979–1997; and (b) 1998–2013 periods

Accordingly, the use of multi-model simulations leads to the question of: "How the accuracy of a single model influences the accuracy of the results?" To address this question, the best performing model (B) and the worst performing one (W) were sequentially removed from consideration. The obtained results are shown in Figure 4.41, which indicates that the inclusion of all the calibrated models is necessary to obtain consistently good simulation results. This is because eliminating the best performing model would actually deteriorate the outcome (Figure 4.41b). However, excluding the worst performing model would enhance the monthly runoff (Figure 4.41a). This leads to the conclusion that the accuracy level of a single model can impact on the overall accuracy of the multi-model combination simulation. This confirms that the application of SAM in runoff estimation might produce values that are more precise than the results from the best of the three considered models, which justifies the implementation of the multi-model technique in the context of rainfall-runoff modeling.

Furthermore, there is a considerable change in the magnitude and timing of the peak discharge occurring between the two periods (Figure 4.41). The monthly discharge differences between two periods illustrate decreases mostly in May. The change in streamflow timing is mainly a result of the anthropogenic intervention. The obtained results regarding the shift in the magnitude and the timing of the river discharge are consistent with the results obtained from others within the study area (Cullen and deMenocal, 2000; Sen et al., 2011).

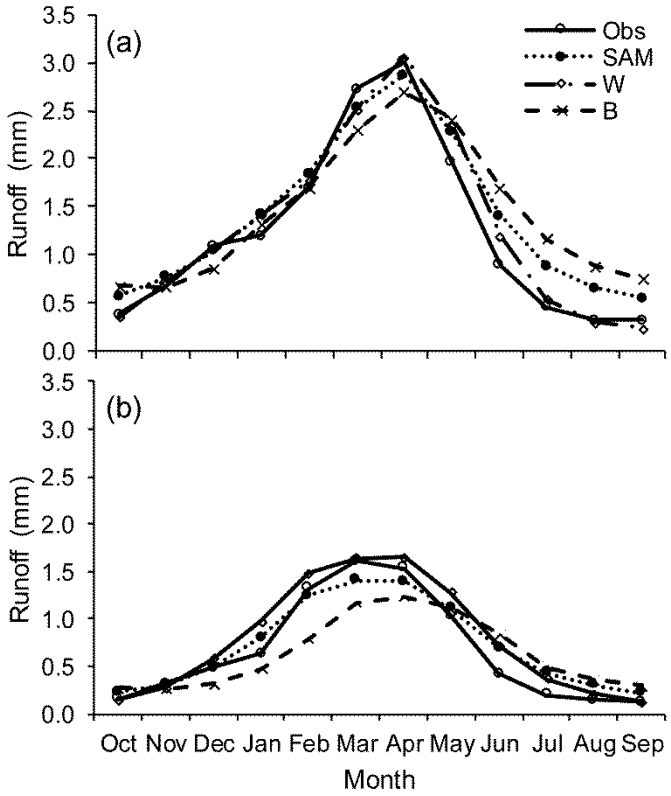

Figure 4.41 Monthly observed (Obs) and simulated runoff using simple average method (SAM), excluding the best model (B) results and eliminating the worst model results (W) for the Dokan hydrological station for the (a) 1979–1997; and (b) 1998–2013 periods

4.8 Climate Change Evaluation

This research characterises the climate change impact uncertainties linked to the planning of reservoirs utilising a methodology similar to that described by Soundharajan et al. (2016). The main variations between the two studies are that a rainfall-runoff model is used to simulate the streamflow series rather than stochastic modeling that as used by Soundharajan et al. (2016). In addition, Soundharajan et al. 2016 did not take into consideration the reservoir capacity-yield-

reliability relationships, which have been considered here. Consequently, the key purpose of this study is to assess the potential impacts of climate change on basin hydrology by considering the impacts of the reservoir operational probability of failure and storage in the water resources system on a typical example reservoir, which is the Dokan multi-purpose dam located in northern Iraq. This is a first attempt to derive the capacity-yield-reliability relationships that can be used to help water resources managers and decision makers to adapt for climate change by characterising the variability of reservoir storage and performance indices, Figure 4.42.

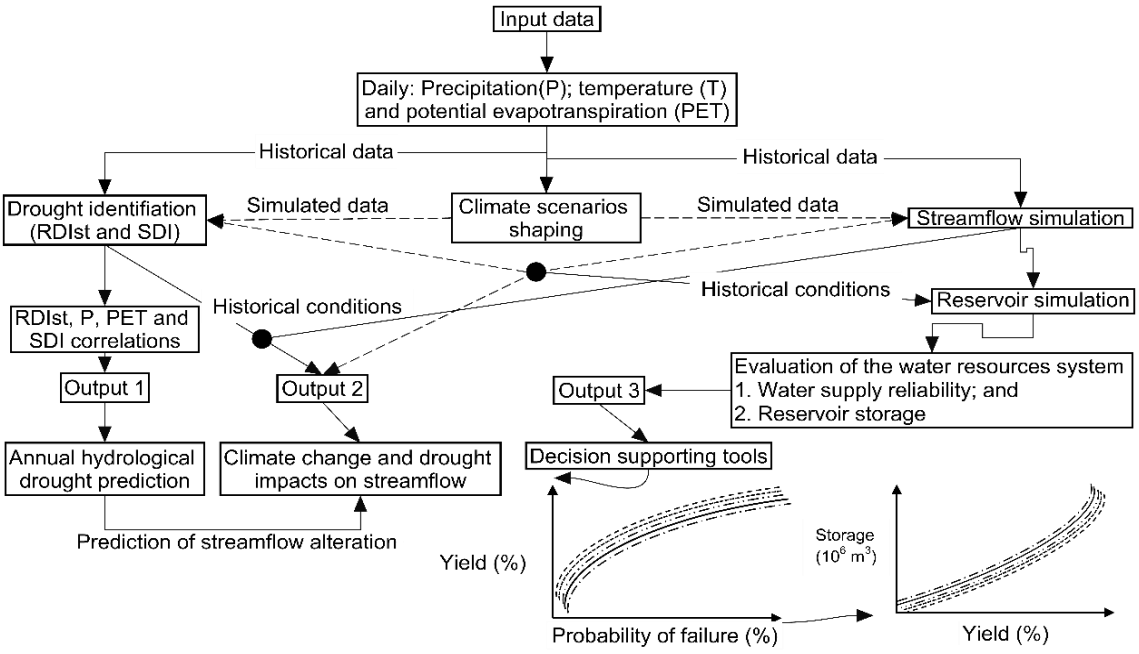

Figure 4.42 The detailed advancement of the objective seven

4.8.1 Rainfall-Runoff Simulation

To specify the normal climatic condition, thirty-five water years (1979–2013) were used, Figure 4.43. Subsequently, a period of twelve water years (1988–2000) is applied for calibration the HBV model and climate change scenarios, whereas 1979–1986 was the validation period. Figure 4.44 visulised the observed against simulated streamflow time series using HBV model for the calibration (1988–2000) and the validation time-periods (1979–1986), respectively.

The statistical performance statistics RMSE, IoA, r, and MAE during the calibration stage of the considered rainfall-runoff model, HBV, were 0.73, 0.99, 0.93, and 0.65, respectively. In comparison, the corresponding values were 0.68, 0.99, 0.84, and 0.60 during the validation period. Simulation results show promising outcomes emphasising that the simulation can be

confidentially applied for more studies, such as running the artificial climatic scenarios and estimating the relative alteration (%) in the average annual streamflow relative to the normal climatic condition. The simulated runoff for the studied period against the observed one is visualised in Figure 4.45. The coefficients associated with equations (3.25) and (3.26) are shown in Figure 4.46a, and Figure 4.46b in that order.

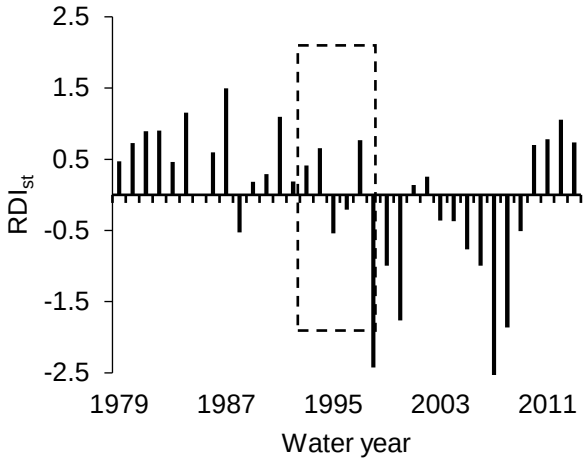

Figure 4.43 The selected time-period that represented (on average) the normal climatic conditions during which no extreme RDI_{st} values were recorded and when (on average) the RDI_{st} value is close to zero

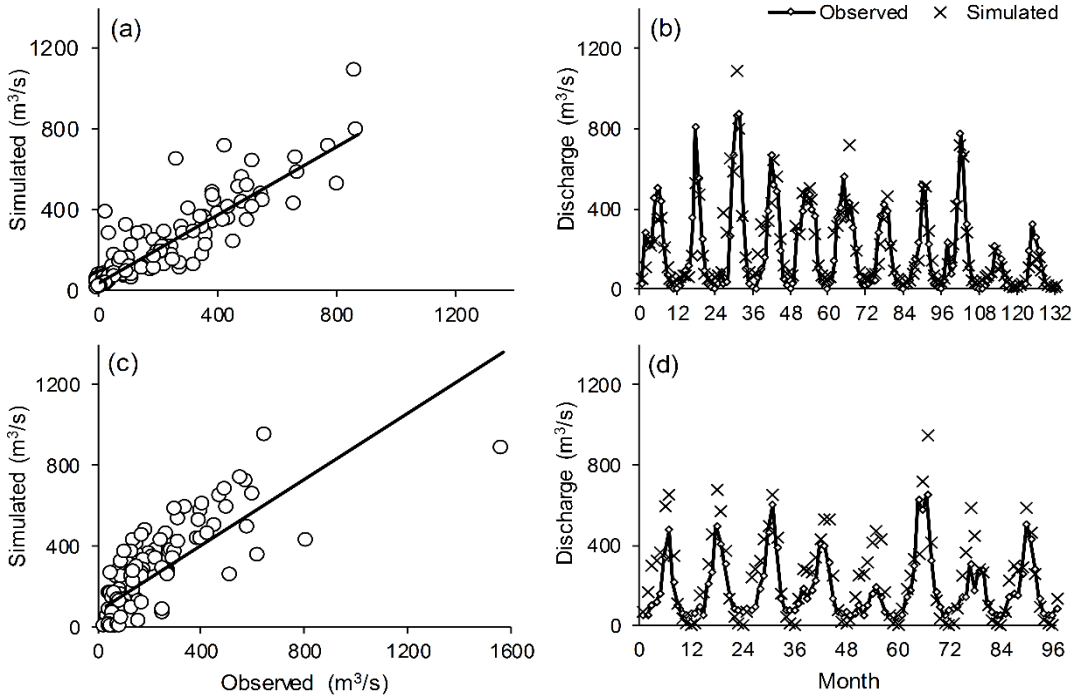

Figure 4.44 Observed against simulated streamflow time series using the Hydrologiska Byråns Vattenbalansavdelning model for (a) and (b) calibration period (1988/1989–1999/2000); and (c) and (d) validation period (1979/1980–1986/1987), respectively

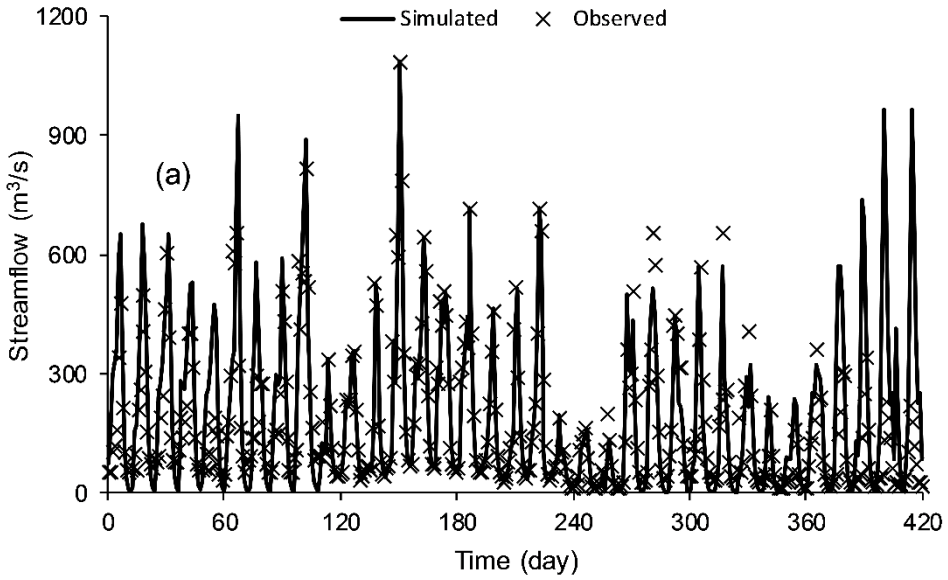

Figure 4.45 Observed against simulated streamflow time series using the Hydrologiska Byråns Vattenbalansavdelning model (Note that there was an outlier (1570 m^3/s), which has been removed

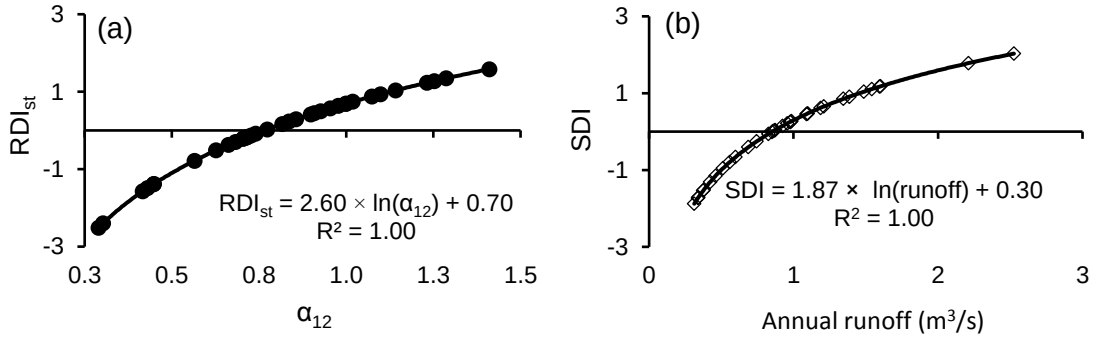

Figure 4.46 (a) Lower Zab River Basin (LZRB) anticipated relationship of the standard reconnaissance drought index (RDI_{st}) and RDI alpha form; (b) LZRB anticipated relationship of streamflow drought index (SDI) and runoff

4.8.2 LARS-WG5.5 Calibration and Validation

The daily weather data for the baseline (1980–2010) were used for LARS-WG5.5 calibration and validation at each of the ten meteorological stations. Some statistical tests and graphical comparison were utilised to evaluate the model. The Kolmogorov-Smirnov (K-S) test is implemented on analysis equivalence of the wet/dry series periodic distributions (WDSeries), daily rainfall distributions (RainD), daily minimum ($T_{min}D$) and maximum ($T_{max}D$) temperature distributions, respectively, computed from the observed and the downscaled data. The analysis estimates a *p*-value, which is utilised to accept or reject the hypotheses that the two sets of data could have stem from the same distribution (i.e. when there is no big change between the

recorded and the modeled climate for that parameter). A very low *p*-value and an equivalent high K-S value mean that the generated climate is unlikely to be similar to the recorded climate, therefore must be rejected. While a *p*-value of 0.05 is the common significant level applied in most statistics, it has suggested that a 0.01 *p*-value used as an acceptable limit of significance (Semenov et al., 2013). There are many reasons for the significant variations between the recorded and simulated data, such as that LARAS-WG model smoothing the recorded data, errors in the recorded data, random variation in the recorded data, and unusual climate phenomenon at a climate station making a specific year's weather very altered.

Assessment of the seasonal distributions of wet/dry spills and the daily rain distribution, in each month, considered very essentially, when applying the downscaling simulation outcomes in impact researches. Therefore, Table 4.16 and Table 4.17 show the K-S test results, during the validation stage, representing the model performance in modeling the seasonal recorded data and the daily rain in each month, respectively. Firstly, it is important to note that LARS-WG5.5 performs very well in fitting the seasonal distribution, as the fit of the wet/dry spells series are ranged from perfect to very good ($1 > p\text{-value} \geq 0.7$), Table 4.16. The performance of LARAS-WG5 in fitting of the wet/dry spells series distributions in the spring "MAM" (March, April, and May) season, is also evaluated as very good ($1 > p\text{-value} \geq 0.7$) to perfect ($p$-value = 1), for the distribution of the wet/dry spells in this order. Yet, the weather generator performance in the summer "JJA" (June, July, and August) season is slightly different. Despite the fact that the model performs perfect in fitting the dry spell distribution in winter "DJF" (December, January, and February), it performs good ($0.7 > p\text{-value} \geq 0.4$) to poor ($0.4 > p$-value) in fitting the wet spell one in many stations. The cause for the poor performance here attributed to the JJA season being a dry one. Since there is no or rare rainfall observed in this season, the model would not be capable of fitting any wet spell and as a result, it would implement poorly. Furthermore, Table 4.17 shows that LARS-WG5.5 performance in modeling distributions of the daily rain, in all months, is ranged from very good to perfect except in the summer season which can be attributed to the same reason for the poor performance in simulating the seasonal distributions that given previously.

To increase the confidence level of the prediction capability of the model, comparisons between the monthly mean and standard deviation (SD) of the observed and the generated precipitation have been implemented for all stations. Figure 4.47 shows that there are good matches between

the modeled and the recorded precipitation in the whole stations. Still, the performance of SD is not as good as that of the average, but the outcomes can be considered reasonably good, as it is identified as being hard to model well SD in most downscaling researches. Moreover, Figure 4.48 shows that LARS-WG5.5 simulated T_{max} and T_{min} monthly mean values very well, which verifies that this version of LARS-WG has a good capability in predicting the extreme air temperature.

From the above, it can urge that the model has a good performance in producing daily precipitation, T_{min}, and T_{max} in most stations and it can be then utilised to predict daily weather values for the ten stations for three future periods of 2011–2030, 2046–2065, and 2080–2099 depending on the seven ensembles GCM and SRA2 scenario.

Table 4.16 The Long Ashton Research Station Weather Generator (LARS-WG5.5) validation results including Kolmogorov-Smirnov (K-S) test (see section 3.5.10) for seasons of wet and dry years series distributions during baseline period of 1980–2010

Sub-basin	Sit name	Seasons for wet years							
		DJF[c]		MAM[d]		JJA[e]		SON[f]	
		K-S	*p*-value	K-S	*p*-value	K-S	*p*-value	K-S	*p*-value
US[a]	Sulymanya	0.278	0.286[4]	0.037	1.000[1]	0.162	0.897[2]	0.158	0.913[2]
	Halabcha	0.336	0.117[4]	0.386	0.047[4]	0.218	0.590[3]	0.243	0.449[3]
	Sachez	0.252	0.403[3]	0.099	1.000[1]	0.137	0.973[2]	0.030	1.000[1]
	Mahabad	0.064	1.000[1]	0.138	0.971[2]	0.326	0.139[4]	0.133	0.979[2]
	Salahddin	0.357	0.082[4]	0.347	0.097[4]	0.093	1.000[1]	0.081	1.000[1]
	Soran	0.215	0.607[3]	0.036	1.000[1]	0.150	0.940[2]	0.128	0.986[2]
DS[b]	Kirkuk	0.490	0.005[4]	0.009	1.000[1]	0.078	1.000[1]	0.126	0.989[2]
	Makhmoor	0.074	1.000[1]	0.190	0.755[2]	0.156	0.920[2]	0.173	0.847[2]
	Erbeel	0.225	0.549[3]	0.094	0.999[2]	0.844	0.000[4]	0.357	0.082[4]
	Chemchamal	0.097	0.999[1]	0.103	0.999[2]	0.175	0.837[2]	0.230	0.520[3]
Sub-basin	Site name	Seasons for dry years							
		DJF[c]		MAM[d]		JJA[e]		SON[f]	
		K-S	p-value	K-S	p-value	K-S	p-value	K-S	p-value
US[a]	Sulymanya	0.037	1.000[1]	0.046	1.000[1]	0.138	0.971[2]	0.066	1.000[1]
	Halabcha	0.040	1.000[1]	0.097	0.999[2]	0.219	0.584[3]	0.110	0.998[1]
	Sachez	0.030	1.000[1]	0.127	0.987[2]	0.057	1.000[1]	0.111	0.998[2]
	Mahabad	0.057	1.000[1]	0.042	1.000[1]	0.084	1.000[1]	0.210	0.637[3]
	Salahddin	0.030	1.000[1]	0.036	1.000[1]	0.123	0.991[2]	0.053	1.000[1]
	Soran	0.032	1.000[1]	0.050	1.000[1]	0.078	1.000[1]	0.135	0.976[2]
DS[b]	Kirkuk	0.896	0.000[4]	0.114	0.997[2]	0.169	0.866[2]	0.114	0.997[2]
	Makhmoor	0.868	0.000[4]	0.200	0.697[3]	0.311	0.176[4]	0.112	0.998[2]
	Erbeel	0.152	0.934[2]	0.101	0.999[2]	0.228	0.531[3]	0.120	0.994[1]
	Chemchamal	0.053	1.000[1]	0.041	1.000[1]	0.049	1.000[1]	0.045	1.000[1]

[a]Upstream; [b]Downstream; [c]Winter season (Dec, Jan, and Feb); [d]Spring season (Mar, Apr, and May); [e]Summer season (Jun, Jul, and Aug); [f]Autumn season (Sep, Oct, and Nov); [1]Perfect fit (*p*-value = 1); [2]Very good fit (1 > *p*-value ≥ 0.7); [3]Good fit(0.7 > *p*-value ≥ 0.4); [4]Poor fit (0.4 > *p*-value)

Table 4.17 The Long Ashton Research Station Weather Generator (LARS-WG5.5) validation results including Kolmogorov-Smirnov (K-S) test (see section 3.5.10) for daily rain distributions during the baseline period of 1980–2010

Sub-basin	Station name	January		February		March		April	
		K-S	*p*-value	K-S	*p*-value	K-S	*p*-value	K-S	*p*-value
US[a]	Sulymanya	0.125	0.989[2]	0.343	1.000[1]	0.038	1.000[1]	0.024	1.000[1]
	Halabcha	0.076	1.000[1]	0.215	0.607[3]	0.113	0.997[2]	0.082	1.000[1]
	Sachez	0.035	1.000[1]	0.088	1.000[1]	0.035	1.000[1]	0.025	1.000[1]
	Mahabad	0.045	1.000[1]	0.106	0.999[2]	0.088	1.000[1]	0.036	1.000[1]
	Salahddin	0.144	0.957[2]	0.176	0.832[2]	0.038	1.000[1]	0.226	0.543[3]
	Soran	0.100	0.999[2]	0.060	1.000[1]	0.093	0.999[2]	0.062	1.000[1]
DS[b]	Kirkuk	0.083	1.000[1]	0.068	1.000[1]	0.032	1.000[1]	0.035	1.000[1]
	Makhmoor	0.041	1.000[1]	0.060	1.000[1]	0.048	1.000[1]	0.145	0.954[2]
	Erbeel	0.048	1.000[1]	0.048	1.000[1]	0.118	0.995[2]	0.022	1.000[1]
	Chemchamal	0.064	1.000[1]	0.095	0.999[2]	0.137	0.973[2]	0.038	1.000[1]
Sub-basin	Station name	May		June		July		August	
		K-S	*p*-value	K-S	*p*-value	K-S	*p*-value	K-S	*p*-value
US[a]	Sulymanya	0.117	0.995[2]	0.325	0.141[4]	0.696	0.000[4]	0.268	0.328[4]
	Halabcha	0.030	1.000[1]	0.696	0.000[4]	0.653	0.000[4]	0.261	0.359[4]
	Sachez	0.208	0.649[3]	0.212	0.625[3]	0.696	0.000[4]	0.478	0.006[4]
	Mahabad	0.169	0.866[2]	0.108	0.999[2]	0.020	1.000[1]	0.037	1.000[1]
	Salahddin	0.154	0.927[1]	0.184	0.789[2]	1.000	0.000[4]	0.696	0.000[4]
	Soran	0.195	0.726[2]	0.069	1.000[1]	0.021	1.000[1]	0.066	1.000[1]
DS[b]	Kirkuk	0.177	0.826[2]	0.348	0.096[1]	[c](-)	[c](-)	1.000	0.000[4]
	Makhmoor	0.095	0.999[2]	0.522	0.002[4]	1.000	0.000[4]	1.000	0.000[4]
	Erbeel	0.025	1.000[1]	0.083	1.000[1]	[c](-)	[c](-)	0.957	0.000[4]
	Chemchamal	0.018	1.000[1]	0.117	0.995[2]	0.175	0.836[2]	0.739	0.000[4]
Sub-basin	Station name	September		October		November		December	
		K-S	*p*-value	K-S	*p*-value	K-S	*p*-value	K-S	*p*-value
US[a]	Sulymanya	0.184	0.789[2]	0.032	1.000[1]	0.143	0.960[2]	0.060	1.000[1]
	Halabcha	0.073	1.000[1]	0.077	1.000[1]	0.246	0.433[3]	0.242	0.454[3]
	Sachez	0.116	0.996[2]	0.021	1.000[1]	0.035	1.000[1]	0.090	1.000[1]
	Mahabad	0.023	1.000[1]	0.068	1.000[1]	0.093	0.999[2]	0.119	0.994[2]
	Salahddin	0.204	0.196[4]	0.276	0.294[4]	0.171	0.856[2]	0.061	1.000[1]
	Soran	0.057	1.000[1]	0.070	1.000[1]	0.034	1.000[1]	0.219	0.584[3]
DS[b]	Kirkuk	0.522	0.002[4]	0.195	0.726[2]	0.151	0.937[2]	0.185	0.783[2]
	Makhmoor	0.248	0.423[3]	0.030	1.000[1]	0.040	1.000[1]	0.040	1.000[1]
	Erbeel	0.319	0.155[4]	0.182	0.799[2]	0.038	1.000[1]	0.042	1.000[1]
	Chemchamal	0.557	0.001[4]	0.038	1.000[1]	0.107	0.999[2]	0.035	1.000[1]

[a]Upstream; [b]Downstream; [c]Below the detected limit; [1]Perfect fit (*p*-value = 1); [2]Very good fit (1 > *p*-value ≥ 0.7); [3]Good fit(0.7 > *p*-value ≥ 0.4); [4]Poor fit(0.4 > *p*-value)

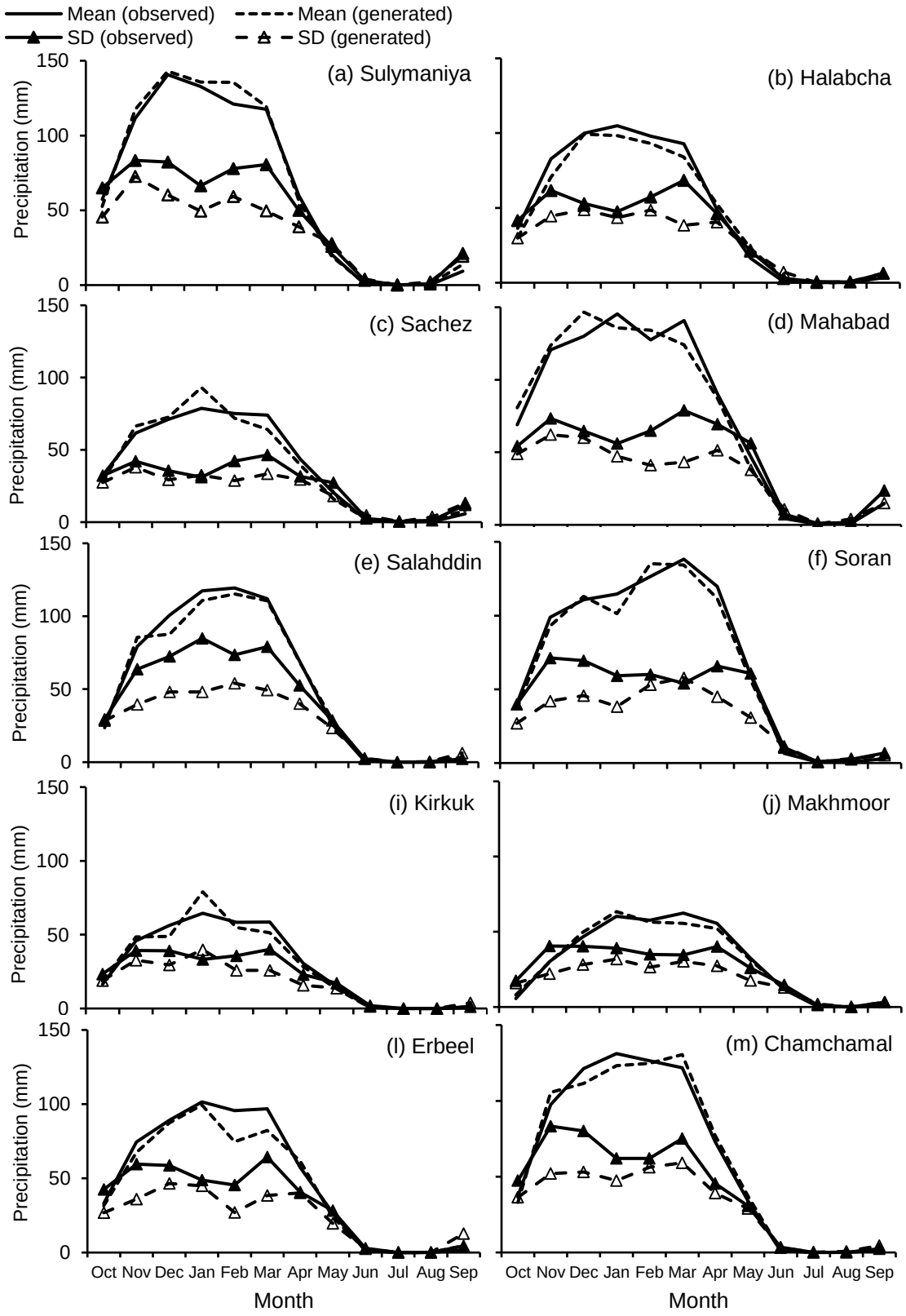

Figure 4.47 Comparison between observed monthly (mean and standard deviation (SD)) precipitation (P) and the corresponding values that generated by LARS-WG5.5 at each meteorological station within the studied basin for the time-period 1980–2010

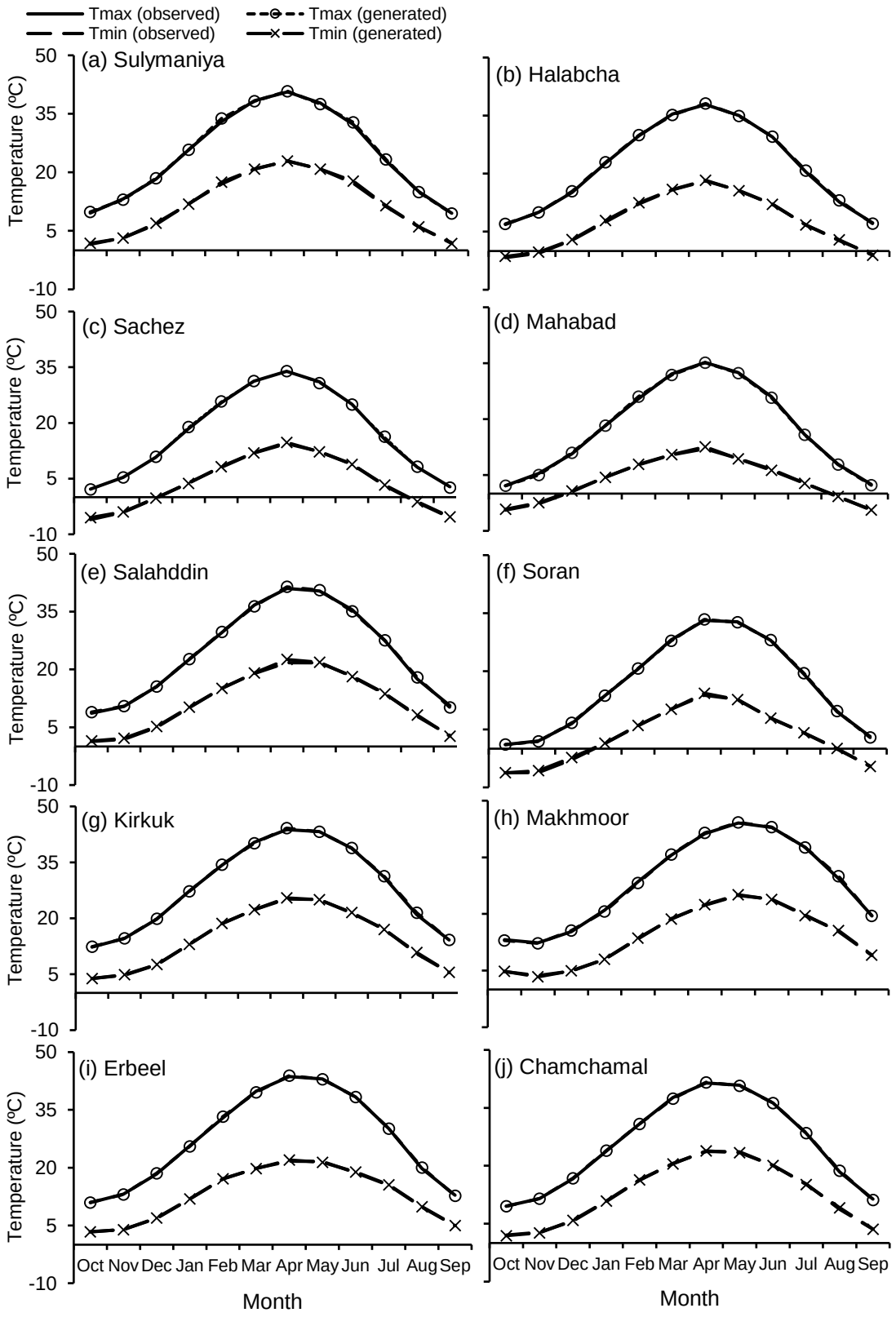

Figure 4.48 Comparison between observed mean monthly (maximum (T_{min}) and minimum (T_{max})) temperature and the corresponding values that generated by LARS-WG5.5 at each meteorological station within the studied basin for the baseline (1980–2010)

4.8.3 Meteorological Variables

Figure 4.9 shows the values of the mean meteorological variables resulted from seven ensembles GCM under SRA2 emission scenario for the three considered future periods. In general, there will be an increasing trend in both T_{min} and T_{max} and a decreasing trend in the P values, and the relative monthly change varies from month to month. The maximum increase in the predicted T_{min} will be varied between 0.54, 3.02, and 4.36 °C, for the three future periods, respectively, Figure 4.9a. The Tmax also predicted to increase with a maximum value of 0.56, 2.49, and 4.70 ºC for the future periods, respectively, Figure 4.9b. The reduction in the precipitation amounts changed between 6.32, 17.33, and 340.18 mm, respectively, Figure 4.9c.

The ensemble means of weather data estimates from seven GCM computed to further clarify the future change during the three periods, and the outcomes were visualised in Figure 4.50. Figure 4.50 (a, b, and c), Figure 4.50 (d, e, and f), and Figure 4.50 (g, h, and i) show the box-whisker plots for Tmin, Tmax, and P distribution data, respectively, that downscaled based on seven ensembles GCM by LARS-WG5.5 in the three considered future time-periods (2011–2030), (2046–2065), and (2080–2099), respectively. Each box-whisker plot denotes the estimate from one GCM. For the period 2080–2099, it has been noticed that there are no logical change trends among several GCM for precipitation predictions. The precipitation predictions from GFCM21, HADCM3, INCM4, IPCM4, and MPEH5 are less than the values of the baseline period. However, T_{min} and T_{max} predictions from all GCM are more than the baseline (1980–2010) period values and showed small differences of the predictions from the seven GCM, which shows that there are small variations in calculating the future extreme temperature by using only one GCM. Unlike 2080–2099 simulations, the predictions of the other two periods from these seven GCM have logical change trends. The predictions of T_{min} and T_{max} are higher than the baseline (1980–2010) period and the temperature predictions from seven GCM have rising trends, in particular, for the periods of 2080–2099 compared to the baseline (1980–2010) climate.

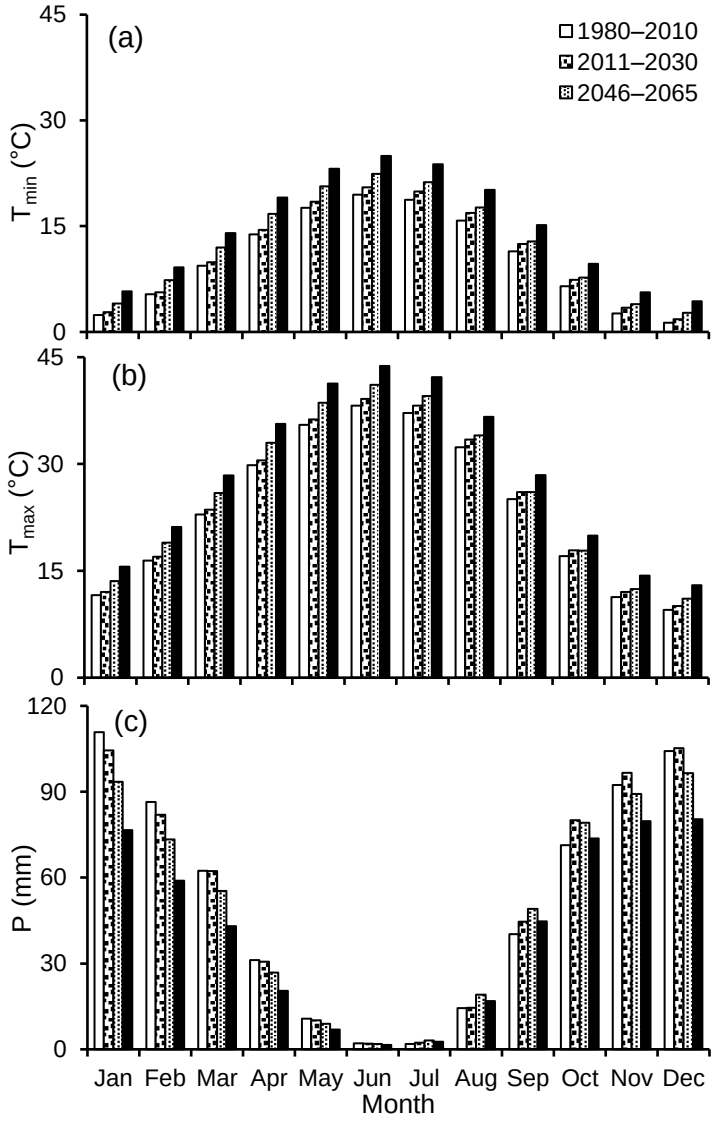

Figure 4.49 Mean monthly (a) minimum temperature (T_{min}); (b) maximum temperature (T_{max}); and (c) precipitation (P), for the baseline (1980–2010), 2010–2030, 2046–2065, and 2080–2099 time-periods that downscaled for seven ensemble general circulation models

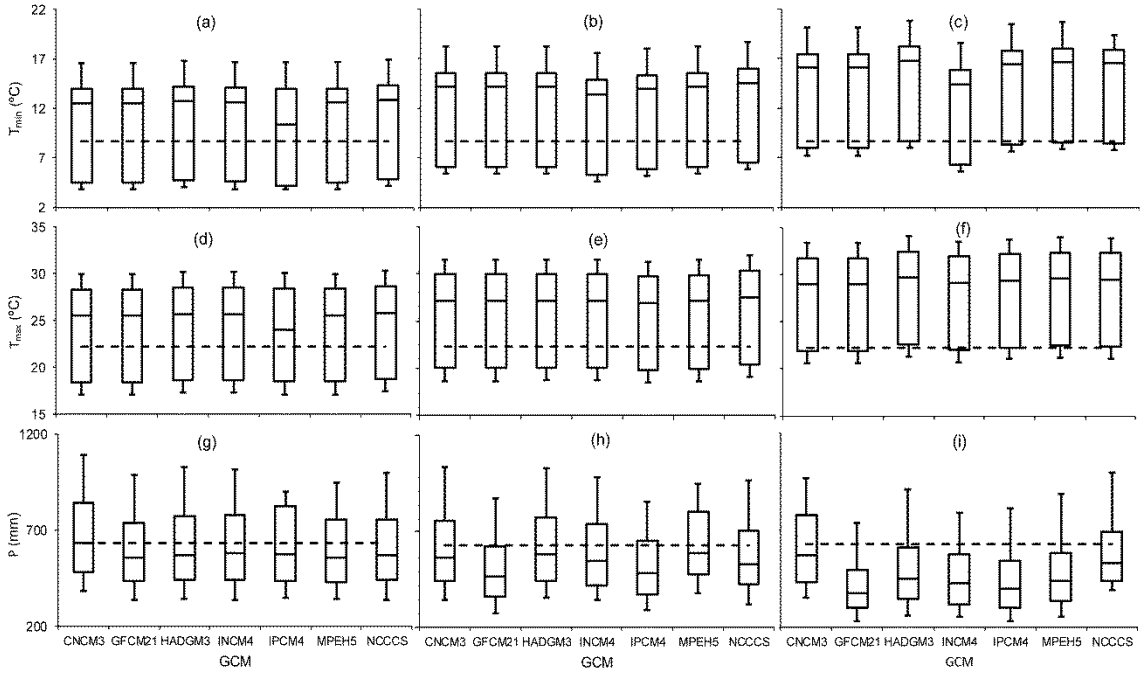

Figure 4.50 Box plot shows the changes in (a), (b), and (c) minimum temperature (T_{min}); (d), (e), and (f) maximum temperature (T_{max}); and (g), (h), and (i) precipitation over the studied basin downscaled from seven GCM using LARS-WG5.5 during the time horizon 2011–2030, 2046–2065, and 2080–2099 compared to the baseline period (1980–2010)

4.8.4 Drought Identification

Figure 4.43 and Figure 4.51 show the selected period for running the DP climate scenario and the alterations in surface runoff simulated by some of the DP climate change scenarios, respectively. A substantial reduction in the inflow to the reservoir would result from climate change. For example, a change of almost 21% in terms of streamflow is expected for an anticipated climate conditions of 10% P reduction and 30% PET increase, which indicated that there is a crucial requirement for pro-active strategies and actions to mitigate climate change influence, anthropogenic intervention, and drought events. Figure 4.52a and Figure 4.52b demonstrate that the anticipated relationships between RDI_{st} and SDI are subject to the potential impact of future P reduction under the collective effects of potential evapotranspiration, and such relationships are very robust with (R^2 = 1.00). Furthermore, Figure 4.52c demonstrates how the change in the hydrological drought index depends on the change in the corresponding meteorological drought.

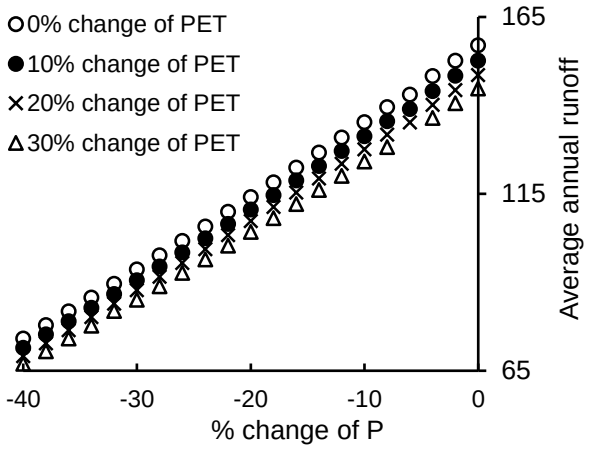

Figure 4.51 The Lower Zab River Basin anticipated (%) streamflow change for selected delta perturbation climatic scenarios. Note: PET is the potential evapotranspiration

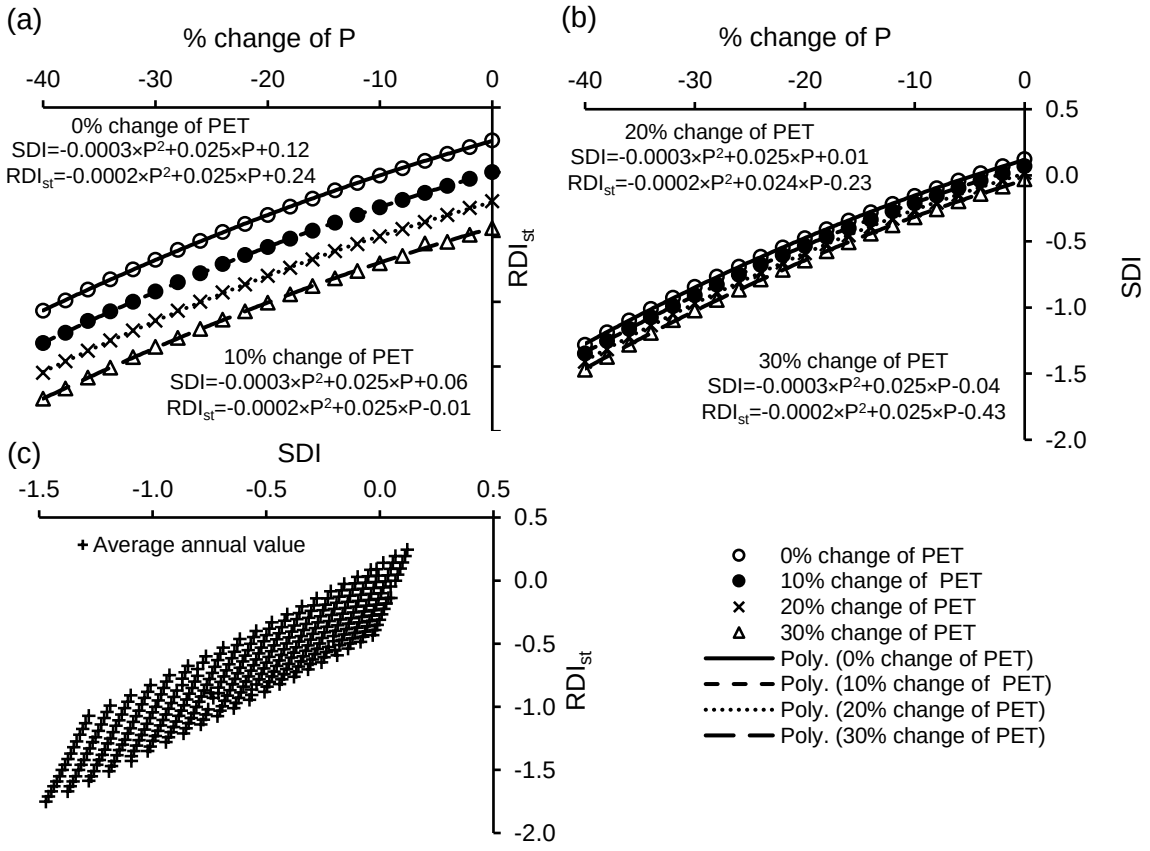

Figure 4.52 Anticipated: (a) standardised reconnaissance drought index (RDI_{st}); (b) streamflow drought index (SDI); and (c) relationship between RDI_{st} and SDI, for Lower Zab River Basin for each delta perturbation scenario. Note: PET is the potential evapotranspiration

Furthermore, to assess the occurrence of the hydro-climatic drought events under GCM scenarios, RDI_{st} and SDI were calculated using the observed and the simulated precipitation, runoff, and potential evapotranspiration data. Figure 4.53 (a and b), Figure 4.50 (c and d), and Figure 4.50 (e and f) present the indices calculated for the baseline (1980–2010), 2011–2030, 2046–2065, and 2080–2099 periods, respectively, that incorporated with the long-term average precipitation (P_{av}) and potential evapotranspiration. A non-regular cyclical configuration of drought and rainy times was detected during all the periods. Hydro-climatic drought phenomena usually increase as precipitation decrease and potential evapotranspiration increase and vice versa. This phenomenon usually happens at the beginning of the rainy season, which reflected by either a decline in precipitation coupled with potential evapotranspiration increase or a delay in precipitation events. In addition, it is anticipated that the severity of drought will dramatically worsen over the coming future. In particular, during the time horizon 2080–2099, the drought severity will increase as the number of months with extended periods of precipitation shortages and potential evapotranspiration growths increase.

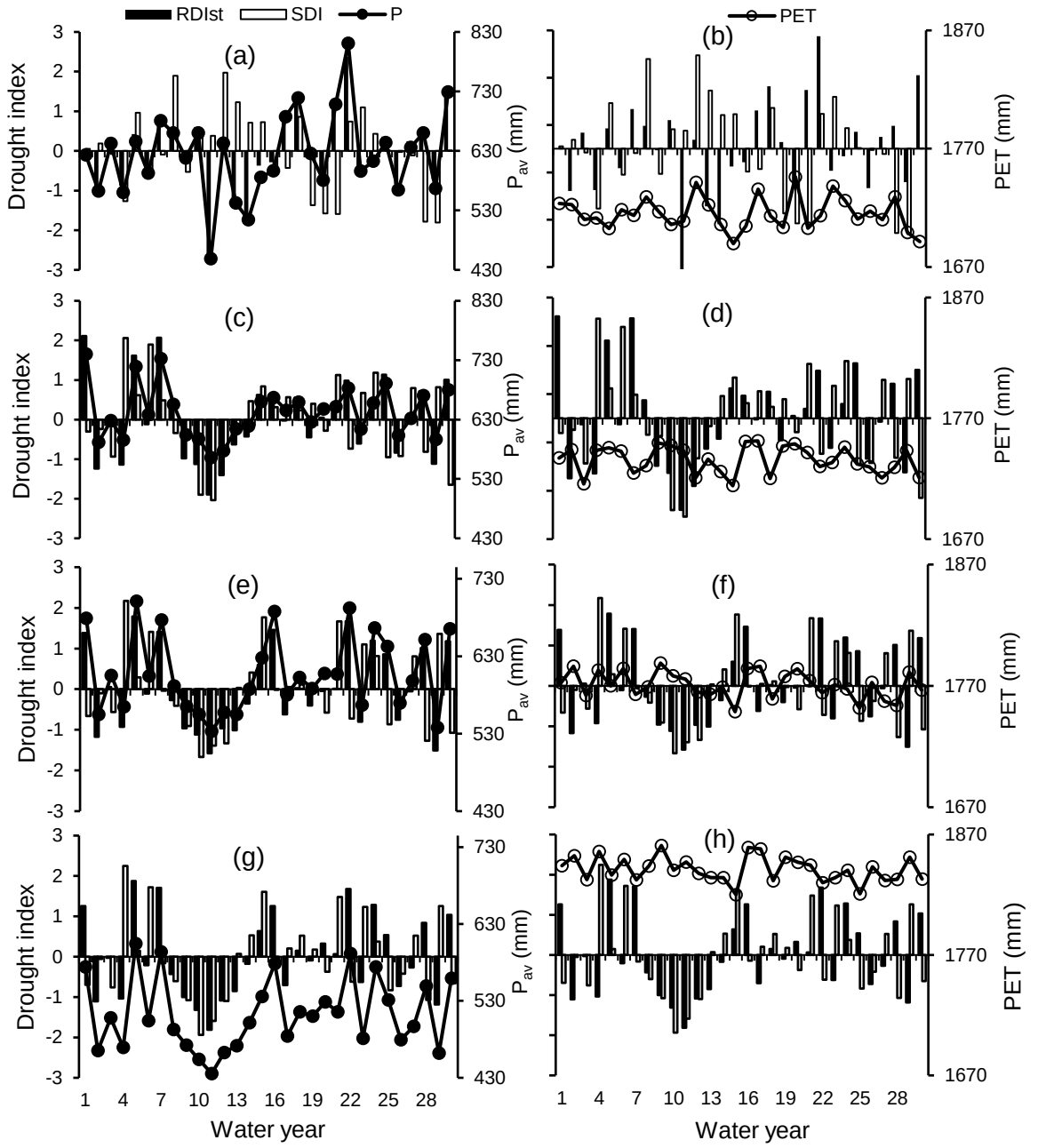

Figure 4.53 Temporal variations of the annual standardised reconnaissance drought index (RDI_{st}) and annual streamflow index (SDI) coupled with the long-term average precipitation (P_{av}) (left graphs) and potential evapotranspiration (PET) (right graphs) for: (a) and (b) baseline (1980–2010); (c) and (d) 2011–2030; (e) and (f) 2046–2065; and (g) and (h) 2080–2099 time horizons, respectively, under the General Circulation Models, over the representative basin

4.8.5 Hydrologic Alteration

4.8.5.1 Delta Perturbation Scenario

Many temporal annual extreme values (i.e. 1-, 3-, 7-, 30-, and 90-days) were estimated for the baseline and climate change scenarios. For group #1, the hydrologic alteration stretched between minimum to maximum. Low levels were noticed in October, March, April, May, and September (Table 4.18). A positive minimum level of alteration was detected in June. A moderate alteration was observed in April for nearly all scenarios with alterations of about -59, -60, and -62% for the F_{10} (20% reduction in P linked with 10% increase in PET); F_{11} (20% reduction in P linked with 20% increase in PET); and F_{12} (20% reduction in P linked with 30% increase in PET) climate change scenario examples, respectively, (Table 4.18). For group #2, the extreme minimum flows exhibited low anomalies. A low anomaly of about -36% was linked to a 30-day minimum flow for F_{12} scenario (20% reduction in P linked with a 30% increase in PET). Regarding the extreme maxima flows, group #2 experienced modest to high alterations. Moderate to high alterations varied from -59 to -73% associated with the 1-day maximum flow for the considered scenarios. The 3-, 7-, and 30-day maxima flows were associated also with moderate to high alterations of -52 to -68%, -46 to -64%, and -42 to -61%, respectively. Low to moderate alterations of -30 and -52% were linked to 90-days.

The temporal percentiles usually represent the potential changes in the basin hydrological characteristics, so that it can be considered as a vital statistical tool. In this study, five temporal percentiles (10^{th}, 25^{th}, 50^{th}, 75^{th}, and 90^{th}), which span the maximum streamflow thresholds, were estimated for the baseline and the climate change scenarios. The estimation results are illustrated in Figure 4.54 for the baseline and the two climate change scenario examples. Figure 4.54a explains that the monthly flow was equivalent to or surpassed the threshold at 10% of the period exhibiting falls ranging between -42 and -53% (May) to between -42 and -54% (September). December, January, and February indicated positive anomalies ranging from 80 to 46% (December) and from 48 to 18% (January) for the two climate change scenario examples, respectively (Figure 4.54b). For the 25^{th} monthly percentiles, the departures were between -43 and -53% (October) to between -49 and -60% (November), Figure 4.54b. However, January, February, and June witnessed positive shifts of 16, 15, and 25% in this order,

based on the first climatic scenario example. The abnormalities related to the monthly median flows (Figure 4.54c) extended between -7 (November) and -12% (February) to between -57 and -64% (April) for the two climate change scenarios, respectively. January experienced positive anomalies.

In contrast to the 75th percentile as shown in Figure 4.54d, the lowest anomalies were observed in January (-9%) and in October (-19%) for the two climate change scenario examples in this order, while the highest drops of between -58 and -65% were associated to April. The 90th monthly percentiles, as Figure 4.54e reveals, were between -70 and -75% (April), between -71 and -76 (May), and between -56 and -64% (June), respectively. The results suggest that climate change will have an adverse impact on the basin in terms of water resources.

Table 4.18 Hydrologic alteration for the middle range of variability approach (RVA) category of the Lower Zab River

Degree of hydrologic alteration (%)												
Month	F_1[a]	F_2[b]	F_3[c]	F_4[d]	F_5[e]	F_6[f]	F_7[g]	F_8[h]	F_9[i]	F_{10}[j]	F_{11}[k]	F_{12}[l]
Parameter group #1 (comprising of monthly median discharge values)												
Oct	-17[m]	-19[m]	-22[m]	-24[m]	-30[m]	-32[m]	-34[n]	-36[n]	-43[n]	-44[n]	-46[n]	-48[n]
Nov	36	32	27	23	14	10	6	3	-7[m]	-11[m]	-14[m]	-16[m]
Dec	41	18	14	10	3	-1[m]	-5[m]	-8[m]	-15[m]	-19[m]	-22[m]	-25[m]
Jan	90	86	83	79	61	58[n]	55	52	34	31	28	25
Feb	48	47	44	41	29	26	23	20	8	6	3	1
Mar	-14[m]	-16[m]	-18[m]	-20[m]	-25[m]	-27[m]	-30[m]	-31[m]	-37[n]	-39[n]	-40[n]	-42[n]
Apr	-41[n]	-43[n]	-45[n]	-47[n]	-49[n]	-51[n]	-53[n]	-54[n]	-57[n]	-59[n]	-60[n]	-62[n]
May	-17[m]	-18[m]	-20[m]	-22[m]	-27[m]	-29[m]	-31[m]	-32[m]	-38[n]	-40[n]	-41[n]	-43[n]
Jun	15	12	9	7	0	-3[m]	-6[m]	-8[m]	-15[m]	-18[m]	-20[m]	-22[m]
Jul	91	83	59	70	64	58	51	45	39	33	27[m]	22[m]
Aug	44	38	19	28	24	19	14	10	5	0	-4[m]	-8[m]
Sep	-11[m]	-15[m]	-22[m]	-21[m]	-24[m]	-27[m]	-30[m]	-33[m]	-36[n]	-39[n]	-41[n]	-44[n]
Parameter group #2 (magnitude and duration of annual extreme)												
n	n-day minimum											
1	0[m]	-5[m]	-8[m]	-11[m]	-16[m]	-19[m]	-22[m]	-24[m]	-30[m]	-32[m]	-35[n]	-37[n]
3	-1[m]	-6[m]	-9[m]	-12[m]	-17[m]	-20[m]	-22[m]	-25[m]	-30[m]	-33[m]	-35[n]	-37[n]
7	-9[m]	-13[m]	-16[m]	-19[m]	-23[m]	-26[m]	-29[m]	-31[m]	-36[n]	-38[n]	-40[n]	-42[n]
30	-3[m]	-6[m]	-22[m]	-11[m]	-16[m]	-19[m]	-21[m]	-24[m]	-29[m]	-31[m]	-34[n]	-36[n]
90	28[m]	20[m]	15[m]	12[m]	5[m]	2[m]	-1[m]	-4[m]	-12[m]	-15[m]	-18[m]	-20[m]
n	n-day maximum											
1	-59[n]	-60[n]	-61[n]	-62[n]	-65[n]	-66[n]	-67[n]	-68[o]	-70[o]	-71[o]	-72[o]	-73[o]
3	-52[n]	-53[n]	-54[n]	-56[n]	-58[n]	-60[n]	-61[n]	-62[n]	-65[n]	-66[n]	-67[n]	-68[o]
7	-46[n]	-48[n]	-49[n]	-50[n]	-54[n]	-55[n]	-56[n]	-57[n]	-61[n]	-62[n]	-63[n]	-64[n]
30	-42[n]	-44[n]	-45[n]	-47[n]	-50[n]	-51[n]	-53[n]	-54[n]	-58[n]	-59[n]	-60[n]	-61[n]
90	-30[m]	-30[m]	-32[m]	-34[n]	-38[n]	-40[n]	-42[n]	-43[n]	-48[n]	-49[n]	-51[n]	-52[n]
BFI[p]	8[m]	6[m]	6[m]	6[m]	7[m]	7[m]	7[m]	7[m]	7[m]	7[m]	7[m]	7[m]

[a, b, c, and d](0% reduction in precipitation (P) linked with 0, 10, 20, and 30% increase in potential evapotranspiration (PET), respectively); [e, f, g, and h](10% reduction in P linked with 0, 10, 20, and 30% increase in PET, respectively); [i, j, k, and l](20% reduction in P linked with 0, 10, 20, and 30% increase in PET, respectively). Degree of alteration: [m]Slight (≤ 33); [n]Modest (34 < > 67); [o]High (≥ 67), [p]Baseflow index

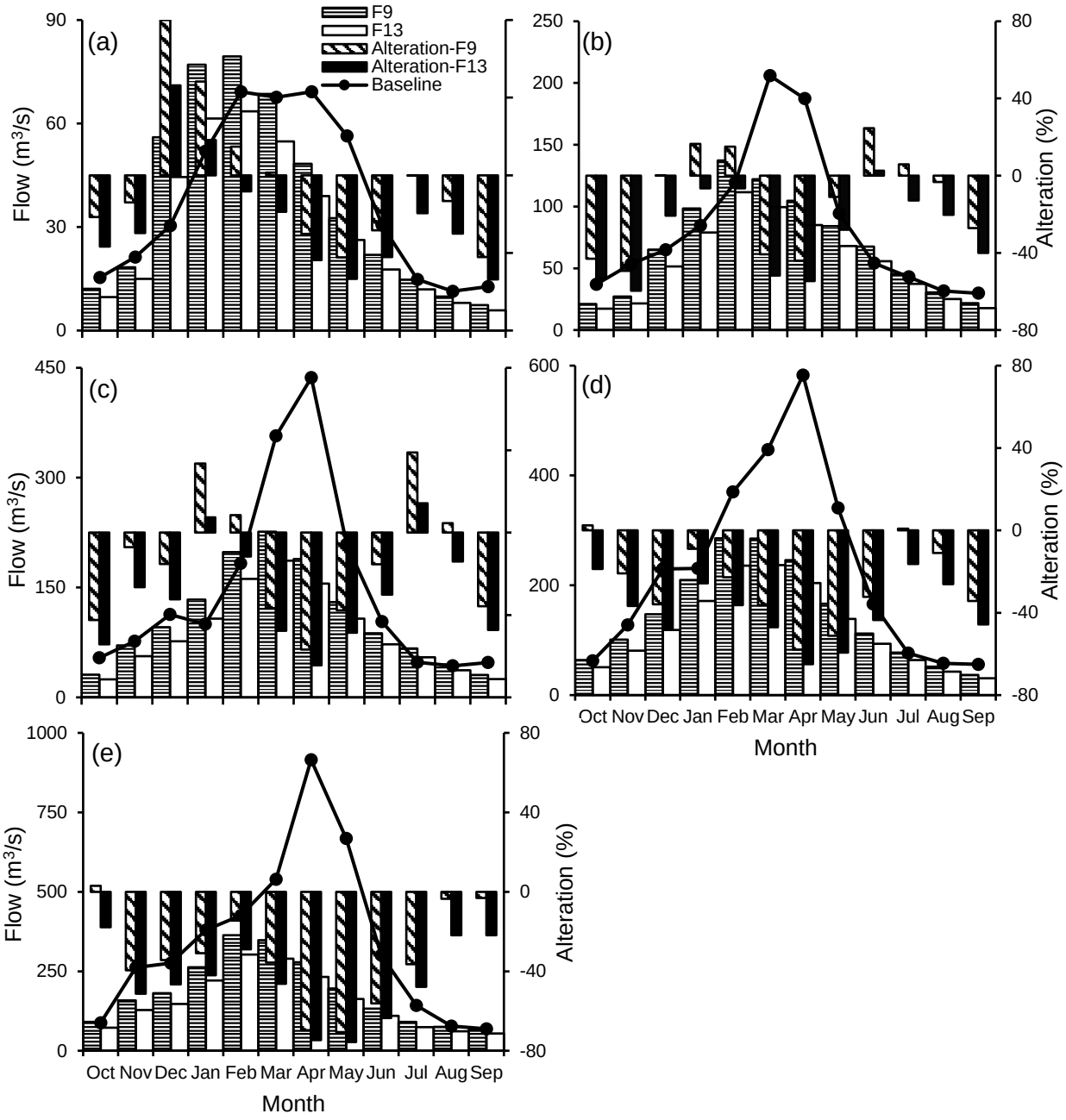

Figure 4.54 Comparison of monthly percentiles between the baseline (1988—2000) and two future climate change scenario examples, which are F_9 (20% reduction in precipitation (P) linked with 0% increase in potential evapotranspiration (PET)) and F_{13} (30% reduction in P linked with 0% increase in PET) coupled with the alteration ratio for the (a) 10^{th}; (b) 25^{th}; (c) 50^{th}; (d) 75^{th}; and (e) 90^{th} percentiles

Moreover, the long-term median monthly streamflow of the baseline and the six climate change scenario examples are illustrated in Figure 4.55. For the baseline (1988—2000), the median flows varied from 43 (September) to 437 m^3/s (April). In comparison, the median flows for the six different climate change scenarios were between 36, 35, 31, 29, 25 and 24 m^3/s (September), and 267, 259, 226, 219, 187, and 181 m^3/s (March), respectively. The noticeable alterations indicate dramatic signatures of the climate change pressures in the basin, which would reduce the basin water resources availability. In addition, Figure 4.55b reveals the overall impact of climate change on the seasonal median flows within the LZRB.

Table 4.19 shows that the long-term median annual streamflow for the baseline and the two climate change scenario examples were estimated at 146, 140, and 117 m^3/s in this order, representing a departure between -4 and -20%. The baseline median flows extended from 43 (August) to 437 m^3/s (April), whereas the corresponding values were between 36 and 31 m^3/s (September) and between 267 and 226 m^3/s (March) for the two climate change scenario examples. The months March, April, and October were related to substantial alterations fluctuating between -25 and -57%. Substantial alterations (mainly during the rainy seasons) illustrate considerable signs of the common impact of climate change, which noticeably would diminish the basin water resources. The 25^{th} percentile anomalies varied between -9 and -23% (May) and between -42 and -52% (November), revealing considerable deviation from the baseline condition. In relation to the 75^{th} percentile, the departures were between -11 (February) and -49% (April) and between -7 (August) and -48% (May) for the two climate change scenario examples, respectively. The months March, April, and May exhibited increases in the 75^{th} percentile fluctuating from -29 to -57%.

Furthermore, considering the climate change impacts on the separated BF, Figure 4.56 shows an example of the BF and the corresponding BF alteration sensitivity analysis under the collective impacts of precipitation and potential evapotranspiration. BF has been estimated based on Mohammed and Scholz (2016) methodology. BF is considerably sensitive to seasonal variations of P values (Figure 4.56a). It can be considered less sensitive to potential evapotranspiration variations (Figure 4.56b). Accordingly, Figure 4.56c compares the long-term mean monthly BF alteration hydrographs for four climatic scenario examples. The hydrograph rising limbs are adjacent to each other between October to February and between June to September, which compares with BF ultimate alteration. A noticeable move was

observed from April to July. Yet, the hydrographs hit the maximum positive alteration in May. The greatest positive alterations were approximately 54, 30, and 7% for the first three climatic scenarios examples, respectively. However, the peak point of the last scenario was -15%, which is considered as the minimum negative alteration.

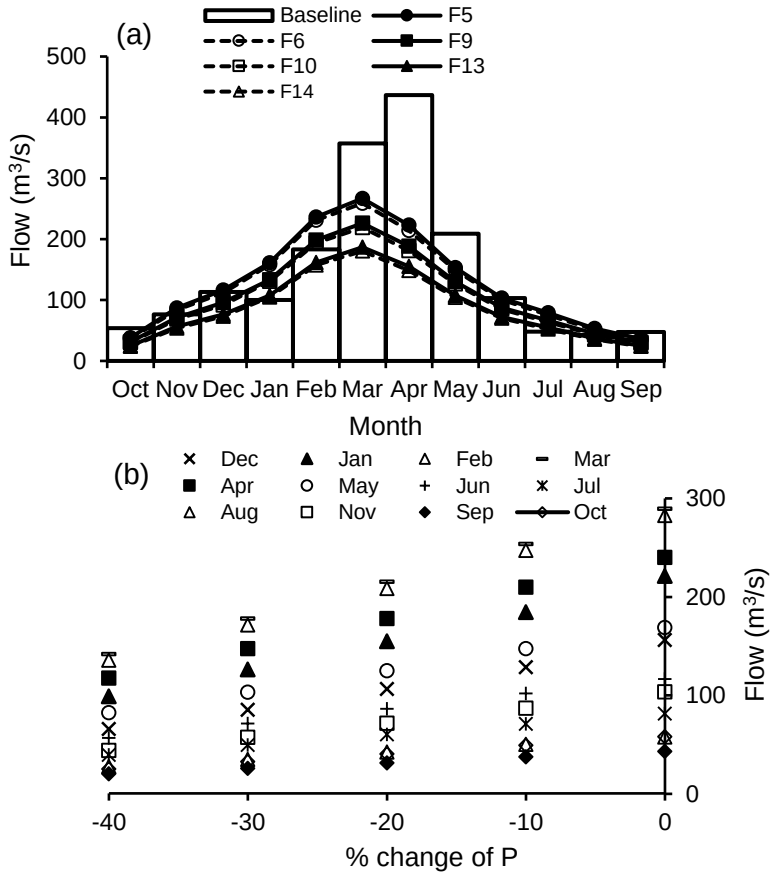

Figure 4.55 (a) Comparison of the long-term monthly median flows between the baseline and some climate change scenario examples, and (b) Anticipated alteration in the long-term mean monthly flow, in the Lower Zab River, due to a reduction in precipitation (P). Note: future F_5 and F_6 (10% reduction in P linked with 0 and 10% increase in potential evapotranspiration (PET), respectively), F_9 and F_{10} (20% reduction in P linked with 0 and 10% increase in PET, respectively), and F_{13} and F_{14} (30% reduction in P linked with 0 and 10% increase in PET, respectively)

Table 4.19 Comparison of some monthly parameters between the baseline (1988—2000) and two of the selected climate change scenarios

[a]P_e	Oct	Nov	Dec	Jan	Feb	Mar	Apr	May	Jun	Jul	Aug	Sep
Baseline												
1[b]	15	20	30	48	48	48	48	48	28	14	11	13
2[c]	38	62	66	90	122	291	219	112	61	46	33	32
3[d]	54	77	113	100	183	357	437	209	104	48	43	48
4[e]	59	95	221	225	360	427	568	317	146	70	55	53
5[f]	97	283	286	397	426	549	1083	781	348	160	79	72
F_5[g]												
1[b]	10	21	68	90	94	72	49	33	22	15	10	8
2[c]	26	36	81	135	202	187	151	102	91	61	41	28
3[d]	38	87	117	161	236	267	223	153	103	79	53	36
4[e]	72	122	161	240	322	305	287	193	130	89	60	42
5[f]	120	196	230	312	448	415	349	248	167	112	100	100
Alteration (%)												
2[c]	-30[i]	-42[j]	22	50	66	-36[j]	-31[i]	-9[i]	51	33	24	-12[i]
3[d]	-30[i]	14	3	61	29	-25[i]	-49[j]	-27[i]	0	64	24	-24[i]
4[e]	22	29	-27[j]	7	-11[i]	-29[i]	-49[j]	-39[j]	-11[i]	27	8	-20[i]
F_9[h]												
1[b]	8	18	56	74	78	59	41	27	18	12	8	7
2[c]	22	30	66	112	169	157	127	86	77	52	35	24
3[d]	31	71	96	134	198	226	189	130	88	67	45	31
4[e]	59	101	134	201	273	259	245	166	112	76	51	36
5[f]	99	163	194	276	382	355	299	212	143	96	82	82
Alteration (%)												
2[c]	-42[j]	-52[j]	0	25	39	-46[j]	-42[j]	-23[i]	28	13	6	-25[i]
3[d]	-43[j]	-7[i]	-15[i]	34	8	-37[j]	-57[j]	-38[j]	-15[i]	39	5	-36[j]
4[e]	0	6	-39[j]	-11[i]	-24[i]	-39[j]	-57[j]	-48[j]	-23[i]	9	-7[i]	-32[i]

[a]Percentile; [b]Minimum; [c]25[th]Percentile; [d]Median; [e]75[th]Percentile; [f]Maximum; [g](10% reduction in precipitation (P) linked with 0% increase in potential evapotranspiration (PET)); [h](20% reduction in P linked with 0% increase in PET); [i]Slight (≤ 33); [j]Modest (34 < > 67)

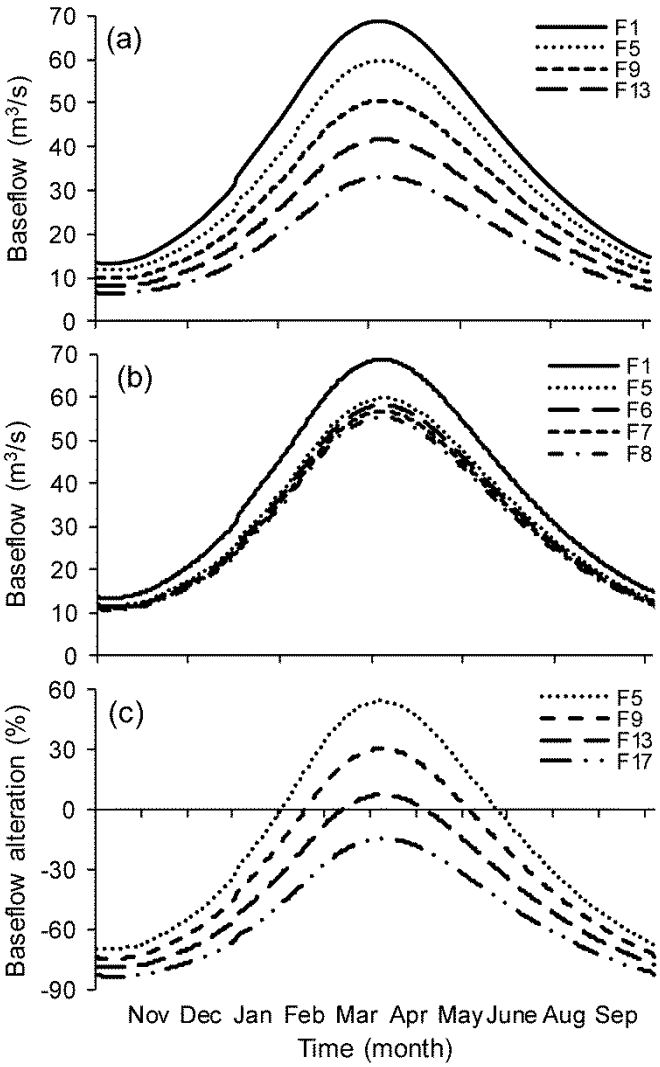

Figure 4.56 (a) Sensitivity analysis for the separated baseflow (BF), with respect to the impact of precipitation (P) reduction; (b) Sensitivity analysis for the separated BF, with respect to the impact of the potential evapotranspiration (PET) increase, using the separation technique that has been proposed by Mohammed and Scholz (2016); and (c) Sensitivity analysis of the BF alteration concerning the impact of the P reduction. Note: Future scenarios F_5 (10% reduction in P linked with 0% increase in PET); and F_6, F_7, and F_8 (10% reduction in P linked with 10, 20, and 30% increase in PET, respectively); and F_9 (20% reduction in P linked with 0% increase in PET)

Additionally, the population of the annual extreme magnitudes is summarised in the box and whisker plots in Figure 4.57, which evidently reveals that there is an extensive variability in the anticipated extreme conditions for each climate change scenario. The effect of climate change on the streamflow estimations mostly follows the impact on the annual extreme magnitudes. Thus, as precipitation and, hence, runoff decreases, the predicted annual minima and maxima decrease as well. Subsequently, a 10% precipitation reduction without any alteration in potential evapotranspiration increase (0% PET) would mean that the 7-days minima magnitude would be reduced by as much as 23%.

Moreover, the C_v, which is estimated as the SD of all daily flows separated by the average yearly flow, increases as the weather become drier and hotter. The ratios of flow reliability to flow predictability had nearly constant values (0.55 to 0.60). Data show that intervals for flood-free seasons increased from 145 to 307 days for the first and the last climatic scenarios, respectively. Figure 4.58 reveals that a significantly ($p < 0.05$) low count has been calculated during December, which means that there is a significant difference between the baseline (1988—2000) and the impacted period, while high values were recorded during the rainy months.

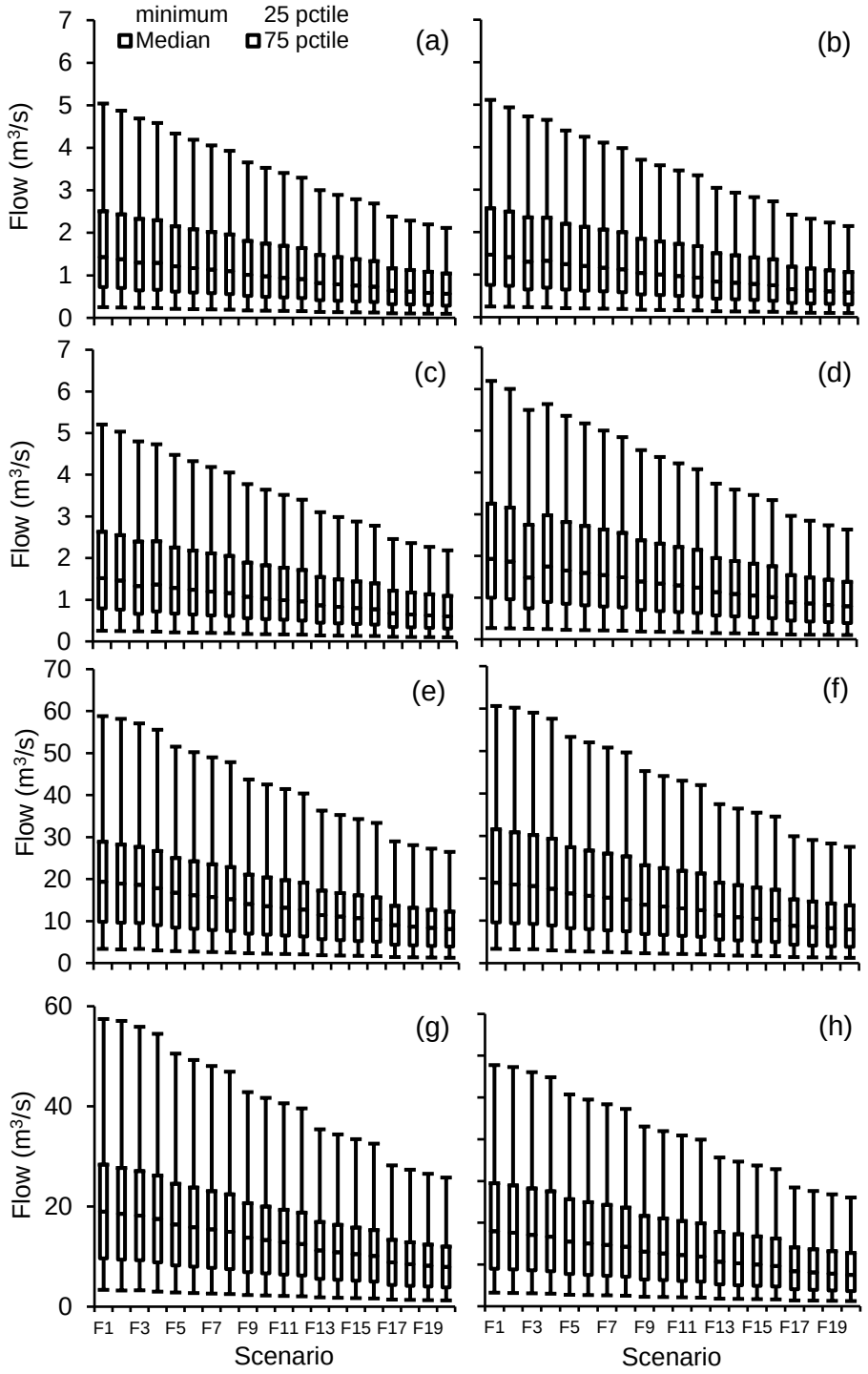

Figure 4.57 Box-whisker plot for the minima and maxima (a) and (e) 1-day; (b) and (f) 3-day; (c) and (g) 7-days; and (d) and (h) 30-days, respectively. Note: future F_1 and F_3 (0% reduction in precipitation (P) linked with 0 and 20% increase in potential evapotranspiration (PET), respectively), F_5 and F_7 (10% reduction in P linked with 0 and 20% increase in PET, respectively), F_9 (20% reduction in P linked with 0% increase in PET), F_{11} and F_{15} (20 and 30% reduction in P, respectively, linked with 20% increase in PET), F_{17} and F_{19} (40% reduction in P linked with 0 and 20% increase in PET, respectively)

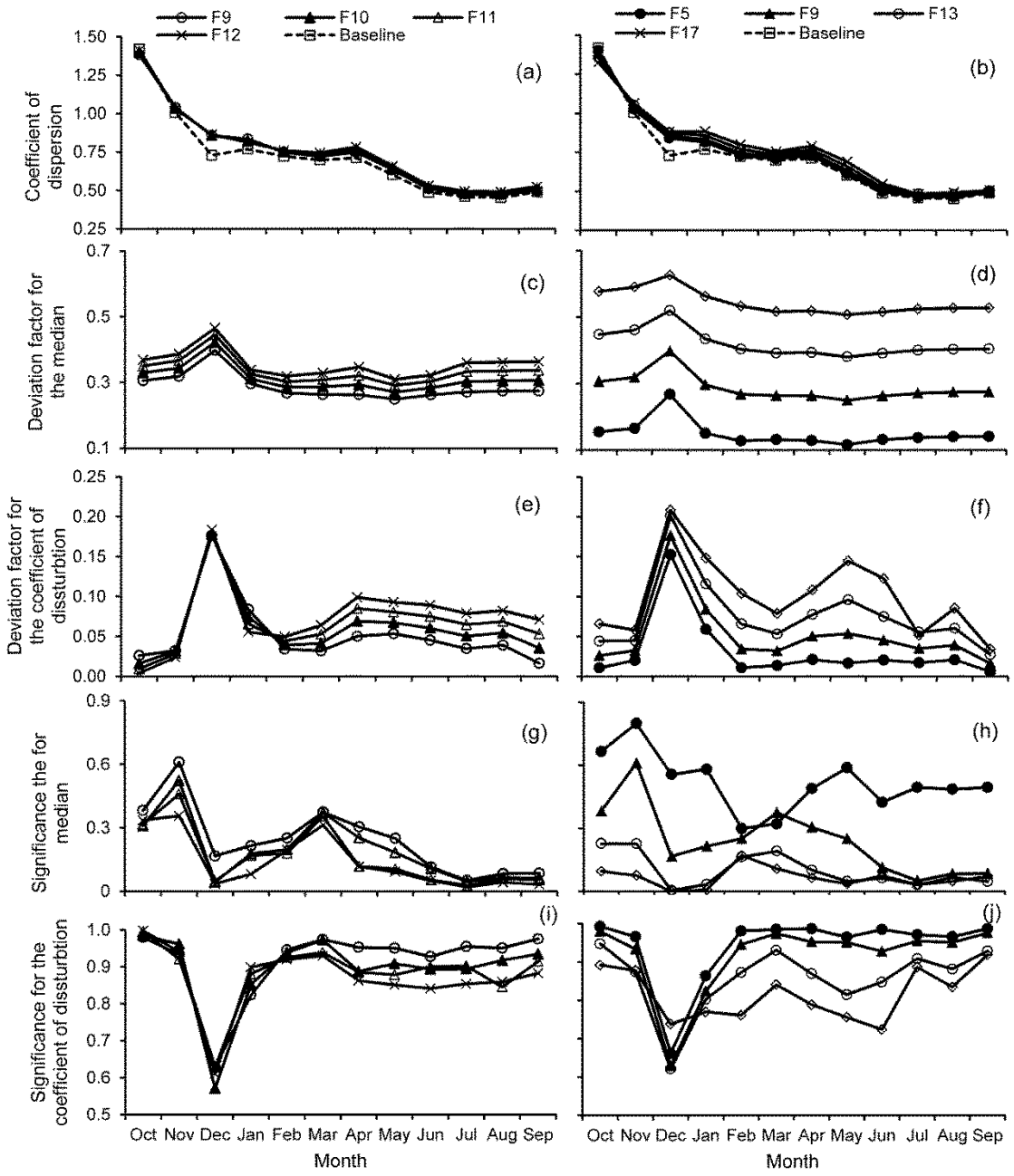

Figure 4.58 The sensitivity analysis of the significance account and the deviation factor for the precipitation (P) reduction and potential evapotranspiration (PET) increase for the (a), (b), (e), and (f) median as well as (c), (d), (g) and (h) coefficient of distribution, respectively. Note: future F_5 and F_9 (10 and 20% reduction in P, respectively, linked with 0% increase in PET), F_{10} and F_{11} (20% reduction in P linked with 10 and 20% increase in PET, respectively), F_{12} (20% reduction in P linked with 30% increase in PET), F_{13} and F_{17} (30 and 40% reduction in P, respectively, linked with 0% increase in PET)

4.8.5.2 General Circulation Model Scenario

Many temporal annual extreme values (i.e. 1-, 3-, 7-, 30-, and 90-days) were estimated for the baseline (1980–2010) and GCM scenario. For group #1, the hydrologic alteration stretched between minimum to maximum. Low levels noticed in October, March, April, May, and September (Table 4.20). A positive minimum level of alteration detected in November and December. A slight alteration anticipated during the time horizon 2011–2030 and 2046–2065. While moderate alteration was observed during 2080–2099, the time-period for nearly all months with alterations of about -36 to -42 between March to September (Table 4.20). For group #2, the extreme minimum flows exhibited low anomalies and a low anomaly of about -28% linked to a 7-day minimum flow for the 2080–2099 time horizon. Regarding the extreme maxima flows, group #2, and experienced low to modest alterations. A moderate anomaly of about -38% linked to a 1-day maximum and 3-day maximum flow for the 2080–2099 time horizon. Moderate alterations varied from -36 to -38% associated with 1-, 3-, and 30-day maximum flow for the 2080–2099 time span.

The temporal percentiles usually represent the potential changes in the basin hydrological characteristics, so that is considered as a vital statistical tool. In this study five temporal percentiles (10^{th}, 25^{th}, 50^{th}, 75^{th}, and 90^{th}) that span the maximum streamflow thresholds, were estimated for the baseline (1980–2010) and GCM scenario, Figure 4.59. The time horizon 2080–2099 linked with the largest alteration. Figure 4.56a explains that the monthly flow was equivalent to or surpassed the threshold at 10% of the period exhibiting falls ranging from -22% (February) to -35% (September) for the time horizon 2080–2099. However, November, December, and January indicated positive anomalies (Figure 4.59a). For the 25^{th} monthly percentiles, the departures were -10% (January) to -38% (September). November and December witnessed positive shifts of 18 and 51% in this order, Figure 4.59b. The abnormalities related to the monthly median flows (Figure 4.59c) extended from -19 (January) to -42% (September), respectively. November and December experienced positive anomalies. In contrast to the 75^{th} percentile (Figure 4.59d), the lowest anomalies were observed in December (-3%), while the highest drops of between -42 was associated to September. The 90^{th} monthly percentiles (Figure 4.59e) were between -4% (November) and -41 (September), respectively. The results suggest that climate change will have an adverse impact overall basin in terms of water resources availability.

Table 4.20 Hydrologic alteration for the middle range of variability approach (RVA) category of the Lower Zab River for the three future time-periods compared to baseline 1980–2010

Degree of hydrologic alteration (%)												
Parameter group #1 (comprising of monthly median discharge values)												
Year ranges	Month											
	Oct	Nov	Dec	Jan	Feb	Mar	Apr	May	Jun	Jul	Aug	Sep
2011–2030	-5^{s}	13^{s}	3^{s}	-6^{s}	-7^{s}	-6^{s}	-7^{s}	-10^{s}	-9^{s}	-9^{s}	-9^{s}	-9^{s}
2046–2065	-4^{s}	13^{s}	25^{s}	12^{s}	3^{s}	-6^{s}	-6^{s}	-8^{s}	-8^{s}	-8^{s}	-8^{s}	-8^{s}
2080–2099	-31^{s}	8^{s}	2^{s}	-20^{s}	-28^{s}	-36^{m}	-38^{m}	-41^{m}	-42^{m}	-42^{m}	-42^{m}	-42^{m}
Parameter group #2 (magnitude and duration of annual extreme)												
Year ranges	n-day minimum					n-day maximum					BFI[a]	
	1	3	7	30	90	1	3	7	30	90		
2011–2030	8^{s}	8^{s}	7^{s}	12^{s}	9^{s}	-8^{s}	-8^{s}	-8^{s}	-6^{s}	-2^{s}	12^{s}	
2046–2065	9^{s}	8^{s}	7^{s}	13^{s}	8^{s}	-8^{s}	-8^{s}	-8^{s}	-6^{s}	-2^{s}	13^{s}	
2080–2099	-27^{s}	-27^{s}	-28^{s}	11^{s}	-26^{s}	-38^{m}	-38^{m}	-37^{m}	-36^{m}	-33^{s}	11^{s}	

[a]Baseflow index; Degree of alteration: ^{S}Slight (≤ 33); ^{m}Modest (34 < > 67); ^{h}High (≥ 67)

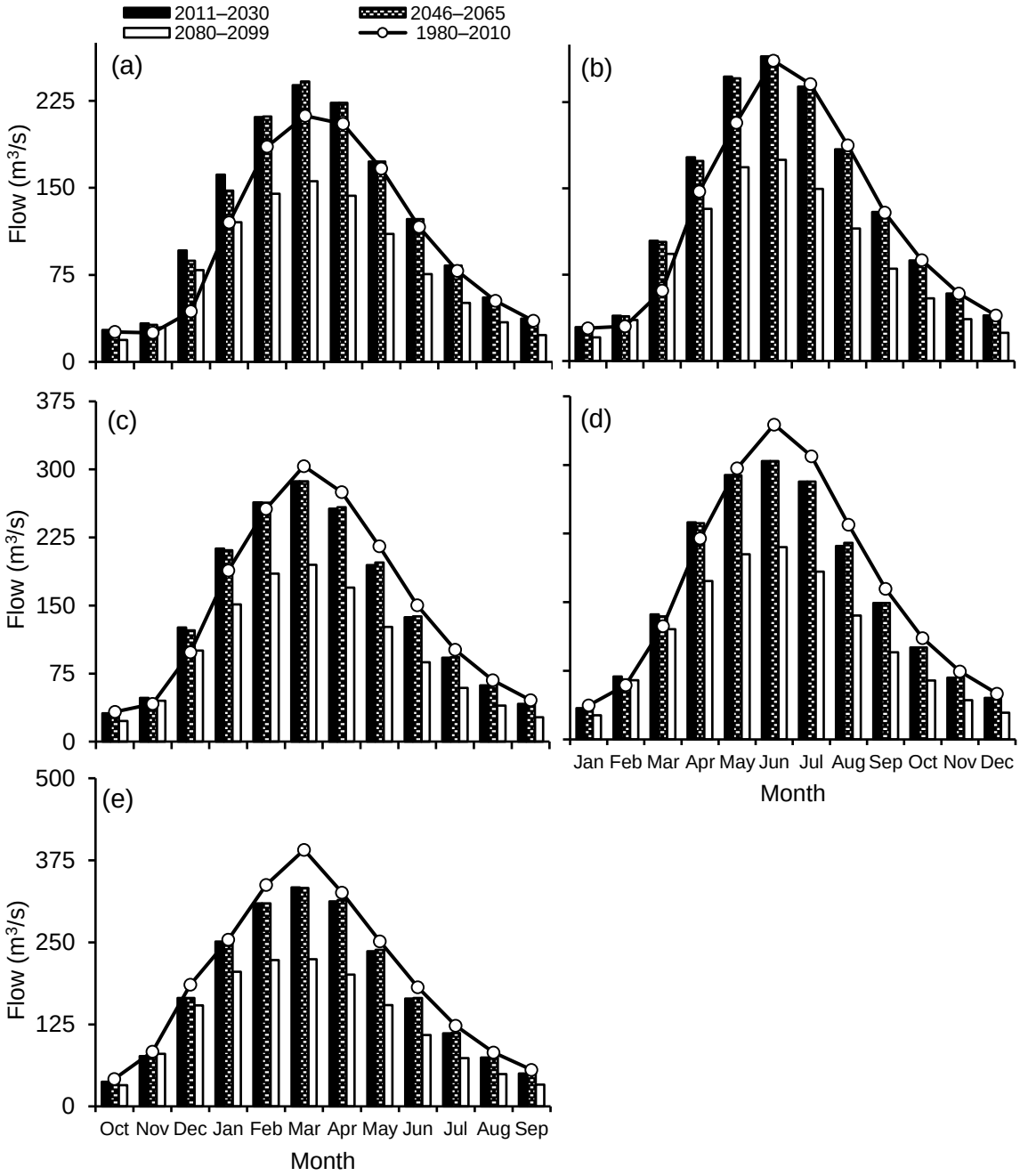

Figure 4.59 Comparison of monthly percentiles between the baseline 1980–2010 and future climate change scenario for the (a) 10th; (b) 25th; (c) 50th; (d) 75th; and (e) 90th percentiles

4.8.6 Reservoir Inflow

Figure 4.60 represents the main steps that suggested, in this study, to derive the reservoir capacity-yield-reliability relationships. Figure 4.61 presents average streamflow hydrographs simulated with weather data predicted by GCM that downscaled using LARS-WG5.5 (left Figures) and delta perturbation methods (right Figures) climate change scenarios, respectively.

To avoid any bias causing by the hydrological simulation procedure, streamflow for the baseline periods, whether it is baseline (1980–2010) or baseline (1988–2000), is represented by simulated streamflow, not by observations. The outcomes displayed how climate change will strongly lead to the reduction in the reservoir inflow. GCM and DP climatic scenarios predict approximately the same decreases in the mean monthly flows, and, consequently, their peak values are almost the same. All GCM show decreases in peak values ranging between 2% (IPCM4) and 10% (GFCM21), Figure 4.61a, 12% (MPEH3) to 37% (GFCM21), Figure 4.61c, and 44% (HADGM3) to 55% (GFCM21), Figure 4.61e, for the three future periods, respectively. By the 2020s horizon and based on the downscaled weather data, there will be a decrease of about 6% in the mean monthly basin runoff, Figure 4.61g, which is identical with the predicted values by DP ($Future_1$ (F_1): 10% P reduction 0% PET), Figure 4.61a. The corresponding decrease for the time horizon 2046–2065 will be nearly 21%, which is identical with DP predicted to decrease (F_8: 10% reduction in P and 30% PET increase, Figure 4.61a). However, the anticipated runoff decrease for the last time horizon is approximately 48%, Figure 4.61d, that is identical with the value resulted from F_{16} (30% P reduction and 30% PET increase, Figure 4.61f). In the worst-case scenario of both GCM and DP, respectively, substantial variations in the inflow between -10 (August), -36 (June), and -55% (July) are anticipated for the three-time horizon, Figure 4.61g, and between -56% and -58% are anticipated for the dry and wet seasons, respectively, Figure 4.61h. In addition, for 2046–2065 future period the peak discharges observed earlier than for the reference period, the lag of about 8 days. However, there is not any change in the time to peak discharges that predicted either by other time horizons or by DP scenario. The inflow peak will decline, and there will be a marked shift in their magnitude, which can result in a dramatic effect on basin water resources availability.

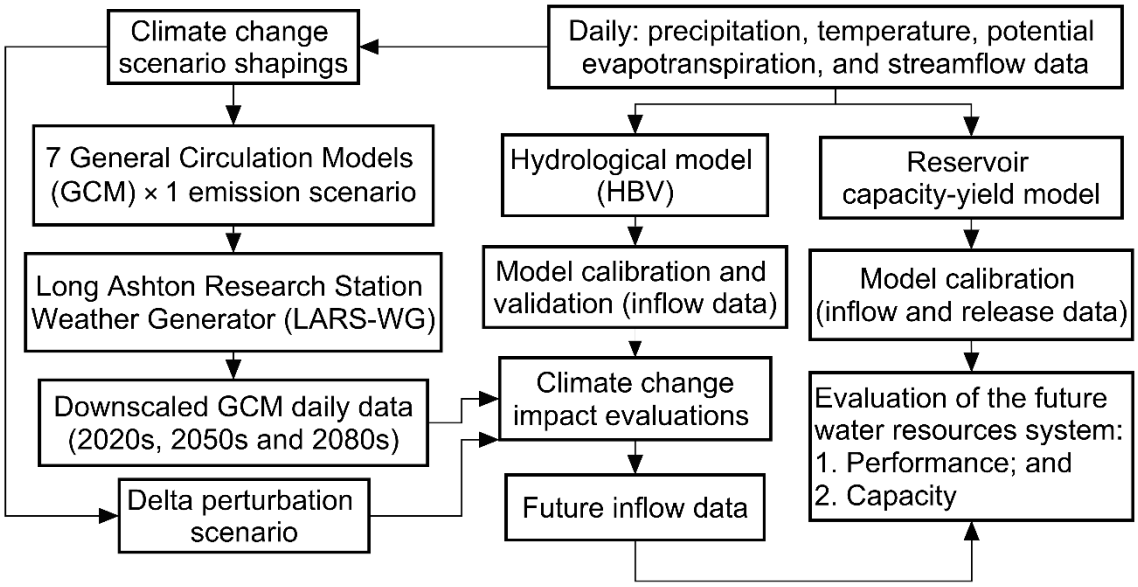

Figure 4.60 The proposed new modeling approach for the evaluation of the potential impacts of climate change on the water resources system, which belongs to the objective eight. Note: HBV is the Hydrologiska Byråns Vattenbalansavdelning hydrological model

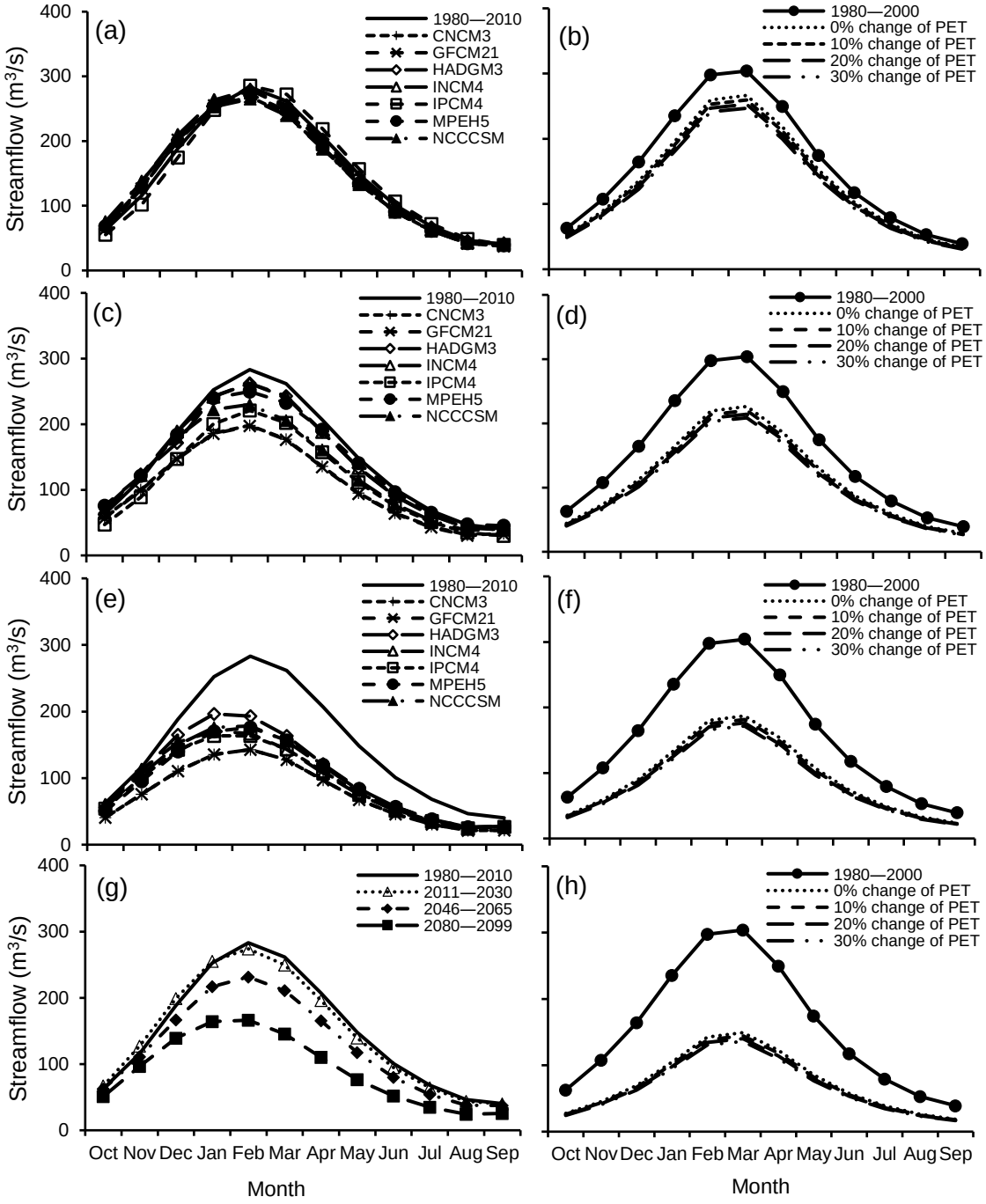

Figure 4.61 Changes in the timing and magnitude of the predicted monthly average inflow to the Dokan reservoir, under the global circulation models (GCM) scenarios (left figures): (a) 2011–2030; (c) 2046–2065; and (e) 2080–2099; time horizon and (g) comparison of the three future time horizons, compared to baseline (1980–2010) values; and delta perturbation scenarios (right figures) (b) 10% increase in precipitation (P); (d) 20% increase in P; (f) 30% increase in P; and (h) 40% increase in P compared to the baseline (1988–2000) values

4.8.7 Reservoir Capacity-Yield-Reliability Relationships

One of the research objectives is the evaluation of reservoir performance sensitivity on water scarcity brought about by climate change. For all the considered scenarios, the future demand for water assumed to continue without major change with respect to the baseline periods. The climate change influence on the Dokan dam operation and its water system assessed by entering the modeled future inflows into the reservoir capacity yield (RCY) model while maintaining the existing operating procedures. To simulate the operations of the Dokan reservoir, HBV simulation of daily streamflow is applied. LWRS-WG5.5 model for down-scaling weather data for GCM and delta perturbations scenarios were applied. Then, RCY model runs to assess the potential impacts of climate change on the reservoir capacity and performance.

Firstly, and under DP scenario, Table 4.21 presents a summary of the potential performance of the Dokan reservoir under the collective impacts of climate change. It is important to notice that the reliability of the reservoir is generally high during the baseline period (1988–2001). Due to precipitation reduction, the reservoir reliability will decline, while the resilience and vulnerability will increase. Figure 4.62b, Table 4.22, and Table 4.23 show the volume required to meet the increase in water demand due to the decline of precipitation and runoff. A 4% precipitation decrease can mean that the existing volume is too little (by as much as 29% for a water yield of 82%), as an example. Moreover, the uncertainty or variability of the reservoir performance is characterised by C_v; i.e. the standard deviation divided by the mean. The uncertainty (C_v) of OPOF, resilience, vulnerability, and the required capacity varied between 0.78–0.07, 0.55–0.40, 0.87–0.47, and 0.46–0.10, respectively. The C_v results indicate that uncertainty/variability of the storage system increase as the basin become drier.

The so-called ‘operational probability of failure’ rates have been determined for each model run and climate change scenario, which led to an amount of OPOF/reliability for each unit time per scenario. The successive range of OPOF involves the possible range of climate change impacts upon the water resources system over the chosen period.

Based on the results of this representative case study, an adaptation operational approach can be implemented, where the policy makers, in particular, in the semi-arid and arid regions, adjust the reservoir operating rules depended on inflow estimations and the current state of reservoir

capacity at each specified period, which can result in a more effective and viable management of reservoirs.

In order to achieve this, RCY model has been utilised to derive the capacity-yield-reliability relationships using the two climate change scenarios. The first relationship is the yield-OPOF, and the second is the capacity-yield (Table 4.22 and Table 4.23). These relationships can be used to test various options against the range of different future scenarios to select the most effective decision on adaptation measure or measures, whether they are structural or non-structural. For example, if the decision-makers target is to supply water for the downstream within 5% OPOF, then by using the first relation/graph they can obtain two values for the expected yield within the range of climate change scenarios. Then, using the second relation/graph, they can investigate whether there will be a need to adopt either a structural or non-structural measure. Furthermore, Table 4.23 shows how much GCM and DP scenarios results are identical.

Table 4.21 Summary of water resources system performance under the collective impacts of precipitation (P) and potential evapotranspiration (PET) for 82% yield

Considered time	Hydro-climatic parameters	Values			
baseline	P (mm)	844.08			
	Inflow (m^3/s)	1009			
	$Inflow_{wet}$ (m^3/s)	2305			
	$Inflow_{dry}$ (m^3/s)	2249			
	Reliability %	99			
	Vurnlibility (10^6 m^3)	426			
	Resilience (month)	3			
% change of P	Hydro-climatic parameters	% change of PET			
		0	10	20	30
0	P (mm)	844.08			
	PET (mm)	1009	1110	1211	1312
	Inflow (m^3/s)	1884	1832	1783	1737
	$Infow_{wet}$ (m^3/s)	1596	1550	1509	1470
	$Inflow_{dry}$ (m^3/s)	289	283	274	267
	Reliability %	92	91	90	88
	Vurnlibility (10^6 m^3)	426	427	428	428
	Resilience (month)	3	5	8	11
10	P (mm)	759.69			
	Inflow (m^3/s)	1623	1576	1531	1490
	$Inflow_{wet}$ (m^3/s)	1371	1331	1294	1260
	$Inflow_{dry}$ (m^3/s)	252	244	237	230
	Reliability %	79	77	74	72
	Vurnlibility (10^6 m^3)	426	427	428	429
	Resilience (month)	22	22	27	23
20	P (mm)	675.26			
	Inflow (m^3/s)	1369	1327	1287	1251
	$Inflow_{wet}$ (m^3/s)	1155	1120	1087	1057
	$Inflow_{dry}$ (m^3/s)	214	207	200	194
	Reliability %	63	58	56	53
	Vurnlibility (10^6 m^3)	430	431	432	433
	Resilience (month)	24	24	32	32
30	P (mm)	590.88			
	Inflow (m^3/s)	1123	1087	1053	1021
	$Inflow_{wet}$ (m^3/s)	946	916	888	862
	$Inflow_{dry}$ (m^3/s)	177	171	165	160
	Reliability %	44	40	37	36
	Vurnlibility (10^6 m^3)	435	436	436	436
	Resilience (month)	33	43	42	45
40	P (mm)	506.44			
	Inflow (m^3/s)	889	858	830	804
	$Inflow_{wet}$ (m^3/s)	748	722	699	677
	$Inflow_{dry}$ (m^3/s)	141	136	131	126
	Reliability %	28	26	24	24
	Vurnlibility (10^6 m^3)	439	440	440	441
	Resilience (month)	61	82	94	73

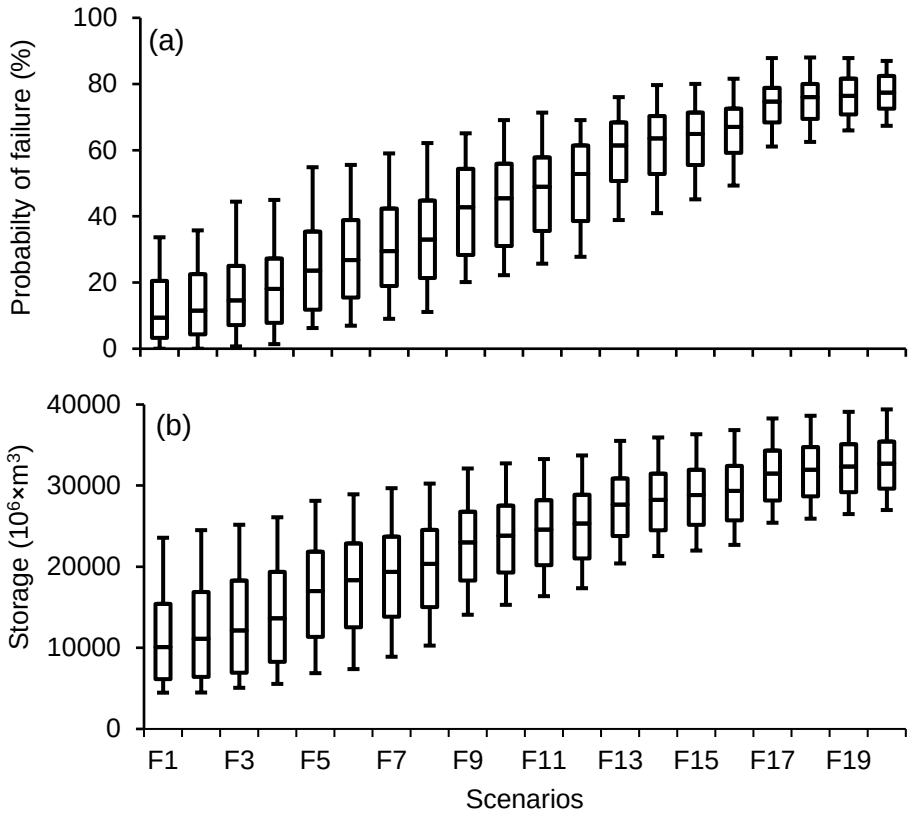

Figure 4.62 Box-plot of the Dokan reservoir; (a) operational probability of failure (OPOF, %); and (b) required storage ($10^6 \times m^3$) under the collective impacts of climate change scenarios. Note: future F_1 and F_3 (0% reduction in precipitation (P) linked with 0 and 20% increase in potential evapotranspiration (PET), respectively), F_5 and F_7 (10% reduction in P linked with 0 and 20% increase in PET, respectively), F_9 and F_{11} (20% reduction in P linked with 0 and 20% increase in PET, respectively), F_{15} (30% reduction in P linked with 20% increase in PET), F_{17} and F_{19} (40% reduction in P linked with 0 and 20% increase in PET, respectively)

Table 4.22 Statistical relationships between yield (Y, %) and operational probability of (reservoir) failure (OPOF, %) and reservoir capacity (C, 10^6 m^3) and yield for different reduction (%) in precipitation (P) and increase (%) in potential evapotranspiration (PET) using delta perturbation climate change scenarios

%		Y (%)[a]			R^2	C (10^6 m^3)[b]			R^2
P	PET	h	i	j		n	o	p	
0	0	-0.018	1.51	71.36	0.99	6.41	–873.30	33302	0.99
	10	-0.007	1.17	71.21	0.99	6.74	–571.30	10968	0.99
	20	-0.008	1.15	69.68	0.99	5.63	–350.80	1303	0.99
	30	-0.005	1.02	68.93	0.99	2.25	226.54	-21846	0.99
10	0	-0.004	0.93	65.25	0.99	-6.83	1727.50	-77136	0.99
	10	-0.001	0.75	65.11	0.99	-7.03	1782.20	-81386	0.99
	20	0.001	0.68	64.08	0.99	-7.06	1906.80	-88811	0.99
	30	0.001	0.65	62.67	0.99	-4.82	1429.30	-69695	0.99
20	0	0.004	0.37	61.92	0.99	-4.48	1224.80	-46423	1.00
	10	0.006	0.24	62.95	0.99	-4.56	1251.10	-48849	0.99
	20	0.007	0.08	64.32	0.99	-4.99	1339.90	-53963	0.99
	30	0.001	-0.18	68.46	0.99	-5.52	1443.90	-59918	0.99
30	0	0.017	-0.99	84.38	0.99	-2.99	905.80	-26026	1.00
	10	0.019	-1.29	91.87	0.99	-3.57	1007.90	-31067	0.99
	20	0.012	-1.59	98.98	0.99	-3.36	982.00	-30995	1.00
	30	0.002	-1.98	109.48	0.99	-3.88	1081.00	-36239	0.99
40	0	0.025	-2.01	111.42	0.99	-2.30	736.50	-13283	0.99
	10	0.034	-3.48	156.36	0.99	-2.48	773.00	-15447	0.99
	20	0.025	-2.20	105.70	0.99	-2.95	859.00	-19765	1.00
	30	0.039	-4.31	181.91	0.99	-2.79	836.30	-19458	1.00

[a]= h × $OPOF^2$ (%) + i × OPOF (%) + j; [b]= n × Y^2 (%) + o × Y (%) + p

Table 4.23 Compared the results of the statistical relationships between the water yield (Y, %) and the operational probability of (reservoir) failure (OPOF, %) and the reservoir capacity (C, 10^6 m^3) and the Y % using seven global circulation models (GCM) for three future time-periods and delta perturbation (DP) scenarios

Year ranges	Climate change scenario for Y (%)[a]							
	GCM			Delta perturbation				
	e	f	g	h	i	j	Change (%)	
							P[b]	PET[c]
1980–2010	0.0034	0.489	70.02	–	–	–	–	–
2011–2030	0.0037	0.455	69.12	-0.001	0.749	65.11	10	10
2046–2065	0.0045	0.362	64.28	0.006	0.224	62.95	20	10
2080–2099	0.0066	-0.162	63.91	-0.024	-1.980	109.48	30	30
Year ranges	Climate change scenario for C (10^6 m^3)[d]							
	GCM			Delta perturbation				
	k	l	m	n	o	p	Change (%)	
							P[b]	PET[c]
1980–2010	-1.21	914.96	-51504	–	–	–	–	–
2011–2030	1.78	234.85	-8491	-4.48	1224.8	-46423	20	30
2046–2065	-1.76	757.48	-23532	-3.57	1007.9	-31067	30	20
2080–2099	-3.62	967.99	-21697	-2.30	736.49	-13283	40	30

[a]= (e or h) × $OPOF^2$ (%) + (f or i) × OPOF (%) + (g or j); [b]precipitation; [c]potential evapotranspiration; [d]= (k or n) × Y^2 (%) + (l or o) × Y (%) + (m or p); Note: all the equations has a correlation coefficient (R^2) more than 0.99

Chapter 5: CONCLUSIONS AND RECOMMENDATIONS

5.1 Conclusions

5.1.1 Drought Analysis

The RDI index is suitable for studying climate instability, evaluation of the meteorological drought severity, and assessment of aridity. This study investigated how the potential evapotranspiration estimates, meteorological station elevation variation, and climatic conditions influenced both the aridity evaluation and the drought severity characterisation, computed through this index. The outcomes and the discussion have been presented in Chapter Four (section 4.4.2) of this thesis. According to the simulation results, the following conclusions have been drawn:

No significant ($p > 0.05$) influence on the standardised (RDI_{st}) and the normalised (RDI_n) forms of the index were detected, through the selected potential evapotranspiration estimates at different elevations for Mediterranean (MD), tropical (TR) and Sahara climates. Slight differences were revealed over many years but these are not considered as important because they do not influence the drought severity indicated by RDI. The different numbers, despite their variations, stay in the identical category of drought, without surpassing a drought severity threshold.

For many regions, such as South Russia, the UK, and East Brazil, RDI_{st}, and RDI_n values are significantly ($p < 0.05$) different for various elevations using the three selected potential evapotranspiration methods compared against PM. The differences are considered significant ($p < 0.05$), since they dramatically affect the drought severity reported by RDI_{st}. The differences would become clearer for shorter periods.

$RDI_{\alpha 12}$ is directly influenced by the selected potential evapotranspiration method at different elevations for all regions. This is why the selection of the potential evapotranspiration method, particularly at high elevations, is important. The application of different approaches may lead to errors in water resources availability predictions of their quality. A significant ($p < 0.05$) deviation has been observed when $RDI_{\alpha 12}$ is computed using different potential evapotranspiration methods. Differences were noticed from region to region and for various elevations.For nearly all the studied cases and for the selected elevations, it was observed that the Hargreaves method performed relatively better than the other methods.

Furthermore, RDI has been suggested in this study as a climatic index to find changes in the drought and aridity of a geographical area, by applying linear regression analysis. The main advantage of the considered method is that RDI integrates into a single index - both precipitation and potential evapotranspiration. In addition, the study shows different durations of RDI (6 and 12 months) for potential periodic climatic variability. Applying the alpha or the normalised form of RDI, more consistent climate variable trends can be identified compared to using time series of potential evapotranspiration and precipitation separately.

The results for RDI_{st} and $RDI_{\alpha 12}$ showed that, currently, semi-arid areas would probably become hyper-arid due to climate change. However, the classification of drought and aridity were presented in this way, to appropriately illustrate the potential climate change impacts and the magnitude of the consequences in the considered geographical regions.

There are regular descending trends in the RDI time series over the last three decades. The long-term time series of this index exposed extra regular trends compared to short-term ones. The declining RDI trend shows more drought severity occurrences over most of the studied regions. In contrast to SPI, which only utilises precipitation time series, RDI takes into account the proportion of precipitation to potential evapotranspiration. Consequently, additional severities would be expected that are more linked to difficult scenarios and influences comprising upward trends in potential evapotranspiration, and its associated parameters in comparison to decreasing trends in either precipitation or precipitation/potential evapotranspiration. Further to the drought frequency increase, the raising of drought extent and duration can be measured. Furthermore, drought episode

severity, special distribution, interval, and many other factors should be considered in the analysis.

The trend of regional aridity most likely does not change for all considered geographical regions. This may be because aridity is considered as a long-term climatic phenomenon, whereas drought is a normal time-based risk, taking into consideration both aridity and water availability inequality. Furthermore, it should be noticed that the calculated trend is based on past climatic conditions as well as drought and aridity categorisations for each area. It can be concluded that both $RDI_{\alpha 12}$ and RDI_{st} are changed as a result of climate variations.

There are insufficient indications for defining downward precipitation trends in the studied regions. The outcomes have highlighted that there are declining or rising trends in annual precipitation, but most of them are not significant. $RDI_{\alpha k}$ trend results in arid and semi-arid areas are comparable to those for precipitation. Furthermore, an examination of meteorological drought trends in Iraq revealed that droughts have increased over the studied basin.

Generally speaking, the study analysis is indicative, it does not result in absolute figures. More studies that focus on trends in precipitation, potential evapotranspiration, precipitation/potential evapotranspiration or aridity, as well as drought indices (especially RDI), would increase the general knowledge concerning these events. A range of possible future conditions could, therefore, be better explained.

This research showed that both precipitation and potential evapotranspiration can have a significant impact on whether an area becomes wetter or drier. As responses occur between precipitation and potential evapotranspiration, it is not a straightforward matter to determine whether and to what extent the former positive or negative trend will influence the latter and vice versa. Hence, it was beneficial in this study to determine the combined impact of using an aridity index.

5.1.2 Hydrograph Analysis

To better understand the potential impact of anthropogenic intervention linked to climate change and drought severity on groundwater involvement to streamflow, a simple but

comprehensive methodology has been presented in Chapter Four (sec. 4.5) of this thesis. Based on the obtained results, the following conclusions are drawn:

A new methodology has been successfully applied to evaluate climate change, anthropogenic activities, and drought phenomena impact on the baseflow (BF) involvement in the total flow (TF). The proposed technique overcomes the drawbacks of previous algorithms and minimises the change between the BF signs. The annual temporal variations of the separated BF show similar patterns for the two studied sub-basins. Very good correlations have been noticed between the separated BF and TF at both the upstream and the downstream locations as well as between the two considered digital filtering algorithms (DFA). The average yearly baseflow index (BFI) of the sub-basins increased from 0.14 to 0.38. This indicates that 14 to 38% of the long-standing Lower Zab River Basin (LZRB) flow can be sustained by groundwater flow. The downstream sub-basin BFI values are approximately double that of the upstream values from October to April. However, they are close to each other from May to September. This variation can be attributed to the differences in the studied hydrological years for each sub-basin and the existence of aquifers with greater releases in the downstream locations compared to the upstream ones. Furthermore, the drainage area of the upstream sub-basin is larger than the area of the downstream one. This leads to an increase of the contribution of both runoff and the interflow to the total river discharge.

During the water year 1987, there was a substantial modification in the flow due to a basin average precipitation increase, which led to a decrease in the involvement of groundwater. Furthermore, about 40 and 60% of the reduction in the average precipitation for the water years 1998–2001 and 2006–2008, respectively, have been reported. This caused substantial drops in the flow by between 52 and 83% respectively, which led to reductions in the contributions of groundwater. Over the water years 1998/1999, 1999/2000, 2000/2001, 2007/2008, and 2008/2009, a considerable increase in the contribution of sub-surface water was recorded, because of seasonal droughts. The matching mean RDI entries were -1.84, -1.67, -1.45, -2.91, and -1.53. Concerning the upstream sub-basin, findings show that the year 1997 had maximum annual BFI values of 0.42 and 0.53 estimated by equations (3.23) and (3.24), respectively. Accordingly, 1997 can be considered as the driest year in the study

period. The downstream part had a maximum yearly BFI of 0.46 and 0.55 using equations (3.23) and (3.24) for the water year 1993.

The recommended approach is useful, simple and supports the preparation of future basin management actions, particularly when challenging hydrological models cannot be applied appropriately, because of a deficiency in observed data. The suggested approach may improve the understanding of the characteristics of BF and clarify how climate change, river control, water use, and transformations in the upstream part of the basin could change the flow regime of the downstream BF. A detailed exploration of the BF contribution to TF is important, because of water resources shortages and corresponding conflicts among different stakeholders and countries.

5.1.3 Streamflow Alteration

A generic methodology has been proposed to enable water resources managers and policy makers to make an informed and robust decision in facing many uncertainties about the future by enhancing their strategies for climate change adaptation. The outcomes and the discussion have been presented in Chapter Four (4.6) of this thesis. The following case study-specific conclusions are drawn:

Climate change will have a more extensive and solid impact on the streamflow hydrological characteristics than human-induced activities. The change in climate will cause a shift of more than one month in the seasonal inflow to the reservoir. The separated BF is considerably sensitive to the seasonal variations of precipitation values, whereas, it is less for the potential evapotranspiration variations.

The effect of climate change on the streamflow estimations generally mirrors the effect on the annual extreme magnitudes. Thus, as precipitation and, hence, runoff decreases, the predicted annual minima and maxima decrease. The region has already experienced increases in drought periods due to precipitation reductions (after 1999).

A non-uniform cyclical characteristic of wet and dry periods was witnessed for the considered period and the seasonal droughts were recorded over the water years 1998/1999, 1999/2000, and 2000/2001. Furthermore, the water year 2007/2008 witnessed a severe

drought, whereas the year 1987/1988 was characterised by a significant ($p < 0.05$) increase in P_{av}. Almost 80% of the streamflow reduction was observed for the water years 1998–2002 and 2006–2008 as a consequence of a sharp drop in P_{av}. A considerable alteration during the non-rainy months is attributed to the effect of human-induced activities and climate change pressure in the region, which led to a decrease in water resources in the basin.

5.1.4 Anthropogenic Interventions Evaluation

The surface runoff in the LZRB has declined considerably due to climate variability and anthropogenic interventions. To evaluate the impacts of these two factors on the river flow over the study basin, hydrologic models simulation, hydrologic sensitivity analysis, and multi-regression have been successfully applied. The outcomes and the discussion have been presented in Chapter Four (section 4.7) of this thesis. The study outcomes indicate that:

Anthropogenic intervention impacts, such as land use and land cover changes, water conservancy project implications, and soil conservation actions may accumulate or counteract each other simultaneously. River alteration, climate variability, and anthropogenic interventions should be considered for future stream basin management strategies to avoid the temporal mismatch between strategies and such changes. There is a big variance in the performance of the considered hydrological models in simulating the runoff.

Simply averaging the single model (SAM) simulation would result in consensus multi-model simulations that are superior to any individual simulations, which confirmed that the SAM multi-model combination technique is a more effective method, since it combines the strengths of different models, and eliminates the weaknesses. More sophisticated multi-model combination approaches improve simulation accuracy. This suggests that further operational hydrologic simulations should incorporate a multi-model combination strategy. Additionally, the multi-model simulation accuracy is dependent on the results of the single models. If a single model simulation accuracy is poor in matching measurements, removing that model from the simulation positively affects the accuracy of the multi-model simulation. Conversely, excluding the best performing model from consideration negatively affects the accuracy of the multi-model simulation. Model combination techniques are still new in

hydrology. However, findings indicate that they may be a preferable alternative to individual model simulation.

This study represents a critical step towards better understanding of the potential effect of climate variability, anthropogenic interventions, and subsequent drought events on streamflow in the LZRB and similar other regions, with arid and semi-arid climates. The research outcomes will benefit engineers and policy-makers in assessing water resources at a basin scale.

5.1.5 Climate Change Evaluation

A comprehensive and generic methodology is proposed to enable water resources managers and policy makers to make an informed and robust decision in facing many uncertainties about the future by enhancing their strategies for climate change adaptation. The outcomes and the discussion have been presented in Chapter Four (section 4.7) of this thesis. The following case study-specific conclusions are drawn:

The LARS-WG5.5 downscaling model has good representation in predicting daily weather data in arid and semi-arid areas; therefore, it can be employed to predict daily values for future time-periods. There will be an increase of approximately 0.54, 3.03, and 4.36 °C and 0.56, 2.49, and 4.70 ºC in T_{min} and T_{max} for the 2011–2010, 2046–2065, and 2080–2099 periods, respectively. However, there will be a decreasing trend of nearly 6.32, 17.33, and 340.18 mm in precipitation values for the three future time-periods and the relative variations will fluctuate from month to month.

It has been noticed that there are no logical alteration trends among several GCM calculations of precipitation for the period 2080–2099. The precipitation predictions from GFCM21, HADCM3, INCM4, IPCM4, and MPEH5 are less than the values of the baseline period (1980–2010). There have been small variations in estimating the future extreme temperature using only one GCM. The predictions of these extremes for the 2046–2065 and 2046–2065 periods using seven GCMs have coherent variation trends compared to the values that were predicted for the 2080–2099 time-period.

Both GCM and DP scenarios predicted nearly the same decreases in the mean monthly flows, and, consequently, their peak values are almost the same. For example, the anticipated decrease in the runoff for the 2080–2099 time horizon was almost 48%, which is equal to the value stemmed from the DP scenario (F_{16}: 30% P reduction and 30% PET increase). The region has already experienced increases in drought periods due to P reductions (after 1999). A non-uniform cyclical characteristic of wet and dry periods was witnessed for the baseline and the future time horizons. It is anticipated that the severity of meteorological and hydrological droughts will dramatically worsen over the coming years; in particular, during the time horizon 2080–2099, the drought severity will increase as the number of months with extended periods of precipitation shortages and potential evapotranspiration growths increase.

Moderate anomalies changed from -36 to -38% were associated with 1-, 3-, and 30-day maximum flows for the 2080–2099 time span. The duration of the flood-free season will increase due to climate change impacts. The effect of climate change on the streamflow estimations generally mirrors the effect on the annual extreme magnitudes. Thus, as the precipitation and, hence, runoff decreases, the predicted annual minima and maxima decrease. The monthly flow was equivalent to or surpassed the threshold at 10% of the period exhibiting falls ranging from -22 % (February) to -35% (September) for the time horizon 2080–2099.

The results provide a basis for enabling future water resources system managers and planners of the Dokan reservoir and similar case studies, in particular, in arid and semi-arid regions, to adapt to climate change taking into consideration as many climate change scenarios as possible. Synthetic scenarios could be supplemented by GCM scenarios, since they permit for a wider range of potential climate change scenarios at the local level, and are easier to build and apply. Additionally, this study should be repeated for other areas and climates, which should lead to a further generalisation of the research conclusions.

5.2 Recommendations for Future Research

For many semi-arid and humid regions such as South Russia, East Brazil, and the UK the values of RDI_{st} and RDI_{n} are significantly ($p < 0.05$) different for various elevations using

the three selected potential evapotranspiration methods compared against the Penman method. The differences are considered significant ($p < 0.05$), since they affect dramatically the drought severity reported by the RDI_{st} index. The difference would become clearer for shorter time-periods. Therefore, it is highly recommended to use time steps shorter than annual periods such as 3, 6, and 9 months for further research in the RDI index.

More studies that focus on trends in precipitation, potential evapotranspiration, precipitation/potential evapotranspiration or aridity, as well as drought indices (especially RDI), would increase the general knowledge concerning these events. A range of possible future conditions could be explained better. Therefore, the study of RDI as a climatic index should be undertaken again for other geographical and climatic zones of interest, considering more meteorological stations to generalise the obtained conclusions.

A detailed exploration of baseflow contribution to total flow is important, because of water resources shortages and corresponding conflicts among different stakeholders and countries. Therefore, it is recommended, for further research, to evaluate aquifer behavior, and corresponding data variability.

The accuracy of the multi-model is related to that of the single models. If single model accuracy is poor in matching observations, removing that model from simulation does affect the multi-model accuracy very much. Whereas, eliminating the best performing model from consideration does negatively affect the multi-model accuracy. More models and larger datasets would enhance the multi-model combination technique outcomes.

It is highly recommended for this research to be undertaken again at other geographical regions and climatic conditions to assess the effect of river damming and climate variability on groundwater contribution to streamflow to generalise the obtained conclusion.

River alteration, climate variability, and anthropogenic interventions, such as land use and land cover changes, water conservancy project implications, and soil conservation actions may accumulate or counteract each other's so that they should be considered for future river basin managing strategies to avoid the temporal mismatch between strategies and such changes.

The delta perturbation permit for a wide range of climate change scenarios at a basin level as well as they are easier to shape and use, therefore it is highly recommended for this study to be undertaken again by combining the results of GCM and DP climate change scenarios.

5.3 Limitations of the Study

Although this research has achieved its main aim there were a number of unavoidable limitations. Firstly, the simple average method was accomplished based on only three hydrological models and a total of thirty-five water years of daily streamflow data. Additional hydrological models and more datasets would enhance the outcomes of multi-model combination performance. Secondly, and due to unavailability of several weather parameters such as wind speed, solar radiation, and relative humidity, a temperature-based method, which is Hargreaves method, has been used to estimate the potential evapotranspiration variable, for the LZRB, so that in the case of the long-term reliable datasets availability of numerous climate parameters, PM estimates should be used. Thirdly, to investigate the sensitivity of the RDI index to the potential evapotranspiration formulations, this research based on a dataset of only 24 meteorological stations representing different elevations and climatic conditions. Therefore, to generalise the obtained conclusions more meteorological stations should be involved.

References

Abebe A, Foerch G (2006) Catchment characteristics as predictors of the dry-weather index (BFI) in Wabi Shebele river basin, East Africa. Paper presented at the Conference on International Agricultural Research for Development, Tropentag 2006, University of Bonn, Bonn. http://citeseerx.ist.psu.edu/viewdoc/download?doi=10.1.1.112.3449&rep=rep1&type=pdf. [Accessed: 8th February 2016]

Adeloye AJ, Soundharajan BS, Ojha CSP, Remesan R (2016) Effect of hedging-integrated rule curves on the performance of the Pong reservoir (India) during scenario-neutral climate change perturbations. *Water Resources Management* 30(2):445–470. doi:10.1007/s11269-015-1171-z

AghaKouchak A, Farahmand A, Melton FS, Teixeira J, Anderson MC, Wardlow BD, Hain CR (2015) Remote sensing of drought: Progress, challenges, and opportunities. *Reviews of Geophysics* 53(2):452–480. doi:10.1002/2014RG000456

Ajami NK, Duan Q, Gao X, Sorooshian S (2006) Multi-model combination techniques for hydrological forecasting: Application to distributed model intercomparison project results. *Journal of Hydrometeorology* 7(4):755–768. doi:10.1175/JHM519.1

Ajami NK, Duan Q, Sorooshian S (2007) An integrated hydrologic Bayesian multi-model combination framework: Confronting input, parameter, and model structural uncertainty in hydrologic prediction. *Water Resources Research* 43(1): W01403. doi:10.1029/2005WR004745

Aksoy H, Gedikli A, Unal NE, Yilmaz M, Eris E, Yoon J, Tayfur G (2016) Rainfall-Runoff model considering microtopography simulated in a laboratory erosion flume. *Water Resources Management* 30(15):5609–5624. doi:10.1007/s11269-016-1439-y

Al-Faraj F, Scholz M (2014) Incorporation of the flow duration curve method within digital filtering algorithms to estimate the baseflow contribution to total runoff. *Water Resources Management* 28(15):5477–5489. doi:10.1007/s11269-014-0816-7

Akin JE (1971) Calculation of mean areal depth of precipitation. *Journal of Hydrology* 12(4):363–376. doi:10.1016/0022-1694(72)90127-8

Allen RG, Pereira LS, Raes D, Smith M (1998) *Crop evapotranspiration: Guidelines for computing crop water requirements*. Food and Agriculture Organization (FAO) Irrigation and Drainage Paper 56, Rome, Italy, 300(9): D05109

Alvarez UFH, Trudel M, Leconte R (2014) Impacts and adaptation to climate change using a reservoir management tool to a Northern watershed: Application to Lievre River watershed, Quebec, Canada. *Water Resources Management* 28(11):3667–3680. doi:10.1007/s11269-014-0694-z

Arnold JG, Allen PM (1999) Automated methods for estimating baseflow and ground water recharge from streamflow records1. JAWRA *Journal of the American Water Resources Association* 35(2):411–424. doi:10.1111/j.1752-1688.1999.tb03599.x

Arnold JG, Muttiah RS, Srinivasan R, Allen PM (2000) Regional estimation of baseflow and groundwater recharge in the upper Mississippi river basin. *Journal of Hydrology* 227(1):21–40. doi:10.1016/S0022-1694(99)00139-0

Asadi A, Vahdat SF (2013) The efficiency of meteorological drought indices for drought monitoring and evaluating in Kohgilouye and Boyerahmad Province, Iran. *International Journal of Modern Engineering Research* (IJMER) 3(4):2407–2411, ISSN: 2249-6645

Asadi Zarch MA, Malekinezhad H, Mobin MH, Dastorani MT, Kousari MR (2011) Drought monitoring by reconnaissance drought index (RDI) in Iran. *Water Resources Management* 25(13):3485–3504. doi:10.1007/s11269-011-9867-1

Asadi Zarch MA, Sivakumar B, Sharma A (2015) Droughts in a warming climate: A global assessment of standardized precipitation index (SPI) and reconnaissance drought index (RDI). *Journal of Hydrology* 526:183–195. doi:10.1016/j.jhydrol.2014.09.071

Ashofteh PS, Haddad OB, Mariño M (2012) Climate change impact on reservoir performance indexes in the agricultural water supply. *Journal of Irrigation and Drainage Engineering* 139(2):85–97. doi:10.1061/(ASCE)IR.1943-4774.0000496

Bardsley T, Wood A, Hobbins M, Kirkham T, Briefer L, Niermeyer J, Burian S (2013) Planning for an uncertain future: Climate change sensitivity assessment toward adaptation planning for public water supply. *Earth Interactions* 17(23):1–26. doi:10.1175/2012EI000501.1

Bastola S, Murphy C, Fealy R (2012) Generating probabilistic estimates of hydrological response for Irish catchments using a weather generator and probabilistic climate change scenarios. *Hydrological Processes* 26(15):2307–2321. doi:10.1002/hyp.8349

Beguería S, López-Moreno JI, Lorente A, Seeger M, García-Ruiz, JM (2003) Assessing the effects of climate oscillations and land-use changes on streamflow in the central Spanish Pyrenees. AMBIO: *A Journal of the Human Environment* 32(4):283–286

Blenkinsop S, Fowler HS (2007) Change in droughts frequency, severity and duration of the British Isles projected by PROUDNES regional climate models. *Journal of Hydrology* 342:50–71. doi:10.1016/j.jhydrol.2007.05.003

Bosona TG, Gebresenbet G (2010) Modeling hydropower plant system to improve its reservoir operation. *International Journal of Water Resources and Environmental Engineering* 2(4):87–94

Bozkurt D, Sen OL (2013) Climate change impacts in the Euphrates–Tigris Basin based on different model and scenario simulations. *Journal of Hydrology* 480:149–161. doi:10.1016/j.jhydrol.2012.12.021

Bozkurt D, Sen OL, Hagemann S (2015) Projected river discharge in the Euphrates-Tigris Basin from a hydrological discharge model forced with RCM and GCM outputs. *Climate Research* 62(2):131–147. doi:10.3354/cr01268

Brekke LD, Maurer EP, Anderson JD, Dettinger MD, Townsley ES, Harrison A, Pruitt T (2009) Assessing reservoir operations risk under climate change. *Water Resources Research* 45(4). doi:10.1029/2008WR006941

Brodie RS, Hostetler S (2005) A review of techniques for analyzing base-flow from stream hydrographs. In *Proceedings of the NZHS-IAH-NZSSS 2005 Conference, 28 November - 2 December 2005, Auckland, New Zealand.* http://data.daff.gov.au/data/warehouse/brsShop/data/iah05_dry-weather_final.pdf. [Accessed: 8th February 2016]

Cai W, Zhang Y, Chen Q, Yao Y (2015) Spatial patterns and temporal variability of drought in Beijing-Tianjin-Tianjin-Hebei metropolitan areas in China. *Advances in Meteorology* 2015, ID 289471:1–14. doi:10.1155/2015/289471

CFSR, Climate Forecast System Reanalysis (2015) Global Weather Data for SWAT [Online] Available from http://globalweather.tamu.edu/home/ [Accessed: 5th September 2015]

Chang J, Wang Y, Istanbulluoglu E, Bai T, Huang Q, Yang D, Huang S (2015) Impact of climate change and human activities on runoff in the Weihe river basin, China. *Quaternary International* 380–381:169–179. doi:10.1016/j.quaint.2014.03.048

Chapman T (1999) A comparison of algorithms for streamflow recession and baseflow separation. *Hydrological Processes* 13(5):701–714. doi:10.1002/(SICI)1099-1085(19990415)13:5<701::AID-HYP774>3.0.CO;2-2

Chatterjee M, Roy D, Das S, Mazumdar A (2014) Assessment of water resources under climate change: Damodar River Basin, India. ARPN *Journal of Engineering and Applied Sciences* 9(11):2183–2191. ISSN 1819-6608

Chen J, Brissette FP, Leconte R (2011) Uncertainty of downscaling method in quantifying the impact of climate change on hydrology. *Journal of Hydrology* 401(3–4):190–202. doi:10.1016/j.jhydrol.2011.02.020

Chen Y, Xu Z (2005) Plausible impact of global climate change on water resources in the Tarim River Basin. *Science in China Series D: Earth Sciences* 48(1):65–73. doi:10.1360/04yd0539

Cheng Y, He H, Cheng N, He W (2016) The effects of climate and anthropogenic activity on hydrologic features in Yanhe River. *Advances in Meteorology* ID 5297158:11. doi:10.1155/2016/5297158

Cigizoglu HK, Bayazit M (2000) A generalized seasonal model for flow duration curve. *Hydrological Processes* 14(6):1053–1067. doi:10.1002/(SICI)1099-1085(20000430)14:6<1053::AID-HYP996>3.0.CO;2-B

Collins WD, Hack JJ, Boville BA, Rasch PJ and others (2004) Description of the NCAR Community Atmosphere Model (CAM3.0). Technical Note TN-464+STR, National Center for Atmospheric Research, Boulder, CO

Cook BI, Smerdon JE, Seager R, Coats S (2014) Global warming and 21st century drying. *Climate Dynamics* 43(9–10):2607–2627. doi:10.1007/s00382-014-2075-y

CSMD, Climate System Modeling Division (2005) An introduction to the first general operational climate model at the National Climate Center. Advances in Climate System Modeling 1, National Climate Center, China Meteorological Administration

Croley TE, Hartmann HC (1985) Resolving Thiessen polygons. *Journal of Hydrology* 76(3–4):363–379

Cullen H M, de Menocal P B (2000) North Atlantic influence on Tigris–Euphrates streamflow. *International Journal of Climatology* 20(8):853–863. doi:10.1002/1097-0088(20000630)20:8<853::AID-JOC497>3.0.CO;2-M

Dahamsheh A, Aksoy H (2007) Structural characteristics of annual precipitation data in Jordan. *Theoretical and Applied Climatology* 88(3):201–212. doi: 10.1007/s00704-006-0247-3

Déqué M, Dreveton C, Braun A, Cariolle D (1994) The ARPEGE/IFS atmosphere model: a contribution to the French community climate modeling. *Climate Dynamics* 10(4):249–266

Dile YT, Srinivasan R (2014) Evaluation of CFSR climate data for hydrologic prediction in data-scarce watersheds: an application in the Blue Nile River Basin. JAWRA *Journal of the American Water Resources Association* 50(5):1226–1241. doi:10.1111/jawr.12182

Diskin MH (1970) On the computer evaluation of Thiessen weights. *Journal of Hydrology* 11(1):69–78

Doll P, Zhang J (2010) Impact of climate change on freshwater ecosystems: A global-scale analysis of ecologically relevant river flow alterations. *Hydrology and Earth System Sciences* 14(5):783–799. doi:10.5194/hess-14-783-2010

Duan Q, Ajami NK, Gao X, Sorooshian S (2007) Multi-model ensemble hydrologic prediction using Bayesian model averaging. *Advances in Water Resources* 30(5):1371–1386. doi:10.1016/j.advwatres.2006.11.014

Dubois J, Boillat JL, Schleiss A (2000) *Routing system–modélisation du routage de crues dans des systèmes hydrauliques à surface libre* (No. LCH-BOOK-2008-009). EPFL-LCH

Ebrahim GY, Villholth KG (2016) Estimating shallow groundwater availability in small catchments using streamflow recession and instream flow requirements of rivers in South Africa. *Journal of Hydrology* 541:754–765. doi: 10.1016/j.jhydrol.2016.07.032

Eckhardt K (2005) How to construct recursive digital filters for baseflow separation. *Hydrological Processes* 19(2):507–515. doi:10.1002/hyp.5675

Edwards DC, McKee TB (2015) Characteristics of 20th century drought in the United States at multiple such scales. *Atmospheric Science paper* 634

Fadhil MA (2011) Drought mapping using geoinformation technology for some sites in the Iraqi Kurdistan region. *International Journal of Digital Earth* 4(3):239–257. doi:10.1080/17538947.2010.489971

Fan Y, Chen Y, Liu Y, Li W (2013) Variation of baseflows in the headstreams of the Tarim River Basin during 1960–2007. *Journal of Hydrology* 487:98–108. doi:10.1016/j.jhydrol.2013.02.037

FAO (2012) *Food and Agriculture Organization of the UN. Adaptation to climate change in semi-arid environments. Experience and lessons from Mozambique*. Retrieved from http://www.fao.org/docrep/015/i2581e/i2581e00.pdf

Foehn A, García Hernández J, Roquier B, Paredes Arquiola J (2016) *RS MINERVE – User's manual v2.6*. RS MINERVE Group, Switzerland

Fowler HJ, Kilsby CG, O'Connell PE (2003) Modeling the impacts of climatic change and variability on the reliability, resilience, and vulnerability of a water resource system. *Water Resources Research* 39(8):1222. doi:10.1029/2002WR001778

Fuka DR,Walter MT, MacAlister C, Degaetano AT, Steenhuis TS, Easton ZM (2014) Using the climate forecasting system reanalysis as weather input data for watershed models. *Hydrological Processes* 28(22):5613–5623. doi:10.1002/hyp.10073

Futter M N Whitehead PG, Sarkar S, Roddad H, Crossman J (2015) Rainfall-runoff modelling of the upper Ganga and Brahmaputra basins using PERSiST. *Environmental Science: Processes and Impacts* 17(6):1070–1081. doi:10.1039/c4em00613e

GADM, Global Administrative Areas Database (2012) Boundaries without limits [Online] Available from http://www.gadm.org [Accessed: 10th March 2015]

Galin VY, Volodin EM, Smyshliaev SP (2003) Atmospheric general circulation model of INM RAS with ozone dynamics. *Russian meteorology and hydrology* 5:13–22

Gao B, Yang D, Yang H (2013) Impact of the Three Gorges Dam on flow regime in the middle and lower Yangtze River. *Quaternary Internationa*l 304:43–50

García Hernández J, Jordan F, Dubois J, Boillat JL, Schleiss A (2007) Routing system II: Flow modelling in hydraulic systems. *Communication* 32:1661–1179

Gedikli A, Aksoy H, Unal NE (2008) Segmentation algorithm for long time series analysis. *Stochastic Environmental Research and Risk Assessment* 22(3):291–302. doi:10.1007/s00477-007-0115-4

Gedikli A, Aksoy H, Unal NE, Kehagias A (2010) Modified dynamic programming approach for offline segmentation of long hydrometeorological time series. *Stochastic Environmental Research and Risk Assessment* 24(5):547–557. doi:10.1007/s00477-009-0335-x

Georgakakos KP, Seo DJ, Gupta H, Schake J, Butts MB (2004) Towards the characterization of streamflow simulation uncertainty through multimodel ensembles. *Journal of Hydrology* 298(1):222–241. doi:10.1016/j.jhydrol.2004.03.037

GFDL-GAMDT, GFDL Global Atmospheric Model Development Team (2004) The new GFDL global atmosphere and land model AM2-LM2: Evaluation with prescribed SST simulations. *Journal of Climate* 17(24):4641–4673

Giannikopoulou AS, Kampragkou E, Gad FK, Kartalidis A, Assimacopoulos D (2014) Drought characterisation in Cyclades complex, Greece. *European Water* 47:31–43

Gibson CA, Meyer JL, Poff NL, Hay LE, Georgakakos A (2005) Flow regime alterations under changing climate in two river basins: Implications for freshwater ecosystems. *River Research and Applications* 21(8):849–864 (2005). doi:10.1002/rra.855

GLCF, Global and Land Cover Facility (2015) Earth science data interface [Online] Available from http://www.landcover.org/data/srtm/ [Accessed: 05th March 2015]

Gordon C, Cooper C, Senior CA, Banks H and others (2000) The simulation of SST, sea ice extents and ocean heat transports in a version of the Hadley Centre coupled model without flux adjustments. *Climate dynamics* 16(2):147–168

Gordon HB, Rotstayn LD, McGregor JL, Dix MR, Kowalczyk EA, O'Farrell SP, Waterman LJ, Hirst AC, Wilson SG, Collier MA, Watterson IG (2002) *The CSIRO Mk3 climate system model*. CSIRO Atmospheric Research, Aspendale

Gordon ND, McMahon TA, Finlayson BL (2004) *Stream hydrology: An introduction for ecologists*. 2nd ed., John Wiley and Sons, Chichester

GR4J, Ge´nie Rural a Daily 4 parameters model (2016) Catchment hydrology research group [Online] Available from https://webgr.irstea.fr/modeles/journalier-gr4j-2/?lang=en [Accessed: 5th June 2016]

Guo Y, Li Z, Amo-Boateng M, Deng P, Huang P (2014) Quantitative assessment of the impact of climate variability and human activities on runoff changes for the upper reaches of Weihe River. *Stochastic Environmental Research and Risk Assessment* 28(2):333–346. doi:10.1007/s00477-013-0752-8

Hargreaves GH, Samani ZA (1982) Estimation of potential evapotranspiration. *Journal of the Irrigation and Drainage Division* 108(3):223–230

Hargreaves GH, Samni ZA (1985) Reference crop evapotranspiration from temperature. *Applied Engineering in Agriculture* 1(2):96–99. doi:10.13031/2013.26773

Hashimoto T, Stedinger JR, Loucks DP (1982) Reliability, resiliency and vulnerability criteria for water resource system performance evaluation. *Water Resources Research* 18(1):14–20. doi:10.1029/WR018i001p00014

He S, Li S, Xie R, Lu J (2016) Baseflow separation based on a meteorology-corrected nonlinear reservoir algorithm in a typical rainy agricultural watershed. *Journal of Hydrology* 535:418–428. doi:10.1016/j.jhydrol.2016.02.010

Heim Jr RR (2002) A review of twenty-century drought indices used in the United State. *Bulletin of the American Meteorological Society* 83(8):1149–1165. doi:10.1175/1520-0477(2002)083<1149:AROTDI>2.3.CO;2

Hoerling MP, Eischeid JK, Quan XW, Diaz HF, Webb RS, Dole RM, Esterling DR (2012) Is a transition to semi-permanent drought conditions imminent in the U.S. Great Plains? *Journal of Climate* 25(24):8380–8386. doi:10.1175/JCLI-D-12-00449.1

Hourdin F, Musat I, Bony S, Braconnot P, Codron F, Dufresne JL, Fairhead L, Filiberti MA, Friedlingstein P, Grandpeix JY, Krinner G (2006) The LMDZ4 general circulation model: climate performance and

sensitivity to parameterized physics with emphasis on tropical convection. *Climate Dynamics* 27(7):787–813

Huo Z, Feng S, Kang S, Li W, Chen S (2008) Effect of climate changes and water-related human activities on annual stream flows of the Shiyang river basin in arid north–west China. *Hydrological Processes* 22(16):3155–31167. doi:10.1002/hyp.6900

HydroOffice (2015) Download [Online] Available from https://hydrooffice.org/Downloads?Items=Software [Accessed: 14th December 2015]

IPCC (2001) *Intergovernmental Panel on Climate Change. Climate Change 2001: Synthesis Report.* Retrieved 12 December 2013, from http://www.ipcc.ch/pdf/climate-changes-2001/synthesis-syr/english/front.pdf

IPCC (2007) Intergovernmental Panel on Climate Change. In: Parry ML, Canziani O F Palutikof JP, van der Linden PJ, Hanson CE (Eds.), *Climate Change 2007: Impacts, adaptation, and vulnerability. Contribution of working group II to the fourth assessment report of the intergovernmental panel on climate change*, Cambridge University Press, Cambridge, pp. 1–976

IPCC (2014) Intergovernmental Panel on Climate Change. Climate Change 2014: Impacts, adaptation, and vulnerability. http: //www.ipcc.ch/report/ar5/wg2. [Accessed: 15th May 2015]

Jagannathan NV, Mohamed AS, Kremer A (2009) *Water in the Arab world: Management perspectives and innovations*. World Bank, Middle East and North Africa Region

Jiang L, Ban X, Wang X, Cai X (2014) Assessment of hydrologic alterations caused by the Three Gorges Dam in the middle and lower reaches of Yangtze River, China. *Water* 6(5):1419–1434. doi:10.3390/w6051419

Jiang S, Ren L,Yang X, Ma M, Liu Y (2014) Multi-model ensemble hydrologic prediction and uncertainties analysis. *Proceedings of the International Association of Hydrological Sciences* 364:249–254

Jiang S; Ren L, Yong B, Singh VP, Yang X, Yuan F (2011) Quantifying the effects of climate variability and human activities on runoff from the Laohahe basin in northern China using three different methods. *Hydrological Processes* 25(16):2492–2505. doi:10.1002/hyp.8002

Joetzjer E, Douville H, Delire C, Ciais P, Decharme B, Tyteca S (2013) Hydrologic benchmarking of meteorological drought indices at interannual to climate change timescales: A case study of the Amazon and Mississippi River Basins. *Hydrology and Earth System Sciences* 17(12):4885–4895. doi:10.5194/hess-17-4885-2013

Jones RN, Chiew FH, Boughton WC, Zhang L (2006) Estimating the sensitivity of mean annual runoff to climate change using selected hydrological models. *Advances in Water Resources* 29(10):1419–1429. doi:10.1016/j.advwatres.2005.11.001

K-1 Model Developers (2004) K-1 Coupled Model (MIROC) description. Center for Climate System Research, University of Tokyo

Kahya E, Kalayci S (2004) Trend analysis of streamflow in Turkey. *Journal of Hydrology* 289(1):128–144. doi:10.1016/j.jhydrol.2003.11.006

Kiehl JT, Gent PR (2004) The community climate system model, version 2. *Journal of Climate* 17(19):3666–3682. doi:10.1175/1520-0442(2004)017<3666:TCCSMV>2.0.CO;2

Kiehl JT, Hack JJ, Bonan GB, Boville BA, Williamson DL, Rasch PJ (1998) The national center for atmospheric rsearch community climate model: CCM3. *Journal of Climate* 11(6):1131–1149. doi:10.1175/1520-0442(1998)011<1131:TNCFAR>2.0.CO;2

Kim BS, Kim BK, Kwon HH (2011) Assessment of the impact of climate change on the flow regime of the Han River basin using indicators of hydrologic alteration. *Hydrological Processes* 25(5):691–704. doi:10.1002/hyp.7856

Kiparsky M, Joyce B, Purkey D, Young C (2014) Potential impacts of climate warming on water supply reliability in the Tuolumne and Merced river basins, California. *PloS one* 9(1):e84946. doi:10.1371/journal.pone.0084946

Lee A, Cho S, Kang DK, Kim S (2014) Analysis of the effect of climate change on the Nakdong river stream flow using indicators of hydrological alteration. Journal of Hydro-environment Research 8(3):234–247. doi:10.1016/j.jher.2013.09.003

Li L, Xu H, Chen X, Simonovic SP (2010) Streamflow forecast and reservoir operation performance assessment under climate change. *Water Resources Management* 24(1):83–104. doi:10.1007/s11269-009-9438-x

Li LJ, Zhang L, Wang H, Wang J, Yang JW, Jiang DJ, Li JY, Qin DY (2007) Assessing the impact of climate change and human activities on streamflow from the Wuding River basin in China. *Hydrological Processes* 21(25):3485–3491. doi:10.1002/hyp.6485

Lim KJ, Engel BA, Tang Z, Choi J, Kim KS, Muthukrishnan S, Tripathy D (2005) Automated web GIS based hydrograph analysis tool, WHAT. JAWRA *Journal of the American Water Resources Association* 41(6):1407–1416. doi:10.1111/j.1752-1688.2005.tb03808.x

Lim KJ, Park YS, Kim J, Shin YC, Kim NW, Kim SJ, Jeon JH, Engel BA (2010) Development of generic algorithm-based optimisation module in WHAT system for hydrograph analysis and model application. *Computers and Geosciences* 36(7):936–944. doi:10.1016/j.cageo.2010.01.004

Linsley RK, Kohler MA, Paulhus JLH (1988) *Hydrology for engineers*. McGraw-Hill, London, UK

Logan KE, Brunsell NA, Jones AR, Feddema JJ (2010) Assessing spatiotemporal variability of drought in the U.S. central plains. *Journal of Arid Environments* 74(2):247–255. doi:10.1016/j.jaridenv.2009.08.008

Longobardi A, Villani P (2008) Baseflow index regionalization analysis in a Mediterranean area and data scarcity context: Role of the catchment permeability index. *Journal of Hydrology* 355(1–4):63–75. doi: 10.1016/j.jhydrol.2008.03.011

Lott DA, Stewart MT (2016) Baseflow separation: A comparison of analytical and mass balance Methods. *Journal of Hydrology* 535:525–533. doi:10.1016/j.jhydrol.2016.01.063

Loukas A, Vasiliades L, Tzabiras J (2008) Climate change effects on drought severity. *Advances in Geosciences* 17:23–29

Lu S, Wu B, Wei Y, Yan N, Wang H, Guo S (2015) Quantifying impacts of climate variability and human activities on the hydrological system of the Haihe River Basin, China. *Environmental Earth Sciences* 73(4):1491–1503. doi:10.1007/s12665-014-3499-8

Ludwig F, van Slobbe E, Cofino W (2014) Climate change adaptation and Integrated Water Resource Management in the water sector. *Journal of Hydrology* 518:235–242. doi:10.1016/j.jhydrol.2013.08.010

Ma Z, Kang S, Zhang L, Tong L, Su X (2008) Analysis of impacts of climate change and human activity on streamflow for a river basin in arid region of northwest China. *Journal of Hydrology* 352(3–4):239–349. doi:10.1016/j.jhydrol.2007.12.022

Mao Y, Nijssen B, Lettenmaier DP (2015) Is climate change implicated in the 2013-2014 California drought? A hydrologic perspective. *Geophysical Research Letters* 42(8):2805–2813. doi:10.1002/2015GL063456

Martin GM, Ringer MA, Pope VD, Jones A, Dearden C, Hinton TJ (2006) The physical properties of the atmosphere in the new Hadley Centre Global Environmental Model (HadGEM1). I. model description and global climatology. *Journal of Climate* 19(7):1274–1301

Matonse AH, Pierson DC, Frei A, Zion MS, Anandhi A, Schneiderman E, Wright B (2013) Investigating the impact of climate change on New York City's primary water supply. *Climatic Change* 116(3–4):437–456. doi:10.1007/s10584-012-0515-4

Maurer EP, Hidalgo HG, Das T, Dettinger MD, Cayan DR (2010) The utility of daily large-scale climate data in the assessment of climate change impacts on daily streamflow in California. *Hydrology and Earth System Sciences* 14(6):1125–1138. doi:10.5194/hess-14-1125-2010

McFarlane NA, Boer GJ, Blanchet JP, Lazare M (1992) The Canadian Climate Centre second-generation general circulation model and its equilibrium climate. *Journal of Climate* 5(10):1013–1044

McKee TB, Doesken NJ, Kleist J (1993) The relationship of drought frequency and duration to time scales. *Proceedings of the 8th Conference on Applied Climatology* 17(22):179–183.

McMahon T, Mein RG (1978) Reservoir capacity and yield. *Development in Water Science* 9, Elsevier, Amsterdam

McMahon TA, Adeloye AJ (2005). *Water resources yield*. Water Resources Publications, Littleton, Colorado, USA

McMahon TA, Adeloye AJ, Zhou SL (2006) Understanding performance measures of reservoirs. *Journal of Hydrology* 324(1):359–382. doi:10.1016/j.jhydrol.2005.09.030

McMahon TA, Mein RG (1986) *River and reservoir yield*. Water Resources Publications, Ft, Collins, Colorado

McMahon TA, Peel MC, Lowe L, Srikanthan R, McVicar TR (2013) Estimating actual, potential, reference crop and pan evaporation using standard meteorological data: a pragmatic synthesis. *Hydrology and Earth System Sciences* 17(4):1331–1363. doi:10.5194/hess-17-1331-2013

McVicar TR, Jupp DL (1998) The current and potential operational uses of remote sensing to aid decisions on drought exceptional circumstances in Australia: A review. *Agricultural systems* 57(3):399–468. doi:10.1016/S0308-521X(98)00026-2

Medbasin 2.1 (2016) Download [Online] Available from http://www.ewra.net/medbasin/ [Accessed: 10th May 2016]

Mei Y, Anagnostou EN (2015) A hydrograph separation method based on information from rainfall and runoff records. *Journal of Hydrology* 523:636–649. doi:10.1016/j.jhydrol.2015.01.083

Miao C, Ni J, Borthwick AG, Yang L (2011) A preliminary estimate of human and natural contributions to the changes in water discharge and sediment load in the Yellow River. *Global and Planetary Change* 76(3–4):196–205. doi:10.1016/j.gloplacha.2011.01.008

Michel D, Pandya A (2009) *Troubled Waters—Climate change, hydropolitics, and transboundary resources*. The Henry L. Stimson Center, Washington DC, USA

Michelangeli PA, Vrac M, Loukos H (2009) Probabilistic downscaling approaches: Application to wind cumulative distribution functions. *Geophysical Research Letters* 36(11):1–6. doi:10.1029/2009GL038401

Miller MP, Buto SG, Susong DD, Rumsey CA (2016) The importance of baseflow in sustaining surface water flow in the Upper Colorado River Basin. *Water Resources Research* 52(5):3547–3562. doi:10.1002/2015WR017963

Minville M, Brissette F, Krau S, Leonte R (2009) Adaptation to climate change in the management of a Canadian water-resources system exploited for hydropower. *Water Resources Management* 23(14):2965–2986. doi:10.1007/s11269-009-9418-1

Mittal N, Mishra A, Singh R, Bhave AG, van der Valk M (2014) Flow regime alteration due to anthropogenic and climatic changes in the Kangsabati River, India. *Ecohydrology and Hydrobiology* 14(3):182–191. doi:10.1016/j.ecohyd.2014.06.002

Mittal N, Bhave AG, Mishra A, Singh R (2016) Impact of human intervention and climate change on natural flow regime. *Water Resources Management* 30(2):685–699. doi:10.1007/s11269-015-1185-6

Mohammed R, Scholz M (2016) Impact of climate variability and streamflow alteration on groundwater contribution to the base flow of the Lower Zab River (Iran and Iraq). *Environmental Earth Sciences* 21(75):1–11. doi:10.1007/s12665-016-6205-1

Mohammed R, Scholz M (2017a) Impact of evapotranspiration formulations at various elevations on the reconnaissance drought index. *Water Resources Management* 31:531–538. doi:10.1007/s11269-016-1546-9

Mohammed R, Scholz M (2017b) The reconnaissance drought index: A method for detecting regional arid climatic variability and potential drought risk. *Journal of Arid Environments* 144:181–191. doi:10.1016/j.jaridenv.2017.03.014

Mohammed R, Scholz M (2017c) Adaptation strategy to mitigate the impact of climate change on water resources in arid and semi-arid regions: A case study. *Water Resources Management* (1–17). doi:10.1007/s11269-017-1685-7

Mohammed R, Scholz M, Nanekely MA, Mokhtari Y (2017a) Assessment of models predicting anthropogenic interventions and climate variability on surface runoff of the Lower Zab River. *Stochastic Environmental Research and Risk Assessment* (1–18). doi:10.1007/s00477-016-1375-7 (in press)

Mohammed R, Scholz M, Zounemat-Kermani M (2017b) Temporal hydrologic alterations coupled with climate variability and drought for transboundary river basins. *Water Resources Management* 31(5):1489–1502. doi:10.1007/s11269-017-1590-0

Moy WS, Cohon JL, ReVelle CS (1986) A programming model for analysis of the reliability, resilience, and vulnerability of a water supply reservoir. *Water Resources Research* 22(4):489–498. doi:10.1029/WR022i004p00489

Mulder G, Olsthoorn TN, Al-Manmi DAMA, Schrama EJO, Smidt EH (2015) Identifying water mass depletion in northern Iraq observed by GRACE. *Hydrology and Earth System Sciences* 19(3):1487–1500. doi:10.5194/hess-19-1487-2015

Nalbantis I (2008) Evaluation of a Hydrological drought index. *European Water* 23(24):67–77

Nash JE, Sutcliffe JV (1970) River flow forecasting through conceptual models, Part 1: A discussion of principles. *Journal of Hydrology* 10(3):282–290. doi:10.1016/0022-1694(70)90255-6

Nathan RJ, McMahon TA (1990) Evaluation of automated techniques for baseflow and recession analysis. *Water Resources Research* 26(7):1465–1473. doi:10.1029/WR026i007p01465

NOAA (2009) National Oceanic and Atmospheric Administration Climate of Iraq. [Online] Available from https://www.ncdc.noaa.gov/oa/climate/afghan/iraq-narrative.html [Accessed: 4th November 2015]

Oguntunde PG, Abiodun BJ, Lischeid G (2011) Rainfall trends in Nigeria, 1901–2000. *Journal of Hydrology* 411(3):207–218. doi:10.1016/j.jhydrol.2011.09.037

Park JY, Kim SJ (2014) Potential impacts of climate change on the reliability of water and hydropower supply from the multipurpose dam in South Korea. JAWRA *Journal of the American Water Resources Association* 50(5):1273–1288. doi:10.1111/jawr.12190

Partington D, Brunner P, Simmons CT, Werner AD, Therrien R, Maier HR, Dandy GC (2012) Evaluation of outputs from automated baseflow separation methods against simulated baseflow from a physically based, surface water-groundwater flow model. *Journal of Hydrology* 458–459:28–39. doi:10.1016/j.jhydrol.2012.06.029

Payne JT, Wood AW, Hamlet AF, Palmer RN, Lettenmaier DP (2004) Mitigating the effects of climate change on the water resources of the Columbia River Basin. *Climatic Change* 62(1):233–256. doi:10.1023/B:CLIM.0000013694.18154.d6

Perrin C, Michel C, Andréassian V (2003) Improvement of a parsimonious model for streamflow simulation. *Journal of Hydrology* 279(1):275–289. doi:10.1016/S0022-1694(03)00225-7

Pope VD, Gallani ML, Rowntree PR, Stratton RA (2000) The impact of new physical parametrizations in the Hadley Centre climate model: HadAM3. *Climate Dynamics* 16(2):123–146

Price K (2011) Effects of watershed topography, soils, land use, and climate on baseflow hydrology in humid regions: A review. *Progress in Physical Geography* 35(4):465–492. doi:10.1177/0309133311402714

Ragab R, Prudhomme C (2002) Climate change and water resources management in arid and semi-arid regions: Prospective and challenges for the 21st century. *Biosystems Engineering* 81(1):3–34. doi:10.1006/bioe.2001.0013

Raje D, Mujumdar PP (2010) Reservoir performance under uncertainty in hydrologic impacts of climate change. *Advances in Water Resources* 33(3):312–326. doi:10.1016/j.advwatres.2009.12.008

Reis J, Culver TB, Block PJ, McCartney MP (2016) Evaluating the impact and uncertainty of reservoir operation for malaria control as the climate changes in Ethiopia. *Climatic Change* 136(3–4):601–614. doi:10.1007/s10584-016-1639-8

Richter BD, Baumgartner JV, Braun DP, Powell J (1998) A spatial assessment of hydrologic alteration within a river network. *Regulated Rivers: Research and Management* 14(4):329–340. doi:10.1002/(SICI)1099-1646(199807/08)14:4<329::AID-RRR505>3.0.CO;2-E

Richter B, Baumgartner J, Wigington R, Braun D (1997) How much water does a river need? *Freshwater Boillogy* 37(1):231–249. doi:10.1046/j.1365-2427.1997.00153.x

RS MINERVE 2.5 software (2016) Download [Online] Available from: https://www.crealp.ch/down/rsm/install2/archives.html [Accessed: 15th June 2016]

Robaa SM, AL-Barazanji ZJ (2013) Trends of annual mean surface air temperature over Iraq. *Nature and Science* 11(12):138–145

Ringer MA, Martin GM, Greeves CZ, Hinton TJ, James PM, Pope VD, Scaife AA, Stratton RA, Inness PM, Slingo JM, Yang GY (2006) The physical properties of the atmosphere in the new Hadley Centre Global Environmental Model (HadGEM1). Part II: aspects of variability and regional climate. *Journal of climate* 19(7):1302–1326

Roeckner E, Arpe K, Bengtsson L, Christoph M and others (1996) *The atmospheric general circulation model ECHAM-4: Model description and simulation of present-day climate*. Max-Planck-Institut für Meteorologie, Hamburg, Germany

Rothamsted Research (2017) Long Ashton Research Station Weather Generator (LARS-WG5.5) [Online] Available from http://www.rothamsted.ac.uk/mas-models/larswg.php [Accessed: 07th March 2017]

Rossi G, Cancelliere A (2013) Managing drought risk in water supply systems in Europe: A review. *International Journal of Water Resources Development* 29(2):272–289. doi:10.1080/07900627.2012.713848

Rumsey CA, Millera MP, Susonga DD, Tillman FD, Anning DW (2015) Regional-scale estimates of baseflow and factors influencing baseflow in the Upper Colorado River Basin. *Journal of Hydrology: Regional Studies* 4:91–107. doi:10.1016/j.ejrh.2015.04.008

Russell GL, Miller JR, Rind D (1995) A coupled atmosphere–ocean model for transient climate change studies. *Atmosphere-ocean* 33(4):683–730

Saha S, Moorthi S, Wu X, Wang J, Nadiga S, Tripp P, Behringer D, Hou YT, Chuang H, Iredell M, Ek M, Meng J, Yang R, Mendez MP, Dool HVD, Zhang Q, Wang W, Chen M, Becker E (2014) The NCEP climate forecast system version 2. *Journal of Climate* 27(6):2185–2208. doi:10.1175/JCLI-D-12-00823.1

Schaefli B, Hingrray B, Musy A (2007) Climate change and hydropower production in the Swiss Alps: quantification of potential impacts and related modeling uncertainties. *Hydrology and Earth System Sciences Discussions* 11(3):1191–1205. doi:10.5194/hess-11-1191-2007

Seibert J, Vis M (2012) Teaching hydrological modeling with a user-friendly catchment–runoff-model software package. *Hydrology and Earth System Sciences* 16(9):3315–3325. doi:10.5194/hess-16-3315-2012

Semenov MA, Stratonovitch P (2010) Use of multi-model ensembles from global climate models for assessment of climate change impacts. *Climate Research* 41(1):1–14. doi:10.3354/cr00836

Semenov MA, Pilkington-Bennett S, Calanca P (2013) Validation of ELPIS 1980-2010 baseline scenarios using the observed European climate assessment data set. *Climate Research* 57:1–9. doi:10.3354/cr01164

Sen OL, Unal A, Bozkurt D, Kindap T (2011) Temporal changes in the Euphrates and Tigris discharges and teleconnections. *Environmental Research Letters* 6(2):1–9. doi:10.1088/1748-9326/6/2/024012

Shadmani M, Marofi S, Roknian M (2012) Trend analysis in reference evapotranspiration using Mann-Kendall and Spearman's Rho tests in arid regions of Iran. *Water Resources Management* 26(1):211–224. doi:10.1007/s11269-011-9913-z

Shahidian S, Serralheiro RP, Serrano J, Teixeira J, Haie N, Santos F (2012) Hargreaves and other reduced-set methods for calculating evapotranspiration. In Irmak, A (Ed.), *Evapotranspiration - Remote Sensing and Modeling* pp.59–80. InTech, Rijeka, Croatia

Shamsnia SA (2014) Comparison of reconnaissance drought index (RDI) and standardized precipitation index (SPI) for drought monitoring in arid and semiarid regions. *Indian Journal of Fundamental and Applied Life Sciences* ISSN: 2231-6345, 4(3):39–44

Sharp E, Dodds P, Barrett M, Spataru C (2015) Evaluating the accuracy of CFSR reanalysis hourly wind speed forecasts for the UK, using in situ measurements and geographical information. *Renewable Energy* 77:527–538. doi:10.1016/j.renene.2014.12.025

Sheffield J, Wood EF, Roderick ML (2012) Little change in global drought over the past 60 years. *Nature* 491(7424):435–438. doi:10.1038/nature11575

Smakhtin VU (2001) Low flow hydrology: A review. *Journal of Hydrology* 240(3–4):147–186. doi:10.1016/S0022-1694(00)00340-1

Soundharajan BS, Adeloye AJ, Remesan R (2016) Evaluating the variability in surface water reservoir planning characteristics during climate change impacts assessment. *Journal of Hydrology* 538:625–639. doi:10.1016/j.jhydrol.2016.04.051

Stagl JC, Hattermann FF (2016) Impacts of climate change on riverine ecosystems: alterations of ecologically relevant flow dynamics in the Danube River and its major tributaries. *Water* 8(12):566. doi:10.3390/w8120566

Stewart MK (2015) Promising new baseflow separation and recession analysis methods applied to streamflow at Glendhu Catchment, New Zealand. *Hydrology and Earth System Sciences* 19(6):2587–2603. doi: 10.5194/hess-19-2587-2015

Suen JP (2010) Potential impacts to freshwater ecosystems caused by flow regime alteration under changing climate conditions in Taiwan. *Hydrobiologia* 649(1):115–128. doi:10.1007/s10750-010-0234-7

Sujono J, Shikasho S, Hiramatsu K (2004) A comparison of techniques for hydrograph recession analysis. *Hydrological Processes* 18(3):403–413. doi:10.1002/hyp.1247

Sun T, Feng ML (2013) Multistage analysis of hydrologic alterations in the Yellow River, China. *River Research and Applications* 29(8):991–1003. doi:10.1002/rra.2586

Tabari H, Taalaee PH (2011) Analysis of trend in temperature data in arid and semi-arid regions of Iran. *Global and Planetary Change* 79(1–2):1–10. doi:10.1016/j.gloplacha.2011.07.008

Tallaksen LM, van Lanen HA (2004) *Hydrological drought – processes and estimation methods for streamflow and groundwater*. Developments in Water Sciences 48. Elsevier, Amsterdam

The Nature Conservancy (2009) *Indicators of hydrologic alteration version 7.1 user's manual*. The Nature Conservancy, June, 76

Thematic mapping (2009) World Borders Dataset [Online] Available from: http://thematicmapping.org/downloads/world_borders.php. [Accessed: 2nd October 2015]

Tigkas D (2008) Drought characterisation and monitoring in regions of Greece. *European Water* 23(24):29–39

Tigkas D, Tsakiris G (2004) Medbasin: A Mediterranean Rainfall-runoff software package. *European Water* 5(6):3–11

Tigkas D, Vangelis H, Tsakiris G (2012) Drought and climatic change impact on streamflow in small watersheds. *Science of the Total Environment* 440:33–41. doi:10.1016/j.scitotenv.2012.08.035

Tigkas D, Vangelis H, Tsakiris G (2015) DrinC: A software for drought analysis based on drought indices. *Earth Science Informatics* 8(3):697–709. doi:10.1007/s12145-014-0178-y

Tsakiris G, Loukas A, Pangalou D, Vangelis H, Tigkas D, Rossi G, Cancelliere A (2007) Drought characterization [Part 1. Components of drought planning. 1. 3. Methodological component]. In Iglesias A, Moneo M, López-Fran cos (Eds.) *Drought management guidelines technical annex* A, CIHEAM / ECMEDA Water, Zaragoza, pp.85–102

Tsakiris G, Vangelis H (2005) Establishing a drought index incorporation evapotranspiration. *European Water* 9(10):3–11

Trzaska S, Schnarr E (2014) *A review of downscaling methods for climate change projections*. United States Agency for International Development by Tetra Tech ARD, pp.1–42

UNESCO, United Nations Educational, Scientific and Cultural Organization (1979) *Map of the world distribution of arid regions: Map at scale 1:25,000,000 with an explanatory note*. MAB Technical Notes 7, UNESCO, Paris

UNESCO, United Nations Educational, Scientific and Cultural Organization (2014) *Integrated Drought Risk Management-DRM National Framework for Iraq*. An analysis report. Retrieved from http://unesdoc.unesco.org/images/0022/002283/228343E.pdf UN-ESCWA

UN-ESCWA and BGR Inventory of Shared Water Resources in Western Asia (2013) United Nations Economic and Social Commission for Western Asia (UN-ESCWA) and Bundesanstalt für Geowissenschaften und Rohstoffe (BGR), Beirut

USGS, United States Geological Survey (2010) *Stream gage descriptions and streamflow statistics for sites in the Tigris river and Euphrates river basins, Iraq*. Data Series 540. Reston, VA: USGS

Vaheddoost B, Aksoy H (2016) Structural characteristics of annual precipitation in Lake Urmia basin. *Theoretical and Applied Climatology* (1–14). doi:10.1007/s00704-016-1748-3

Vallam P, Qin XS, Yu JJ (2014) Uncertainty quantification of hydrologic model. APCBEE *Procedia* 10:219–223. doi:10.1016/j.apcbee.2014.10.042

Vangelis H, Tigkas D, Tsakiris G (2013) The effect of PET method on reconnaissance drought index (RDI) calculation. *Journal of Arid Environments* 88:130–140. doi:10.1016/j.jaridenv.2012.07.020

Velázquez JA, Anctil F, Ramos MH, Perrin C (2011) Can a multi-model approach improve hydrological ensemble forecasting? A study on 29 French catchments using 16 hydrological model structures. *Advances in Geosciences* 29:33–42. doi:10.5194/adgeo-29-33-2011

Vicente-Serrano SM, Schrier G, Begueria S, Azorin-Molina C, Lopez-Moreno J (2015) Contribution of precipitation and reference evapotranspiration to drought indices under different climates. *Journal of Hydrology* 526:42–54. doi:10.1016/j.jhydrol.2014.11.025

Vicente-Serrano SM, Begueria S, Lopez-Moreno JI (2010) A Multiscalar drought index sensitive to global warming: The standardized precipitation evapotranspiration index. *Journal of Climate* 23(7):1696–1718. doi:10.1175/2009JCLI2909.1

Vicente-Serrano SM, Lopez-Moreno JI, Beguería S, Lorenzo-Lacruz J, Sanchez-Lorenzo A, García-Ruiz, JM, Azorin-Molina C, Morán-Tejeda E, Revuelto J, Trigo R, Coelho F (2014) Evidence of increasing drought severity caused by temperature rise in southern Europe. *Environmental Research Letters* 9(4):044001. doi:10.1088/1748-9326/9/4/044001

Vicuna S, Dracup JA (2007) The evolution of climate change impact studies on hydrology and water resources in California. *Climatic Change* 82(3):327–350. doi:10.1007/s10584-006-9207-2

Viviroli D, Archer DR, Buytaert W, Fowler HJ, Greenwood G, Hamlet AF, Huang Y, Koboltschnig G, Litaor I, López-Moreno JI, Lorentz S (2011) Climate change and mountain water resources: overview and recommendations for research, management, and policy. *Hydrology and Earth System Sciences* 15(2):471–504. doi:10.5194/hess-15-471-2011

Viviroli D, Durr HH, Messerli B, Meybeck M, Weingartner R (2007) Mountains of the world, water towers for humanity: Typology, mapping, and global significance. *Water Resources Research* 43(7):W07447. doi:10.1029/2006WR005653

Wan L, Xia J, Hong S, Bu H, Ning L, Chen J (2015) Decadal climate variability and vulnerability of water resources in arid regions of Northwest China. *Environmental Earth Sciences* 73(10):6539–6552. doi:10.1007/s12665-014-3874-5

Wang B, Wan H, Ji Z, Zhang X, Yu R, Yu Y, Liu H (2004) Design of a new dynamical core for global atmospheric models based on some efficient numerical methods. *Science in China Series A: Mathematics* 47:4–21

Wang W, Shao Q, Yang T, Peng S, Xing W, Sun F, Luo Y (2013) Quantitative assessment of the impact of climate variability and human activities on runoff changes: A case study in four catchments of the Haihe River basin, China. *Hydrological Processes* 27(8):1158–1174. doi.org/10.1002/hyp.9299

Wang Y, Rhoads BL,Wang D (2016) Assessment of the flow regime alterations in themiddle reach of the Yangtze River associatedwith damconstruction: potential ecological implications. *Hydrological Processes* 30(21):3949–3966. doi:10.1002/hyp.10921

Watts RJ, Richter BD, Opperman JJ, Bowmer KH (2011) Dam reoperation in an era of climate change. *Marine and Freshwater Research* 62(3):321–327

Welderufael WA, Woyessa YE (2010) Stream flow analysis and comparison of methods for baseflow separation: Case study of the Modder River basin in central South Africa. *European of Water* 31:3–12

Wilby RL, Dawson CW, Murphy C, O'Connor P, Hawkins E (2014) The statistical DownScaling model-decision centric (SDSM-DC): Conceptual basis and applications. *Climatic Research* 61(3):251–268. doi:10.3354/cr01254

WMO, World Meteorological Organization (2009) *Manual of low-flow estimation and prediction*. Operational Hydrology Report Number 50, World Meteorological Organization (WMO) Report Number 1029, WMO, Geneva

Xu CY, Singh VP (2001) Evaluation and generalization of temperature-based methods for calculating evaporation. *Hydrological Processes* 15(2):305–319. doi:10.1002/hyp.119

Yan Y, Yang Z, Liu Q, Sun T (2010) Assessing effects of dam operation on flow regimes in the lower Yellow River. *Procedia Environmental Sciences* 2:507–516. doi:10.1016/j.proenv.2010.10.055

Yang T, Zhang Q, Chen YD, Tao X, Xu CY, Chen X (2008) A spatial assessment of hydrologic alteration caused by dam construction in the middle and lower Yellow River, China. *Hydrological Processes* 22(18):3829–3843. doi: 10.1002/hyp.6993

Ye X, Zhang Q, Liu J, Li X, Xu CY (2013) Distinguishing the relative impacts of climate change and human activities on the variation of streamflow in the Poyang Lake catchment, China. *Journal of Hydrology* 494:83–95. doi: 10.1016/j.jhydrol.2013.04.036

Yoo C (2006) Long-term analysis of wet and dry years in Seoul, Korea. *Journal of Hydrology* 318(1–4):24–36. doi:10.1016/j.jhydrol.2005.06.002

Zarch MAA, Sivakumar B, Sharma A (2015) Droughts in a warming climate: A global assessment of standardized precipitation index (SPI) and reconnaissance drought index (RDI). *Journal of Hydrology* 526:183–195. doi:10.1016/j.jhydrol.2014.09.071

Zhang L, Dawes WR, Walker GR (2001) Response of mean annual evapotranspiration to vegetation changes at catchment scale. *Water Resources Research* 37(3):701–708. doi:10.1029/2000WR900325

Zhang Q, Xu CY, Yang T (2009) Variability of Water Resource in the Yellow River Basin of Past 50 Years, China. *Water Resources Management* 23(6):1157–1170. doi:10.1007/s11269-008-9320-2

Zhao F, Zhang L, Xu Z, Scott DF (2010) Evaluation of methods for estimating the effects of vegetation change and climate change on streamflow. *Water Resources Research* 46(3):W03505. doi:10.1029/2009WR007702

Zheng Z, Lu W, Chu H, Cheng W, Zhao Y (2014) Uncertainty analysis of hydrological model parameters based on the bootstrap method: A case study of the SWAT model applied to the Dongliao River Watershed, Jilin Province, Northeastern China. *Science China Technological Sciences* 57(1):219–229. doi:10.1007/s11431-013-5385-0

Appendix A Climate Forecasting System Reanalysis Datasets and Land-Based Datasets Correlation

Table A1 Relationships between the land-based meteorological station datasets and the climate forecasting system reanalysis datasets

Meteorological variable		Station ID	Mean	SD[a]	Max[b]	Min[c]	RMSE[d]	Corr coffe[e]
Precipitation		Makhmool	8.30	2.64	12.39	4.35	2.15	0.62
		358438	8.20	2.54	10.73	1.86		
		Kirkuk	8.29	3.39	14.47	3.71	2.72	0.54
		354444	8.11	2.77	10.84	1.81		
Temperature	Max[b]	Makhmool	29.32	0.50	30.00	28.40	0.36	0.90
		358438	29.09	0.63	30.13	28.33		
		Kirkuk	29.27	0.59	30.39	28.59	0.30	0.91
		354444	29.09	0.63	30.13	28.33		
	Min[c]	Makhmool	16.52	0.54	17.85	16.09	2.38	0.90
		358438	14.15	0.56	15.64	13.72		
		Kirkuk	17.22	0.54	18.32	16.40	0.20	0.98
		354444	17.06	0.58	18.27	16.38		

[a]Standard deviation; [b]Maximum; [c]Minimum; [d]Root mean square error; and [c]Correlation coefficient

Appendix B Published Journal Papers

Paper 1

Environ Earth Sci (2016)75:1392
DOI 10.1007/s12665-016-6205-1

ORIGINAL ARTICLE

Impact of climate variability and streamflow alteration on groundwater contribution to the base flow of the Lower Zab River (Iran and Iraq)

Ruqayah Mohammed[1] · **Miklas Scholz**[2]

Received: 9 February 2016 / Accepted: 14 October 2016

Abstract Overall water resources evaluations including groundwater contributions to river flow are critical for assessing climate change and drought impacts on basin hydrological responses. By utilising precipitation, daily stream flow and simulated river discharge alteration data, this study introduces a simple but comprehensive methodology to better understand the potential impact of river regulation coupled with climate variability and drought on groundwater involvement. The Lower Zab River basin in northern Iraq has been selected as a representative case study to demonstrate the new methodology. Three of the most commonly used base flow separation methods were assessed: Eckhardt algorithm, flow duration curve and Chapman filtering algorithm. In addition, the indicators of hydrologic alteration method and the reconnaissance drought index have been applied. The results demonstrated that some of the underground water responds to precipitation events. A noticeable increase in groundwater contribution has been observed during the hydrological years between 1998–2001 and 2006–2008 as a result of a sharp decline in the average precipitation. However, the opposite has been observed during the hydrological year 1987, which impacted negatively on the basin water resources availability. The reservoir release through the dry periods causes the observed variations in base flow index (BFI) values between the pre- and post-river damming time periods. Considering the BFI long-term seasonal variation, index values started to rise in April and reached their maximum by the end of June. A steady decline has been recorded between August and September.

Keywords Climatology · Environmental assessment · Groundwater contamination and vulnerability · Hydrogeology · Surface water · Water management

✉ Miklas Scholz
miklas.scholz@tvrl.lth.se

[1] Civil Engineering Research Group, School of Computing, Science and Engineering, The University of Salford, Newton Building, Peel Park Campus, Salford, Greater Manchester M5 4WT, UK

[2] Division of Water Resources Engineering, Department of Building and Environmental Technology, Faculty of Engineering, Lund University, P.O. Box 118, 221 00 Lund, Sweden

Published online: 25 October 2016

Introduction

Background

Separation of streamflow hydrographs into dry-weather or base flow and direct run-off components is a useful technique to understand the groundwater contribution to rivers, in particular, when concerned with a varied range of water resources organisation matters (Brodie and Hostetler 2005; Lu et al. 2015). Such techniques also have been utilised to quantify the groundwater element of hydrological budgets and to assist in the estimation of recharge rates. The direct run-off component represents the additional streamflow contributed by sub-surface flow and surface flow, whereas the base flow component represents steady groundwater flow contributions to river discharge. Brodie and Hostetler (2005) argued that the exploration of groundwater inputs to watercourses is important when discussing matters such as the water resources supply probability of failure, water distribution and design of water storages, hydroelectric power generation and water needs for ecosystems.

Various techniques have been developed to isolate the base flow from the overall run-off hydrograph, which is

traditionally categorised into three basic techniques: graphical base flow isolation, filtering algorithms frequency analysis and recession analysis (Brodie and Hostetler 2005; WMO 2009; Welderufael and Woyessa 2010). Tallaksen and van Lannen (2004) pointed out that Nathan and McMahon (1990) distinguished between methods for continuous separation regarding different components of flow.

Graphical methods separate the base flow component on a discharge hydrograph by connecting an intersection point of base flow and direct flow upon the hydrograph rising limb lowest flow point to a point on the falling limb where it is assumed all flows are changed to base flow (Linsley et al. 1988; Welderufael and Woyessa 2010). These techniques partition base flow in different ways that vary in their complexity and involve the constant flowrate, constant slope and concave technique (Brodie and Hostetler 2005). Conversely, Lim et al. (2005) confirmed that the main drawback of these techniques is that they do not provide consistent outcomes even with similar flow data.

The filtering techniques are the most regularly used methods in river flow separation, which splits the base flow by a filtering or processing procedure (Eckhardt 2005; Lim et al. 2005, 2010; Welderufael and Woyessa 2010). These methods have been recommended for providing reproducible results, can easily be automated, and should be linked to the base flow react of a river basin (Arnold et al. 2000; Eckhardt 2005). For the purpose of this paper, two of the recursive digital filtering techniques have been used: the Eckhardt (2005) and Chapman (1999) methods. The latter is one of the most commonly used recursive filtering algorithms for base flow separation.

The frequency duration or flow duration curve method represents the relationship between the magnitude and the frequency of daily, weekly or monthly discharges for a specific river watershed (Cigizoglu and Bayazit 2000). It is another widespread approach to analyse the characteristics of a river and used to estimate the time percentage the stream discharge is equal or exceed a historical period (Welderufael and Woyessa 2010). If the contributions of groundwater are minor, the curve slope at the lower end tends to be steep, whereas a flat curve indicates significant base flow.

A number of indices can be provided by flow duration curves to describe the streamflow rating or regionalisation purposes. If the flow exceeds 50% of the time, the median Q50 value gives an average measure (Gordon et al. 2004). The Q90 or Q95 values are commonly used as low flow indices. The ratio of Q90/Q50 can be utilised as an index of base flow. Various techniques have been developed to isolate the base flow from the overall run-off hydrograph.

Hydrograph recession analysis is considered as one of the widely used techniques for separation of the base flow at a basin scale (Sujono et al. 2004). The main focus of the recession study is on the recession curve that is the falling limb of the hydrograph, which follows the stream crest when discharge reduces. Recession parts are chosen from the hydrographic value and can be separately or simultaneously analysed to obtain and understand the processes which impact dry-weather conditions. For a single hydrograph recession, a semi-logarithmic plot is originally applied for isolating a hydrograph into linear elements of river flow, interflow and dry-weather flow. When assessing a set of hydrograph recessions at a certain basin at the same time, a master recession curve is usually applied. Along with the graphical method, the fitting procedure also might be performed mathematically.

The base flow index (BFI) is the percentage of base flow to total flow estimated from a hydrograph separation approach. It was initially developed in a low flow analysis in the UK (Abebel and Foerch 2006) for describing the hydrological reaction of soils and geology of the basin. A high BFI value would expose the basin ability to feed flow of the stream during prolonged dry time periods. The BFI is associated with many characteristics of the river basin such as soil type and geology, topography, vegetation and climate (Tallaksen and van Lannen 2004; Longobardi and Villani 2008; Welderufael and Woyessa 2010; Price 2011). The index can change between 0.15 and 0.20 for an impervious basin to larger than 0.95 for a basin with a high storage volume and a steady flow system (WMO 2009).

Representative case study region

The Lower Zab River (also known as Little Zab River and Lesser Zab River) is one of the main tributaries of the Tigris River in the Erbil governorate in the north-east of Iraq. The river is situated with its tributaries between latitudes 36°50′N and 35°20′N, and longitudes 43°25′E and 45°50′E (Saeedrashed and Guven 2013) as shown in Fig. 1. The current study examines the daily flow rate for the hydrological years between 1931 and 2013 at Dokan station, which is considered as a key hydrometric gauging station (Latitude 35°53′00″N and Longitude 44°58′00″E). A vast majority of rivers have highly altered discharges as a result of water resources development and use; for example, the Lower Zab River has artificially relatively high flows during summer due to releases of water from the Dokan reservoir storage to supply irrigation and urban users.

Rationale, aim, objectives and significance

Particular activities that can affect dry-weather may contain river flow regulations, where river discharge is controlled through infrastructure elements such as dams, weirs or locks. Discharges from surface water storage structures

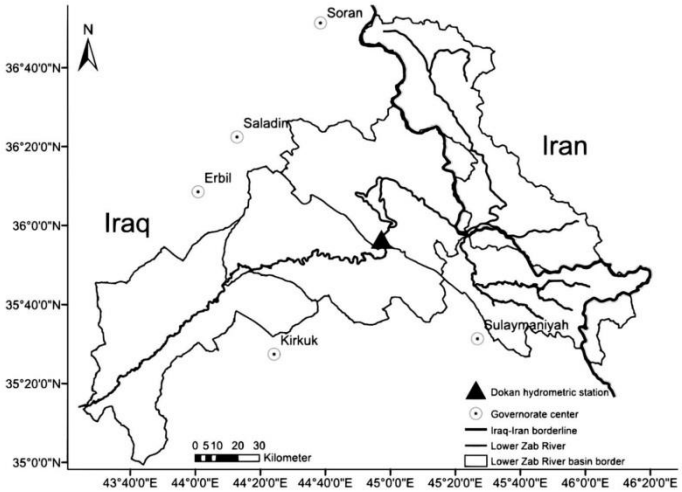

Fig. 1 Overview of the Lower Zab River basin shapefile showing the Dokan hydrometric station location

for downstream stakeholders can make up the bulk of river during dry times reducing the groundwater contribution, which in turn decreases the dry-weather index. Many researchers argued that dry-weather assessment should be performed in unregulated reaches, or at least the regulated basin area should be $\leq$10% of the basin area of the river gauge (Al-Faraj and Scholz 2014). This study explores the effects of weather variability and anthropogenic interventions on river flow alteration. Then the sensitivity of groundwater to such changes will be assessed. This will be achieved through a new generic methodology to enable engineers and water resources policy makers to make informed and robust decisions on adaptation and mitigation strategies in the face of climate variability.

The aim is to assess to what extent upstream river damming will alter the base flow pattern of the downstream part of the river basin by assessing the effect of river regulation on the base flow analysis. This will be achieved by addressing the following objectives:

- To develop a generic and simplified methodology for studying the impacts of river damming linked to climate change and drought on the groundwater contribution to river flow;
- To integrate the Eckhardt digital filtering algorithm (Eckhardt 2005) with the flow duration curve to derive α, which is the filter parameter of the Lower Zab River basin (Fig. 1);
- To compare the obtained results with the base flow that was gained from the Chapman (1999) digital filtering algorithm;
- To quantify the base flow contribution to the Lower Zab River (Fig. 1) flow as a function of time; and
- To evaluate the sensitivity of the groundwater contribution to river flows.

The flowchart visualised in Fig. 2 reveals how the above research objectives can be integrated to achieve the main research aim.

This study represents a critical step towards better understanding of the potential impact of river damming and streamflow alteration, climate change and drought events on groundwater contributions to river flow. The research outcomes will benefit engineers and decision makers in evaluating the contribution of groundwater at a basin scale.

Methods

The current research considers two recursive digital filtering algorithms coupled with the frequency duration function. The filtering algorithms are the one proposed by Eckhardt (2005) and a filtering algorithm by Chapman (1999). Both methods were utilised to isolate the dry-weather flow of the upper Lower Zab River basin from the daily mean streamflow as recorded at the inlet of the Dokan reservoir (Latitude 35°53′00″N and Longitude 44°58′00″E).

The Eckhardt (2005) method is applied to accomplish low pass filtering on the hydrograph to isolate the base flow, depending on Eq. (1):

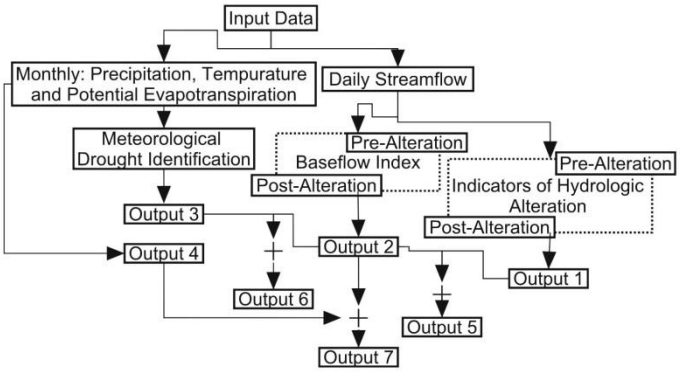

Fig. 2 New methodology for assessing the impacts of river damming as well as climate change and drought events on the groundwater contribution to river flow

$$BF_t = \frac{(1 - BFI_{max}) \times \alpha \times BF_{t-1} + (1 - \alpha) \times BFI_{max} \times TF_t}{1 - \alpha \times BFI_{max}} \quad (1)$$

where BF (m^3/s) is the separated base flow, BFI_{max} is the long-term percentage of dry-weather to total river flow, TF (m^3/s) is the total streamflow, α is the filter parameter, and t is the time step subject to $BF_t \leq TF_t$.

The Eckhardt recursive method needs to identify two parameters (Eckhardt 2005): (i) the recession constant α, which can be resulted from recession curves statistical assessment of the hydrograph and (ii) the maximum amount of the base flow index BFI_{max}, which cannot be observed, but optimised based on the outcomes of other techniques. In this study, BFI_{max} was considered to be 0.25.

The second recursive digital filtering algorithm (Chapman 1999) is represented by Eq. (2):

$$DF_t = \frac{3 \times \alpha - 1}{3 - \alpha} \times TF_{t-1} + \frac{2}{3 - \alpha} \times (TF_t - TF_{t-1}) \quad (2)$$

where DF_t (m^3/s) is the direct run-off, TF (m^3/s) is the total streamflow, α is the filter parameter, and t is the step of time.

However, the flow duration curve known as frequency duration curve is defined as a plot, which shows the ratio of time that a river discharge is possible to be equal or exceed some certain flow values. Such a curve depicts the catchment ability to provide flows of different values. The shape of the upper and lower areas of the plot is particularly important in assessing the channel and catchment attributes. The high flow region shape specifies the kind of flood system the catchment is expected to characterise, whilst the shape of the low flow area characterises the capacity of the catchment to endure dry seasons' low discharges.

The curve appearance is highly affected by a basic time unit that is used in drawing it. For example, when average daily discharges are used, then the resultant curve will be steep, whereas when a long period average flow such as a flow monthly mean is used, the resulting curve will be flat owing to averaging of short-term peaks with the intervening smaller flows during this month. Maximum values are progressively averaged out, as the period of time gets longer, e.g., for a flow duration curve depended on yearly discharges at a long record station.

To plot the flow duration curve, many steps have to be followed. Firstly, average daily discharges need to be sorted from the largest to the smallest number, involving a total of n values. Secondly, each discharge value should be assigned a rank M, starting with 1 for the largest daily discharge value. Thirdly, the exceedance probability using Eq. (3) has to be calculated.

$$P = \left(\frac{M}{n+1}\right) \times 100 \quad (3)$$

where P is the probability that a specific discharge will be equal to or exceed a specific percentage of time; M is the ranked (dimensionless) location on the listing; and n is the (dimensionless) figure of events for a period of the record.

Commonly, the Q50 is considered as the median discharge. A discharge $\geq$ Q50 is interpreted as low flow. The ratio of Q90/Q50 represents a proportion of the streamflow contribution from groundwater aquifers or the corresponding ratio of the base flow element (Smakhtin 2001; Welderufael and Woyessa 2010; Stewart 2015).

Taking into consideration the generic methodology that has been suggested and utilised in this study, the results of the FDC analysis have been coupled with the Eckhardt algorithm to obtain the α value after taking $BFI_{max} = 0.25$, which has been suggested by Eckhardt (2005) for perennial

rivers with porous aquifers. Firstly, the long-term average yearly ratio of the total run-off from the dry-weather flow was determined after estimating the Q90 and Q50 values by using the flow duration curve analysis, coupling the Eckhardt recursive digital filtering algorithm with the flow duration curve. Based on $\alpha = 0.925$ as a starting value (Arnold and Allen 1999; Smakhtin 2001), the daily river flow is filtered for different values of filter parameter α until the BFI is equal to the Q90/Q50 ratio. Various dry-weather time series were obtained through using the filtered α value. After that, linear regression models were undertaken between the yearly BFI and the annual run-off for pre-regulated, post-regulated and integrated time periods to investigate the impact of river damming on the dry-weather contribution.

Results and discussion

Eckhardt integrated with flow duration curve

Three time periods have been considered in the current research. Pre-river damming is considered as the first time period covering the water years from 1931 to 1965. The post-river damming is the second studied time period that spans from 1966 to 2013, whereas the hydrological years 1931–2013 is the third time period, which is referred here as an integrated time period.

According to the outcome of the daily FDC at Dokan location for the pre- and post-river damming, the integrated time periods indicated that the Q90 and Q50 discharges were 35 and 101, 31 and 100, and 33 and 100 m^3/s, respectively. Accordingly, the BFI, which is the Q90/Q50 ratio, were nearly 35, 31, and 33%, respectively, representing volumes of water that the river might be gaining from sub-surface flow or other delayed shallow groundwater sources regarding the studied periods.

This indicates that the BFI of the pre-regulated period was moderately greater than the values computed for both the post-regulated and the integrated time periods. This can be attributed to the reduction in the groundwater involvement in the total Lower Zab River flow as a result of water being released from the reservoir during the dry period, which in turn reduces the BFI. Therefore, more consideration should be given to evaluate the aquifer characteristics and comprehend the aspects that might cause such alterations for improving managing of sub-surface resources within the basin.

Impact assessment of river regulation on dry-weather separation

For the pre-regulated time period between 1931 and 1965, and taking into consideration Eckhardt's digital filtering algorithm, outcomes reveal that the filter parameter α with a value of 0.982 produces a BFI that is the same as the one obtained from the FDC study. The yearly base flow volumes over this period fluctuate between 0.632 billion cubic meters (bcm) recorded in 1958 and 2.826 bcm observed in 1953. The corresponding yearly base flow depth varies between nearly 30 and 132 mm a year. The long-term yearly mean base flow volume and the matching standard deviation were 1.478 and 0.512 bcm in this order (Figs. 3a, c).

Whereas the annual base flow magnitudes calculated by the Chapman algorithm over the same hydrological time periods varied between 1.38 bcm recorded in 1958 and 5.71 bcm observed in 1953, the corresponding yearly base flow changed between approximately 65 mm a year and about 266 mm a year. The long-term yearly mean base flow storage and the corresponding standard deviation were 2.91 and 1.05 bcm, respectively (Figs. 3b, d).

Based on the established linear regression model expressed in Eqs. (4) and (5), Table 1 shows the linear regression models between the separated base flow and the total surface run-off for the two considered algorithms. Figure 3 reveals high coefficients of determination (R^2) of 0.99 and 0.92 for the Eckhardt and the Chapman algorithms in this order.

For the post-regulated time period that spans from the hydrological years 1965–2013, and based on the outcome of the Eckhardt algorithm, the annual base flow magnitudes vary between 0.437 bcm recorded in 2006 and 3.647 bcm observed in 1968. The matching yearly base flow changed from nearly 21 mm per year to nearly 170 mm per year. The long-term yearly mean base flow storage and the corresponding standard deviation were 1.45 and 0.70 bcm, respectively (Figs. 3a, c). However, the annual base flow magnitudes obtained from the Chapman algorithm varied from 0.871 bcm observed in 2006 to 7.077 bcm measured in 1968. The corresponding yearly base flow changed between about 40 mm per year to about 330 mm per year. The long-term yearly mean base flow volume and the conforming standard deviations were 2.88 and 1.31 bcm, respectively (Figs. 3b, d).

Additionally, a high R^2 of 0.99 was observed for the developed linear model Eq. (6). Table 1 indicates the association between the separated base flow and total flow for the two studied algorithms (Fig. 3e). Moreover, Fig. 3c and d characterises the base flow, which is separated by the two considered filtering algorithms for the pre- and post-damming time periods. The obtained results indicate that the two studied recurrence filtering algorithms are strongly correlated. The $R^2 = 0.91$ and 0.99 for the base flow values obtained from the two algorithms. The created linear regression models are expressed in Eqs. (7) and (8) (Table 1).

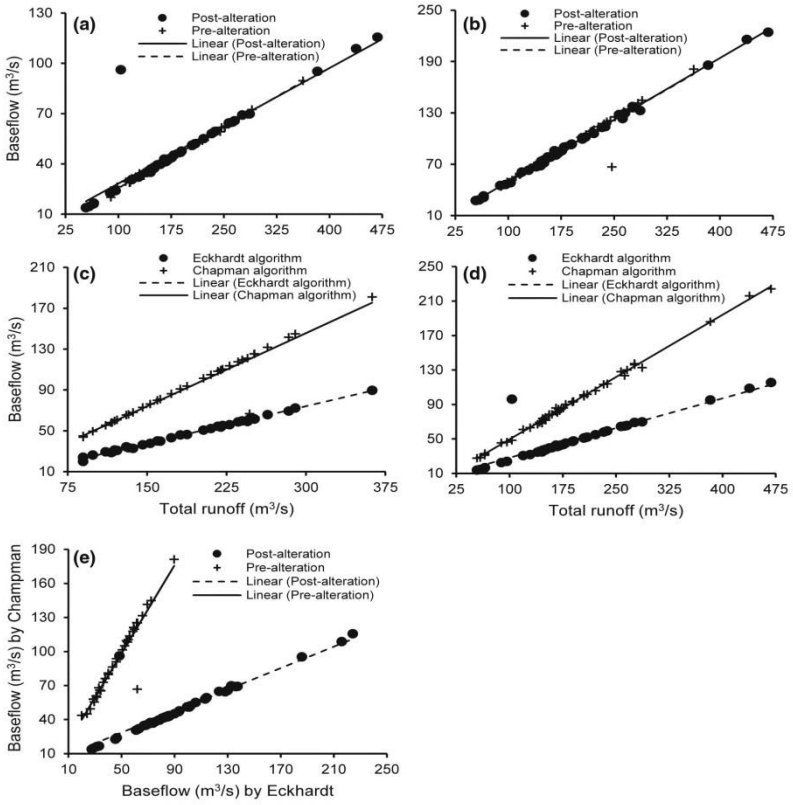

Fig. 3 The linear regression models for the relationships between the separated base flow and the total runoff **a** using the Eckhardt method; and **b** applying the Chapman recursive digital filtering algorithm for the time periods **c** pre-alteration; **d** post-alteration; and **e** the relationship between the two considered methods

Furthermore, Fig. 4 shows the long-term variations of the total flow and the separated base flow volumes coupled with the BFI for the considered time periods. The derived base flows for all studied periods show almost similar patterns. However, a noticeable variation has been observed for the BFI for the post-alteration time period, which can be due to the water released from the river basin storage system.

Assessment of base flow index linked to climate variability and drought phenomena

The detection of the potential effects of climate variability on the meteorological and hydrological variables, and base flow index (BFI) over the upper part of the study area can be considered as a substantial step in the analysis of the impact of climate change on basin water resources availability. The main consequence of climate change is that wet and dry years are characterised by high and low flows in that order.

Yoo (2006) proposed that wet years are defined as periods in which the annual basin precipitation is more than the mean precipitation (P_{av}) + 0.75 × standard deviation (SD), whereas dry years are characterised by precipitation that is no more than the $P_{av}-0.75 \times SD$. Therefore, hydrological years with annual precipitation values between these two thresholds can be considered as normal years: $P_{av}-0.75 \times SD \leq P \leq P_{av} + 0.75 \times SD$ (Yang

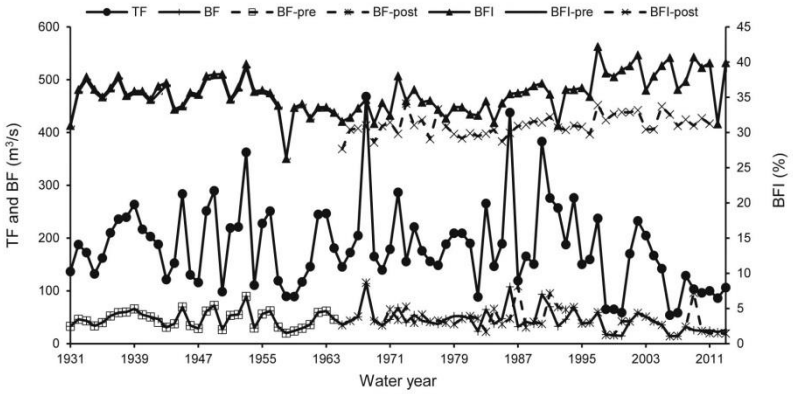

Fig. 4 Long-term monthly variation of total flow (TF), base flow (BF) and base flow index (BFI) at Dokan hydrometric station estimated by the Eckhardt filtering algorithm coupled with the flow duration curve (FDC) for the three studied time periods

Table 1 Developed linear regression models for the three considered time periods using both the Eckhardt algorithm linked to the flow duration curve and the Chapman digital algorithm

Equation		R^2	Time period	Algorithm
No.	Formulation			
4	$BF^a = 0.482 \times TF^b + 1.40$	0.99	Pre-alteration	Eckhardt
5	$BF = 0.476 \times TF + 2.74$	0.92		Chapman
6	$BF = 0.482 \times TF + 1.40$	0.99	Post-alteration	Eckhardt
7	$BF = 0.23 \times BF + 5.24$	0.79		Chapman
8	$BF\text{-Chapman} = 0.51 \times BF\text{-Eckhardt} - 0.15$	0.99		
9	$BF = 0.24 \times TF + 1.24$	0.99	Pre-alteration	Eckhardt
10	$BF = 0.48 \times TF + 1.40$	0.99	Post-alteration	
11	$BF = 0.24 \times TF + 1.78$	0.97	Integrated	
12	$BF = 0.28 \times TF + 2.74$	0.92	Pre-alteration	Chapman
13	$BF = 0.48 \times TF + 1.40$	0.99	Post-alteration	
14	$BF = 0.24 \times TF + 1.78$	0.97	Integrated	

[a] Base flow

[b] Total run-off

et al. 2008). Figure 5 shows BFI time series for both wet and dry year thresholds.

Figure 5 also reveals that the water year 1987 witnessed a significant ($p < 0.05$) increase in the basin average precipitation of about 44% more than the normal water year maximum threshold. The considerable increase in the amount of precipitation results in a dramatic change in the river flow to about 118% (Fig. 6; Table 2), which in turn reduces the contribution of the groundwater to the total flow to the river. Whereas the complete opposite was noticed for the hydrological periods between 1998 and 2001, and between 2006 and 2008. These two periods witnessed a sharp decline in the basin average precipitation to about 40 and 60%, respectively. The decrease of average precipitation led to a dramatic reduction in the Lower Zab River streamflow by approximately 66, 77 and 79% (corresponding annual mean flow volumes of 0.35×10^9 m^3, 0.31×10^9 m^3 and 0.34×10^9 m^3) (Table 3) for the water years 1998/1999, 1999/2000 and 2000/2001, which in turn increases the groundwater contribution, which is represented by the BFI. However, the hydrological years 2006/2007, 2007/2008 and 2008/2009 witnessed about 52, 80 and 83% streamflow reductions with corresponding 0.76×10^9 m^3, 0.29×10^9 m^3 and 0.31×10^9 m^3 annual

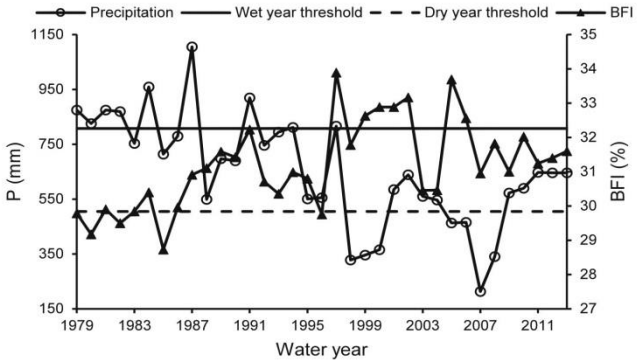

Fig. 5 Long-term base flow index (BFI) with both wet and dry year thresholds coupled with long-term average precipitation for the time periods between 1979 and 2014

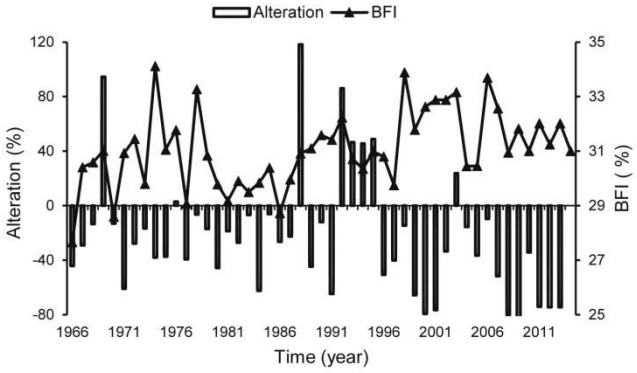

Fig. 6 Annual median anomaly of the Lower Zab River basin flows linked with the long-term base flow index (BFI) for the time period between 1966 and 2014

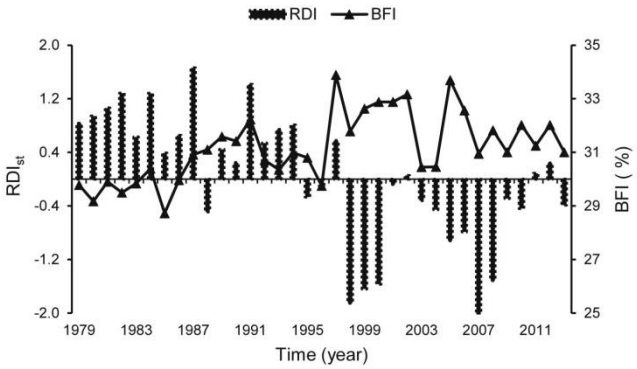

Fig. 7 Annual median anomaly of the Lower Zab River basin flows linked with the long-term base flow index (BFI) for the time period between 1966 and 2014. The reconnaissance drought index (RDI) coupled with the long-term base flow index (BFI) for the Lower Zab River basin between 1979 and 2014

Table 2 Annual river flows, storage volumes, means of changed to unchanged storage ratios, and median anomalies between the periods 1979–1980 and 1987–1988

Water year	Flow (m^3/s)	Storage ($\times 10^9$ m^3)	Percentage change	
			Long-term mean yearly storage	Anomaly
1979–1980	148	4.68	0.79	−46
1980–1981	189	5.96	1.00	−19
1981–1882	210	6.61	1.11	−27
1982–1983	190	6.00	1.01	−7
1983–1984	88	2.79	0.47	−62
1984–1985	268	8.46	1.42	−6
1985–1986	148	4.66	0.78	−26
1986–1987	190	5.98	1.01	−23
1987–1988	436	13.75	2.31	+118

Table 3 Annual river flows, storages, means of changed to unchanged storage rations, and median anomalies between the period 1998–1999 and 2008–2009

Water year	Flow (m^3/s)	Storage ($\times 10^9$ m^3)	Percentage change	
			Long-term mean yearly storage	Anomaly
1998–1999	66	2.08	0.35	−66
1999–2000	65	2.04	0.34	−79
2000–2001	59	1.87	0.31	−77
2001–2002	171	5.40	0.91	−34
2002–2003	233	7.36	1.24	+24
2003–2004	205	6.46	1.09	−15
2004–2005	170	5.37	0.90	−37
2005–2006	170	5.38	0.90	−10
2006–2007	144	4.53	0.76	−52
2007–2008	54	1.70	0.29	−80
2008–2009	59	1.85	0.31	−83

mean flow volumes, respectively (Table 3). Furthermore, between 1991 and 2013, the natural flow regime witnessed a steep decline during which the flow alteration varied between −75 and 86% with corresponding 0.31×10^9 m^3 and 1.24×10^9 m^3 maximum and minimum annual mean storage volumes, respectively. Accordingly, the BFI increased from nearly 31 to almost 35%.

Figure 7 presents the RDI_{st} values calculated for the case study region based on data from 1979 to 2014 in addition to long-term average BFI and indicates that a non-uniform cyclic pattern of drought and wet periods was observed for the study area concerning the studied time span. Noticeable droughts on a seasonal basis were observed for five years during the considered historical record, particularly for 1998/1999, 1999/2000, 2000/2001, 2007/2008 and 2008/2009 (average RDI values: −1.84, −1.67, −1.45, −2.91 and −1.53, respectively), which were also reported by many previous studies such as Fadhil (2011) and UNESCO (2014). Based on the observed drought phenomena over the study area, the groundwater contribution was increased dramatically from about 30–35%.

Figure 8 shows that the basin potential to recharge the Lower Zab River with water from aquifers started to increase dramatically from April until reaching the maximum value by the end of June, remaining constant until the middle of August and starting to decline slightly until the end of September. In addition, during the dry season, the BFI values revealed generally relatively high magnitudes of fluctuation, and they took relatively long time periods before reaching the peak point. Findings indicate that during the last few decades, climate change and drought phenomena have negatively affected the Lower Zab River storage water availability.

Conclusions and recommendations

The long-term mean annual BFI of the studied geographical region varied from 31, 33 and 35% for the pre-alteration, post-alteration and integrated time periods, respectively. The obtained results suggest that 31, 33, and 35% of the long-term discharge in the Lower Zab River basin results from both the groundwater contribution and shallow sub-surface flow. The rather small variations in

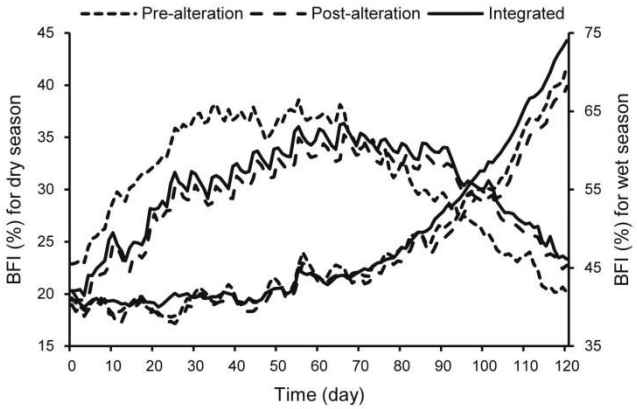

Fig. 8 Wet and dry seasonal variations of the base flow index (BFI) at Dokan hydrometric station estimated by the Eckhardt filtering algorithm coupled with the flow duration curve for the three studied time periods

base flow contribution between the pre-alteration and the post-alteration time period resulted from water released from the reservoir during the dry period to cover the downstream water requirements. Therefore, more consideration must be given to the assessment of the characteristics of aquifers and understanding the factors that might lead to such variations. This could lead to improvements in the management of groundwater resources within the basin. This is because it is critical to investigate the base flow contribution to total discharge as a result of the pressing requirement for logical use of water resources and strong competition among several of the riparian nations. Furthermore, the proposed methodology can lead a better appreciation of the signature of the base flow and enlighten how the river damming, transformation and water utilisation in the upper part of the basin might alter the flow pattern of the base flow of the lower part of the basin.

The base flow index values increased in April and peaked by the end of June. A gradual decrease has been recorded between August and September. The water year 1987 witnessed a significant increase in the basin average precipitation of about 44% more than the normal water year maximum threshold. This resulted in a considerable change of the river flow to about 118% in addition to the reduction in the groundwater contribution to the total flow of the river. Furthermore, the water years for periods between 1998 and 2001 and 2006–2008 witnessed a sharp decline in the basin average precipitation to about 40 and 60%, respectively. This led to a considerable reduction in the river flow by approximately 52 and 83%, which in turn increased the groundwater contributions.

Seasonal droughts, which were observed during five years during the considered historical records (particularly for 1998/1999, 1999/2000, 2000/2001, 2007/2008 and 2008/2009 corresponding average RDI values of −1.84, −1.67, −1.45, −2.91 and −1.53, respectively) resulted in a dramatic increase in terms of the corresponding groundwater contribution.

During the last few decades, there was a dramatic alteration in the river flow in particular during the non-rainy months. The variation might be attributed to the influence of both river damming and climate variability pressure in the upper part of the case study area, which in turn decreased the basin storage system availability from both surface and underground sources. Research findings imply that river alteration and climate variability should be considered for future stream basin managing strategies to escape the temporal disparity between strategy and such changes. Therefore, the proposed methodology is a rather practical and simple tool for the formulation of future river basin managing strategies, when difficult hydrological methods cannot be simulated through hydrological models, because of lack of measured data. Furthermore, the research should also be undertaken again for other regulated river basins located in different climatic zones to evaluate the impact of river damming and climate change on ground water contribution to streamflow.

Acknowledgements The research presented has been financially supported by the Iraqi Government. Thanks go to Furat Al-Faraj, Amjad Hussain and Al-Isawi Rawaa (all based at The University of Salford) for their kind help and support.

References

Abebel A, Foerch G (2006) Catchment characteristics as predictors of dry-weather index (BFI) in Wabi Shebele river basin, East Africa. Paper presented at the Conference on International Agricultural Research for Development, Tropentag 2006, University of Bonn, Bonn. http://citeseerx.ist.psu.edu/viewdoc/download?doi=10.1.1.112.3449&rep=rep1&type=pdf. Accessed 8 Feb 2016

Al-Faraj F, Scholz M (2014) Incorporation of the flow duration curve method within digital filtering algorithms to estimate the base flow contribution to total runoff. Water Resour Manag 28(15):5477–5489

Arnold JG, Allen PM (1999) Validation of automated methods for estimating baseflow and groundwater recharge from stream flow records. J Am Water Resour Assoc 35(2):411–424. doi:10.1111/j.1752-1688.1999.tb03599.x

Arnold JG, Muttiah RS, Srinivasan R, Allen PM (2000) Regional estimation of base flow and groundwater recharge in the upper Mississippi river basin. J Hydrol 227(1–4):21–40. doi:10.1016/S0022-1694(99)00139-0

Brodie RS, Hostetler S (2005) A review of techniques for analyzing base-flow from stream hydrographs. Proceedings of the NZHS-IAH-NZSSS 2005 Conference, 28 November–2 December 2005, Auckland, New Zealand. http://data.daff.gov.au/data/warehouse/brsShop/data/iah05_dry-weather_final.pdf. Accessed 8 Feb 2016

Chapman T (1999) A comparison of algorithms for streamflow recession and baseflow separation. Hydrol Process 13(5):701–714. doi:10.1002/(SICI)1099-1085(19990415)13:5<701:AID-HYP774>3.0.CO;2-2

Cigizoglu HK, Bayazit M (2000) A generalized seasonal model for flow duration curve. Hydrol Process 14(6):1053–1067. doi:10.1002/(SICI)1099-1085(20000430)14:6<1053:AID-HYP996>3.0.CO;2-B

Eckhardt K (2005) How to construct recursive digital filters for base flow separation. Hydrol Process 19:507–515

Fadhil MA (2011) Drought mapping using geoinformation technology for some sites in the Iraqi Kurdistan region. Int J Digit Earth 4(3):239–257. doi:10.1080/17538947.2010.489971

Gordon NC, McMahon TA, Finlayson BL, Gippel CJ, Nathan RJ (2004) Stream hydrology: an introduction for ecologists, 2nd edn. Wiley, Chichester

Lim KJ, Engel BA, Tang Z, Choi J, Kim KS, Muthukrishnan S, Tripathy D (2005) Automated web GIS based hydrograph analysis tool, WHAT. J Am Water Res Assoc 41(6):1407–1416

Lim KJ, Parka YS, Kima J, Shina Y, Kimb NW, Kime SJ, Jeon JH, Engel BA (2010) Development of generic algorithm-based optimisation module in WHAT system for hydrograph analysis and model application. Comput Geosci 36(7):936–944. doi:10.1016/j.cageo.2010.01.004

Linsley RK, Kohler MA, Paulhus JLH (1988) Hydrology for engineers. McGraw-Hill, London

Longobardi A, Villani P (2008) Dry-weather index regionalization analysis in a Mediterranean area and data scarcity context: role of the catchment permeability index. J Hydrol 355(1):63–75

Lu S, Wu B, Wei Y, Yan N, Wang H (2015) Quantifying impacts of climate variability and human activities on the hydrological system of the Haihe River Basin, China. Hydrol Earth Syst Sci 73:1491–1503

Nathan RJ, McMahon TA (1990) Evaluation of automated techniques for baseflow and recession analysis. Water Resour Res 26(7):1465–1473. doi:10.1029/WR026i007p01465

Price K (2011) Effects of watershed topography, soils, land use, and climate on base flow hydrology in humid regions: a review. Prog Phys Geogr 35(4):465–492. doi:10.1177/0309133311402714

Saeedrashed Y, Guven A (2013) Estimation of geomorphological parameters of Lower Zab River-Basin by using GIS-based remotely sensed image. Water Res Manag 27(1):209–219. doi:10.1007/s11269-012-0179-x

Smakhtin VU (2001) Low flow hydrology: a review. J Hydrol 240(3–4):147–186. doi:10.1016/S0022-1694(00)00340-1

Stewart MK (2015) Promising new baseflow separation and recession analysis methods applied to streamflow at Glendhu catchment, New Zealand. Hydrol Earth Syst Sci 19(6):2587–2603. doi:10.5194/hess-19-2587-2015

Sujono J, Shikasho S, Hiramatsu K (2004) A comparison of techniques for hydrograph recession analysis. Hydrol Process 18(3):403–413. doi:10.1002/hyp.1247

Tallaksen LM, van Lanen HAJ (2004) Hydrological drought—processes and estimation methods for streamflow and groundwater. Developments in water sciences, vol 48. Elsevier, Amsterdam

UNESCO (2014) United Nations Educational, Scientific and Cultural Organization. Integrated drought risk management-DRM National framework for Iraq. An analysis report. http://unesdoc.unesco.org/images/0022/002283/228343E.pdf UN-ESCWA and BGR (United Nations Economic and Social Commission for Western Asia; Bundesanstalt für Geowissenschaften und Rohstoffe) Inventory of shared water resources in Western Asia, Beirut

Welderufael W, Woyessa Y (2010) Stream flow analysis and comparison of methods for base flow separation: case study of the Modder River basin in central South Africa. Eur Water 8(2):107–119

WMO (2009) World Meteorological Organization. Manual of low-flow estimation and prediction, operational hydrology Report Number 50, World Meteorological Organization (WMO) Report Number 1029, WMO, Geneva

Yang T, Zhang Q, Xu C-Y, Chen X (2008) A spatial assessment of hydrologic alteration caused by dam construction in the middle and lower Yellow River, China. Hydrol Process 22(18):3829–3843. doi:10.1002/hyp.6993

Yoo C (2006) Long term analysis of wet and dry years in Seoul, Korea. J Hydrol 318(1–4):24–36

Paper 2

Water Resour Manage (2017) 31:531–548
DOI 10.1007/s11269-016-1546-9

Impact of Evapotranspiration Formulations at Various Elevations on the Reconnaissance Drought Index

Ruqayah Mohammed[1] · **Miklas Scholz**[1,2]

Received: 27 January 2016 / Accepted: 14 November 2016 /
Published online: 22 November 2016

Abstract Numerous drought indices with various intricacy have been utilised in several climatic regions. Presently, the reconnaissance drought index (RDI), which is considered as a powerful index of meteorological drought, is acquisitioning approval primarily in semi-arid and arid climatologic areas. Because RDI is based on precipitation (P) and evapotranspiration (ET), it assesses the ET estimation effects on the characterisation of drought severity computed by RDI. The current study sheds light on the impact of the ET methods, and the elevation and climate conditions on the RDI annual results, (particularly, the alpha form of the index ($RDI_{\alpha 12}$)), using three of the most widespread experimental ET estimates with low data requirements. These techniques are known as Thornthwaite, Hargreaves, and Blaney-Criddle, and are utilised in addition to the Food and Agriculture Organization Penman-Monteith reference technique. Data from 24 stations for the period from 1979 to 2014 cover different elevations and climatic conditions. No significant ($P > 0.05$) impacts on both the standardised (RDI_{st}) and normalised (RDI_n) forms of the RDI were detected by applying the considered ET methods at various elevations for various climatic conditions. However, the $RDI_{\alpha 12}$ is directly influenced with a significant ($P < 0.05$) deviation that has been observed by various ET methods at different elevations and climate conditions. Accordingly, consideration should be paid to the ET estimation methodologies, in particular at high elevations. The use of various approaches may lead to flaws in availability of water resources and water quality forecasts.

Keywords Agriculture · Aridity evaluation · Elevation indicator · Irrigation · Penman-Monteith · Water resources management

✉ Miklas Scholz
miklas.scholz@tvrl.lth.se

[1] School of Computing, Science and Engineering, Civil Engineering Research Group, The University of Salford, Newton Building, Greater Manchester M5 4WT, UK

[2] Division of Water Resources Engineering, Department of Building and Environmental Technology, Faculty of Engineering, Lund University, P.O. Box 118, 221 00 Lund, Sweden

1 Introduction

1.1 Background

One of the main water-related hazards is drought (Giannikopoulou et al. 2014), which should be considered as a three-dimensional event characterised by its severity, duration and affected area (Tsakiris and Vangelis 2005; Vangelis et al. 2013; Zarch et al. 2015). Despite the fact that there is no commonly agreed definition of the term drought, a commonly acceptable one describes the event as a considerable decline of the water availability during a lengthy time period and over a spacious region (Tigkas 2008).

For identifying, quantifying and monitoring of drought, there are different suggested methodologies. One of the most popular methods, which are distinctive collections of indicators involving meteorological, hydrological and other data, is the estimation of drought indices (Tsakiris and Vangelis 2005; Tigkas 2008; Vangelis et al. 2013; Giannikopoulou et al. 2014). Drought indices might be categorised into two main groups: the common indices and the more detailed ones. The former gives an outline of the drought event and its strength, while the latter are generally beneficial for related drought occurrences to the prospective destructions from drought in different areas of the environment, society and overall economy (Tigkas 2008; Tigkas et al. 2012). The indices are vital and practical elements for characterising drought and supporting policy makers for moderating its impacts on various water consumption sections, since they facilitate intricate interrelationships between several climatic variables. Noticeably, indices make it easier to transfer climate anomaly information to a wide range of audiences and assisting scientists in quantitative weather abnormality evaluations in terms of their intensity, frequency, areal extent and duration (Vangelis et al. 2013; Giannikopoulou et al. 2014). Moreover, when drought indices are utilised, the time steps are adapted and the thresholds of each index selected are considered for representing the levels of drought severity.

A high number of meteorological drought indices with different intricacy have been utilised in various climatic conditions of the world for many objectives. Examples for some of the most common drought indices are as follows: Crop moisture index (CMI), deciles, Palmer drought severity index (PDSI), Palmer hydrological drought index (PHDI), percent of normal, standardized anomaly index (SAI), rainfall anomaly index (RAI), standardized precipitation index (SPI) and soil moisture drought index (SMDI), and surface water supply index (SWSI) as well as indices linked to the normalised difference vegetation index (NDVI). For more details of the most common indices that are used during the last few decades, readers may refer to many studies such as Heim (2002). Moreover, McVicar and Jupp (1998) as well as AghaKouchak et al. (2015) reviewed the current and potential operational uses of remote sensing to aid decisions on drought assessment.

The World Meteorological Organization (WMO) has put forward the SPI as a universal drought index because of its capacity to be estimated for various reference periods adapting to the different response times of typical hydrological parameters to precipitation shortages (Vicente-Serrano et al. 2015). The index allows detection of different drought categories affecting different systems and areas. However, there are deficiencies associated with its failure to identify drought conditions determined not by a shortage of precipitation but by a higher than normal atmospheric evaporative demand. The failure of the SPI to capture a raised evaporative demand associated with climate change is challenging (Tsakiris and Vangelis 2005; Cook et al. 2014). Therefore, recent drought trend studies (Shahidian et al. 2012; Vicente-Serrano et al. 2014) and drought scenarios under potential climate change projections

(e.g., Hoerling et al. 2012; Cook et al. 2014) depend on drought indices that take into account precipitation and the atmospheric evaporative demand. Applying such indices, Cook et al. (2014) showed that increased ET_o not only intensifies drying in areas where precipitation is already decreased, it also drives regions into drought that would otherwise experience little drying or even wetting from precipitation trends alone.

Tigkas et al. (2012, 2015) introduced a summary of the RDI theory with some practical applications, the RDI is founded on the P, which is observed, and the ET, which is estimated. The RDI can be calculated for any time step, and can be effectively related with agricultural drought and directly linked to the climate conditions of the area. Generally, in case of higher temperatures, water demand is increasing; therefore, the RDI could be amended to be used as an indicator for future drought risk assessment related to the various sectors of water use. So, that the RDI is suitable for climate instability conditions studies.

Viviroli et al. (2007) assessed the typology, mapping, and global significance of mountains. The team also made recommendations regarding further research on climate change and mountain water resources (Viviroli et al. 2011). However, their research was more concerned with the potential changes in water resources as a result of climate change, as well as corresponding implications for water resources management, climate change adaptation and water policy.

Drought severity and aridity evaluation are impacted on by the potential impacts of ET methods, meteorological station elevation variations and climate conditions. A growing number of researchers in the field of water resources have recently used the RDI as a drought severity evaluation index (e.g., Tigkas et al. 2012; Vangelis et al. 2013; Giannikopoulou et al. 2014; Cai et al. 2015; Zarch et al. 2015), and they only used the standardised form without taking into consideration other forms and/or if there will be any change in the drought severity evaluation, if the ET methods changed and/or if the weather stations within the same basin have different elevations in addition to the impact of the regional climate conditions. For example, although Vangelis et al. (2013) assessed the potential impact of different ET methods on the drought severity computed by RDI, they only used data from semi-arid climates of the Mediterranean region and only for two meteorological stations without taking into consideration other semi-arid climatic conditions such as tropical and continental in addition to Sahara and humid conditions. Furthermore, they have just focused on the RDIst without giving any attention to the RDIα12. Therefore, to fill the acknowledge gap, this study has focused, in particular, on the alpha form, which is used for aridity evaluation attempting to answer the following questions:

1. How can the ET method(s) impact on the RDI index outcomes, which in turn can change the drought severity and aridity evaluation?
2. If the elevations of the meteorological stations that are located within the same basin would change, how would this alter the evaluation of the drought and aridity of the basin?
3. For regional drought severity and aridity assessments, would changing climatic conditions impact on the ET estimations?

1.2 Rationale, Aim and Objectives

The current study target is to assess the potential impact of ET methods, elevation and climate conditions on the spatiotemporal variability of the RDI. The motivation to study the RDI index is the fact that it is depended on a combination of P and ET, which is considered more realistic than using P only. In addition, the RDI is a newly developed drought index and is used in

several areas all over the word, particularly in semi-arid and arid regions, and became the acquisitioning base as a result of its low data requirements, high sensitivity, resilience and suitability for climate instability (Rossi and Cancelliere 2013; Vicente-Serrano et al. 2015; Zarch et al. 2015). The RDI provides physically thorough theoretical grounds for evaluation of the meteorological drought severity and aridity assessment. Therefore, it is important to evaluate the ET estimation impact, elevation and climate conditions on the aridity and drought severity characterization estimated by this index.

Accordingly, the main aim of the current research is to shed light on the three basic components of the RDI index, in particular, its $RDI_{\alpha 12}$ form. The corresponding objectives are as follows:

- to study the sensitivity of the RDI index;
- To compare the selected methods Hargeaves (HG), Thornthwaite (ThW) and Blaney-Criddle (BC) with the FAO Penman-Monteith (PM) methodology for reference purposes;
- To assess the impact of elevation variations for different climate conditions; and
- To highlight the use of RDI as an aridity and climatic index.

To address these objectives, meteorological data from twenty-four stations all over the world describing semi-arid (Mediterranean (MD), Tropical (TR), and Continental (CN)), Sahara, and humid climatic conditions, representing both mountainous regions and lowlands, have been selected.

2 Theory

2.1 Evapotranspiration Estimation

The evapotranspiration (*ET*) estimation methods can be split into three main groups. The first one is known as hydrologic or water balance methods, which comprises physical techniques, and its application is restricted to the workshop environment.

The second group comprises analytical methods that are based on climatic parameters; in this group, evapo-transpiration processes are expressed by equations, which concentrate on the two key climatic component mass transport and energy balance. The PM and the Priestley-Taylor methodologies are recognized models of this group (Shahidian et al. 2012; Vangelis et al. 2013).

Empirical methods belong to the last group. The underlying assumption is that temperature is a good indicator of the evaporative influence of the atmospheric temperature. These methods became very common as a result of their low data requirements. The HG, ThW and BC equations are the most widely used methods representing this category, which has been considered in this study (see section 3). The following sub-sections provide short descriptions of all the aforesaid ET estimates.

2.1.1 Hargreaves Method

The Hargreaves method is an attractive methodology for the *ET* estimation as it is simple and reliable, requires only a few data is easy-to-compute and has a minimum impact associated with arid weather station results. This method is temperature-based, as it requires only the minimum and maximum values of temperature. The reader may refer to many researches such

as Hargreaves and Samani (1982, 1985) for more details regarding this method. For a specific latitude and day, R_A is usually estimated from published tables or calculated applying a group of equations (Xu and Singh 2001; Vangelis et al. 2013).

$$ET = 0.0230 \times R_A \times {T_m}^{1/2} \times (T_m + 17.80) \tag{1}$$

2.1.2 Thornthwaite Method

This method is one of the temperature-based empirical formula for calculation of *ET*, which is estimated on a monthly basis, and is given by Eq. (2).

$$ET = 16 \times \left(\frac{N}{12}\right) \times \left(\frac{m}{30}\right) \times \left(10 \times \frac{T_m}{I}\right)^a \tag{2}$$

where N is the average monthly possible sunshine hour (hr/day), m is the number of days of each month, T_m is the mean monthly temperature (C°), and α is estimated by Eq. (3).

$$a = 6.75 \times 10^{-7} \times I^3 - 7.71 \times 10^{-5} \times I^2 + 1.79 \times 10^{-2} \times I + 0.49 \tag{3}$$

where I is a heat index for the year calculated according to Eq. (4).

$$I = \sum_{i=1}^{12} \left(\frac{T_{(i)m}}{5}\right)^{1.514} \tag{4}$$

Given the observed monthly average temperatures at a meteorological station, a prediction of the monthly evaporation of the year can be obtained. Despite the fact that this formula is shown by many researches to underestimate *ET*, it has been accepted widely around the globe (Vangelis et al. 2013).

2.1.3 Blaney–Criddle Method

The Blaney–Criddle method is popular and widely used, especially in semi-arid and arid climates, due to its simplicity and ease-of-use. The general form is shown in Eqs. (5) and (6).

$$ET = k \times p \times f \tag{5}$$

$$f = (0.46 \times T_m + 8.13) \tag{6}$$

where ET is the evapotranspiration (mm) from the reference crop, T_m is the average temperature (°C), k is a monthly coefficient representing consumption, p is the ratio of the mean number of daylight hours in the day for the specified month over the total of daylight hours in

the year, which is a function of the latitude of the study area and the month required. Despite the fact that the p value is normally estimated through tables, it can also be computed according to Eq. (7) (Vangelis et al. 2013).

$$p = 100 \times \left(\frac{\sum_{i=d}^{d_2} N_i}{\sum_{i=1}^{365} N_i} \right) \tag{7}$$

where N_i is the theoretical number of daytime hours i, and d_1 and d_2 are the last days of the month.

2.1.4 Food and Agriculture Organization Penman-Monteith Method

The FAO Penman-Monteith method is primarily applied to estimate the reference evapotranspiration (ET) as indicated in Eq. (8) according to McMahon et al. (2013).

$$ET = \frac{0.408 \times (R_n - G) + \gamma \times \frac{900}{T_m + 273} u_2 \times (e_s - e_a)}{\Delta + \gamma \times (1 + 0.34 \times u_2)} \tag{8}$$

where ET is the reference evapotranspiration (mm/day), R_n is the net radiation at the crop surface (MJ/m^2/day), G is the soil heat flux density (MJ/m^2 × day), u_2 is the wind speed at 2-m elevation (m/s), e_s is the saturation vapour pressure (kPa), e_a is the natural vapour pressure (kPa), e_s-e_a is the saturation vapour pressure deficit (kPa), Δ is the slope vapour pressure curve (kPa/°C) and γ is the psychrometric constant (kPa/°C).

2.2 The Reconnaissance Drought Index (RDI)

This index can be formulated in alpha ($RDI_{\alpha k}$), normalised (RDI_n) and standard (RDI_{st}) forms. The RDI_{st} can be used for drought severity assessments, whereas $RDI_{\alpha k}$ can be applied as an aridity index. The index is mainly founded on the aggregated P and ET theories (Vangelis et al. 2013). The RDI is normally estimated using Eq. (9).

$$RDI_{\alpha_0^i} = \frac{\sum_{j=1}^{12} P_{ij}}{\sum_{j=1}^{12} ET_{ij}}, i = 1 \text{ to} N \text{and} j = 1 \text{ to } 12 \tag{9}$$

where P_{ij} and ET_{ij} represent precipitation and evapotranspiration of the j-th month of the i-th water year (the water year in, for example, Iraq begins in October), and N is the obtained weather data total year number.

The values of $RDI_{\alpha k}$ match both the gamma and the lognormal distributions in various positions for various time scales for which they were examined (Tigkas 2008). Through applying the former distribution, RDI_{st} can be computed by utilising Eq. (10).

$$RDI_{st}^{i} = \frac{y^{j} - \bar{y}}{\hat{\sigma}_{y}} \tag{10}$$

where y_i is the $\ln(\alpha_{ki})$, is its arithmetic mean and σ_y is the corresponding standard deviation. Equation (11) can be used to calculate RDI_{st} in the case of the gamma distribution application (Tigkas 2008).

$$g(x) = \frac{1}{\beta^{\gamma} \times \Gamma(\gamma)} x^{\gamma-1} e^{-\frac{x}{\beta}} \text{for } x > 0 \tag{11}$$

where γ and β are the shape and scale parameters, respectively, and $\Gamma(\gamma)$ is the gamma function. The spatiotemporal extent of the gamma probability distribution parameters γ and β can be predicted for 3, 6, 9 and 12 months. The γ and β are estimated by the maximum likelihood method as shown in Eqs. (12) to (14).

$$\gamma = \frac{1}{4A}\left(1 + \sqrt{1 + \frac{4A}{3}}\right) \tag{12}$$

$$\beta = \frac{\bar{x}}{\gamma} \tag{13}$$

$$A = \ln\left(\bar{x}\right) - \frac{\sum \ln(x)}{N} \tag{14}$$

When the cumulative precipitation datasets for the selected reference period contain zeros, the gamma function cannot be defined for $x = 0$. Therefore, a composite cumulative probability function (Eq. (15)) might be utilised.

$$H(x) = q + (1-q) \times G(x) \tag{15}$$

where q is the likelihood of zero precipitation and $G(x)$ is the gamma distribution cumulative probability. The probability of zero precipitation (q) can be computed by m/N if m is the zeros number in the α_k time series. The gamma distribution cumulative probability $G(x)$ is replaced by the cumulative probability $H(x)$.

Compared to the natural conditions, a positive value of RDI_{st} relates to a wet period. The drought severity increases when RDI_{st} numbers are minimal and it can be classified into mild, moderate, severe and extreme classes. The respective limits of RDI_{st} are −0.5 to −1.0, −1.0 to −1.5, −1.5 to −2.0, and <−2.0, respectively. The RDI can be estimated for different time steps such as 3-, 6-, 9- and

12-month (Tigkas et al. 2012). This indicates a variable quality of RDI compared to other drought indices since it is computed for pre-determined reference periods. Additionally, arid regions are defined into dry sub-humid, semi-arid, arid and hyper-arid classes, and the corresponding limits of $RDI_{\alpha 12}$ are 0.50 to 0.75, 0.20 to −0.50, 0.03 to 0.20, and <0.03, respectively (UNESCO 1979).

3 Materials, Data and Methods

3.1 Climate Forecasting System Reanalysis Data

The climate forecasting system reanalysis data are based on a dataset created by the National Centres for Environmental Prediction (NCEP) as a part of the climate forecast system (Dile and Srinivasan 2014; Saha et al. 2014). These data are applied in this study to gain historical data and to investigate its applicability for drought severity assessments.

The CFSR dataset supersedes the previous NCEP/NCAR reanalysis dataset that has been immensely utilised in previous down-scaling research (e.g., Wilby et al. 1998; Michelangeli et al. 2009; Higgins et al. 2010; Maurer et al. 2010). The CFSR dataset covers the period from 1979 to the present, and has a resolution of nearly 0.25 degrees around the equator and to 0.5 degrees in non-tropical regions (Higgins et al. 2010). Concerning data reliability in watershed-scale modeling, Fuka et al. (2014) confirmed that applying the CFSR data as input to the hydrological model produces discharge simulations that are as accurate as or even better than models derived thought popular stations, particularly in the case that the stations are located greater than 10 km from the area of interest. Additionally, gathering representative weather data for basin-scale hydrological simulations might be challenging and time-consuming. This is because the land-based meteorologiacl stations do not usually adequately cover the climate occurring over a basin for many reasons such as that they might be located far from the area of interest and are associated with missing data.

For the purpose of this article, the CFSR dataset has been applied for two different elevations representing typical lowland and mountainous stations that were selected from semi-arid (MD, TR, and CN), Sahara and humid climatic regions (Fig. 1). Table 1 shows the categories and locations of the chosen stations. For example, the gridded station labelled "HL" is situated at an elevation (1677 m) representing a mountainous area in the East of Al-Sudan (22° 0′ 36″N, 36° 15′ 0″E), while the station that is labelled "LL" is situated at a low elevation (40 m) in the UK (52° 55′ 12″ N, 3° 45′ 0″ W). The average yearly precipitation and temperature for the first location is 1118 mm and 24.7 °C, respectively. The corresponding means for the second station are 155 mm and 9.1 °C, respectively. Reliable monthly data of minimum and maximum temperature, precipitation, relative humidity and wind speed were sourced.

Initially, the data were examined for their validity, minor emendations and filling of some gaps were implemented depending on customary statistical practices. After that, ET was estimated by the three considered methods (Fig. 2).

The next step involved the calculation of annual values of $RDI_{\alpha 12}$, RDI_{st}, and RDI_{n}, depending on ET values estimated by various methods with the aid of the software tool called drought indices calculator (DrinC) as reported by Tigkas et al. (2015).

3.2 Data Analysis

ArcGIS 10.3 has been used for gridded meteorological station projections on the world borders Shapefile that has been downloaded from Thematic Mapping (2009).

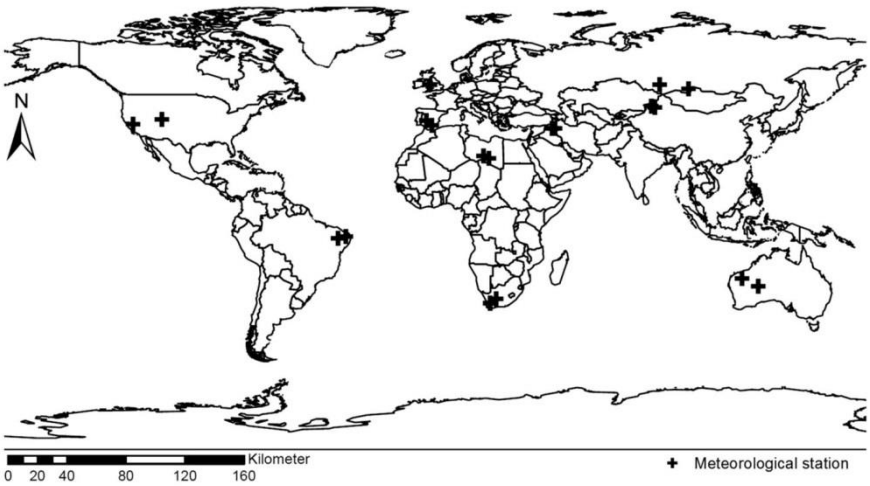

Fig. 1 The locations of the selected meteorological stations

Statistical analyses for the daily data, including monthly and annually average values, corrections and gap filling were performed using the Statistical Program for Social Sciences (SPSS) 20. One-way ANOVA analysis has been achieved using Daniel's XL Toolbox, which is a free, open-source add-in for Excel. Whereas, estimating ET and RDI were accomplished with a specialized software package named DrinC (Tigkas et al. 2012, 2015).

3.3 Evaluation of the Performance

The root mean square error (*RMSE*) and the mean bias error (*MBE*) are two of the most widely accepted statistical indicators, which have been selected to compare the effect of various *ET* estimates on various RDI form values. Equation (16) is used to compute *RMSE*.

$$\mathrm{RMSE} = \sqrt{\frac{1}{n}\sum_{i=1}^{n}\left(X_{ob,i}-X_{est,i}\right)^2} \tag{16}$$

The *MBE* is estimated by Eq. (17).

$$MBE = \frac{1}{n}\sum_{i=1}^{n}\left(X_{ob,i}-X_{es.,i}\right) \tag{17}$$

where n represents the total number of observations (in both equations), X_{ob} and X_{es} are the estimated values by the equation used as a standard in each case and the computed value by each equation under review, this is because there are no measured data available. The ideal value of both *RMSE* and *MBE* is zero (Vangelis et al. 2013).

Table 1 Statistical performance indicators of the annual reconnaissance drought index for the normalised values (RDI_n) estimated by various evapotranspiration methods against the reference method for different locations all over the world

Wider region	St[a] ID	Lat[b] (°)	Long[c] (°)	El[d] (m)	RMSE[e]			MBE[f]		
					1[g]	2[h]	3[i]	1[g]	2[h]	3[i]
Mediterranean										
South Africa	LL[j]	-32.63	19.69	485	42	54	50	2	3	2
	HL[k]	-31.07	22.19	1382	33	33	36	1	1	1
North Iraq	LL[j]	35.75	44.06	306	18	57	29	0	3	1
	HL[k]	35.75	45.25	1458	36	37	52	1	1	3
West Australia	LL[j]	-26.07	124.68	485	51	90	48	3	8	2
	HL[k]	-22.95	118.43	820	54	91	54	3	8	3
South USA	LL[j]	37.31	-120.00	361	57	47	51	3	2	3
	HL[k]	39.18	-108.75	1382	50	43	54	3	2	3
Tropical										
East China	LL[j]	44.49	82.81	409	71	82	84	5	7	7
	HL[k]	44.18	84.38	1316	109	112	110	12	13	12
East Brazil	LL[j]	-6.71	-36.88	440	49	79	53	2	6	3
	HL[k]	-7.34	-39.69	918	36	42	61	1	2	4
Continental										
South Russia	LL[j]	38.87	-5.31	403	102	57	62	10	3	4
	HL[k]	36.99	-3.13	1360	369	108	107	136	12	11
South East Spain	LL[j]	52.92	86.25	438	35	40	43	1	2	2
	HL[k]	51.36	97.50	1208	68	58	57	5	3	3
Arid										
Sahara	LL[j]	24.82	17.19	146	26	74	21	1	6	0
	HL[k]	24.20	19.38	604	25	59	21	1	4	0
Al-Sudan	LL[j]	19.83	34.34	390	48	150	26	2	23	1
	HL[k]	22.01	36.25	1677	42	55	27	2	3	1
Humid										
UK	LL[j]	52.92	-3.75	40	25	59	21	1	4	0
	HL[k]	52.92	-4.06	717	26	74	21	1	6	0
Norway	LL[j]	6.56	61.35	490	50	86	82	2	7	7
	HL[k]	8.13	61.35	1652	53	115	112	3	13	13

Values of RME and MBE are multiplied by 10^{-3}

[a] Station, [b] Latitude, [c] Longtude, [d] Elevation, [e] Root mean square error, [f] Mean bias error, [g] Hargreaves method, [h] Thornthwaite method, [i] Blaney-Criddle method, [j] Low land, [k] High land

4 Results and Discussion

The selection of the best ET estimate for a specific climate and elevation is important. This is required since the application of different approaches may result in flaws in estimations of water resources availability. Therefore, one of the study objectives is to analyse the ET estimate impacts on aridity and drought evaluations. It is critical to note that for all climatic conditions, ThW produced lower values, except for humid climate as HG is linked to lower ET values, whereas the PM had the highest ones. Differences of about 1000, 500, 750, 1000 and 1250 mm in terms of mean values were calculated for MD, TR, CN, Sahara and humid

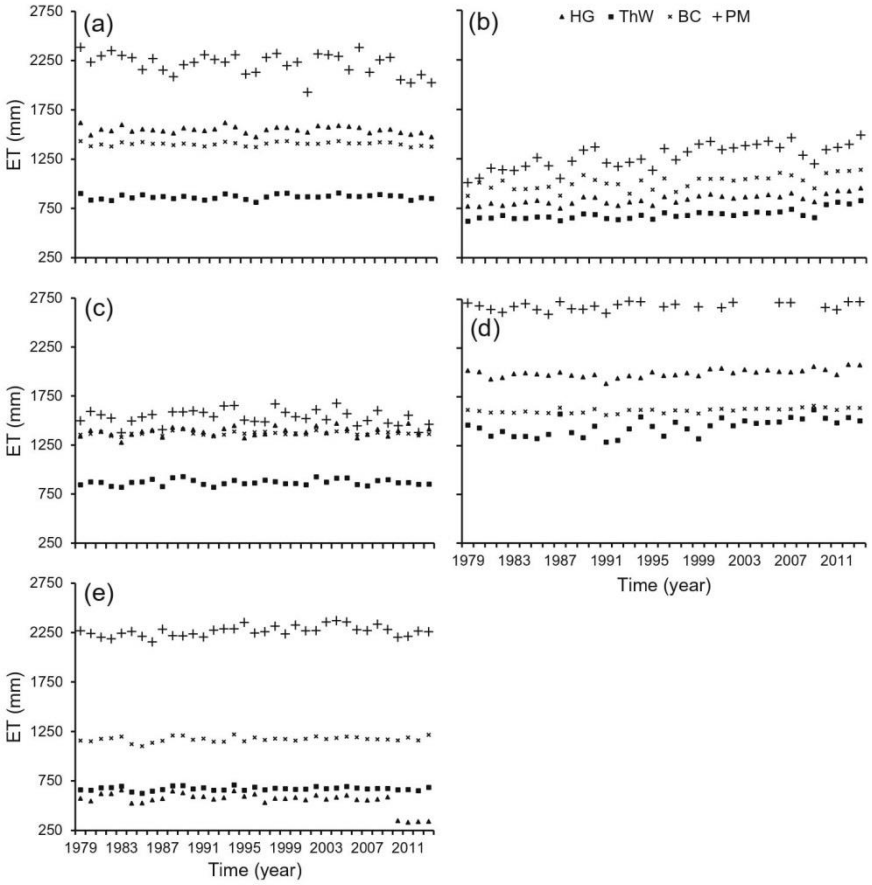

Fig. 2 The evapotranspiration (ET) estimated by various methods for different climatic conditions: (**a**) Mediterranean, (**b**) tropical, (c) continental, (**d**) Sahara and (**e**) humid

climates, respectively. The HG and PM formulas follow the same annual pattern with rather alike variations around their average numbers in the same periods. However, a diverse variation pattern is followed by ThW. This result confirms findings by Vangelis et al. (2013).

The difference among all locations is that the amounts estimated by ThW are mostly lower than the values calculated by the other two methods for MD, TR, CN and Sahara climates. Moreover, it can be observed that ThW strongly underestimates ET under dry and arid conditions and at elevated elevations since the equation does not take into account the air saturation deficit, it is mainly calibrated for temperate climates at low elevations.

Whereas BC estimates rather accurately with no large under- or over-estimates the majority of the time series, the obtained results using BC are close to the numbers produced by HG, particularly for the MD, TR and CN regions. Moreover, for the humid regions, the BC methodology was linked to the best findings (similar to the full equation of PM). Accordingly, the HG could be considered as the main method to estimate ET for almost all selected regions due to its suitability for climate change studies. The superiority of the HG is supported by several research studies in the field (Vangelis et al. 2013; Tigkas et al. 2015).

Then, and to evaluate the potential impacts of ET methods on the drought severity assessment, Tables 1 and 2 show the RDI_n and RDI_{st} values, which could be considered approximately the same regardless of elevation and ET estimation used for most of MD, TR and Sahara climates. Slight variations, which appear for few years are not significant, because they do not impact on drought severity as indicated by the RDI index. The different numbers, despite their variations, are in the same drought severity category without surpassing a drought severity threshold. No significant differences ($P > 0.05$) (part of the analysis are not presented)

Table 2 Statistical performance indicators of the annual reconnaissance drought index for the standardised values (RDI_{st}) estimated by various evapotranspiration methods against the reference method for different locations all over the world

Wider region	Station ID	El[a] (m)	RMSE[b]			MBE[c]		
			1[d]	2[e]	3[f]	1[d]	2[e]	3[f]
Mediterranean								
South Africa	LL[g]	485	2	3	3	21	34	26
	HL[h]	1382	66	70	69	4	5	5
North Iraq	LL[g]	306	34	92	40	1	8	2
	HL[h]	1458	111	75	126	12	6	16
West Australia	LL[g]	485	78	140	78	6	20	6
	HL[h]	820	91	174	83	8	32	7
South USA	LL[g]	361	99	89	49	10	8	2
	HL[h]	1382	142	108	159	20	12	25
Tropical								
East China	LL[g]	409	62	102	91	4	10	8
	HL[h]	1316	240	162	164	58	26	27
East Brazil	LL[g]	440	213	302	214	41	91	45
	HL[h]	918	6	83	68	3	7	5
Continental								
South East Spain	LL[g]	438	70	60	63	5	4	39
	HL[h]	1208	154	97	93	24	9	9
South Russia	LL[g]	403	543	199	247	295	40	61
	HL[h]	1360	417	122	124	174	15	15
Arid								
Sahara	LL[g]	146	23	49	31	1	2	1
	HL[h]	604	12	30	10	0	1	0
Al-Sudan	LL[g]	390	23	40	18	1	2	0
	HL[h]	1677	70	67	38	5	4	1
Humid								
UK	LL[g]	40	1320	533	504	1742	284	254
	HL[h]	717	698	433	447	488	188	200
Norway	LL[g]	490	180	307	298	32	94	89
	HL[h]	1652	232	596	607	54	355	368

Values of RME and MBE are multiplied by 10^{-3}

[a] Elevation, [b] Root mean square error, [c] Mean bias error, [d] Hargreaves method, [e] Thornthwaite method, [f] Blaney-Criddle method, [g] Low land, [h] High land

were noted for RDI_n and RDI_{st} values produced by the numerous ET methodologies for most of the MD, TR and Sahara areas. However, this could not the case for smaller periods such as 3, 6, and 9 months, therefore, it is suggested to use such periods for further research.

Furthermore, RDI_{st} and RDI_n values for many other geographical regions such as South Russia, UK and East Brazil are significantly ($P < 0.05$) different for various elevations using the three ET methods compared to PM (Tables 1 and 2). The differences are considered important since they affect drought severity reported by the RDI_{st}, and different values give completely different drought severity categories for almost all periods. This would become

Table 3 Statistical performance indicators of the annual reconnaissance drought index for the initial values α_k at k = 12 months ($RDI_{\alpha 12}$) estimated by various evapotranspiration methods against the reference method for different locations all over the world

Wider region	St[a] ID	El[b]	RMSE[c]			MBE[d]			ANOVA[e]		
			1[f]	2[g]	3[h]	1[f]	2[g]	3[h]	1[f]	2[g]	3[h]
Mediterranean											
South Africa	LL[i]	485	52	187	69	50	35	5	*	*	*
	HL[j]	1382	31	115	41	29	13	2	*	*	*
North Iraq	LL[i]	306	40	79	56	37	6	3	61	*	*
	HL[j]	1458	63	599	208	58	359	43	125	*	*
West Australia	LL[i]	485	25	49	23	-23	2	1	213	69	270
	HL[j]	820	89	31	77	-78	1	6	*	581	*
South USA	LL[i]	361	79	299	86	71	89	7	72	*	*
	HL[j]	1382	29	293	74	24	86	5	227	*	*
Tropical											
East China	LL[i]	409	111	186	52	102	35	3	*	*	144
	HL[j]	1316	385	900	167	369	811	28	*	*	622
East Brazil	LL[i]	440	166	247	229	159	61	53	*	*	*
	HL[j]	918	87	341	130	84	116	17	91	*	*
Continental											
South Russia	LL[i]	403	137	245	271	-50	60	73	404	*	*
	HL[j]	1360	2273	632	190	1583	399	36	*	*	944
South East Spain	LL[i]	438	24	171	25	23	29	6	270	*	230
	HL[j]	1208	183	502	47	172	251	2	*	*	280
Arid											
Sahara	LL[i]	146	16	4	3	1	0	0	280	*	81
	HL[j]	604	2	5	3	1	0	0	150	*	*
Al-Sudan	LL[i]	390	5	3	9	2	0	0	180	*	61
	HL[j]	1677	2	8	7	2	0	0	140	*	*
Humid											
UK	LL[i]	40	209	403	1437	-124	162	2064	268	*	*
	HL[j]	717	478	549	1703	-458	302	2901	*	*	*
Norway	LL[i]	490	644	1326	2891	-515	1758	8355	141	*	*
	HL[j]	1652	279	395	893	231	156	797	106	388	*

Values of RME, MBE and ANOVA are multiplied by 10^{-3}

[a] Station, [b] Elevation, [c] Root mean square error, [d] Mean bias error, [e] One-way ANOVA analysis at 0.05 significant level, [f] Hargreaves method, [g] Thornthwaite method, [h] Blaney-Criddle method, [i] Low land, [j] High land

* < 0.05

even clearer for shorter periods such as 3, 6 and 9 months, which is why it is highly recommended to use such periods for future research.

Regional aridity evaluations can alter due to many factors such as the specific ET method used and weather station elevations. Table 3 reveals the following: No significant aridity variations were found with respect to different ET estimates for different elevations in the West Australia, East Brazil, Sahara and Al-Sudan geographical regions. Figure 3a, b show the results for only West Australia as an example. Marginal differences, which are revealed for

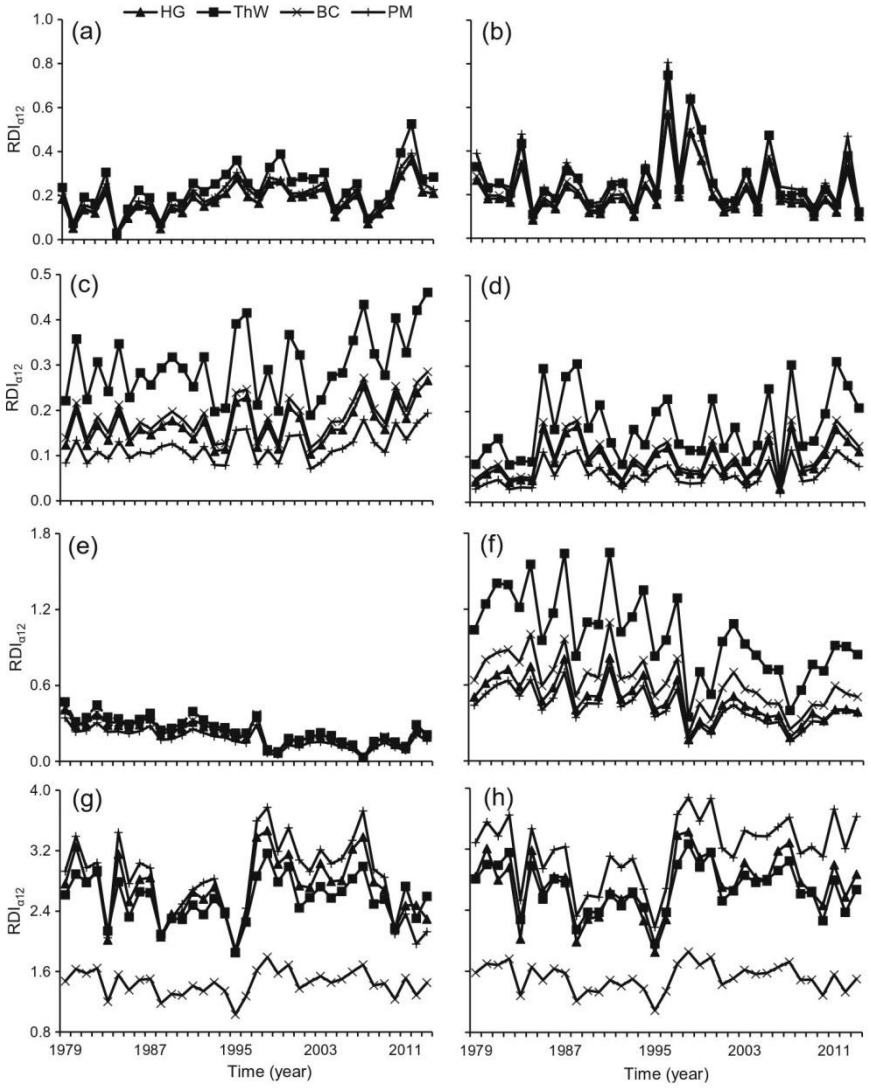

Fig. 3 The alpha reconnaissance drought index ($RDI_{\alpha 12}$) values estimated by various evapotranspiration (ET) methods for two different elevations each in (**a**) and (**b**) West Australia, (**c**) and (**d**) South Africa, (**e**) and (**f**) North Iraq, and (**g**) and (**h**) UK

many years, cannot be seen as important since they do not influence aridity evaluation. The different numbers, despite their fluctuations, stay constant for the two main elevations in the same aridity class without exceeding any threshold value. However, this could not be the case for smaller periods of time. This is why $RDI_{\alpha 12}$ values for shorter reference periods than the annual one are recommended.

For the MD and CN climatic conditions in South Africa, South USA and South East Spain, Fig. 3c, d as well as Table 3 present results for South Africa as an example confirming that there is considerable variation in $RDI_{\alpha 12}$ values for different elevations using different ET estimates, which in turn affect significantly regional aridity assessments. Despite the fact that values of $RDI_{\alpha 12}$ produced by the HG and BC methods are not similar to the results of the reference method, they are rather identical and the most significant ($P < 0.05$) deviations are shown by the ThW method.

Moreover, no significant ($P > 0.05$) differences were detected in the $RDI_{\alpha 12}$ values estimated by the ET methods (particularly, the HG method) at low elevations in North Iraq (Fig. 3e, f), East China and South Russia. Whereas at mountainous locations, significant ($P < 0.05$) $RDI_{\alpha 12}$ values were noted using different ET estimates (Table 3).

Regarding $RDI_{\alpha 12}$ for humid climatic conditions such as the UK, Fig. 3g, h as well as Table 3 show that at both elevations the selected methods are underestimating ET (particularly, the BC method) so that using such methods can lead to completely different aridity categories for mountainous locations.

Another objective of this study was to present $RDI\alpha_{12}$ as a climatic index. Figure 4a shows the $RDI_{\alpha 12}$ values for different climatic conditions. Note that $RDI_{\alpha 12}$ is significantly ($P < 0.05$) higher for humid areas regarding the whole time series and linked to higher fluctuations compared to other climatic conditions. Furthermore, $RDI_{\alpha 12}$ is higher for the mountainous locations for the complete time series and related to higher variability compared with lowland

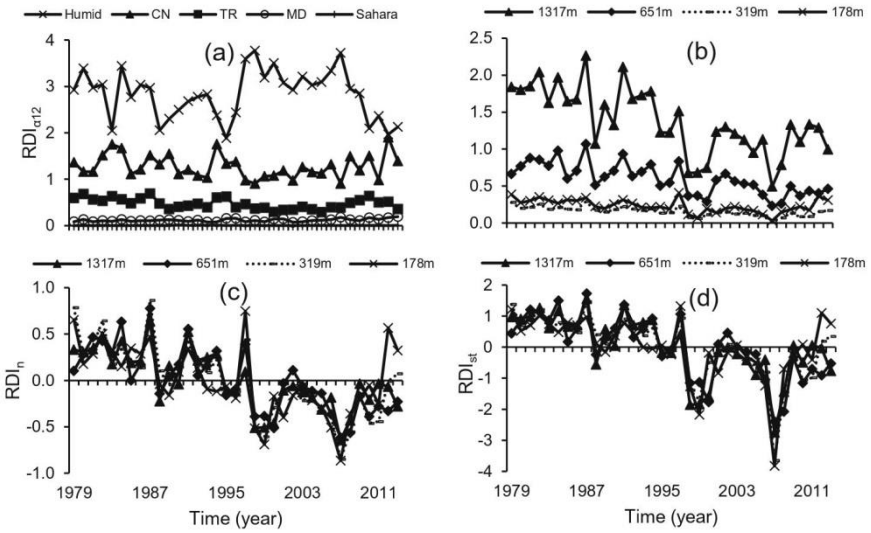

Fig. 4 **a** The annual reconnaissance drought index alpha form ($RDI_{\alpha 12}$) form values for different climatic conditions; **b** different elevations; **c** The normalised annual reconnaissance drought index (RDI_n) values for different elevations; and **d** The standardised annual reconnaissance drought (RDI_{st}) index values for different elevations

locations (Fig. 4b). Eventually, and for explanation purposes, Fig. 4c, d represent how RDI_{st} and RDI_n values at a specific region and climate condition can be changed with considerable fluctuations corresponding to different elevations.

Apart from the above, the authors suggest using any of the examined ET methods for RDI_{st} and RDI_n estimations with the aim to circumvent the ThW equation, particularly for mountainous locations. Furthermore, the HG method provides the most accurate results. Since RDI utilises the critical part of evapotranspiration but retaining the need for data to a minimum, the HG and BC methods are the most appropriate choices for computing ET for the RDI in many regions (particularly in semi-arid and arid ones). However, in the case of the long-term reliable datasets availability of several weather parameters, researchers should use PM estimates.

5 Conclusions and Recommendations

The following conclusions could be drawn: No significant ($P > 0.05$) influence on RDI_{st} and RDI_n was detected through the selected ET estimates at different elevations for the MD, TR and Sahara climates. Slight differences revealed for many years cannot be seen as important, because they do not impact drought severity indicated by RDI. The different numbers, despite their variations, stay in the identical category of drought severity without surpassing a drought severity threshold. However, this could not be the case for smaller periods of time, so that it is highly recommended to use shorter time steps such as 3, 6 and 9 months for further research.

In addition, for many regions such as South Russia, the UK, and East Brazil, RDI_{st} and RDI_n values are significantly ($P < 0.05$) different for various elevations using the three selected ET methods compared against PM. The differences are considered significant ($P < 0.05$), since they affect dramatically the drought severity reported by RDI_{st}. The difference would become clearer for shorter time periods. Therefore, it is highly recommended to use time steps such as 3, 6 and 9 months for further research.

Furthermore, $RDI_{\alpha 12}$ is directly influenced by the selected ET method at different elevations for all regions. This is why the method of ET, particularly at high elevation, is important. Accordingly, the application of different approaches may lead to errors in water resources availability and water quality predictions. A significant ($P < 0.05$) deviation has been observed when the $RDI_{\alpha 12}$ is computed using different ET methods. Differences were noted from region to region and for various elevations. Furthermore, for nearly all cases studied and for the selected elevations, it has been observed that the HG method performed relatively better than the others. This research should be undertaken again for other regions and climatic conditions to evaluate the impact of elevation on the choice of ET method and the calculation of the $RDI_{\alpha 12}$. Assessments for shorter reference time periods than the annual time step are also recommended. This should lead to a further generalisation of the research conclusions.

Acknowledgements The research presented has been financially supported by the Iraqi Government. Thanks go to Dr. Furat Al-Faraj assisted in the early stage of this research.

Compliance with Ethical Standards

Conflict of Interest The authors declare that they have no conflict of interest.

References

Aghakouchak A, Farahmand A, Melton FS et al (2015) Remote sensing of drought: progress, challenges and opportunities. Rev Geophys 53(2):452–480

Cai W, Zhang Y, Chen Q, Yao Y (2015) Spatial patterns and temporal variability of drought in Beijing-Tianjin-Hebei metropolitan areas in China. Adv Meteorol 2015(289471):1–14

Cook BI, Smerdon JE, Seager R, Coats S (2014) Global warming and twenty-first century drying. Clim Dyn 43(9):2607–2627

Dile YT, Srinivasan R (2014) Evaluation of CFSR climate data for hydrologic prediction in data-scarce watersheds: an application in the Blue Nile River basin. J Am Water Resour Assoc (JAWAR) 50(5): 1226–1241

Fuka DR, Walter MT, MacAlister C et al (2014) Using the climate forecasting system reanalysis as weather input data for watershed models. Hydrol Process 28(22):5613–5623

Giannikopoulou AS, Kampragkou E, Gad FK et al (2014) Drought characterisation in Cyclades complex, Greece. Eur Water 47:31–43

Hargreaves GH, Samani ZA (1982) Estimation of potential evapotranspiration. J Irrig Drain Div, Proceeding of the American Society of Civil Engineering 108:223–230

Hargreaves GH, Samni ZA (1985) Reference crop evapotranspiration from temperature. Trans Am Soc Agric Eng 51(4):1295–1310

Heim RR (2002) A review of twenty-century drought indices used in the united state. Bull Am Meteorol Soc 83(8):1149–1165

Higgins RW, Kousky VE, Silva VBS et al (2010) Intercomparison of daily precipitation statistics over the United States in observations and in NCEP reanalysis products. J Clim 23(17):4637–4650

Hoerling MP, Eischeid JK et al (2012) Is a transition to semi-permanent drought conditions imminent in the U.S. Great Plains? J Clim 25:8380–8386

Maurer EP, Hidalgo HG, Das T et al (2010) The utility of daily large-scale climate data in the assessment of climate change impacts on daily streamflow in California. Hydrol Earth Syst Sci 14(6):1125–1138

McMahon TA, Peel MC, Lowe L et al (2013) Estimating actual, potential, reference crop and pan evaporation using standard meteorological data: a pragmatic synthesis. Hydrol Earth Syst Sci 17:1331–1363

McVicar TR, Jupp DLB (1998) The current and potential operational uses of remote sensing to aid decisions on drought exceptional circumstances in Australia: a review. Agric Syst 57(3):399–468

Michelangeli PA, Vrac M, Loukos H (2009) Probabilistic downscaling approaches: application to wind cumulative distribution functions. Geophys Res Lett 36(11):1–6

Rossi G, Cancelliere A (2013) Managing drought risk in water supply systems in Europe: a review. Int J Water Resour Dev 29(2):272–289

Saha S, Moorthi S, Wu X et al (2014) The NCEP climate forecast system version 2. J Clim 27(6):2185–2208

Shahidian Sh, Serralheiro R, Serrano J et al. (2012) Hargreaves and other reduced-set methods for calculating evapotranspiration. In: Irmak A (ed) Evapotranspiration: remote sensing and modelling. InTech, pp 50–80. ISBN 978–953–307-808-3

Thematic mapping (2009) [Online] Available from: http://thematicmapping.org/downloads/world_borders.php. [Accessed: 2nd October 2015]

Tigkas D (2008) Drought characterisation and monitoring in regions of Greece. Eur Water 23(24):29–39

Tigkas D, Vangelis H, Tsakiris G (2012) Drought and climatic change impact on streamflow in small watersheds. Sci Total Environ 440:33–41

Tigkas D, Vangelis H, Tsakiris G (2015) DrinC: a software for drought analysis based on drought indices. Earth Sci Inform 8(3):697–709

Tsakiris G, Vangelis H (2005) Establishing a drought index incorporation evapotranspiration. Eur Water 9(10):3–11

United Nations Educational, Scientific and Cultural Organization (UNESCO) (1979) Map of the world distribution of arid regions: Map at scale 1:25,000,000 with explanatory note. MAB Technical Notes 7, UNESCO, Paris

Vangelis H, Tigkas D, Tsakiris G (2013) The effect of PET method on reconnaissance drought index (RDI) calculation. J Arid Environ 88:130–140

Vicente-Serrano SM, Lopez-Moreno J, Begueria S et al (2014) Evidence of increasing drought severity caused by temperature rise in southern Europe. Environ Res Lett 9:044001

Vicente-Serrano SM, Schrier GVD, Begueria S et al (2015) Contribution of precipitation and reference evapotranspiration to drought indices under different climates. J Hydrol 526:42–54

Viviroli D, Durr HH, Messerli B et al (2007) Mountains of the world, water towers for humanity: typology, mapping, and global significance. Water Resour Res 43(7):1–13

Viviroli D, Archer DR, Buytaert W et al (2011) Climate change and mountain water resources: overview and recommendations for research, management and policy. Hydrol Earth Syst Sci 15(2):471–504

Wilby LR, Hassan H, Hanaki K (1998) Statistical downscaling of hydrometeorological variables using general circulation model output. J Hydrol 205(1–2):1–19

Xu CY, Singh VP (2001) Evaluation and generalization of temperature-based methods for calculating evaporation. Hydrol Process 15(2):305–319

Zarch MAA, Sivakumar B, Sharma A (2015) Droughts in a warming climate: Aglobal assessment of standardized precipitation index (SPI) and reconnaissance drought index (RDI). J Hydrol 526:183–195

Paper 3

Stoch Environ Res Risk Assess
DOI 10.1007/s00477-016-1375-7

ORIGINAL PAPER

Assessment of models predicting anthropogenic interventions and climate variability on surface runoff of the Lower Zab River

R. Mohammed[1] · M. Scholz[1,2] · M. A. Nanekely[1] · Y. Mokhtari[1]

Abstract Multi-regression, hydrologic sensitivity and hydrologic model simulations were applied to quantify the climate change and anthropogenic intervention impacts on the Lower Zab River basin (LZRB). The Pettitt, precipitation-runoff double cumulative curve (PR-DCC) and Mann–Kendall methods were used for the change points and significant trend analyses in the annual streamflow. The long-term runoff series from 1979 to 2013 was first divided into two main periods: a baseline (1979–1997) and an anthropogenic intervention period (1998–2013). The findings show that the mean annual streamflow changes were consistent using the three methods. In addition, climate variability was the main driver, which led to streamflow reduction with contributions of 66–97% during 2003–2013, whereas anthropogenic interventions caused reductions of 4–34%. Moreover, to enhance the multi-model combination concept and explore the simple average method (SAM), Hydrologiska Byrans Vattenbalansavdelning (HBV), Génie Rural a Daily 4 parameters (GR4J) and Medbasin models have been successfully applied.

Keywords Climate change · Human-induced impacts · Hydrologic sensitivity analysis · Multi-model combination technique · Multi-regression · Runoff simulation

✉ M. Scholz
miklas.scholz@tvrl.lth.se

[1] Civil Engineering Research Group, School of ComputingScience and Engineering, University of Salford, Newton Building, Peel Park Campus, Salford, Greater Manchester M5 4WT, UK

[2] Division of Water Resources Engineering, Faculty of Engineering, Lund University, P.O. Box 118, 221 00 Lund, Sweden

1 Introduction

1.1 Background

Alterations in streamflow as a result of climate change linked with the anthropogenic interventions have long been the main focus of hydrological studies (Guo et al. 2014; Jiang et al. 2011). Generally speaking, the climate change is considered as the focal factor changing precipitation patterns. However, anthropogenic interventions have affected the water resources temporally and spatially. The impacts of these two factors on streamflow are sensitive, particularly in semi-arid and arid geographical regions, which resulted in serious environmental degradations and water crisis (Zhang et al. 2001; Miao et al. 2011; Chang et al. 2015). Hence, assessing factors that impact on alterations of river flow have drawn considerable concerns.

A growing number of studies focus on evaluating the ratio of climate change and anthropogenic interventions on basin streamflow (Jiang et al. 2011; Wang et al. 2012; Ye et al. 2013; Guo et al. 2014; Jiang et al. 2015; Mao et al. 2015; Cheng et al. 2016; Huang et al. 2016). Such impacts vary based on geographical region; accordingly, they are commonly explored at a regional scale such as on sub-basin or basin scale. For instance, Ma et al. (2008) predicted that climate variability accounted for over 64% of the reduction in average yearly streamflow, mainly as a result of precipitation decline.

The impacts of anthropogenic interventions and climate variability can be quantified through adopting the following steps: firstly, determining the change points in climatic data since it would influences the results in assessing other factors (Cheng et al. 2016). Specifying such points can be achieved by using statistical methods such as the Mann–Kendall trend analysis (M–K) (Chen and Xu 2005; Kahya

Published online: 29 December 2016

and Kalayci 2004; Mao et al. 2015), the Pettitt's analysis or the precipitation-runoff double cumulative curve technique (Jiang et al. 2011; Guo et al. 2014; Vaheddoost and Aksoy 2016). Accordingly, the hydrological years before the alteration are considered as a baseline, then the impact of the climate change period can be isolated from the baseline period. The second step is to apply methods that determine the climate change effects. Hence, the reminder of the effects is then attributed to other factors such as land use land cover, direct withdrawal of water from surface or subsurface flow for municipal, industrial production and irrigation purposes, and other different purposes which are considered as anthropogenic interventions (Zhao et al. 2010).

In order to identify the impacts of climate variability and anthropogenic interventions on streamflow, a large number of methodologies have been proposed (Li et al. 2007; Ma et al. 2008; Miao et al. 2011; Wang et al. 2012; Guo et al., 2014; Chang et al. 2015; Cheng et al. 2016). The rainfall-runoff model simulation is usually considered as the most widely spread method (Futter et al. 2015; Jiang et al. 2011; Jones et al. 2004; Zhang et al. 2001). For example, Li et al. (2007) suggested a framework to predict the mean runoff sensitivity on precipitation and potential evapotranspiration. The technique was then employed to evaluate the anthropogenic interventions and climate change impacts on streamflow (Li et al. 2007; Zhang et al. 2001). However, some modernistic endeavours have been developed to address this environmental issue using linear regression analysis (Li et al. 2007; Zhao et al. 2010).

A rainfall-runoff simulation is an estimated explanation of the problematical hydrologic phenomena that happen in the environment. Such model is a potentially powerful tool to solve practical hydrological challenges. In addition, the model is considered as an effective method for understanding the complex water cycle processes.

Rainfall-runoff models have advanced from empirical models to conceptual ones and thus to distributed models. Hydrological estimation accuracy has improved over time. However, there are often diverse modelling uncertainties such as model parameters as well as data and model structural errors (Jiang et al. 2014). Uncertainties in hydrological modelling have been studied previously (Ajami et al. 2007; Duan et al. 2007; Vallam et al. 2014; Zheng et al. 2014). Zheng et al. (2014) demonstrated that hydrological model parameter uncertainties have great impacts on the model simulation results. The uncertainties in model simulation during wet periods are relatively higher than those during dry periods.

Numerous rainfall-runoff models are available, and each model describes the processes of hydrological events. There is currently no single model that can describe the principles of basin rainfall-runoff covering all conditions. Therefore, multi-model approaches depend on the results of several models, and can improve the accuracy of hydrological prediction through a reduction of the model structure uncertainty.

This study focuses on applying a simple multi-model approach to perform streamflow simulations and uncertainty analyses. As a representative case study, the Lower Zab River basin (LZRB), which is considered one of the important basins in the northern part of Iraq, contributing to the flow rate of the Tigris River (Fig. 1). In addition, there are four other basin regions, which are the Diyala, Khabur, Upper Zab (Greater Zab) and Uzem. Over the past few years, the northern area of Iraq has been severely impacted by climatic variations, water shortage, drought phenomena and some casual flood events. Droughts have negatively impacted the wide range of areas in the studied region. However, floods only sometimes happened over the winter season due to of heavy rainfall and the lack of dams and artificial drainage networks, which result in socio-economic damages in the region (Sen et al. 2012; Al-Ansari 2013; Saeedrashed and Guven 2013; Al-Ansari et al. 2014; Devi et al. 2015). To date, the LZRB runoff has significantly declined during recent water years as reported by various studies (Chen and Xu 2005; Saeedrashed and Guven 2013). Anthropogenic interventions such as dam and reservoir constructions, irrigation and drainage systems, land use and land cover alterations in addition to climate change have been considered to be the main reasons for the decline in the LZRB runoff (Bozkurt and Sen 2012; Bozkurt et al. 2015). An evaluation of the relative contributions of anthropogenic interventions and climate change to streamflow alteration in the LZRB has not been performed, yet.

1.2 Rationale, aim, objectives and significance

Land use and land cover have been demonstrated universally to be the main factors impacting on river basin flow (Li et al. 2007; Huo et al. 2008; Miao et al. 2011; Wang et al. 2012; Guo et al. 2014; Chang et al. 2015). However, detailed assessments on the long-term change in streamflow to the LZRB and the distinct contribution of anthropogenic interventions and climate change have not been reported upon. The main target of the current study is to answer the following question: To what extent do anthropogenic interventions and climate change impact on the alteration of runoff within the LZRB? The answer depends on three of the most commonly accepted runoff simulation methods applied in this study, which are the Medbasin, GR4J and HBV models. Accordingly, the objectives of the study are as follows:

- To analysis the basin streamflow temporal variations;

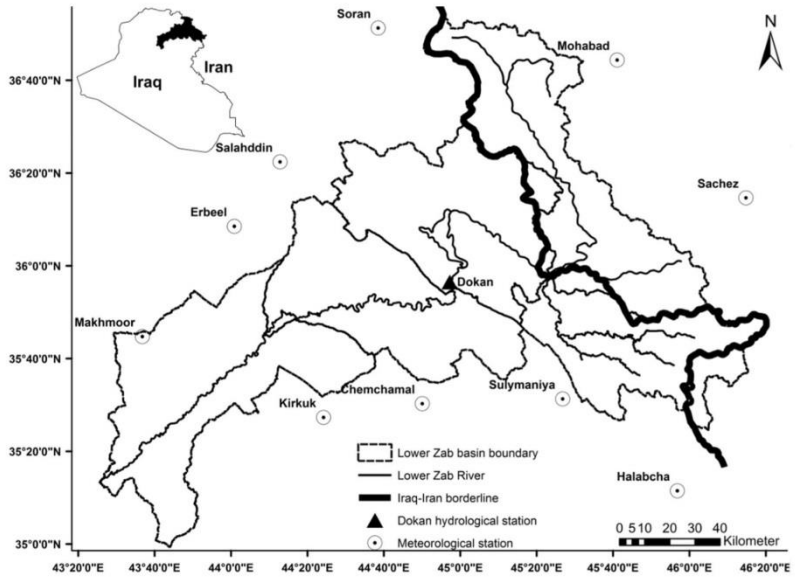

Fig. 1 Locations of the selected meteorological stations

- To detect critical change points and trends of annual basin streamflow;
- To understand the main driving factors for the recorded streamflow alterations;
- To assess the relative contributions of climate change and anthropogenic interventions such as land use change, reservoir construction and in-channel damming on basin streamflow; and
- To evaluate how the accuracy of multi-model simulation is influenced by the seasonal variations of hydrological processes, and the accuracy level of individual member models.

The models applied (Sect. 2.5) have different structural assumptions and data requirements. They were selected to ensure that they cover a wide range of possibilities to maximise the benefits obtained from combining their outputs. The results of this study can be used for regional water resources evaluation and utilisation as well as managing benchmarks by shading light on the abrupt changes and trends of historical hydrological data for the whole studied geographical region and similar ones elsewhere. In the next section available data and methods are introduced, followed by various runoff simulation approach descriptions. The obtained results are then discussed, and key conclusions are drawn.

2 Available data and methods

2.1 Representative case study

The Lower Zab River (also known as Little Zab River and Lesser Zab River) is one of the main tributaries of the Tigris River in the Erbil governorate in the north-east of Iraq. The basin is divided between Iraq and Iran with a total area of 19,846 km^2. About 75% of this area is located in Iraq. The entire length of 370 km covers areas between the south-east and south-west of Iraq on one side and north-western Iran and northern Iraq on the other side before joining the Tigris near Fatha city, which is located about 220 km north of Baghdad (Tsakiris et al. 2007). The river and its tributaries are located between latitudes 36°50′N and 35°20′N, and longitudes 43°25′E and 45°50′E (Saeedrashed and Guven 2013; Seibert and Vis 2012) as shown in Fig. 1. The considered river basin is situated in a semi-arid to arid climate zone. The annual precipitation within

the basin is approximately 720 mm. The current study is restricted to the basin upper part with an overall drainage area of 14,924 km^2.

This research examines the daily flow rate for the hydrological years between 1979 and 2013 at Dokan station, which is considered as a key hydrometric gauging station (latitude 35°53′00″N and longitude 44°58′00″E). The considered area has suffered from drought in recent years. The water year 2008 was the driest. The Lower Zab River has relatively high flows during summer due to releases of water from the Dokan reservoir to supply the agricultural industry and urban users.

2.2 Data collection and analysis

Daily meteorological data from seven stations with elevations ranging from 319 to 1536 m (Table 1) were available for the period between 1979/1980 and 2012/2013. The data were assigned to the watershed and subsequently adjusted to the average elevation of the watershed. The collected information comprises daily streamflow data accessible for Dokan station (latitude 35°53′00″N and longitude 44°58′00″E) for a duration of 35 years. The representative sub-basin area for this part of the study is 14,924 km^2. The data were obtained from the Ministry of Agriculture and Water Resources in the Kurdistan region of Iraq (personal communication).

ArcGIS 10.3 has been used for meteorological and hydrological station location projections, Thiessen network computations and river basin delineation. Table 1 reveals the latitude, longitude and elevation of the meteorological stations covering the studied basin. Additionally, statistical analyses for the daily meteorological and hydrological data, including trend analysis, monthly and annual average values, corrections and gap filling, were performed using the Statistical Program for Social Sciences (SPSS) 20. The Pettitt test has been performed using XLSTAT, which is an add-in for Excel. Table 2 reveals Mann–Kendall test findings for the key meteorological variables. The estimation of potential evapotranspiration PET (mm) was accomplished based on the Food and Agriculture Organization Penman–Monteith standard method (Allen et al. 1998), which was calculated depending on the reference evapotranspiration ET_o (mm) calculator version 3.2 (FAO 2012).

In order to achieve an accurate estimation of the spatial distribution of rainfall, it is necessary to use interpolation methods. The weighing mean method is often considered as the most important one for engineering praxis. This method assigns weights at each gauging station in proportion to the basin area, which is closest to that station. To set up the method, the following steps have been accomplished using ArcGIS. The creation of a shapefile of the named watershed polygons as a function of the land cover image has been achieved by downloading the relevant information from the Global Land Cover Facility.

This step was followed by the creation of two shapefiles. The first one is the basin border polygon, while the second one is the point shapefile that represents meteorological stations. Each point representation is linked to a value of the long-term precipitation. A Thiessen network was created to estimate the area of each station polygon (a_i). This has been achieved depending on the following: (a) connecting the adjacent stations with lines; (b) constructing perpendicular bisectors of each line, and (c) extending the bisectors and applying them to form polygons around each station. Table 3 lists the station addresses with corresponding average precipitation and potential evapotranspiration and the sub-area sizes.

Rainfall and potential evapotranspiration values for each gauging station were multiplied by the area of each polygon a_i (km^2). The next step required the computation of the average values of the average precipitation P_m (mm) and average potential evapotranspiration PET_m (mm) by

Table 1 Overview of basin station locations

Station name	Longitude (°)	Latitude (°)	Elevation (m)
Kirkuk	44.40	35.47	319
Chem-Chamal	44.83	35.52	701
Sulymanya	45.45	35.53	885
Halabcha	45.94	35.44	651
Makhmoor	43.60	35.75	306
Salahddin	44.20	36.38	1088
Erbeel	44.00	36.15	1088
Soran	44.63	36.87	1132
Mahabad	45.70	36.75	1356
Sachez	46.26	36.25	1536

Table 2 Station addresses with corresponding average precipitations and the sub-area sizes

Station ID	Sub-area (km^2)	Av[a] P[b] (mm)	Av[a] PET[c] (mm)
Sulymaniya	4479.57	772	1989
Mohabad	2593.31	886	920
Soran	1463.30	813	1433
Chem-Chamal	2827.46	738	2075
Sachez	1182.79	462	1550
Salahddin	1641.07	652	2058
Halabcha	735.60	585	980

[a] Average

[b] Precipitation

[c] Potential evapotranspiration

Table 3 Long-term average monthly to long-term annual precipitation ratios

Station name	Percentage of long-term annual precipitation ratio					
	October	November	December	January	February	March
Kirkuk	4.94	13.41	16.89	17.83	16.96	16.56
Chem-Chamal	5.17	13.14	16.53	17.48	16.91	16.21
Sulymanya	4.53	12.16	16.42	18.63	17.42	16.83
Halabcha	3.87	10.92	16.33	18.01	19.01	17.55
Makhmoor	6.78	13.11	15.66	17.09	15.56	17.11
Salahddin	4.09	12.18	15.82	18.10	18.14	16.92
Erbeel	5.87	12.93	15.91	17.27	16.53	16.48
Soran	5.04	12.19	13.78	13.91	15.62	16.66
Mohabad	5.88	11.91	14.26	15.76	16.19	16.65
Sachez	4.17	11.27	15.27	16.80	17.04	17.94

Station name	Percentage of long-term annual precipitation ratio					
	April	May	June	July	August	September
Kirkuk	9.06	4.09	0.17	0.00	0.00	0.10
Chem-Chamal	9.92	4.38	0.13	0.00	0.00	0.12
Sulymanya	9.75	4.05	0.10	0.00	0.00	0.11
Halabcha	10.64	3.39	0.12	0.02	0.00	0.14
Makhmoor	9.53	4.73	0.17	0.00	0.00	0.25
Salahddin	10.82	3.70	0.10	0.00	0.00	0.13
Erbeel	10.26	4.31	0.18	0.00	0.00	0.26
Soran	14.74	6.91	0.73	0.08	0.11	0.23
Mohabad	12.26	6.32	0.41	0.07	0.05	0.25
Sachez	11.20	5.78	0.25	0.05	0.01	0.22

summing up all values obtained from the previous step and dividing the corresponding number by the total basin area according to Eq. (1). Stations are distributed both inside and outside basin polygons (Fig. 1). Only one average value M per station has been provided to keep the procedure simple.

$$M_m = \frac{\sum_{i=1}^{n} a_i \times M_i}{\sum_{i=1}^{n} a_i} \quad (1)$$

where M_m is the average value of the basin precipitation P (mm) or PET (mm), a_i (km^2) is the meteorological station area, and M_i (mm) is the average value of the station polygon M.

Furthermore, the ratios of the long-term average monthly precipitation to the long-term average annual precipitation for the studied hydrologic year period, which started from October, are listed in Table 3. Data analysis outcomes show that the accumulated precipitation over the wet months, which are from October to May, accounts to nearly 99.5% of the entire yearly precipitation. However, the aggregated precipitation during the dry months, which are from June to September, contributes to just about 0.5% of the total precipitation.

2.3 Potential evapotranspiration estimation

The FAO Penman–Monteith method is primarily applied to estimate ET_o as indicated in Eq. (2).

$$ET_o = \frac{0.408 \times (R_n - G) + \gamma \times \frac{900}{T_m+273} u_2 \times (e_s - e_a)}{\Delta + \gamma \times (1 + 0.34 \times u_2)} \quad (2)$$

where ET_o (mm/day) is the reference evapotranspiration, R_n (MJ/m^2/day) is the net radiation at the crop surface, G (MJ/m^2 $\times$ day) is the soil heat flux density, γ (kPa/°C) is the psychrometric constant, T_m (°C) is the mean air temperature, u_2 (m/s) is the wind speed at 2-m elevation, e_s (kPa) is the saturation vapour pressure, e_a (kPa) is the natural vapour pressure, $e_s - e_a$ (kPa) is the saturation vapour pressure deficit, and Δ (kPa/°C) is the slope vapour pressure curve.

2.4 Analysis of trends and change points

The normality of meteorological and hydrological datasets was investigated with the Kolmogorov–Smirnov analysis as a first step before conducting change tests using

statistical techniques. Depending on these tests, most meteorological and hydrological data series applied in this research do not follow a normal distribution at a significance level p of 0.05. Regarding the non-normal distribution attributes of datasets utilised in the current research, two widespread distribution-free non-parametric techniques (Pettitt test and Mann–Kendall (M–K) analysis) were applied to identify the variations of streamflow, precipitation, mean air temperature and potential evapotranspiration time series in the LZRB. The former was utilised for identifying monotonic trends or slow trends, whereas the latter was applied to identify sudden changes in the average level. A brief description of these two tests can be found below.

Firstly, for trend detection in the considered datasets, the Mann–Kendall analysis was considered. The M–K analysis is a distribution-free technique for evaluating if there is a monotonic upward or downward trend of the considered parameter over time (Dahamsheh and Aksoy 2007; Seibert and Vis 2012). A monotonic downward (upward) trend indicates that the parameter consistently decreases (increases) during the studied time period. However, the trend might or might not be linear. The M–K analysis can be applied instead of a parametric linear regression test, which can be used to analysis if the slope of the computed linear regression line is different from zero. The regression test requires that the residuals from the fitted regression line are normally distributed. Such an assumption is not required by the M–K test, which is a non-parametric distribution-free test. For more details about the M–K test, readers may refer to previous studies (Robaa and AL-Barazanji 2013; Seibert and Vis 2012).

Secondly, the Pettitt test has been applied for change point identification. Change point identifications are considered as important in the analysis of runoff datasets for the purpose of studying the impacts of anthropogenic interventions and climate change. The Pettitt test is a distribution-free method to calculate the existence change points for the average of a time series, if the specific change time is unidentified. This analysis has been commonly applied to assess alterations in hydrological and weather data (Velázquez et al. 2011; Zhang et al. 2001).

The PR-DCC can illustrate the consistency of runoff and precipitation data (Jiang et al. 2011). In general, the curve is a straight line. A variation in the trend of the curve could deduce that the properties of streamflow or precipitation have altered. The PR-DCC technique might be applied to test homogeneity of hydrological data and is often seen as an efficient tool for the detection of the hydrological system variations as a result of anthropogenic interventions (Huo et al. 2008; Velázquez et al. 2011; Zhang et al. 2001). As an auxiliary method for the change point detection in the precipitation and runoff series, the PR-DCC method was used in the current study.

By using change point test and trend analysis, the streamflow dataset is divided into a baseline period dataset and an anthropogenic interventions period dataset (Jiang et al. 2011). In this study, the Pettitt's test for change point identification of the streamflow time series is tested for re-approval of the change points identified using PR-DCC. Depending on the separated periods, the impacts of anthropogenic interventions and climate change on streamflow can be divided by using streamflow simulation methods as outlined in the next section.

2.5 Rainfall-runoff simulation methods

2.5.1 Hydrological model descriptions

For the purposes of planning, designing or management of river discharges, rainfall-runoff models have been used widely to acquire streamflow data since such data are not easily available. These models comprise of a series of equations that endeavour to mimic the diversity of the interrelated events, which participate in hydrological process. The hydrological models might be categorised based on many criteria such as procedure description, solution mechanism and scale. Various categories are applied in the literature, for example, lumped and distributed models, continuous-time and event-based models as well as conceptual and black-box models (Tigkas and Tsakiris 2004; Aksoy et al. 2016).

For the simulation of basin runoff depending on a set of weather parameters, the current research utilised three of the most commonly used conceptual models, which are the Medbasin rainfall-runoff, GR4J and HBV rainfall-runoff models (Tabari and Taalaee 2011; Tigkas et al. 2012). The Medbasin model integrates the two lumped hydrological models Medbasin-D and Medbasin-M for daily (D) and monthly (M) data, respectively, with tools for forecasting different climatic variations and drought scenarios. The Medbasin-M model is based on two calibration parameters, the total capacity of the soil storage S_{max} (mm) and the coefficient of deep percolation C. The monthly delay factor a adjusts the distribution of the monthly runoff (Tigkas and Tsakiris 2004). A favourable computation of S_{max} (mm) can be accomplished by Eq. (3). Monthly precipitation P (mm) and PET (mm) data are utilised as input data for the rainfall-runoff modelling process.

$$S_{max} = 25.4 \times \left(\frac{1000}{CN} - 10\right) \tag{3}$$

where S_{max} (mm) is the total capacity of the soil storage and CN is the curve number that is based on many factors

such as land use and land cover, previous moisture conditions in the basin and soil infiltrability.

The GR4J is a daily-lumped four parameter rainfall-runoff model that is used both for precipitation and potential evapotranspiration data as input for meteorological variables. The model belongs to the family of soil moisture accounting models, and shows a good robustness in comparative studies and was also extensively tested for various climatic regions including the USA, Australia and France. The model calibration is relatively simple because of the low number of parameters (Perrin et al. 2003).

The HBV is an example of a semi-distributed conceptual model simulating daily discharge depending on daily rainfall and air temperature and monthly estimates of potential evaporation as input. Air temperature data are used for calculating snow accumulation.

As a first step for simulation of runoff, the rainfall-runoff models were calibrated depending on the recorded dataset of the baseline period. Subsequently, the usual time series of streamflow was rebuild for the anthropogenic period. After that, the anthropogenic intervention impacts on streamflow have been estimated through subtracting the recorded streamflow from the rebuild streamflow as shown in Eq. (4).

$$\Delta R_{anthropogenic} = R_a - R_{ar} \tag{4}$$

where $\Delta R_{anthropogenic}$ (mm/month) indicates the change in mean annual runoff as a result of the anthropogenic interventions effect, R_a (mm/month) refers the observed runoff of the anthropogenic intervention period, and R_{ar} (mm/month) is the rebuild runoff series for the anthropogenic interventions period.

2.5.2 Simple average method

The simple average technique is considered the simplest method of combining the results of many single hydrological models (Ajami et al. 2006; Duan et al. 2007; Velázquez et al. 2011). An equal weight is assigned to the results of all of the considered models. This method can produce estimates that are better than those of the single models. The accuracy of the SAM method depends mainly on the number of models involved and on the actual estimating capability of the specific models included. The combined predicted streamflow R from N hydrological models can be computed by Eq. (5).

$$R_{SAM_t} = \frac{1}{N}\sum_{j=1}^{N} R_{sim_{i,t}} \tag{5}$$

where R_{SAM_t} is the multi-model streamflow simulated by SAM at time t, N is the number of models under consideration and $R_{sim_{i,t}}$ is the model streamflow simulation for i model and t time.

2.5.3 Method of hydrologic sensitivity analysis

The analysis of hydrologic sensitivity might be defined as the ratio variation in average streamflow in response to the average P and PET variations in an annual time step (Velázquez et al. 2011). The basin water balance can be expressed with Eq. (5). The change of ΔS (mm) can reasonably be neglected on the average yearly time scale. It follows that ΔS can be set as zero for a lengthy time period (i.e. 10 water years or more) (Guo et al. 2014; Jiang et al. 2014). Long-term average yearly actual evapotranspiration AET (mm) can be predicted by Eqs. (5) and (6) according to Zhang et al. (2001).

$$P = E + R + \Delta S \tag{6}$$

where P (mm) is precipitation, E (mm) represents evapotranspiration, R (mm) is streamflow, and ΔS (mm) is basin water volume change. According to Zhang et al. (2001), long-term average annual actual evapotranspiration (AET) can be calculated as shown in Eq. (7).

$$\frac{E}{P} = \frac{1 + \omega \times \alpha_k^{-1}}{1 + \omega \times \alpha_k^{-1} + \alpha_k} \tag{7}$$

where E (mm) is evapotranspiration, P (mm) is precipitation, w is the coefficient of the available water for plants related to the vegetation type (Zhang et al. 2001) and α_k^i is defined in Eq. (8).

$$\alpha_k^i = \frac{\sum_{j=1}^{12} P_{ij}}{\sum_{j=1}^{12} PET_{ij}} \quad i = 1 \text{ to } N \text{ and } j = 1 \text{ to } 12 \tag{8}$$

where α_k^i is the initial value (α_k) of RDI index; P_{ij} (mm) and PET_{ij} (mm) are precipitation and potential evapotranspiration of the j-th month of the i-th year; and N is the overall number of years for the available data set.

The values of α_k match both the gamma and the log-normal distributions in various positions for various time scales for which they were examined, previously (Tigkas et al. 2012). Note that ω is the coefficient of plant-available water as a function of the crop type (Zhang et al. 2001). The parameter ω can be calibrated with the support of the annual long-term AET estimated from Eqs. (7) and (8). Precipitation perturbations and potential evapotranspiration can result in water balance alterations. Through considering a hydrologic sensitivity analysis, the average yearly streamflow alteration as a result of climate change can be predicted using Eq. (9) (Jiang et al. 2011).

$$\Delta R_{climate} = \beta \times \Delta P + \gamma \times \Delta PET \tag{9}$$

where $\Delta R_{climate}$ (mm/month), ΔP (mm) and ΔPET (mm)

indicate variations in streamflow, precipitation and potential evapotranspiration, respectively; β and γ are the streamflow coefficients of sensitivity to precipitation and potential evapotranspiration in this order, which can be expressed by Eqs. (10) and (11) (Li et al. 2007).

$$\beta = \frac{1 + 2\alpha_{12}^{-1} + 3\omega\alpha_{12}^{-1}}{\left(1 + \alpha_{12}^{-1} + \omega\left(\alpha_{12}^{-1}\right)^2\right)^2} \tag{10}$$

where β is the streamflow coefficient of sensitivity to precipitation, a_{12} is the 1/annual dryness index and w is the coefficient of available water for plants related to the vegetation category (Zhang et al. 2001).

$$\gamma = -\frac{1 + 2\omega\alpha_{12}^{-1}}{\left(1 + \alpha_{12}^{-1} + \omega\left(\alpha_{12}^{-1}\right)^2\right)^2} \tag{11}$$

where γ is the streamflow coefficient of potential evapotranspiration, w is the coefficient of plant-available water related to the vegetation category (Zhang et al. 2001) and α_{12} is the 1/annual dryness index.

2.5.4 Multi-regression method

In this method, streamflow is integrated with P and PET at a monthly time scale for the baseline time period as shown in Eq. (12). Based this equation, the natural streamflow of the anthropogenic interventions can be expressed as shown in Eqs. (13) and (14).

$$R_b = aP_b + bPET_b + c \tag{12}$$

where R_b (m^3/s) refers to the baseline period observed streamflow; P_b (mm) and PET_b (mm) represent the precipitation and potential evapotranspiration of the baseline period; and a, b, and c are three constants predicted using least-square regression analysis.

$$\overline{R_a} = aP_a + bPET_a + c \tag{13}$$

where $\overline{R_a}$ (mm/month) expresses the reconstructed streamflow for the anthropogenic intervention period; P_a (mm) and PET_a (mm) represent the anthropogenic intervention period precipitation and potential evapotranspiration, respectively; and a, b, and c are three parameters estimated using least-square regression analysis.

$$\Delta R_{anthropogenic} = R_a - \overline{R_a} \tag{14}$$

where $\Delta R_{anthropogenic}$ (mm/month) indicates the average annual streamflow alteration owing to the anthropogenic intervention effects, R_a (mm/month) represents the recorded streamflow subject to anthropogenic intervention period, and $\overline{R_a}$ (mm/month) indicates the change in mean annual runoff due to anthropogenic interventions.

2.5.5 Model evaluation criteria

The root mean square error (RMSE), statistical methods index of agreement (IoA), correlation coefficient (r), and coefficient of Nash–Sutcliffe (NSCE (Jones et al. 2004)) were used to assess the model performance (Eqs. (15) to (18)). Accordingly, the impacts of anthropogenic interventions and climate change on streamflow can be quantified as Eqs. (15) to (18).

$$RMSE = \sqrt{\frac{1}{n}\sum_{i=1}^{n}\left[(R_{obs})_i - (R_{sim})_i\right]^2} \tag{15}$$

$$IoA = 1 - \frac{\sum_{i=1}^{n}\left[(R_{obs})_i - (R_{sim})_i\right]^2}{\sum_{i=1}^{n}\left[\left|(R_{obs})_i - \bar{R}_{obs}\right| + \left|(R_{sim})_i - \bar{R}_{obs}\right|\right]^2} \tag{16}$$

$$r = \sqrt{\frac{\sum_{i=1}^{n}\left[(R_{obs})_i - \bar{R}_{obs}\right]\left[(R_{obs})_i - \bar{R}_{sim}\right]}{\left\{\sum_{i=1}^{n}\left[(R_{obs})_i - \bar{R}_{obs}\right]\right\}^{0.5}\left\{\sum_{i=1}^{n}\left[(R_{sim})_i - \bar{R}_{sim}\right]\right\}^{0.5}}} \tag{17}$$

$$NSCE = 1 - \frac{\sum_{i=1}^{n}\left[(R_{sim})_i - (R_{obs})_i\right]^2}{\sum_{i=1}^{n}\left[(R_{obs})_i - \overline{R_{obs}}\right]^2} \tag{18}$$

where RMSE is the root mean square error (dimensionless), IoA is the index of agreement (dimensionless), r is the coefficient of correlation (dimensionless), $R_{obs(i)}$ is the recorded streamflow (mm/month) at time step i, $R_{sim(i)}$ is the predicted streamflow (mm/month) at time step i, $\overline{R_{obs}}$ is the average amount of the recorded values (mm/month), and n is the data point number.

2.5.6 Separation effect framework

The impacts of these two factors on streamflow can be estimated using the following equations:

$$\Delta R_{total} = R_a - R_b \tag{19}$$

$$\Delta R_{total} = \Delta R_{anthropogenic} + \Delta R_{climate} \tag{20}$$

$$E_{anthropogenic} = \frac{\Delta R_{anthropogenic}}{|\Delta R_{total}|} \times 100\% \tag{21}$$

$$E_{climate} = \frac{\Delta R_{climate}}{|\Delta R_{total}|} \times 100\% \tag{22}$$

where ΔR_{total} (mm/month) is the total change of streamflow, R_a (mm/month) represents the streamflow subject to anthropogenic interventions, R_b (mm/month) refers to the baseline period observed streamflow, $\Delta R_{anthropogenic}$ (mm/month) indicates the average annual streamflow alteration owing to the anthropogenic intervention effects, $\Delta R_{climate}$ (mm/month) indicates variations in streamflow, $E_{anthropogenic}$ (%) expresses the impact of anthropogenic interventions on streamflow,$|\Delta R_{total}|$ indicates the absolute

value of ΔR_{total},.and $E_{climate}$ (%) indicates the impact of climate change on streamflow.

3 Results and discussion

3.1 Long-term meteorological and hydrological data changes

Long-term trends in hydrological processes are potentially influenced by changing climate and anthropogenic interventions (Al-Ansari 2013; Al-Ansari et al. 2014). Investigating such trends might support the identification of anthropogenic intervention starting points. Yearly mean air temperature, precipitation, potential evapotranspiration and streamflow data were analysed applying the M–K test to detect long-term trends for the time period between 1979 and 2013.

During the last 35 analysed years, the whole LZRB displayed a rising trend of mean air temperature with a maximum value of +0.67 C° for one decade, while a declining precipitation trend (Fig. 2) with a maximum decrease of 151 mm per decade was noted. The LZRB yearly precipitation is around 720 mm. The maximum precipitation (1222 mm) was recorded for 1987/1988, while the corresponding minimum (250 mm) was assigned to 2007/2008 (Fig. 2). The mean annual precipitation changed spatially from 56 mm at Kirkuk station to 1369 mm at Sulymaniya station. The upper basin had higher precipitation values than the lower one.

An evident trend of air temperature increase during the last half century led to a significant increase in the potential evapotranspiration for the entire LZRB. Based on the trend analysis (Table 4), the increase in PET rate was 39 mm per decade. With an average value of 1065.3 mm, the computed potential evapotranspiration for the basin changed from 962 mm in 1982/1983 to 1110 mm in 2007/2008 (Fig. 2).

The obtained results indicate that the climate in the studied region is getting warmer and drier. The annual precipitation decreased. The yearly average air temperature increased and the annual runoff depth decreased. These findings are largely in agreement with previous studies (Al-Ansari 2013; Al-Ansari et al. 2014; Fadhil 2010; Robaa and AL-Barazanji 2013).

The coefficient of runoff is expressed as the percentage of the streamflow compared to the precipitation over a specific time period, and has been selected to represent the LZRB hydro-climatic conditions (Fig. 3). The corresponding coefficient of runoff for the entire period of study was 0.22. A declining trend at a rate of -0.009 per decade was noted. The decline in the coefficient of runoff (Fig. 3) indicates that the streamflow yield has become weaker during the last four decades as estimated previously (Al-Ansari 2013; Al-Ansari et al. 2014).

3.2 Hydrological variable change point detection

The upstream annual runoff of the LZRB has an average of 169 m^3/s for the 35-year hydrological period (1979 to 2013). The minimum was 54 m^3/s for the water year 2007/2008. Nearly 436 m^3/s were noted as the maximum for the year 1987/1988 (Fig. 2). Over the studied time period, mean streamflow runoff of the LZRB exhibited a significant decline (-0.334 at $\alpha = 95\%$) decline at a rate of -38 m^3/s per decade.

The annual runoff change point series was determined using the Pettitt and PR-DCC tests. Figures 4 and 5 show the change point years of the runoff and precipitation time series for the Pettitt and PR-DCC methods, respectively. The water

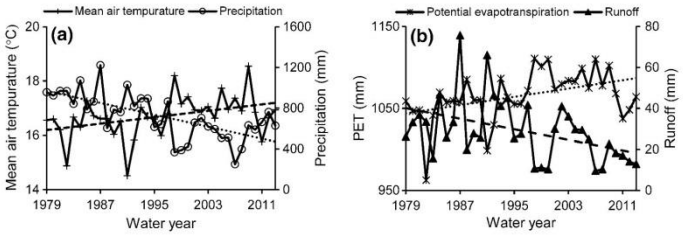

Fig. 2 Annual values and trends of **a** mean air temperature and precipitation; and **b** potential evapotranspiration (PET) and runoff in Lower Zab River basin for the time period between 1979 and 2014

Table 4 Statistical properties of the meteorological variables after applying a non-parametric test for the decadal change

Station name	Mean air temperature (°C)		Precipitation (mm)		Potential evapotranspiration (mm)	
	M–K[a]	*P* value	M–K[a]	*P* value	M–K[a]	*P* value
Kirkuk	0.422**	<0.01	−0.553**	<0.01	0.420**	<0.01
Chem-Chamal	0.345**	<0.01	−0.412**	<0.01	0.139	0.24
Sulymanya	0.358**	<0.01	−0.301**	<0.01	0.201	0.09
Halabcha	0.572**	<0.01	−0.522**	<0.01	0.316**	<0.01
Makhmoor	0.462**	<0.01	−0.536**	<0.01	0.243	0.04
Salahddin	0.452**	<0.01	−0.472**	<0.01	0.220	0.06
Erbeel	0.351**	<0.01	−0.371**	<0.01	0.203	0.09
Soran	0.380**	<0.01	−0.426**	<0.01	0.241*	0.05
Mahabad	0.603**	<0.01	−0.573**	<0.01	0.525**	<0.01
Sachez	0.079	0.50	−0.328**	0.01	0.193	0.10

Negative (−) and positive values indicate the decreasing and increasing trends, respectively

** Correlation is significant at the 0.01 level (2-tailed); and

* Correlation is significant at the 0.05 level (2-tailed)

[a] Mann–Kendall non-parametric test

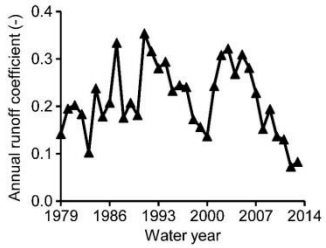

Fig. 3 Annual runoff coefficient for the 1979–2014 period in Lower Zab River basin

year 1997/1998 is considered as a change point for the studied time series. The obtained results are found to be consistent with the findings of many other researchers with respect to this study area. For example, Sen et al. (2012) explained through an analysis based on NCEP/NCAR reanalysis data that due to climate change the study region witnessed a statistically ($p < 0.05$) significant shift in the streamflow during the same period of time. In addition, Bozkurt and Sen (2012) investigated the hydro-climatic effects of future climate change in the study region using the results of different dynamically down-scaled GCM (ECHAM5, CCSM3 and HadCM3) emission scenario (A1FI, A2 and B1) simulations. They found that the annual surface runoff of the headwater area declined dramatically by about 25 to 55%).

The aggregate yearly runoff and precipitation shown in Fig. 5a indicates that before 1997, runoff and precipitation were relatively regular, but after 1997, the properties of runoff or precipitation altered. Integrating the PR-DCC analysis and the Pettitt test, the year 1997 could be seen as the change point reflecting the impact of both climate change and anthropogenic interventions on runoff and precipitation. Accordingly, the period between 1979 and 1997 was considered as the baseline period during which the anthropogenic interventions impacted on runoff were less recognisable. In order to fully appreciate the effects of climate and other influences on streamflow over the two periods, the variations in the correlation of streamflow and precipitation were investigated (Fig. 5b).

The period from 1998 to 2013 was seen as the anthropogenic intervention period, and was grouped into three hydrological sub-periods: 1998–2002, 2003–2008 and 2009–2013. For these hydrological periods, changes in average yearly streamflow, precipitation, and PET were estimated (Table 5). During the periods 1998–2002, 2003–2008 and 2009–2013, the mean annual precipitation declined by −42, −43 and −30%, and the potential evapotranspiration increased by 4, 3.5 and 1%, whereas streamflow decreased by −44, −37 and −55% in this order.

The runoff intra-annual alteration is associated with the monthly cycle of precipitation, mean air temperature and catchment water-related non-climatic drivers. In order to further comprehend the intra-annual availability of streamflow and precipitation, the mean monthly precipitation and streamflow data between the baseline period (1979–1997) and the anthropogenic intervention period (1998–2013) have been compared with each other (Fig. 6). Noticeable changes in both precipitation and streamflow were seen for the two considered time periods. The average monthly precipitation and streamflow between 1998 and 2013 declined compared with the corresponding data for the baseline period. The decreases were greatest for June,

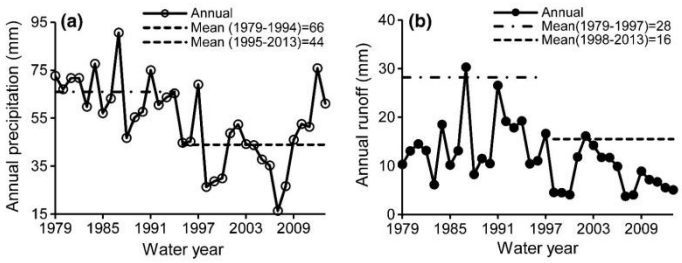

Fig. 4 Pettitt test for detecting a change in the annual: **a** precipitation; and **b** runoff

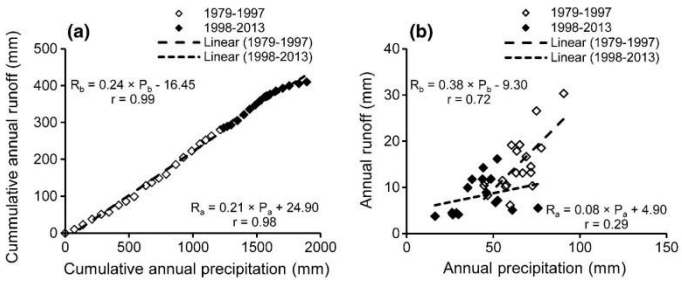

Fig. 5 **a** Precipitation-runoff double cumulative curve (PR-DCC) of annual precipitation and runoff in the Lower Zab River basin; **b** and correlation between precipitation and runoff for the two considered time period

Table 5 Changes in mean annual precipitation, potential evapotranspiration and runoff during recent hydrological time periods

Duration	Unit	1998–2002	2003–2008	2009–2013
Precipitation	mm/a	507	496	611
	Change in mm/a	−83.98	−36.3	−90.9
	Relative change in %	−42	−43	−30
Potential evapotranspiration	mm/a	1106	1088	1064
	Change in mm/a	−7.79	6.53	−9.51
	Relative change in %	+4	+3.5	+1
Recorded runoff	mm/a	8	9	7
	Change in mm/a	−2.90	−2.67	−0.96
	Relative change in %	−44	−37	−55

July and August (irrigation season), and were smallest during the winter months. Hence, the decrease in streamflow within the post-alteration period might be due to basin-related non-climate drivers as indicated in the past (Al-Ansari 2013; Al-Ansari et al. 2014). The application of the same statistical methods for a case study in Northern China was similarly successful (Jiang et al. 2011).

3.3 Calibration and validation

3.3.1 Overview

Over the baseline time period, few anthropogenic interventions impacted on streamflow within the LZRB. Accordingly, it was treated as a baseline to compute the climate change impacts and anthropogenic interventions on streamflow for the non-climate drivers' period utilising the considered techniques. Figure 7 displays scatter diagram relationships between monthly runoff and precipitation for the time periods 1979–1997 ($r = 0.50$) and 1998–2013 ($r = 0.44$). The correlation between monthly runoff and precipitation for 1979–1997 is better than that for 1998–2013. Additionally, the coefficients of runoff for the baseline period were more than the ones for the climate change and anthropogenic intervention periods. The obtained results demonstrated that the runoff was considerably affected by drought events due to climate change linked with upstream non-climatic drivers such as river

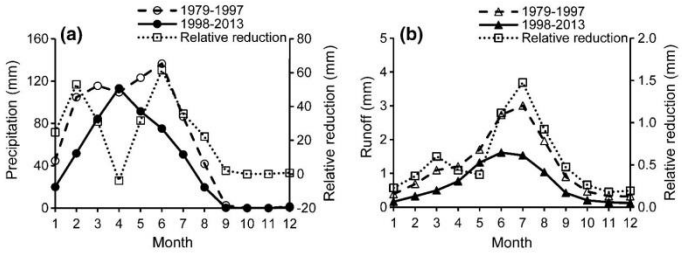

Fig. 6 Average monthly **a** precipitation and **b** runoff for the baseline (1979–1997) and the altered periods between 1998 and 2013

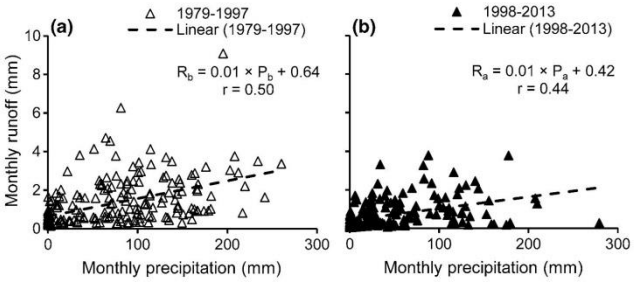

Fig. 7 Monthly relationship between precipitation and runoff for the **a** 1979–1997, and **b** 1998–2013 periods

regulation, land use changes, water withdrawal and inter-basin water transfer schemes (Al-Ansari 2013; Al-Ansari et al. 2014).

3.3.2 The multi-regression equation

Depending on the monthly precipitation and PET of the baseline period, a multi-regression equation was developed as indicated by Eq. (23).

$$R = 0.013 \times P + 0.0034 \times PET - 0.05 \quad (23)$$

where R (mm) is the monthly streamflow, P (mm) is precipitation, and PET (mm) represents the potential evapotranspiration.

Figure 8a, b indicate good promise between monthly recorded and predicted streamflow data applying Eq. (23) for the Dokan hydrologic station during the considered time periods 1979–1997 and 1998–2013, respectively. The value of the coefficient of correlation was 0.52 at a significance level of 0.001. The NSCE coefficient was 0.30. The obtained measures of performance show that the multi-regression model might not predicted streamflow precisely. The natural runoff series was rebuilt after considering the precipitation and PET of the anthropogenic interventions period as input. Using the rebuild runoff time series, the impacts of human activities and climate variability on streamflow were tested.

3.3.3 Method for the hydrologic sensitivity analysis

The coefficient of plant-available water to crop type w is the main variable in the hydrologic sensitivity analysis. This parameter has been calibrated through equating long-term annual AET computed using Eq. (9) and the baseline period for the water balance Eq. (1979–1997). Considering $w = 1$, the outcomes of yearly AET predicted by Eq. (9) are acceptable and reasonable (Fig. 9). Thus $w = 1$ has been specified for the LZRB. When w is set to 1, the coefficients of sensitivity values $\frac{\partial R}{\partial P}$ and $\frac{\partial R}{\partial PET}$ (where R (mm/month) is the monthly streamflow) were 0.0167 and 0.0141 in this order, which indicate that the runoff change was more subtle to precipitation compared to potential evapotranspiration.

3.3.4 Method of hydrologic simulation

The calibration time period for the hydrologic model was 1988–1999, while 1979–1986 was the validation period. The obtained results from the three used models show a good promise between monthly recorded and predicted

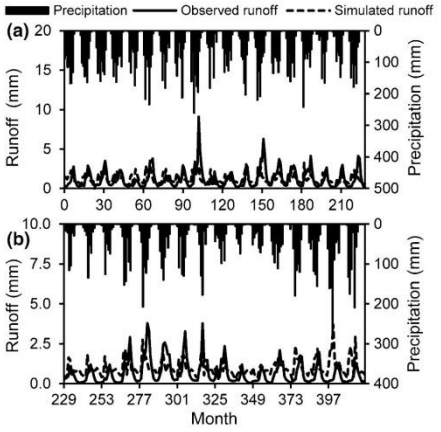

Fig. 8 Monthly observed and simulated runoff by multi-regression method at the Dokan hydrologic station for the **a** 1979–1997; and **b** 1998–2013 periods, respectively

runoff data at the Dokan hydrologic station from 1979 to 1997 (Fig. 10a). Table 6 shows the performance measures for the calibration and validation time periods using the GR4J, Medbasin and HBV simulation models. The calibrated rainfall runoff model was used to rebuild the streamflow datasets for the anthropogenic interventions period between 1998 and 2013 (Fig. 10b) with actual weather and hydrologic input data. With the rebuild streamflow dataset of the anthropogenic intervention period and the corresponding recorded streamflow dataset, it makes it possible to quantitatively assess the impacts of non-climate drivers and climate variability on streamflow.

Figures 8b and 10b compared recorded and predicted streamflow data for the Dokan hydrologic station for the hydrological years between 1998 and 2013. The impacts of anthropogenic interventions and climate variability on streamflow were assessed depending on both the conceptual framework and the simulated findings of the various applied models. The simulation methods provided relatively consistent computations of the mean streamflow ratio change for the hydrological period between 1998 and 2013 (Table 7). The data show that climate change makes the greatest impact. These findings are in broad agreements with previous estimations (Ajami et al. 2006; Al-Ansari 2013).

3.4 Comparison of simple average method and single model predictions

In order to examine the simple average method performance, firstly, a set of numerical experiments were computed using the three hydrological models. Figure 11a shows the linear regression between observed and simulated runoff for various model predictions regarding the Dokan hydrological station. Figure 11b reveals that HBV is the best model in terms of correlation coefficient, whereas the Medbasin model is the weakest. Then the SAM has been utilised to estimate the streamflow (Fig. 11b). Figure 11 reveals that the statistics from the single model simulations are almost always worse than those of the SAM, W and B simulations. The results confirm that just simply averaging the single model simulations would lead to an enhancement of the simulation level of accuracies, which is consistent with previous research

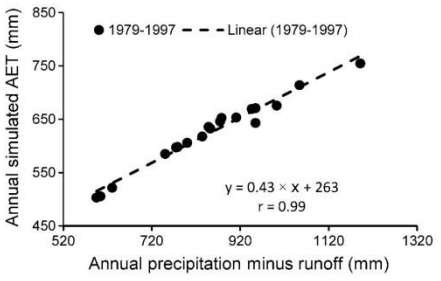

Fig. 9 Scatter diagram and correlation of annual actual evapotranspiration (AET) estimated from a water balance equation and predicted using Eq. (6) for the time period between 1979 and 1997

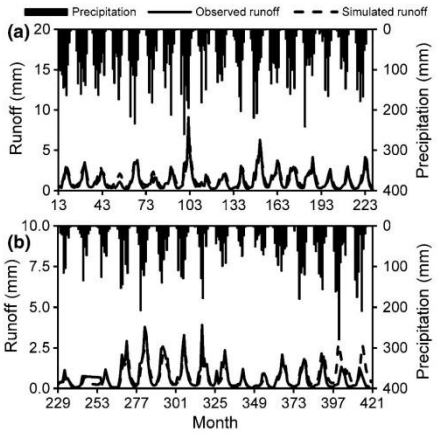

Fig. 10 Monthly observed and simulated runoff using SAM multi-model technique at the Dokan hydrological station for the **a** 1979–1997; and **b** 1998–2013 periods

Table 6 Performance measures for the calibration and validation time periods using the GR4J, Medbasin, and HBV simulation models

Model	Time period	Statistical performance			
		RMSE[a]	IoA[b]	R[c]	NSCE[d]
Medbasin	Calibration	2.69	0.96	0.94	88
	Validation	5.99	0.66	0.50	83
GR4J	Calibration	0.79	0.90	0.82	67
	Validation	1.00	0.90	0.84	50
HBV	Calibration	0.542	0.99	0.89	80
	Validation	0.446	0.99	0.94	50

[a] Root mean square error

[b] Index of agreement

[c] Correlation coefficient

[d] Nash–Sutcliffe coefficient

(Ajami et al. 2006; Georgakakos et al. 2004). Hence, excluding the worst performing model leads to an improvement of the correlation compared to the single hydrological model.

Furthermore, hydrological parameters such as flowrate are known to have a special annual cycle. The hydrologic model simulation accuracies for different months often mimic this yearly cycle (Fig. 12), which shows the performance of the individual model simulations for the studied basin during various months for the two considered time periods. Figure 12 reveals that a model might perform well for some months, but poorly for other months, when compared to competing models.

Accordingly, the use of multi-model simulations leads to the question of how the accuracy of a single model influences the accuracy of the results. To address this question, the best performing model (B) and the worst performing one (W) were sequentially removed from consideration. The obtained results are shown in Fig. 13, which indicates that the inclusion of all the calibrated models is necessary to obtain consistently good simulation results. This is because eliminating the best performing model would actually deteriorate the outcome (Fig. 13b). However, excluding the worst performing model would enhance the monthly runoff (Fig. 13a). This leads to the conclusion that the accuracy level of a single model can impact on the overall accuracy of the multi-model combination simulation. This confirms that the application of the SAM in runoff estimation might produce values that are

Table 7 Climate change and anthropogenic interventions impacts on mean annual runoff (R) during recent hydrological periods using different rainfall-runoff simulation methods

Duration		Unit	1998–2002	2003–2008	2009–2013
Runoff total alteration		mm/a	−6.54	−5.52	−8.08
Multi-regression method	$\Delta R_{anthropogenic}$	mm/a	−1.93	−1.88	−0.97
		%	−30	−34	−12
	$\Delta R_{climate}$	mm/a	−4.61	−3.64	−7.11
		%	−71	−66	−88
Hydrological sensitivity	$\Delta R_{anthropogenic}$	mm/a	−1.94	1.41	3.27
		%	−30	−26	−40
	$\Delta R_{climate}$	mm/a	4.60	4.10	4.81
		%	−70	−74	−60
Medbasin model	$\Delta R_{anthropogenic}$	mm/a	−0.29	−0.67	−2.36
		%	−4	−12	−29
	$\Delta R_{climate}$	mm/a	−6.25	−4.85	−5.72
		%	−96	−88	−71
GR4J model	$\Delta R_{anthropogenic}$	mm/a	−1.03	−0.72	−0.43
		%	−16	−14	−5
	$\Delta R_{climate}$	mm/a	−5.51	−4.73	−7.65
		%	−84	−86	−95
HBV model	$\Delta R_{anthropogenic}$	mm/a	−0.60	−0.14	−3.10
		%	−9	−3	−38
	$\Delta R_{climate}$	mm/a	−5.94	−5.38	−4.98
		%	−91	−97	−62
SAM[a]	$\Delta R_{anthropogenic}$	mm/a	−0.35	−0.23	−0.69
		%	−5	−4	−8
	$\Delta R_{climate}$	mm/a	−6.19	−5.29	−7.39
		%	−95	−96	−92

[a] Simple average method

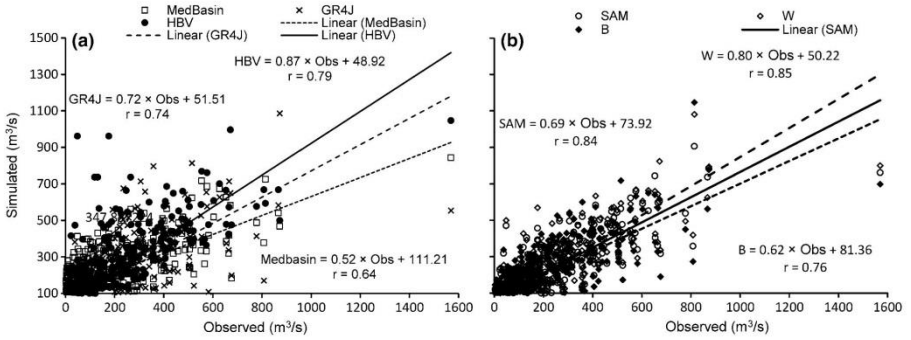

Fig. 11 Linear regression between observed and simulated runoff: **a** Medbasin, GR4J and HBV models; **b** simple average model (SAM), excluding the best model (B) and the worst model (W) simulation results, for the Dokan hydrological station

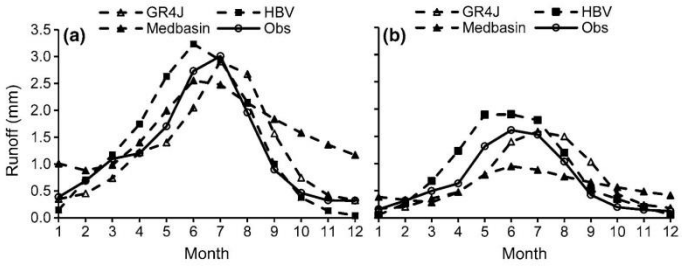

Fig. 12 Monthly observed (Obs) and simulated runoff using Medbasin, GR4J, and HBV models at the Dokan hydrological station for the **a** 1979–1997; and **b** 1998–2013 periods

more precise than the results from the best of the three considered models, which justifies the implementation of the multi-model technique in the context of rainfall-runoff modelling.

Furthermore, there is a considerable change in the magnitude and timing of the peak discharge occurring between two time periods (Fig. 13). The monthly discharge differences between two periods illustrate decreases mostly in May. The change in streamflow timing is mainly a result of anthropogenic intervention. The obtained results regarding the shift in the magnitude and the timing of the river discharge are consistent with the results obtained from others within the study area (Cullen and deMenocal 2000; Sen et al. 2012).

4 Conclusions and recommendations

The surface runoff in the LZRB has declined considerably as a result of climate variability and anthropogenic interventions. In order to evaluate the impacts of these two factors on the river flow over the study basin, hydrologic models simulation, hydrologic sensitivity analysis and multi-regression have been successfully applied.

The study outcomes indicate that the aggregated precipitation between October and May, which are the wet months, accounts for nearly 99.5% of the total annual precipitation. In contrast, the aggregated precipitation contributes only to nearly 0.5% of the entire precipitation during the dry months, which are June to September.

The hydrological periods 1998–2002 and 2006–2008 witnessed a sharp decline in the average precipitation for the studied basin, which in turn caused a reduction in the streamflow by more than 80%. This statistically significant alteration during the non-rainy months attributed to the influence of both anthropogenic interventions and climate variability pressure to the upper part of the case study area, which in turn decreased the watershed storage system availability. An abrupt change reflecting the climate change impacts on streamflow was recorded for the year 1997. This change was due to the rapid anthropogenic developments in the basin. During the hydrological years between 1998 and 2013, the mean annual runoff declined by 95% compared with the baseline period from 1979 to 1997.

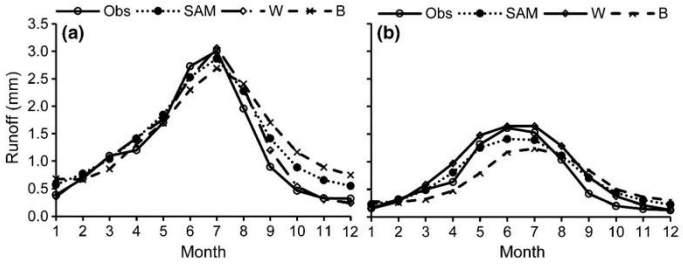

Fig. 13 Monthly observed (Obs) and simulated runoff using simple average method (SAM), excluding the best model (B) results and eliminating the worst model results (W) for the Dokan hydrological station for the **a** 1979–1997; and **b** 1998–2013 periods

Based on the three considered methods for simulating the anthropogenic interventions and climate change impacts on streamflow from 1998 to 2013, climate change was the leading factor for the decline (66 to 97%) of streamflow. Climate change was the main factor reducing runoff for the periods 1998–2002, 2003–2008 and 2008–2013. Anthropogenic intervention impacts such as land use and cover changes, water conservancy project implications, and soil conservation actions might accumulate or counteract each other simultaneously, and further research on these challenges is recommended. Furthermore, research findings imply that river alteration, climate variability and anthropogenic interventions should be considered for future stream basin managing strategies to avoid the temporal mismatch between strategies and such changes.

The simulation outcomes reveal that there is a big variance in the performance of the considered hydrological models in simulating the runoff. Simply averaging the single model simulation would result in consensus multi-model simulations that are superior to any individual simulations which confirmed that the SAM multi-model combination technique is applicable tool to extract the strengths from different models whereas avoiding the weaknesses. More sophisticated multi-model combination approaches can improve the simulation accuracy. This suggests that further operational hydrologic simulations should incorporate a multi-model combination strategy. The multi-model simulation accuracy is associated with that of the single models. On the one hand, if single model simulation accuracy is poor in matching measurements, removing that model from simulation does impact the accuracy of multi-model simulations very much. On the other hand, excluding the best performing model from consideration does negatively impact the accuracy of multi-model simulation.

The current research is based on the hydrological simulation of only three models and a total of 35 years of daily runoff data. More models and larger datasets can enhance the multi-model combination outcomes, but this needs to be explored further. Model combination techniques are still new in hydrology. However, initial findings indicate that they might be a preferable alternative to individual model simulation. This study represents a critical step toward better understanding of the potential effect of climate variability, anthropogenic interventions and subsequent drought events on streamflow in the LZRB and similar other regions with arid and semi-arid climate. The research outcomes will benefit engineers and policy-makers in assessing water resources at a basin scale.

Acknowledgements The research presented has been financially supported by the Iraqi Government. Thanks go to Amjad Hussain (The University of Salford) for his kind help and support.

References

Ajami NK, Duan Q, Gao X, Sorooshian S (2006) Multi-model combination techniques for hydrological forecasting: application to distributed model intercomparison project results. J Hydrometeorol 7(4):755–768. doi:10.1175/JHM519.1

Ajami NK, Duan QY, Sorooshian S (2007) An integrated hydrologic Bayesian multi-model combination framework: confronting input, parameter, and model structural uncertainty in hydrologic prediction. Water Resour Res 43:W01403

Aksoy H, Gedikli A, Unal NE, Yilmaz M, Eris E, Yoon J, Tayfur G (2016) Rainfall-runoff model considering microtopography simulated in a laboratory erosion flume. Water Res Manag. doi:10.1007/s11269-016-1439-y

Al-Ansari NA (2013) Management of water resources in Iraq: perspectives and prognoses. Engineering 5:667–684. doi:10.4236/eng.2013.58080

Al-Ansari NA, Ali AA, Knutsson S (2014) Present conditions and future challenges of water resources problems in Iraq. J Water Res Prot 6(12):1066–1098. doi:10.4236/jwarp.2014.612102

Allen RG, Pereira LS, Raes D, Smith M (1998) Crop evapotranspiration: guidelines for computing crop water requirements. Food

and Agriculture Organization (FAO) Irrigation and Drainage Paper 56, first ed, Rome

Bozkurt D, Sen OL (2012) Climate change impacts in the Euphrates-Tigris Basin based on different model and scenario simulations. J Hydrol 480:149–161. doi:10.1016/j.jhydrol.2012.12.021

Bozkurt D, Sen OL, Hagemann S (2015) Projected river discharge in the Euphrates-Tigris Basin from a hydrological discharge model forced with RCM and GCM outputs. Clim Res 62(2):131–147. doi:10.3354/cr01268

Chang J, Wang YM, Istanbulluoglu E, Bai T, Hunang Q, Yang D, Huang S (2015) Impact of climate change and human activities on runoff in the Weihe river basin, China. Quat Int 380–381:169–179

Chen YN, Xu ZX (2005) Plausible impact of global climate change on water resources in the Tarim River Basin. Sci China Ser D (Earth Sci) 48(1):65–73

Cheng Y, He H, Cheng N, He W (2016) The effects of climate and anthropogenic activity on hydrologic features in Yanhe River. Adv Meteorol. doi:10.1155/2016/5297158

Cullen HM, deMenocal PB (2000) North Atlantic influence on Tigris–Euphrates streamflow. Int J Climatol 20:853–863

Dahamsheh A, Aksoy H (2007) Structural characteristics of annual precipitation data in Jordan. Theor Appl Climatol 88(3):201–212. doi:10.1007/s00704-006-0247-3

Devi GK, Ganasri BP, Dwarakish GS (2015) A review on hydrological models. international conference on water resources, coastal and ocean engineering (ICWRCOE'15). Aquat Proc 4:1001–1007. doi:10.1016/j.aqpro.2015.02.126

Duan QY, Ajami NK, Gao XG, Sorooshian S (2007) Multi-model ensemble hydrologic prediction using Bayesian model averaging. Adv Water Res 30:1371–1386. doi:10.1016/j.advwatres.2006.11.014

Fadhil MA (2010) Drought mapping using geoinformation technology for some sites in the Iraqi Kurdistan region. Int J Digit Earth 4(3):239–257

FAO (2012) Adaptation to climate change in semi-arid environments. Experience and lessons from Mozambique. Environment and Natural Resources Management Series. Food and Agriculture Organization (FAO) of the United Nations, Rome, pp. 1–83. http://www.fao.org/docrep/015/i2581e/i2581e00.pdf. Accessed 19 July 2016

Futter MN, Whitehead PG, Sarkar BS, Roddad CH, Crossman J (2015) Rainfall runoff modelling of the Upper Ganga and Brahmaputra basins using PERSiST. Environ Sci Process Impacts. doi:10.1039/c4em00613e

Georgakakos KP, Seo DJ, Gupta H, Schake J, Butts MB (2004) Characterizing streamflow simulation uncertainty through multimodel ensembles. J Hydrol 298:222–241. doi:10.1016/j.jhydrol.2004.03.037

Guo Y, Li Z, Amo-Boateng M, Deng P, Huang P (2014) Quantitative assessment of the impact of climate variability and human activities on runoff changes for the upper reaches of Weihe River. Stoch Environ Res Risk Assess 28(2):333–346

Huang SZ, Liu DF, Huang Q, Chen Y (2016) Contribution of climate variability and human activities to the variation in runoff in Wei River Basin, China. Hydrol Sci J 61(6):1026–1039

Huo Z, Feng S, Kang S, Li W, Chen S (2008) Effect of climate changes and water-related human activities on annual stream flows of the Shiyang river basin in arid north–west China. Hydrol Process 22:3155–31167

Jiang S, Ren L, Yong B, Singh VP, Yang X, Yuan F (2011) Quantifying the effects of climate variability and human activities on runoff from the Laohahe basin in northern China using three different methods. Hydrol Process 25:2492–2505

Jiang S, Ren L, Yang X, Ma M, Liu Y (2014) Mulit-model ensemble hydrologic prediction analysis. In: Evolving water resources systems: understanding, predicting and managing water-society interaction proceedings of ICWRS 2014, Bologna, Italy, June 2014 (IAHS Publ 364, 2014)

Jiang C, Xiong L, Wang D, Liu P, Guo S, Xu C-Y (2015) Separating the impacts of climate change and human activities on runoff using the Budyko-type equations with time-varying parameters. J Hydrol 522:326–338

Jones RN, Chiew FHS, Boughtom WC, Zhang L (2004) Estimating the sensitivity of mean annual runoff to climate change using selected hydrological models. Adv Water Res 29:1419–1429

Kahya E, Kalayci S (2004) Trend analysis of streamflow in Turkey. J Hydrol 289:128–144

Li LJ, Zhang L, Wang H, Wang J, Yang JW, Jiang DJ, Li JY, Qin DY (2007) Assessing the impact of climate change and human activities on streamflow from the Wuding River basin in China. Hydrol Process 21:3485–3491

Ma ZM, Kang SZ, Zhang L, Tong L, Su XL (2008) Analysis of impacts of climate change and human activity on streamflow for a river basin in arid region of northwest China. J Hydrol 352:239–349

Mao Y, Nijssen B, Lettenmaier DP (2015) Is climate change implicated in the 2013–2014 California drought? A hydrologic perspective. Geophys Res Lett 42(8):2805–2813

Miao C, Ni J, Borthwick AGL, Yang L (2011) A preliminary estimate of human and natural contributions to the changes in water discharge and sediment load in the Yellow River. Glob Planet Change 76:196–205

Perrin C, Michel C, Andréassian V (2003) Improvement of a parsimonious model for streamflow simulation. J Hydrol 279:275–289

Robaa SM, AL-Barazanji ZJ (2013) Trends of annual mean surface air temperature over Iraq. Nat Sci 11(12):138–145

Saeedrashed Y, Guven A (2013) Estimation of geomorphological parameters of lower Zab River-Basin by using GIS-based remotely sensed image. Water Res Manag 27(1):209. doi:10.1007/s11269012-0179-x

Seibert J, Vis M (2012) Teaching hydrological modeling with a user-friendly catchment-runoff-model software package. Hydrol Earth Syst Sci 16:3315–3325. doi:10.5194/hess-16-3315-201

Sen OL, Unal A, Bozkurt D, Kindap T (2012) Temporal changes in the Euphrates and Tigris discharges and teleconnections. Environ Res Lett 6(2):1–9. doi:10.1088/1748-9326/6/2/024012

Tabari H, Taalaee PH (2011) Analysis of trend in temperature data in arid and semi-arid regions of Iran. Glob Planet Change 72:1–10

Tigkas D, Tsakiris G (2004) Medbasin: a Mediterranean rainfall-runoff software package. Eur Water 5(6):3–11

Tigkas D, Vangelis H, Tsakiris G (2012) Drought and climatic change impact on streamflow in small watersheds. Sci Total Environ 440:33–41

Tsakiris G, Loukas A, Pangalou D, Vangelis H, Tigkas D, Rossi G, Cancelliere A (2007) Drought characterization [Part 1. Components of drought planning. 1. 3. Methodological component]. In: Iglesias A, Moneo M, López-Fran cos A (eds) Drought management guidelines technical annex CIHEAM/ECMEDA Water, Zaragoza, pp 85–102 (Options Méditerranéennes: Série B. Etudes et Recherches; n. 58)

UN-ESCWA and BGR Inventory of Shared Water Resources in Western Asia (2013) United Nations Economic and Social Commission for Western Asia (UN-ESCWA) and Bundesanstalt für Geowissenschaften und Rohstoffe (BGR), Beirut

Vaheddoost B, Aksoy H (2016) Structural characteristics of annual precipitation in Lake Urmia basin. Theor Appl Climatol. doi:10.1007/s00704-016-1748-3

Vallam P, Qin XS, Yu JJ (2014) Uncertainty quantification of hydrologic model. APCBEE Procedia 10:219–223

Velázquez JA, Anctil F, Ramos MH, Perrin C (2011) Can a multi-model approach improve hydrological ensemble forecasting? A study on 29 French catchments using 16 hydrological model structures. Adv Geosci 29:33–42. doi:10.5194/adgeo-29-33-2011

Wang W, Shao Q, Yang T, Peng S, Xing W, Sun F, Luo Y (2012) Quantitative assessment of the impact of climate variability and human activities on runoff changes: a case study in four catchments of the Haihe River basin, China. Hydrol Process. doi:10.1002/hyp.9299

Ye X, Zhang Q, Liu J, Li X, Xu CY (2013) Distinguishing the relative impacts of climate change and human activities on variation of streamflow in the Poyang Lake catchment, China. J Hydrol 494:83–95

Zhang L, Dawes WR, Walker GR (2001) Response of mean annual evapotranspiration to vegetation changes at catchment scale. Water Resour Res 37(3):701–708

Zhao F, Zhang L, Xu ZX, David FS (2010) Evaluation of methods for estimating the effects of vegetation change and climate change on streamflow. Water Resour Res 46:W03505

Zheng Z, Wen-Xi LU, Hai-Bo C, Wei-Guo C, Ying Z (2014) Uncertainty analysis of hydrological model parameters based on the bootstrap method: a case study of the SWAT model applied to the Dongliao River Watershed, Jilin Province, Northeastern China. Sci China Technol Sci 57(1):219–229

Paper 4

Water Resour Manage (2017) 31:1489–1502
DOI 10.1007/s11269-017-1590-0

Temporal Hydrologic Alterations Coupled with Climate Variability and Drought for Transboundary River Basins

Ruqayah Mohammed[1] · Miklas Scholz[1,2] · Mohammad Zounemat-Kermani[3]

Received: 31 December 2015 / Accepted: 10 February 2017 /
Published online: 28 February 2017

Abstract Climate change (CC) and drought episode impacts linked with anthropogenic pressure have become an increasing concern for policy makers and water resources managers. The current research presents a comprehensive methodology but simple approach for predicting the annual streamflow alteration based on drought indices and hydrological alteration indicators. This has been achieved depending on the evaluation of drought severity and CC impacts during the human intervention periods to separate the influence of climatic abnormality and measure the hydrologic deviations as a result of streamflow regulation configurations. As a representative case study, the Lesser Zab River Basin in northern Iraq has been chosen. In order to analyse the natural flow regime, 34 hydrological years of streamflow (1931–1965) prior to the main dam construction were assessed. The Indicators of Hydrologic Alteration (IHA) method has been applied to quantify the hydrological alterations of various flow characteristics. In addition, an easy approach for hydrological drought prediction in relatively small basins grounded on meteorological parameters during the early months of the hydrological year has been presented. The prediction was accomplished by implementing the one-dimensional drought examination and the reconnaissance drought index (RDI) for evaluating the severity of meteorological drought. The proposed methodology is founded on linear regression relations connecting the RDI of 3, 6, and 12 months and the streamflow drought index (SDI). The results are critical for circumstances where an early exploration of meteorological drought is obtainable. Outcomes assist water resources

Electronic supplementary material The online version of this article (doi:10.1007/s11269-017-1590-0) contains supplementary material, which is available to authorized users.

✉ Miklas Scholz
miklas.scholz@tvrl.lth.se

[1] Division of Water Resources Engineering, Department of Building and Environmental Technology, Faculty of Engineering, Lund University, P.O. Box 118, 221 00 Lund, Sweden

[2] School of Computing, Science and Engineering, Civil Engineering Research Group, The University of Salford, Newton Building, Greater Manchester M5 4WT, UK

[3] Department of Water Engineering, Shahid Bahonar University of Kerman, Kerman, Iran

managers, engineers, policy makers and decision-makers responsible for mitigating the effects of CC.

Keywords Hydrological alteration indicator · Climate change · Decision-making · Reconnaissance drought index · Streamflow drought index · Water resources management

1 Introduction

1.1 Background

One of the main water-related hazards is drought (Mishra and Singh 2010), which is commonly considered as a three-dimensional episode categorised by its severity, duration and impacted region (Tsakiris and Vangelis 2005; Mohammed and Scholz 2017). There are numerous proposed methodologies for drought identifying, quantifying and monitoring. The most widespread methods, which are distinctive collections of indicators involving meteorological, hydrological and other data, are the drought indices (Tsakiris and Vangelis 2005; Mohammed and Scholz 2017).

Drought indices are vital and practical elements for characterising drought and supporting policy makers in mitigating its impacts on various water sectors. Noticeably, indices make it easier to transfer climate anomaly information to a wide range of audiences and assisting scientists in the evaluation of quantitative weather abnormalities in terms of their intensity, frequency, areal extent and duration (Mishra and Singh 2010; Yu et al. 2013).

A high number of meteorological drought indices with different intricacy have been utilised for various climatic conditions and objectives. Examples of the most common indices are as follows: Palmer drought severity index (PDSI), Palmer hydrological drought index (PHDI), standardised precipitation index (SPI), rainfall anomaly index (RAI), standardized anomaly index (SAI), deciles, percent of normal, crop moisture index (CMI), soil moisture drought index (SMDI), and surface water supply index (SWSI) as well as such indices based on the normalised difference vegetation index (NDVI). For more details of the most common indices, interested readers may refer to Heim (2002).

The SPI is considered by The World Meteorological Organisation as a universal drought index because of its capacity to be estimated for various reference periods adapting to the different response times of typical hydrological characteristics to precipitation (Vicente-Serrano et al. 2015). The index permits exposure of various drought classifications affecting different regimes and regions. Still, there are shortages related to its failure to detect drought conditions estimated not by a shortage of precipitation (P) but by a higher than normal aerial evaporative requirement, which is challenging (Tsakiris and Vangelis 2005; Cook et al. 2014). Therefore, recent drought trend studies (Shahidian et al. 2012; Vicente-Serrano et al. 2015) and drought scenarios under potential CC projections (Cook et al. 2014) depended on drought indices that take into account P and the aerial evaporative requirement.

Tigkas et al. (2015) introduced a brief overview of the theoretical basis of the reconnaissance drought index (RDI) together with some practical applications with a specialised software package called drought indices calculator (DrinC). The RDI is founded on two meteorological parameters, P, which is observed, and the potential evapotranspiration (PET), which is estimated.

Furthermore, cyclical river flow components anomaly such as high and low flows resulted from natural (i.e. climate change (CC)) and man-made (i.e. river damming) climatic conditions has produced enormous concerns expressed by hydrologists due to consequences for riverine ecosystems (Suen 2008; Doll and Zhang, 2010; Al-Faraj and Scholz 2014; Mittal et al. 2016). For estimation of the natural and altered hydrologic systems, a simple tool, which is known as the Indicator for Hydrologic Alteration (IHA), has been developed by The Nature Conservancy (The Nature Conservancy 2009). Through calculating the hydrologic characteristics for the pre-impact and post- impact periods, the IHA can be utilised to assess how the stream system would be altered due to river regulation such as dam building.

Literature exposes that considerable research work has been undertaken to assess the hydrologic anomalies of natural flow regimes (Yan et al. 2010; Gao et al. 2013; Sun and Feng 2013; Jiang et al. 2014; Wang et al. 2016). Yet, most of the recent research has focused on the streamflow alteration from an ecological point of view (Suen 2008; Doll and Zhang 2010; Kim et al. 2011; Lee et al. 2014; Mittal et al. 2014; Stagl and Hattermann 2016) and not from a hydrological one. In addition, they did not consider to incorporate anthropogenic interventions, CC and drought event impacts within a comprehensive study.

Therefore, the prime aim of the study is to evaluate the streamflow hydrological anomalies due to anthropogenic interventions such as dam building, incorporated with CC and drought phenomena impacts, attempting to assess to what extent the anthropogenic intervention impacts linked with natural climatic phenomena would alter basin hydrological properties. Based on the authors' best knowledge, this is a novel effort at exploring the anthropogenic interventions, CC and drought severity effects on the basin hydrologic features.

1.2 Aim and Objectives

The major aim of this research is to investigate the impacts of CC and anthropogenic interventions on streamflow alteration in addition to the prediction of hydrological drought for relatively small basins based on meteorological data. The corresponding objectives are (a) to introduce a methodology for applying the climate forecasting system reanalysis (CFSR) dataset to attain historical meteorological data and to assess its applicability on CC studies, drought event estimations, and hydrological alteration detections; (b) to investigate the characteristics of spatio-temporal change of meteorological data at monthly and annual time scales; (c) to analyse the response of PET to the temperature variations; (d) to assess the temporal alteration of hydrologic regimes related to CC impacts coupled with anthropogenic interventions over the whole watershed; (e) to evaluate the potential CC impact, drought phenomenon and anthropogenic interventions on streamflow volume; and (f) to present a generic and simplified method for hydrological drought prediction in relatively small basins based on weather data.

2 Theory

2.1 Trend Investigation

In order to detect a trend in long time series of hydro-climatologic data, there are different tests that can be used such as parametric and non-parametric methods (Duhan and Pandey 2013). In

this research, parametric (linear regression) and non-parametric (Mann-Kendall (M-K)) were used. The former method is distinguished by its simplicity and requires variables to be normally distributed (Tabari and Taalaee 2011). However, the latter technique has the advantage of not assuming any data distribution and is similarly powerful to its parametric competitors (Zhang et al. 2008). The following section briefly explains the applied methods.

2.2 Parametric Method

Simple linear regression is often performed to investigate the relationship between variables of interest and obtain the change of hydro-climatologic variables with time. A positive slope indicates a rising trend, whereas a negative slope is indicative of a decreasing trend. Another advantage for this test is that it gives a measure of significance founded on the hypothesis test regarding the slope and also delivers the magnitude of the degree of alteration (Hirsch et al. 1991). By multiplying the slope by the number of years, the total change during the period under observation can be received.

2.3 Non-Parametric Method

The M-K test is a non-parametric method for assessing if there is a monotonic downward or upward trend of the parameter under consideration with time (Tabari and Taalaee 2011). A monotonic upward (downward) tendency indicates that the parameter consistently rises (declines) during the period. However, the trend might or might not be linear. The M-K test can be applied instead of a linear regression analysis, which can be applied to investigate if the slope of the predicted linear regression line is unlike zero. The regression analysis demands that the residuals from the fitted regression line are normally distributed. Such an assumption is not required by the M-K test. For more details about M-K test, readers may refer to previous studies (Tabari and Taalaee 2011; Robaa and AL-Barazanji 2013).

2.4 Reconnaissance Drought Index (RDI)

The reconnaissance drought index (RDI) can be shown in the alpha ($RDI_{\alpha k}$), normalised (RDI_n) and the standard (RDI_{st}) forms. The RDI_{st} can be used to assess the drought severity, whereas the $RDI_{\alpha k}$ can be used as an aridity index. The index is mainly founded on the aggregated P and PET theories. The $RDI_{\alpha k}$ is normally estimated for the *i*-th year at a time basis of *j* successive months. The values of $RDI_{\alpha k}$ match both the lognormal and the gamma distributions in various positions.

A positive value of RDI_{st} relates to a wet period. In comparison, a negative value is indicative of a dry period in comparison to the natural conditions of the study region. The drought severity phenomena increase when RDI_{st} values are minimal. The drought severity can be classified into mild, moderate, severe and extreme classes. The corresponding limit values of RDI_{st} are -0.5 to -1.0, -1.0 to -1.5, -1.5 to -2.0, and < -2.0, respectively. The RDI is estimated for a hydrological year in 3-, 6-, 9- and 12-month reference time periods. This indicates a variable quality of RDI compared to other drought indices since it is computed for pre-determined reference periods of time (Tigkas and Vangelis 2013).

2.5 Hydrological Drought Index

The hydrological drought index (SDI) is founded on the cumulative streamflow volumes $S_{i,k}$ for each reference period k of the i-th hydrological year. For most small basins, streamflow may follow a skewed probability distribution. This can be approximated well by gamma distribution functions. The distribution is then transformed into normal. The SDI index can be defined by applying a two-parameter lognormal distribution.

A value of SDI greater than zero relates to a non-drought period. In comparison, a negative value is indicative of a drought period in comparison to the natural conditions of the study region. The hydrological drought severity increase when SDI values are minimal. The hydrological drought severity can be classified into mild, moderate, severe and extreme classes. The corresponding limit values of SDI are 0.0 to -1.0, -1.0 to -1.5, -1.5 to -2.0, and < -2.0, respectively (Nalbantis 2008; Nalbantis and Tsakiris 2009). An integer number ranging from 0 (non-drought) to 4 (extreme drought) is usually considered.

3 Materials and Methods

3.1 Representative Case Study Region

The Lower Zab River (also known as Little Zab River and Lesser Zab River) is one of the main tributaries of the Tigris River, and is situated with its tributaries between latitudes 36°50′ N and 35°20′ N, and longitudes 43°25′ E and 45°50′ E (Mohammed and Scholz 2016); see also Online Resource 1.1. The Lower Zab River originates from the Zagros Mountains in Iran, and flows about 370 km south-east and south-west through north-western Iran and northern Iraq before joining the Tigris near Fatha city, which is located about 220 km north of Baghdad (Mohammed et al. 2017), with a total length of approximately 302 km and about 80 km south of the Greater Zab River.

There are a number of tributaries contributing to the river discharge such as the Banah and Qazlaga. The catchment area of the Lower Zab Basin (LZRB) and its tributaries is approximately 19,254 km^2 with nearly 76% of the basin located in Iraq. The mean annual storage of the Lower Zab at Dokan and at the downstream station of Altun Kupri-Goma is about 6 billion cubic meters (BCM) and 7.8 BCM in this order. The corresponding mean contribution to the Tigris of 191 m^3/s and 249 m^3/s for the two stations, respectively (Mohammed et al. 2017).

Online Resource 1.2 indicates the average annual flow variability of the river Zab, which is characterised by regular oscillation of dry and wet periods at both gauging stations (USGS 2010). The mean, maximum and minimum discharges of the Lower Zab are 227, 3420 and 6 m^3/s, respectively (Al-Ansari et al. 2014; Mohammed et al. 2017). The Lower Zab crosses rather diverse ecological and climatic zones. Annual P along the river course decreases from more than 1000 in the Iranian Zagros to less than 200 mm at the confluence with the river Tigris. Moreover, mean temperatures follow the same gradient. The mountain valleys are usually subjected to colder winters than the corresponding foothill areas. However, summers in the latter are usually hotter (NOAA 2009).

Dokan is the main dam that has been constructed in the Iraqi portion of the LZRB, whereas Iran is recently constructing one dam with two others in the planning phase. The Dokan, which is a multi-purpose arch dam, was constructed between 1957 and 1961 upstream from Dokan town with a maximum capacity of approximately 6970 million cubic meters (MCM), crest

height of 116 m above the river bed (516 m) and a length of 360 m. The main dam functions are to control the discharge of the Lower Zab, store water for irrigation and to provide hydroelectric power.

3.2 Climate Forecasting System Reanalysis Data

Gathering representative weather data for basin-scale hydrological simulations might be challenging and take a lot of time. This is because the land-based meteorological stations do not usually adequately cover the climate observed over a basin for many reasons such as that they might be located far from the area of interest and are associated with missing data, which holds true for the case study area.

Accordingly, this research introduces a procedure for utilising the CFSR global methodological dataset (Saha et al. 2010) to gain historical meteorological data and investigate its applicability for hydrologic alteration, drought severity assessment and CC studies. The CFSR data are based on a dataset created by the National Centres for Environmental Prediction (NCEP) as a part of a climate forecast system (Chen and Emily 2014; Dile and Srinivasan 2014; Saha et al. 2014).

The CFSR dataset supersedes the previous National Centers for Environmental Prediction (NCEP)/National Center for Atmospheric Research (NCAR) reanalysis dataset that has been immensely utilised in previous down-scaling research (e.g., Michelangeli et al. (2009) and Maurer et al. (2010)). Recent research in water resources (Srinivasan 2014; Adeloye et al. 2016; Soundharajan et al. 2016; Mohammed and Scholz 2017) dependent on the CFSR dataset. For example, Mohammed and Scholz (2017) confirmed the CFSR data reliability by applying the dataset to evaluate the potential effect of evapotranspiration formulations at different elevations and climatic conditions on the RDI index. The CFSR dataset covers the period from 1979 to 2014 with a spatial resolution of $0.5° \times 0.5°$ (Soundharajan et al. 2016). Concerning data reliability in watershed-scale modelling, Fuka et al. (2013) confirmed that applying the CFSR data as input to the hydrological model produces streamflow, which are as accurate as or even better than models derived through popular meteorological stations, particularly in the case that the stations are located greater than 10 km from the area of interest.

3.3 Information Availability and Application of the Method to the Case Study

Daily meteorological data from 30 stations were available for the period between 1979/80 and 2013/14. Daily streamflow data were accessible for Dokan station for the duration of 82 years.

ArcGIS 10.3 has been used for meteorological station location projections, Thiessen network computations, spatial analysis of the meteorological data and river basin delineation using the world borders, Iraqi Shapefiles and Lower Zab River basin files, which have been downloaded from Thematic Mapping (2009), the database of Global Administrative Areas (GADM 2012), the Global and Land Cover Facility (GLCF 2015), which is a centre for land cover science with a concentrate on study using remotely sensed satellite data and products to access land cover change for regional to universal systems, respectively.

Statistical analyses for the daily data, including monthly and annual average values, corrections and gap filling were performed using the Statistical Program for Social Sciences (SPSS) 20. Online Resource 1.3 shows the categories of the meteorological stations for the studied basin. Online Resources 1.4 and 1.5 reveal both the parametric and non-parametric

tests for the meteorological variables. The estimation of PET and RDI was accomplished with a specialised software package named DrinC (Tigkas et al. 2015).

In order to achieve an accurate estimation of the spatial distribution of rainfall, it is necessary to use interpolation methods. The weighing mean method was considered as the most important one for engineering praxis (Fiedler 2003). This method assigns weights at each gauging station in proportion to the basin area, which is closest to that station.

To set up the method, the following steps have been accomplished using ArcGIS 10.3. The creation of a shapefile of the named watershed polygons as a function of the land cover image has been achieved by downloading the relevant information from GLCF (2015)

This step was followed by creation of two shapefiles. The first one is the basin border polygon, while the second one is the point shapefile that represents meteorological stations. Each representative point involved a value of the long-term P.

A Thiessen network (Online Resource 1.6) was created to estimate the area of each station polygon (a_i). This has been achieved depending on the following: (a) Connecting the adjacent stations with lines; (b) Constructing perpendicular bisectors of each line, and (c) The bisectors are extended and applied to form the polygon around each station. Online Resource 1.7 lists the station addresses with corresponding average P and the sub-area sizes.

Rainfall values for each gauging station (P_i) are multiplied by the area of each polygon (a_i). The next step required the computation of the average values of the P_{av} by summing up all values obtained from the previous step and dividing the number by the total basin area according to equation (1).

$$P_{av} = \frac{\sum_{i=1}^{n} a_i \times P_i}{\sum_{i=1}^{n} a_i} \tag{1}$$

where P_{av} is the average value of the basin P (mm), P_i is the average value of the station polygon P (mm) and a_i is the meteorological station area. Stations are distributed both inside and outside the polygons (Online Resource 1.6). Only one P value per station has been provided to keep the procedure simple. To evaluate the deviation of the natural flow regime that resulted from CC and drought phenomena linked to the anthropogenic interventions, the Indicators of Hydrologic Alteration software version7.1 (Richter et al. 1998; The Nature Conservancy 2009) has been utilised.

The daily Lower Zab River flow rate ranged from 1931 to 2013 and was measured at the Iraqi side of the river. The entire records were separated into two prime categories: natural flow period and changed flow period. The first hydrological alteration has occurred in the water year 1965, which was considered as a reference water year. Accordingly, the period between 1931 and 1964 represent the pre-regulated period. However, the period that covers the hydrologic years between 1965 and 2013, which was considered as the post-regulated period.

The time intervals selected depended on the degree of anthropogenic interventions such as increasing water requirements and reservoir constructions in addition to the impact of CC. The first period between 1965 and 2013 represents the entire period since the first reservoir was constructed. The period between 1979 and 2014 was characterised by variation in climate involving two sub-periods (1979–1987 and 1998–2008). The developed methodology enhanced understanding of the separate elements of the hydrologic variations in the streamflow. Furthermore, Online Resource 1.8 shows the normal P years during the studied period.

4 Results and Discussion

4.1 Historical Trends of the Meteorological Parameters

This research is based on the CFSR global methodological dataset, which is used to investigate its applicability for streamflow alteration estimations, drought severity computations and CC studies. The considered datasets represent various elevations, which ranged from 178 m to 2420 m over the case study basin. Online Resource 1.6 visualises the spatial distribution of the stations. Online Resource 1.3 shows the categories and locations of the chosen meteorological stations.

Before using the dataset, it is critical to assess its validity by assessing the correlation coefficients between variables collected from land-based stations and the CFSR. Online Resource 1.9 indicates that there is a strong correlation between the two datasets.

In order to detect the decadal trend of the key meteorological parameters, both parametric and non-parametric tests have been accomplished. Online Resource 1.4 reveals the analysis for P and air temperature for 30 meteorological stations over the studied area for the period between 1979 and 2014. Based on the outcome of the statistical analysis. Online Resource 1.10 shows the trend for the mean air temperature, P and PET over the basin. The analysis reveals that there is a significantly positive trend in annual T_{max} at about 90% ($p < 0.01$) and 10% ($p < 0.05$) of the stations, respectively. Moreover, significant warming trends in annual T_{max} varied from 1.909 °C to 0.370 °C per decade. The trend rates of T_{max} have been usually stronger than those in the T_{min} series. Some previous studies have reported similar conclusions in the selected region (Robaa and AL-Barazanji 2013; UNESCO 2014).

Regarding the historical changes for the third meteorological variable PET, the statistical analysis showed that the long-term PET has increased significantly by nearly 77 ($p < 0.01$) and 23% ($p < 0.05$) of the considered stations, respectively, with a decadal growth that reached its maximum value that is approximately 36 mm (Online Resource 1.5). Both changes have contributed significantly to the reduction of the streamflow and indicated that the lower Zab river basin has witnessed CC. Variation in climate produced an alteration in precipitation, air temperature and PET, which widened the gap between the basin water storage availability and the corresponding water demand.

4.2 Drought Identification and Classification

For the purpose of drought occurrence detection, the RDI (Tsakiris and Vangelis 2005) was calculated using the available data for P and the estimated values of PET. The index is classified as a meteorological drought index because it depends essentially on meteorological parameters observed for various meteorological stations. To evaluate different types of droughts, a three-month RDI (3 RDI) is computed for a short-term meteorological drought evaluation, a six-month RDI (6 RDI) is estimated for agricultural drought, and a 12-month RDI (12 RDI) is used as an intermediate long-term drought index for hydrological drought analyses and applications (USGS 2010).

Online Resource 1.11 presents the RDI_{st} values estimated for the studied area based on data from 1979 to 2014 as well as long-term P_{av} and indicates that a non-uniform cyclic pattern of drought and wet periods was observed for the studied area concerning the studied time span. Evident seasonal droughts were recorded for five years during the examined record; particularly for 1998/1999, 1999/2000, 2000/2001, 2007/2008 and 2008/2009 (average RDI values -

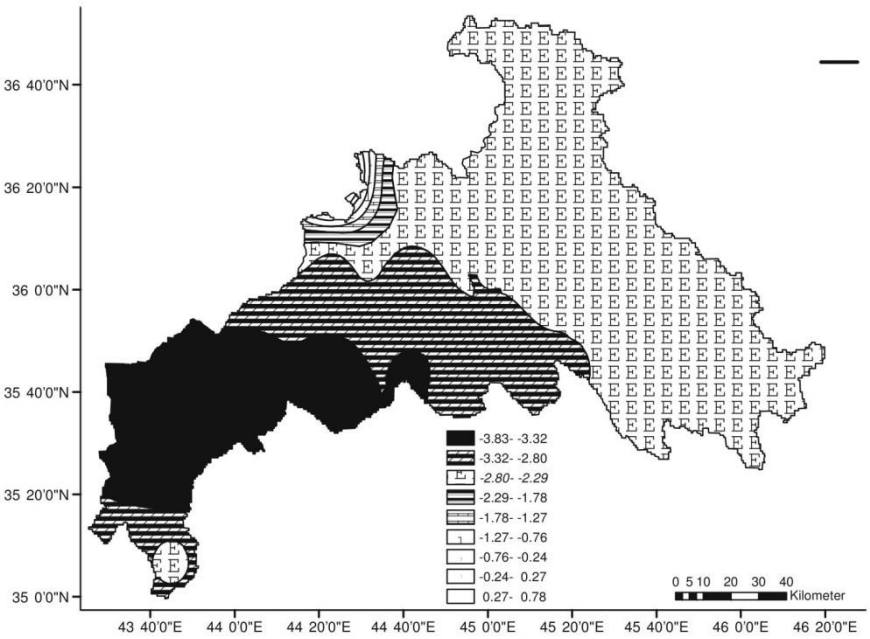

Fig. 1 The spatial distribution of the worst drought that occurred in the case study region during the water years 2007 and 2008

1.84, -1.67, -1.45, -2.91 and -1.53, respectively), which were also reported by many earlier studies such as Fadhil (2011) and UNESCO (2014). Figure 1 shows the spatial distribution of the worst drought that occurred in the region during the water year 2007/2008. Generally speaking, droughts usually happen at the beginning of the wet season, which is reflected by either a decline in the P amount or a delay in P events.

As the RDI analysis shows, the drought severity over the studied basin has worsened significantly during the past twelve years. The RDI values computed between 1998 and 2011 show that critical droughts happened as the number of months with extended periods of P shortage increased. As shown in the P trend and the long-term analysis, the drought phenomenon was accompanied by a decrease in P. In addition, the P trend from the beginning of 2000 indicates that the region has been experiencing a reduction in rainfall and water resources in addition to an increase in drought periods.

4.3 Assessment of Anthropogenic Interventions Linked to Climate Variability

The potential effects of CC detection on the hydro-climatologic variables can be considered as a substantial step in the CC impacts analysis linked with anthropogenic interventions. The main consequence of CC is that the wet and dry years are characterised by high and low flows in that order. Yoo (2006) proposed that the proper periods in which annual basin P is more than Average P (P_{av}) + 0.75 × Standard Deviation (SD) are considered as wet years, whereas, years with annual P no more than P_{av}-0.75 × SD are considered as dry years. Therefore, hydrological years with annual P values between these two thresholds are considered as normal years P_{av}-

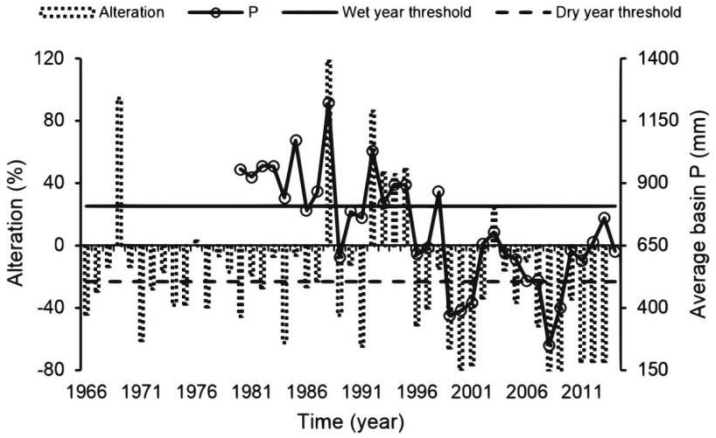

Fig. 2 Annual median anomaly for the time period between 1966 and 2014 with both wet and dry year thresholds coupled with long-term average precipitation over the study area for the time span between 1979 and 2014

$0.75 \times SD \leq P \leq P_{av} + 0.75 \times SD$ (Yang et al. 2008). Figure 2 shows streamflow time series corresponding to normal hydrological years with wet and dry year thresholds.

On one hand, the annual alteration ratio of the entire changed timespan (1964–2013) compared to the long-term median yearly discharge for the unchanged period (1932–1964) was calculated according to equation (2).

$$\text{LZR flow alteration } \% = \frac{\text{LZR altered flow -LZR unaltered flow}}{\text{LZR unaltered flow}} \times 100 \qquad (2)$$

where $LZR_{altered}$ and $LZR_{unaltered}$ (m^3/s) are the median yearly changed discharge and long-term median annual natural flow for the entirely unaltered condition in this order. Figure 2 shows the anomalies of the median annual flow for the post-regulation condition based on the long-term pre-regulation median annual flow.

On the other hand, Fig. 2 reveals that the water year 1987 experienced a significant increase in the basin P_{av} of nearly 44% more than the normal year maximum threshold. The considerable increase in P results in a substantial alteration in the streamflow to about 118%, with the corresponding annual mean flow volume of 2.31×10^9 m^3 (Online Resource 1.12). However, the entire opposite was recorded for the hydrological periods 1998–2001 and 2006–2008 (Online Resource 1.13). These two periods experienced a steep decline in the basin P_{av} to nearly 40 and 60% in that order. The reduction in P_{av} led to a substantial decline in the Lower Zab streamflow by around 66, 77 and 79% with the corresponding yearly mean flow volumes of 0.35×10^9, 0.31×10^9, and 0.34×10^9 m^3 for the period between 1998 and 2001. However, the hydrological period between 2006 and 2008 experienced approximately 52, 80 and 83% streamflow reductions with 0.76×10^9, 0.29×10^9 and 0.31×10^9 m^3 annual mean flow volumes. Furthermore, between 1991 and 2013, the normal flow regime has been experienced a sharp reduction during which the flow alteration fluctuated between -75 and 86% with 0.31×10^9 and 1.24×10^9 m^3 maximum and minimum yearly average storage volumes in that order. Findings of this research proved that CC has negatively affected the Lower Zab river storage water availability.

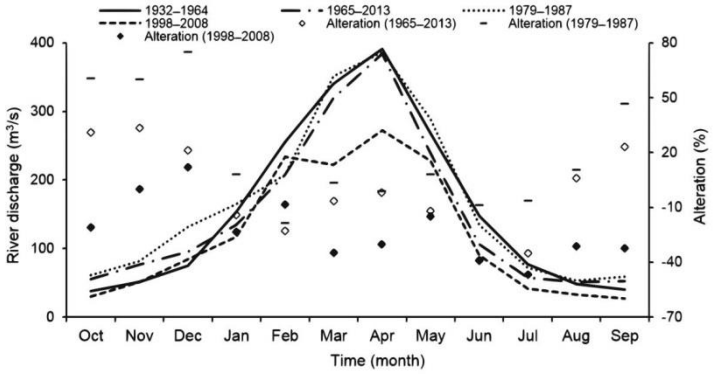

Fig. 3 The long-term median monthly flows of the pre-altered and the three altered time scales coupled with their anomies

Moreover, the alteration in monthly median flows corresponding to the long-term natural flow regime and the three changed time scales and their related alteration is visualised in Fig. 3. The alteration during the two altered time spans of the periods 1965–2013 and 1979–1987 could be considered relatively close to each other, particularly through the rainy months. The small variations can be assigned to the CC impacts, which was noticeable from the water year 1998 onward. The dramatic alteration during the non-rainy months assigned to the effect of human-induced and CC pressure in the upper part of the studied area, which in turn decreases watershed storage system availability.

4.4 Predicting Equation

For the reference periods of 3, 6, and 12 months, RDI_{st} estimations were achieved. The linear regression lines between RDI_{st} (3, 6, and 12 months) and SDI (12 months) for the water years 1979/80 to 2013/14 are presented in Fig. 4. The evapotranspiration values needed for the RDI calculations were estimated applying the FAO Penman-Monteith methodology (Allen et al. 1998). This equation has been increasingly gaining acceptance and is used throughout the world for reference evapotranspiration estimations (Shahidian et al. 2012). The method requires the measurement of several climatic variables such as temperature, relative humidity, solar radiation and wind speed, which are available for this research.

As the reference periods become longer, the regression equations reveal better fits, as represented by higher correlation coefficients (Fig. 4). This can be expected, because an improve correlation is obtained by including extra data associated to the hydrological drought of the assessed year. This has been achieved for a reference period of up to 9 months by which P and streamflow co-exist. Regression equations can introduce predicts with rather high variability. Accordingly, each SDI prediction should be treated only as a representative value, particularly if it is calculated applying data from the first trimester of the water year. It follows that, this relatively simple method, which introduces findings with substantial variability, demonstrates to be valuable since pro-active measures to mitigate the effects of droughts are decided upon the class of severity category of the expected drought event and not on the absolute SDI value.

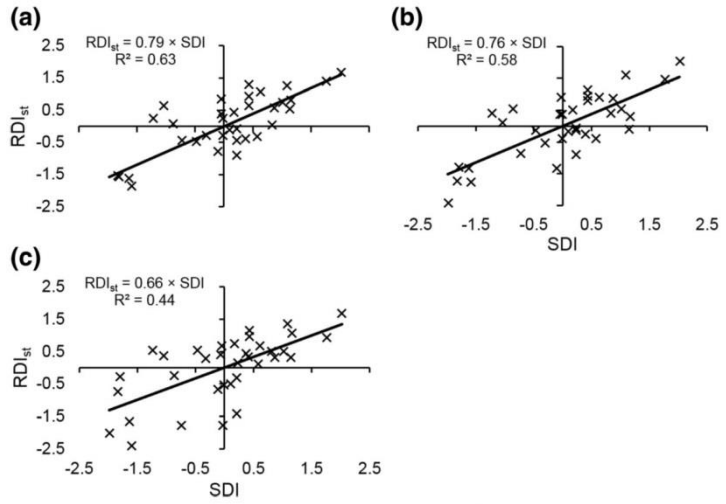

Fig. 4 Annual streamflow drought index (SDI) forecasting equations based on the standardised reconnaissance drought index (RDI_{st}) for the reference time periods of 12, 6 and 6 months: (**a**) RDI_{st} (12 months) – SDI (12 months), (**b**) RDI_{st} (6 months) – SDI (12 months) and (**c**) RDI_{st} (3 months) – SDI (12 months), respectively

5 Conclusions

The current research presents a generic method to support water resources managers to create informed and robust judgements on adaptation and mitigation policies in the face of CC. The following case study-specific conclusions could be drawn:

- The regular periodic drought and rainy periods were recorded for the considered period.
- Noticeable droughts on a seasonal basis were observed for five years during the considered historical records, particularly in 1998/1999, 1999/2000 and 2000/2001.
- The P trend along with the RDI_{st} calculation, beginning from 2000, reveals that the region has been witnessing a P decline and water resources as well as drought period increases.
- During the water year 2007/2008, the drought severity has worsened dramatically.
- The hydrological year 1987/1988 experienced a substantial rise in the basin P_{av} due to considerable streamflow alteration.
- The hydrological periods 1998–2002 and 2006–2008 experienced a steep P_{av} reduction over the studied basin, which caused a streamflow reduction by more than 80%.
- The dramatic alteration during the non-rainy months attributed to the effect of human-induced and CC pressure in the upper part of the studied area, which in turn reduced the watershed storage capacity.

Acknowledgements The research presented has been financially supported by the Iraqi Government via Babylon University (PhD studentship for the lead author).

Compliance with Ethical Standards

Conflict of Interest The authors declare that they have no conflict of interest.

References

Adeloye AJ, Soundharajan BS, Ojha CSP, Remesan R (2016) Effect of hedging-integrated rule curves on the performance of the pong reservoir (India) during scenario-neutral climate change perturbations. Water Resour Manag 30(2):445–470. doi:10.1007/s11269-015-1171-z

Al-Ansari NA, Ali AA, Knutsson S (2014) Present conditions and future challenges of water resources problems in Iraq. J Wat Res Prot 6(12):1066–1098. doi:10.4236/jwarp.2014.612102

Al-Faraj F, Scholz M (2014) Assessment of temporal hydrologic anomalies coupled with drought impact for a transboundary river flow regime: the Diyala watershed case study. J Hydrol 517:64–73

Allen RG, Pereira LS, Raes D, Smith M (1998) Crop evapotranspiration: Guidelines for computing crop water requirements. Food and Agriculture Organization (FAO) Irrigation and Drainage Paper 56, first ed, Rome

Chen M, Emily B (2014) The NCEP climate forecast system version 2. J Clim 27(6):2185–2208

Cook BI, Smerdon JE, Seager R, Coats S (2014) Global warming and 21st century drying. Clim Dyn 43(9): 2607–2627

Dile YT, Srinivasan R (2014) Evaluation of CFSR climate data for hydrologic prediction in data-scarce watersheds: an application in the Blue Nile River Basin. J Am Water Resour Assoc 50(5):1226–1241

Doll P, Zhang J (2010) Impact of climate change on freshwater ecosystems: a global-scale analysis of ecologically relevant river flow alterations. Hydrol Earth Syst Sci 14(5):783–799

Duhan D, Pandey A, Gahalaut KPS, Pandey RP (2013) Spatial and temporal variability in maximum, minimum and mean air temperatures at Madhya Pradesh in central India. Compt Rendus Geosci 345:3–21

Fadhil MA (2011) Drought mapping using Geoinformation technology for some sites in the Iraqi Kurdistan region. Int J Digit Earth 4(3):239–257

Fiedler FR (2003) Simple, practical method for determining station weights using Thiessen polygons and isohyetal maps. J Hydrol Eng 8(4):219–221

Fuka DR, Walter MT, MacAlister C, Degaetano AT, Steenhuis TS, Easton ZM (2013) Using the climate forecasting system reanalysis as weather input data for watershed models. Hydro Proc 28(22):5613–5623

GADM (2012) Global Administrative Areas database. http://www.gadm.org. Accessed 10 March 2015

GLCF (2015) Global and Land Cover Facility. http://www.landcover.org/data/srtm/ Accessed 50 March 2015

Gao D, Yang H (2013) Impact of the Three Gorges Dam on flow regime in the middle and lower Yangtze River Bing. Quat Int 304(2013):43–50

Heim RR Jr (2002) A review of twenty-century drought indices used in the United States. Bull Am Meteorol Soc 83(8):1149–1165

Hirsch RM, Alexander RB, Smith RA (1991) Selection of methods for the detection and estimation of trends in water quality. Water Res Res 27(5):803–814

Jiang BX, Wang X, Cai X (2014) Assessment of hydrologic alterations caused by the Three Gorges Dam in the middle and lower reaches of Yangtze River, China. Water 6(5):1419–1434

Kim BS, Kim BK, Kwon HH (2011) Assessment of the impact of climate change on the flow regime of the Han River basin using indicators of hydrologic alteration. Hydrol Process 25(5):691–704. doi:10.1002/hyp.7856

Lee A, Cho S, Kang DK, Kim S (2014) Analysis of the effect of climate change on the Nakdong river stream flow using indicators of hydrological alteration. J Hydro-Environ Res 8(3):234–247. doi:10.1016/j.jher.2013.09.003

Maurer EP, Hidalgo HG, Das T, Dettinger MD, Cayan DR (2010) The utility of daily large-scale climate data in the assessment of climate change impacts on daily streamflow in California. Hydrol Earth Syst Sci 14(6):1125–1138

Michelangeli PA, Vrac M, Loukos H (2009) Probabilistic downscaling approaches: application to wind cumulative distribution functions. Geophys Res Lett 36(11):1–6

Mishra KA, Singh VP (2010) A review of drought concepts. J Hydrol 391(1–2):202–216

Mittal N, Mishra A, Singh R, Bhave AG, van der Valk M (2014) Flow regime alteration due to anthropogenic and climatic changes in the Kangsabati River, India. Ecohydrol Hydrobiol 14(3):182–191

Mittal N, Bhave AG, Mishra A, Singh R (2016) Impact of human intervention and climate change on natural flow regime. Water Resour Manag 30(2):685–699. doi:10.1007/s11269-015-1185-6

Mohammed R, Scholz M (2016) Impact of climate variability and streamflow alteration on groundwater contribution to the base flow of the Lower Zab River (Iran and Iraq). Environ Earth Sci 75:1392. doi:10.1007/s12665-016-6205-1

Mohammed R, Scholz M (2017) Impact of evapotranspiration formulations at various elevations on the reconnaissance drought index. Water Res Manag 31(1):531–548. doi:10.1007/s11269-016-1546-9

Mohammed R, Scholz M, Nanekely MA, Mokhtari Y (2017) Assessment of models predicting anthropogenic interventions and climate variability on surface runoff of the Lower Zab River. Stoch Environ Res Risk Assess. doi:10.1007/s00477-016-1375-7

Nalbantis I (2008) Drought and streamflow. Eur Water 23(24):65–76

Nalbantis I, Tsakiris G (2009) Assessment of hydrological drought revisited. Water Res Manag 23(5):881–897

NOAA (2009) National Oceanic and Atmospheric Administration Climate of Iraq. https://www.ncdc.noaa.gov/oa/climate/afghan/iraq-narrative.html. Accessed 4 November 2015

Richter B, Baumgartner JV, Braun DP, Ponell J (1998) A spatial assessment of hydrologic alteration within a river network. Regul Riv: Res Manag 14(4):329–340

Robaa SM, AL-Barazanji ZJ (2013) Trends of annual mean surface air temperature over. Iraq Nat Sci 11(12):138–145

Saha S, Moorthi S, Pan HL, Behringer D, Stokes D, Grumbine R, Hou YT, Chuang HY, Juang HMH, Sela J, Iredell M, Treadon R, Keyser D, Derber J, Ek M, Lord S, Dool HVD, Kumar A, Wang W, Long C, Chelliah M, Xue Y, Schemm JK, Ebisuzaki W, Xie P, Higgins W, Chen Y, Wu X, Wang J, Nadiga S, Kistler R, Woollen J, Liu H, Gayno G, Wang J, Kleist D, Van Delst P, Meng J, Wei H, Yang R, Chen M, Zou CZ, Han Y, Cucurull L, Goldberg M, Liu Q, Rutledge G, Tripp P, Reynolds RW, Huang B, Lin R, Zhou S (2010) The NCEP climate forecast system reanalysis. Bull Am Meteorol Soc 91(8):1015–1057

Saha S, Moorthi S, Wu X, Wang J, Nadiga S, Tripp P, Behringer D, Hou YT, Chuang H, Iredell M, Ek M, Meng J, Yang R, Mendez MP, Doll HVD, Zhang Q, Wang W (2014) The NCEP climate forecast system version 2. J Clim 27(6):2185–2208

Shahidian S, Serralheiro R, Serrano J, Teixeira J, Haie N, Santos F (2012) Hargreaves and other reduced-set methods for calculating evapotranspiration. In: Evapotranspiration – 15 Remote Sensing and Modeling (ed) Irmak, A., InTech, Rijeka, pp 60–80

Soundharajan BS, Adeloye AJ, Remesan R (2016) Evaluating the variability in surface water reservoir planning characteristics during climate change impacts assessment. J Hydrol 538:625–639. doi:10.1016/j.jhydrol.2016.04.051

Stagl JC, Hattermann FF (2016) Impacts of climate change on riverine ecosystems: alterations of ecologically relevant flow dynamics in the Danube River and its major tributaries. Water 8(12):566. doi:10.3390/w8120566

Suen JP (2008) Potential impacts to freshwater ecosystems caused by flow regime alteration under changing climate conditions in Taiwan. Hydrol Earth Syst Sci Discuss 5(6):3005–3032

Sun T, Feng ML (2013) Multistage analysis of hydrologic alterations in the Yellow River, China. River Res Appl 29(8):991–1003. doi:10.1002/rra.2586

Tabari H, Taalaee PH (2011) Analysis of trend in temperature data in arid and semi-arid regions of Iran. Glob Planet Change 72:1–10

Thematic Mapping (2009). http://thematicmapping.org/downloads/world_borders.php. Accessed 2 October 2015

The Nature Conservancy (2009) Indicators of hydrologic alteration version 7.1 user's manual. The Nature Conservancy, June, 76

Tigkas D, Vangelis H, Tsakiris G (2015) DrinC: a software for drought analysis based on drought indices. Earth Sci Inform 8(3):697–709

Tsakiris G, Vangelis H (2005) Establishing a drought index incorporation evapotranspiration. Eur Wat 9(10):3–11

UNESCO (2014) United Nations Educational, Scientific and Cultural Organization. Integrated Drought Risk Management-DRM National Framework for Iraq. An analysis report. Retrieved from http://unesdoc.unesco.org/images/0022/002283/228343E.pdf UN-ESCWA and BGR (United Nations Economic and Social Commission for Western Asia; Bundesanstalt für Geowissenschaften und Rohstoffe) (2013) Inventory of Shared Water Resources in Western Asia, Beirut

USGS (2010) U.S. Geological Survey. Stream Gage Descriptions and Streamflow Statistics for Sites in the Tigris River and Euphrates River Basins, Iraq. Data Series 540

Vicente-Serrano SM, Schrier GVD, Begueria S, Azorin-Molina C, Lopez-Moreno J (2015) Contribution of precipitation and reference evapotranspiration to drought indices under different climates. J Hydrol 526:42–54

Wang Y, Rhoads BL, Wang D (2016) Assessment of the flow regime alterations in the middle reach of the Yangtze River associated with dam construction: potential ecological implications. Hydrol Process 30(21):3949–3966. doi:10.1002/hyp.10921

Yan Y, Yang Z, Liu Q, Sun T (2010) Assessing effects of dam operation on flow regimes in the lower Yellow River. Proc Environ Sci 2:507–516. doi:10.1016/j.proenv.2010.10.055

Yang T, Zhang Q, Xu C-Y, Chen X (2008) A spatial assessment of hydrologic alteration caused by dam construction in the middle and lower Yellow River, China. Hydrol Process 22(18):3829–3843

Yoo C (2006) Long term analysis of wet and dry years in Seoul, Korea. J Hydrol 318(1–4):24–36

Yu W, Shao M, Ren M, Zhou H, Jiang H, Li D (2013) Analysis on spatial and temporal characteristics drought of Yunnan Province. Acta Ecol Sin 33(3):317–324

Journal of Arid Environments 144 (2017) 181–191

Contents lists available at ScienceDirect

Journal of Arid Environments

journal homepage: www.elsevier.com/locate/jaridenv

The reconnaissance drought index: A method for detecting regional arid climatic variability and potential drought risk

Ruqayah Mohammed [a], Miklas Scholz [a, b, *]

[a] Civil Engineering Research Group, School of Computing, Science and Engineering, The University of Salford, Newton Building, Peel Park Campus, Salford, Greater Manchester M5 4WT, United Kingdom
[b] Division of Water Resources Engineering, Department of Building and Environmental Technology, Faculty of Engineering, Lund University, P.O. Box 118, 221 00 Lund, Sweden

ARTICLE INFO

Article history:
Received 12 November 2016
Received in revised form
17 March 2017
Accepted 24 March 2017
Available online 18 April 2017

Keywords:
Climate change
Decision-making
Drought indicator
Hydrological processes
Trend detection
Water resources management

ABSTRACT

The impact of climate variability on water demand and availability in drylands is substantial. Establishing methods to analyse precipitation (P) and evapotranspiration data sets may generate useful tools that assist in drought recognition and regional variations therein. The authors developed an index that simultaneous integrates both these variables in climate variability analysis. This study proposes the alpha and normalised forms of the reconnaissance drought index (RDI) as a single climatic index for the recognition of geographical areas with differing drought characteristics and potential weather variability. The prime application is that the RDI combines in a single index both P and potential evapotranspiration. A more consistent trend of climate variability can be identified by applying time series of different durations of RDI compared to using time series of P and potential evapotranspiration separately. The researchers explore this approach using meteorological data form 24 locations representing arid, semi-arid (Mediterranean (MD), tropical (TR), continental (CN)), and humid climatic conditions. The method is then tested through application to the semi-arid Lower Zab River basin (LZRB) in Iran and Iraq. Findings show that many regions such as the LZRB will face major droughts, indicating that there is an urgent requirement to advance water management strategies.

1. Introduction

1.1. Background

Long-term trends in hydrological processes are potentially influenced by changing climate and anthropogenic interventions (Al-Ansari, 2013; Al-Ansari et al., 2014). Investigating such trends might support identification of such changes. Defining the climate of a region is normally based on the long-term pattern of variations in meteorological variables such as mean air temperature, P, humidity and wind. The long-term impacts of climate change (CC) are expected to affect land use, agriculture, water resources, society and environmental sustainability. Accordingly, such changes can strengthen present pressure and extreme events, thus increasing water resources system hazards and overall uncertainty (Loukas et al., 2008; Logan et al., 2010). The fifth assessment report of the Intergovernmental Panel on Climate Change (IPCC) explained that the impacts of global warming on natural and human systems are observed on all continents and across the oceans (IPCC, 2014). Hydrological cycle alterations are considered to be one of the greatest CC impact such as floods, drought and storms (IPCC, 2007; Michel and Pandya, 2009). By the end of the 21st century, it is more likely that the global mean air temperature will increase by 1.4 °C to nearly 5.8 °C (IPCC, 2001). However, the Middle East and North Africa will likely encounter a decrease in rainfall and runoff between 10 and 25%, and between 10 and 40%, respectively, and an increase in evaporation between 5 and 20% (World Bank, 2009).

Both P and mean air temperature can be basic parameters to characterise regional climate and designate alterations in climate. However, these parameters display changeable trends for various regions. Accordingly, a compound index that integrates these parameters can be very critical for analysis of the overall climate. Evapotranspiration is considered as a more descriptive weather parameter for replacing air temperature in water resources

* Corresponding author. Division of Water Resources Engineering, Department of Building and Environmental Technology, Faculty of Engineering, Lund University, P.O. Box 118, 221 00 Lund, Sweden.
E-mail address: miklas.scholz@tvrl.lth.se (M. Scholz).

http://dx.doi.org/10.1016/j.jaridenv.2017.03.014
0140-1963/

management owing to its involvement in water balance studies. Analysing long-term time series of both P and potential evapotranspiration (PET) of a region can result in one of the following combinations: ++, +0, +−, 0+, 00, 0−, −+, −0 and −−, where + indicates a rise, − indicates a decline and 0 indicates no alteration for the considered parameters. It is not clear, if alterations will lead to wetter or drier climates. Trends in the availability of water may be inferred by the recorded rise of P and/or PET. Accordingly, a more beneficial method would be to study simultaneously the two key variable alterations applying a single index that will respond positively as PET decreases or P increases and vice versa.

A large number of weather-related drought indices with varying intricacy have been utilised in many climatic conditions for many purposes. Examples of some of these indices are as follows: crop moisture index (CMI), deciles, palmer drought severity index (PDSI), palmer hydrological drought index (PHDI), percent of normal, standardized anomaly index (SAI), rainfall anomaly index (RAI), standardized precipitation index (SPI), soil moisture drought index (SMDI), and surface water supply index (SWSI). Interested readers might refer to Heim (2002) for more details regarding meteorological indices. Since SPI can be estimated using various time periods adapted to the various response times of standard hydrological parameters to P delicences, the World Meteorological Organization (WMO) has put forward the SPI as a widespread index to be used (Vicente-Serrano et al., 2015). The SPI allows findings of different drought classes to impact on diverse systems and regions. However, its ability to capture a raised evaporative requirement related to CC is problematic (Tsakiris and Vangelis, 2005; Cook et al., 2014). Consequently, recent drought trend studies (Shahidian et al., 2012; Vicente-Serrano et al., 2014) under probable CC predictions (e.g., Hoerling et al., 2012; Cook et al., 2014) are dependent on indices of drought that take into consideration P and the evaporative demand of the atmosphere. Applying such indices, Cook et al. (2014) exhibited that raised evapotranspiration not only strengthens the process of regions becoming dryer, but also leads regions to experience droughts that would else witness slight drying or wetting.

Currently, a rather recently developed index, the RDI, has been suggested (Tsakiris and Vangelis, 2005; Tsakiris et al., 2007a). This

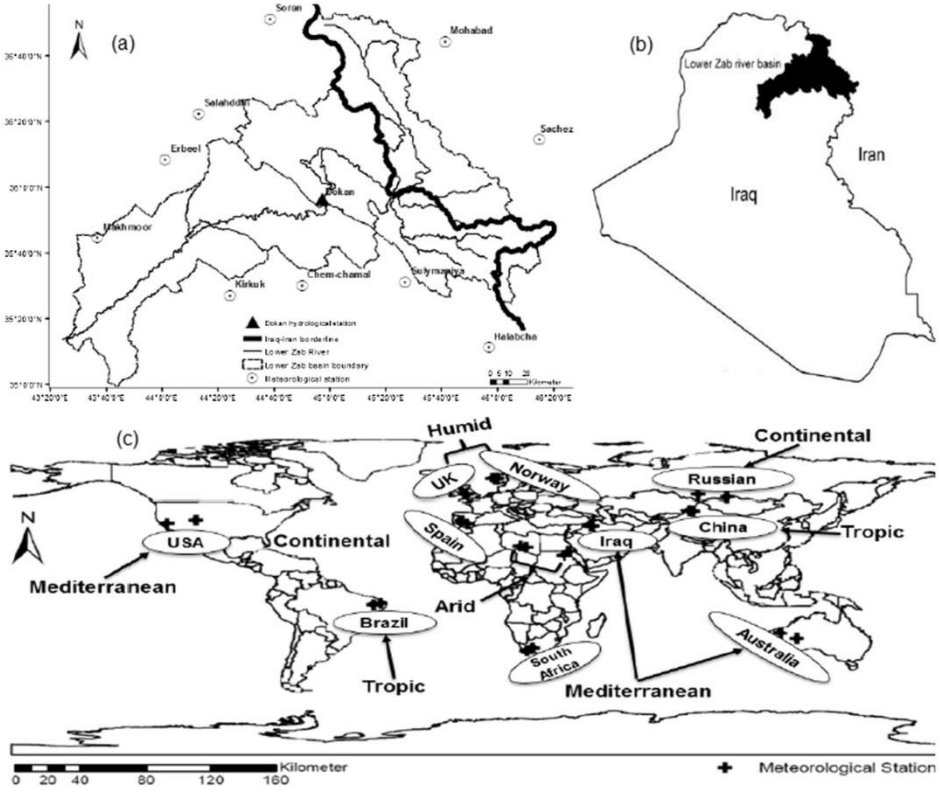

Fig. 1. (a) Meteorological stations distributed over the Lower Zab River Basin shown on (b) the map of Iraq and (c) the locations of the selected meteorological regions.

index is applied in many areas all over the word, in particular in semi-arid and arid regions, and is characterised by high sensitivity and resilience as well as its low data needs (Tigkas et al., 2012; Asadi and Vahdat, 2013; Rossi and Cancelliere, 2013; Asadi Zarch et al., 2015; Vicente-Serrano et al., 2015). The RDI is physically sound and can be estimated for any time period (Tsakiris et al., 2007b). Tigkas et al. (2012, 2015) published brief explanations of the hypothetical basis for the RDI and many other drought-related indices together with some practical applications with a specialised software package named Drought Indices Calculator (DrinC), which was established to provide a simple interface for the estimation of drought indices. Generally speaking, if there is a rise in temperature, water demand is increasing; therefore, the RDI could be modified to be used as an index for future drought risk evaluation associated with various water sectors. Therefore, the RDI is suitable for studies on climate instability.

Recently, a high number of studies in the water resources field have applied the RDI index for drought severity assessments (e.g., Tigkas et al., 2012; Vangelis et al., 2013; Giannikopoulou et al., 2014; Cai et al., 2015; Zarch et al., 2015). However, they only applied the standardized expression (RDI_{st}) without taking into consideration other forms such as the initial ($RDI_{\alpha 12}$) and the normalised (RDI_n) expressions. More recently, Mohammed and Scholz (2017) assessed the impacts of evapotranspiration estimates, meteorological station elevation, and climate condition on both drought severity and aridity evaluated by the RDI index. However, they did not discuss or highlight the particular use of the $RDI_{\alpha 12}$ expression; either as an aridity index or as a CC detection index, and how this form and other forms of the RDI can be efficiently used to investigate the impacts of CC on the regional climate. Therefore, to acknowledge this apparent gap in understanding, this study assessed the climate variability occurrence and its effects on the aridity of a geographical region depending on the RDI forms ($RDI\alpha_{12}$ and RDI_n) as a single climatic index.

1.2. Rationale, aim and objectives

There is an indication that climate variabilities are now represented by meteorological and hydrologic droughts. In contrast to various drought studies of stream flow, bounded drought research depends on meteorological drought indices with minimum data requirements concerning land use, hydrology, meteorology, agro-hydrology and water management (Blenkinsop and Fowler, 2007; Loukas et al., 2008). This research will investigate whether the increasing trend of droughts and regional aridity (IPCC, 2001), as explained above, is likely to remain at the same categories as a result of the potential impacts of CC or whether it will be altered. The authors try to understand the past and present severity of

Table 1
Categories of the selected meteorological stations form different climate conditions in addition to the Lower Zab River basin (LZRB) case study.

Wider Region	Station ID	Latitude (°)	Longitude (°)	Elevation (m)
Mediterranean				
South Africa	LL[a]	−32.63	19.69	485
	HL[b]	−31.07	22.19	1382
North Iraq	LL[a]	35.75	44.06	306
	HL[b]	36.25	46.26	1536
West Australia	LL[a]	−26.07	124.68	485
	HL[b]	−22.95	118.43	820
South USA	LL[a]	37.31	−120.00	361
	HL[b]	39.18	−108.75	1382
Tropical				
East China	LL[a]	44.49	82.81	409
	HL[b]	44.18	84.38	1316
East Brazil	LL[a]	−6.71	−36.88	440
	HL[b]	−7.34	−39.69	918
Continental				
South East Spain	LL[a]	38.87	−5.31	438
	HL[b]	36.99	−3.13	1208
South Russia	LL[a]	52.92	86.25	403
	HL[b]	51.36	97.50	1360
Arid				
Sahara	LL[a]	24.82	17.19	146
	HL[b]	24.20	19.38	604
Al-Sudan	LL[a]	19.83	34.34	390
	HL[b]	22.01	36.25	1677
Humid				
UK	LL[a]	52.92	−3.75	40
	HL[b]	52.92	−4.06	717
Norway	LL[a]	6.56	61.35	490
	HL[b]	8.13	61.35	1652
Semi-arid climate				
LZRB case study (Upstream)	Sulymanya	35.53	45.45	885
	Halabcha	35.44	45.94	651
	Sachez	36.25	46.26	1536
	Mahabad	36.75	45.70	1356
	Salahddin	36.38	44.20	1088
	Soran	36.87	44.63	1132
LZRB case study (Downstream)	Kirkuk	35.47	44.40	319
	Makhmoor	35.75	43.60	306
	Erbeel	36.15	44.00	1088
	Chem-Chamal	35.52	44.83	701

[a]Low land; and
[b]High land.

Table 2
Drought and aridity classifications based on both the standardized reconnaissance drought index (RDI_{st}) and the alpha reconnaissance drought index ($RDI_{\alpha 12}$) values.

No.	RDI_{st} range	Drought classes	$RDI_{\alpha 12}$ range	Aridity classes
1	≥2.0	Extremely wet	≤0.03	Hyper-arid
2	1.99–1.50	Very wet	0.03–0.2	Arid
3	1.49–1.00	Moderately wet	0.2–0.5	Semi-arid
4	0.99–0.00	Normal	0.5–0.65	Dry sub-humid
5	0.00 to −0.99	Near normal	≥0.65	Humid
6	−1 – −1.49	Moderately dry		
7	−1.5 – −1.99	Severely dry		
8	≤−2.0	Extremely dry		

aridity and associated drought conditions by rebuilding climatic records of CC to estimate future categories of these two phenomena using simple regression equations. This should help to understand whether aridity and droughts increase or decrease in severity in the future.

The main aim of the current research is to shed light on the RDI as a climate index, in particular, its $RDI_{\alpha 12}$ and RDI_n forms. The corresponding objectives are as follows:

- To assess representative meteorological data from 24 stations all over the world describing semi-arid (MD, TR and CN), Sahara and humid climatic conditions, representing both mountainous regions and lowlands (Fig. 1 and Table 1);
- To analysis meteorological data from a particular case study for the purpose of an accurate evaluation of CC impacts (Fig. 1 and Table 1);
- To evaluate CC impacts on aridity and droughts on different climatic conditions; and
- To highlight the use of RDI as an aridity and climatic index.

Table 3
Statistical properties of meteorological variables representing the non-parametric test for different climatic conditions in addition to the Lower Zab River basin (LZRB) as semi-arid representative case study.

Wider Region	Station ID	Meteorological parameter					
		T^b_m (°C)		P^c (mm)		PET^d (mm)	
		M-K[a]	*p*-value	M-K[a]	*p*-value	M-K[a]	p-value
Mediterranean							
South Africa	LL[e]	−0.005	0.966	0.264*	0.026	−0.240*	0.042
	HL[f]	−0.059	0.619	0.193	0.102	−0.247*	0.037
North Iraq	LL[e]	0.462**	<0.010	−0.536**	<0.010	0.243	0.040
	HL[f]	0.079	0.500	−0.328**	0.010	0.193	0.100
West Australia	LL[e]	0.103	0.386	−0.099	0.402	0.103	0.386
	HL[f]	0.227	0.055	0.334**	0.005	0.113	0.341
South USA	LL[e]	−0.005	0.966	0.025	0.831	0.129	0.274
	HL[f]	0.032	0.787	0.045	0.701	−0.015	0.898
Tropical							
East China	LL[e]	0.603**	<0.010	−0.365**	0.002	0.257*	0.030
	HL[f]	0.318**	0.007	−0.560**	<0.010	0.587**	<0.010
East Brazil	LL[e]	0.486**	<0.010	−0.066	0.580	0.129	0.274
	HL[f]	0.412**	0.001	−0.365**	0.002	−0.274*	0.012
Continental							
South East Spain	LL[e]	0.042	0.723	0.146	0.217	−0.092	0.435
	HL[f]	0.220	0.063	0.126	0.287	−0.045	0.701
South Russia	LL[e]	0.163	0.168	−0.055	0.639	0.19	0.108
	HL[f]	0.106	0.371	−0.277*	0.019	0.447**	<0.010
Arid							
Sahara	LL[e]	0.439**	<0.010	0.153	0.196	0.308**	0.009
	HL[f]	0.371**	0.002	0.069	0.560	0.153	0.196
Al-Sudan	LL[e]	0.250**	0.034	−0.008	0.943	0.106	0.371
	HL[f]	0.244**	0.039	−0.197	0.097	0.156	0.187
Humid							
UK	LL[e]	0.445**	<0.010	0.133	0.262	0.113	0.341
	HL[f]	0.455**	<0.010	0.113	−0.244	0.113	0.034
Norway	LL[e]	0.136	0.250	0.005	0.966	0.185	0.118
	HL[f]	0.069	0.560	0.002	0.989	0.185	0.118
Semi-arid climate							
LZRB case study (Upstream)	Sulymanya	0.358**	<0.010	−0.301**	<0.010	0.201	0.090
	Halabcha	0.572**	<0.010	−0.522**	<0.010	0.316**	<0.010
	Sachez	0.079	0.500	−0.328**	0.010	0.193	0.100
	Mahabad	0.603**	<0.010	−0.573**	<0.010	0.525**	<0.010
	Salahddin	0.452**	<0.010	−0.472**	<0.010	0.220	0.060
	Soran	0.380**	<0.010	−0.426**	<0.010	0.241*	0.050
LZRB case study (Downstream)	Kirkuk	0.422**	<0.010	−0.553**	<0.010	0.420**	<0.01
	Makhmoor	0.462**	<0.010	−0.536**	<0.010	0.243	0.040
	Erbeel	0.351**	<0.010	−0.371**	<0.010	0.203	0.090
	Chem-Chamal	0.345**	<0.010	−0.412**	<0.010	0.139	0.240

[a]Mann–Kendall.
[b]Mean air temperature.
[c]Precipitation.
[d]Potential evapotranspiration.
[e] Low land; and
[f]High land.
Note: Negative (−) and positive (+) values indicate the decreasing and increasing trends, respectively.
**Correlation is significant at the 0.01 level (2-tailed); and
* Correlation is significant at the 0.05 level (2-tailed).

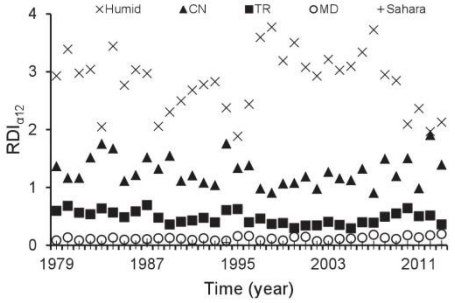

Fig. 2. The time series of 35 water years of the alpha form representing Mediterranean (MD), tropical (TR), conventional (CN), Sahara and humid climate conditions.

This research should support engineers and managers in understanding the impact of CC on surface water systems for different climatic zones, and identifying effective climate adaptation measures.

2. Methodology and data availability

2.1. Representative case study region

The impacts of CC are universal in range and differ from one climatic zone to another, and thus have important consequences on the extreme hydrological events and water resources (Asadi Zarch et al., 2015). Since drought is commonly considered as a local episode, the influences of CC on such events might vary through the world; therefore, it can be supposed that the drought occurrence and trends display numerous configurations in various climatic conditions or arid regions. Although all dry regions are relatively susceptible to droughts, the strength of each region to the challenge of such an event is different. For example, within the same level of drought severity, arid geographical regions are in a more vulnerable situation compared to those with other climatic conditions such as humid areas. Accordingly, for an accurate evaluation of CC effects on water resources, it would be necessary to shape the overall outlines and trends of droughts within each region, which is the main motivation for the current research.

The main target of this investigation is to evaluate the spatio-temporal variations of drought phenomena in different climatic conditions all over the word. In order to study the problem and

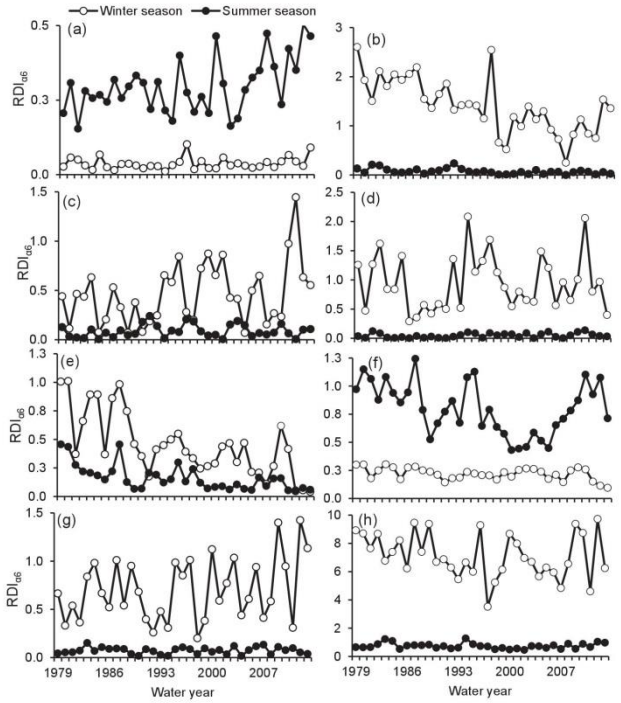

Fig. 3. Time series for 35 water years of the alpha form for: (a) South Africa; (b) North Iraq; (c) West Australia; (d) South USA; (e) East China; (f) East Brazil; (g) South-East Spain; and (h) South Russia.

achieve the main goal, meteorological data from 24 locations that represent different climatic conditions and elevations all over the word have been selected.

In addition, the Lower Zab River Basin (LZRB) has been chosen as a suitable case study to shed light on semi-arid regions (Table 1). The magnitude of problems plaguing the LZRB has a great deal in common with other transboundary watersheds such as Rhine, Volta and Senegal, where the problems of shared water resources utilisation in a sustainable manner is expected to exacerbate under the collective impact of uncertainty surrounding CC.

The Lower Zab River (Little Zab River or Lesser Zab River as well) is a key tributary of the Tigris River, and is located between latitudes 36°50′ N and 35°20′ N, and longitudes 43°25′ E and 45°50′ E (Mohammed et al., 2017b); Fig. 1a and b. The Lower Zab River originates from the Zagros Mountains in Iran, and flows about 370 km south-east and south-west through north-western Iran and northern Iraq before joining the Tigris near Fatha city, which is located about 220 km north of Baghdad (Mohammed and Scholz, 2016; Mohammed et al., 2017a), with a total length of approximately 302 km and about 80 km south of the Greater Zab River. There are number of tributaries contributing to the river discharge such as the Banah and Qazlaga. The catchment area of the LZRB and its tributaries is approximately 20,605 km^2 with nearly 76% of the basin located in Iraq. Annual P along the river decreases from ≥1000 mm in the Iranian Zagros to less than 200 mm at the confluence with the River Tigris. Mean temperatures follow the same gradient. The mountain valleys are usually subjected to colder winters than the corresponding foothill areas. However, summers in the latter are usually hotter (NOAA, 2009).

The basin covers a range of relatively large watersheds and a wide range of climatic and hydrologic conditions. The upstream and downstream developments vary widely. This suggests a considerably wide range of uncertainties in CC impacts on water resources availability. A severe drought over the basin was reported by Mohammed et al. (2017b) during the water year 2007/2008 as a result of about 80% reduction in P. The extended drought conditions seem to have had a disastrous impact on the lives of the people in the country. The limited access to water has led among others to the erosion of livelihoods and decrease in crop production.

2.2. Data availability and analysis

The climate forecasting system reanalysis (CFSR) data are based on a dataset created by the National Centres for Environmental Prediction (NCEP) as a part of the climate forecast system (Dile and Srinivasan, 2014; Saha et al., 2014). These data are applied in this study to gain historical data and to investigate its applicability for drought and aridity assessments. The CFSR dataset covers the period from 1979 to 2014 with a spatial resolution of 0.5° × 0.5° (Soundharajan et al., 2016). The CFSR data supersedes the previous NCEP/National Center for Atmospheric Research reanalysis dataset that has been immensely utilised in previous down-scaling studies. Recent water resources research (Soundharajan et al., 2016; Mohammed and Scholz, 2017; Mohammed et al., 2017b) considered the CFSR dataset. For example, Mohammed and Scholz (2017) confirmed the reliability of the CFSR by applying these data to evaluate the potential effect of evapotranspiration formulations at different elevations and climatic conditions on the RDI index. Additionally, concerning data reliability in watershed-scale modelling, Fuka et al. (2014) proved that applying the CFSR data as input to a hydrological model is appropriate. The researcher proved that the obtained results are as accurate as or even better than the results that derived through using land-based meteorological station data, particularly, where the stations are located further than 10 km from the area of interest.

ArcGIS 10.3 has been used for meteorological station location projections on the world borders shape file. The LZRB shape file has been downloaded from Thematic Mapping (2009). Yearly mean air temperature, P and potential evapotranspiration data were analysed by applying the Mann-Kendal (M-K) test to detect long-term trends for the time period between 1979 and 2013. Statistical analyses for the meteorological data including the M-K trend analysis, regression analysis, monthly and annually average values, corrections, and gap filling were performed using the Statistical Program for Social Sciences (SPSS) 23. The estimation of RDI were accomplished with a specialised software package named DrinC (Tigkas et al., 2012, 2015). Due to unavailability of evapotranspiration records the calculator version 3.2 (FAO, 2012) has been used to for the estimation of this variable by the Food and Agriculture Organization Penman-Monteith standard method (Allen et al., 1998).

2.3. Reconnaissance drought index

The RDI can be formulated in alpha ($RDI_{\alpha k}$), normalised (RDI_n) and standard (RDI_{st}) forms. The RDI_{st} can be used for drought severity assessments, whereas $RDI_{\alpha k}$ can be applied as an aridity index. This index is mainly founded on the aggregated P and PET theories (Vangelis et al., 2013). Online Resource 1.1 explains the

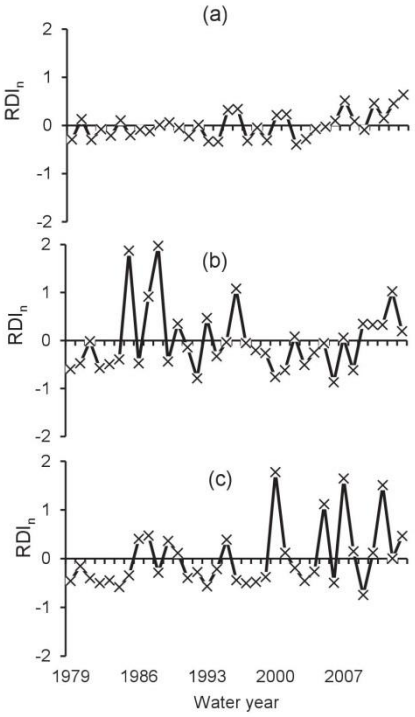

Fig. 4. Time series of 35 water years of the alpha form representing arid and humid climates: (a) Libya; (b) Al-Sudan; (c) United Kingdom; and (d) Norway.

mathematical basis of the RDI index. The RDI has been applied extensively for drought identification, quantification and observation. The severity of drought can be evaluated through the estimation of the RDI_{st}. The method is widely used, in particular, in semi-arid and arid geographical areas (Asadi Zarch et al., 2011; Tigkas et al., 2012).

A positive value of RDI_{st} relates to a wet period, whereas a negative one is indicative of a dry period compared to the natural climatic conditions of the study area. Drought severity can be classified into eight classes based on the RDI_{st} values and it increases when RDI_{st} numbers are minimal (Table 2). The RDI is estimated for a water year in 1-, 3-, 6-, 9- and 12-month reference time durations. This indicates a variable quality of RDI compared to other indices representing drought, since it is computed for predetermined reference durations. On the other hand, the $RDI_{\alpha 12}$ is based on the ratio of annual P and PET, which makes it attractive in that it is conceptually and operationally simple and is based solely on the two main parameters that define aridity. UNESCO (1979) proposed a classification of climate zones based on aridity expressed as an index, in which arid regions are defined into many classes based on the limited values of $RDI_{\alpha 12}$ as shown in Table 2.

3. Results and discussion

3.1. Long-term changes of meteorological data

Table 3 contains the statistical properties of the key meteorological variables representing the non-parametric test for the decadal change for different climatic conditions in addition to the semi-arid specific case study. The table displays the three-dimensional distribution of raising and declining as well as non-significant trends for the studied areas. The mean air temperature time series show that the majority of non-significant trends are situated in most of the MD and CN areas, while the TR, arid and most of the humid climatic conditions show significantly positive trends. Positive trends are commonly found for the United Kingdom. Most of the MD and TR regions reveal significant trends for both P and PET.

As an example for representing semi-arid areas, LZRB displayed a rising trend of mean air temperature with a maximum value of 0.67 °C for one decade, while a declining P trend (Online Resource 1.2) with a maximum decrease of 151 mm per decade was noted. The LZRB yearly P is around 720 mm. The maximum P (1222 mm) was recorded for 1987/1988, while the corresponding minimum (250 mm) was assigned to 2007/2008. The mean annual P changed spatially from 56 mm at Kirkuk station, which is located at the lower part of the basin, to 1369 mm at Sulymaniya station, which is situated at the upper basin. This indicates that the upper sub-basin, which is characterised by high elevations (compared to the lower part), had higher P values than the lower.

An evident trend of mean air temperature increase during the last half century led to a significant ($p < 0.05$) rise in the potential evapotranspiration for the entire LZRB (Table 3). Based on the trend analysis, the increase in PET rate was 39 mm per decade. With an average value of about 1065 mm, the computed potential evapotranspiration for the basin changed from 962 mm in 1982/1983 to 1110 mm in 2007/2008 (Online Resource 1.2). The obtained results indicate that the semi-arid climate, as represented by the specific case study, is getting warmer and drier due to CC. The annual P decreased and the yearly average air temperature increased (Table 3). The findings regarding LZRB are largely in agreement with previous studies (Al-Ansari, 2013, Al-Ansari et al., 2014; Fadhil, 2011; Robaa and AL-Barazanji, 2013).

3.2. Reconnaissance drought index as a climate index

Examples for the use of RDI as a climate index are presented in this sub-section. To highlight this function of the RDI index, Fig. 2 shows the alpha values for five geographical regions concerning various climatic conditions representing MD, TR, CN, Sahara and humid climate, respectively. The most important point is that the $RDI_{\alpha 12}$ values are considerably higher for the humid areas regarding the whole time series and associated with higher variability in comparison with other climatic conditions. Moreover, a more comprehensive exposure of CC could be performed through assessing shorter reference periods compared to the annual time period.

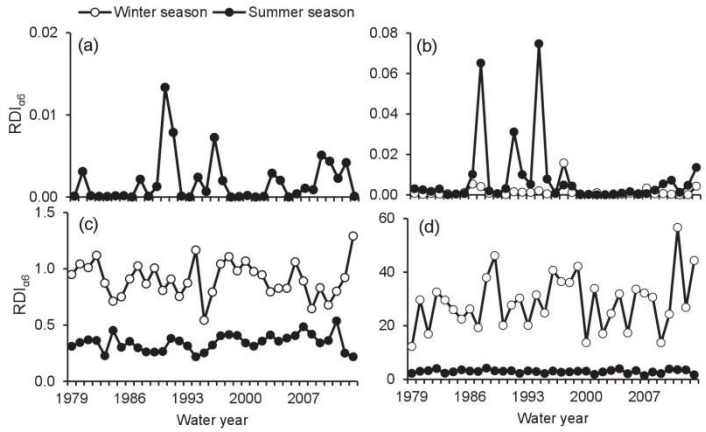

Fig. 5. The normalised reconnaissance drought index (RDI) concerning a time series of 35 water years for: (a) an annual reference time period; (b) the winter season (October to March) and (c) the summer season (April to September).

Figs. 3 and 4 present a thirty-five-year time series of $RDI_{\alpha 12}$ for winter and summer seasons at different locations for various climatic conditions. Generally speaking, due to a steep reduction in P during summer time, the alpha values are much lower than the corresponding winter values for nearly all the considered locations and climatic conditions. The alpha form of RDI incorporates both cumulative P and potential evapotranspiration. Therefore, it has been used in the above example as a climate alteration detection index.

The RDI_n might be applied additionally for the identification of substantial trends, therefore, displaying signals of climatic variability. Fig. 5 presents the annual and the 6-month periods (October to March; April to September) for the RDI_n values concerning different geographical regions and various climatic conditions.

3.3. Drought and aridity trends, and future scenarios

For the purpose of trend identification in $RDI_{\alpha 12}$ and RDI_{st} time series, linear regression tests have been applied. The trend analysis outcomes were used to shape drought and aridity scenarios (optimistic scenario) referring to the next three decades, assuming that these trends will continue without change (Tables 4 and 5). Based on the data analysis, drought trends will remain approximately the same for arid regions and decrease in humid regions such as Norway and the UK, while, semi-arid areas will change from normal to extremely dry conditions.

The $RDI_{\alpha 12}$ values coincided with the aridity index that is applied for climate classification. In general, the decreasing trend of P and increasing trend of PET resulted in a negative aridity trend and vice versa. In most studied cases, the regional aridity trends showed the same trends as for P, indicating that the aridity trends could mainly be determined by the P trends and to a lesser extent by PET trends (Online Resources 1.3 and 1.4). The humid areas showed an increasing trend in annual $RDI_{\alpha 12}$ index, which means that these regions became wetter, while some of the semi-arid locations showed decreasing trends in $RDI_{\alpha 12}$. At some stations, the increasing trends in PET were accompanied with increasing

Table 4
Trend analysis representing climate change impacts on drought index calcification for different climate conditions in addition to the Lower Zab River basin (LZRB) as a specific semi-arid case study.

Wider Region	Station ID	Time			Change/decadal
		Past	Present	Future	
Mediterranean					
South Africa	Low land	−0.71[5]	0.662[4]	1.838[2]	0.392
	High land	−0.433[5]	0.411[4]	1.134[3]	0.241
North Iraq	Low land	1.13[3]	−1.08[6]	−2.02[8]	−0.063
	High land	0.73[4]	−0.71[5]	−1.94[7]	−0.41
West Australia	Low land	−0.78[5]	0.736[4]	2.04[1]	0.433
	High land	0.111[3]	−0.11[5]	−0.296[5]	−0.062
South USA	Low land	0.024[4]	0.07[4]	0.031[4]	−0.013
	High land	−0.13[5]	0.119[4]	0.332[4]	0.071
Tropical					
East China	Low land	1.390[3]	−1.310[6]	−3.620[8]	−0.770
	High land	0.960[4]	−0.895[5]	−2.490[8]	−0.530
East Brazil	Low land	0.970[4]	−0.920[5]	−2.540[8]	−0.540
	High land	0.360[4]	−0.340[5]	−0.940[5]	−0.200
Continental					
South East Spain	Low land	−0.311[5]	0.295[4]	0.814[4]	0.173
	High land	−0.224[5]	0.214[4]	0.589[4]	0.125
South Russia	Low land	−0.079[5]	0.075[4]	0.207[4]	0.044
	High land	0.743[4]	−0.71[5]	−1.949[7]	−0.413
Arid					
Sahara	Low land	−0.423[5]	0.179[4]	0.695[4]	0.172
	High land	−0.423[5]	0.179[4]	0.695[4]	0.172
Al-Sudan	Low land	−0.423[5]	0.179[4]	0.695[4]	0.172
	High land	−0.423[5]	0.179[4]	0.695[4]	0.172
Humid					
UK	Low land	−0.985[5]	0.929[4]	2.570[1]	0.547
	High land	−0.937[5]	0.883[4]	2.443[1]	0.520
Norway	Low land	0.319[4]	−0.304[5]	−0.838[5]	−0.178
	High land	0.292[4]	−0.276[5]	−0.762[5]	−0.162
Semi-arid					
LZRB case study (upstream)	Sulymanya	0.66[4]	−0.64[5]	−1.75[7]	−0.37
	Halabcha	1.26[3]	−1.19[6]	−2.24[8]	−0.07
	Sachez	0.73[4]	−0.71[5]	−1.94[7]	−0.41
	Mahabad	1.21[3]	−1.13[6]	−3.15[8]	−0.67
	Salahddin	0.23[4]	−0.22[5]	−0.42[5]	−0.013
	Soran	1.00[3]	0.80[4]	0.63[5]	−0.056
LZRB case study (downstream)	Kirkuk	1.14[3]	−1.07[6]	−2.01[8]	−0.063
	Makhmoor	1.13[3]	−1.08[6]	−2.02[8]	−0.063
	Erbeel	0.83[4]	−0.78[5]	−1.47[6]	−0.046
	Chem-Chamal	0.86[4]	−0.82[5]	−2.26[8]	−0.480

[1]Extremely wet.
[2]Very wet.
[3]Moderately wet.
[4]Normal.
[5]Near normal.
[6]Moderately dry.
[7]Severely dry; and
[8]Extremely dry.

Table 5
Trend analysis representing climate change impacts on the aridity calcification for different climate conditions in addition to the Lower Zab River basin (LZRB) as a specific semi-arid climatic case study.

Wider Region	Station ID	Time			Change/decade
		Past	Present	Future	
Mediterranean					
South Africa	Low land	0.136[2]	0.199[2]	0.253[3]	0.018
	High land	0.074[2]	0.110[2]	0.137[3]	0.009
North Iraq	Low land	0.580[4]	0.200[3]	0.030[1]	−0.010
	High land	0.380[3]	0.240[3]	0.120[3]	−0.040
West Australia	Low land	0.113[2]	0.229[3]	0.328[3]	0.03
	High land	0.210[3]	0.203[3]	0.197[2]	−0.002
South USA	Low land	0.385[3]	0.354[3]	0.327[3]	−0.009
	High land	0.305[3]	0.326[3]	0.344[3]	0.006
Tropical					
East China	Low land	0.531[4]	0.958[5]	1.324[5]	0.122
	High land	2.428[5]	1.406[5]	0.530[4]	−0.292
East Brazil	Low land	0.781[5]	0.491[3]	0.242[3]	−0.083
	High land	0.612[4]	0.521[4]	0.442[4]	−0.026
Continental					
South East Spain	Low land	0.212[3]	0.272[3]	0.323[3]	0.017
	High land	0.570[3]	0.675[5]	0.765[5]	0.030
South Russia	Low land	1.206[5]	1.241[5]	1.271[5]	0.011
	High land	4.933[5]	1.815[5]	−0.858[1]	−0.891
Arid					
Sahara	Low land	0.0034[1]	0.004[1]	0.005[1]	0.000
	High land	0.0042[1]	0.004[2]	0.004[1]	0.000
Al-Sudan	Low land	0.011[1]	0.004[1]	−0.002[1]	−0.002
	High land	0.022[1]	0.012[1]	0.003[1]	−0.003
Humid					
UK	Low land	2.202[5]	3.749[5]	5.075[5]	0.442
	High land	2.230[5]	3.700[5]	4.960[5]	0.420
Norway	Low land	6.263[5]	5.528[5]	4.898[5]	−0.210
	High land	3.660[5]	3.350[5]	3.083[5]	−0.089
Semi-arid climate					
LZRB case study (upstream)	Sulymanya	1.130[5]	0.750[5]	0.420[3]	−0.110
	Halabcha	0.860[5]	0.340[3]	0.110[3]	−0.150
	Sachez	0.380[3]	0.240[3]	0.120[3]	−0.040
	Mahabad	0.620[4]	0.240[3]	0.570[4]	−0.110
	Salahddin	0.300[3]	0.350[3]	0.380[3]	0.000
	Soran	0.800[5]	0.790[5]	0.430[3]	−0.120
LZRB case study (downstream)	Kirkuk	0.230[3]	0.080[2]	0.020[1]	0.000
	Makhmoor	0.580[4]	0.200[3]	0.030[1]	−0.010
	Erbeel	0.320[3]	0.150[3]	0.070[2]	−0.010
	Chem-Chamal	0.480[3]	0.270[3]	0.090[2]	−0.060

[1]Hyperarid.
[2]Arid.
[3]Semi-arid.
[4]Dry sub-humid; and
[5]Humid.

trends in P, which requires further research to determine the parameters that contributed to such change. A trend analysis of the most sensitive parameters of PET may highlight some of the causes of increasing and decreasing trends in PET.

Through shedding light on semi-arid regions, in particular those that are more vulnerable to the impact of CC, a case study has been selected. Tables 4 and 5 show that the Dokan, which is the upstream sub-basin, has been classified as moderately wet-normal, while it is categorised as nearly normal-moderately dry at the present time. However, it is expected to become severely-extremely dry over the next thirty years. The downstream sub-basin has altered from moderately wet to normal over the past three decades to near normal-moderately dry at present, and it is expected to convert to moderately-extremely dry during the next thirty years. Taking into consideration the past, present and future aridity variations over the LZRB, it can be noticed that the upstream sub-basin is expected to become semi-arid over the next few decades as a result of human-induced links to CC (Table 5). However, the downstream sub-basin is most likely to change from semi-arid to hyper-arid.

4. Conclusions and recommendations

The RDI has been suggested in this study as a climatic index to find changes in the drought and aridity of a geographical area by applying linear regression analysis. The main advantage of the considered method is that the RDI integrates in a single index both P and PET. In addition, the study shows different durations of the RDI (6 and 12 months) for potential periodic climatic variability. Applying the alpha or the normalised form of RDI, more consistent climate variable trends can be identified compared to using time series of potential evapotranspiration and P separately.

The results for RDI_{st} and $RDI_{\alpha 12}$ showed that currently semi-arid areas would probably become hyper-arid due to CC. However, the classification of drought and aridity are presented in this way to appropriately illustrate the potential CC impacts and the magnitude of the consequences in the considered geographical regions.

There are regular descending trends in the RDI time series over the last three decades. The long-term time series of this index exposed extra regular trends compared to short-term ones. The declining RDI trend shows more drought severity occurrences over

most of the studied regions. In contrast to SPI, which utilises P time series only, RDI takes into account the proportion of P to potential evapotranspiration. Consequently, additional severities would be expected that are more linked to difficult scenarios and influences comprising upward trends in PET and its associated parameters in comparison to decreasing trends in either P or P/PET. Further to the drought frequency increase, raising of drought extent and duration can be measured. Furthermore, drought episode severity, special distribution, interval and many other factors should be considered in the analysis.

The trend of regional aridity does most likely not change for all considered geographical regions. This might be because aridity is considered as a long-term climatic phenomenon, whereas drought is a normal time-based risk, taking into consideration both aridity and water availability inequality. Furthermore, it should be noted that the calculated trend is based on past climatic conditions as well as drought and aridity categorisations for each area. It can be concluded that both $RDI_{\alpha 12}$ and RDI_{st} are changed as a result of climate variations.

There are insufficient indications for defining downward P trends in the studied regions. The outcomes have highlighted that there are declining or raising trends in annual P, but most of them are not significant. The $RDI_{\alpha k}$ trend results in arid and semi-arid areas are comparable to those for P. Furthermore, an examination of meteorological drought trends in Iraq revealed that droughts have increased over the studied basin.

Generally speaking, the study analysis is indicative and does result in absolute figures. More studies that focus on trends in P, PET, P/PET or aridity as well as drought indices (especially RDI) would increase the general knowledge concerning these events. A range of possible future conditions could be explained better. Therefore, it is highly recommended that this research should be undertaken again for other geographical and climatic zones of interest taking more meteorological stations into account.

This research showed that both P and PET can have a significant impact on whether an area becomes wetter or drier. As responses occur between P and PET, it is not a straightforward matter to determine whether and to what extent the former positive or negative trend will influence the latter and vice versa. Hence, it was beneficial in this study to determine the combined impact of using an aridity index.

Acknowledgement

The study has been financed by the Iraqi Government and Babylon University via a PhD scholarship for the lead author.

Appendix A. Supplementary data

Supplementary data related to this article can be found at http://dx.doi.org/10.1016/j.jaridenv.2017.03.014.

References

Al-Ansari, N.A., 2013. Management of water resources in Iraq: perspectives and prognoses. Eng 5, 667–684. http://dx.doi.org/10.4236/eng.2013.58080.

Al-Ansari, N.A., Ali, A.A., Knutsson, S., 2014. Present conditions and future challenges of water resources problems in Iraq. J. Water Resour. Prot. 6 (12), 1066–1098. http://dx.doi.org/10.4236/jwarp.2014.612102.

Allen, R.G., Pereira, L.S., Raes, D., Smith, M., 1998. Crop Evapotranspiration: Guidelines for Computing Crop Water Requirements, first ed. Food and Agriculture Organization (FAO) Irrigation and Drainage Paper 56, Rome, Italy.

Asadi, A., Vahdat, S.F., 2013. The efficiency of meteorological drought indices for drought monitoring and evaluating in Kohgilouye and Boyerahmad Province, Iran. Int. J. Mod. Eng. Res. 3 (4), 2407–2411.

Asadi Zarch, M.A., Malekinezhad, H., Mobin, M.H., Dastorani, M.T., Kousari, M.R., 2011. Drought monitoring by reconnaissance Drought Index (RDI) in Iran. Water Resour. Manage 25 (13), 3485–3504.

Asadi Zarch, M.A., Sivakumar, B., Sharma, A., 2015. Droughts in a warming climate: a global assessment of Standardized precipitation index (SPI) and Reconnaissance drought index (RDI). J. Hydrol. 526, 183–195.

Blenkinsop, S., Fowler, H.S., 2007. Change in droughts frequency, severity and duration of the British Isles projected by PROUDNES regional climate models. J. Hydrol. 342, 50–71.

Cai, W., Zhang, Y., Chen, Q., Yao, Y., 2015. Spatial patterns and temporal variability of drought in Beijing-Tianjin-Hebei metropolitan areas in China. Adv. Meteorol. 2015. ID 28947, 14 pages.

Cook, B.I., Smerdon, J.E., Seager, R., Coats, S., 2014. Global warming and 21st century drying. Clim. Dyn. 43 (9–10), 2607–2627. http://dx.doi.org/10.1007/s00382-014-2075-y.

Dile, Y.T., Srinivasan, R., 2014. Evaluation of CFSR climate data for hydrologic prediction in data-scarce watersheds: an application in the Blue Nile River Basin. J. Am. Water Resour. Assoc. (JAWAR) 50 (5), 1226–1241. http://dx.doi.org/10.1111/jawr.12182.

Fadhil, M.A., 2011. Drought mapping using Geoinformation technology for some sites in the Iraqi Kurdistan region. Int. J. Digit. Earth 4 (3), 239–257. http://dx.doi.org/10.1080/17538947.2010.489971.

FAO, 2012. Food and Agriculture Organization of the UN. Adaptation to Climate Change in Semi-arid Environments. Experience and Lessons from Mozambique. In: Environment and Natural Resources Management Series. Rome. pp. 1–83. Retrieved from. http://www.fao.org/docrep/015/i2581e/i2581e00.pdf.

Fuka, D.R., Walter, M.T., MacAlister, C., Degaetano, A.T., Steenhuis, T.S., Easton, Z.M., 2014. Using the climate forecasting system reanalysis as weather input data for watershed models. Hydrol. Process 28 (22), 5613–5623. http://dx.doi.org/10.1002/hyp.10073.

Giannikopoulou, A.S., Kampragkou, E., Gad, F.K., Kartalidis, A., Assimacopoulos, D., 2014. Drought characterisation in cyclades complex, Greece. Eur. Water 47, 31–43.

Heim Jr., R.R., 2002. A Rev. twenty-century drought indices used United State. Bull. Am. Meteorol. Soc. 83 (8), 1149–1165. http://dx.doi.org/10.1175/1520-0477(2002)083<1149:AROTDI>2.3.CO;2.

Hoerling, M.P., Eischeid, J.K., Quan, X.W., Diaz, H.F., Webb, R.S., Dole, R.M., Esterling, D.R., 2012. Is a transition to semi-permanent drought conditions imminent in the U.S. Great Plains? J. Clim. 25 (24), 8380–8386. http://dx.doi.org/10.1175/JCLI-D-12-00449.1.

IPCC, 2001. Intergovernmental Panel on Climate Change. Climate Change 2001: Synthesis Report. Retrieved 12 December, 2013, from. http://www.ipcc.ch/pdf/climate-changes-2001/synthesis-syr/english/front.pdf.

IPCC, 2007. Intergovernmental Panel on climate change. In: Parry, M.L., Canziani, O.F., Palutikof, J.P., van der Linden, P.J., Hanson, C.E. (Eds.), Climate Change 2007: Impacts, Adaptation and Vulnerability. Contribution of Working Group II to the Fourth Assessment Report of the Intergovernmental Panel on Climate Change. Cambridge University Press, Cambridge, pp. 1–976.

IPCC, 2014. Intergovernmental Panel on Climate Change. Climate Change 2014: Impacts, Adaptation, and Vulnerability. Retrieved 05 May, 2014, from at. http://www.ipcc.ch/report/ar5/wg2.

Logan, K.E., Brunsell, N.A., Jones, A.R., Feddema, J.J., 2010. Assessing spatiotemporal variability of drought in the U.S. central plains. J. Arid. Environ. 74 (2), 247–255.

Loukas, A., Vasiliades, L., Tzabiras, J., 2008. Climate change effects on drought severity. Adv. Geosci. 17, 23–29.

Michel, D., Pandya, A. (Eds.), 2009. Troubled Waters—climate Change, Hydropolitics, and Transboundary Resources. The Henry L. Stimson Center, Washington, DC, USA.

Mohammed, R., Scholz, M., 2016. Impact of climate variability and streamflow alteration on groundwater contribution to the baseflow of the Lower Zab River (Iran and Iraq). Environ. Earth. Sci. 75 (21), 1392. http://dx.doi.org/10.1007/s12665-016-6205-1.

Mohammed, R., Scholz, M., 2017. Impact of evapotranspiration formulations at various elevations on the reconnaissance drought index. Water Resour. Manage 31 (1), 531–548. http://dx.doi.org/10.1007/s11269-016-1546-9.

Mohammed, R., Scholz, M., Nanekely, M.A., Mokhtari, Y., 2017a. Assessment of models predicting anthropogenic interventions and climate variability on surface runoff of the Lower Zab River. Stoch. Env. Res. Risk. A 1–18. http://dx.doi.org/10.1007/s00477-016-1375-7 (in press).

Mohammed, R., Scholz, M., Zounemat-Kermani, M., 2017b. Temporal hydrologic alterations coupled with climate variability and drought for transboundary river basins. Water Resour. Manage 1–4. http://dx.doi.org/10.1007/s11269-017-1590-0.

NOAA, 2009. National Oceanic and Atmospheric Administration Climate of Iraq. https://www.ncdc.noaa.gov/oa/climate/afghan/iraq-narrative.html (accessed 04.11.15).

Robaa, S.M., AL-Barazanji, Z.J., 2013. Trends of annual mean surface air temperature over Iraq. Nat. Sci. 11 (12), 138–145.

Rossi, G., Cancelliere, A., 2013. Managing drought risk in water supply systems in Europe: a review. Int. J. Water Resour. D. 29 (2), 272–289.

Saha, S., Moorthi, S., Wu, X., Wang, J., Nadiga, S., Tripp, P., Behringer, D., Hou, Y.T., Chuang, H., Iredell, M., Ek, M., Meng, J., Yang, R., Mendez, M.P., Doll, H.V.D., Zhang, Q., Wang, W., 2014. The NCEP climate forecast system version 2. J. Clim. 27 (6), 2185–2208. http://dx.doi.org/10.1175/JCLI-D-12-00823.1.

Shahidian, S., Serralheiro, R.P., Serrano, J., Teixeira, J., Haie, N., Santos, F., 2012. Hargreaves and other reduced-set methods for calculating evapotranspiration. In: Irmak, A., In Tech, Rijeka (Eds.), Evapotranspiration – 15 Remote Sensing and Modeling. Croatia, pp. 60–80.

Soundharajan, B.S., Adeloye, A.J., Remesan, R., 2016. Evaluating the variability in surface water reservoir planning characteristics during climate change impacts assessment. J. Hydrol. 538, 629–639. http://dx.doi.org/10.1016/j.jhydrol.2016.04.051.

Thematic Mapping, 2009. http://thematicmapping.org/downloads/world_borders.php/ (accessed 2.10.15).

Tigkas, D., Vangelis, H., Tsakiris, G., 2012. Drought and climatic change impact on streamflow in small watersheds. Sci. Total Environ. 440, 33–41.

Tigkas, D., Vangelis, H., Tsakiris, G., 2015. DrinC: a software for drought analysis based on drought indices. Earth Sci. Inf. 8 (3), 697–709.

Tsakiris, G., Vangelis, H., 2005. Establishing a drought index incorporation evapotranspiration. Eur. Water 9 (10), 3–11.

Tsakiris, G., Pangalou, D., Vangelis, H., 2007a. Regional drought assessment based on the reconnaissance Drought Index (RDI). Water Res. Manage 21 (5), 821–833.

Tsakiris, G., Loukas, A., Pangalou, D., Vangelis, H., Tigkas, D., Rossi, G., Cancelliere, A., 2007b. Drought characterization [Part 1. Components of drought planning. 1. 3. Methodological component]. In: Iglesias, A., Moneo, M., López-Fran cos A (Eds.), Drought Management Guidelines Technical Annex. CIHEAM/ECMEDA Water 2007, Zaragoza, pp. 85–102 (Options Méditerranéennes: Série B. Etudes et Recherches; n. 58).

United Nations Educational, Scientific and Cultural Organization (UNESCO), 1979. Map of the World Distribution of Arid Regions: Map at Scale 1:25,000,000 with Explanatory Note. MAB Technical Notes 7. UNESCO, Paris.

Vangelis, H., Tigkas, D., Tsakiris, G., 2013. The effect of PET method on Reconnaissance Drought Index (RDI) calculation. J. Arid. Environ. 88, 130–140.

Vicente-Serrano, S.M., Lopez-Moreno, J.I., Beguería, S., Lorenzo-Lacruz, J., Sanchez-Lorenzo, A., García-Ruiz, J.M., Azorin-Molina, C., Morán-Tejeda, E., Revuelto, J., Trigo, R., Coelho, F., 2014. Evidence of increasing drought severity caused by temperature rise in southern Europe. Environ. Res. Lett. 9 (4), 044001. http://dx.doi.org/10.1088/1748-9326/9/4/044001.

Vicente-Serrano, S.M., Schrier, G.V.D., Begueria, S., Azorin-Molina, C., Lopez-Moreno, J., 2015. Contribution of precipitation and reference evapotranspiration to drought indices under different climates. J. Hydrol. 526, 42–54.

World Bank, 2009. Water in the Arab World: Management Perspectives and Innovations. Retrieved from. http://siteresources.worldbank.org/INTMENA/Resources/Water_Arab_World_full.pdf.

Zarch, M.A.A., Sivakumar, B., Sharma, A., 2015. Droughts in a warming climate: aglobal assessment of standardized precipitation index (SPI) and reconnaissance drought index (RDI). J. Hydrol. 526, 183–195. http://dx.doi.org/10.1016/j.jhydrol.2014.09.071.

Paper 6

Water Resour Manage
DOI 10.1007/s11269-017-1685-7

Adaptation Strategy to Mitigate the Impact of Climate Change on Water Resources in Arid and Semi-Arid Regions: a Case Study

Ruqayah Mohammed[1] · **Miklas Scholz**[1,2,3]

Received: 23 January 2017 / Accepted: 20 April 2017

Abstract Climate change and drought phenomena impacts have become a growing concern for water resources engineers and policy makers, mainly in arid and semi-arid areas. This study aims to contribute to the development of a decision support tool to prepare water resources managers and planners for climate change adaptation. The Hydrologiska Byråns Vattenbalansavdelning (The Water Balance Department of the Hydrological Bureau) hydrologic model was used to define the boundary conditions for the reservoir capacity yield model comprising daily reservoir inflow from a representative example watershed with the size of 14,924 km^2 into a reservoir with the capacity of 6.80 Gm^3. The reservoir capacity yield model was used to simulate variability in climate change-induced differences in reservoir capacity needs and performance (operational probability of failure, resilience, and vulnerability). Owing to the future precipitation reduction and potential evapotranspiration increase during the worst case scenario (−40% precipitation and +30% potential evapotranspiration), substantial reductions in streamflow of between −56% and −58% are anticipated for the dry and wet seasons, respectively. Furthermore, model simulations recommend that as a result of future climatic conditions, the reservoir operational probability of failure would generally increase due to declined reservoir inflow. The study developed preparedness plans to combat the consequences of climate change and drought.

✉ Miklas Scholz
miklas.scholz@tvrl.lth.se

Ruqayah Mohammed
ruqaya2008@yahoo.com

[1] Civil Engineering Research Group, School of Computing, Science and Engineering, The University of Salford, Newton Building, Peel Park Campus, Salford, Greater Manchester M5 4WT, UK

[2] Division of Water Resources Engineering, Department of Building and Environmental Technology, Faculty of Engineering, Lund University, P.O. Box 118, 221 00 Lund, Sweden

[3] Department of Civil Engineering Science, School of Civil Engineering and the Built Environment, University of Johannesburg, Kingsway Campus, PO Box 524, Aukland Park, Johannesburg 2006, South Africa

Published online: 27 April 2017

Keywords Alteration measure · Precipitation · Reservoir operation and reliability · Sustainable development · Water resources availability · Weather variability

1 Introduction

1.1 Background

It is expected that climate variability will intensify the water resources stress (IPCC, 2014) such as the alteration in the river flow seasonality (Vicuna and Dracup, 2007; Minville et al. 2009) as well as reservoir planning properties (capacity) and performance (reliability, resilience and vulnerability). Such change is likely to lead to a negative effect on water resources management.

A growing number of researchers have explored climate change impacts on reservoirs (Fowler et al. 2003; Li et al. 2010; Park and Kim 2014). The majority of these scientists argued that due to climate change, there will be an increase in the storage capacity requirements in addition to the deterioration of its performance. Only a few researchers have focused on reservoir management adaptation to climate variability (McMahon et al. 2006; Li et al. 2010; Minville et al. 2009) and confirmed that the impact of such change on streamflow should be considered through a re-examination of reservoir operating rules.

The vast majority of researchers have investigated climate change impacts based on the results of large-scale general circulation models (GCM) that have been downscaled to the basin-scale applying statistical or regional (i.e. dynamical) downscaling procedures. However, Chen et al. (2011) claimed that there are many sources of uncertainty involved in climate change studies and the major sources of uncertainty are linked to GCM and greenhouse gasses emissions scenarios (GGES) in addition to the uncertainties that stem from a downscaling method. Therefore, to avoid the GCM and downscaling uncertainties and challenges, many studies (e.g., Tigkas et al. 2012; Vangelis et al. 2013; Reis et al. 2016) proposed delta perturbation (change factor) concepts, in which plausible alterations in meteorological variables are assumed. Then, by using a suitable rainfall-runoff model, the impacts of these changes on the streamflow can be predicted.

1.2 Aim, Objectives and Novelty

The aim of this research is to develop a methodology that can be used as part of a decision support tool to enable engineers and policy makers to prepare effectively for climate change adaptation, particularly in arid and semi-arid regions. The prime objectives are to (1) estimate the anticipated climate change impacts on runoff; (2) calculate the probable relative alteration in the annual streamflow availability of the downstream country under the collective impacts of climate change; (3) predict standardised reconnaissance drought index (RDI_{st}) and streamflow drought index (SDI) values under the collective climate change impacts; (4) derive the anticipated relationships that link RDI_{st} and SDI with the potential future variations of precipitation (P) and potential evapotranspiration (PET); (5) evaluate the reservoir operational probability of failure (OPOF) under the collective climate change impacts; and (6) develop relationships that integrate capacity-yield-reliability.

This research characterises the climate change impact uncertainties linked to the planning of reservoirs utilising a methodology similar to that described by Soundharajan et al. (2016). The

main variations between the two studies are that a rainfall-runoff model is used to simulate the streamflow series rather than stochastic modeling that as used by Soundharajan et al. (2016). In addition, Soundharajan et al. 2016 did not take into consideration the reservoir capacity-yield-reliability relationships, which have been considered here. Consequently, the key purpose of this study is to assess the potential impacts of climate change on basin hydrology by considering the impacts of the reservoir operational probability of failure and storage in the water resources system on a typical example reservoir, which is the Dokan multi-purpose dam located in northern Iraq. The study attempts to answer the following question: How well would the adaptation measures, whether they are structural or non-structural, work across the range of climate change uncertainty? Successful adaptation measures may subsequently be used as supporting tools in mitigating climate change impacts on water resources. This is a first attempt to derive the capacity-yield-reliability relationships that can be used as part of an adaptation strategy for climate change by characterising the variability of reservoir storage and performance indices.

1.3 Case Study Description

The Lower Zab River (also known as Little and Lesser Zab) is one of the main streams of the Tigris River in the Erbil governorate located in the north-east of Iraq. The river and its tributaries are situated between latitudes 36°50′ N and 35°20′ N, and longitudes 43°25′ E and 45°50′ E (Mohammed and Scholz 2016); Fig. 1. The River originates from the Zagros Mountains in Iran and flows about 370 km southeast and southwest through north-western Iran and northern Iraq before joining the Tigris near Fatha city, which is located about 220 km north

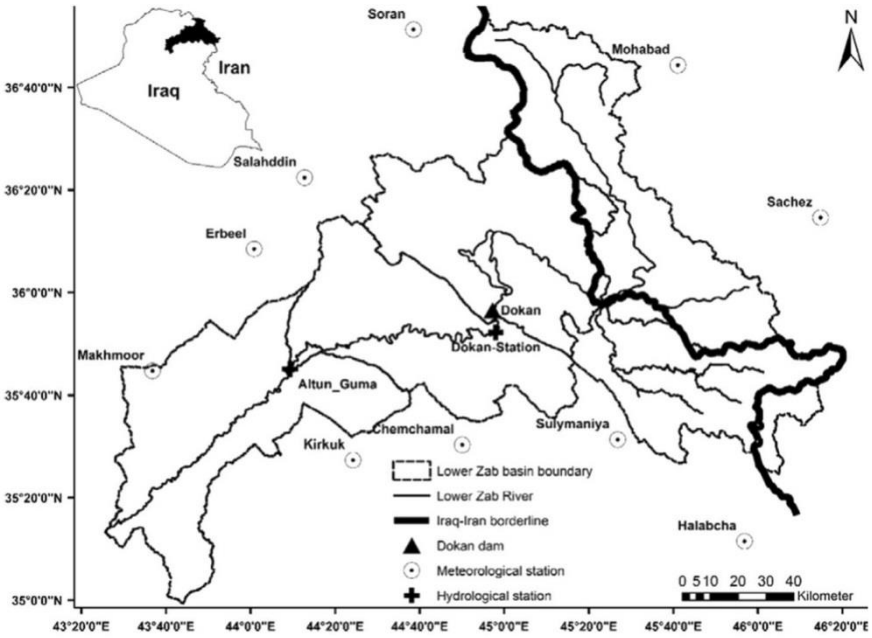

Fig. 1 Location of the studied basin

of Baghdad (Mohammed and Scholz 2016), with a total length of approximately 302 km. The catchment area of the River is approximately 19,254 km^2 with nearly 76% located in Iraq. The mean annual storage of the river at Dokan and Altun Kupri-Goma is about 6 billion cubic meters (BCM) and 7.8 BCM in this order (Mohammed et al. 2017); Fig. 1. Dokan is the main dam that has been constructed within the upstream portion of the basin. The main function of the dam is to control the discharge of the Lower Zab, store water for irrigation purposes and to provide hydroelectric power.

2 Material and Methods

2.1 Identification of Drought

Drought is considered one of the leading water-related hazards (Mohammed and Scholz 2017). For drought identifying and quantifying there are many recommended approaches. However, indices are considered as one of the most popular methods (Vangelis et al. 2013; Mohammed and Scholz 2017). A high number of meteorological drought indices with different intricacy have been utilised in various climatic conditions (Mohammed and Scholz 2017). Latest drought trend studies (Sheffield et al. 2012; Vicente-Serrano et al. 2014) and drought scenarios under possible climate change predictions (e.g., Cook et al. 2014) depend on indices that take into consideration evapotranspiration and precipitation such as the reconnaissance drought index (RDI), which is considered in this study.

2.1.1 Reconnaissance Drought Index

The RDI is a newly developed meteorological drought index, which is mainly applied in arid and semi-arid geographical regions. The RDI is based on P, which is observed, and the PET, which is estimated. Tigkas et al. (2015) introduced a brief overview of the theoretical basis of RDI together with some practical applications with a specialised software package called drought indices calculator (DrinC).

This RDI can be formulated as the alpha ($RDI_{\alpha k}$), normalised (RDI_n) and standardised (RDI_{st}) forms. The RDI_{st} is frequently applied for drought severity evaluations, whereas $RDI_{\alpha k}$ can be applied as an aridity index, which is mainly founded on the aggregated P and PET theories (Vangelis et al. 2013; Mohammed and Scholz 2017). The RDI is normally estimated using Eq. (1).

$$RDI_{\alpha_o^i} = \frac{\sum_{j=1}^{12} P_{ij}}{\sum_{j=1}^{12} PET_{ij}} \quad i = 1 \text{ to } N \text{ and } j = 1 \text{ to } 12 \tag{1}$$

where P_{ij} and PET_{ij} represent precipitation and potential evapotranspiration of the j^{th} month of the i^{th} water year, which in Iraq starts in October, and N is the climate data total year number.

The values of $RDI_{\alpha k}$ match both the gamma and the lognormal distributions in various positions for a variety of examined time scales. Through applying the former distribution, RDI_{st} can be calculated applying Eq. (2).

$$RDI_{st}^i = \frac{Y_i}{\hat{\sigma}_y} \tag{2}$$

where y^i is the $\ln(\alpha_{ki})$, $\bar{y}$ is its arithmetic mean and σ_y is the corresponding standard deviation.

Equation (3) can be applied to compute RDI_{st} in the gamma distribution application.

$$g(x) = \frac{1}{\beta^{\gamma} \times \Gamma(\gamma)} x^{\gamma-1} e^{\frac{x}{\beta}} \text{ for } x > 0 \tag{3}$$

where γ and β are the shape and scale parameters, respectively, and $\Gamma(\gamma)$ is the gamma function. The spatiotemporal extent of the gamma probability distribution parameters γ and β can be predicted for 3, 6, 9 and 12 months. The γ and β are estimated by the maximum likelihood method as shown in Eqs. (4) to (6).

$$\gamma = \frac{1}{4A}\left(1 + \sqrt{1 + \frac{4A}{3}}\right) \tag{4}$$

$$\beta = \frac{\overline{x}}{\gamma} \tag{5}$$

$$A = \ln\left(\overline{x}\right) - \frac{\sum \ln(x)}{N} \tag{6}$$

When the cumulative precipitation data sets for the selected reference period contains zeros, the gamma function cannot be defined for $x = 0$. Therefore, a composite cumulative probability function (Eq. (7)) might be utilised.

$$H(x) = q + (1-q) \times G(x) \tag{7}$$

where q is the likelihood of zero precipitation and G(x) is the gamma distribution cumulative probability. The probability of zero precipitation (q) can be computed by m/N if m is zero in the α_k time series. The gamma distribution cumulative probability G(x) is replaced by the cumulative probability H(x).

A positive value of RDI_{st} relates to a wet period. On the other hand, a negative value is indicative of a dry period in comparison to the natural conditions of the region. Drought severity phenomena increase when RDI_{st} values are minimal. The severity of drought can be classified into (extremely, severely, moderately) dry, near normal, normal, (moderately, very and extremely) wet classes based on the corresponding boundary RDI_{st} value ranges ≤ -2.00, -1.5 to -1.99, -1 to -1.49, 0.00 to -0.99, 0.99 to 0.00, 1.49 to 1.00, 1.99 to 1.5, and ≥ 2.00, respectively (Tigkas et al. 2012; Vangelis et al. 2013; Mohammed and Scholz 2017).

2.1.2 Hydrological Drought Index

Given a monthly time series streamflow storage V_{ij} for a specific water year, the corresponding cumulative value can be obtained according to Eq. (8), which was developed by Nalbantis (2008).

$$S_{i,k} = \sum_{j=1}^{3k} V_{i,j} \text{ for } i = 1, 2, \ldots.., n; j = 1, 2, \ldots.., 12; k = 1, 2, 3, 4 \tag{8}$$

where S_{ij} is the aggregate streamflow storage for the i^{th} water year and the k^{th} reference period, k = 1 for the period October–December, k = 2 for October–March, k = 3 for October–June, and k = 4 for October–September.

The SDI founded on the discharge aggregated capacities $S_{i,k}$ for each period k of the i^{th} water year can be defined according to Eq. (9).

$$SDI_{i,k} = \frac{S_{i,k} - \overline{M}_k}{SD_k} \quad \text{for } i = 1, 2, \ldots\ldots, n; \text{ and } k = 1, 2, 3, 4 \tag{9}$$

where $\bar{M}_k$ and SD_k are the cumulative streamflow storage means and the standard deviation of the period k, respectively, since they are calculated over a long time. Although many values founded on logical criteria could be used, the truncation level is set to $\bar{M}_k$ in this definition.

For most small basins, the streamflow follows a skewed probability distribution. This can be estimated by gamma distribution functions. The distribution is then converted into normal. Appling the two-parameter lognormal distribution, the SDI index is defined as shown in Eq. (10).

$$SDI_{i,k} = \frac{Y_{i,k} - \overline{Y}_{i,k}}{S_{y,k}} \quad \text{for } i = 1, 2, \ldots.; \text{ and } k = 1, 2, 3, 4 \tag{10}$$

where the natural logarithms of cumulative streamflow with mean $\bar{y_k}$ and standard deviation S_{ik} can be estimated according to Eq. (11).

$$y_{i,k} = \ln\left(S_{i,k}\right) \text{ for } i = 1, 2, \ldots.., \text{and } k = 1, 2, 3, 4 \tag{11}$$

A value of SDI greater than zero relates to a non-drought period. In comparison, a negative value is indicative of a drought period in comparison to the natural conditions of the study region. The hydrological drought severity phenomena increase when SDI values are minimal, and it follows that the same classification for drought severity can be used as the one for the RDI index. Usually, an integer number from 0 (non-drought) to 4 (extreme drought) is considered.

2.1.3 Reservoir Capacity-Yield Simulation and Performance Indices

As a first step for reservoir capacity-yield (RCY) performance evaluation, the Hydrologiska Byråns Vattenbalansavdelning (HBV) rainfall-runoff models were calibrated depending on the recorded dataset of the baseline period. The HBV is an example of a semi-distributed conceptual model simulating daily discharge depending on daily rainfall, temperature, and potential evaporation as input. Air temperature data are used for calculating snow accumulation. Subsequently, the RCY simulation was performed applying Eq. (12) (McMahon and Adeloye 2005)

$$\begin{aligned} &S_{t+1} = S_t + Q_t - D_t - \Delta E_t - L_t \\ &(\text{Subject to } 0 \le S_{t+1} \le C) \end{aligned} \tag{12}$$

where S_{t+1} and S_t are reservoir storage volumes at the end and beginning of a time period t, respectively; Q_t is the inflow over period t; D_t is the actual water yield over the period t; ΔE_t is the reservoir net evaporation loss within the period t; L_t represents other losses; and C is the reservoir active capacity.

During the simulation procedures, the reservoir S_o is typically assumed to be full (McMahon and Adeloye 2005), and the downstream demand is usually considered as a specific fraction of

the mean inflow. The usual period is one month, but any other period can be used. The calculation of the reservoir OPOF can be summarised as follows: (a) assume the reservoir is initially full ($S_o = C$); (b) apply Eq. (12) month by month on the historical flows; (c) plot (S_{t+1}) against time on a monthly time scale; and (d) compute the OPOF by using Eq. (14).

The storage size estimated through RCY analysis varies little with the starting month. By the RCY analysis, the vulnerability of the reservoir is estimated by ignoring the constraint on Eq. (12) and then choosing the maximum negative value of (S_{t+1}) during the analysis period, whereas the resilience is estimated by computing the maximum consecutive number of empty months during the analysis (Moy et al. 1986).

Following simulation, three appropriate performance measures were assessed (McMahon and Adeloye 2005; McMahon et al. 2006): (1) The time-based reliability (R_e) can be defined as the percentage of the entire period under investigation during which a reservoir is capable of providing the full demand without any deficiencies, as indicated in Eq. (13).

$$R_e = 1 - \mathrm{OPOF} \tag{13}$$

where R_e is the reservoir reliability (%) and OPOF is the operational probability of failure (%), which is defined as the ratio of time units during which the reservoir is effectively empty to the total number of time units applied in the analysis (Eq. (14)).

$$\mathrm{OPOF} = \frac{N_e}{N} \tag{14}$$

where N_e is the time unit number during which the reservoir is empty, and N is the total number of time units in the streamflow time series. There is no limitation on the OPOF but many studies considered 5% to be an acceptable limitation (McMahon and Adeloye 2005).

(2) The resilience ρ describes the reservoir's ability to recover from failure and can be expressed based on Eq. (14) as discussed previously (Fowler et al. 2003; Park and Kim 2014). Moy et al. (1986) defined it as the maximum number of consecutive periods of shortage that occur prior to recovery.

$$\rho = \sum_{t=1}^{N} Y_t \tag{15}$$

where Y_t is the number representing the continuous shortage indicator, $Y_t = 1$, if there is a shortage during period t, $Y_t = 0$, and $t = 1, 2, \ldots, N$, which is the total number of time units in the stream flow time series sequence of failure periods.

(3) The vulnerability ν is a criterion to determine the significance of failure. Mathematically, it is expressed by Eq. (16) as shown in the past (Fowler et al. 2003; Park and Kim 2014).

$$v = \max(Df_t) \tag{16}$$

where v is the system vulnerability, and Df_t is the deficit at time t (McMahon and Adeloye 2005; McMahon et al. 2006).

2.1.4 Data Availability and Methodology Application

Figure 2 reveals the considered methodology and visualises how the research objectives can be integrated, which can be summarised in the following seven steps:

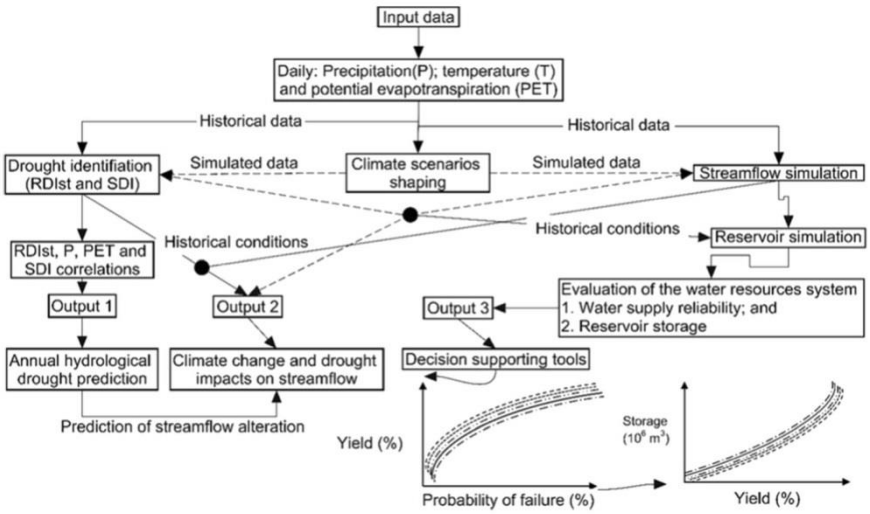

Fig. 2 Research methodology flow chart

(1) Thirty-five hydrological years (1979–2013) were utilised to estimate the RDI_{st} values, specify the normal climatic conditions and then evaluate the regression coefficients a_1, b_1, a_2, and b_2 of Eqs. (17) and (18).

$$RDI_{st} = a_1 \times \ln(RDI_{\alpha 12}) + b_1 \tag{17}$$

$$SDI = a_2 \times \ln(\text{runoff}) + b_2 \tag{18}$$

where RDI_{st}, $RDI_{\alpha 12}$, and SDI are the RDI standardised form, the RDI alpha representation, and the streamflow drought index, respectively.

(2) Using daily P, T, and PET, the HBV model was calibrated and validated for the normal water years.

(3) For assessing the model performance, the following criteria have been used (Eqs. (19) to (22)):

$$RMSE = \sqrt{\frac{1}{n}\sum_{i=1}^{n}\left[(R_{obs})_i - (R_{sim})_i\right]^2} \tag{19}$$

$$IoA = 1 - \frac{\sum_{i=1}^{n}\left[(R_{obs})_i - (R_{sim})_i\right]^2}{\sum_{i=1}^{n}\left[\left|(R_{obs})_i - \overline{R}_{obs}\right| + \left|(R_{sim})_i - \overline{R}_{obs}\right|\right]^2} \tag{20}$$

$$r = \sqrt{\frac{\sum_{i=1}^{n}\left[(R_{obs})_i - \overline{R}_{obs}\right]\left[(R_{obs})_i - \overline{R}_{sim}\right]}{\left\{\sum_{i=1}^{n}\left[(R_{obs})_i - \overline{R}_{obs}\right]\right\}^{0.5}\left\{\sum_{i=1}^{n}\left[(R_{sim})_i - \overline{R}_{sim}\right]\right\}^{0.5}}} \tag{21}$$

$$\mathrm{MAE} = \frac{1}{n}\sum_{i=1}^{n}\left|(R_{obs})_i - (R_{sim})_i\right| \quad (22)$$

where RMSE is the root mean square error (dimensionless), IoA is the index of agreement (dimensionless), r is the correlation coefficient (dimensionless), MAE is the mean absolute error, $R_{obs(i)}$ is the recorded streamflow (mm/month) at time step i, $R_{sim(i)}$ is the predicted streamflow (mm/month) at time step i, $\bar{R}_{obs}$ is the average amount of the recorded values (mm/month), and n is the data point number.

(4) The delta perturbations in P (dP) of 0–40% (2% step) and PET perturbations (dPET) of 0–30% (2% step) were used for the streamflow alteration analysis. Twelve years (1988–2000), which are characterised by an average value of RDI_{st} close to zero, were applied for running the climate change scenarios. Although the delta perturbations method does not accommodate future alterations in the probability distribution of climatic characteristics and seasonality (and therefore the streamflow), it is, however, an effective technique in detecting tipping points at which a water storage structure such as a reservoir is expected to fail disastrously in providing water demand.
(5) The expected relative alteration in the annual streamflow (%) depends on each climate change scenario, which was estimated relative to the reference average annual streamflow.
(6) The predicted streamflow series input to the RCY model. The corresponding outputs of the model are evaluated using the indicators of reliability, resilience, and vulnerability, with reference to the imposed demands.
(7) The RCY model has been utilised to develop the capacity-yield-reliability relationship for the selected time period (the 2020s). The first relation linked yield (%) with OPOF (%), and the second linked capacity($10^6 \times m^3$) with yield(%). These relations can be applied to test various adaptation strategies, whether they are structural or non-structural, against the range of different future scenarios to select the most effective adaptation measures.

3 Results and Discussion

3.1 Rainfall–Runoff Simulation

In this section, the obtained results will be identified and discussed. Descriptions of the hydrological simulation results, drought and climate change impacts, and basin water supply future performances will be provided.

The HBV model has been calibrated and validated for the periods of 1988–1999 and 1979–1986, respectively. The statistical performance indicators RMSE, IoA, r and MAE during calibration were 0.73, 0.99, 0.93 and 0.65 in this order. The corresponding values were 0.68, 0.99, 0.84 and 0.60 during the validation period. Simulation results show promising outcomes emphasising that the simulation can be confidentially applied for more studies such as simulating the artificial climatic scenarios and estimating the relative alteration (%) in the average annual streamflow relative to the normal climatic conditions. The simulated runoff for the studied period against the observed one is visualised in Fig. 3a. The coefficients associated with Eqs. (17) and (18) are shown in Fig. 3b and c in that order.

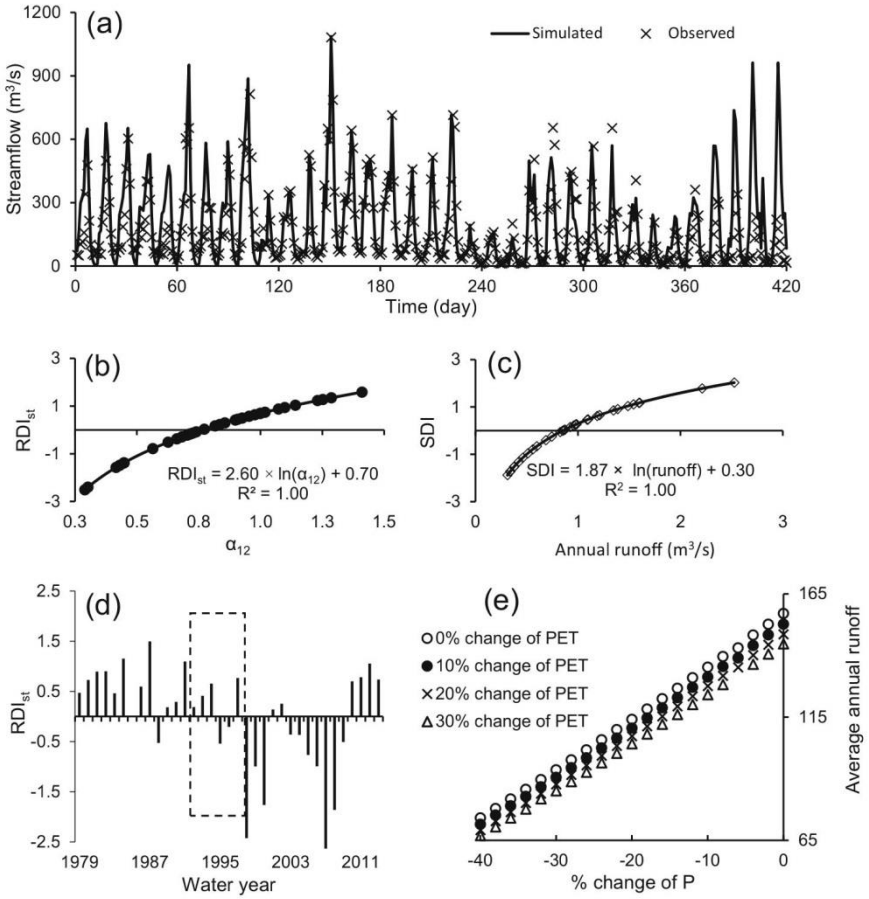

Fig. 3 **a** Observed against simulated streamflow time series using the Hydrologiska Byråns Vattenbalansavdelning model (Note that there was an outlier (1570 m^3/s), which has been removed.); **b** The Lower Zab River Basin (LZRB) anticipated relationship of the standardised reconnaissance drought index (RDI_{st}) and RDI alpha form; **c** The LZRB anticipated relationship of streamflow drought index (SDI) and runoff; **d** The selected simulation period for climate change scenarios; and **e** The LZRB anticipated (%) streamflow change for selected climate change scenarios

3.2 Drought and Climate Change Impacts

Figure 3d shows the period of time that has been selected for the simulation. Based on the simulation results, Fig. 3e reveals that there will be a substantial reduction in the streamflow due to the potential impacts of climate change, which in turn would result in a dramatic alteration on the LZRB water resources availability. For example, a change of almost −21% in terms of streamflow is expected to result in an anticipated climate condition of −10% P and +30% PET. The research outcomes indicated that there is a crucial requirement for pro-active strategies and actions to mitigate climate change influences, anthropogenic interventions, and drought events. Furthermore, Fig. 4a and b demonstrate that the anticipated RDI_{st} and SDI relationships are subject to the potential impact of future P reduction under the collective

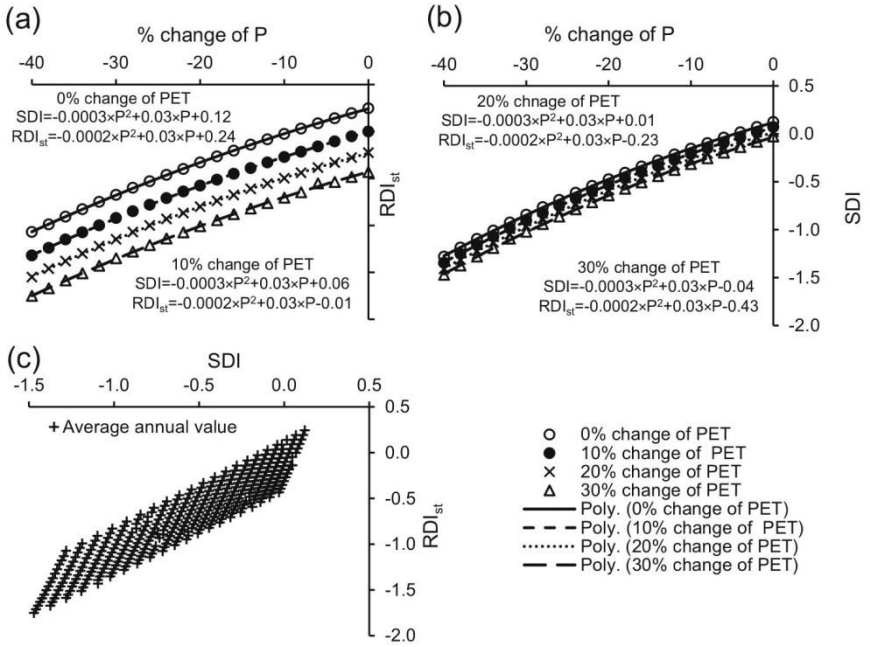

Fig. 4 Anticipated: **a** Standardised reconnaissance drought index (RDI_{st}); **b** streamflow drought index (SDI); and **c** Relationship between RDI_{st} and SDI, for the upper Lower Zab River Basin (LZRB) for each climate change scenarios

effects of PET. Fig. 4c demonstrates that both RDI_{st} and SDI changes depend on drought severity in the same way.

3.3 Future Performance of Water Supply

Figure 5 shows the reservoir inflow magnitude and timing, which prove how climate change will strongly lead to the reduction in the reservoir inflow. In the worst case scenario, substantial variations in inflow between −56% and −58% are anticipated for the dry and wet seasons, respectively. The inflow peak will decline, and there will be a marked shift in their magnitude, which can result in a dramatic effect on basin water resources availability.

One of the research objectives is an evaluation of water supply performance sensitivity on water scarcity brought about by climate change. For all considered scenarios, the future demand for water is assumed to continue without major change with respect to the baseline period. The climate change influence on the Dokan dam operation and its water system were assessed by entering modeled future inflows into the RCY model while maintaining the existing operating procedures. In order to simulate the operations of the Dokan reservoir, the HBV simulations of daily streamflow were applied to mimic water resources in the RCY model. The delta perturbations of climate change scenarios were applied. Then, the RCY model was run to assess the potential impacts of climate change on water resources availability, indicators and water supply capacity. After that, indicators were used for both the climate change scenarios and the baseline periods (Fig. 6a).

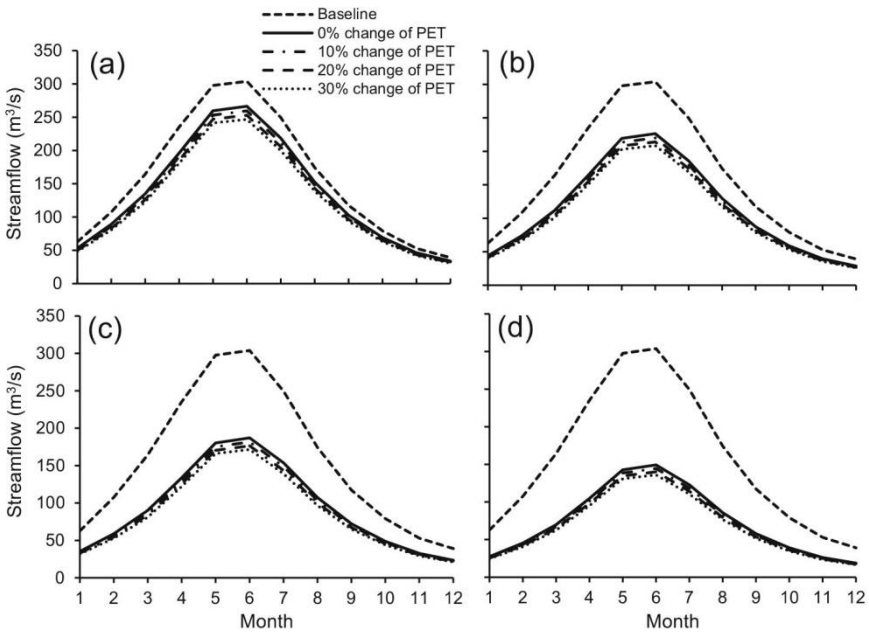

Fig. 5 Changes in the timing and magnitude of monthly average inflow to Dokan reservoir under the delta perturbation climate change scenarios for (**a**) 10% increase in precipitation (P); (**b**) 20% increase in P; (**c**) 30% increase in P; and (**d**) 40% increase in P; compared to the baseline values

Fig. 6 Box plots indicating (**a**) the Dokan reservoir operational probability of failure (OPOF, %); and (**b**) the required storage ($10^6 \times m^3$) for the reservoir

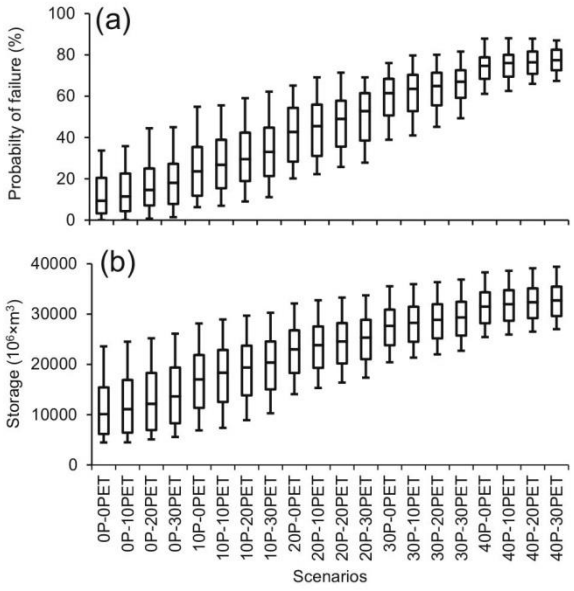

Table 1 presents a summary of the potential performance of the water resources system. It is important to note that the reliability of the water supply system is generally high during the baseline scenario. The reliability and resilience will decline, while the vulnerability will increase as a result of P reduction. However, Fig. 6b and Table 2 show that the volume required to meet the increase in water demand due to the decline of P and runoff. A 4% P decrease can mean that the existing volume is too little (by as much as 29% for a water yield of 82%), as an example. Moreover, the uncertainty or variability of the reservoir performance is

Table 1 Summary of water resources system performance under the collective impacts of precipitation (P) and potential evapotranspiration (PET) with for 82% yield

Considered time	Hydro-meteorological parameters	Values			
Baseline	P (mm)	844.08			
	Inflow (m^3/s)	1009			
	$Inflow_{wet}$ (m^3/s)	2305			
	$Inflow_{dry}$ (m^3/s)	2249			
	Reliability %	99			
	Vurnlibility (10^6 m^3)	426			
	Resilience (month)	3			
% change of P	Hydro-meteorological parameters	% change of PET			
		0	10	20	30
0	P (mm)	844.08			
	PET (mm)	1009	1110	1211	1312
	Inflow (m^3/s)	1884	1832	1783	1737
	$Infow_{wet}$ (m^3/s)	1596	1550	1509	1470
	$Inflow_{dry}$ (m^3/s)	289	283	274	267
	Reliability %	92	91	90	88
	Vurnlibility (10^6 m^3)	426	427	428	428
	Resilience (month)	3	5	8	11
10	P (mm)	759.69			
	Inflow (m^3/s)	1623	1576	1531	1490
	$Inflow_{wet}$ (m^3/s)	1371	1331	1294	1260
	$Inflow_{dry}$ (m^3/s)	252	244	237	230
	Reliability %	79	77	74	72
	Vurnlibility (10^6 m^3)	426	427	428	429
	Resilience (month)	22	22	27	23
20	P (mm)	675.26			
	Inflow (m^3/s)	1369	1327	1287	1251
	$Inflow_{wet}$ (m^3/s)	1155	1120	1087	1057
	$Inflow_{dry}$ (m^3/s)	214	207	200	194
	Reliability %	63	58	56	53
	Vurnlibility (10^6 m^3)	430	431	432	433
	Resilience (month)	24	24	32	32
30	P (mm)	590.88			
	Inflow (m^3/s)	1123	1087	1053	1021
	$Inflow_{wet}$ (m^3/s)	946	916	888	862
	$Inflow_{dry}$ (m^3/s)	177	171	165	160
	Reliability %	44	40	37	36
	Vurnlibility (10^6 m^3)	435	436	436	436
	Resilience (month)	33	43	42	45
40	P (mm)	506.44			
	Inflow (m^3/s)	889	858	830	804
	$Inflow_{wet}$ (m^3/s)	748	722	699	677
	$Inflow_{dry}$ (m^3/s)	141	136	131	126
	Reliability %	28	26	24	24
	Vurnlibility (10^6 m^3)	439	440	440	441
	Resilience (month)	61	82	94	73

Table 2 Statistical relationships between yield (Y, %) and operational probability of failure (OPOF, %) and reservoir capacity (C, 10^6 m^3) and yield for different reduction (%) in precipitation (P) and increase (%) in potential evapotranspiration (PET) using incremental climate change scenarios

%		Y (%)[a]			R^2	C (10^6 m^3)[b]			R^2
P	PET	a_3	b_3	c_3		a_4	b_4	c_4	
0	0	−0.018	1.51	71.36	0.99	6.41	− 873.3	33,302	0.99
	10	−0.007	1.17	71.21	0.99	6.74	− 571.3	10,968	0.99
	20	−0.008	1.15	69.68	0.99	5.63	− 350.8	1302.6	0.99
	30	−0.005	1.02	68.93	0.99	2.25	226.54	−21,846	0.99
10	0	−0.004	0.93	65.25	0.99	−6.83	1727.5	−77,136	0.99
	10	−0.001	0.75	65.11	0.99	−7.03	1782.2	−81,386	0.99
	20	0.001	0.68	64.08	0.99	−7.06	1906.8	−88,811	0.99
	30	0.001	0.65	62.67	0.99	−4.82	1429.3	−69,695	0.99
20	0	0.004	0.37	61.92	0.99	−4.48	1224.8	−46,423	1.00
	10	0.006	0.24	62.95	0.99	−4.56	1251.1	−48,849	0.99
	20	0.007	0.08	64.32	0.99	−4.99	1339.9	−53,963	0.99
	30	0.001	−0.18	68.46	0.99	−5.52	1443.9	−59,918	0.99
30	0	0.017	−0.99	84.38	0.99	−2.99	905.8	−26,026	1.00
	10	0.019	−1.29	91.87	0.99	−3.57	1007.9	−31,067	0.99
	20	0.012	−1.59	98.98	0.99	−3.36	982	−30,995	1.00
	30	0.002	−1.98	109.48	0.99	−3.88	1081	−36,239	0.99
40	0	0.025	−2.01	111.42	0.99	−2.30	736.5	−13,283	0.99
	10	0.034	−3.48	156.36	0.99	−2.48	773	−15,447	0.99
	20	0.025	−2.20	105.70	0.99	−2.95	859	−19,765	1.00
	30	0.039	−4.31	181.91	0.99	−2.79	836.3	−19,458	1.00

[a] $= a_3 \times OPOF^2$ (%) + $b_3 \times$ OPOF (%) + c_3;

[b] $= a_4 \times Y^2$ (%) + $b_4 \times$ Y (%) + c_4

characterised by C_v; i.e. the standard deviation divided by the mean. The uncertainty (C_v) of the OPOF, resilience, vulnerability and the required capacity varied between 0.78–0.07, 0.55–0.40, 0.87–0.47 and 0.46–0.10, respectively, which indicate that their uncertainty/variability increase as the basin become drier.

The so-called 'operational failure' rates have been determined for each model run and climate change scenario, which led to an amount of OPOF/reliability for each unit time per scenario. The successive range of OPOF involves the possible range of climate change impacts upon the water resources system over the chosen period. As the simulation results indicate that through combining adaptation measures, whether they are structural or non-structural, into water resources simulation (supply side), their effectiveness will be determined across a range of climate change and climate change variability by evaluating how each of the simulations react to a given adaptation strategy in terms of decrease (or otherwise) of OPOF, and how much of the distribution is moved away from a pre-determined and undesirable level of hazard. The developed approaches can be used to evaluate how well an adaptation measure would work within the uncertainty of a climate change range, and can, therefore, be used as a support tool for managing water resources.

Based on the results of this representative case study, an adaptation operational approach can be inferred, where the policy makers, in particular, in the semi-arid and arid regions, adjust the reservoir operating rules based on inflow estimations and the current state of reservoir capacity at each specified period, which can result in a more effective and viable management of reservoirs. In order to achieve this, the RCY model has been utilised

to derive the capacity-yield-reliability relations for the 2020s period. The first one concerns the yield-OPOF relationships (Table 2), and the second considers the capacity-yield (Table 2). These relationships can be used to test various options against the range of different future scenarios to select the most effective adaptation measure or measures, whether they are structural or non-structural. For example, if the decision-makers target is to supply water for the downstream within 5% OPOF, then by using the first graph they can obtain two values of the expected rate of yield within the range of climate change scenarios. Then, using the second operational tool, they can investigate whether there will be a need to adapt either a structural or non-structural measure.

4 Conclusions and Recommendations

Based on the representative case study for arid and semi-arid regions results, it can be inferred that an adaptation operational method, where the policy makers adjust the reservoir operating rules, based on the predicted inflow and the current state of reservoir capacity at each specified period. This can result in a more effective and viable management of the reservoir. This study tried to estimate the potential impacts of climate change on the Dokan reservoir operation, which is located in a semi-arid region using the HBV and RCY models under delta perturbations of climate change scenarios.

One of the most important impacts of the anticipated climate variation in the reservoir area is the alteration of the hydrologic environment and the performance of the water resources system if the present operation modes remain to be used. The HBV model outputs recommend a critical decrease in the values of the Dokan reservoir inflow due to a decrease in P and increase in the PET, which in turn decreases the current capacity. For instance, a reduction of about 21% in streamflow is expected to result in 10% P reduction and 30% PET increase. Additionally, for the worst case scenario, a substantial decline in inflow ranged between 56% and 58%, are estimated for the dry and wet seasons in this order. The inflow maximum magnitude will decrease, and there will be a noticeable shift in their values, which can cause a dramatic effect on basin water resources availability. Moreover, a 4% P decrease can mean that the existing capacity is too little (by as much as 29% for a water yield of 82%). Variations in reservoir inflow will impact on water utilisation purposes such as water supply, hydropower, irrigation, downstream water quality enhancement and recreational uses. Accordingly, to moderate the negative hydrologic influences and to apply the positive effects, the potential climate change impact should be examined by water resources organisations in the future.

Alterations in future monthly reservoir inflows require modifications of some of the reservoir management processes to use water more efficiently. If existing operational rules continue to be operated unchanged, projected climate change would further lead to a decline in the ability to supply water to all stakeholders. In addition, the research results show potential decreases in the water supply reliability and increases in the resilience to nearly 22% and 86%, respectively, due to dam inflow decreases. However, with higher mean temperatures and extended crop growing periods, it is expected that the demands for irrigation would also rise, which will intensify the increasing demand, owing to an increase in population. Therefore, any alteration that would improve the ability of the system to accomplish the water needs for one sector would essentially require compromises from other stakeholders. Subsequently, it is essential to assess the monthly water supply to get the most out of profit, which means that the supply system organised by the multi-purpose reservoir should have operating policies that can

be adjusted to potential hydrological and climatic alterations. The inflow increase will provide the chance to reallocate preservation storage under a climate change scenario.

The estimation of the existing water demand in the RCY model is a study limitation. Despite the fact that water demand prediction is vital to evaluate water resources systems in the future, this project and its outcomes should be seen as an initial examination of the climate change impacts on the dam water supply reliability. In order to facilitate adaptation to climate change, basin managers ought to have a quantitative basis for establishing the adaptation strategies. Accordingly, results provide a basis for enabling future water resources system managers and planners of the Dokan reservoir and similar case studies, in particular, in arid and semi-arid regions to adapt to climate change.

Acknowledgements The research has been financed by the Iraqi government via a Ph.D. scholarship for the lead author via Babylon University.

References

Chen J, Brissette FP, Leconte R (2011) Uncertainty of downscaling method in quantifying the impact of climate change on hydrology. J Hydrol 401(3–4):190–202. doi:10.1016/j.jhydrol.2011.02.020

Cook BI, Smerdon JE, Seager R, Coats S (2014) Global warming and 21st century drying. Clim Dyn 43(9–10): 2607–2627. doi:10.1007/s00382-014-2075-y

Fowler HJ, Kilsby CG, Connell PEO (2003) Modeling the impacts of climatic change and variability on the reliability, resilience, and vulnerability of a water resource system. Water Resour Res 39(8):1222. doi:10.1029/2002WR001778

IPCC (2014) Intergovernmental panel on climate change. Climate change 2014: impacts, adaptation, and vulnerability. http://www.ipcc.ch/report/ar5/wg2. Accessed 15 May 2015

Li L, Xu H, Chen X, Simonovic SP (2010) Streamflow forecast and reservoir operation performance assessment under climate change. Water Resour Manag 24:83–104

McMahon TA, Adeloye AJ (2005) Water resources yield. Water Resources Publications, Littleton

McMahon TA, Adeloye AJ, Zhou SL (2006) Understanding performance measures of reservoirs. J Hydrol 324: 359–382

Minville M, Brissette F, Krau S, Leonte R (2009) Adaptation to climate change in the management of a Canadian water resources system exploited for hydropower. Water Resour Manag 23:2965–2986

Mohammed R, Scholz M (2016) Impact of climate variability and streamflow alteration on groundwater contribution to the base flow of the Lower Zab River (Iran and Iraq). Environ Earth Sci 75:1392. doi:10.1007/s12665-016-6205-1

Mohammed R, Scholz M (2017) The reconnaissance drought index: a method for detecting regional arid climatic variability and potential drought risk. J Arid Environ (in press)

Mohammed R, Scholz M, Zounemat-Kermani M (2017) Temporal hydrologic alterations coupled with climate variability and drought for transboundary river basins. Water Resour Manag 31:1489–1502. doi:10.1007/s11269-017-1590-0

Moy W, Cohon JL, ReVelle CS (1986) A programming model for analysis of the reliability, resilience, and vulnerability of a water supply reservoir. Water Resour Res 22(4):489–498

Nalbantis I (2008) Drought and streamflow. Eur Water 23(24):65–76

Park JY, Kim SJ (2014) Potential impacts of climate change on the reliability of water and hydropower supply from a multipurpose dam in South Korea. J Am Water Resour Assoc (JAWRA) 50(5):1273–1288

Reis J, Culver TB, Block PJ, McCartney MP (2016) Evaluating the impact and uncertainty of reservoir operation for malaria control as the climate changes in Ethiopia. Clim Chang 136:601–614. doi:10.1007/s10584-016-1639-8

Sheffield J, Wood EJ, Roderick ML (2012) Little change in global drought over the past 60 years. Nature 491: 435–438

Soundharajan BS, Adeloye AJ, Remesan R (2016) Evaluating the variability in surface water reservoir planning characteristics during climate change impacts assessment. J Hydrol 538:625–639. doi:10.1016/j.jhydrol.2016.04.051

Tigkas D, Vangelis H, Tsakiris G (2012) Drought and climatic change impact on streamflow in small watersheds. Sci Total Environ 440:33–41

Tigkas D, Vangelis H, Tsakiris G (2015) DrinC: a software for drought analysis based on drought indices. Earth Sci Inform 8(3):697–709. doi:10.1007/s12145-014-0178-y

Vangelis H, Tigkas D, Tsakiris G (2013) The effect of PET method on reconnaissance drought index (RDI) calculation. J Arid Environ 88:130–140

Vicente-Serrano SM, Lopez-Moreno JI, Beguería S, Lorenzo-Lacruz J, Sanchez-Lorenzo A, García-Ruiz JM, Azorin-Molina C, Morán-Tejeda E, Revuelto J, Trigo R, Coelho F (2014) Evidence of increasing drought severity caused by temperature rise in southern Europe. Environ Res Lett 9(4):044001. doi:10.1088/1748-9326/9/4/044001

Vicuna S, Dracup JP (2007) The evolution of climate change impact studies on hydrology and water resources in California. Clim Chang 82:327–350. doi:10.1007/s10584-006-9207-2

Appendix C Data Requested Official Letters

University of Salford MANCHESTER

Salford, 2 September 2015

Ministry of Agriculture and Water Resources-KRG-General Directorate of Dams and Reservoirs,
Ministry of Agriculture and Water Resources-KRG-Dokan Dam Directorate,
Ministry of Planning-KRG, and
Ministry of Environmental-KRG

To Whom It May Concern

Dear Sir or Madam,

Request for information on the impact of climate change on water resources availability in Iraq.

We have several Iraqi students (funded by the Iraqi Ministry of Higher Education) working towards a PhD degree under my supervision here at The University of Salford. We would highly appreciate, if you could help us in gathering some of the information related to the impact of climate change on water resources availability in Iraq and corresponding adaptation and mitigation strategies. The information we may need include:

1. Daily and monthly records for the following meteorological variables:
   a. Precipitation,
   b. Maximum and Minimum Temperature,
   a. Humidity,
   b. Wind Speed,
   a. Solar, and
   a. Evaporation
   from the stations: Sulymanyah, Erbeel, Salahddin, Kirkuk, Makhmoor, Halabcha, Soran, Halabcha, and Tus.

2. Daily and monthly flow at the following gauging stations along Little Zab River: Little Zab at Dokan, Little Zab at Dokan Village, and Little Zab at Altun Kupri-Goma Zardela.

3. All information related to Dokan dam and its reservoir such as:
   a. Daily and monthly:
      a.1 Inflow and outflow from Dokan dam,
      a.2 Evaporation from Dokan reservoir, and
      a.3 Precipitation at Dokan reservoir
   b. The tabulated values of the relationships between storage, surface area, and water level
   c. The dam hydraulic properties such as maximum, minimum, normal and dead water level
   d. The dam structural properties such as length, width, height and type
   e. A diagrammatic scheme for the dam

4. Hydrological studies about the Little Zab River Basin

5. All local studies done to analysis climate change and drought impacts on the Little Zab River Basin water resources

6. All available FAO (and other UN organizations) studies carried out on water resources availability as well as the effect of drought and climate change on Little Zab River Basin

7. Actions that were taken by local authorities to tackle and mitigate climate change and drought influences on the Little Zab River Basin water resources

8. Proposed and planned irrigation projects upstream and downstream of Dokan dam.

We assure you that any information that we collect will only be used for research purposes and we are happy to sign any non-disclosure agreement with you if necessary. The outcome of the research will be supplied to you for free.

Yours Sincerely,

University of Salford MANCHESTER
School of Computing, Science & Engineering
07 SEP 2015

Prof. Miklas Scholz
cand ing, BEng (equiv), PgC, MSc, PhD, CWEM, CEnv, CSci, CEng, FIEA, MIEMA, PCIWEM, FICE, Fellow of IWA
Chair in Civil Engineering and Head of the Civil Engineering Research Group
Phone: 0044 161 2955921; E-mail:m.scholz@salford.ac.uk

University of Salford, The Crescent, Salford, M5 4WT, United Kingdom
t: +44 (0)161 295 5000 www.salford.ac.uk

University of Salford MANCHESTER

January 15, 2016

To: The Environmental Protection and Improvement Broad-Erbil Environment Directorate

Facilitation for obtaining the required information from your relevant departments

Dear Sir/Madam,

We have a number of worldwide students, are working towards their PhD degrees under my supervision here at the University of Salford, Greater Manchester, UK.

Miss Ruqayah Mohammed is one of our students who work toward this. We would highly appreciate if you could help us in gathering some of the information concerning an approach for possibility of applying the "Assessment of the effect of climate change in anticipated water resources availability and adaptation measures: Application of Lower Zab River basin in arid climate zone".

We assure you that any information we collect will only be used for research purposes and we are happy to sign Non-Disclosure agreement with you, if any.

The outcomes of the research may be given to you if you need it.

Many thanks and looking forward for your help.

Yours Sincerely,

University of Salford MANCHESTER
School of Computing, Science & Engineering
20 JAN 2016

Professor Miklas Scholz

cand ing, BEng (equiv), PgC, MSc, PhD, CWEM, CEnv, CSci, CEng, FHEA, FIEMA, FCIWEM, FICE, Fellow of IWA

Chair in Civil Engineering and Head of the Civil Engineering Research Group

Address: Civil Engineering Research Group, School of Computing, Science and Engineering, The University of Salford, Newton Building, Greater Manchester M5 4WT, UK

Phone: 0044 161 2955921

Mobile: 0044 7765464263

Fax: 0044 161 2955575

E-mail: m.scholz@salford.ac.uk

Web: http://www.salford.ac.uk/computing-science-engineering/our-academics/miklas-scholz

Board of Protection & Improvement of Environment

Student has asked us pertaining Enviro-issues

University of Salford MANCHESTER

Miss Ruqayah visited the planning department, ~~last~~ based on her request the information and has been given to her.
Sincerely, March 2nd 2016

January 15, 2016

To: The Environmental Protection and Improvement Broad

Environment Protection and improvement board
Sanaan. A. Mohammed

Facilitation for obtaining the required information from your relevant departments

دەستەی پاراستن وچاککردنی ژینگە
فەرمانگەی کارگێڕی ودارایی وياسايی
بەشی خوێندن

Dear Sir/Madam,

We have a number of worldwide students, are working towards their PhD degrees under my supervision here at the University of Salford, Greater Manchester, UK.

Miss Ruqayah Mohammed is one of our students who work toward this. We would highly appreciate if you could help us in gathering some of the information concerning an approach for possibility of applying the "Assessment of the effect of climate change in anticipated water resources availability and adaptation measures: Application of Lower Zab River basin in arid climate zone".

We assure you that any information we collect will only be used for research purposes and we are happy to sign Non-Disclosure agreement with you, if any.

The outcomes of the research may be given to you if you need it.

Many thanks and looking forward for your help.

University of Salford MANCHESTER
School of Computing, Science & Engineering
20 JAN 2016

Yours Sincerely,

Professor Miklas Scholz

cand ing, BEng (equiv), PgC, MSc, PhD, CWEM, CEnv, CSci, CEng, FHEA, FIEMA, FCIWEM, FICE, Fellow of IWA

Chair in Civil Engineering and Head of the Civil Engineering Research Group

Address: Civil Engineering Research Group, School of Computing, Science and Engineering, The University of Salford, Newton Building, Greater Manchester M5 4WT, UK

Phone: 0044 161 2955921

Mobile: 0044 7765464263

Fax: 0044 161 2955575

E-mail: m.scholz@salford.ac.uk

Web: http://www.salford.ac.uk/computing-science-engineering/cse-academics/miklas-scholz

University of Salford, The Crescent, Salford, M5 4WT, United Kingdom
t: +44 (0)161 295 5000 www.salford.ac.uk

University of Salford MANCHESTER

January 15, 2016

To: The Ministry of Agriculture and Water Resources, General Directorate of Water Resources

Facilitation for obtaining the required information from your relevant departments

Dear Sir/Madam,

We have a number of worldwide students, are working towards their PhD degrees under my supervision here at the University of Salford, Greater Manchester, UK.

Miss Ruqayah Mohammed is one of our students who work toward this. We would highly appreciate if you could help us in gathering some of the information concerning an approach for possibility of applying the "Assessment of the effect of climate change in anticipated water resources availability and adaptation measures: Application of Lower Zab River basin in arid climate zone".

We assure you that any information we collect will only be used for research purposes and we are happy to sign Non-Disclosure agreement with you, if any.

The outcomes of the research may be given to you if you need it.

Many thanks and looking forward for your help.

Yours Sincerely,

University of Salford MANCHESTER
School of Computing, Science & Engineering
20 JAN 2016

Professor Miklas Scholz

cand ing, BEng (equiv), PgC, MSc, PhD, CWEM, CEnv, CSci, CEng, FIIEA, ~~FIEMA, FCIWEM, FICE,~~ Fellow of IWA

Chair in Civil Engineering and Head of the Civil Engineering Research Group

Address: Civil Engineering Research Group, School of Computing, Science and Engineering, The University of Salford, Newton Building, Greater Manchester M5 4WT, UK

Phone: 0044 161 2955921

Mobile: 0044 7765464263

Fax: 0044 161 2955575

E-mail: m.scholz@salford.ac.uk

Web: http://www.salford.ac.uk/computing-science-engineering/cse-academics/miklas-scholz

For whom concerned
we supported that
water resources data
up to (2016) is given as
thesis by G.D. of Water Res
(both surface & ground waters)
for ascertaining
investigation's studies
Muhammad Rizgar
Hussain A Rasool

Assessment of the Effect of Climate Change in Anticipated Water Resources Availability Measures in Arid Climate Zones

A thesis submitted in partial fulfillment of the requirement for the degree of Doctor of Philosophy

By

Ruqayah Kadhim Mohammed

B.Sc., M.Sc.

School of Computing Science and Engineering

University of Salford

Manchester

UK

September 2017